HIGH FREQUENCY INVERTER-TRANSFORMER-CYCLOCONVERTER

SYSTEM FOR DC TO AC(3-PHASE) POWER CONVERSION

A thesis submitted for the degree of Doctor of philosophy

by

Asghar Karamat

Department of Electrical Engineering and Electronics

Brunel , The University of West London , England

March 1991

Dedicated to My :

1- Mother and late Father with respect

2- wife Nahid and Daughter Shima

3- Sister and Brothers

ACKNOWLEDGMENTS

I wish to express my deep and sincere gratitude to my supervisor , Mr. T. Thompson , for his enlightened supervision , kind assistance , encouragement and constructive suggestions throughout the course of this research work .

I wish to thank professor G. Musgrave Head of Department of Electrical Engineering and Electronics , Brunel university , for providing research facilities .

Thanks are due to Dr. P. Mehta and Dr. Mohammed Darwish for their valuable assistance , discussions and also due to Dr. Mostafa Darwish for his many helps .

The author is also grateful to :

Mr. J. Newton , Mr. M. Rafati and colleagues for their willing help in providing devices and equipments relating to this work .

Departmental secretary , Mrs. P. Phillips .

The staff of Brunel university computer centre for the excellent provision of computing facilities .

I express my thanks due to Urmia University , IRAN , for providing this opportunity and financial support .

I wish to thank and acknowledge my wife , Nahid , for her continuous encouragement and help during this study and difficult times .

Finally , I wish to express my everlasting gratitude to my parents for their invaluable help and guidance to make me prepared for this study in the past .

ABSTRACT :

This thesis is concerned with a 3-phase multistage high frequency link DC to AC power conversion with a novel inverter-cycloconverter circuitry . The conversion system is composed of a high frequency PWM inverter , step-up high frequency transformer and cycloconverter with bidirectional switching devices .

In first stage the DC voltage of the power source , say a submarine battery, is inverted to a system of 3-phase sinusoidally modulated 1 kHz alternative wave forms . For this purpose a suggested optimized PWM technique for 3-phase inverter operation is adopted , in which harmonic components up to 17 th (17 kHz) are eliminated from the inverter output voltages.

In the second stage , for DC input isolation from AC output and also for a voltage transfomation (here stepping-up) a high frequency (size reduced) transformer is employed . Generalized high frequency operation , influence and side effects of the transformer on overall system design & performanc is investigated .

In the final stage the 1 kHz -to- 50 Hz conversion process is accomplished by a 3-phase cycloconverter . The proposed "nonlinear modulation strategy" for cycloconverter output voltage and associated harmonic analysis is demonstrated , in which the hamonic components up to 38th (1.9 kHz) are eliminated fom the conversion system output voltage .

To assess the suggested functioning principles for the inverter & cycloconverter , the prototype conversion system was developed . Some design criteria and switching device selection are presented , together with different voltage & current wave forms of the prototype system under resistive & inductive load (induction motor) and their respective spectra .

Contents

Chapter 3

Chapter 5

Design & Performance of the prototype System 193

Chapter 6

Appendixes

Abbreviations:

AC	Alternative Current
CRD	Capacitor Resistor Diode(snubber)
D	Drain (MOSFET)
DC	Direct Current
EMI	Electro-Magnetic Interference
G	Gate(MOSFET)
GOSS	Grain Oriented Silicon Steel
GTO	Gate Turn Off thyristor
H.D	Harmonic Distortion
h.f	high frequency
HVDC	High Voltage Direct Current
k Hz	kilo Hertz
M Hz	Mega Hetz
MOSFET	Metal Oxide Semiconductor Field Effect Transistor
PRI	Parallel Resonant Inverter
PWM	Pulse Width Modulation
S	Source(MOSFET)
SIT	Static Induction Transistor
SITH	Static Induction Thyristor
SMES	Super-Conducting Magnetic Energy Storage
SMPC	Switched mode Power Conversion
SPICE	Simulation Program with Integrated Circuit Emphasis
SRI	Series Resonant Inverter
T.H.D	Total Harmonic Distortion
UPS	Uninterruptible Power Supply
vol.	volume
ZVS	Zero Voltage Switching
ZCS	Zero Current Switching

List of Principal Symbols:

A	ampere
A	area(m^2)
A_n	transfer matrix coefficients
A_n	cycloconverter switching pattern amplitude
A_1 & A_2	load line trajectory
a_n	Fourier Series coefficients in general
A	area(m^2)
B	magnetic flux density(Tesla)
B_r	remanent density
B_{max}	maximum density
B_s	saturation density
b_n	Fourier Series coefficients in general
C	capacitance(Farad)
C_f	filter capacitor
C_r	resonant capacitor
C_s	snubber capacitor
C_{gs}	MOSFET gate to source capacitor
C_{gd}	MOSFET gate to drain capacitor
C_{ds}	MOSFET drain to source capacitor
C_p	primary interwinding capacitance
C_s	secondary interwinding capacitance
C_t	total interwinding capacitance
C°	teperature
D1,D2,D3,...	antiparallel diodes
D11,D22,....	snubber circuit diodes
di/dt	rate of change of instantaneous current

E	source voltage(volt)
E	energy(J)
$f_{11}..f_{lk}...f_{mn}$	cycloconverter switching function
f_c	carier wave frequency
f_i	cycloconverter input frequency
f_m	modulating wave frequency
f_o	cycloconverter output frequency
f_r	resonance frequency
f_{rotor}	rotor frequency
f_{stator}	stator frequency or supply frequency
F1,F2,F3	switching functions in direct 3-phase conversion
h	heat transfer coefficient
H	magnetizing force or magnetic field intensity
i	instantaneous current(A)
I_a,I_b,I_c	cycloconverter input current
I_A,I_B,I_C	cycloconverter output current
I_{ah}	input current harmonics
I_C	collector current
I_d	dual converter output current
I_D	drain current
I_ϕ	primary magnetizing current
k	constant
L	inductance(H)
L_c	winding length
L_e	magnetic path length
L_f	filter inductor
L_m	primary magnetizing inductance
L_{mt}	mean turn length

L_p	primary leakage inductance
L_r	resonant inductor
L_s	secondary magnetizing inductance
L_S	snubber inductance(turn-on)
m	number of input phases
M	modulation index
n	number of output phases
n_1,n_2	transformer turns numbers
N	number of pulses over a quarter cycle
N_P	primary turns
N_r	rotor speed (round per minute)
N_s	synchronous speed(round per minute)
N_S	secondary turns
p	number of pole pairs
p_d	dielectric loss
p_e	eddy current loss
p_h	hysteresis loss
p_i	input power
p_o	output power
p_r	prototype power
Q_o	quality factor
R	ratio of input to output frequency
R	resistance
R	ratio of carrier wave to modulating wave frequency
Re	transformer core loss shunt resistance
R_g	gate resistance
R_o	load resistance
R_p	primary resistance

R_s	secondary resistance
R_S	snubber circuit resistance
S	slip(per unit)
$S_1,S_2,.....,S_{18}$	semiconductor switches
t	transformer sheet thickness
T_1,T_2	semiconductor switches
T_a	ambient temperature
t_d(off)	delay time on switch turn-OFF
t_d(on)	delay time on switch turn-ON
t_f	switching fall time
T_{on}	switch on(conduction) time
t_r	switching rise time
T_s	switching period(on + off)
T_o	operating temperature
u_{AN},u_{BN}	average voltage during device switching
dv/dt	rate of change of the instantaneous voltage
v_{ab},v_{bc},v_{ca}	3-phase inverter line voltages
v_{an},v_{bn},v_{cn}	3-phase inverter phase voltages
$v_{a'n},v_{b'n},v_{c'n}$	3-phase rectifier phase voltages
v_{AN},v_{BN}	cycloconverter input voltages
v_{ANh}	output voltage harmonics
v_C	voltage across the capacitor
V_{CE}	transistor Collector to Emitter voltage
V_d	dual converter output voltage
V_{DC}	phase controlled converter output voltage

V_{DS}	MOSFET drain to source voltage
V_{GS}	MOSFET gate to source voltage
v_{in}	input voltage
$v_{(\,harm.\,)}$	harmonic voltage amplitude
$v_{(\,harm.\,)}$	harmonic voltage amplitude
V_m	maximum source voltage
v_{no}	inverter third harmonic voltage
v_o	output voltage
$v_{o\text{-}p}$	positive group output voltage
v_R	voltage across the resistor
v_{spike}	spike voltage
$v_2, v_3, \ldots, v_n$	harmonic voltage amplitude
y	lamination sheet thickness(meter)
Z_{AB}, Z_{BC}, Z_{CA}	3-phase load impedances

Greek letters

α	delay firing angle(inverter-phase R)
$\alpha_1,\alpha_2,...,\alpha_k$	pulse width in proposed modulation strategy
α_p	delay firing angles for the positive converter
α_n	delay firing angles for the negative converter
β	delay firing angle(inverter-phase Y)
γ	delay firing angle(inverter-phase B)
δ	magnetic skin dept
δ	pulse width
Δ	proportional to
ε	dielectric constant
η	efficiency
θ	phase shift between waveforms(in phase modulation)
θ	permissible temperature(C°)
μ	absolute permeability(H/m)
μ_o	magnetic space constant = $4\pi.10^{-7}$ (H/m)
μ_r	relative permeability(per unit)
ρ	resistivity(Ω.m)
Φ	core flux(Wb)
Φ_m	maximum flux(Wb)
$d\Phi/dt$	rate of change of the magnetic flux(Wb/sec.=volt)
ω	source angular frequency(rad/sec.)
ω_c	carrier wave angular frequency(rad./sec.)
ω_o	output voltage angular frequency(rad./sec.)

Chapter 1

Introduction

1. Switched Mode Power Conversion (SMPC)

1.1 General

In a general sense , power conversion can be defined as a process(series of action , changes , manipulations) that converts one form of energy(Electrical , Thermal , Radiant , ...) to another on a continuous basis . There are many types of devices which can provide such a function with varing degrees of cost , reliability , complexity and efficiency .

Here , only power converters which perform energy translation electrically and in a dynamic fashion , are the area of interest . Generally the linear(dissipative) and switched mode (nondissipative) are two alternatives for delivery of electric power from a DC source in a controllable manner .

Linear power conversion is based on the presence of a series linear element , either a resistor (mechanical control) , or a transistor used in linear mode (electronic control) such that the total load current is passed through the series linear element and more power is lost in the controlling device Fig.1-1(a) . Thus , linear power conversion even in its ideal form is dissipative and inefficient (according to the maximum power transfer theorem $\eta(max)=50\%$).

In switched mode power conversion , the controlling device is an ideal switch either closed or open Fig. 1-1(b) . By controlling the ratio of the time intervals spent in the closed and open position (T_{on}/T_s) the power flow to the load can be controlled in a very efficient way , ideally 100% , because when the device is fully on it has only a small saturation voltage drop across it (0.3 to 1.0).

In the off condition the reverse leakage current is usually negligible so that the power loss is nearly zero . A detailed comparison between linear and switched mode power conversion may be found in [1] .

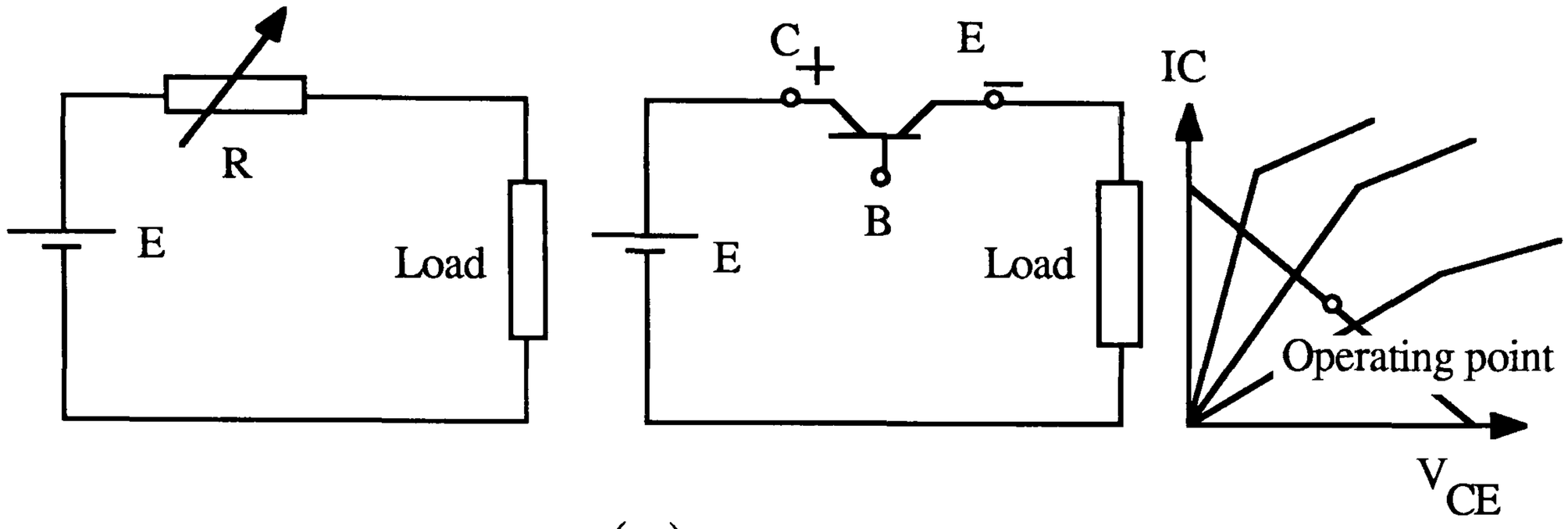

(a)

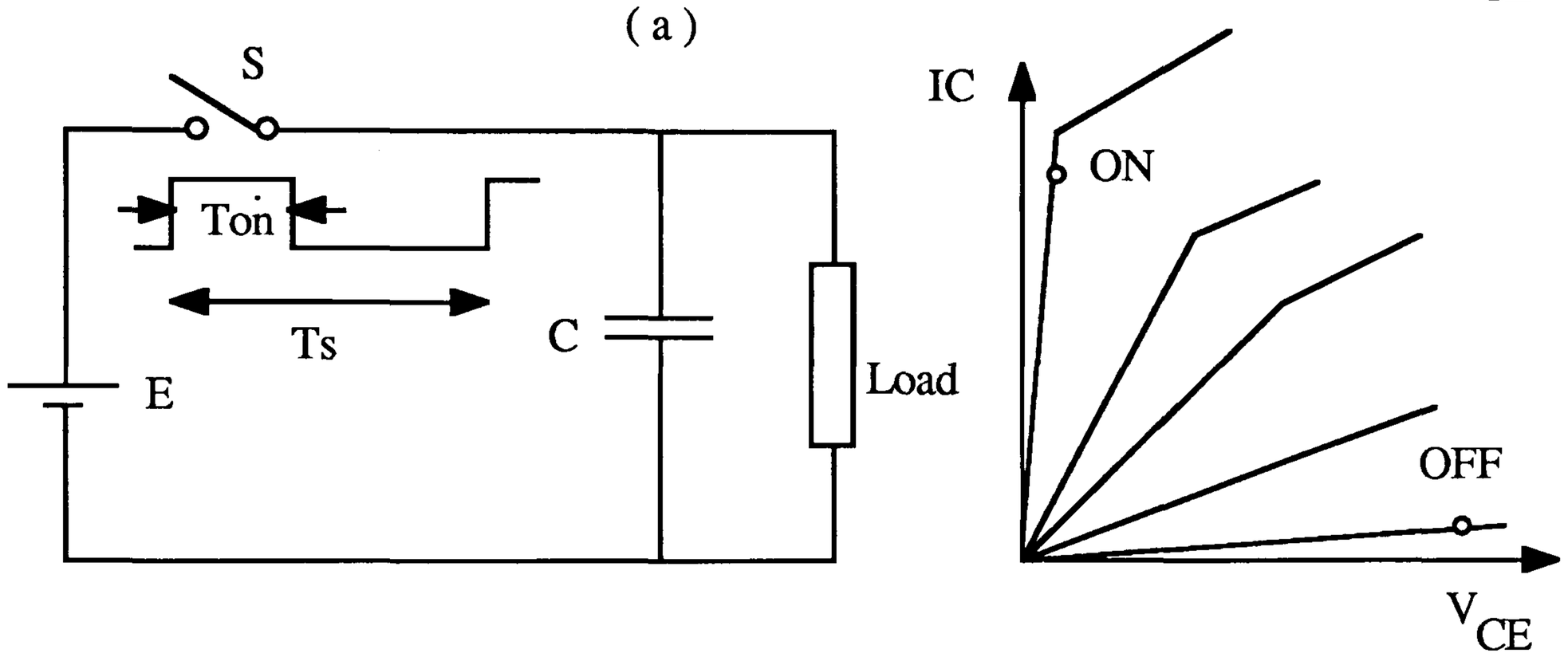

(b)

Fig. 1.1 Power conversion circuits :

(a) - linear (dissipative) (b) - switch mode (nondissipative)

A general switched mode power conversion (SMPC) system has components including , Inductors , Capacitors , Transformers , Semiconductor Switches , and associative Controllers (microcomputers , microprocessors) as shown in Fig. 1-2.

In SMPC systems , the semiconductor switches ; Bipolar Junction Transistor (BJT) , Metal Oxide Semiconductor Field Effect Transistor (MOSFET) , ...and Gate Turn-Off Thyristors (GTO) , that controlling the dynamic transfer of power from input to output , are either fully ON or fully OFF , with very short transition times from one of these states to the other .

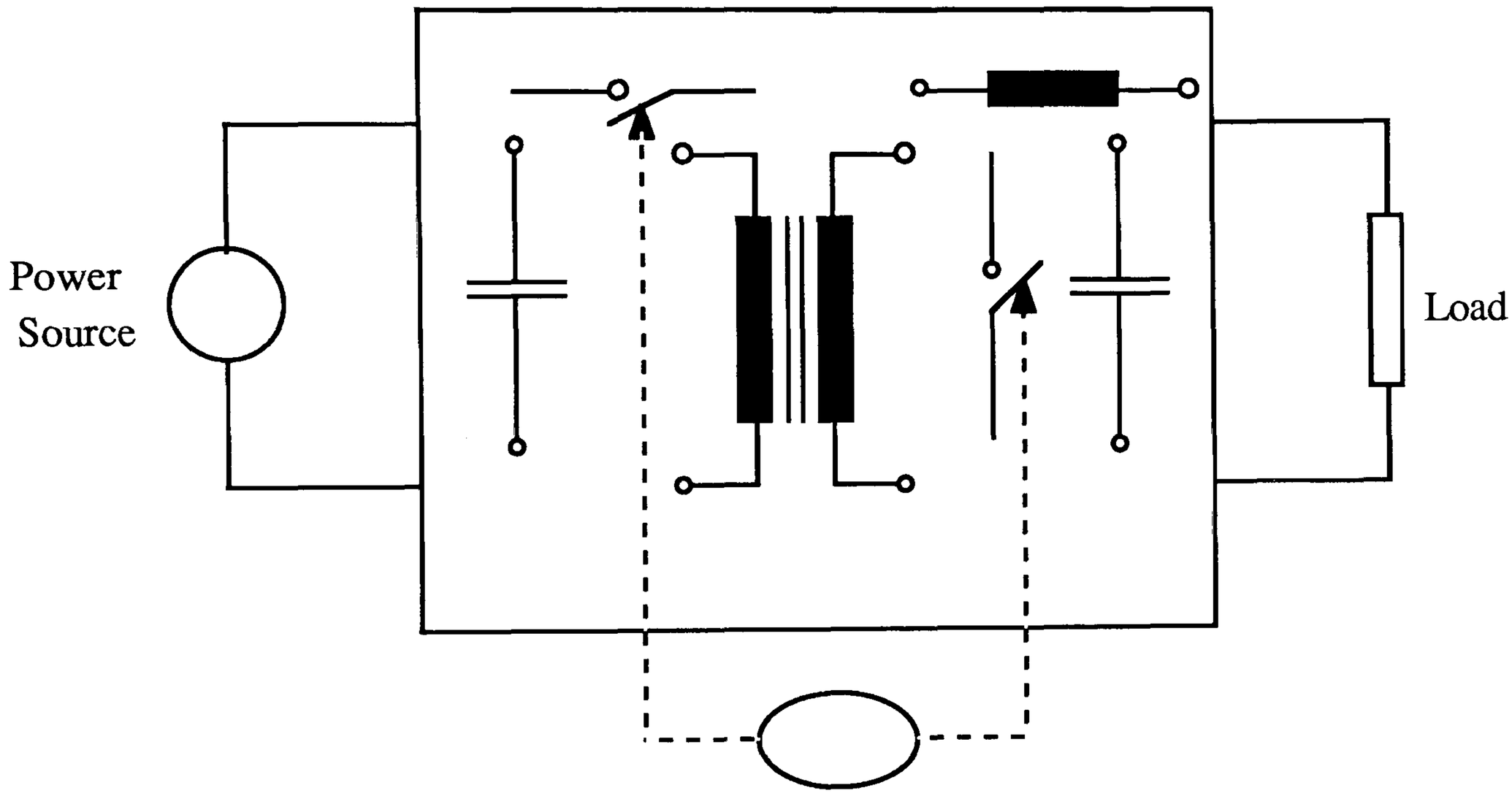

Fig. 1-2 General switched mode power conversion(SMPC) system

1.2 SMPC with high frequency link

The basic objective of high frequency power conversion is size reduction , that is , having compact and lighter weight power converters for following applications :

Mainframe computers , airborne and mobile equipments , artificial satellite , artificial organs for biological replacement , space stations , space vehicles , robotics , ships and submarines (in link with the work presented in this thesis) .

Reducing the physical size with result of less surface area for system cooling, necessitates higher efficiencies for achieving higher power densities. On the other hand higher efficiency dictates lower conversion loss in all devices and components .

In SMPC circuits , magnetic elements and capacitors play the major roles of energy storage / transfer and ripple filtering . Since the required values and volumes of magnetic elements (Transformers and Inductors) and Capacitors decrease as the operating frequency is increased , it is imperative to design converter circuits capable of operating at high power and high frequencies to achieve high power density and element size reduction .

It should be emphasized that , the operation of any converter at very high frequencies (k Hzs and M Hz) is strongly influenced by the effects of parasitic elements such as interconnected and leakage inductances , interwinding capacitances , skin effect in conductors , and proximity effect in inductors .

Some parasitics such as the leakage inductance of the transformers can be constructively used as a part of circuit [1] , [2] , [3] . When the resonant elements are placed on the primary side of the transformer , the leakage inductance and interwinding capacitances act as an independent parasitic elements between the resonant elements (L_r & C_r) and out-put filter . If the resonant capacitor be pushed appropriately through the transformer to the secondary then the leakage inductance and interwinding capacitances values can be added to resonant elements . The result is a welcomed absence of the voltage spikes on all the windings . Other parasitics may have adverse effects on the circuit performance and should be

minimized . The effects of high frequency operation in transformers will be studied in chapter 3 .

During the last decade , different topologies which use a high frequency AC link for DC-to-DC and DC-to-AC power conversion with different control requirement , have been presented in [4] , [5] , ... , [12] .

Reference [13] illustrates a DC-to-AC power conversion technique which employes two high frequency inverters operating with *frequency modulation* . The link frequency is typically of the order of a few kilohertz and low frequency (50 Hz) output power is obtained from the high frequency inverters through a suitable Transformer -Cycloconverter circuitry with following block diagram .

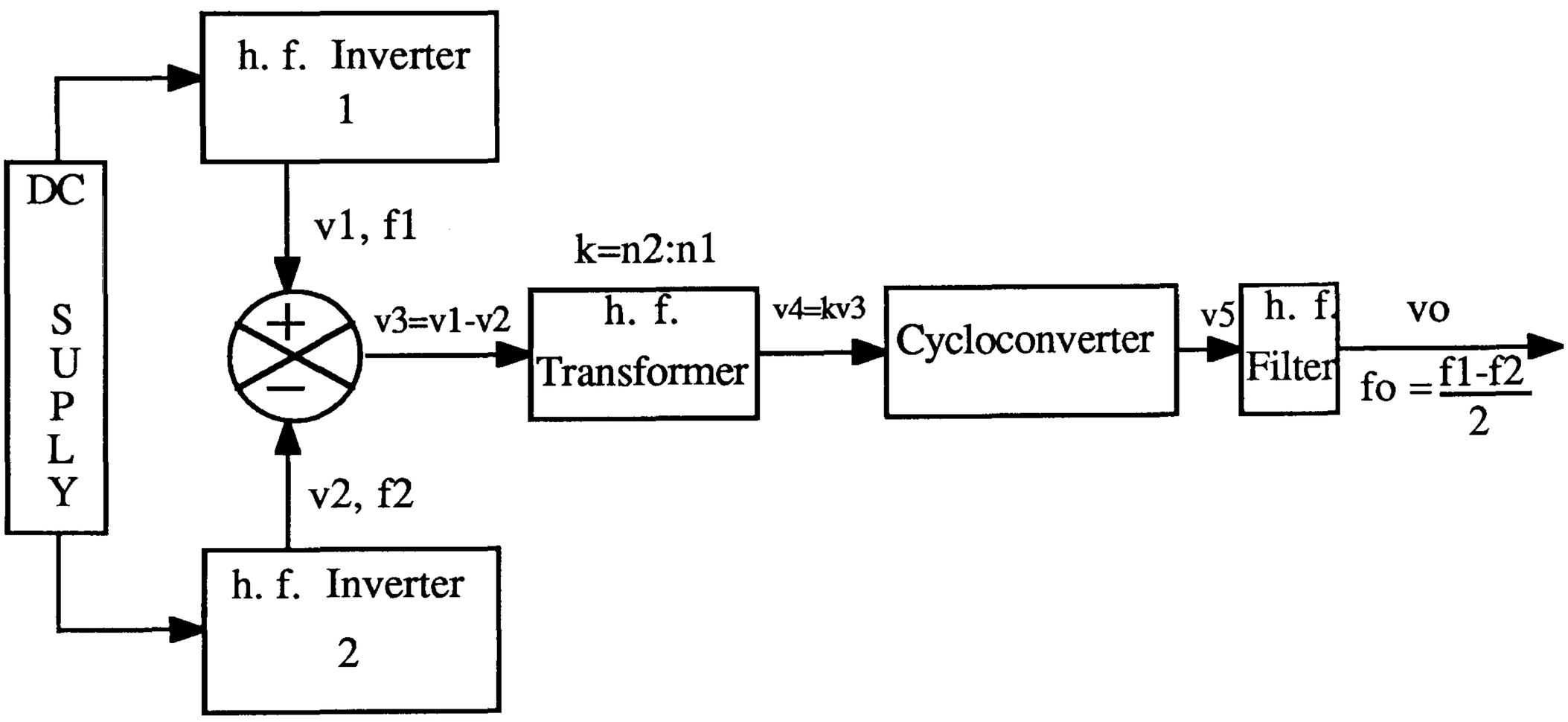

Fig. 1.3 DC-to-AC power conversion based on ***frequency modulation***

A brief mathematical system description is :

$$v_1 = V_m.Sin(\omega_c+\omega_o)t\ ,\ v_2 = V_m.Sin(\omega_c-\omega_o)t\ ,\ v_3 = v_1-v_2\ ,\ v_4 = k.v_3 \qquad (1\text{-}1)$$

$$v_4 = kV_m\left[Sin(\omega_c+\omega_o)t\ -\ Sin(\omega_c-\omega_o)t\right] = \left[2kV_mSin(\omega_o t)\right].Cos(\omega_c t) \qquad (1\text{-}2)$$

v_5 can be obtained by multiplying v_4 and a square wave v_s with unit amplitude and in phase with $Cos(\omega_c t)$. Afther some arithmetic manipulation :

$$v_5 = v_o + v_{(harmon.)} \qquad (1\text{-}3)$$

$$v_o = \frac{4kV_m}{\pi}.Sin(\omega_o t) \qquad (1\text{-}4)$$

$$v_{(harmon.)} = -\sum_{m=1}^{\infty}\left[Sin(2m\omega_c+\omega_o)t - Sin(2m\omega_c-\omega_o)t\right](-1)^m\left(\frac{2kV_m}{\pi}\right)\left[\frac{1}{2k-1} - \frac{1}{2k+1}\right] \qquad (1\text{-}5)$$

If $f_1 = f_c + f_o = 20.1$ kHz , $f_2 = f_c - f_o = 20$ kHz , then in (1-4) the v_o is required output with $f_o = (f_1 - f_2)/2 = 50$ Hz and (1-5) shows harmonic components starting with $2f_c+f_o = 40.15$ k Hz and $2f_c - f_o = 40.05$ k Hz , so unwanted components can be easily filtered.

Reference [14] shows a controllable DC-to-DC and DC-to-AC power conversion process employing two high frequency Inverters operating with *phase-modulation strategy* , Fig. 1-4 , with following mathematical description

$$v1(\omega t) = \frac{4V_m}{\pi}\sum_{n=1,3,5}^{\infty}\frac{Sin(\frac{n\pi}{2})}{n}.Cos\left[n(\omega_c t-\theta)\right] \qquad (1\text{-}6)$$

$$v1(\omega t) = \frac{4V_m}{\pi}\sum_{n=1,3,5}^{\infty}\frac{Sin(\frac{n\pi}{2})}{n}.Cos\left[n(\omega_c t+\theta)\right] \qquad (1\text{-}7)$$

$$v3(\omega t) = v1(\omega t) - v2(\omega t) \qquad (1\text{-}8)$$

$$v3(\omega t) = \frac{8V_m}{\pi}\sum_{n=1,3,5}^{\infty}\frac{Sin(\frac{n\pi}{2})}{n}.Sin(n\theta).Sin(n\omega_c t) \qquad (1\text{-}9)$$

Suppressing of harmonics by tank circuit :

$$v4(\omega t) = \frac{8V_m}{\pi}.Sin(\theta).Sin(\omega_c t) \qquad (1\text{-}10)$$

$v_4(\omega t)$ after passing through full bridge rectifier is processed to $v_5(\omega t)$ which can be obtained by multiplying $v_4(\omega t)$ with a unit square wave $v_s(\omega t)$ having the same phase relationship:

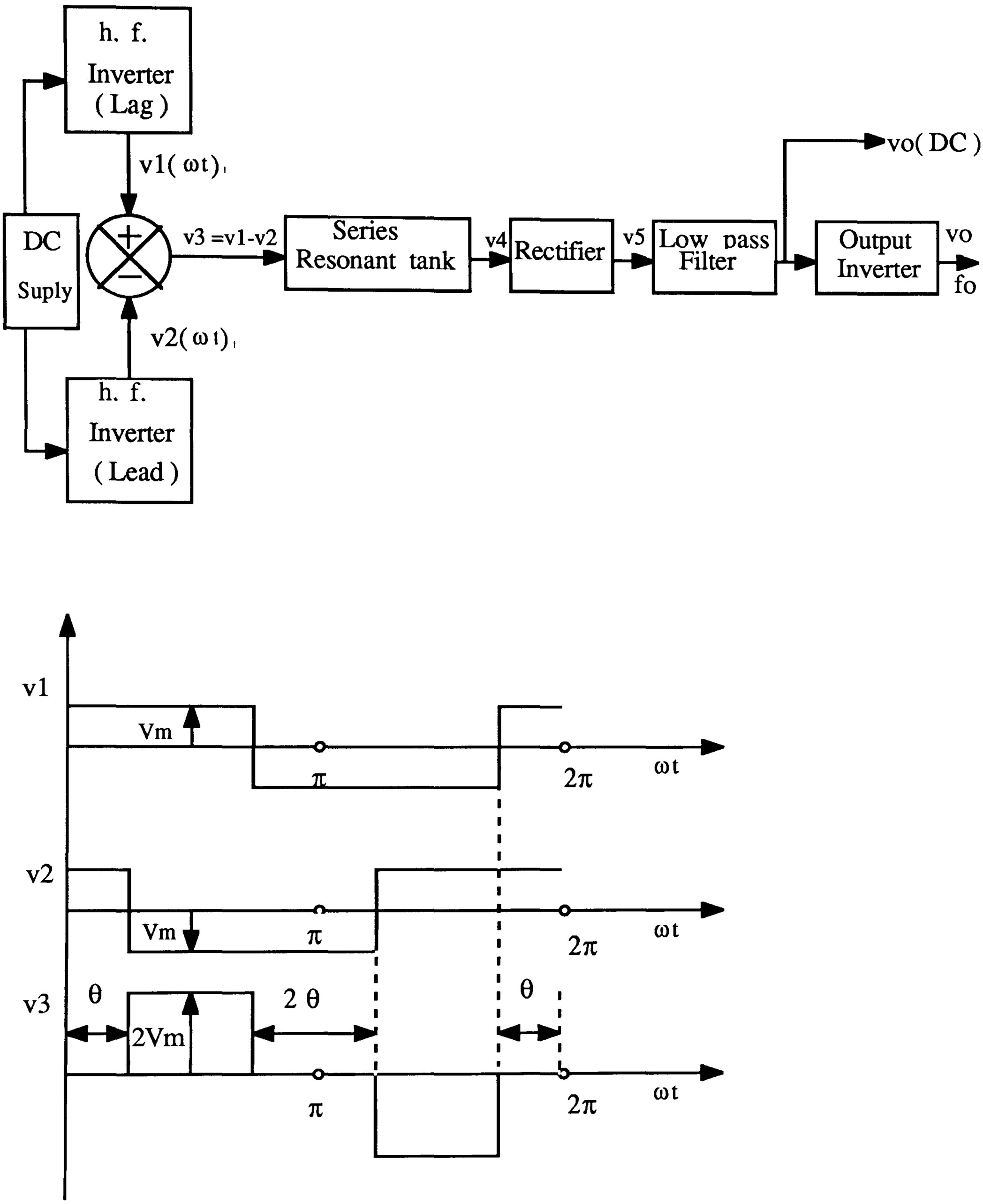

Fig. 1.4 DC-to-(DC & AC) power conversion based on ***phase modulation***

$$v5(\omega t) = \frac{16V_m}{\pi^2}.Sin(\theta) \; - \; v_{(harmoni.)} \qquad (1\text{-}11)$$

$$v_{(harmoni.)} = \frac{32V_m}{\pi^2}Sin(\theta).\left\{ \sum_{n=3,5,7}^{\infty} \left[\frac{1}{(n+1)(n-1)} \right].Cos(n\omega_c t) \right\} \qquad (1\text{-}12)$$

after suppressing terms containing ωc yields :

$$V_{out(DC)} = \frac{16V_m}{\pi^2}.Sin(\theta) \qquad (1\text{-}13)$$

The output of the output Inverter is yielded from (1-12) with frequency of fo and modulation index of M . Phase modulation [14] has some advantages over frequency modulation [13] :

1- Control range is extended to include zero output ($\theta = 0^\circ$)

2 - Power factor of the system is unity when $\theta = 90^\circ$ and zero when $\theta = 0^\circ$.

1-3 SMPC with Resonant Topologies

Generally , when the conversion frequency of conventional pulse width-modulation(PWM) power converters increase and approaches to 100 k Hzs , the switching losses and switch stresses become excessive due to the forced commutation and consequently , simultaneous presence of a high current and high voltage during turn-on and turn-off , Fig. 1-5 .

On the other hand , industrial applications strongly demand high frequency operation in off-line power conversion , because they offer higher power density , faster transient response , and size reduction in energy storage/transfer components .

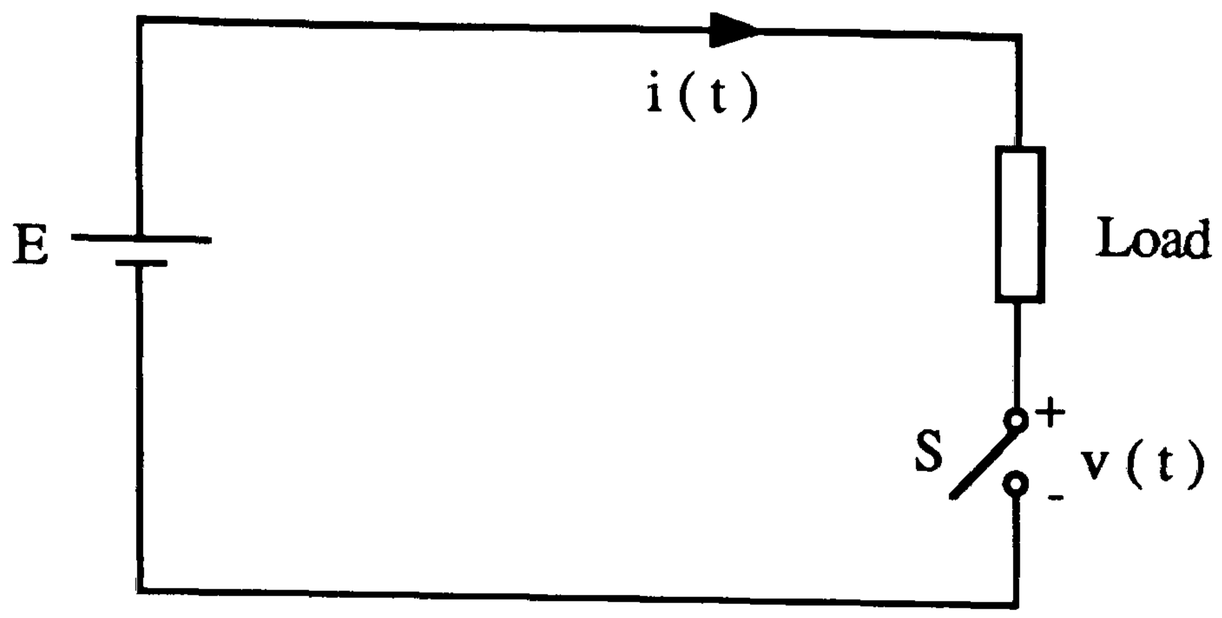

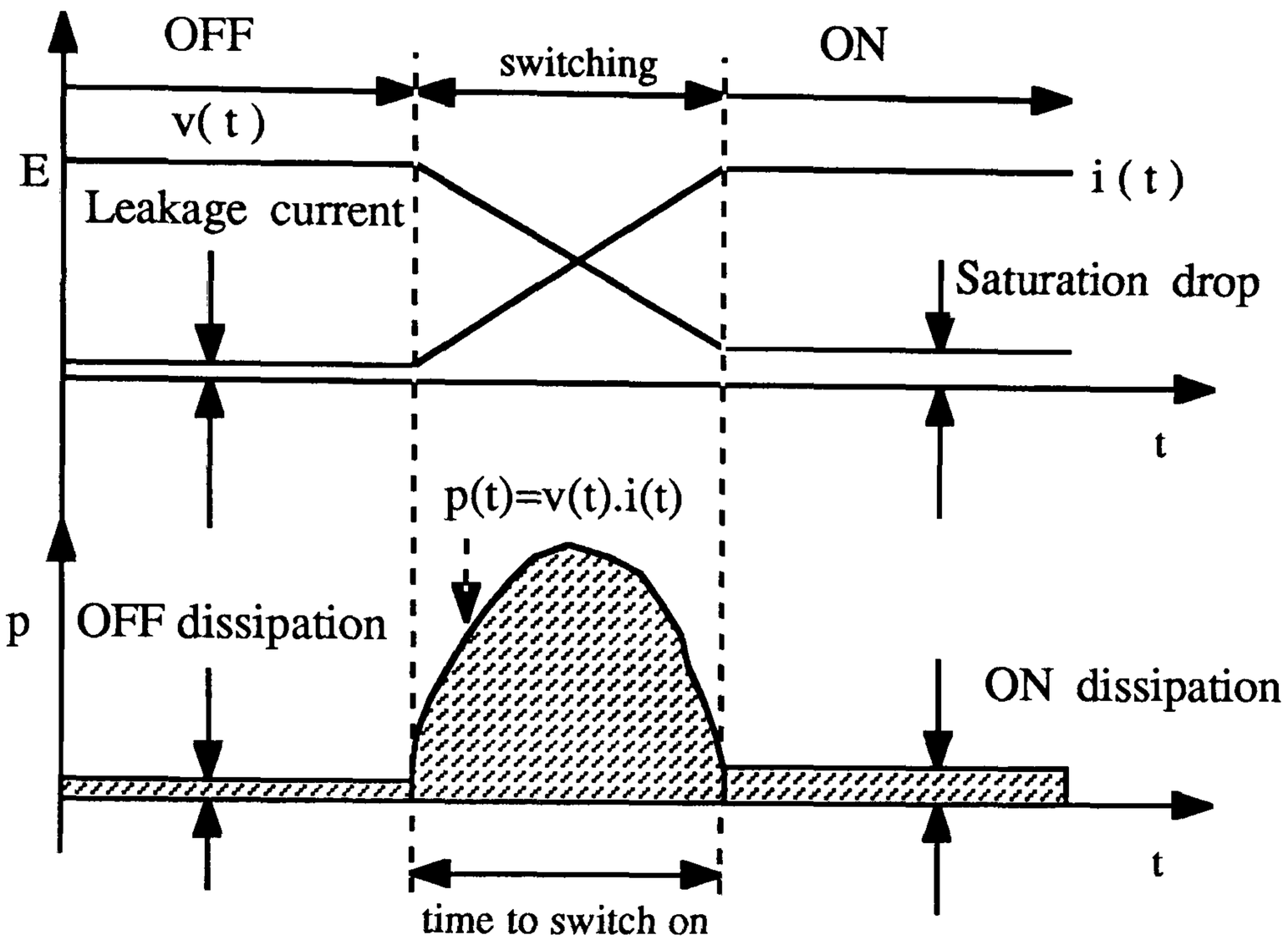

Fig. 1-5 General device switching & associated power loss characteristics

The fundamental departure from the conventional forced commutation approach was the "zero-current switching" technique reported in [15] , then "resonant switches" was proposed by Liu and Lee in [16] . By adding a high frequency resonant circuit around the switch it is possible to shape the switch current and voltage wave forms so that a high current and a high voltage are not present at the same time.

Depending on how the high frequency resonant circuit is connected to the switch , the resonant or quasi-resonant technique eliminates either turn-on or turn-off switching losses .

1.3.1 Zero Current & Zero Voltage Switching:(ZCS) & (ZVS)

In the zero-current switched (ZCS) resonant converters [17] the current of the transistor is shaped by a resonant network , so that it is reduced to zero prior to turn-off to eliminate turn-off losses . In the zero-voltage switched (ZVS) resonant converters [17] the voltage wave form of the transistor is shaped by a resonant network , so that the voltage reduces to zero prior to turn-on to eliminate turn-on losses .

For clear understanding Fig. 1-6 shows the Buck converter with the conventional , ZCS and ZVS versions and their equivalent [18] . In Fig. 1-6 (b) ,when switch is conducting , Inductor L and Capacitor C constitute a series resonant circuit with it's oscillation initiated by the turn-on of S . Current through S is sinusoidal and reduced to zero before S is turned-off .

Similar events take place in Fig. 1-6 (d) . Fig. 1-6 (c) & (e) are equivalent circuit of ZC & ZV resonant switches . Each of these topologies represent a high frequency sub-circuit obtaining from a resonant converter by replacing voltage sources and filter capacitors with short circuits , and filter inductors with open circuits [19] .

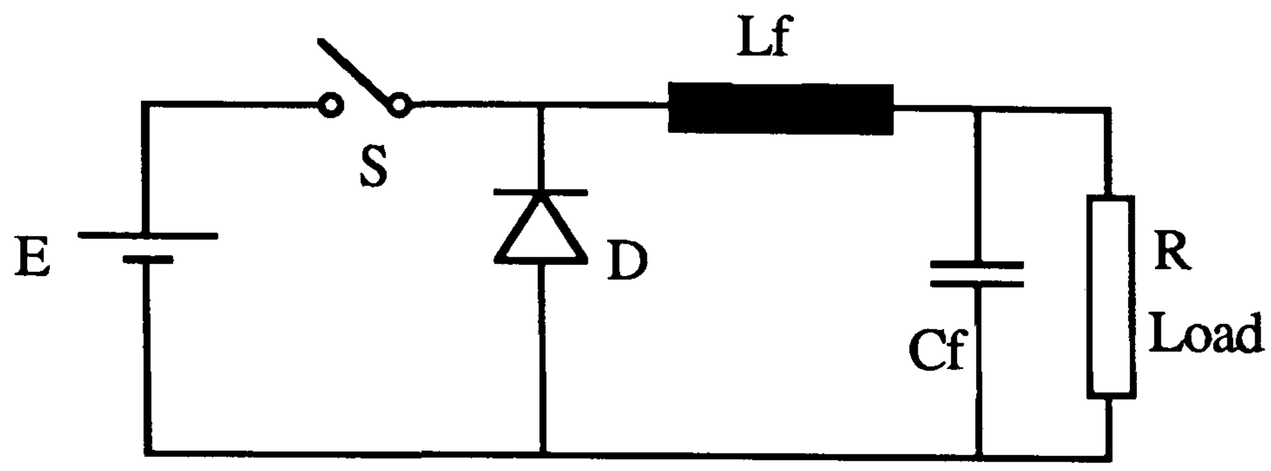

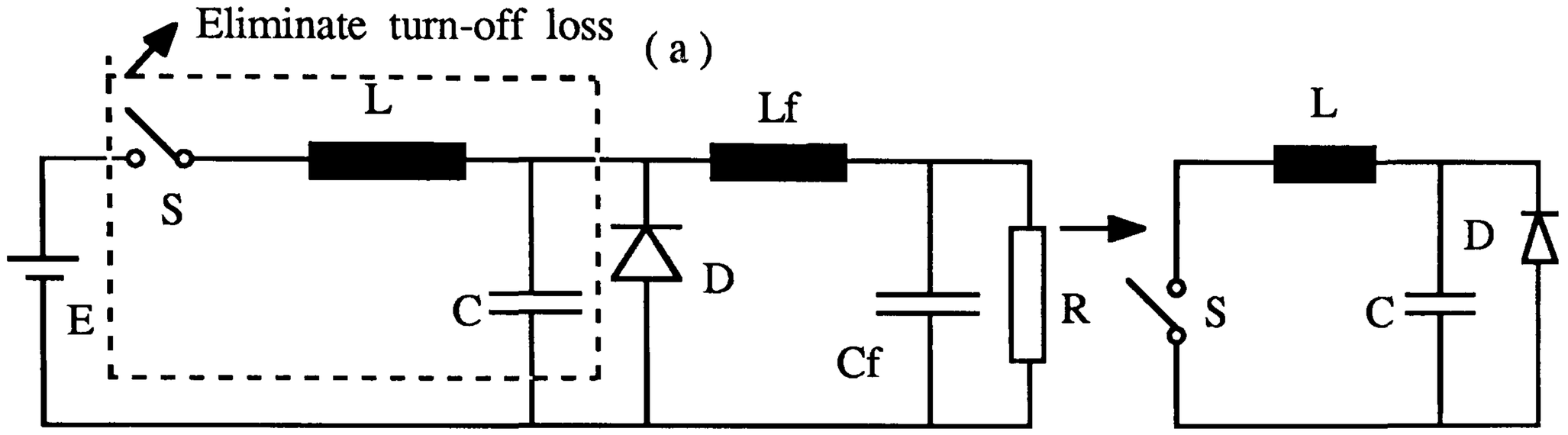

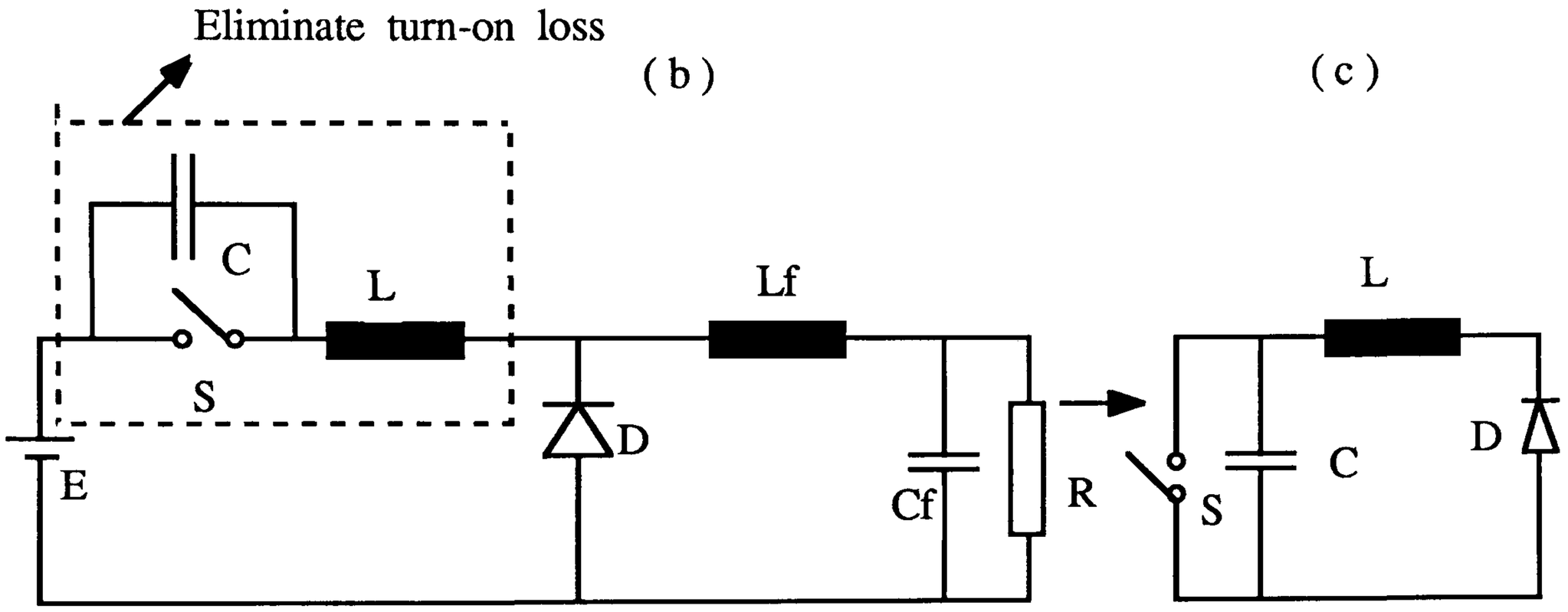

Fig. 1-6 Buck converter (a)- conventional (b)- ZCS (d)- ZVS

The load line trajectory for a inductive load with conventional and resonant switching is shown in Fig. 1-7 . In the conventional switching (path A1 & A2) the path goes through a high stress region where the switch

is subject to high voltage and high current simultaneously , but in the resonant switching the path B moves along either the voltage axis or the current axis , consequently , the switching stresses and losses are eliminated .

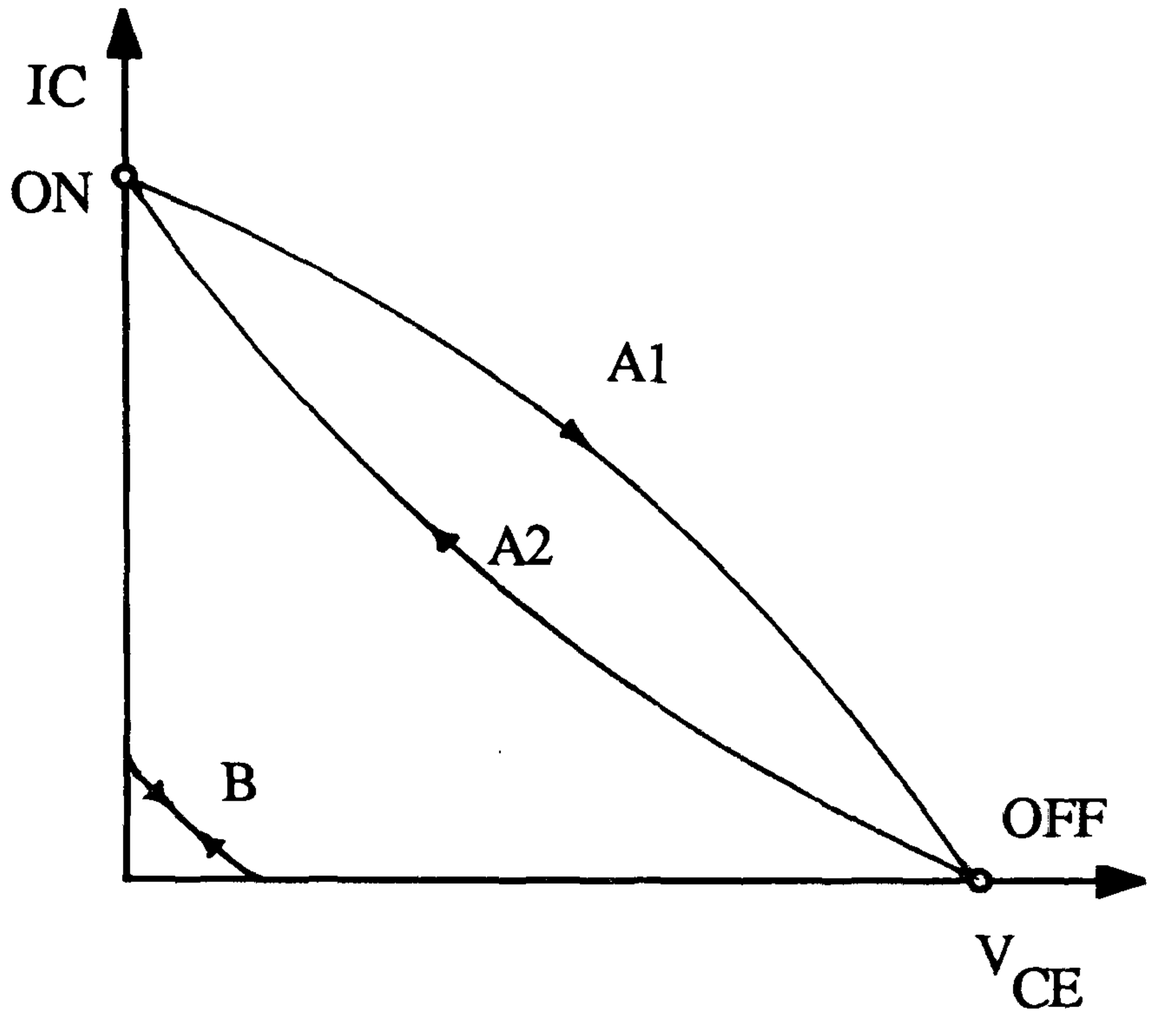

Fig. 1-7 Load line trajectory for inductive load :

A , A2 for conventional switching & B for resonant switching

1.4 Uninterruptible Power Supply (UPS)

An UPS system is a device which is placed between the user's equipment input and the power-source output , to act as a reserve source of energy in the event of a complete power failure or mains disturbances (missing cycles , sags , spikes and transients) .

Most of the equipment served by the utility can tolerate short term voltage variations or disturbances with out affecting the operation or life of the equipment . There is however growing use of computer and other critical equipments that are more sensitive to input power quality than almost all others.

Once a computer system stops for very short duration due to a power disturbance or failure ; the result may be malfunction , production of "bad data" , and total system shut down . Nevertheless , in general , voltage can fall to zero as long as it recovers with in 0.5 cycles or 8.33 milliseconds , and it can drop to 30% below normal for up-to 0.5 seconds . This is due to stored energy built in to the computer power supply filters and motors [20] .

The need for a UPS will always be determined by comparing the danger , inconvenience and expense caused by unpredicted power problems against the cost of installing and maintaining UPS system itself [20-chapter 2] ,[21]

1.4.1 General application of UPS systems

In general the following are the most common areas of applications :

1- where power interruptions endanger lives and property ; hospital diagnostic , intensive-care systems , industrial safety monitors and process control systems where quality and continuity of supply are of vital importance , stock-market quotation , bank transfers , air-line reservations , and alarms and surveillance equipment .

2- where power interruptions cost time and money ; computer complexes , remote terminals , and instrumentation centres .

3- where power interruptions disrupt critical data networks ; military installations , automatic production lines , satellite and radar communications , pipe-line and electrical distribution monitoring systems .

1.4.2 UPS technology

There are basically two types of power conditioning devices available to provide the reserve energy source :

1-static UPS system

2-rotary UPS system

In addition there are 3 types of operating principle; "on-line" , "off-line" and "hybrid" [22] . Each type has its own advantages and disadvantages .

1.4.2.1 static UPS system

Fig. 1-8 shows typical static UPS , OFF-line and ON-line [23] . In Fig.1-8 (a) OFF-line UPS provides power for less sensitive loads such as lighting , heating , systems and motors that only require protection against complete mains failure . Under normal conditions the load is powered directly by the input AC supply , and is only driven by the inverter on failure of the mains supply . The transfer to the inverter is automatic and is normally performed by a mechanical device such as contactor .

ON-line UPS , Fig. 1-8 (b) eliminates any switching of load between the failed mains and inverter output . This system protect the sensitive loads against of whole range of daily occurrence hazards to include ; line disturbances , over voltage spikes , voltage sags and drop-outs .

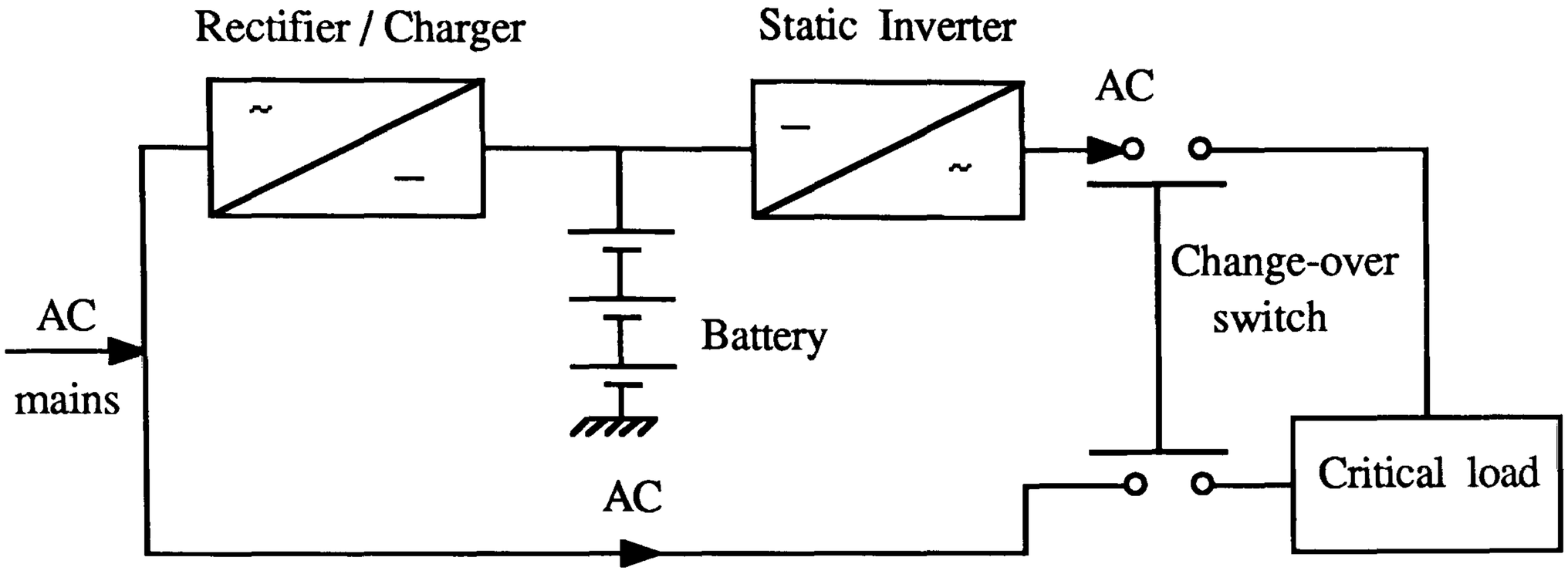

(a) OFF-line (stand-by) UPS

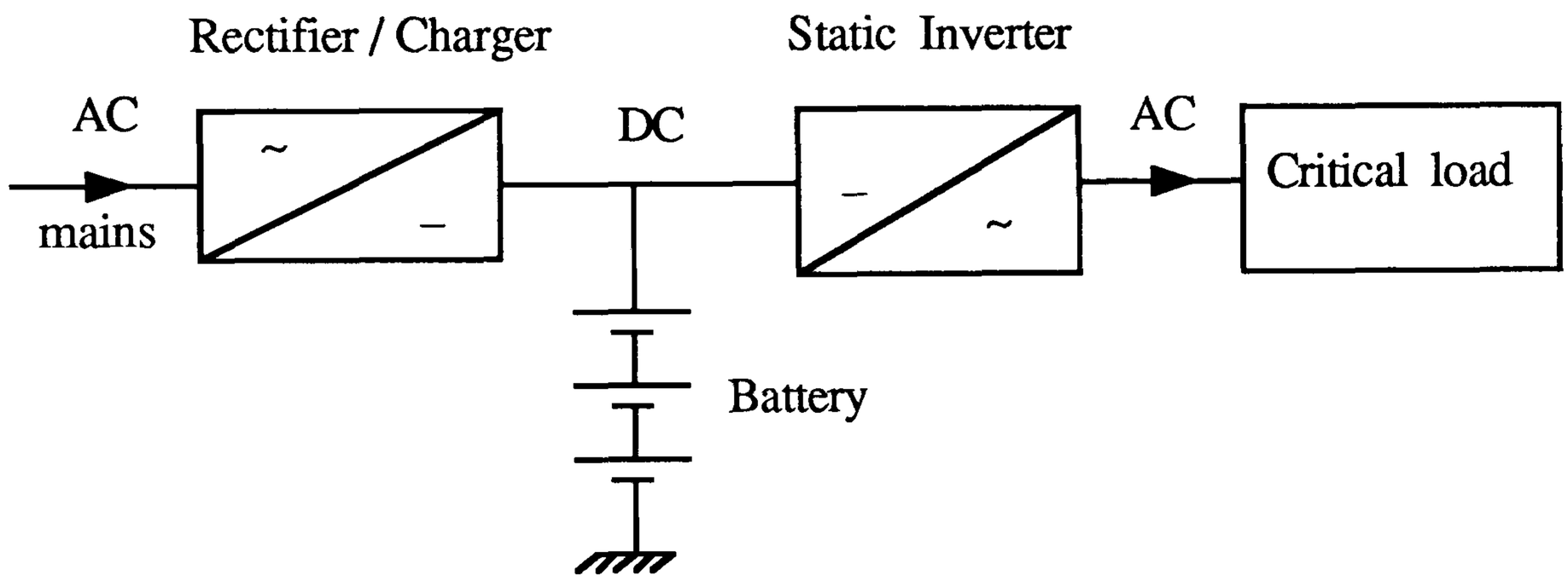

(b) ON-line UPS

Fig. 1-8 Static UPS systems (a)- OFF-line (b)- ON-line

1.4.2.2 Rotary UPS system

Although the majority of UPS in use today are of the static variety , a number of very reliable and useful systems using rotating components . Fig. 1-9 shows typical rotary UPS (a) [20] and hybridized static-rotary (b) [24] .

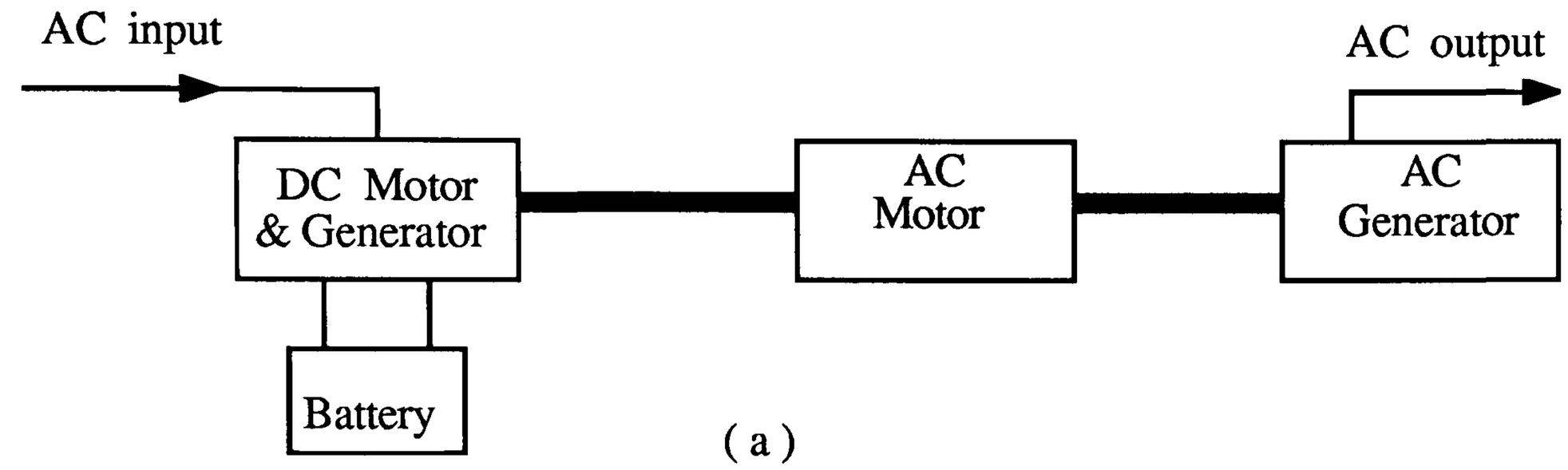

(a)

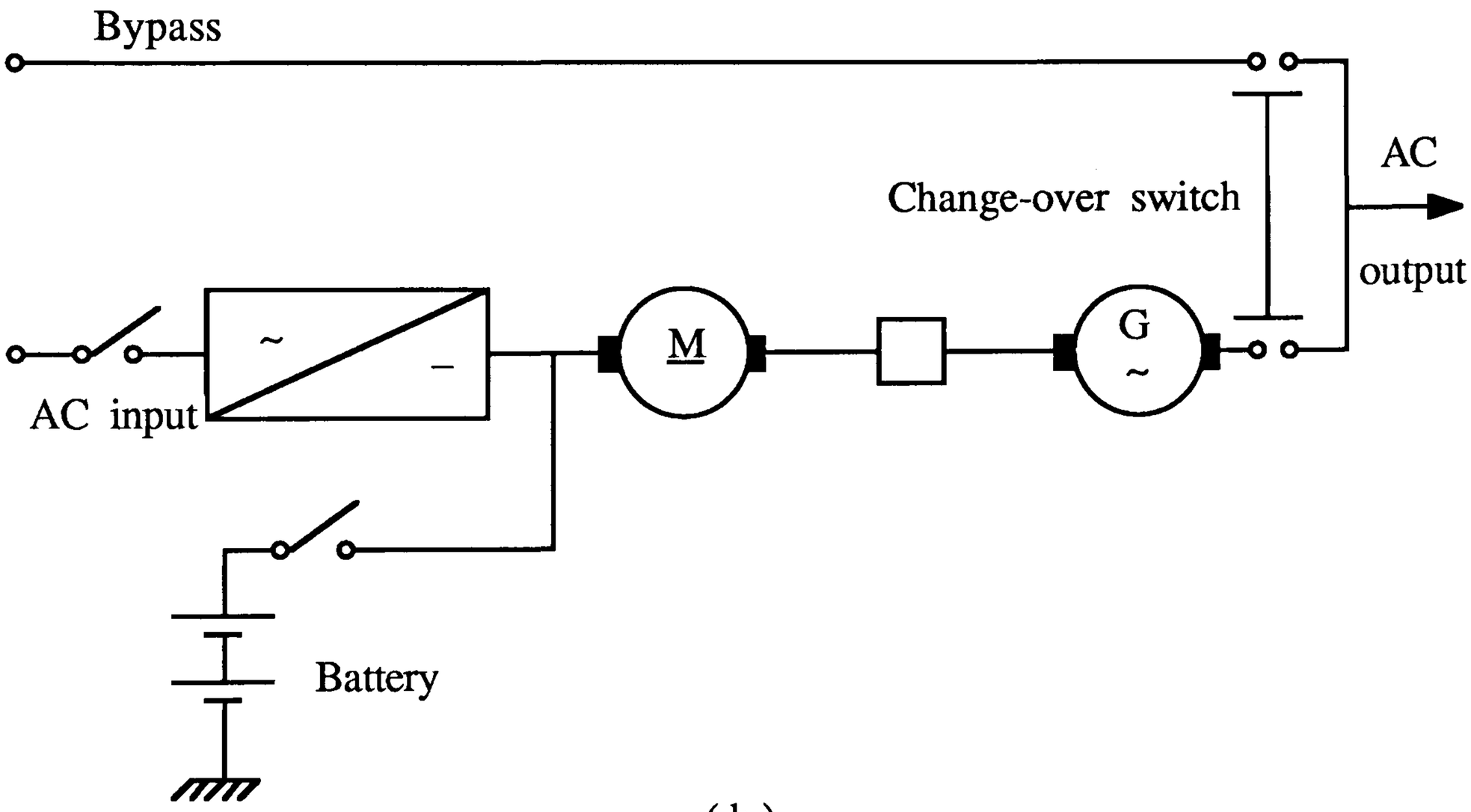

(b)

Fig. 1-9 (a)- Rotary & (b)- Hybridized (static-rotary) UPS system

The rotary system fulfils the same basic requirements as the static UPS . The DC / AC converter of the rotary system consists of a DC motor with shunt field control driving a separately exited AC alternator mounted on a common shaft with or with out a fly wheel . Stable frequency operation is achieved by regulating the speed of the DC motor and the output voltage of the AC alternator is regulated by the use of an automatic voltage regulator .

Further development of rotary UPS includes a synchronous machine in which the motor and the generator windings are located on a single common frame . The rotor is DC exited and has a damper winding which provides a low impedance to high frequency harmonic currents . This construction of machine offers the advantages of a reduction in size and weight , improvement of efficiency, reduction of source impedance and increase of system reliability . Detailed study about rotary and hybrid version of UPS systems may be found in [20] .

A full optimum voltage and harmonic control PWM technique for 3-phase UPS systems has been presented in [25] .

1.4.3 Other type of UPS system (Triport UPS system)

This system employs the versatility of reversible charger / inverter and combine some of the benefits of both OFF-line and ON-line systems . Basically it consists of a ferro-resonant Transformer [26] and a single-phase square wave inverter . The Transformer has two primary windings , one of them is connected to the mains through a static transfer switch and the other connected to the output of inverter and the secondary winding connected to the load as Fig. 1-10 shows.

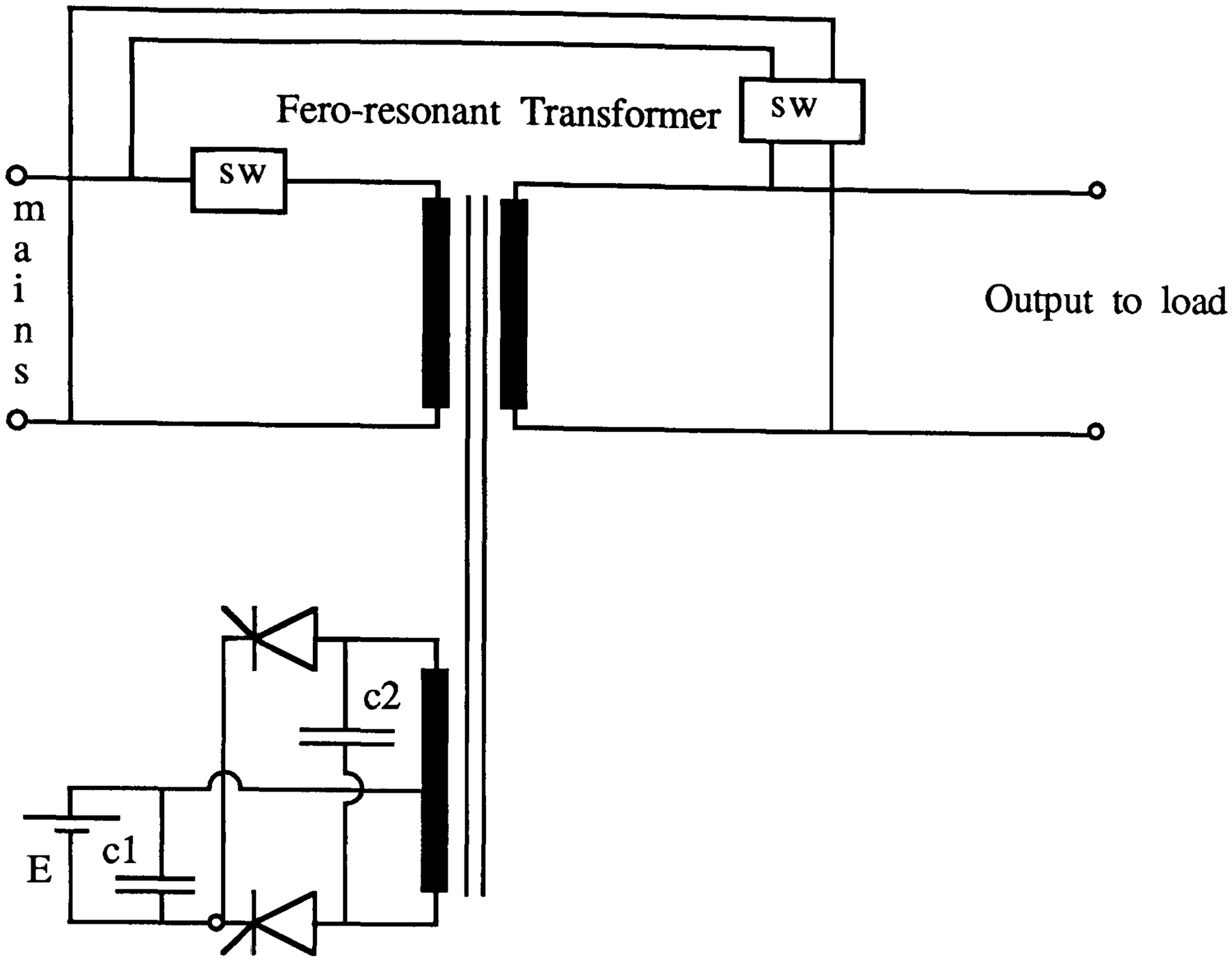

Fig. 1-10 Triport UPS system

under normal condition , the load and ferro-resonant transformer and consequently the battery charger are powered from the mains . During mains disturbance transfer switch disconnect the mains , allowing inverter to rebuilt AC power from the battery without any interruption [27] , [28] and [29] .

1.5 Superconducting Magnetic Energy Storage (SMES)

To satisfy the need for a power conditioner (future large scale UPS system) and peak power , several technologies including compressed air , under - ground pumped hydro-storage , batteries , and superconducting magnetic energy storage [30] , [31] are available . In each of these technologies , except SMES , the Electrical energy is converted to another form , Mechanical or Chemical , through several transformations and then back to Electrical . The conversion processes are inherently inefficient (65% to 75%) . SMES may be as high as 95% efficient because there is no conversion of energy from one form to other [32] .

Research on SMES started in 1970 at the university of Wisconsin(U.S.A) and industrial participation in the development of commercially feasible SMES began in 1980 by Bechtel company [33] . The general schematic of a SMES and it's components [32] is shown in Fig. 1-11 .

The current in the superconducting coil will be on the order of several kilo-ampers . Since power systems normally operate at low current levels so a transformer is needed to convert the high voltage and low current of the AC system to the low voltage and high current required by the coil . The individual semiconductor elements can only carry a few thousand amperes so many must be used in parallel .

The converter is an AC-to-DC rectifier and DC-to-AC inverter that changes the alternating current from the utility in to the direct current that must flow continuously in the coil . Here extremely reliable protection measures are required because , unlike other energy sources , an open coil circuit could result in huge economic loss . Since the AC-to-DC and DC-to-AC conversion processes are very efficient , losses attributable to these conversion will be between 3% and 8% of the energy charge .

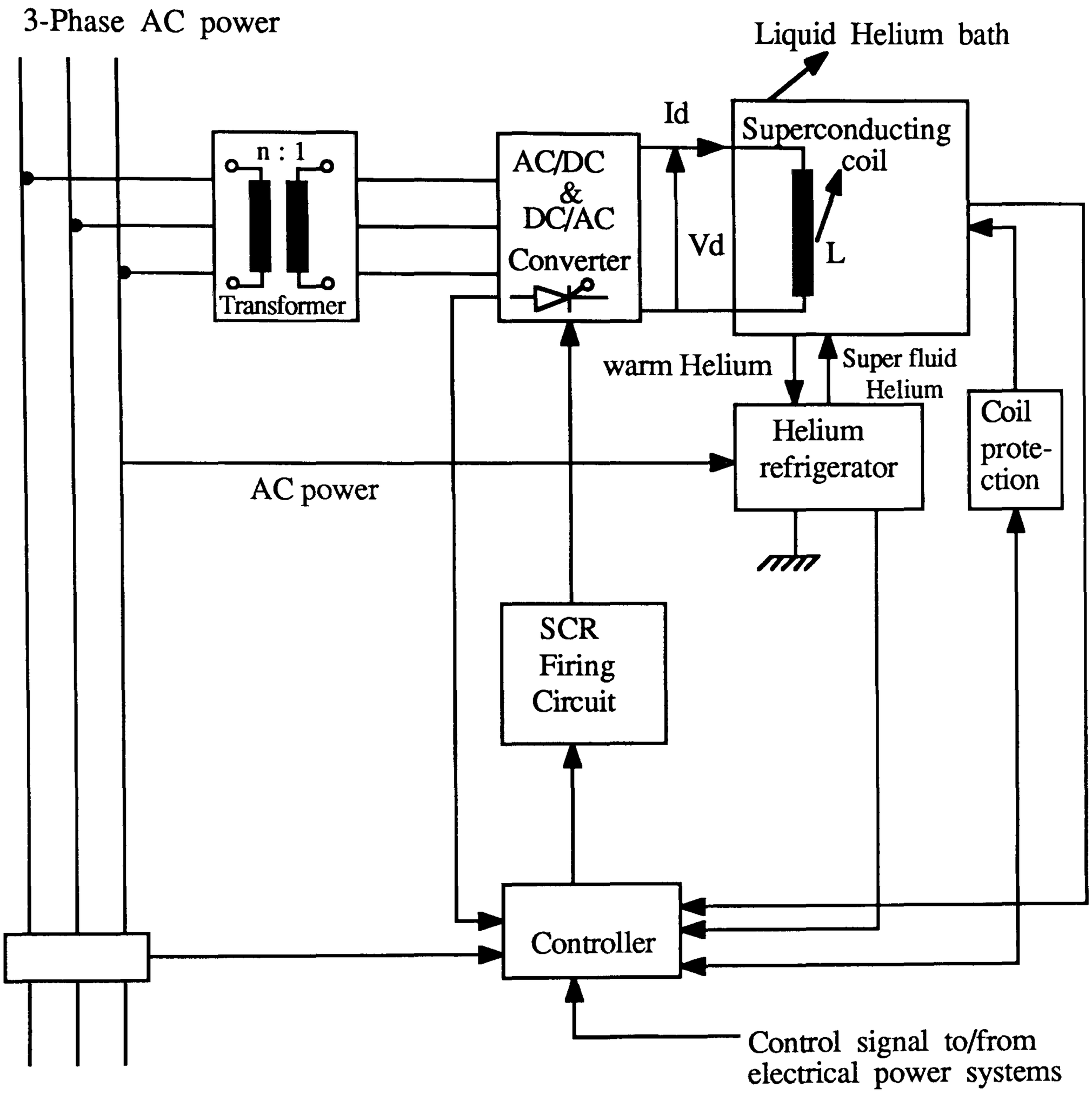

Fig. 1-11 General Super-Conducting Magnetic Enegy Storage System

During normal operation the coil will be charged to maximum Amps , storage the maximum energy :

$$E = \frac{1}{2}LI^2 \qquad (1\text{-}14)$$

where : E = stored energy , L = coil inductance , I = coil current

and when energy be required by the power line the coil will be discharged . The converter delay angle of α (0° to 180° degrees ideally) is the key to the control of rate of charge and discharge . The SMES , in addition to it's use in the load leveling of a system , may also be used as a power supply for large scale UPS systems or as a system stabilizer that damps power oscillation by mean of the rapid charge and discharge of energy .

1.6 Future developments

Power conditioning technology , particularly in applications , has progressed rapidly over the past 15 to 20 years due mainly to the growing importance and needs for computer related and other critical loads . The UPS market is expected to grow [34] at a rate of about 30% per year in units over the next several years , tilted in favour of the smaller units [20] and compact UPS capable of powering more load units .

At present , the volume of a typical UPS is divided in to four main sections :

1- switching devices (rectifier , inverter)

2- control and filter circuit

3- battery

4- transformer

The proportion of the total volume occupied by each of the four sections is shown in Fig. 1-12 .

Since the transformer occupy about one third of the volume of a UPS system [27] the reduction of battery and the transformer size are the main

research targets. It may become economical to store sufficient electromagnetic energy using superconductivity to eliminate the need for storage batteries or fly wheels for momentary power loss protection [20] & [35] .

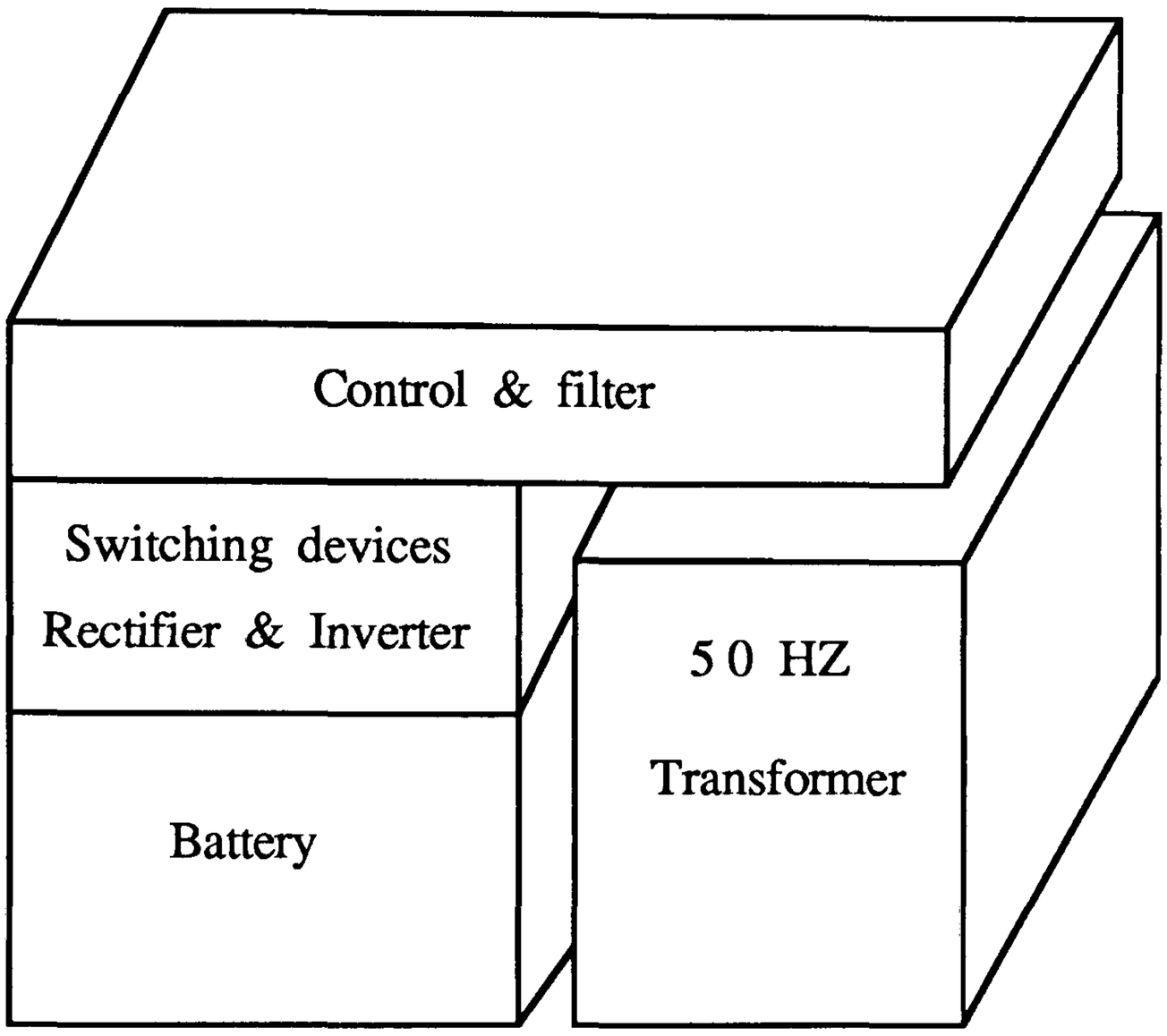

Fig. 1-12 Component distribution in a conventional 50 HZ UPS

1.7 Multi-stage power conversion

The remarkable progress in high frequency switching power-Electronics , mainly concerned with new power semiconductor switches ; MOSFET , IGBT , GTO thyristor , Static Induction Transistor & Thyristor , and control devices has made possible the development of high frequency switched mode power conversion with high frequency AC link and DC link .

Recently , high performance and high power density DC(solar array)-to-AC power conversion systems with a high frequency transformer & AC link have become of major interest in telecommunication , space / satellite stations and decentralized residential solar photovoltaic generation systems [36] & [37].

The multi-stage sine-wave modulated AC power conditioning system with high frequency link , which is composed of a PWM or series / parallel resonant h. f. inverter , h. f. transformer for isolation & voltage transformation (up/down) and a synchronous switching cycloconverter with bidirectional switching devices becomes more attractive and efficient .

Fig. 1-13 (a) shows the conventional UPS and DC-to-AC conversion which has simple structure , but it has following disadvantages :

1- The size of the isolation transformer is large.

2- the size of the output filter for removing low order harmonics is high.

3- the transient response to fluctuation of the load or input voltage is not good.

4- acoustic noise occurs from the transformer & filter reactor.

In Fig. 1-13 (b) , the h. f. inverter output is a pulse-width modulated h. f. voltage . The h. f. transformer provides isolation between DC and AC parts , and probably steps of the voltage , the cycloconverter output's is a modulated voltage whose frequency is the same as the commercial AC line frequency by converting the polarity of rectangular pulses output by the inverter .

Since the system is operated with h. f. link , the transformer and filter component size can be reduced . Moreover by employing a high frequency link in

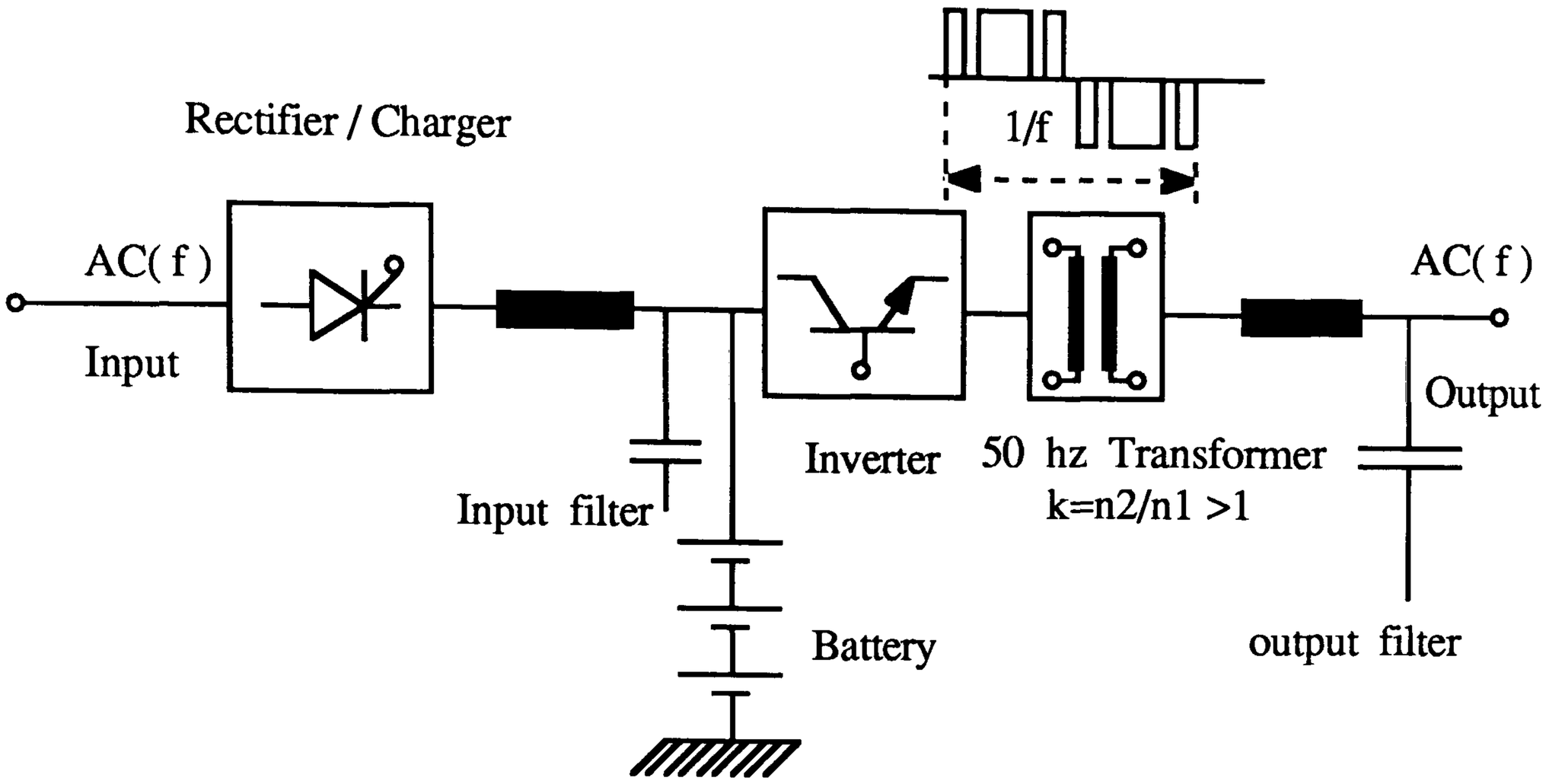

(a) Block diagram of conventional UPS

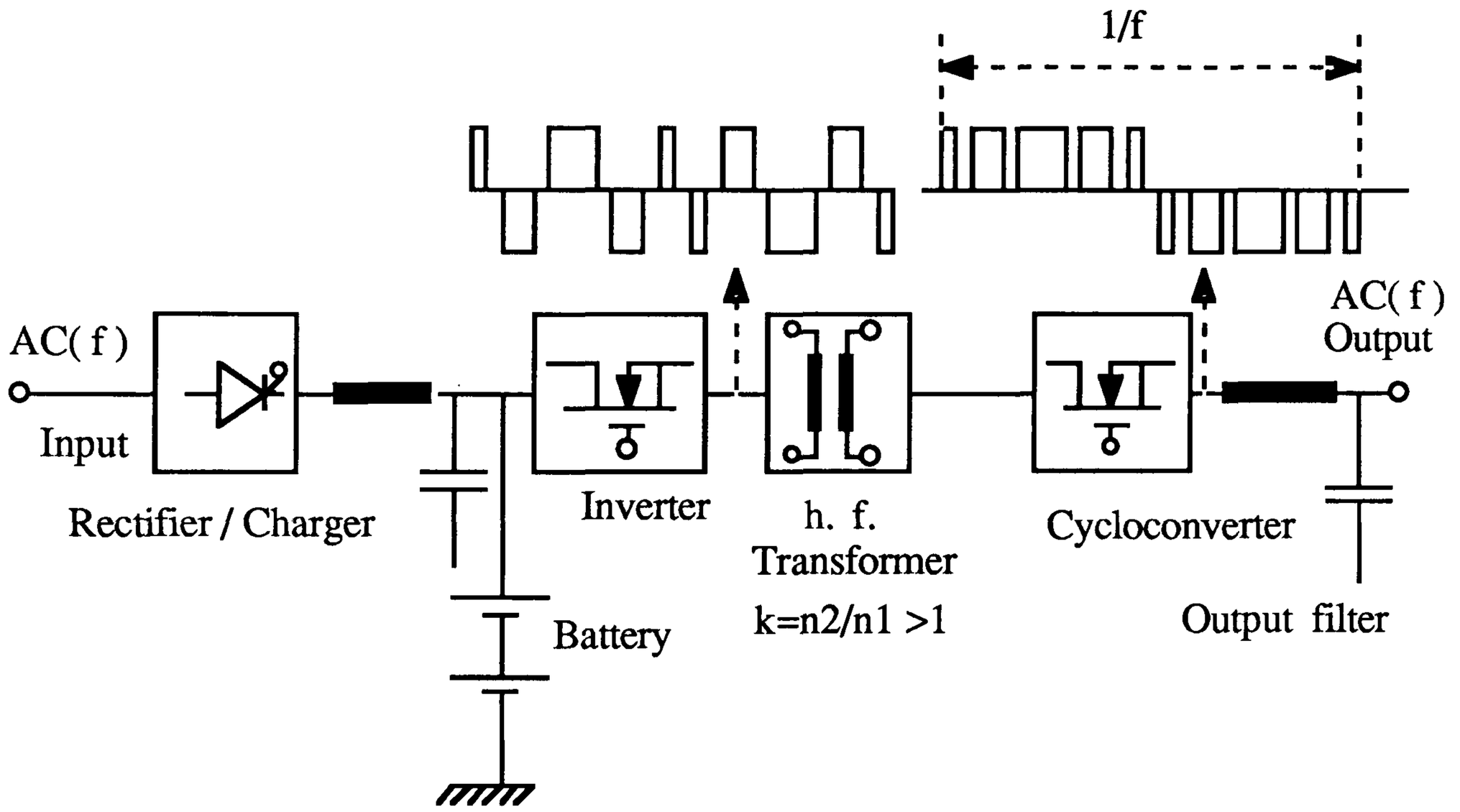

(b) Block diagram of multi-stage h. f. link power conversion

Fig. 1-13 Multistage power conversion (a)-conventional (b)-with h. f. link

excess of 20 k Hz , acoustic noise is reduced and transient is improved .

Generally there are 4 different topologies are practically acceptable for multi-stage DC-to-AC power conversion either with DC link or h. f. AC link . Fig.1-14 schematicly represents these topologies .

The systems shown in Fig. 1-14 , can be divided in to two unidirectional and bidirectional groups . High frequency inverter can be chosen either the PWM or series / parallel resonant configuration .

The topology of Fig. 14- (a) will be fully discussed in chapter 4 and the cases of 14 -(b) & 14-(c) have been discussed in [36] & [13] respectively . **The topology of 14-(d) , with cycloconverter supplied by sinusoidal wave form , is subject of the research reported in this thesis .**

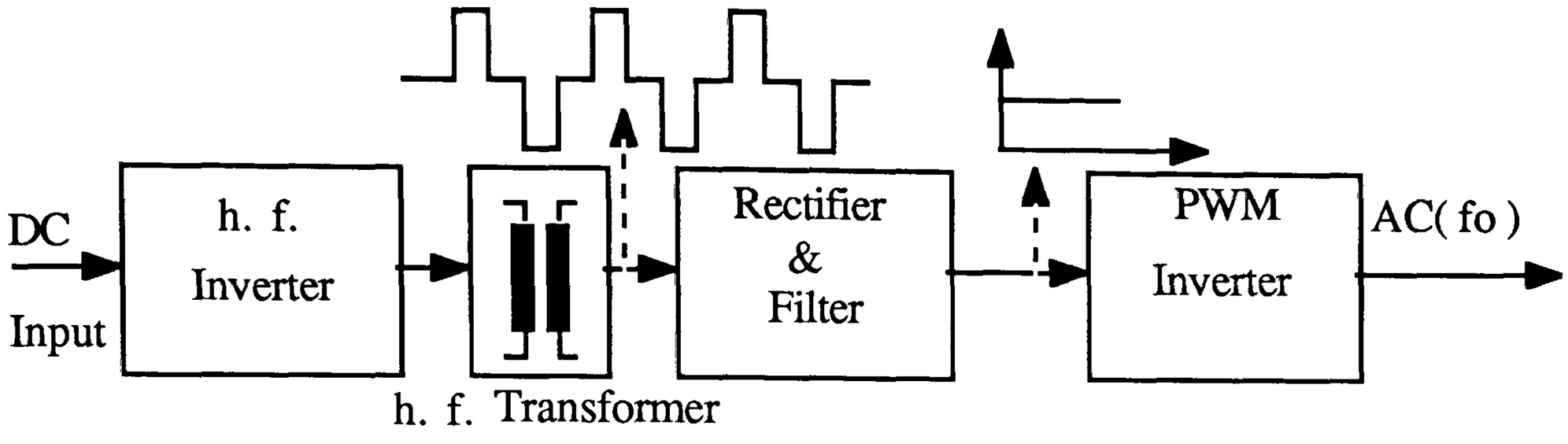

(a) DC link , " PWM Inverter" type

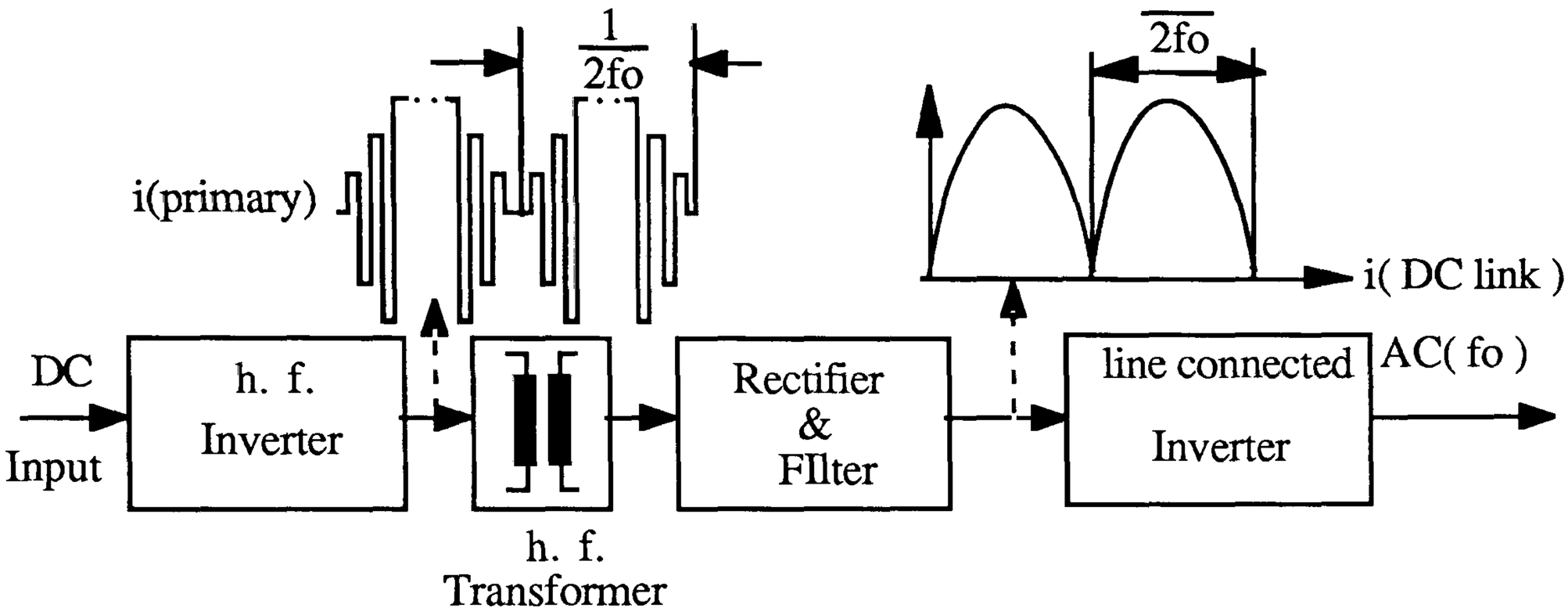

(b) DC link , "line connected Inverter" type

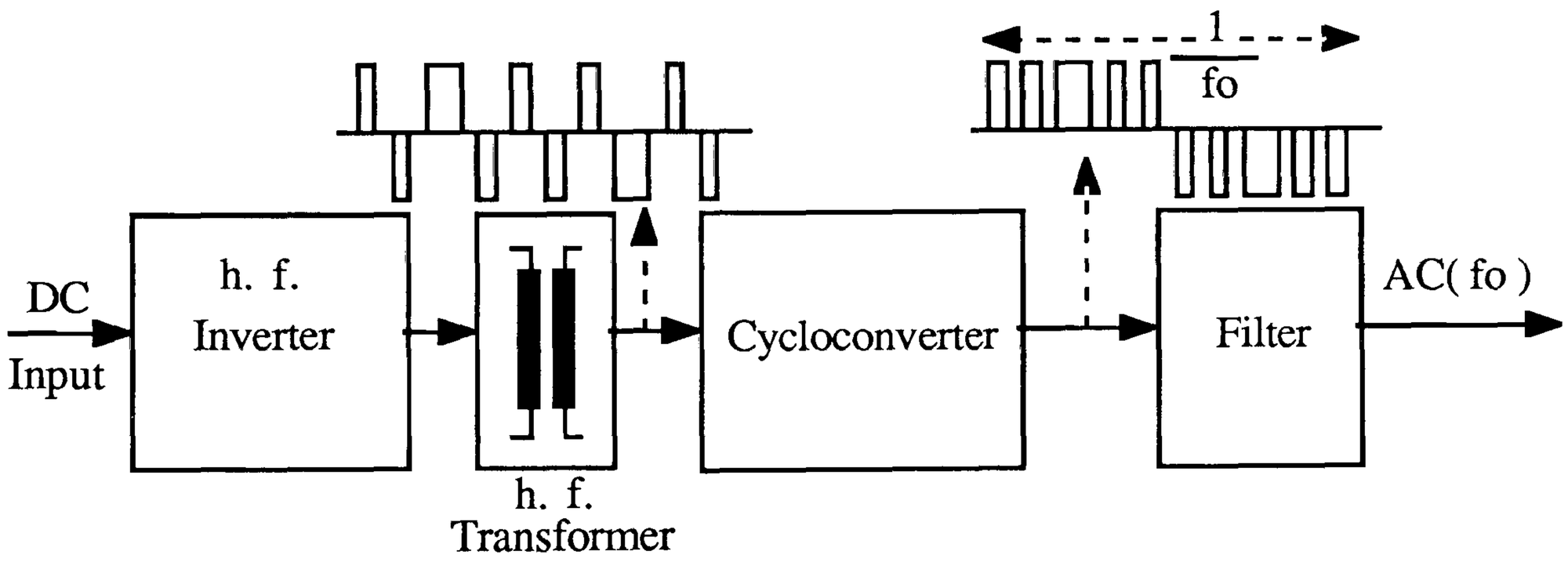

(c) AC link , "rectifier-mode cycloconverter" type

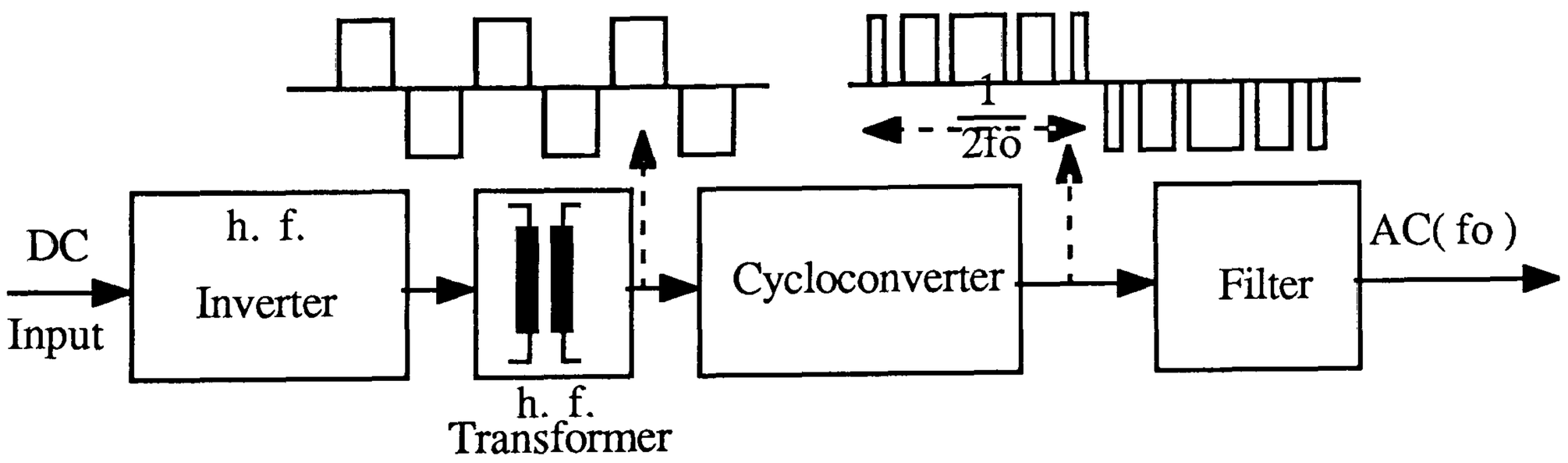

(d) AC link , "Phase controlled-mode cycloconverter" type

Fig. 1-14 Possible topologies for multi-stage DC / AC power conversion

1.8 Research background & proposed system

On the basis of section 1-7 discussion , for proposed system with 3-phase version , the possible configurations are proposed through Fig. 1-15 (a , b , c , d) in coming pages .

The principles of (3-phase)-to-(3-phase) in Fig. 1-15 (a) , (1-phase)-to-(3-phase) in Fig. 1-15 (b) , indirect (1-phase)-to-(3-phase) in Fig. 1-15 (c) and direct (3-phase)-to-(3-phase) in FIg. 1-15 (d) will be fully discussed in chapter 4 . **The case of Fig.1-15(a) is the subject of study in this thesis .**

S7 , S8 , ..., S17 , S18 = bidirectional switches

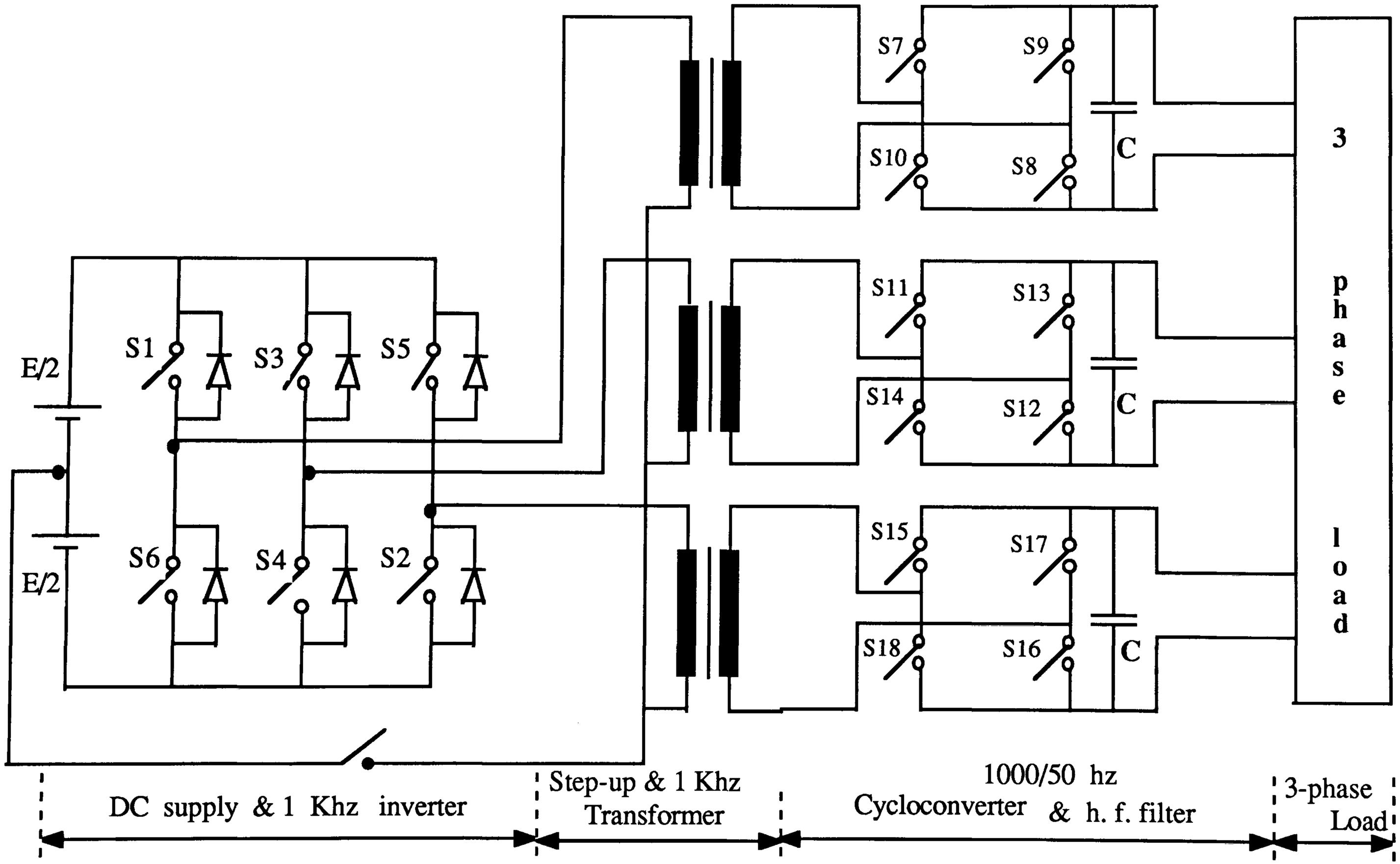

Fig. 1-15 Multi-stage DC-to-AC conversion (a)

S5 , S6 , ... , S13 , S14 = bilateral switches

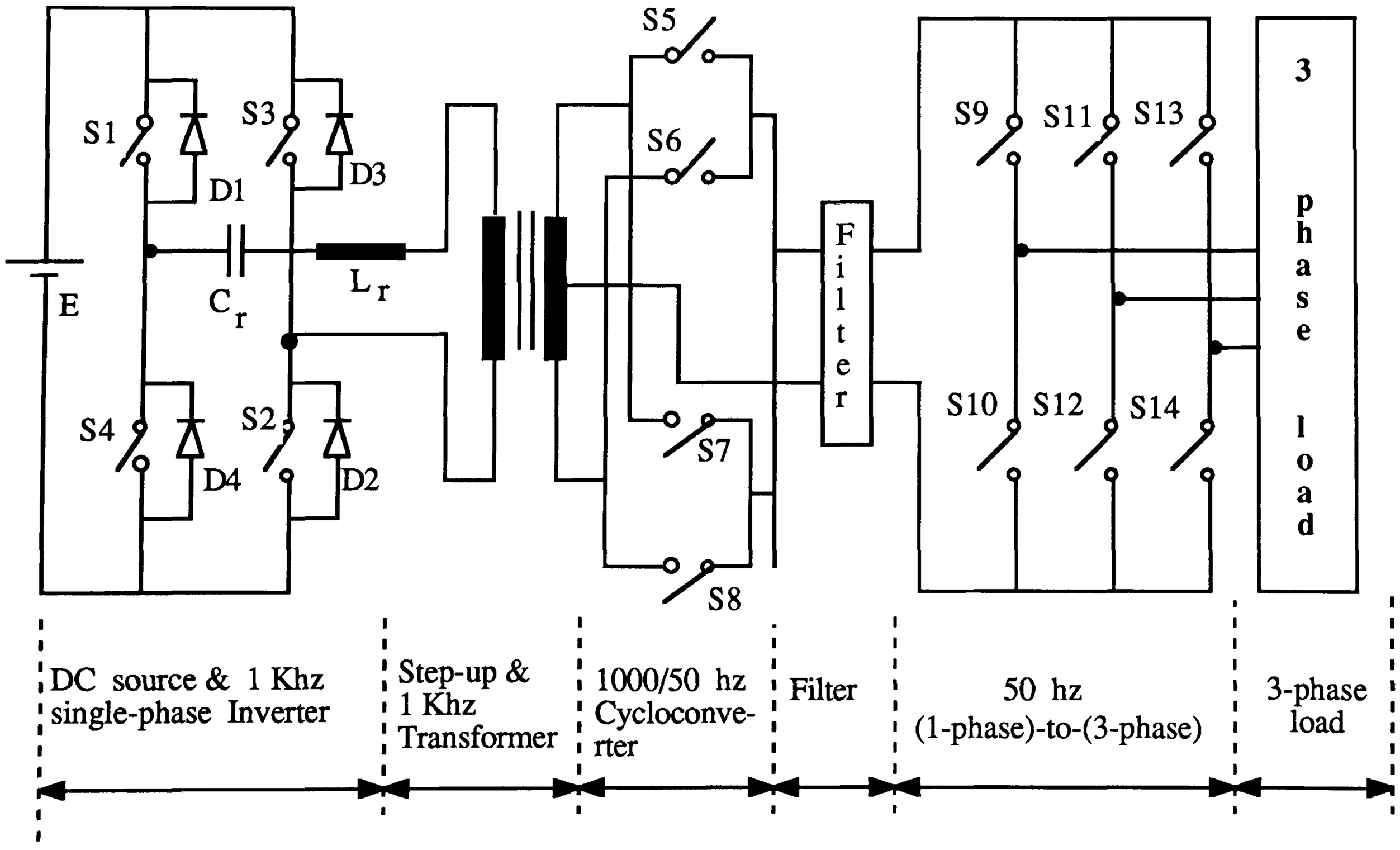

Fig. 1-15 Multi-stage DC-to-AC conversion (b)

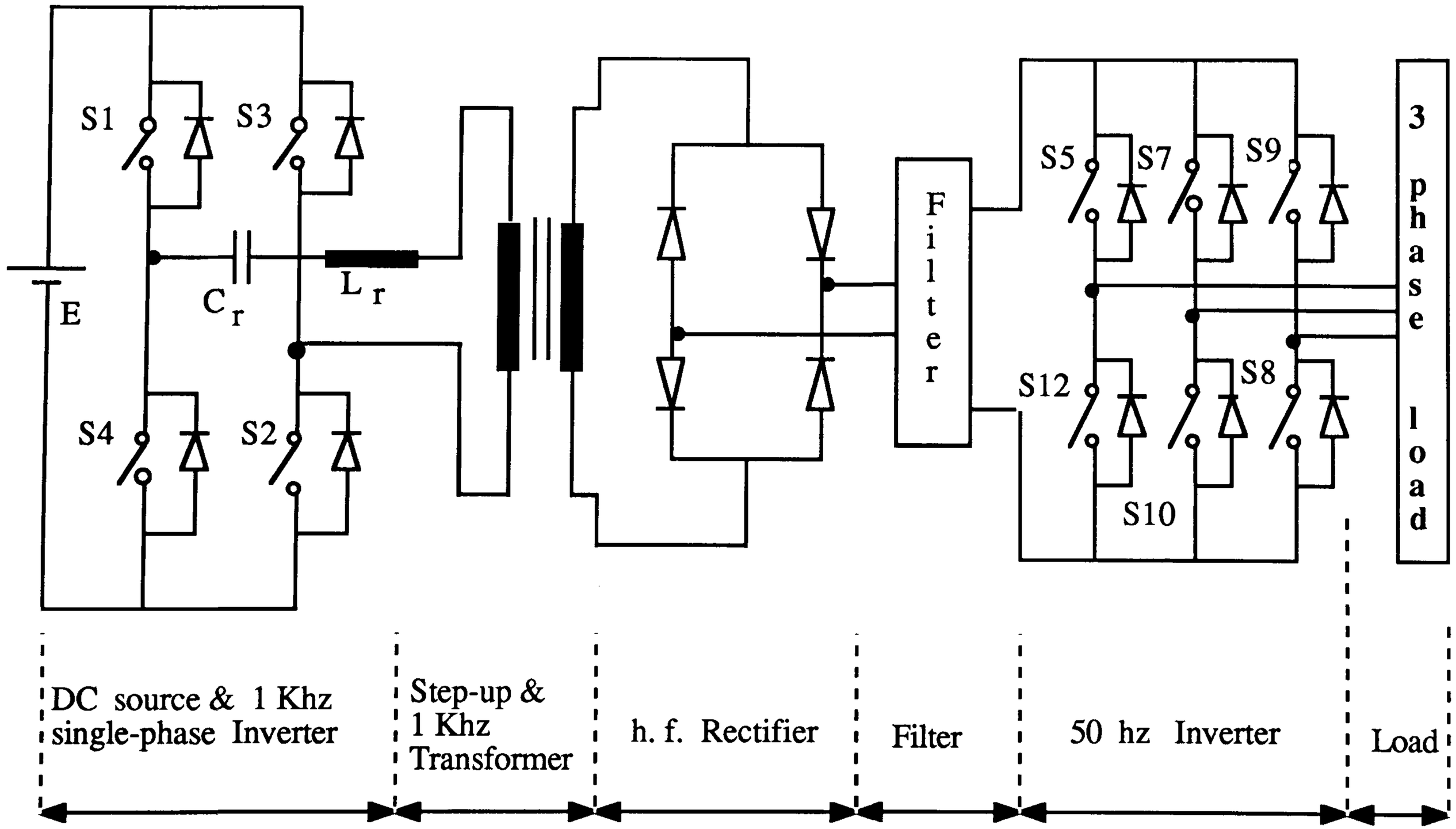

Fig. 1-15 Multi-stage DC-to-AC conversion (c)

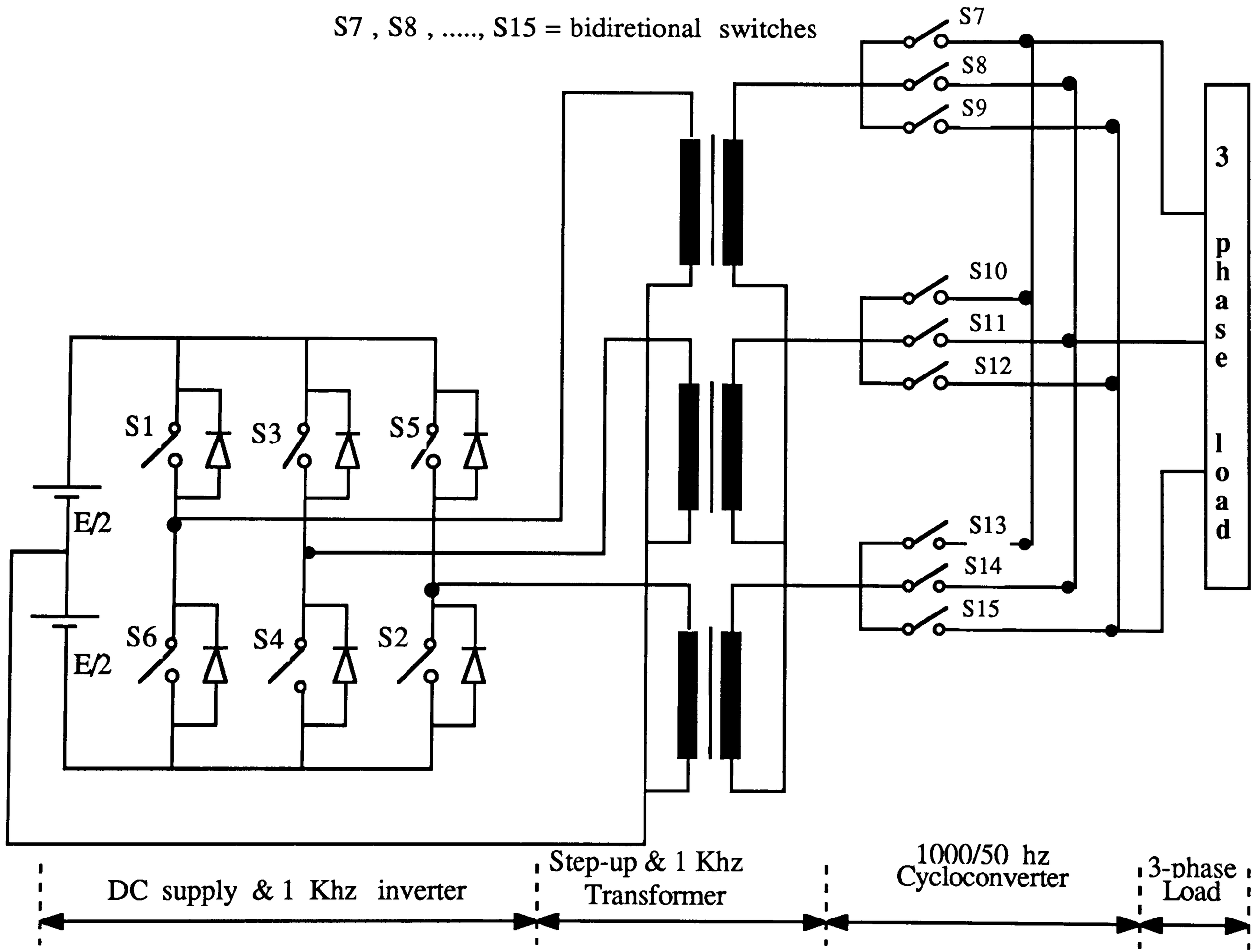

Fig. 1-15 Multi-stage DC-to-AC conversion (d)

1.9 References :

1- M. Brown *" Practical switching power supply design "* MOTOROLA series in solid state Electronics , 1990 , Academic press Inc. .

2- D. C. Hopkins , M. M. Jovanovic , F. C. Lee , and F. W. Stephenson *" Hybridized off-line 2-MHz zero-current-switched quasi-resonant converter "* IEEE transactions on Power Electronics , Vol. 4 , No. 1 , Janu. 1989 , pp.147-154 .

3- M. M. Jovanovic , D. C. Hopkins , F. C. Lee *" Evaluation and design of Megahertz-frequency off-line zero-current-switched quasi-resonant converters "* IEEE transactions on Power Electronics , Vol. 4 , No. 1 , Janu. 1989 , pp. 136-146 .

4- P. M. Espelage abd B. K. Bose *" High frequency link power conversion "* IEEE Trans. on Industry Applications , Vol. IA-13 , No. 5 , Sept./Oct. 1977 , pp. 387-394 .

5- L. Gyugyi , F. Cibulka *" The high frequency base converter - A new approach to static high power conversion "* IEEE Trans. on Industry Application , Vol. IA-15 , No. 4 , July/August 1979 , pp. 420-429 .

6- S. Manias , P. D. Ziogas , and G. Olivier *" Bilateral DC-to-AC converters employing a high frequency link "* IEE Proc. , Vol. 134 , Pt. B , No. 1 , Jan. 1987 , pp. 15-23 .

7- K. Alhaddad , T. Krishnan , V. Rajagopalan*" DC-to-DC converter with high frequency link "* IEEE Trans. on Industry Applications , Vol. IA-22 , No. 2 , March/April 1986 , pp. 244-254 .

8- P. D. Ziogas , Y. Kang , V. R. stefanovic " ***Rectifier-Inverter frequency changers with suppressed DC link components*** " IEEE Trans. on Industry Applications , Vol. IA-22 , No. 6 , Nov./Dec. 1986 , pp. 1027-36 .

9- V. T. Ranganathan , P. D. Ziogas , V. R. Stefanovic " ***A regulated DC-to-DC voltage source converter using a high frequency link*** " IEEE IAS Annual meeting conference record , Oct. 1981 , pp. 917-924 .

10- S. Manias and P. D. Ziogas " ***A novel sine wave in AC-to-DC converter with high frequency transformer isolation*** " IEEE Trans. on Industrial Electronics , Vol. IE-32 , No. 4 , Nov. 1985 , pp.430-438 .

11- R. L. Steigerwald and R. E. Tompking " ***A comparison of high frequency link schemes for interfacing a DC source to a utility grid*** " IEEE IAS Annual meeting conference record , Oct. 1982 , pp. 759-766 .

12- F. C. Schwarz and J. B. Klaassens" ***A 95% efficient 1 Kw DC converter with an internal frequency of 50 KHZ*** " IEEE Trans. on Industrial Electronics and control instrument. , Vol. IECI-25 , No. 4 , Nov. 1978 , pp. 326-333 .

13- V. T. Ranganathan , P. D. Ziogas , V. R. Stefanovic " ***A DC-to-AC power conversion technique using twin resonant high frequency links*** " IEEE Trans. on Industry Applications , Vol. IA-19 , No. 3 , May/June 1983 , pp. 393-400

14- I. J. Pitel " ***Phase modulated resonant power conversion techniques for high frequency link inverters*** " IEEE Trans. on industry Applications , Vol. IA-22 , No. 6 , Nov./Dec. 1986 , pp. 1044-51 .

15- E. E. Buchanan and E. J. Miller ***"Resonant switching power conversion technique"*** IEEE Power Electronics Specialist conference , 1975 , pp. 188-193 .

16- K. H. Liu and F. C. Lee ***" Resonant switches-A unified approach to improve performance of switching converters "*** IEEE Int. Telecom. Energy conference , 1984 proc. , pp.344-351 .

17- K. H. Liu , R. Oruganti , and F. C. Lee ***" Quasi-resonant converters - Topologies and characteristics "*** IEEE Trans. on Power Electronics , Vol. PE-2 , No. 1 , Jan. 1987 , pp. 62-71 .

18- W. A. Tabisz and F. C. Lee ***" Zero-voltage-switching multi-resonant technique "*** IEEE Trans. on Power Electronics , Vol. 4 , No. 4 , Oct. 1989 , pp. 450-458

19- K. D. Ngo ***" Generalization of resonant switches and quasi-resonant DC-to-DC converters "*** IEEE Power Electronics Specialist conference record, 1987 , pp. 395-403

20- D. C. Griffith ***" Uninterruptible Power Supplies "*** Marcel Dekker , New-york 1989

21- Ian West ***" Uninterruptible power sources for computer installation "*** IEE , Electronics & Power , July/August 1983 , pp. 571-74

22- Khan and Maning ***" recent developments in Uninterruptible power supply technology "*** 24th Universities Power Engineering conference , Belfast , 1989 .

23- Mike Taylor *" Choosing the right UPS "* IEE , Electronic & Power , July 1987 , pp. 461-467

24- W. P. Harris *" UPS systems static or rotary "* IEE , Electronics & Power , July 1987 , pp. 465-467 .

25- P. D. Ziogas *" Optimum voltage and harmonic control PWM techniques for three phase static UPS system "* IEEE Trans. on Industry Application , Vol. IA-16 , No. 4 , July/August 1980 , pp. 542 - 546 .

26- Ray Barlow *" The ferroresonant line conditioner "* IEE , Electronics & Power , June 1986 , pp.445-447 .

27- P. Mehta , M. Darwish *" UPS . An overview of present and future technique"* PEMC (Power Electronics & Motion Control) , 1990 , pp. 781 - 785

28- M. Z. U. Khan and C. D. Maning *" Recent developments in uninterruptible power supply technologies "* UPEC , 1989 , pp. 197-201 .

29- S. Martizen , M. Castro , R. Antoranz , F. Aldana *" off-line Uninterruptible Power Supply with zero transfer time using integrated magnetics "* IEEE Industrial Electronics , Vol. 36 , No. 3 , August -1989 , pp. 441-445 .

30- W. V. Hassen Zahl *" Superconducting Magnetic Energy Storage "* Proc. IEEE , Vol. 71 , No. 9 , Sept. 1983 , pp. 1089-1098 .

31- J. D. Rogers , M. H. Barron , H. J. Boenig , A. L. Criscoulo , J. W. Dean , R. I. Schemer *" Superconducting Magnetic Energy Storage "* Proc. 1982 ASC , IEEE Trans. on Magnetics , Vol. Mag.-19 , May 1983 , pp. 1078-1080 .

32- W. Hassen Zahl *" Superconducting Magnetic Energy Storage "* IEEE Trans. on Magnetics , Vol. 25 , No. 2 , March 1989 , pp. 750-757 .

33- R. J. Loyd , T. E. Walsh , E. R. Kimmy , B. E. Dick *" An Overview of the SMES ETM program "* IEEE Trans. on Magnetics , Vol. 25 , No. 2 , March 1989 , pp.1569-1575 .

34- R. Chauprade *" Inverters for Uninterruptible Power Supply "* IEEE Trans. on Industry Applications , Vol. IA-13 , No. 4 , pp.281-297 , July/August 1977 , pp.281-297 .

35- *" The European Market for Uninterruptible Power Supplies from 200 VA to 200 KVA "* published by EXTIN , August 1988 .

36- A. K. S. Bhat and S. B. Dewan *" DC-to-Utility interface using sinewave resonant inverter "* IEE Proc. , Vol. 135 , Pt. B , No. 5 , Sept. 1988 , pp. 193 - 201

37- A. Cocconi , S. C'uk , R. D. Middlebrook *" high frequency isolated 4 Kw Photovoltaic inverter for utility interface"* PCI/Motor Conference Proceedings , 1983 , pp. 39-59 .

Chapter 2

Inverters &The Prototype System Inverter

(proposed modulation strategy)

2.1 Inverters , General

Since "energy storage" can only be obtained in the form of DC (battery , fuel cell [1] , solar array , other DC sources) , inverters accomplish the DC-to-AC conversion process .

Application of inverters include the following areas :

1- variable speed AC motor drives .

2- induction heating .

3- stand by power supplies (off-line) .

4- uninterruptible power supplies (on-line) .

5- air craft and space craft power supplies .

6- output of HVDC transmission lines .

7- photovoltaic application for utility interface .

2.2 Type of Inverters

Inverters can be broadly classified in to two types :

1- Single phase inverters 2- 3-phase inverters

each type can be subdivided in to mainly two categories depending on the type of power semiconductor switch commutation :

1- pulse width modulation (PWM) inverters with forced commutated operation .

2- resonant inverters with naturally commuted operation .

For the proposed work the pulse width modulation inverter will be studied with 3-phase and half-bridge mode of connection . Moreover , in order to achieve any selected transformation ratio of voltage or current of inverter , and provide complete isolation between it's DC input and AC output a transformer

is employed on output side of the inverter . The high frequency orientated operation of this transformer (emergence of significant parasitic elements) and drastic side effects on the operation of the prototype system will be taken in to consideration in chapters 3 & 5 .

2.3 Half bridge and Full bridge Inverters

Inverters provide single phase or three phase AC balance system either by half bridge or full bridge mode of connections . Theoretically any poly-phase AC system may be derived [2] ,[3] . Fig. 2-1 shows the basic structure of a single phase inverter .

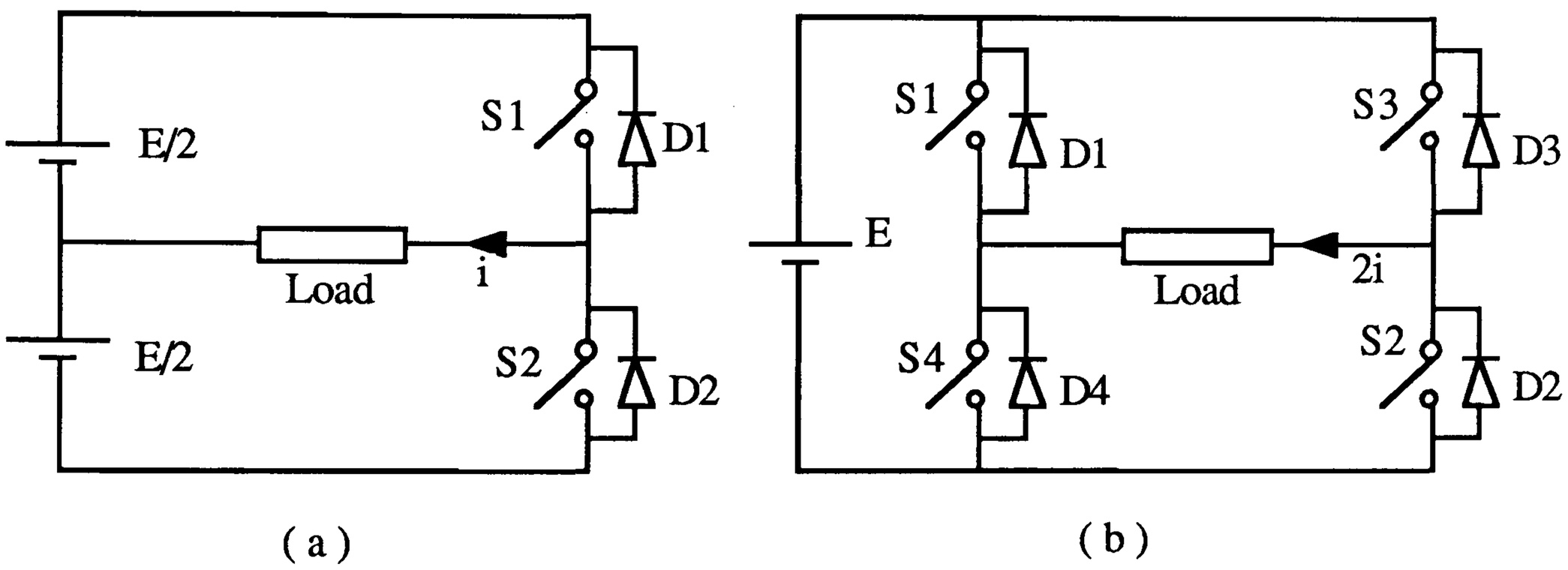

Fig. 2-1 Single phase inverter (a)- half bridge (b)- full bridge

With resistive loads , the antiparallel diodes (D1 , D2 ,..., D4 in Fig. 2-1) across the MOSFETs have no functions . If the load is non-resistive (mainly inductive) the current in each arm of the inverter would be delayed on it's voltage since the conduction time of the MOSFETs and diodes depends on the load power factor , details in [23] . When the diodes conducts , the trapped electric energy is fed back to the DC source , thus preventing voltage instability . For this reason these diodes are called as a feed back diodes. For the Inverter-Transformer system , the effect of different power factors ; resistive with

Cos(Φ)=1 , inductive and capacitive with Cos(Φ)=0.0 lagging & leading respectively , is shown in Fig. 2-2 . (further discussion in Appendix C)

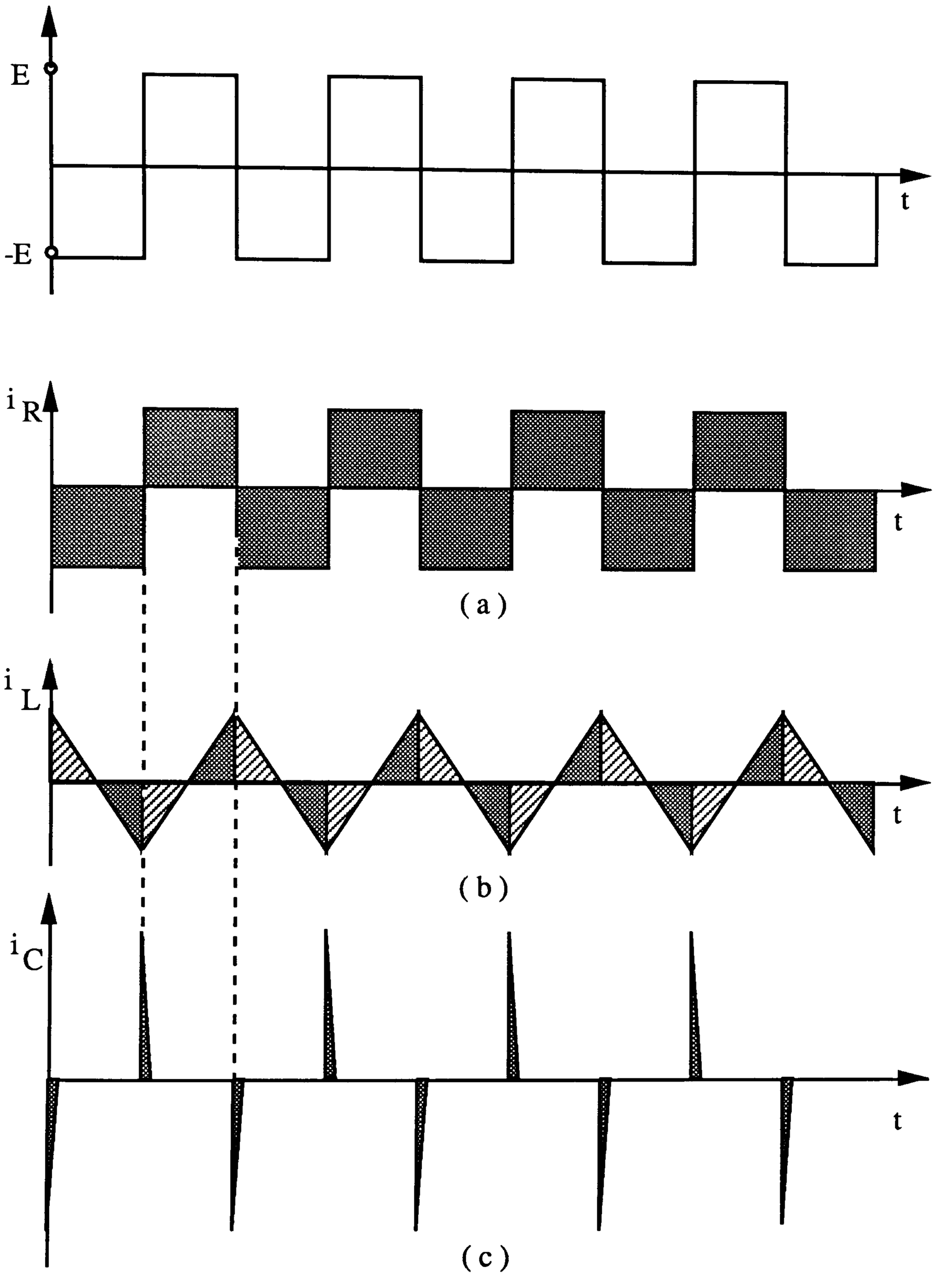

Energy from source to load Energy from load to source

Fig. 2-2 Voltage and current waveforms of an inverter for pure :
(a)-Resistive (b)-Inductive (c)-Capacitive loads

In the half bridge circuit , S1 and S2 conduct alternately , i.e. ,when S1 is on , S2 is off and vice versa . The voltage appearing across any open switch is equal to the E and the peak current through any conducting switch is the half of average source current $i = \frac{E}{2R}$.

In the full bridge circuit , switches S1 and S2 are closed simultaneously during the first half-cycle of the conversion process , and then S3 and S4 are closed simultaneously during the second half cycle . The voltage appearing across any open switch is equal to the E and the peak current through any conducting switch is $2i = \frac{E}{R}$, so for full bridge inverter with resistive load , the out put power is 4 times higher and the fundamental current component is twice than that of half bridge inverters .

2.4 Three Phase Inverters

Three phase inverters are normally used for high power application . Three single phase half bridge (6 MOSFETs) or three single phase full bridge (12 MOSFETs) inverters can be connected in parallel to form a 3-phase inverter . Fig. 2-3 shows the most common connection of the 3-phase half bridge inverter .

The gating signals of single phase inverters should be advanced or delayed by 120° with respect to each other in order to obtain three phase balanced (fundamental) voltages . The three outputs may then be brought to a three phase transformer . The transformer primary windings must be isolated from one another , the secondary windings may be connected in star or delta to supply the load circuit .

In order to eliminate triplen harmonics (n=3 , 6, 9 , ...) the transformer secondary is normally in delta . When S1 is switched on , terminal a is connected to the positive of the DC input voltage . When S4 is switched on , terminal a is brought to the negative terminal of DC source and the same happens to terminals b and c .

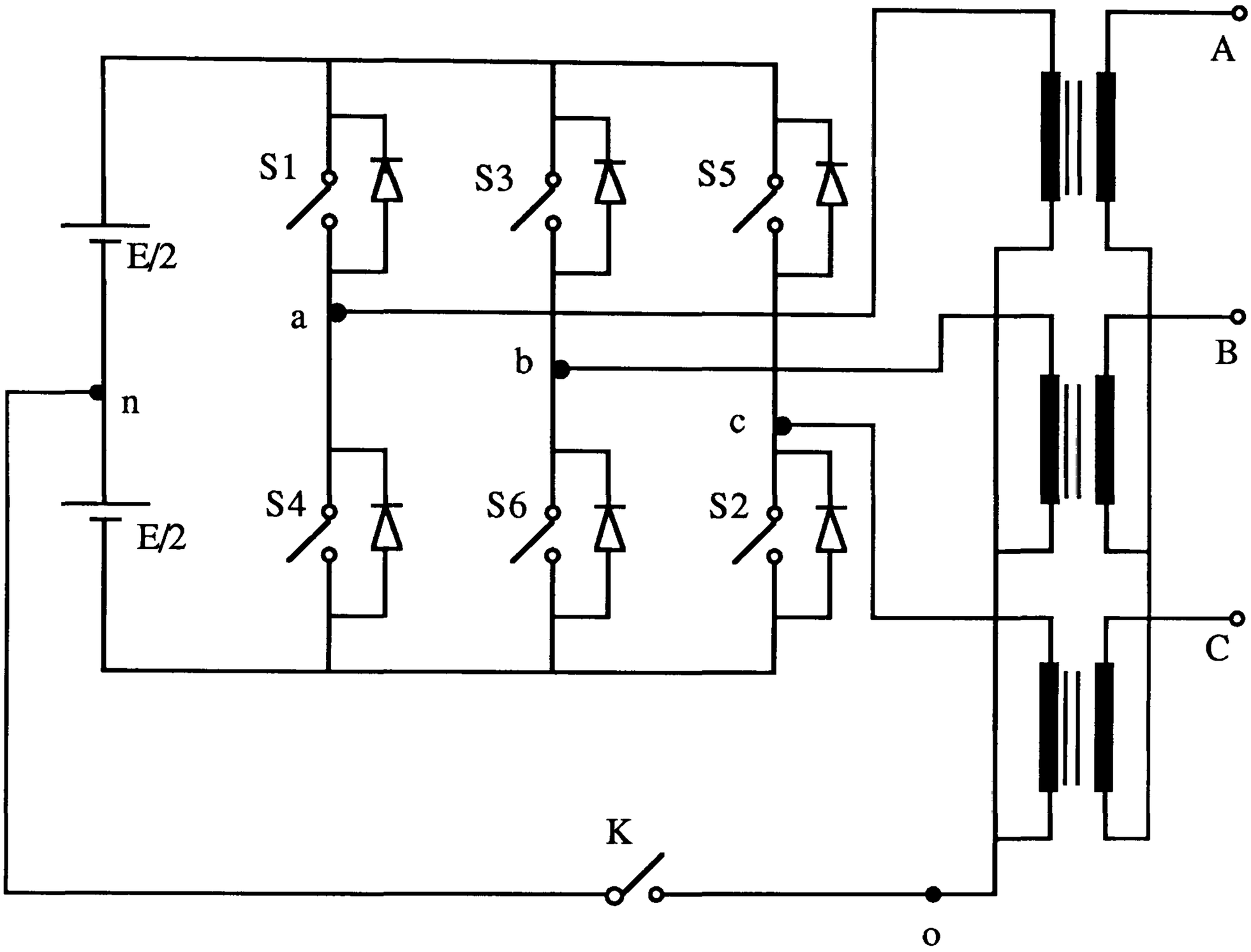

Fig. 2-3 General 3-phase half bridge inverter with isolating & stepping transformer

There are 6R modes of conduction for creation a cycle of inverter out put voltage , where R is the number of pulses per full cycle of out-put voltage . The MOSFETs are numbered in the sequence of gating them (i.e. , 123 - 234 - 345 - 456 - 561 - 612) when each MOSFET conducts for 180° (R=1) . For proposed system inverter R=9 , thus for creation of one cycle there will be 54 modes of conduction , table 2-10 .

2.5 Voltage Control of Single Phase Inverters

In many Industrial applications , it is often required to control the output voltage of inverters . The techniques available differ in the harmonic content that they produce in the inverter output voltage , thus the acceptable harmonic content is the factor that determines the choice of technique . There are number of strategies employing pulse width modulation (PWM) and may be listed as :

1- single pulse width modulation .
2- multi-pulse width modulation(uniform pulse width modulation-UPWM [4])
3- sinusoidal pulse width modulation : natural sampled PWM, regular sampled PWM(symmetrical & asymmetrical) and optimized PWM [5] , [6] .
4- modified sinusoidal pulse width modulation [7] .
5- staircase pulse width modulation [8] , [9] .

The optimized PWM will be employed for proposed system inverter .

2.5.1 Single pulse width modulation

Fig. 2-4 shows the output voltage of single pulse width modulation on full bridge inverter .

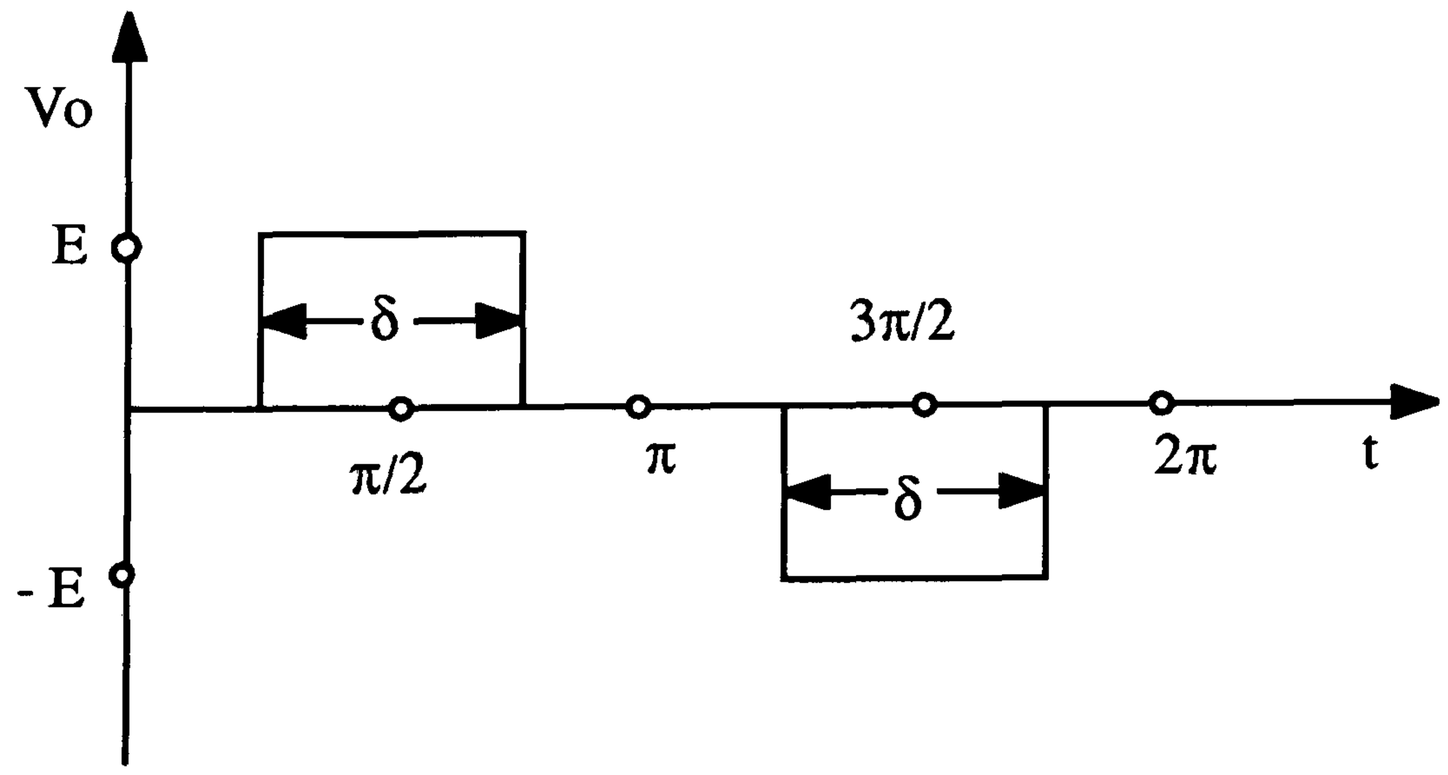

Fig. 2-4 Single pulse width modulation

This wave form may be analysed according to Fourier Series .

$$v_o(t) = \sum_{n=1,3,5}^{\infty} \left[a_n \mathrm{Sin}(n\omega t) + b_n \mathrm{Cos}(n\omega t) \right] \qquad (2\text{-}1)$$

$$a_n = \frac{2}{\pi}\int_0^{\pi} E.\mathrm{Sin}(n\omega t)d(\omega t) = \frac{2E}{\pi}\int_{\frac{\pi-\delta}{2}}^{\frac{\pi+\delta}{2}} \mathrm{Sin}(n\omega t)d(\omega t) = \frac{4E}{n\pi}\mathrm{Sin}(\frac{n\delta}{2}) \qquad (2\text{-}2)$$

$$b_n = \frac{2}{\pi}\int_0^{\pi} E.\mathrm{Cos}(n\omega t)d(\omega t) = \frac{2E}{\pi}\int_{\frac{\pi-\delta}{2}}^{\frac{\pi+\delta}{2}} \mathrm{Cos}(n\omega t)d(\omega t) = 0 \qquad (2\text{-}3)$$

$$v_o(t) = \sum_{n=1,3,5}^{\infty} a_n \mathrm{Sin}(n\omega t) = \sum_{n=1,3,5}^{\infty} \left[\frac{4E}{n\pi}\mathrm{Sin}(\frac{n\delta}{2}) \right].\mathrm{Sin}(n\omega t) \qquad (2\text{-}4)$$

In (2-4) , the output voltage , $V_o(t)$ is controlled by varing δ from 0° to 180° .

2.5.2 Multiple pulse width modulation

This method is also called uniform pulse width modulation(UPWM) , since the width and space between pulses are equal , Fig. 2-5 .

The harmonic content can be significantly reduced by increasing number of pulses in each half cycle of output voltage . The $v_o(t)$ wave form Fourier Series coefficients are determined by deriving an expression for a general pair of pulses situated at $\omega t = \alpha_m$ and $\omega t = \pi + \alpha_m$, and then combining the effects of all such pairs of pulses in the cycle .

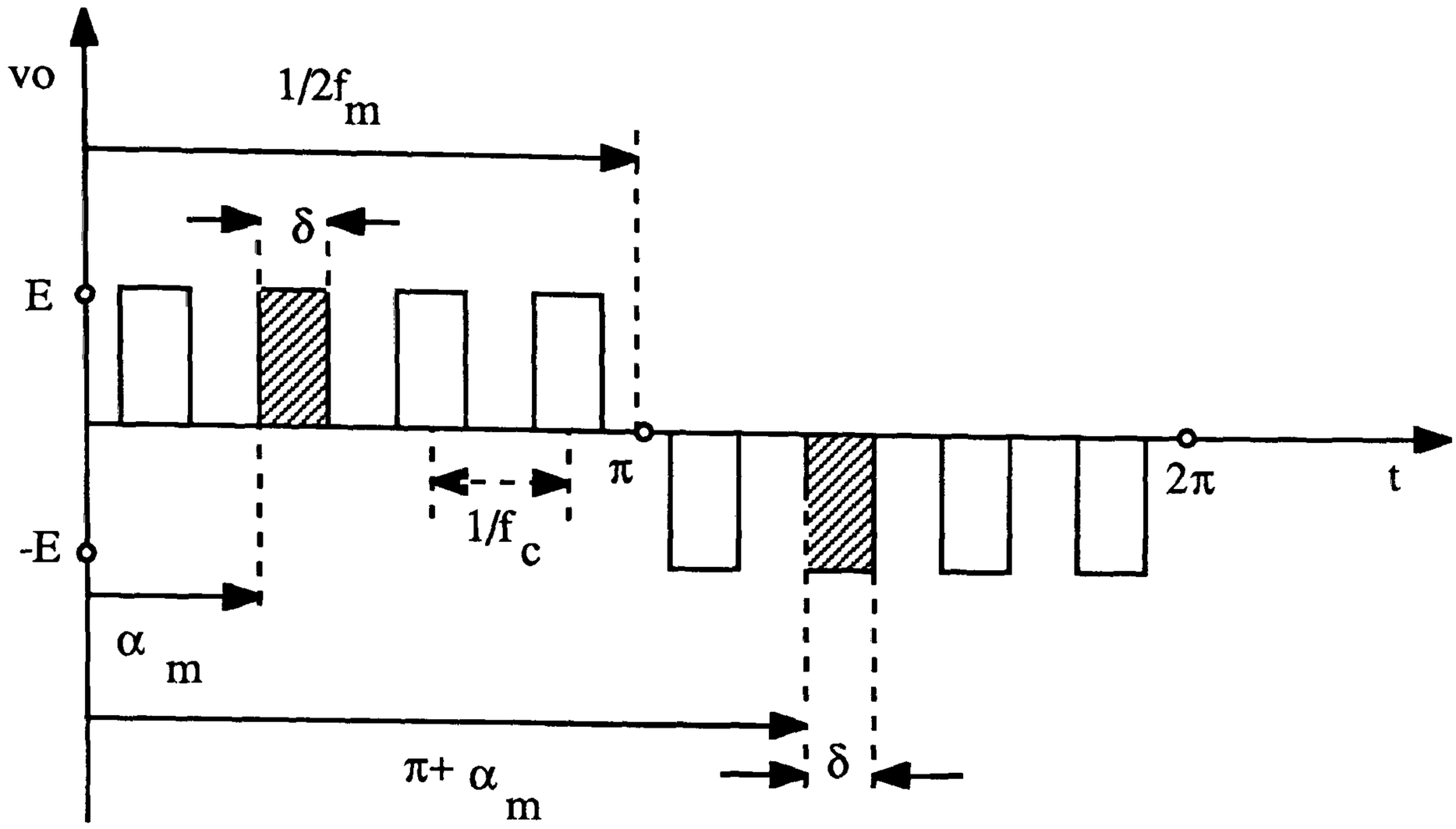

Fig. 2-5 Multiple pulse width modulation

$$v_o(t) = \sum_{n=1,3,5}^{\infty} \left[A_n \mathrm{Sin}(n\omega t) + B_n \mathrm{Cos}(n\omega t) \right] \qquad (2\text{-}5)$$

The Fourier coefficients for a pair of pulses are :

$$a_n = \frac{2}{\pi}\int_{\alpha_m}^{\alpha_m+\delta} E\mathrm{Sin}(n\omega t)d(\omega t) = \frac{2E}{n\pi}\left[\mathrm{Cos}(n\alpha_m) - \mathrm{Cos}\left(n(\alpha_m+\delta)\right)\right] = \frac{4E}{n\pi}\mathrm{Sin}(n\frac{\delta}{2}).\mathrm{Sin}\left(n(\alpha_m+\frac{\delta}{2})\right)$$

$$(2\text{-}6)$$

$$b_n = \frac{2}{\pi}\int_{\alpha_m}^{\alpha_m+\delta} E\mathrm{Cos}(n\omega t)d(\omega t) = \frac{2E}{n\pi}\left[-\mathrm{Sin}(n\alpha_m) + \mathrm{Sin}\left(n(\alpha_m+\delta)\right)\right] = \frac{4E}{n\pi}\mathrm{Sin}(n\frac{\delta}{2}).\mathrm{Cos}\left(n(\alpha_m+\frac{\delta}{2})\right)$$

Then : $(2\text{-}7)$

$$A_n = \sum_{m=1,2}^{R}\left[\frac{4E}{n\pi}\mathrm{Sin}(n\frac{\delta}{2})\mathrm{Sin}\left(n(\alpha_m+\frac{\delta}{2})\right)\right] \qquad (2\text{-}8)$$

$$B_n = \sum_{m=1,2}^{R}\left[\frac{4E}{n\pi}\mathrm{Sin}(n\frac{\delta}{2})\mathrm{Cos}\left(n(\alpha_m+\frac{\delta}{2})\right)\right] \qquad (2\text{-}9)$$

Where :

$R = f_c/f_m$ or R = number of pulses per one cycle

f_c = carier frequency

f_m = output voltage frequency

By substituting (2-8) & (2-9) in to (2-5) the output voltage results :

$$v_o(t) = \sum_{n=1,3,5}^{\infty}\left[\sum_{m=1,2}^{R}\left[\frac{4E}{n\pi}\mathrm{Sin}(n\frac{\delta}{2})\mathrm{Sin}\left(n(\alpha_m+\frac{\delta}{2})\right)\right]\right].\mathrm{Sin}(n\omega t) +$$

$$\sum_{n=1,3,5}^{\infty}\left[\sum_{m=1,2}^{R}\left[\frac{4E}{n\pi}\mathrm{Sin}(n\frac{\delta}{2})\mathrm{Cos}\left(n(\alpha_m+\frac{\delta}{2})\right)\right]\right].\mathrm{Cos}(n\omega t) \qquad (2\text{-}10)$$

By changing R and varing δ the $V_o(t)$ and harmonic contents are controlled .

2.5.3 Sinusoidal pulse-width modulation (Naturally sampled)

Unlike the multiple pulse width modulation that the width of pulses was the same , here the width of each pulse is varied in proportion to the amplitude of a sine wave evaluated at the centre of the same pulse [10] , Fig. 2-6 .

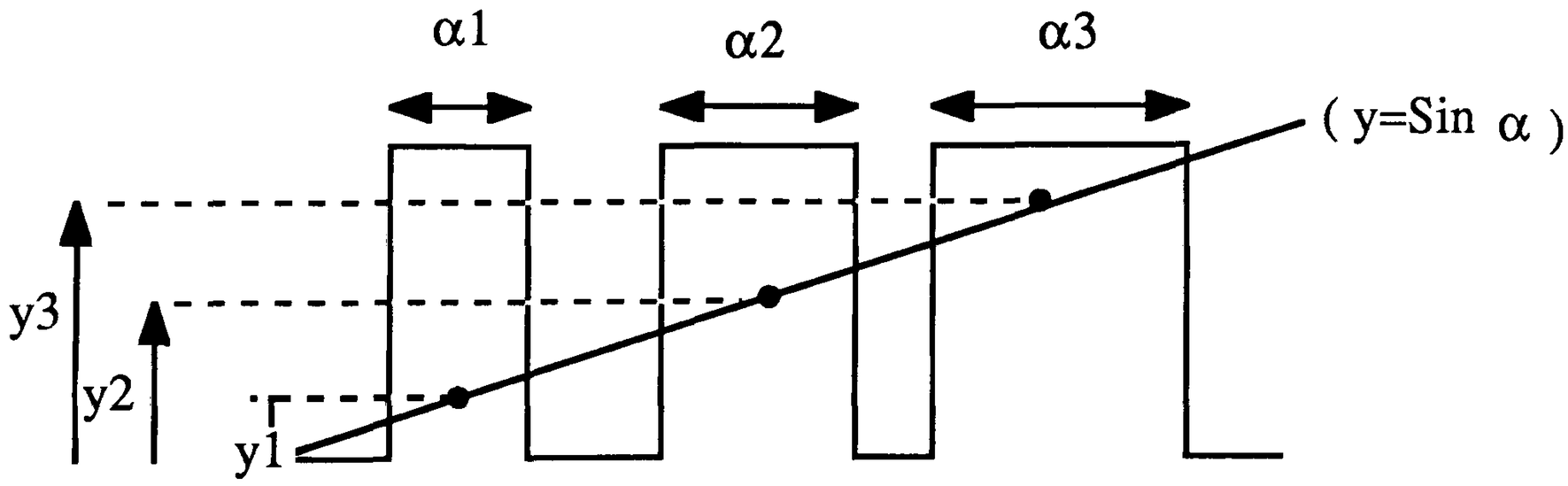

Fig. 2-6 Sinusoidal PWM principle

$$\frac{\alpha_1}{y_1} = \frac{\alpha_2}{y_2} = \frac{\alpha_3}{y_3} = \mathrm{cte.} \qquad (2\text{-}11)$$

In this strategy the output voltage is controlled efficiently , moreover distortion factor and low order harmonics are reduced significantly [7] .

In sinusoidal PWM , a sinusoidal modulating wave is compared directly with a triangular carrier wave (Sampling signal) to determine the switching instants , and therefore the resultant pulse widths , Fig . 2-7 .

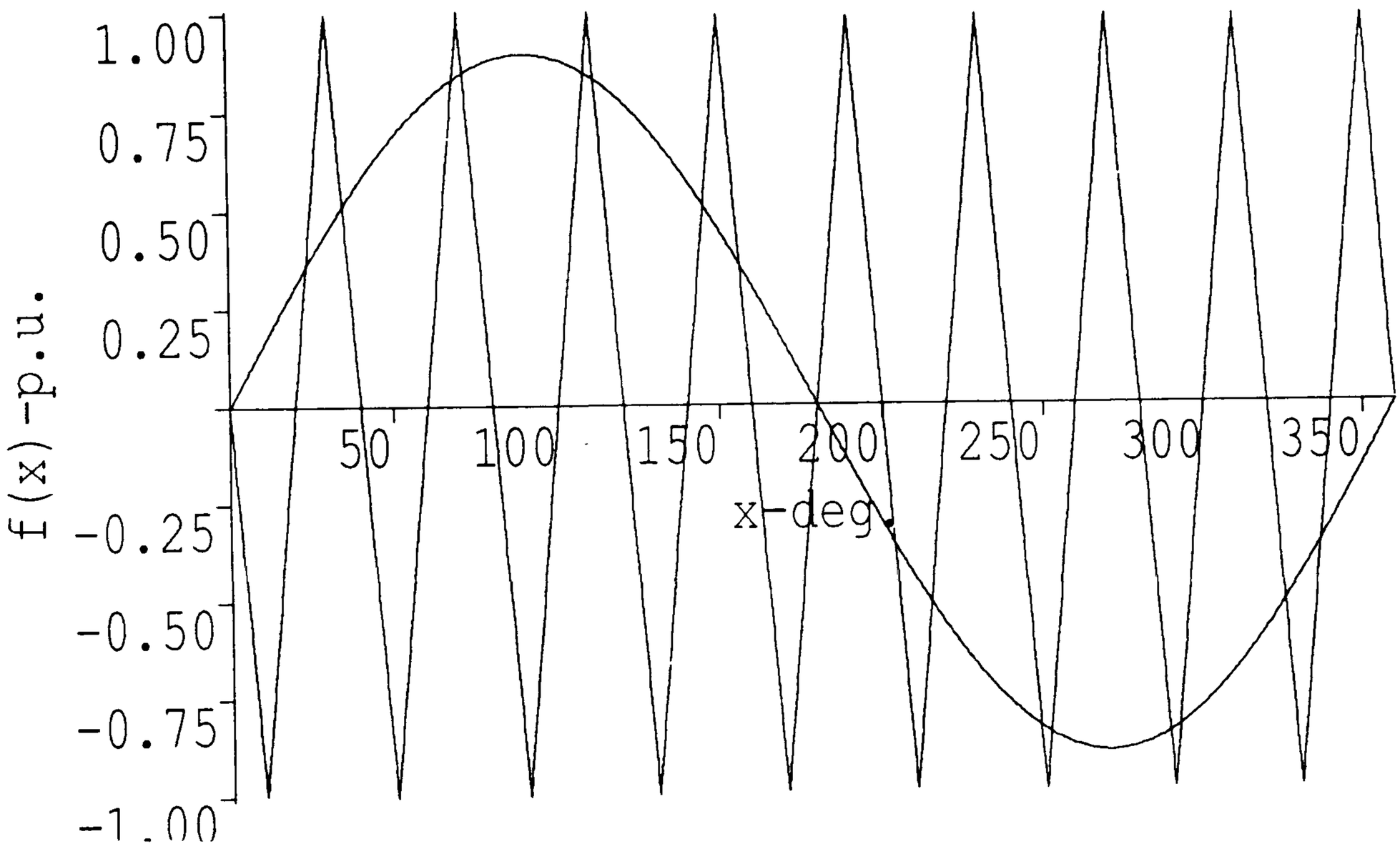

Fig. 2-7 Modulating & carrier wave

Each switching point is determined via a non-linear equation expressing the equality at the switching point of the carrier wave and modulating sine wave as follow (with reference to Fig. 2-7)

Modulating wave :

$$y = M\sin(\alpha) \qquad (2\text{-}12)$$

Carrier wave :

$$y_1 = 4(k-1) - \frac{2R}{\pi}\alpha \qquad \text{Negative going transitions}$$

$$y_2 = 2 - 4k + \frac{2R}{\pi}\alpha \qquad \text{positive going transitions}$$

$$k = 1, 2, 3, \ldots\ldots, R \qquad (2\text{-}13)$$

Where :

$$\alpha = \omega_m t$$

$$\omega_m = 2.\pi.f_m$$

$$R = \frac{f_c}{f_m} \qquad (2\text{-}14)$$

f_m = is frequency of modulating wave

f_c = is frequency of carrier wave

M = is modulating index

R = is frequency ratio or pulse numbers forming one out-put cycle

Thus the 2R switching points are given by the solution of following set :

$$M\sin(\alpha) = 4(k\text{-}1) - \frac{2R}{\pi}\alpha$$

$$M\sin(\alpha) = 2\text{-}4k + \frac{2R}{\pi}\alpha \qquad (2\text{-}15)$$

k = 1, 2 , 3 , ..., R

2.6 Discussion on M,R

For modulation index less than unity , the number of pulses in the resulting PWM wave is always equal to the frequency ratio R . For M > 1 , the number of pulses may be less than R . As modulation index increases beyond unity , pulses are successively dropped and pulse numbers decreases . For significantly large M , the pulse number becomes 1 and , finally , a square wave results .

To utilize fully the harmonic minimization capabilities of PWM control , it is desirable the inverter to operate at the maximum permissible switching frequency over the widest possible inverter output frequency range .

For low values of R the following consideration should be taken in to account :

1- R should be an integer , this means that the two intersecting wave forms are synchronous , and therefore discontinuities and fluctuations are avoided. Subharmonics or " beat frequency " effects can be produced if the modulating and carrier frequencies are not synchronized [11]

2- R should be an odd number , ensuring that the positive and negative half-cycle have the same wave form , which means that the output voltage contains no even harmonics .

3- The harmonic of the order R will be dominant , thus in a 3-phase system it can be eliminated if R is chosen as a multiple of 3 .

4- with a high value of the frequency ratio it is possible to cancel or reduce a number of low order harmonics . but at the same time a high frequency ratio results in relatively high switching losses in MOSFETs .

5- As has been shown in [12] by a 3-dimension model , the harmonic distortion(H.D.)* decreases with increasing M till unity , and increases there-after. Harmonic distortion also decreases with increasing of R .

Fig. 2.8 shows the 3-dimensional relationship(variation) between R , M , Total Harmonic Distortion (T.H.D)** .

(*) $$H.D = \frac{\sqrt{\sum_{2}^{\infty}\left(\frac{v_n}{n}\right)^2}}{v_1}$$

(**) $$T.H.D = \frac{\sqrt{\sum_{2}^{\infty}(v_n)^2}}{v_1}$$

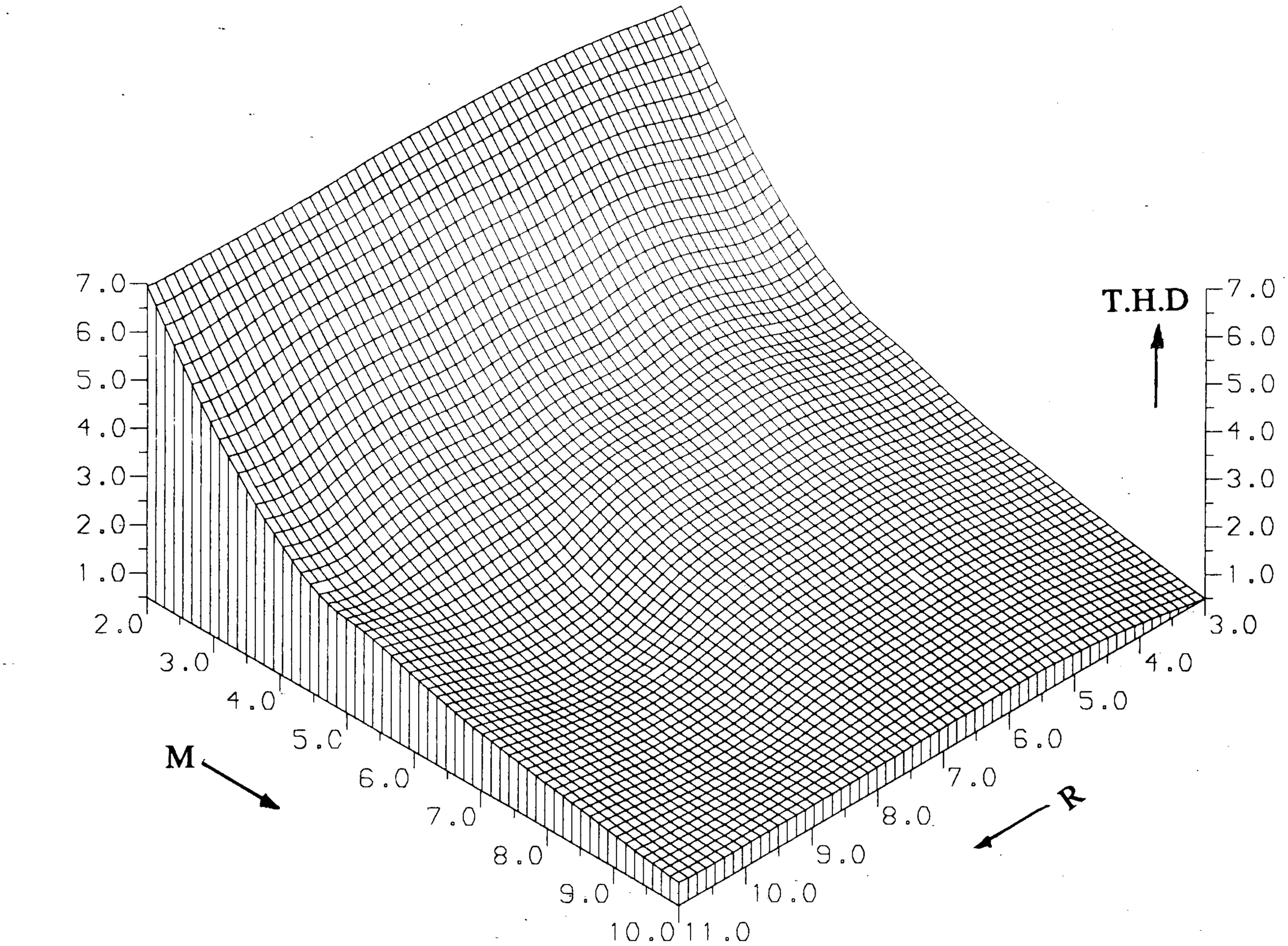

Fig. 2-8 3-Dimensional relationship between R , M , T.H.D. in sinusoidal PWM

2.7 PWM inverter for proposed system

A sinusoidal PWM method is applied to the three phase half bridge prototype system inverter (Fig. 2-3) for obtaining switching instants . The set of equations (2-15) is used here by the following specifications :

$$M\sin(\alpha) = 4(k-1) - \frac{2R}{\pi}\alpha$$

$$M\sin(\alpha) = 2-4k + \frac{2R}{\pi}\alpha \qquad (2\text{-}16)$$

$$k = 1, 2, 3, \ldots\ldots\ldots\ldots, R$$

$$M = 0.9$$

$$f_m = 1000 \text{ hz inverter output voltage frequency} \qquad (2\text{-}17)$$

$$R = 9$$

By substituting (2-17) in to (2-16) :

$$0.9\sin(\alpha) = 4(k-1) - \frac{18}{\pi}\alpha$$

$$0.9\sin(\alpha) = 2-4k + \frac{18}{\pi}\alpha \qquad (2\text{-}18)$$

$$k = 1, 2, \ldots\ldots\ldots\ldots\ldots, 9$$

The $2R = 18$ switching angles ; $\alpha0, \alpha1, \alpha2, \alpha3, \ldots\ldots\ldots\ldots, \alpha17$ & $\alpha18$ for v_{an} formation are obtained from solving of (2-18) by computer . Then by referring to Fig. 2-9 and considering 3-phase symmetry & quarter cycle symmetry property the switching angles for v_{bn} ; $\beta0$ ' $\beta1, \beta2, \beta3, \ldots\ldots\ldots\ldots\ldots$, $\beta17$ & $\beta18$ and vcn ; $\gamma0, \gamma1, \gamma2, \gamma3, \ldots\ldots\ldots\ldots\ldots, \gamma17$ & $\gamma18$ are arranged in following tables :

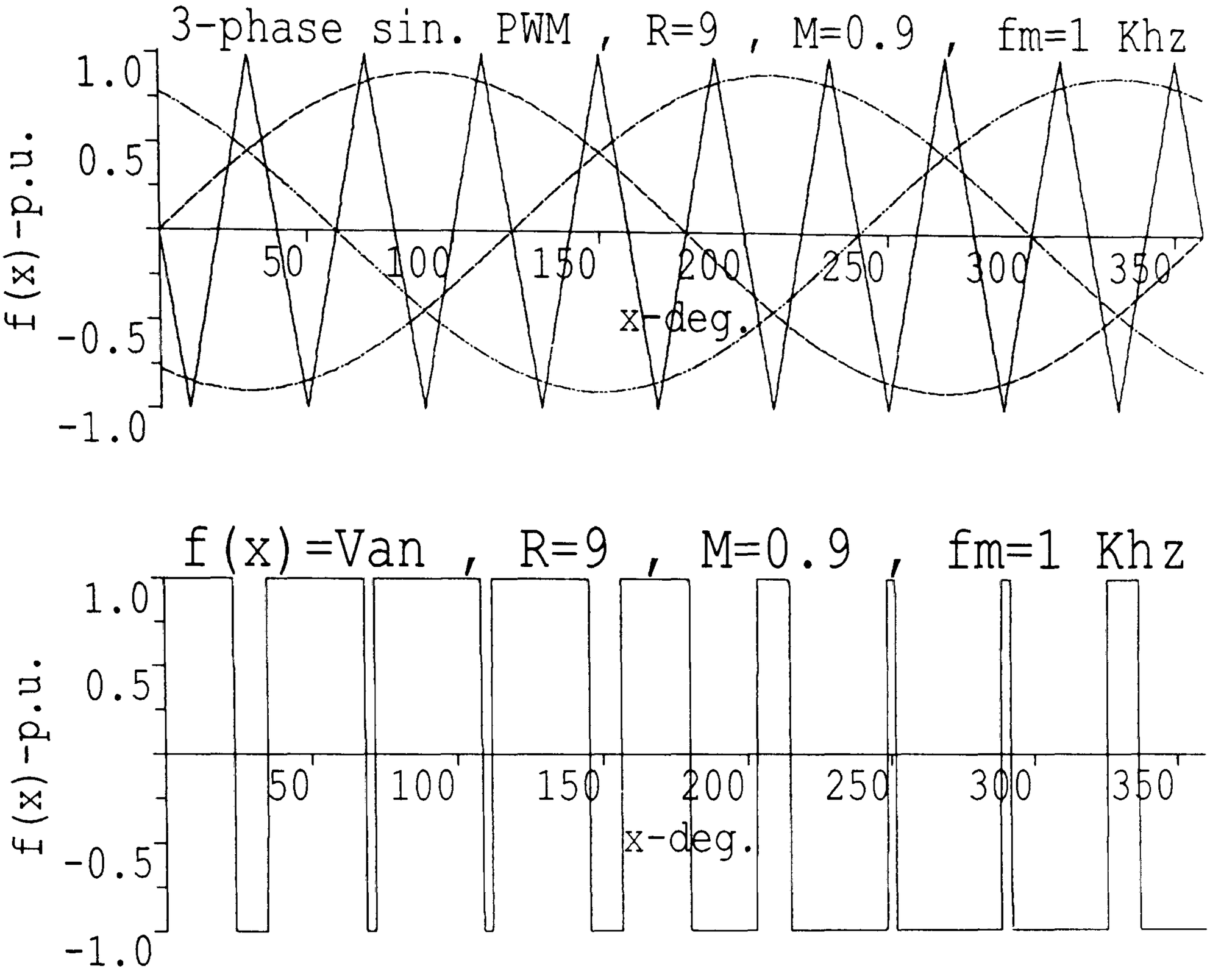

Fig. 2-9 3-phase inverter (Fig. 2-3) phase voltages

Table 2-1 Switching angles for v_{an} formation

Switching angles	Relationship with α1 , α2 , α3 , α4	Degrees
α0	0	0.00000
α1	α1	23.6001
α2	α2	34.8000
α3	α3	68.3995
α4	α4	71.4995
α5	180–α4	108.500
α6	180–α3	111.600
α7	180–α2	145.200
α8	180–α1	159.399
α9	180	180.000
α10	180+α1	203.600
α11	180+α2	214.800
α12	180+α3	248.399
α13	180+α4	251.499
α14	360–α4	288.590
α15	360–α3	291.699
α16	360–α2	325.200
α17	360–α1	336.400
α18	360	360.000

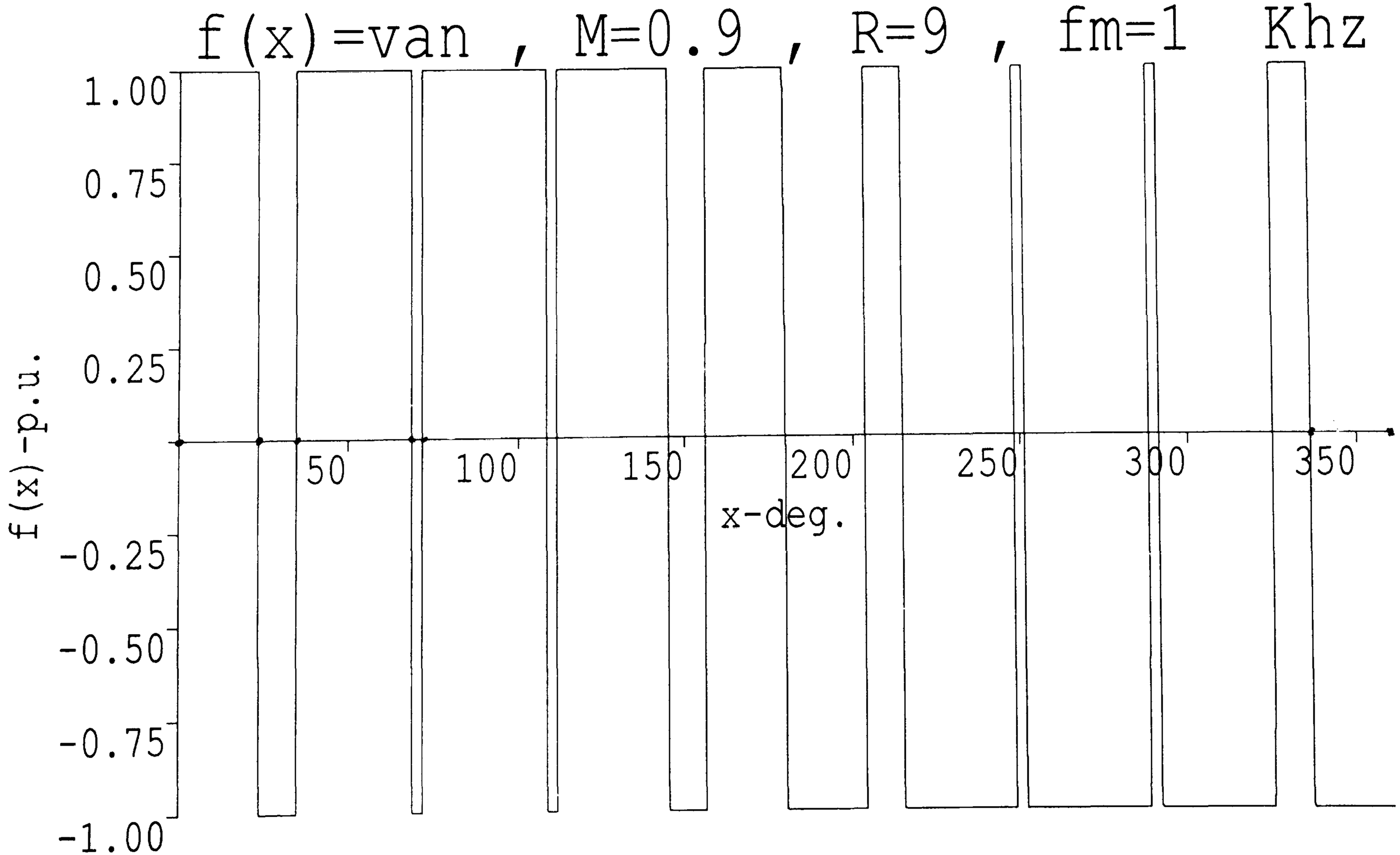
f(x)=van , M=0.9 , R=9 , fm=1 Khz
1.00
0.75
0.50
0.25
-0.25
-0.50
-0.75
-1.00
f(x)-p.u.
50
100
150
200
250
300
350
x-deg.

Fig. 2-10

Table 2-2 Switching angles for v_{bn} formation

Switching angles	Relationship with α1 , α2 , α3 , α4	Degrees
β0	α3–60	8.4000
β1	α4–60	11.500
β2	120–α4	48.500
β3	120–α3	51.600
β4	120–α2	85.500
β5	120–α1	96.500
β6	120	120.00
β7	120+α1	143.60
β8	120+α2	154.80
β9	120+α3	188.40
β10	120+α4	191.50
β11	300–α4	228.50
β12	300–α3	231.60
β13	300–α2	265.20
β14	300–α1	276.40
β15	300	300.00
β16	300+α1	323.71
β17	300+α2	334.80
β18	360	360.00

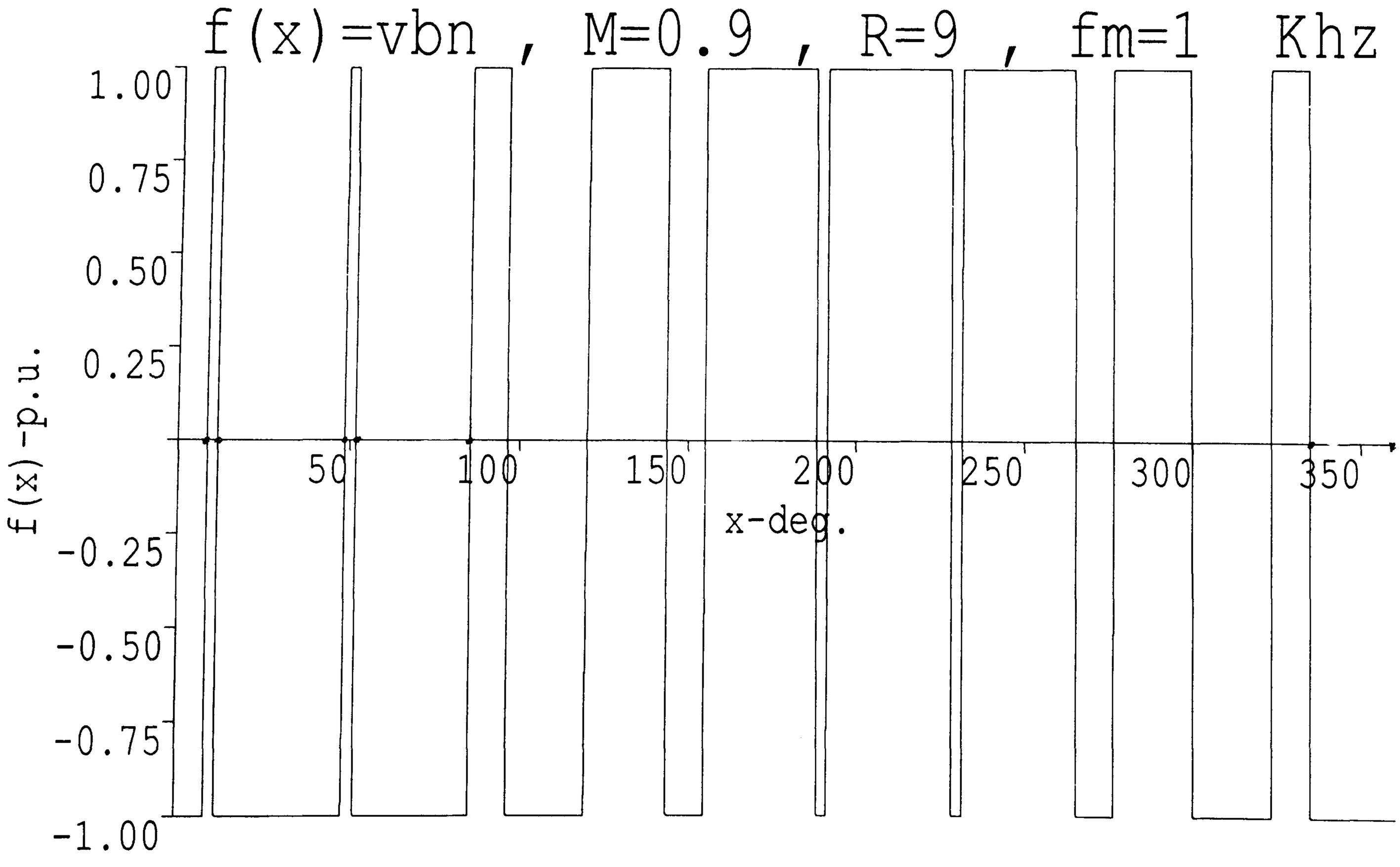
f(x)=vbn , M=0.9 , R=9 , fm=1 Khz
1.00
0.75
0.50
0.25
-0.25
-0.50
-0.75
-1.00
f(x)-p.u.
50
100
150
200
250
300
350
x-deg.

Fig. 2-11

Table 2-3 Switching angles for v_{cn} formation

Switrching angles	Relationship with $\alpha1$, $\alpha2$, $\alpha3$, $\alpha4$	Degrees
$\gamma0$	60–$\alpha2$	25.200
$\gamma1$	60–$\alpha1$	34.400
$\gamma2$	60	60.000
$\gamma3$	60+$\alpha1$	83.600
$\gamma4$	60+$\alpha2$	94.800
$\gamma5$	60+$\alpha3$	128.40
$\gamma6$	60+$\alpha4$	131.50
$\gamma7$	240–$\alpha4$	168.50
$\gamma8$	240–$\alpha3$	171.60
$\gamma9$	240–$\alpha2$	205.20
$\gamma10$	240–$\alpha1$	216.40
$\gamma11$	240	240.00
$\gamma12$	240+$\alpha1$	263.60
$\gamma13$	240+$\alpha2$	274.80
$\gamma14$	240+$\alpha3$	308.40
$\gamma15$	240+$\alpha4$	311.50
$\gamma16$	420–$\alpha4$	348.50
$\gamma17$	420–$\alpha3$	351.60
$\gamma18$	360	360.00

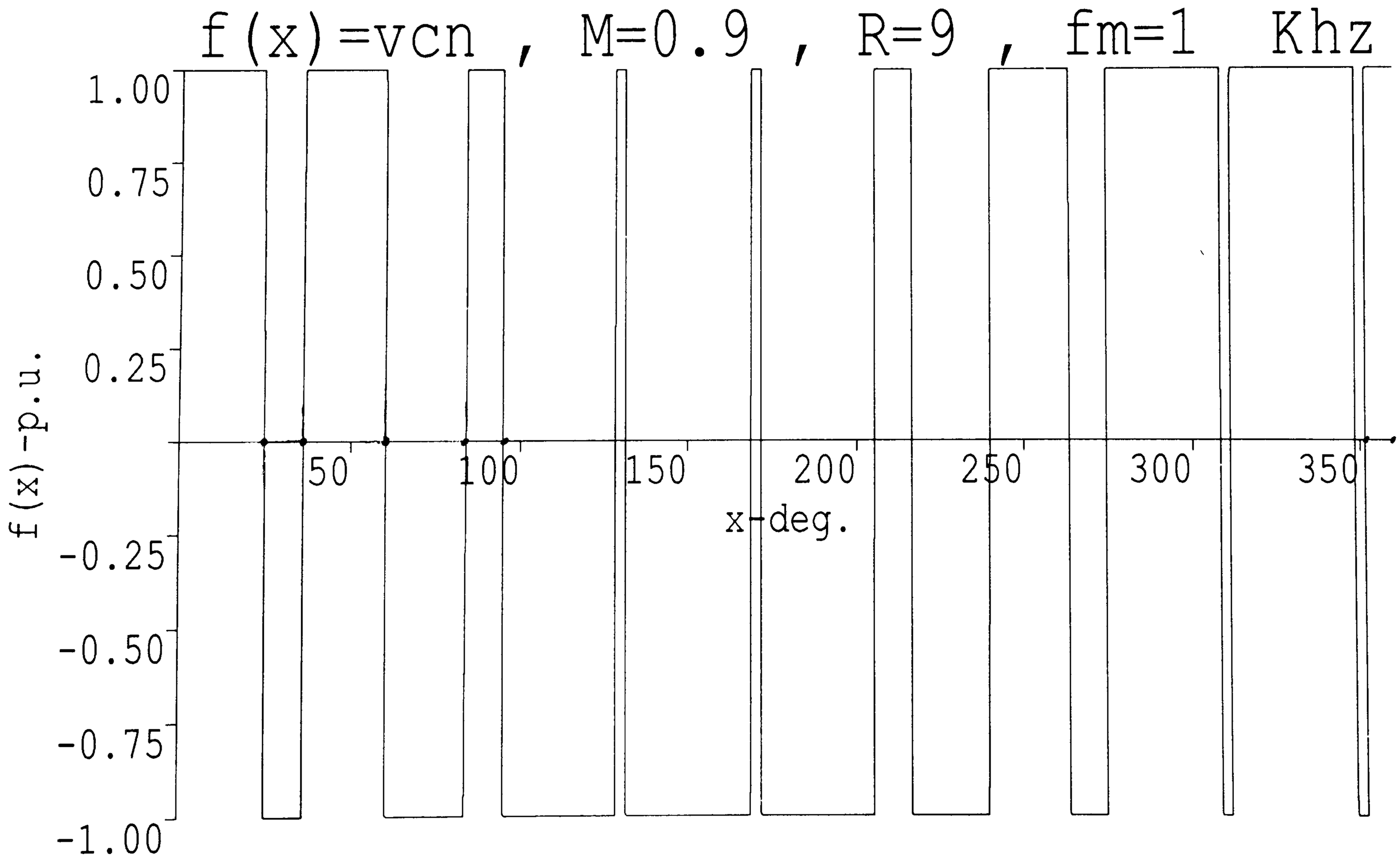
f(x)=vcn , M=0.9 , R=9 , fm=1 Khz
1.00
0.75
0.50
0.25
-0.25
-0.50
-0.75
-1.00
f(x)-p.u.
50
100
150
200
250
300
350
x-deg.

Fig. 2-12

2.8 Other waveforms of inverter

Based on Fig. 2-3 the following relationship can be derived by assuming.

i- balanced resistive load.

ii- the n is zero voltage reference point .

$$v_{ab} = v_{an} - v_{bn}$$

$$v_{bc} = v_{bn} - v_{cn} \qquad (2\text{–}19)$$

$$v_{ca} = v_{cn} - v_{an}$$

$$\begin{bmatrix} v_{ao} \\ v_{bo} \\ v_{co} \end{bmatrix} = \frac{1}{3}\begin{bmatrix} 2 & -1 & -1 \\ -1 & 2 & -1 \\ -1 & -1 & 2 \end{bmatrix}\cdot\begin{bmatrix} v_{an} \\ v_{bn} \\ v_{cn} \end{bmatrix} \qquad (2\text{–}20)$$

The third harmonic (when in Fig. 2-3 the K is open) is :

$$v_{no} = \frac{1}{3}\left[(v_{ao} + v_{bo} + v_{co}) - (v_{an} + v_{bn} + v_{cn})\right] \qquad (2\text{-}21)$$

The respective waveforms are shown in next pages .

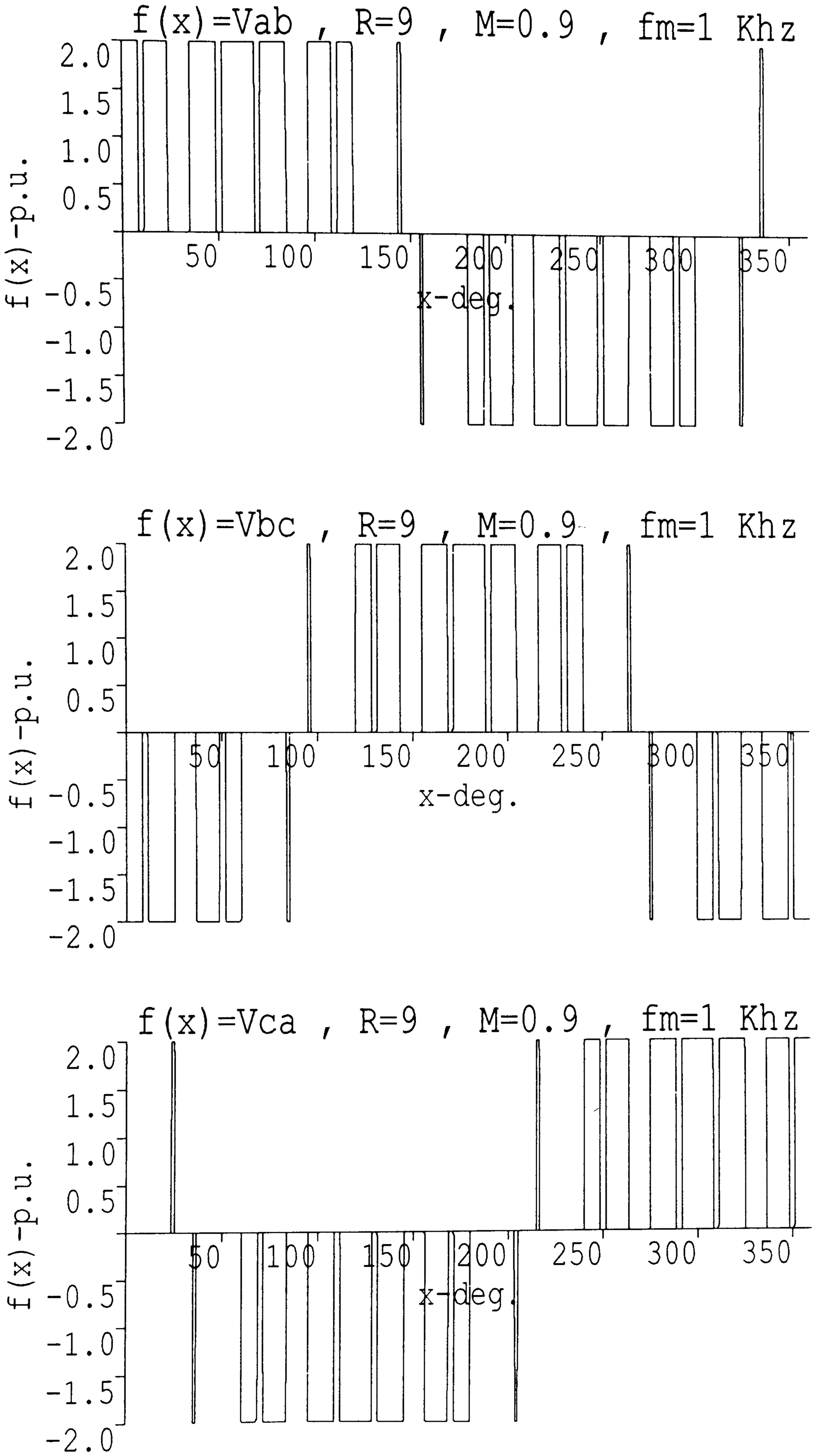

Fig. 2-13 3-phase inverter line voltages

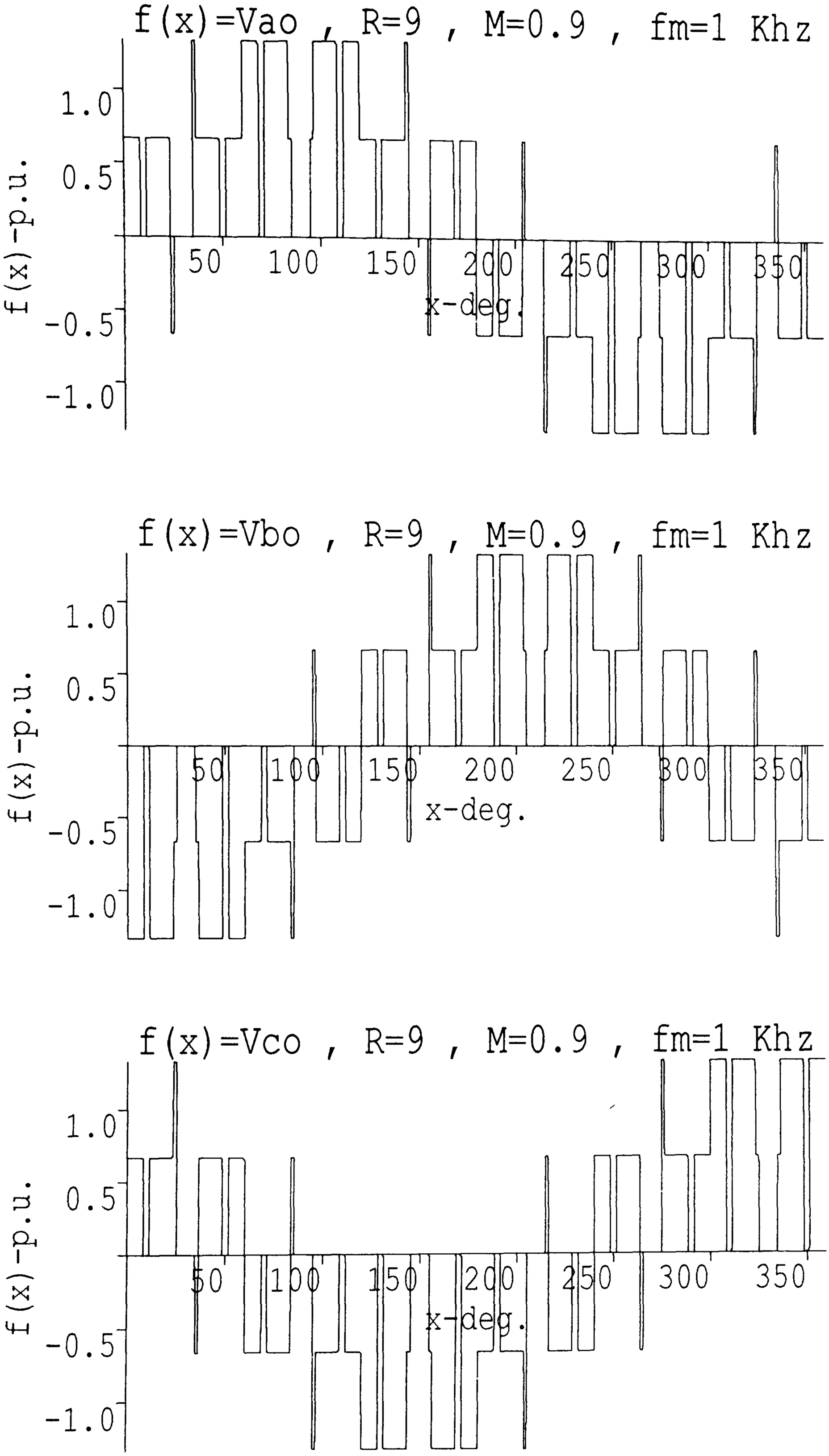
f(x)=Vao , R=9 , M=0.9 , fm=1 Khz
f(x)-p.u.
1.0
0.5
-0.5
-1.0
50
100
150
200
250
300
350
x-deg.
f(x)=Vbo , R=9 , M=0.9 , fm=1 Khz
f(x)-p.u.
1.0
0.5
-0.5
-1.0
50
100
150
200
250
300
350
x-deg.
f(x)=Vco , R=9 , M=0.9 , fm=1 Khz
f(x)-p.u.
1.0
0.5
-0.5
-1.0
50
100
150
200
250
300
350
x-deg.

Fig. 2-14

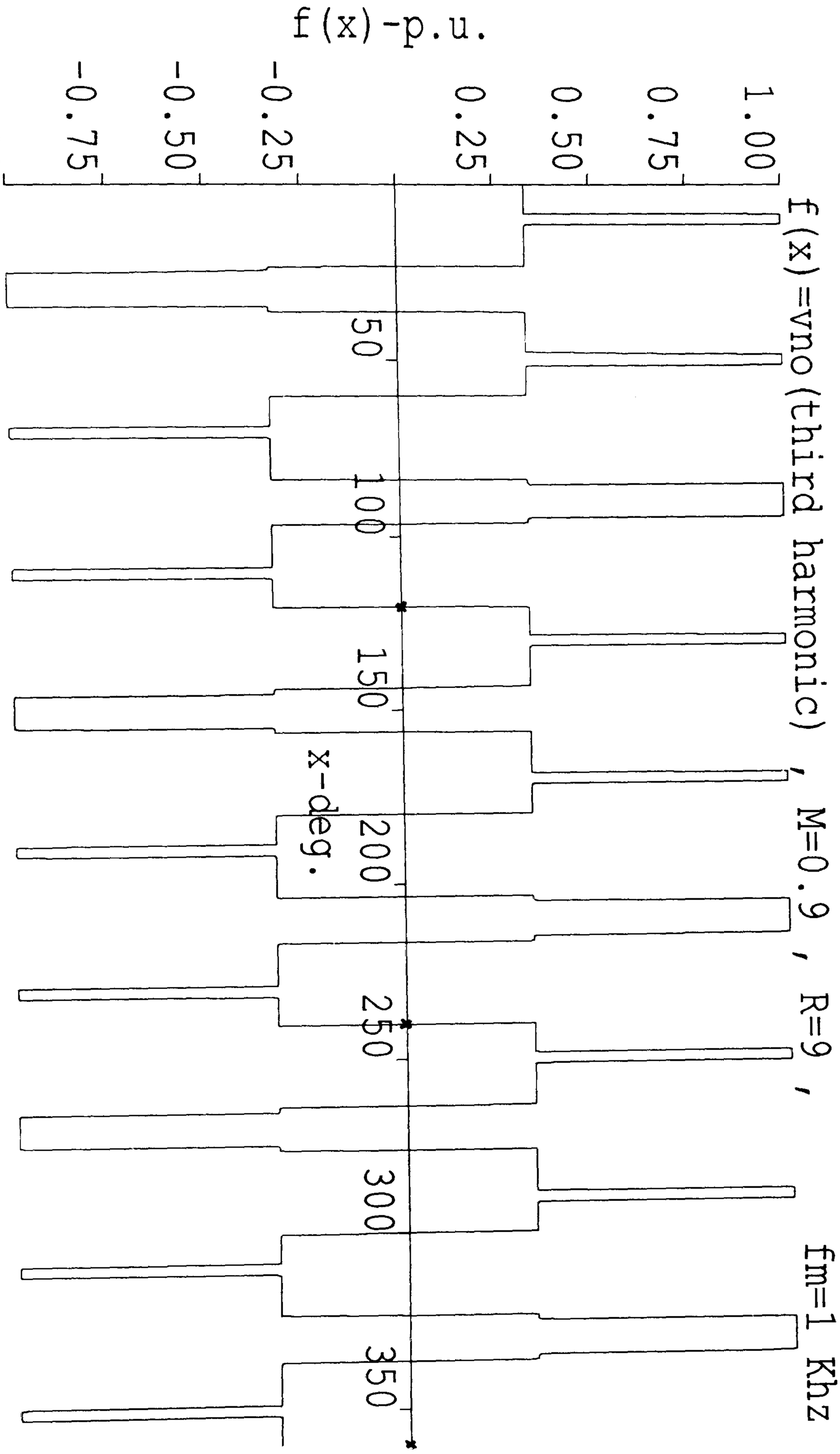

Fig. 2-15 third harmonic (v_{no}) waveform

2.9 Harmonic spectrum of output voltage (v_{an})

The harmonic spectrum of the v_{an} waveform (analysed by Fourier Series) is shown in Fig. 2-16 . In Table 2-4 the amplitude of low order and predominant components is presented .

Table 2-4 The v_{an} harmonic component amplitudes

Harmonic Order	Harmonic Amplitude
1	0.901369
3	0.002669
5	0.011683
7	0.266405
9	0.710470
11	0.267798
13	0.005674
15	0.176882
17	0.256467
19	0.255778
21	0.159450
23	0.127635
25	0.163148

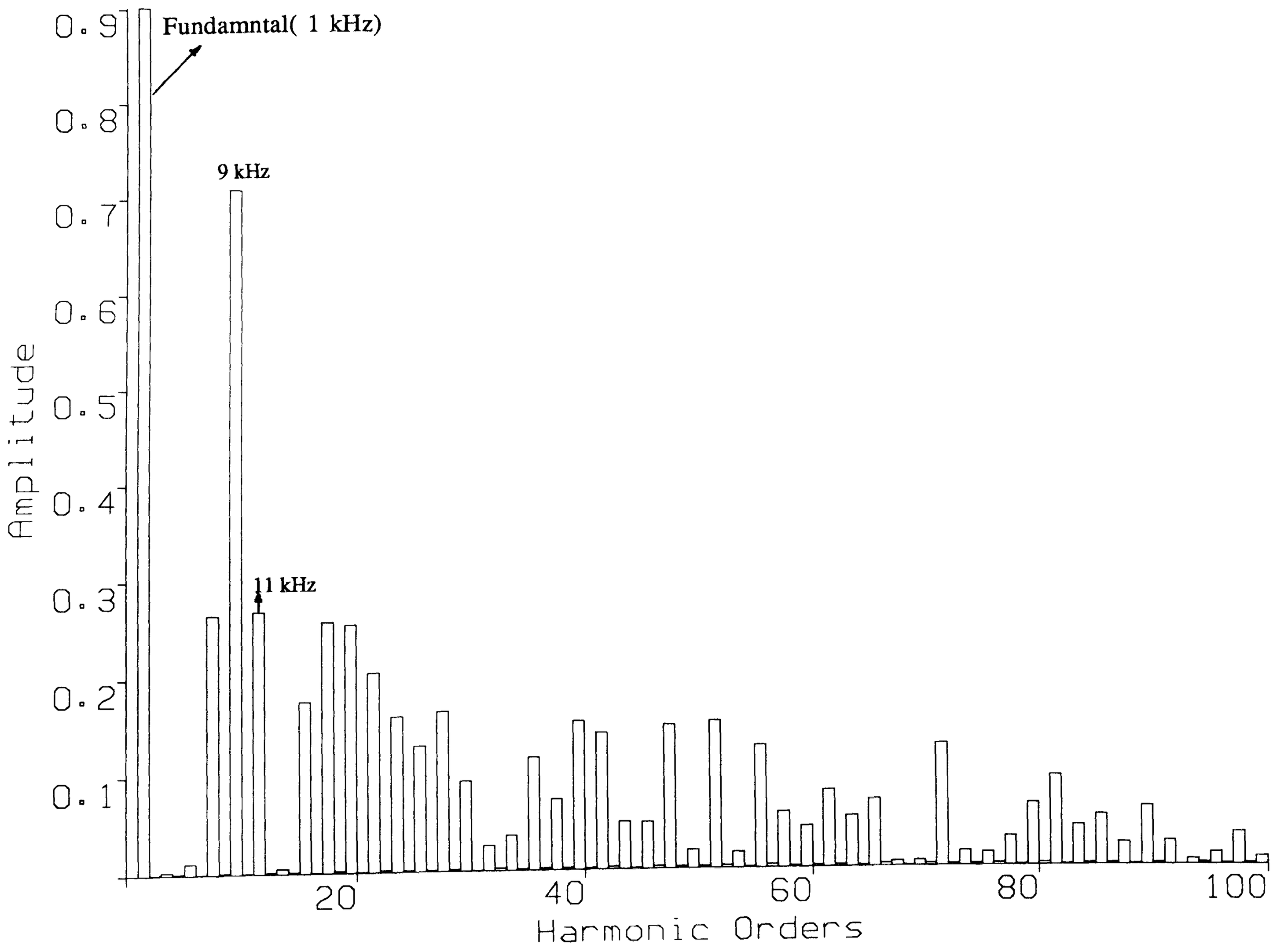

Fig. 2-16 inverter phase voltage(v_{an}) harmonic spectrum

2.10 Harmonic elimination importance

The output voltage waveform of ideal inverters should be sinusoidal . Nevertheless , the waveforms of practical inverters are nonsinusoidal and contain certain harmonics , for example : the output of conventional PWM inverters is square wave (2 level on half bridge , 3 level on full bridge) and for resonant inverters the output voltage is approximately sinusoidal .

The total harmonic distortion (T.H.D.) factor is defined as a measure of closeness in shape between a waveform and it's fundamental component :

$$\text{T.H.D.} = \frac{\sqrt{v_2^{\,2} + v_3^{\,2} + v_4^{\,2} + \ldots . v_n^{\,2}}}{v_1} = \frac{1}{v_1}\left(\sum_{n=2,3,..}^{\infty} v_n^{\,2} \right)^{\frac{1}{2}} \qquad (2-22)$$

Where v_1 is the rms value of the fundamental component of the output voltage , and v_n ($n \neq 1$) is the rms value of the n th harmonic . In some application (fast response power supplies) T.H.D. may be varied from 0. 05 ..... , and this requires a low pass filter at inverter output to eliminate the higher harmonics .

As it is clear from resonant L-C filtering circuits ($f_r = \frac{1}{2\pi\sqrt{LC}}$) , the low order harmonics is accompanied weight and bulky filter elements . Thus if low order harmonics in the output voltage can be reduced or eliminated by other means (unfiltered inverter) , the size of the filter can be reduced . This also improves the speed of response to load change of the entire inverter filter system .

2.11 Harmonic elimination and voltage control of PWM inverters

For the harmonic elimination and control process of the output voltage of the 3-phase inverters , the Fig. 2 - 17 is used as a simplified reference circuit .

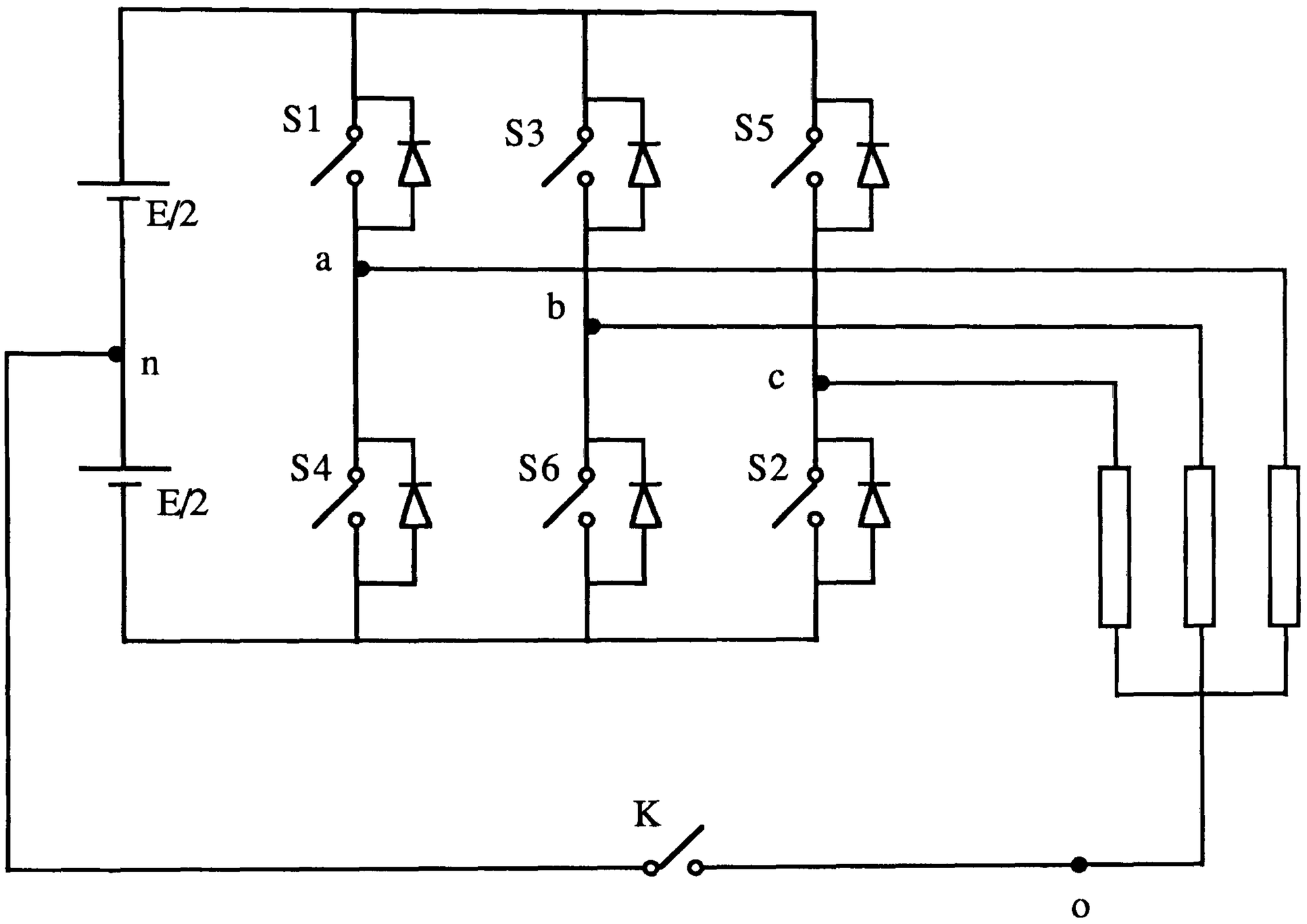

Fig. 2-17 The simplified 3-phase half bridge inverter

A generalized quarter-wave symmetric PWM switching pattern can be defined as shown in Fig. 2 -18 , where the odd switching angles $\alpha 1$, $\alpha 3$,... define the negative going transitions and $\alpha 2$, $\alpha 4$, ... define the positive going transitions .

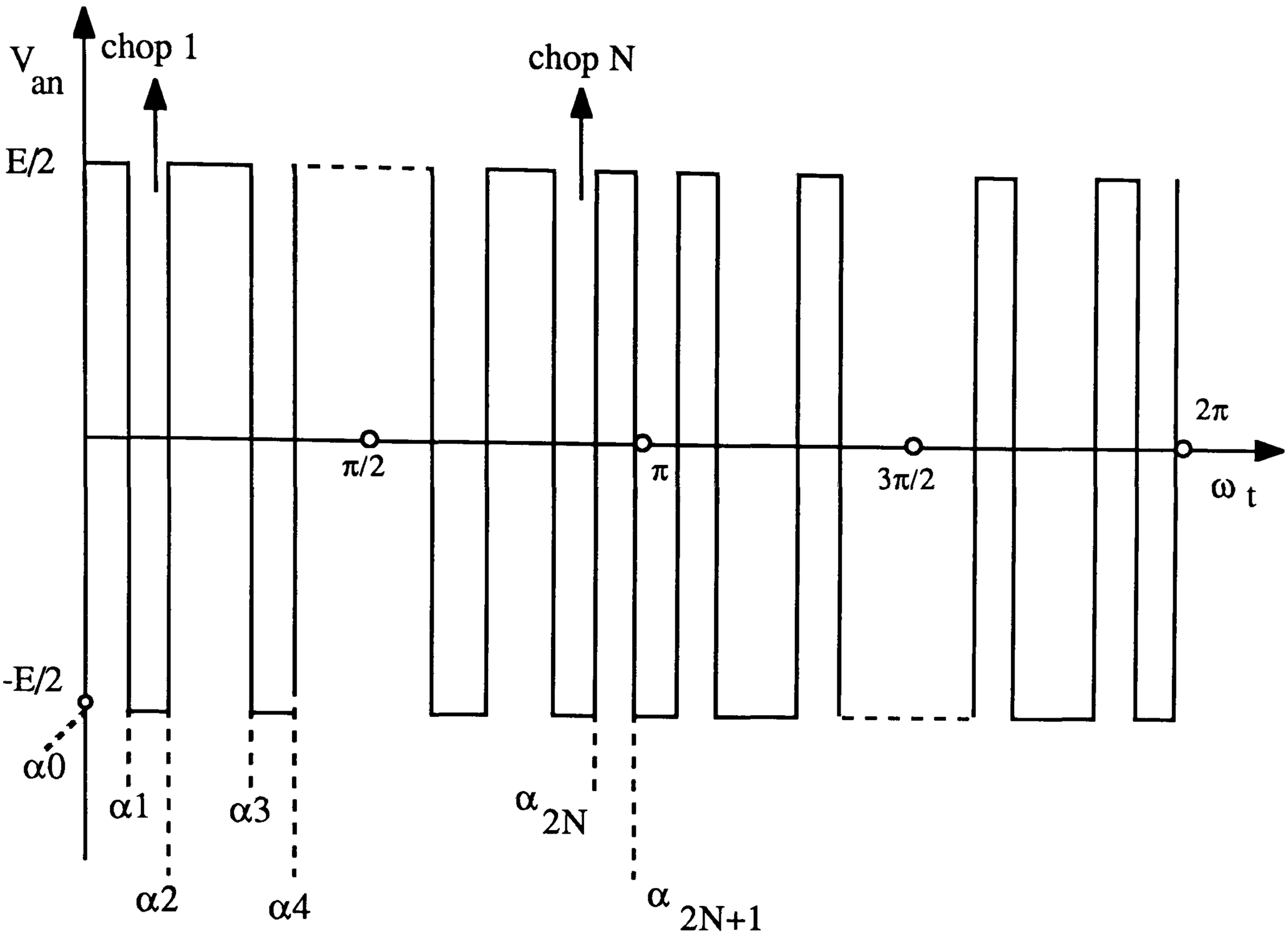

Fig. 2-18 Generalized output voltage waveform of single phase half bridge inverter

The $v_{an}(\omega_t)$, $v_{bn}(\omega_t)$, and $v_{cn}(\omega_t)$ will be referred as the inverter phase voltages, where the following relationships are valid between them.

$$v_{an}(\omega t) = v_{an}(\omega t+2\pi)$$

$$v_{an}(\omega t) = v_{an}(\pi-\omega t)$$

$$v_{an}(\omega t) = -v_{an}(\pi+\omega t) \qquad (2\text{-}23)$$

$$v_{bn}(\omega t) = v_{an}(\omega t - \frac{2}{3}\pi)$$

$$v_{cn}(\omega t) = v_{an}(\omega t + \frac{2}{3}\pi)$$

The first three are the character of the wave : periodic , with quarter-cycle symmetry , and half-cycle antisymmetry . The last two requirments shows the symmetric three-phase character of the inverter voltages . The $v_{ab}(\omega t)$, $v_{bc}(\omega t)$ and $v_{ca}(\omega t)$ define the line voltages of inverter .

When the inverter is commutated N(number of switching angles) times over a quarter cycle , the expansion of $v_{an}(\omega t)$ in a fourier series yields only odd-sinusoidal components [13] & [14] .

$$v_{an}(\omega t) = \sum_{n=1,3,5}^{\infty} \left[a_n \mathrm{Sin}(n\omega t) + b_n \mathrm{Cos}(n\omega t) \right] \qquad (2\text{-}24)$$

where :

$$b_n = 0.0$$

$$a_n = V_{max}(n) = \frac{4E}{n\pi} \left[1 + 2\sum_{k=1}^{N} (-1)^k \mathrm{Cos}(n\alpha_k) \right] \qquad (2\text{-}25)$$

$$n = 1 , 3 , 5 , \ldots\ldots\ldots\ldots$$

N = number of pulses over a quarter cycle

The term α_k denotes the commutation angles ($k = 1 , 2 , \ldots\ldots , N$) , such that :

$$0 < \alpha_1 < \alpha_2 < \ldots\ldots < \alpha_k < \alpha_N < \frac{\pi}{2} \qquad (2\text{–}26)$$

The (2-25) may be shown in a expanded form :

$$a_n = V_{max}(n) = \frac{4E}{n\pi} \left[1 - 2\mathrm{Cos}(n\alpha_1) + 2\mathrm{Cos}(n\alpha_2) - 2\mathrm{Cos}(n\alpha_3) + 2\mathrm{Cos}(n\alpha_4) - \ldots\ldots\ldots \right]$$

(2-27)

It is clear from (2-25) that , there are N degrees of freedom in controlling the amplitudes of the component harmonics , making it possible to eliminate N low order harmonics (put related $a_n = 0.0$) or eliminate (N-1) low order and to control the amplitude of the fundamental wave between the limits :

$$0 \leq V_{max}(1) < \frac{4}{\pi}E \quad \text{or} \quad 0 \leq v_{max}(1) < 1.2732E \qquad (2\text{-}28)$$

For elimination N low order harmonics following set can be arranged :

$$\begin{aligned} f_1(\alpha) &= 1 + 2\sum_{k=1}^{N}(-1)^k \cos(n_1\alpha_k) = 0 \\ f_2(\alpha) &= 1 + 2\sum_{k=1}^{N}(-1)^k \cos(n_2\alpha_k) = 0 \\ &\cdots\cdots\cdots\cdots\cdots\cdots\cdots\cdots \\ &\cdots\cdots\cdots\cdots\cdots\cdots\cdots\cdots \\ f_N(\alpha) &= 1 + 2\sum_{k=1}^{N}(-1)^k \cos(n_N\alpha_k) = 0 \end{aligned} \qquad (2\text{-}29)$$

The (2-29) represent a system of N nonlinear equations . In solving that numerically [15] & [16] the main concern is the convergence of iteration results (for example in using Newton-Raphson method asigning an initial guess for the N angles , which is the most difficult step of solution) . So there is a trial and error process , rather than a guarantee for convergence to a solution .

After determining the optimized switching angles , they can subsequently be programmed in to the microprocessor memory and used to generate the PWM waveform in real-time . A number of solutions have been reported with different computer facilities [13] , [17] and [18] .

In ref. [13] , the system of equations has been solved for N = 2 & N= 5 for half bridge and full bridge inverters . Ref. [17] is more interesting for programmed PWM techniques , and [19] gives the trajectories of switching angles with N = 9 for high performance induction motor type loads .

Here the control of fundamental wave amplitude between the limits given in (2-28) and eliminating of 5th , 7th , 11th components by varing of $\alpha 1$, $\alpha 2$, $\alpha 3$ and $\alpha 4$ [18] , is shown in Fig. 2-19 .

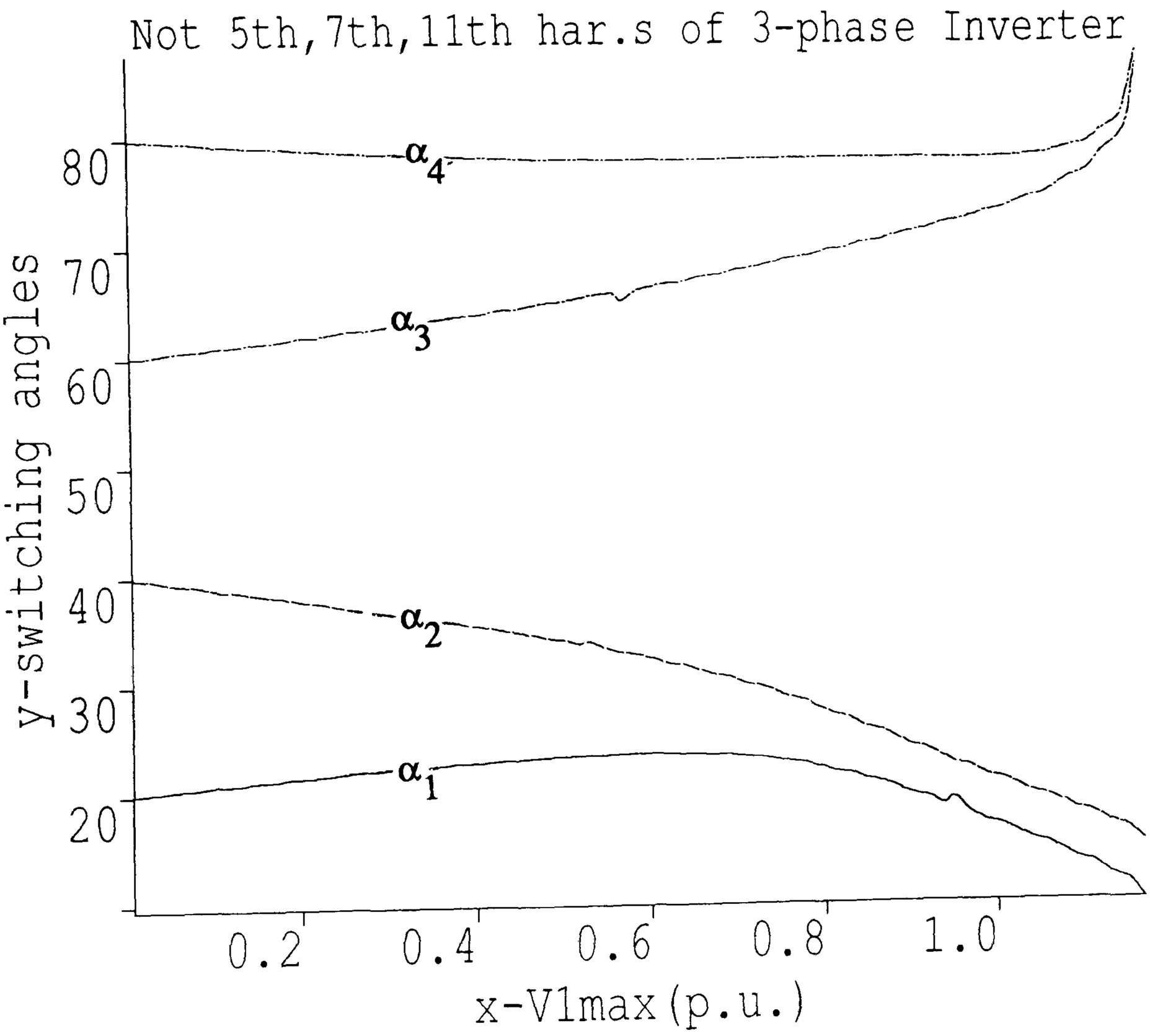

Fig. 2-19 Trajectories of switching angles for 3-phase inverter

2.12 *Harmonic elimination for prototype 3-phase half bridge system with N=4 and $V_{max}(1)$ =1.17 p.u.*

In determining the N angles over a quarter-cycle , with a view to eliminating N harmonics , a set of nonlinear equations , based on (2-25) should be solved . Since the prototype system is 3-phase & half bridge , the triplen harmonics (v_{3k} , k=1 , 2 , 3 , ...) produce no current in it and need not be eliminated . putting N=4 in (2-25) yields .

$$\begin{aligned} &V_{max}(5)=0\\ &V_{max}(7)=0\\ &V_{max}(11)=0\\ &V_{max}(13)=0 \end{aligned} \qquad (2\text{-}30)$$

or in a expanded form :

$$\begin{aligned} &0.5 - \cos(5\alpha_1) + \cos(5\alpha_2) - \cos(5\alpha_3) + \cos(5\alpha_4) = 0.0\\ &0.5 - \cos(7\alpha_1) + \cos(7\alpha_2) - \cos(7\alpha_3) + \cos(7\alpha_4) = 0.0\\ &0.5 - \cos(11\alpha_1) + \cos(11\alpha_2) - \cos(11\alpha_3) + \cos(11\alpha_4) = 0.0\\ &0.5 - \cos(13\alpha_1) + \cos(13\alpha_2) - \cos(13\alpha_3) + \cos(13\alpha_4) = 0.0 \end{aligned} \qquad (2\text{-}31)$$

This set , (2-31) was solved by using **NAG(Numerical Algorithm Groups) routines in University computer center(Computer program in Appendix A)** with following results :

$$\begin{aligned} &\alpha1 = 10.548153^\circ\\ &\alpha2 = 16.094384^\circ\\ &\alpha3 = 30.905343^\circ\\ &\alpha4 = 32.864859^\circ\\ &V_{max}(1) = 1.17 \text{ p.u.} \end{aligned} \qquad (2.33)$$

2.13 Waveforms construction for prototype system inverter

With reference to Fig. 2-17 , related relationships of (2-19) , (2-20) , (2-21) , (2-23) and based on obtained angles of (2-32) the inverter phase & line voltages and associated tables of switching angles are arranged as follows :

Table 2-5 Switching angles for v_{an} *(harmonic eliminated) formation*

Switching angles	Relationship with $\alpha1$, $\alpha2$, $\alpha3$, $\alpha4$	Degrees
$\alpha0$	0	0.00000
$\alpha1$	$\alpha1$	10.5482
$\alpha2$	$\alpha2$	16.0944
$\alpha3$	$\alpha3$	30.9053
$\alpha4$	$\alpha4$	32.8649
$\alpha5$	180–$\alpha4$	147.135
$\alpha6$	180–$\alpha3$	149.095
$\alpha7$	180–$\alpha2$	163.906
$\alpha8$	180–$\alpha1$	169.452
$\alpha9$	180	180.000
$\alpha10$	180+$\alpha1$	190.548
$\alpha11$	180+$\alpha2$	196.094
$\alpha12$	180+$\alpha3$	210.905
$\alpha13$	180+$\alpha4$	212.865
$\alpha14$	360–$\alpha4$	327.135
$\alpha15$	360–$\alpha3$	329.095
$\alpha16$	360–$\alpha2$	343.906
$\alpha17$	360–$\alpha1$	349.452
$\alpha18$	360	360.000

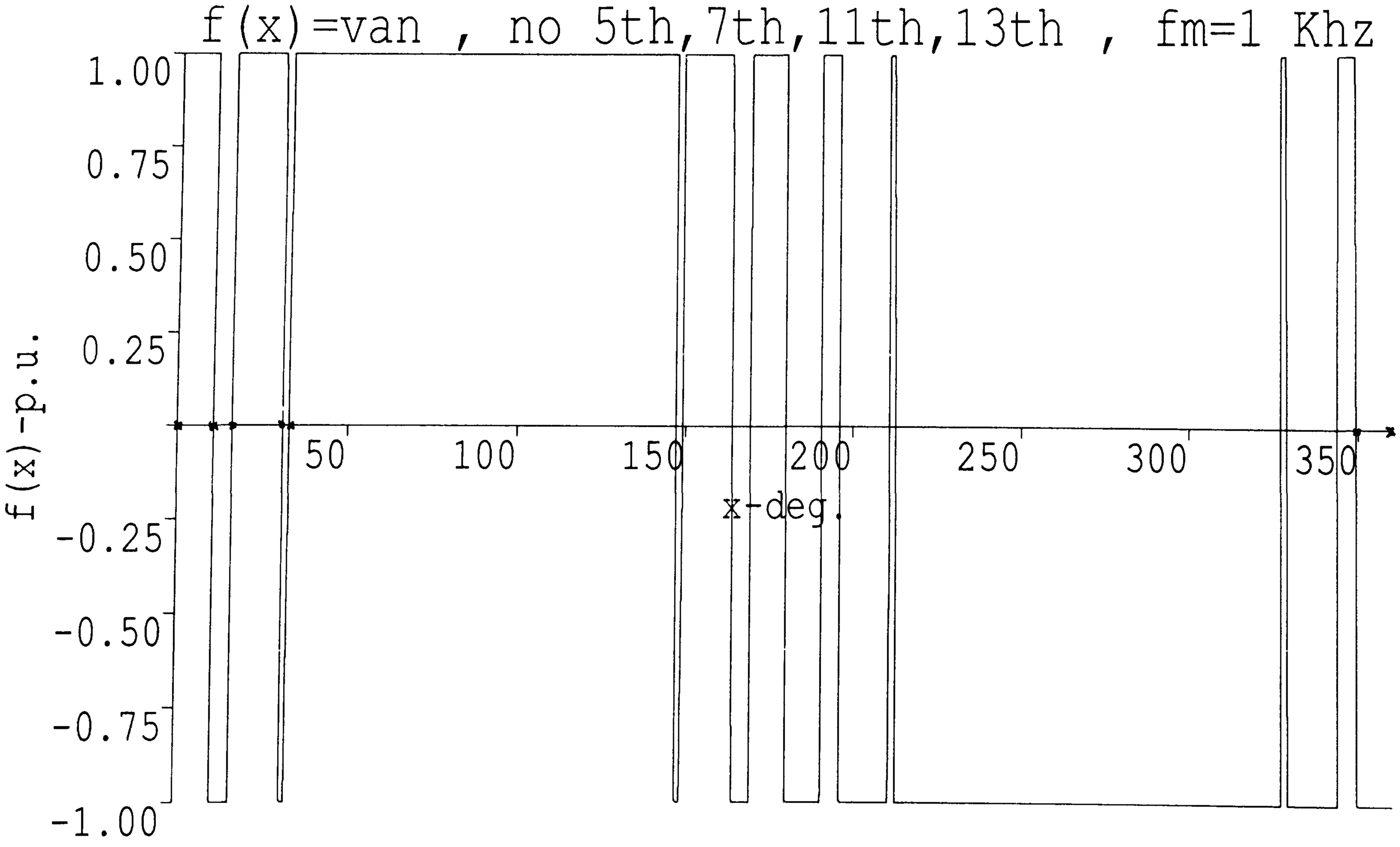
f(x)=van , no 5th,7th,11th,13th , fm=1 Khz
1.00
0.75
0.50
0.25
-0.25
-0.50
-0.75
-1.00
f(x)-p.u.
50
100
150
200
250
300
350
x-deg.

Fig. 2-20

Table 2-6 Switching angles for v_{bn}*(harmonic eliminated) formation*

Switching angles	Relationship with α1 , α2 , α3 , α4	Degrees
β0	120–α4	87.1351
β1	120–α3	89.0947
β2	120–α2	103.906
β3	120–α1	109.452
β4	120	120.000
β5	120+α1	130.548
β6	120+α2	136.094
β7	120+α3	150.905
β8	120+α4	152.865
β9	300–α4	267.135
β10	300–α3	269.095
β11	300–α2	283.906
β12	300–α1	289.452
β13	300	300.000
β14	300+α1	310.548
β15	300+α2	316.094
β16	300+α3	330.905
β17	300+α4	332.865
β18	360	360.000

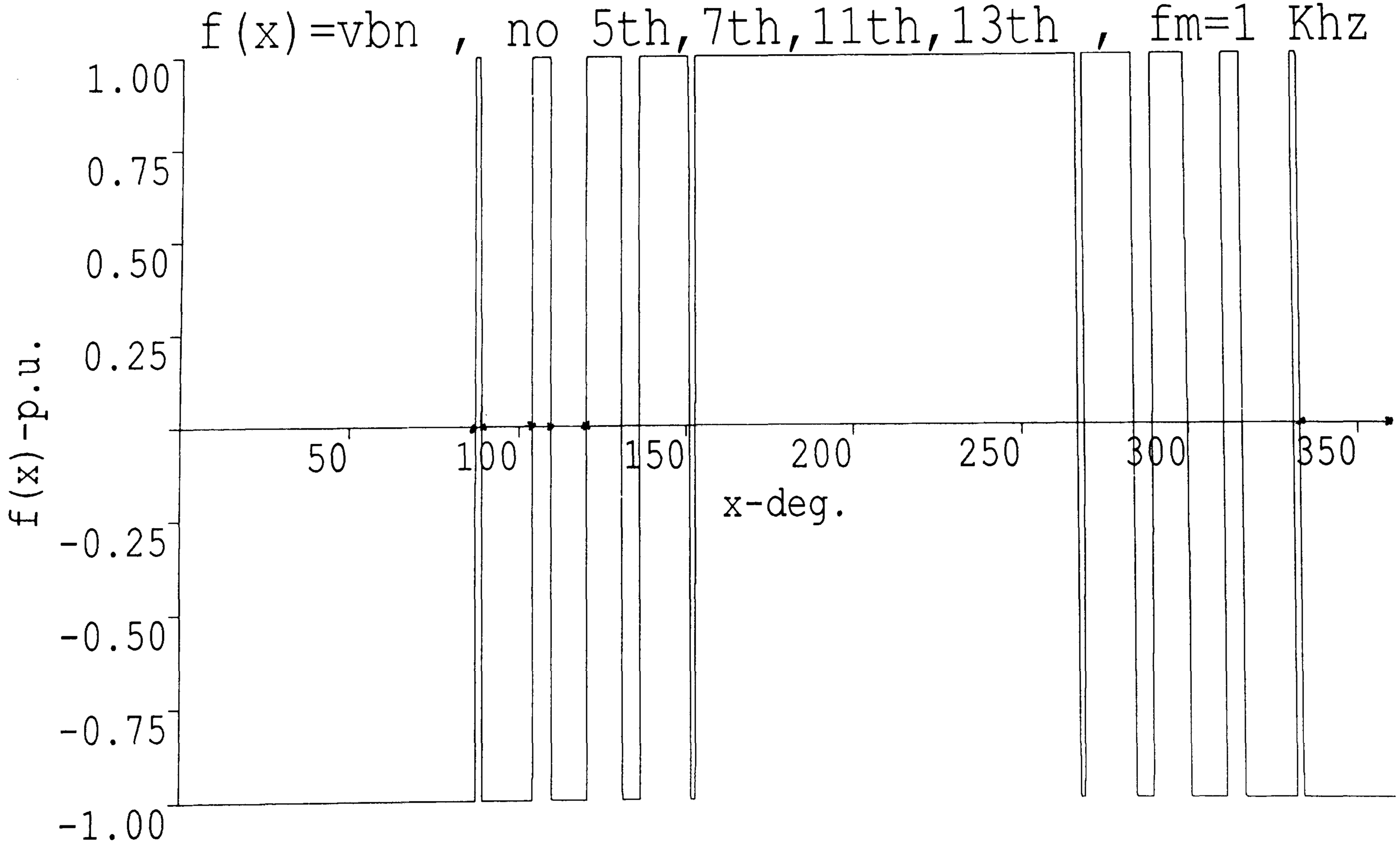
f(x)=vbn , no 5th,7th,11th,13th , fm=1 Khz
1.00
0.75
0.50
0.25
-0.25
-0.50
-0.75
-1.00
f(x)-p.u.
50
100
150
200
250
300
350
x-deg.

Fig. 2-21

Table 2-7 Switching angles for v_{cn} *(harmonic eliminated) formation*

Switching angles	Relationship with $\alpha1, \alpha2, \alpha3, \alpha4$	Degrees
γo	$60-\alpha4$	27.1351
$\gamma1$	$60-\alpha3$	29.0947
$\gamma2$	$60-\alpha2$	43.9056
$\gamma3$	$60-\alpha1$	49.4518
$\gamma4$	60	60.0000
$\gamma5$	$60+\alpha1$	70.5480
$\gamma6$	$60+\alpha2$	76.0944
$\gamma7$	$60+\alpha3$	90.9053
$\gamma8$	$60+\alpha4$	92.8649
$\gamma9$	$240-\alpha4$	207.135
$\gamma10$	$240-\alpha3$	209.095
$\gamma11$	$240-\alpha2$	223.906
$\gamma12$	$240-\alpha1$	229.452
$\gamma13$	240	240.000
$\gamma14$	$240+\alpha1$	250.548
$\gamma15$	$240+\alpha2$	256.094
$\gamma16$	$240+\alpha3$	270.905
$\gamma17$	$240+\alpha4$	272.865
$\gamma18$	360	360.000

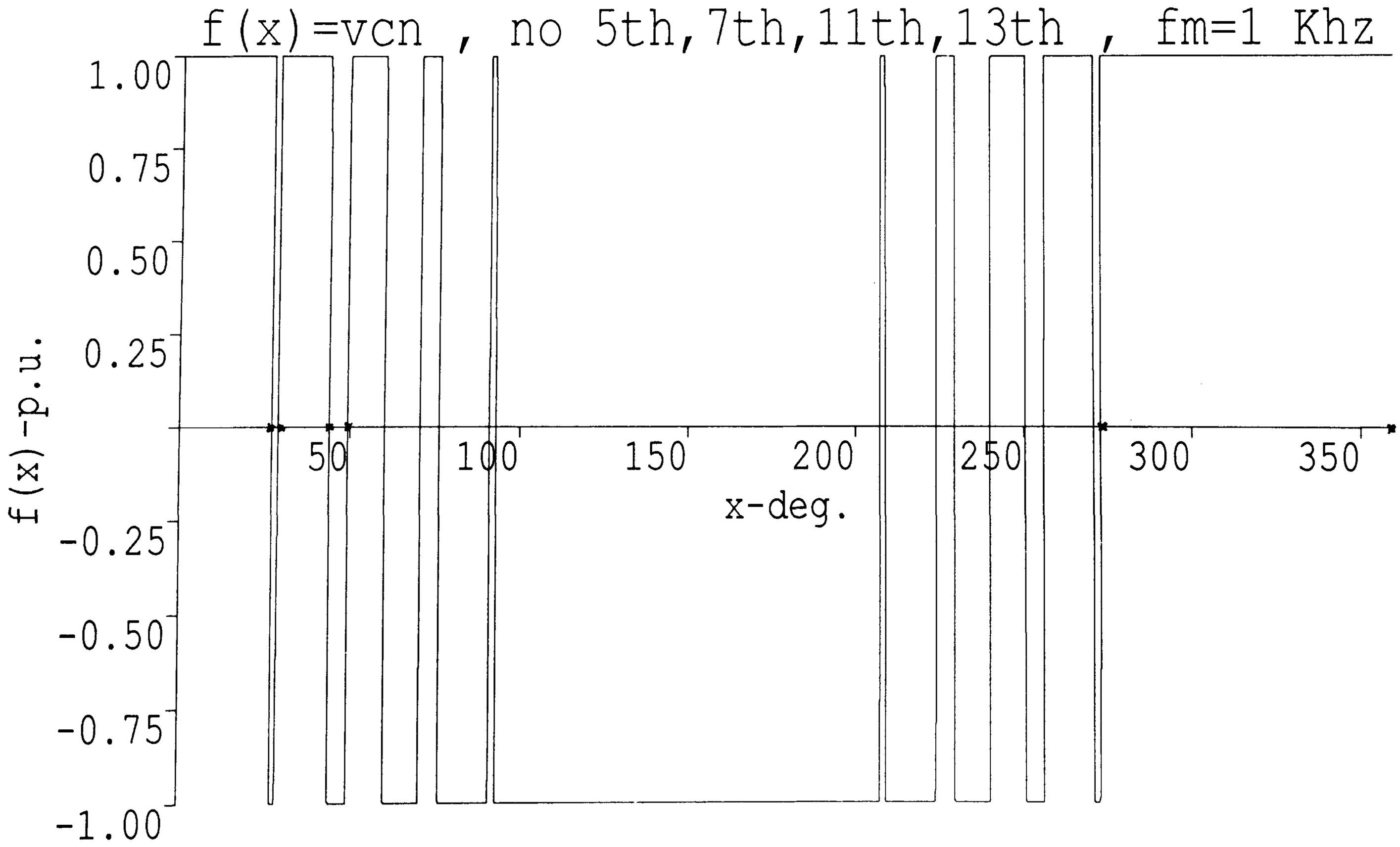
f(x)=vcn , no 5th,7th,11th,13th , fm=1 Khz
1.00
0.75
0.50
0.25
-0.25
-0.50
-0.75
-1.00
f(x)-p.u.
50
100
150
200
250
300
350
x-deg.

Fig. 2-22

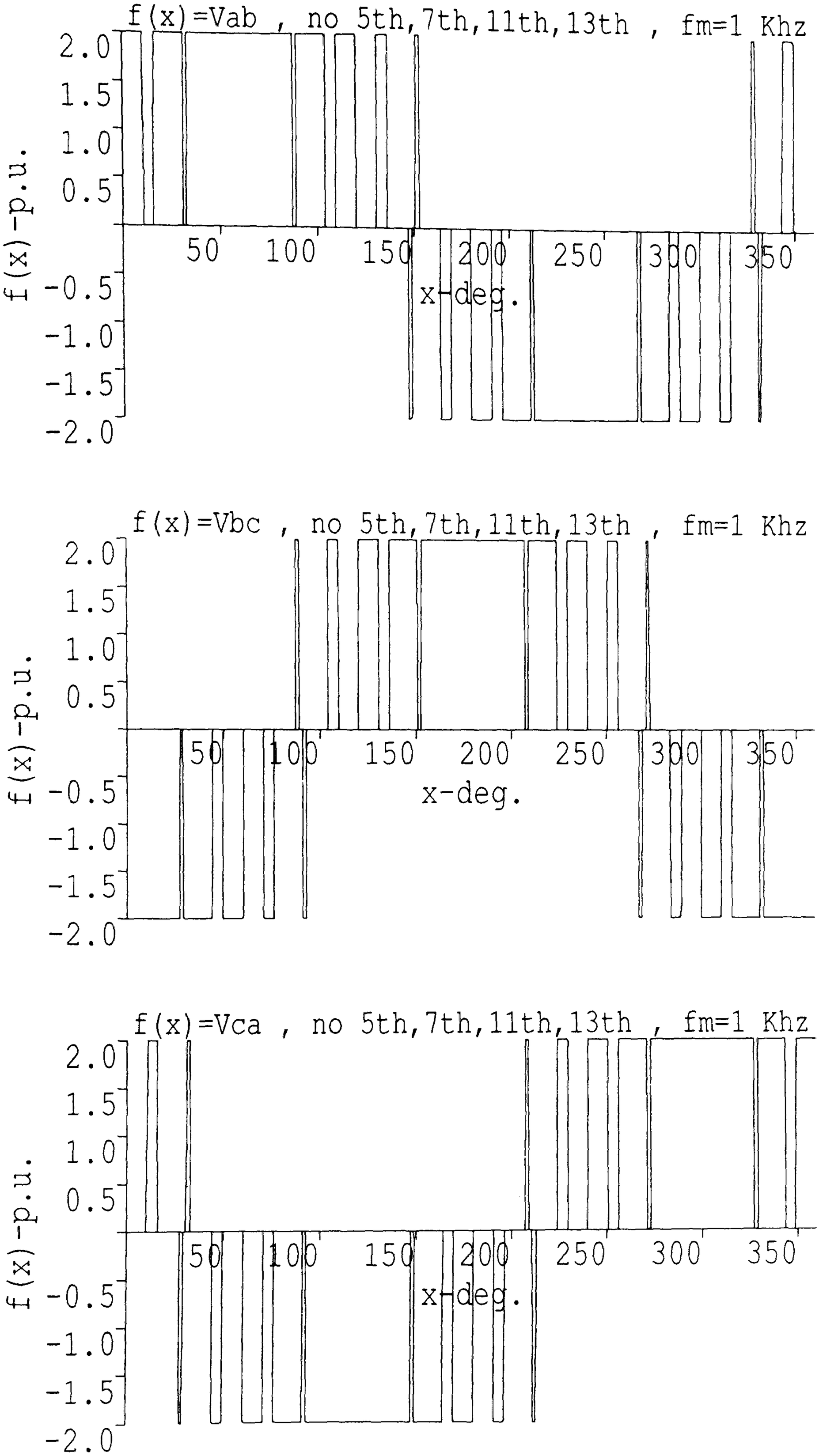

Fig. 2-23 3-phase inverter (Fig 2-17) line voltages

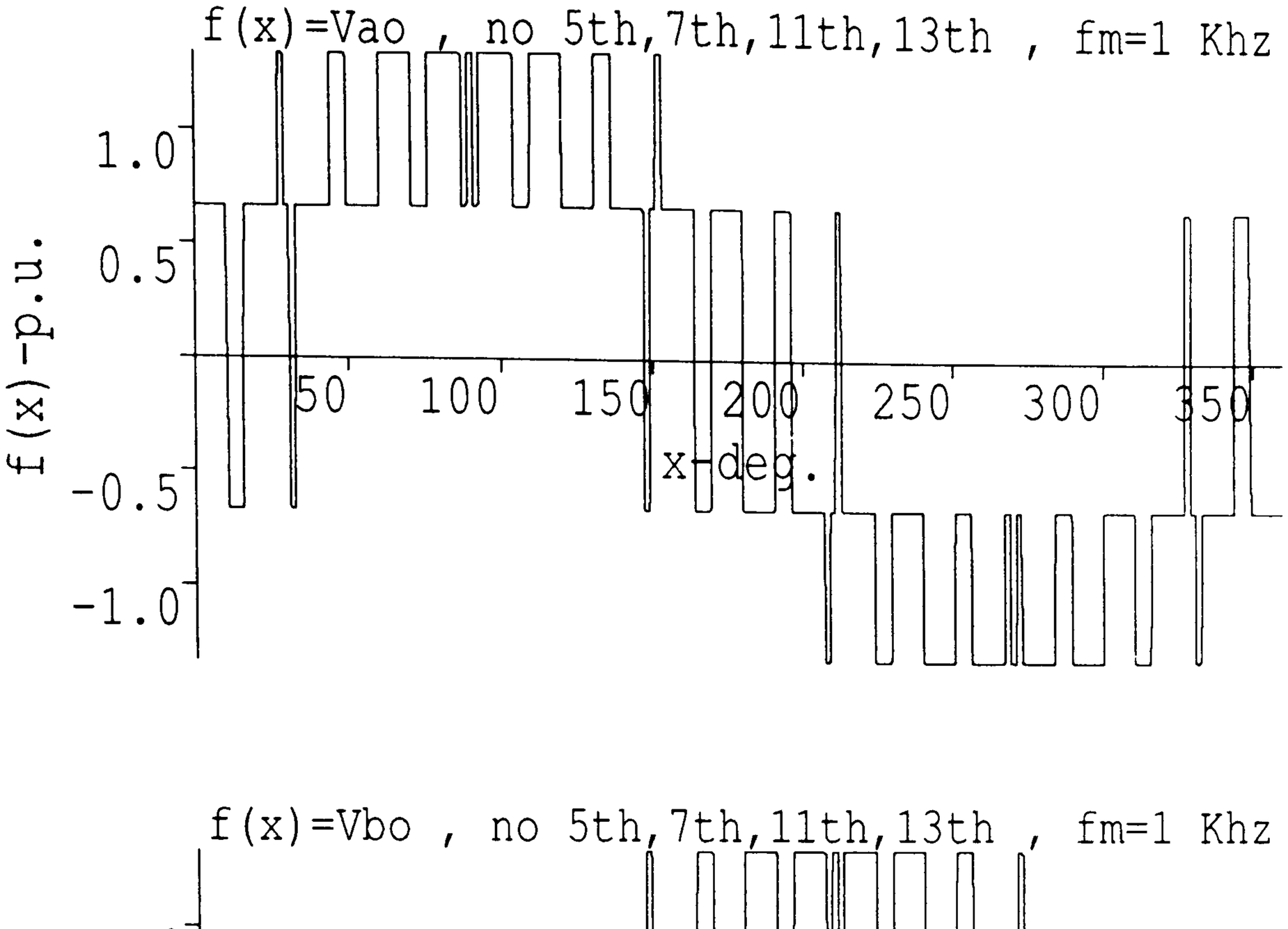
f(x)=Vao , no 5th,7th,11th,13th , fm=1 Khz
1.0
0.5
-0.5
-1.0
f(x)-p.u.
50
100
150
200
250
300
350
x-deg.

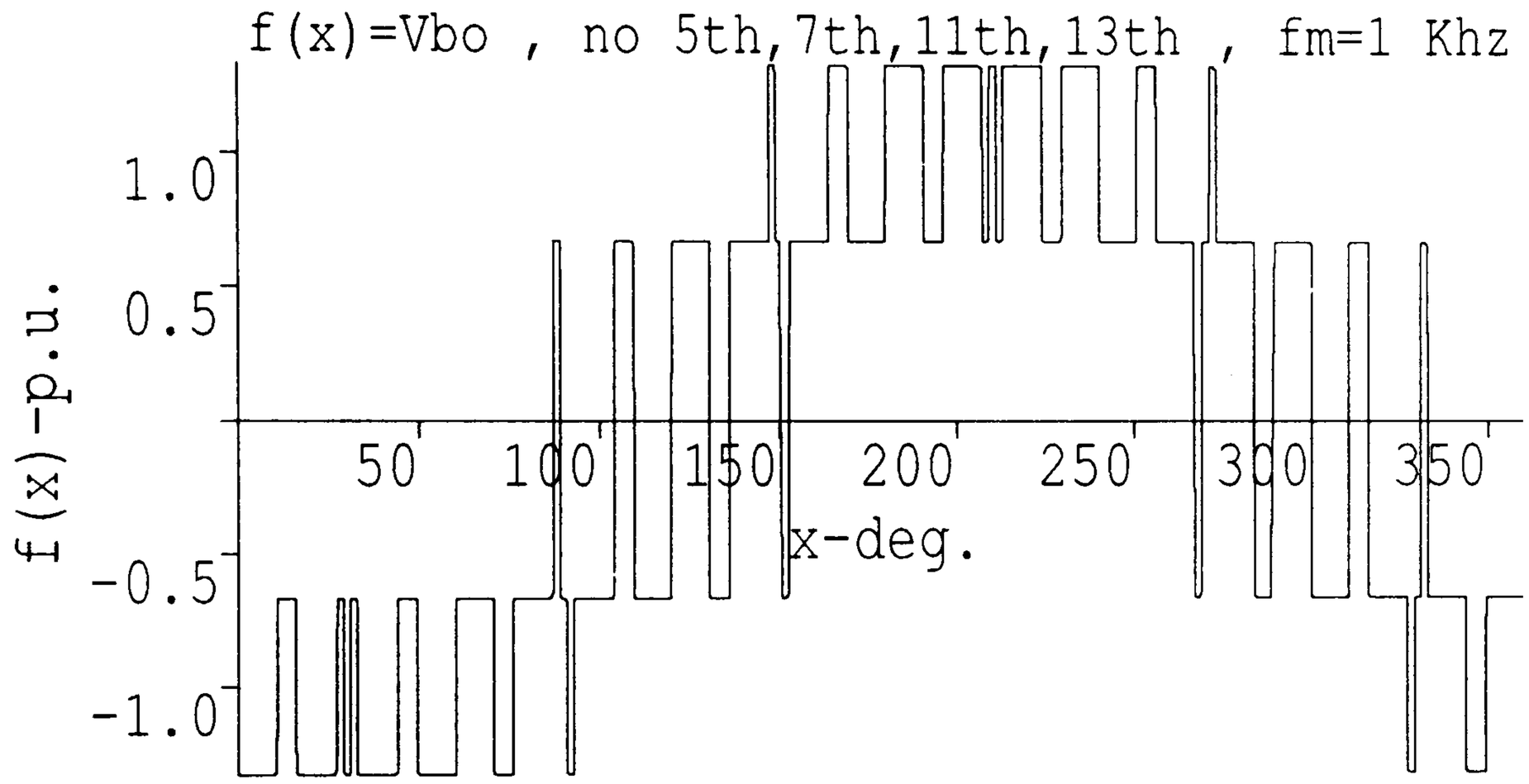
f(x)=Vbo , no 5th,7th,11th,13th , fm=1 Khz
1.0
0.5
-0.5
-1.0
f(x)-p.u.
50
100
150
200
250
300
350
x-deg.

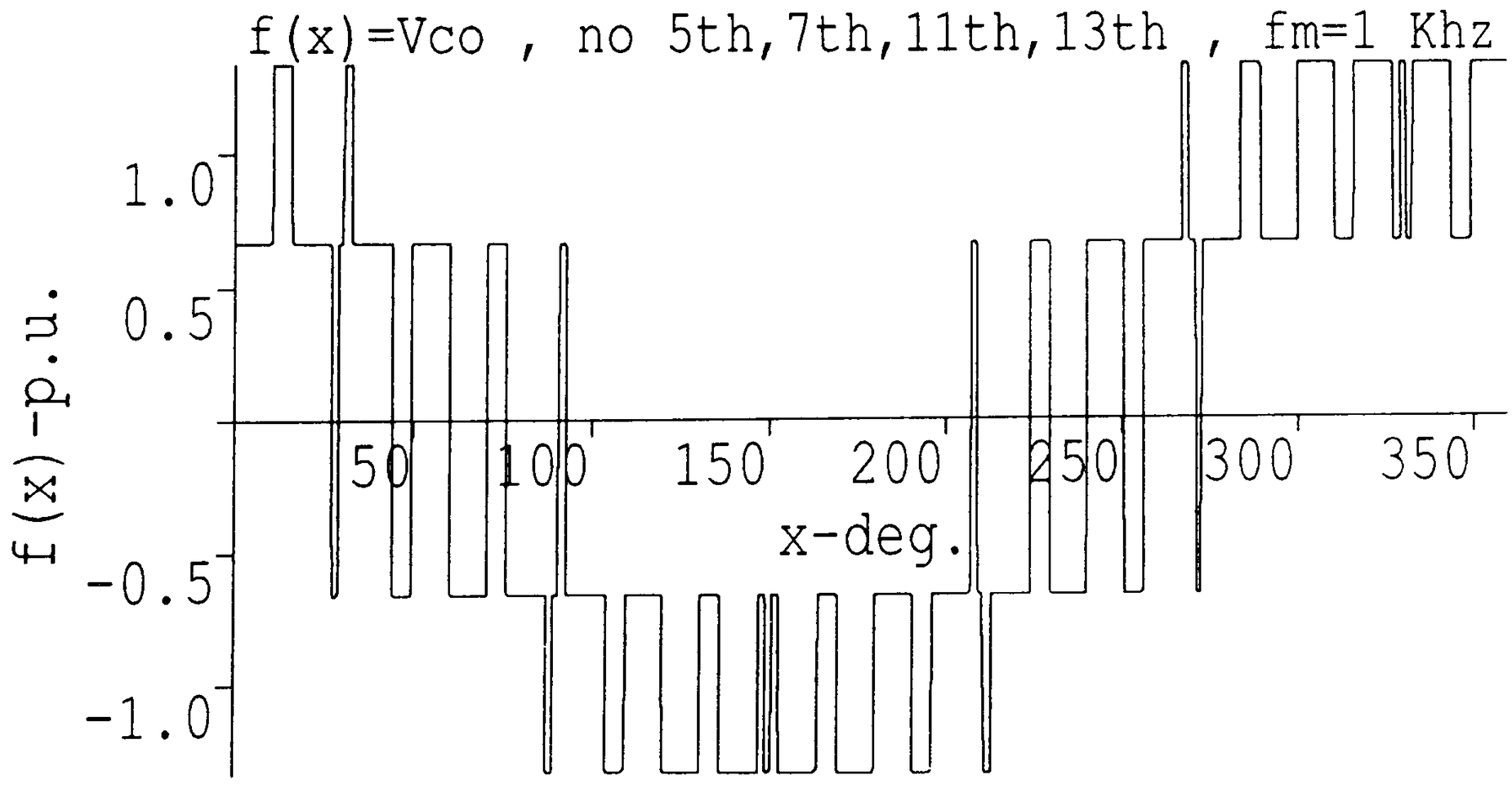
f(x)=Vco , no 5th,7th,11th,13th , fm=1 Khz
1.0
0.5
-0.5
-1.0
f(x)-p.u.
50
100
150
200
250
300
350
x-deg.

Fig. 2-24

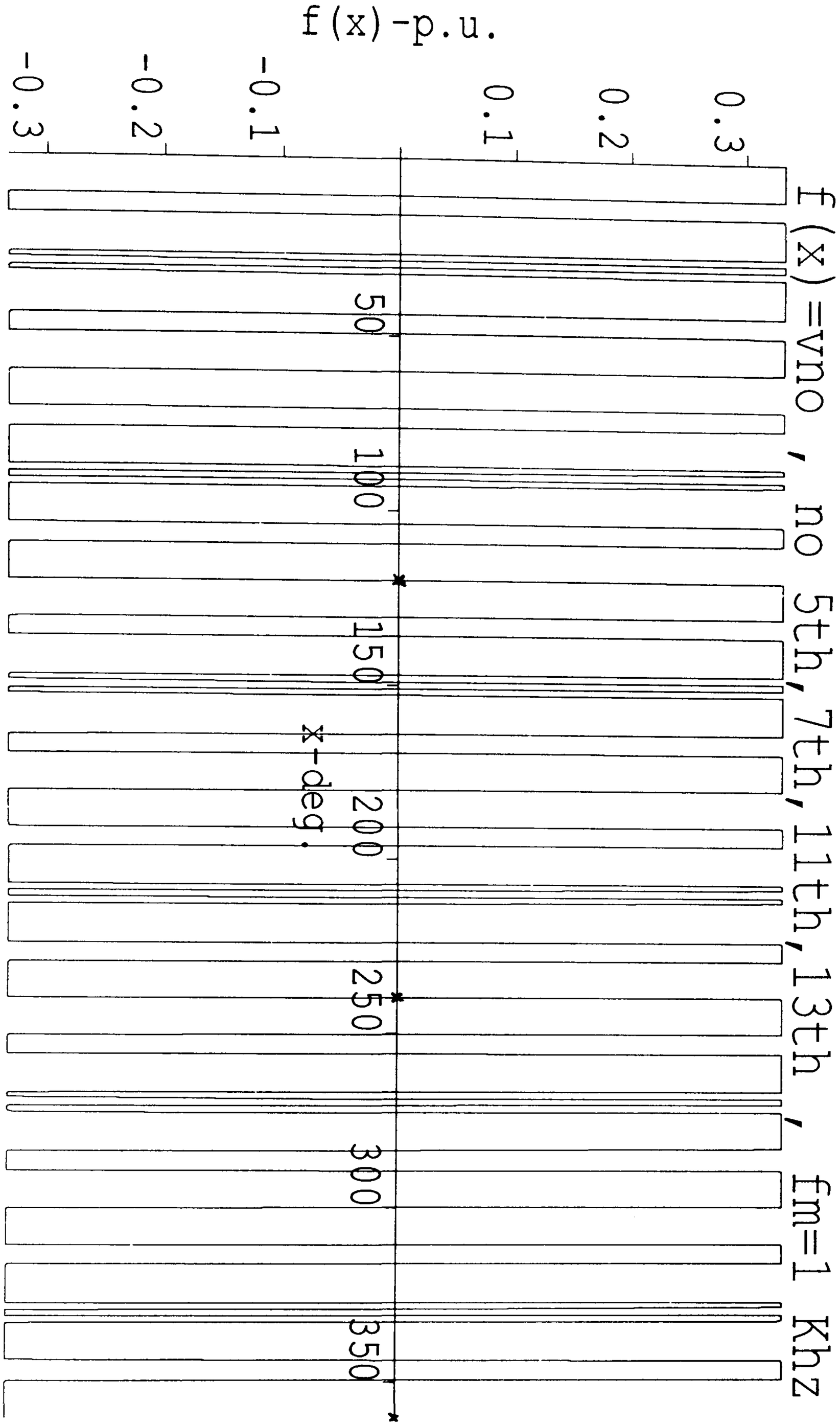

Fig. 2-25 Third harmonic (v_{no}) waveform

2.14 Harmonic spectrum of output voltages (v_{an} & v_{ab})

The harmonic spectrum of v_{an} waveform (analysed by Fourier Series) is shown in Fig. 2-26(a) . The harmonic spectrum of v_{ab}(line voltage) is represented in Fig. 2-26(b) where triplen components are eliminated and amplitudes should be multiplied by $\sqrt{3}$. In Table 2-8 the amplitude of low order and predominant components is presented .

Table 2-8 The v_{an} harmonic component amplitudes

Harmonic Order	Harmonic Amplitude
1	1.170470
3	0.180014
5	0.000040
7	0.000060
9	0.017429
11	0.000080
13	0.000224
15	0.085448
17	0.237163
19	0.349063
21	0.329534
23	0.195669
25	0.055028

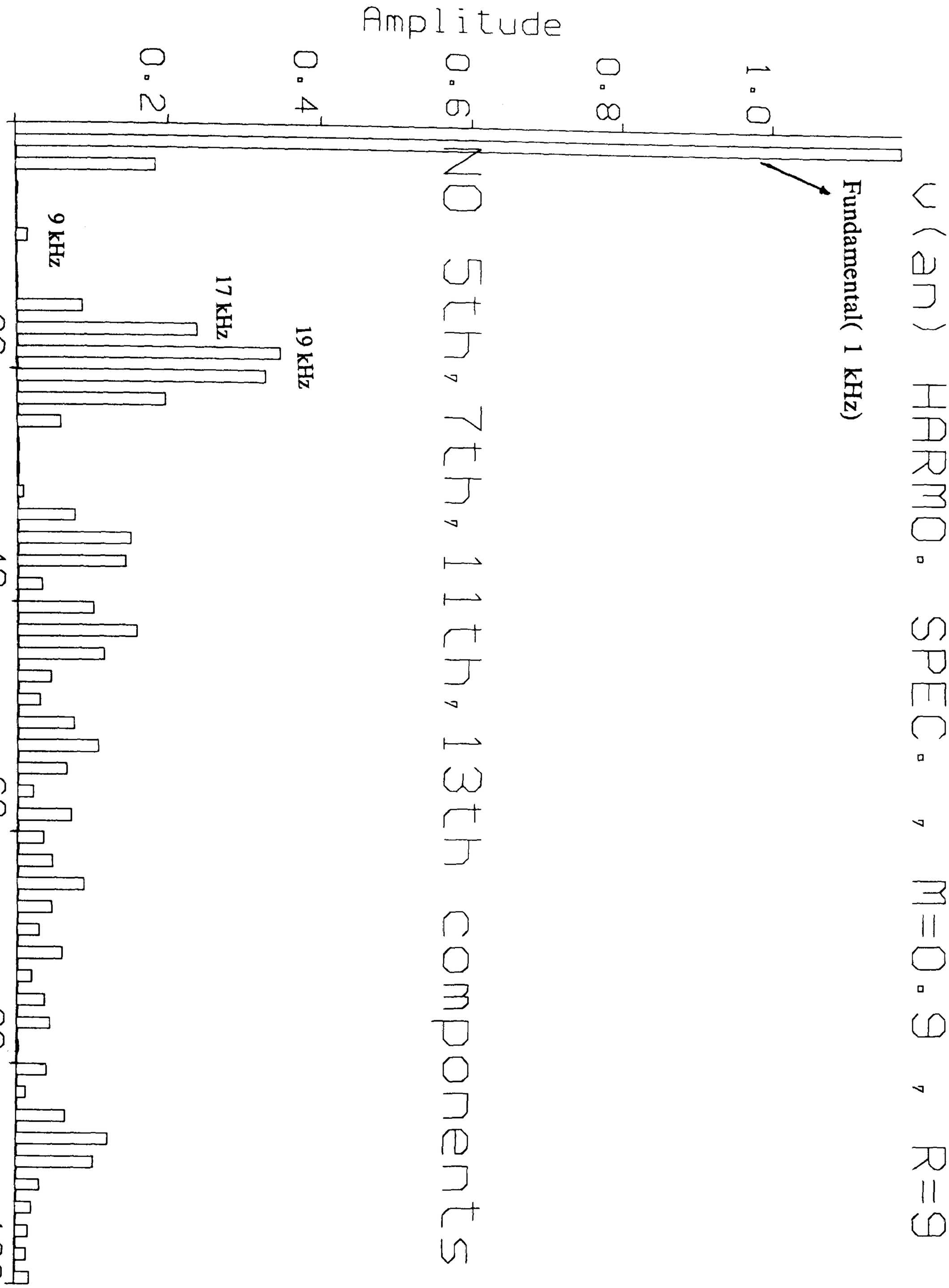

Fig. 2-26(a) inverter phase voltage(v_{an}) harmonic spectrum

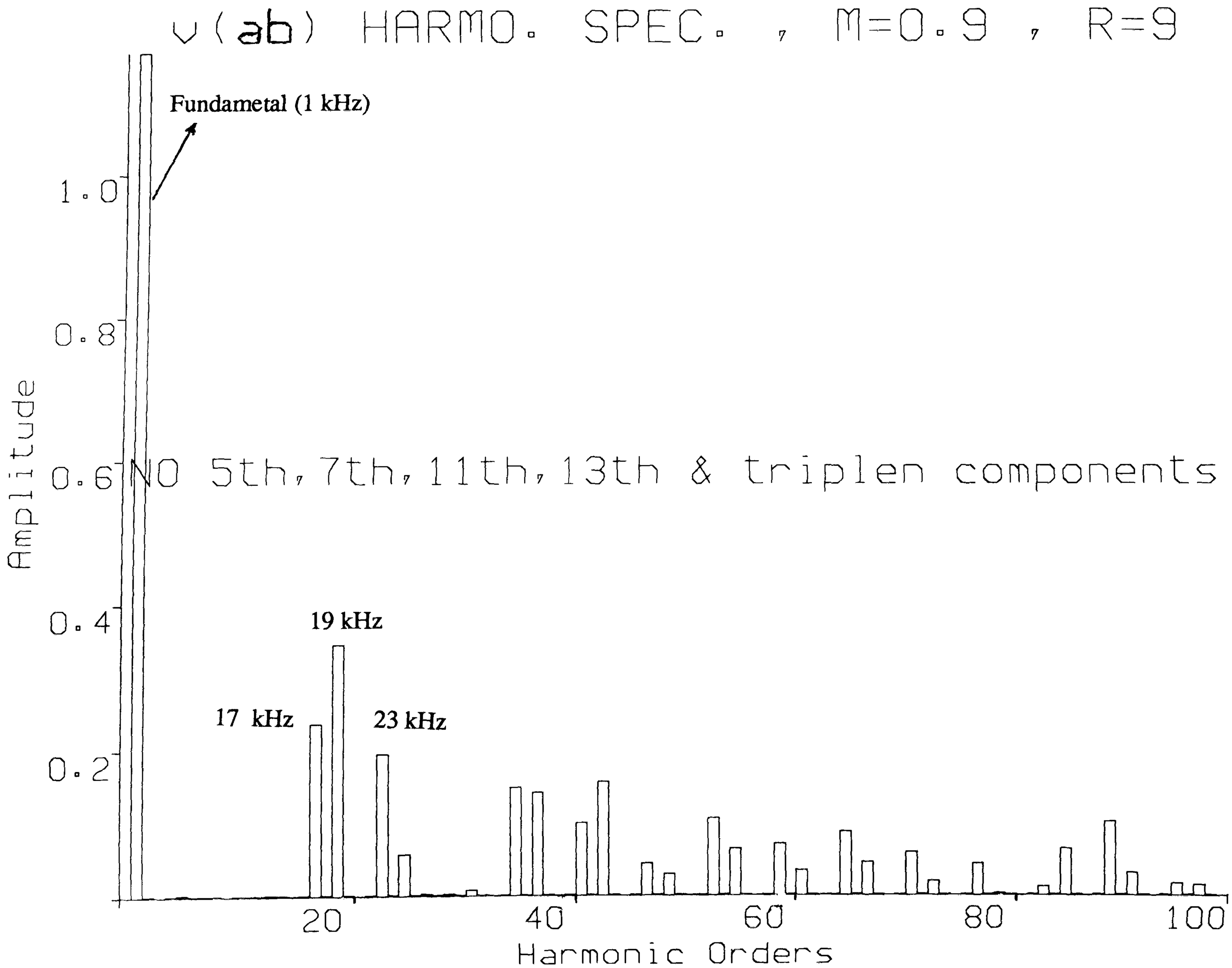

Fig. 2-26(b) inverter line voltage(v_{ab}) harmonic spectrum

2.15 Spectrum comparison before and after harmonic elimination

The comparison between v_{an} harmonic spectrums before and after low order component elimination is presented in Table 2-9 .

Table 2-9 The v_{an} harmonic spectrum comparison before & after eliminatrion

Harmonic Order	Harmonic Amplitude No Elimination	Harmonic Amplitude 5, 7, 11, 13 th Eliminated
1	0.901369	1.170470
3	0.002669	0.180014
5	0.011683	0.000000
7	0.266405	0.000000
9	0.710470	0.017429
11	0.267798	0.000000
13	0.005674	0.000000
15	0.176882	0.085448
17	0.256467	0.237163
19	0.255778	0.349063
21	0.159450	0.329534
23	0.127635	0.195669
25	0.163148	0.055028

In prototype 3-phase half bridge inverter there are no :

1- DC components (because of area symmetry) .

2- Even harmonics (because of half-wave symmetry) .

3- Odd cosine terms (because of quarter-wave symmetry)

4- Triplen components (because of 3-phase symmetry) .

5- 5th , 7th , 11th , 13th components (because of elimination process) .

2.16 Microprocessor implementation of prototype system inverter

By considering of α , β and γ switching angles for modulation of v_{an} (Fig. 2-20) , v_{bn} (Fig. 2-21) and v_{cn} (Fig. 2-22) waveforms , Table 2-10 is made up which illustrates that there are 54 conduction stages (6R & R=9) for creation of one cycle of 3-phase , symmetric and 1 k Hz AC waveforms from DC source . The prototype system inverter is shown in Fig. 2-27 for convenience .

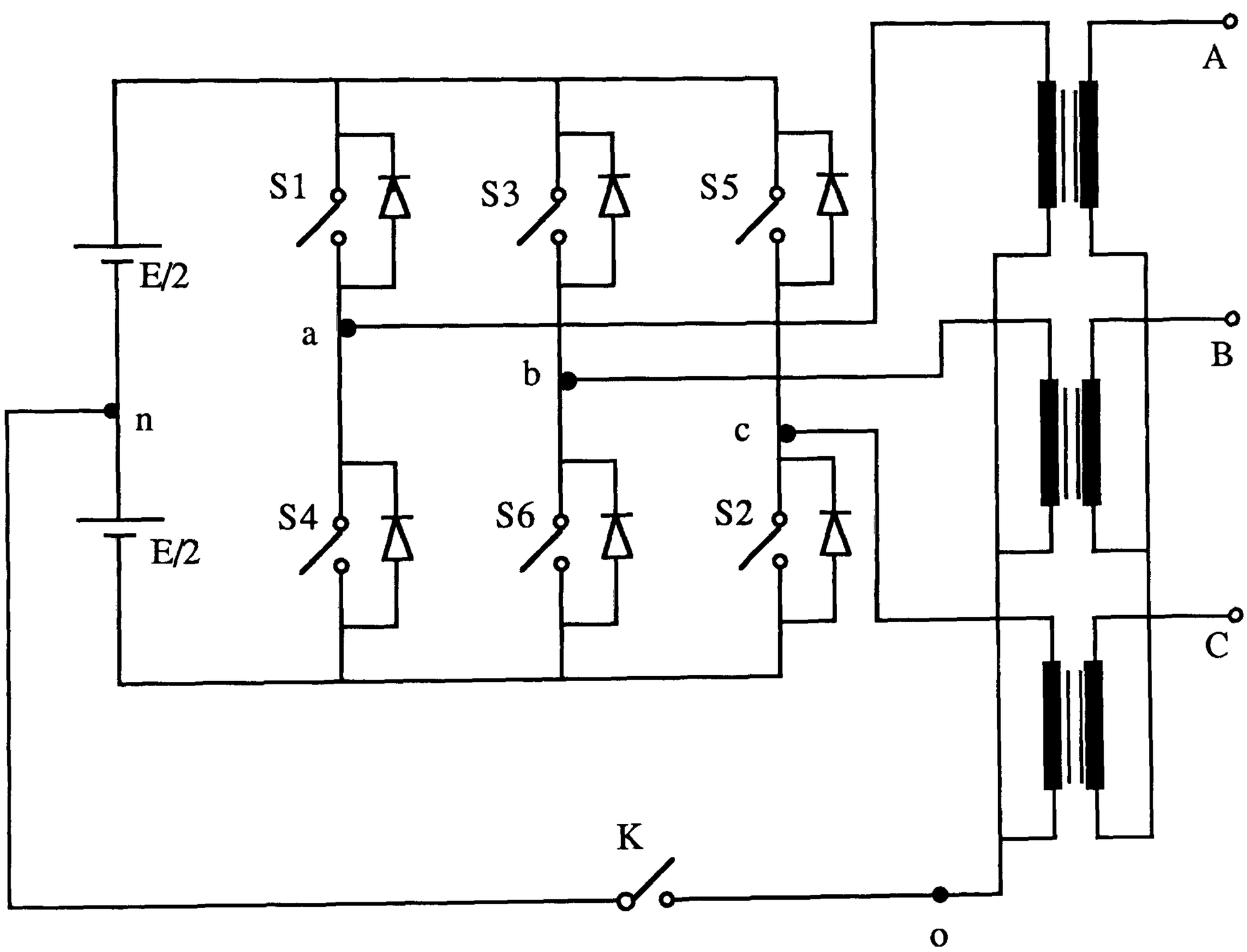

Fig. 2-27 3-phase half bridge inverter with isolating & stepping transformer

Table 2-10 one cycle switching sequences for 3-phase 1 Khz half bridge inverter

Stage	S1	S2	S3	S4	S5	S6	Conduction Duration (degrees)	Step ↓	Conduction Duration (μse)
1	1	0	0	0	1	1	α1–α0=10.5482	α1	29.30000
2	0	0	0	1	1	1	α2–α1=5.54620	α2	15.40555
3	1	0	0	0	1	1	γ1–α2=11.0407	γ1	30.66944
4	1	1	0	0	0	1	γ2–γ1=1.959600	γ2	5.444444
5	1	0	0	0	1	1	α3–γ2=1.810600	α3	5.027777
6	0	0	0	1	1	1	α4–α3=1.959600	α4	5.444444
7	1	0	0	0	1	1	γ3–α4=11.04070	γ3	30.66944
8	1	1	0	0	0	1	γ4–γ3=5.546200	γ4	15.40555
9	1	0	0	0	1	1	γ5–γ4=10.54820	γ5	29.30000
10	1	1	0	0	0	1	γ6–γ5=10.54820	γ6	29.30000
11	1	0	0	0	1	1	γ7–γ6=5.546200	γ7	15.40555
12	1	1	0	0	0	1	β1–γ7=11.04070	β1	30.66944
13	1	1	1	0	0	0	β2–β1=1.95900	β2	5.444444
14	1	1	0	0	0	1	γ8–β2=1.81060	γ8	5.027777
15	1	0	0	0	1	1	γ9–γ8=1.95960	γ9	5.444444
16	1	1	0	0	0	1	β3–γ9=11.0411	β3	30.66944
17	1	1	1	0	0	0	β4–β3=5.54600	β4	15.40555
18	1	1	0	0	0	1	β5–β4=10.5480	β5	29.30000
19	1	1	1	0	0	0	β6–β5=10.5480	β6	29.30000
20	1	1	0	0	0	1	β7–β6=5.54600	β7	15.40555
21	1	1	1	0	0	0	α5–β7=11.0410	α5	30.66944
22	0	1	1	1	0	0	α6–α5=1.96000	α6	5.444444
23	1	1	1	0	0	0	β8–α6=1.81000	β8	5.027777
24	1	1	0	0	0	1	β9–β8=1.96000	β9	5.444444
25	1	1	1	0	0	0	α7–β9=11.0410	α7	30.66944
26	0	1	1	1	0	0	α8–α7=5.54600	α8	15.40555
27	1	1	1	0	0	0	α9–α8=10.5480	α9	29.30000
28	0	1	1	1	0	0	α10–α9=10.548	α10	29.30000
29	1	1	1	0	0	0	α11–α10=5.546	α11	15.40555
30	0	1	1	1	0	0	γ10–α11=11.041	γ10	30.66944

Table 2-10 (continue)

Stage	S1	S2	S3	S4	S5	S6	Conduction Duration (degree)	Step ↓	Conduction Duration (μse)
31	0	0	1	1	1	0	γ11–γ10=1.96	γ11	5.444444
32	0	1	1	1	0	0	α12–γ11=1.81	α12	5.027777
33	1	1	1	0	0	0	α13–α12=1.96	α13	5.444444
34	0	1	1	1	0	0	γ12–α13=11.04	γ12	30.66944
35	0	0	1	1	1	0	γ13–γ12=5.546	γ13	15.40555
36	0	1	1	1	0	0	γ14–γ13=10.54	γ14	29.30000
37	0	0	1	1	1	0	γ15–γ14=10.54	γ15	29.30000
38	0	1	1	1	0	0	γ16–γ15=5.546	γ16	15.40555
39	0	0	1	1	1	0	β10–γ16=11.04	β10	30.66944
40	0	0	0	1	1	1	β11–β10=1.96	β11	5.444444
41	0	0	1	1	1	0	γ17–β11=1.81	γ17	5.027777
42	0	1	1	1	0	0	γ18–γ17=1.96	γ18	5.444444
43	0	0	1	1	1	0	β12–γ18=11.04	β12	30.66944
44	0	0	0	1	1	1	β13–β12=5.546	β13	15.40555
45	0	0	1	1	1	0	β14–β13=10.54	β14	29.30000
46	0	0	0	1	1	1	β15–β14=10.54	β15	29.30000
47	0	0	1	1	1	0	β16–β15=5.546	β16	15.40555
48	0	0	0	1	1	1	α14–β16=11.04	α14	30.66944
49	1	0	0	0	1	1	α15–α14=1.96	α15	5.444444
50	0	0	0	1	1	1	β17–α15=1.81	β17	5.027777
51	0	0	1	1	1	0	β18–β17=1.96	β18	5.444444
52	0	0	0	1	1	1	α16–β18=11.04	α16	30.66944
53	1	0	0	0	1	1	α17–α16=5.546	α17	15.40555
54	0	0	0	1	1	1	α18–α17=10.54	α18	29.30000

The different practical waveforms about the prototype system inverter will be presented in chapter 5 .

2.17 Resonant inverters

There is increasing demand for smaller and lighter power processing equipment for DC-to-DC or DC-to-AC conversion . The natural approach is to raise the converter's operating frequency . PWM inverters fail to accommodate such a requirement owing to high frequency harmonic components associated with the square wave current or voltage wave forms . Moreover the power dissipation in the switching device of PWM inverters increases significantly at high frequency because of the their forced commutation operation .

As a result , resonant power conversion employing a high frequency link emerges as a leading technique and resonant inverters being superior to conventional PWM iverters due to possessing several attractive features such as :

1- light wight .

2- fast response .

3- high reliability .

4- naturally sinusoidal voltage and current wave forms .

5- reduced EMI (electromagnetic interference) .

6- simple circuit implementation .

Features 1 , 2 result from link operation at high frequency levels . While features 3 , 4 , 5 , 6 are common to all circuits in which the commutation of the current in the MOSFETs occurs naturally in the course of circuit operation .

The resonant inverters are based on resonant current oscillation on a L-C-R circuit with **under damped** [$R < 2(L/C)^{1/2}$] mode of operation [20] , [21] & [22] , which is exited from a fixed DC supply through a half bridge or full bridge inverter , Fig. 2-28 .

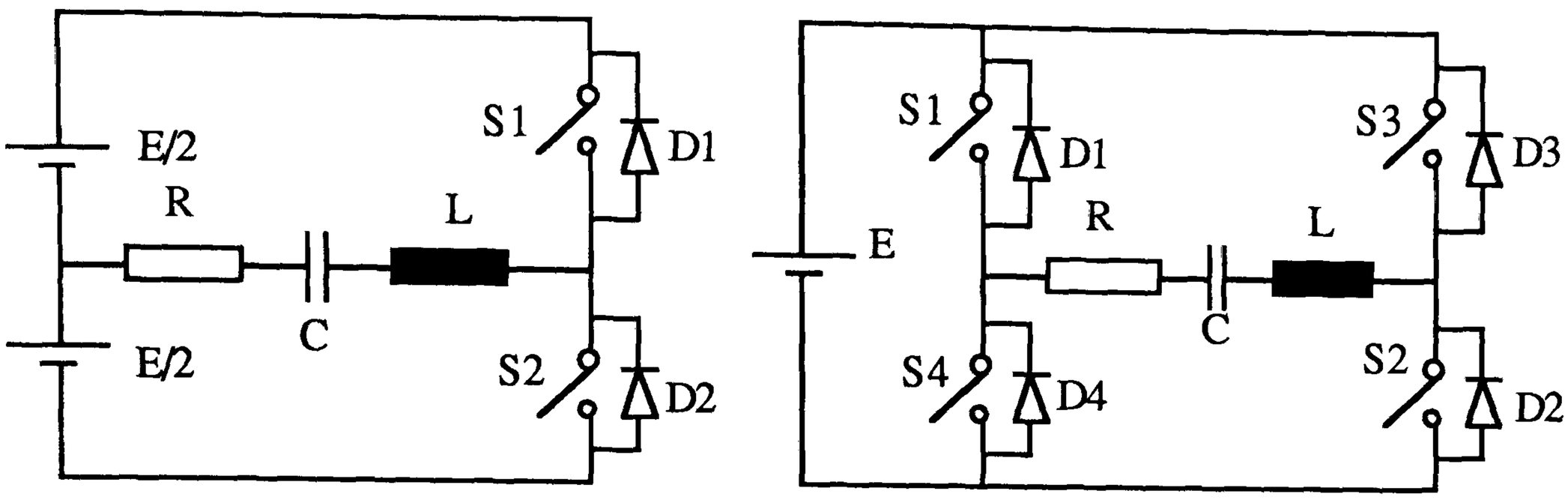

(a) (b)

Fig. 2-28 Series resonant inverter (a)- half bridge (b)- full bridge

This type of inverter produces an approximately sinusoidal wave form at high output frequency , up to several hundred k Hz and is commonly used in relatively fixed output load application , for example ; induction heating , ultrasonic generator , fluorescent lighting .

2.18 Series resonant & Parallel resonant inverters

In general , resonant converters are classified in to two types , depending on the manner by which energy is extracted from the resonant tank . These two types are :

1- The series resonant converters(SRCs)

2- The parallel resonant converters(PRCs)

In the SRCs , Fig. 2-29 (a) , the load (output converter) is connected to the h. f. link circuit in series with link capacitor in which power transfer from the source to the load is accomplished through series resonance . The steady-state and the dynamic properties of SRCs have been analysed in many literature [23] , [24] & [25] .

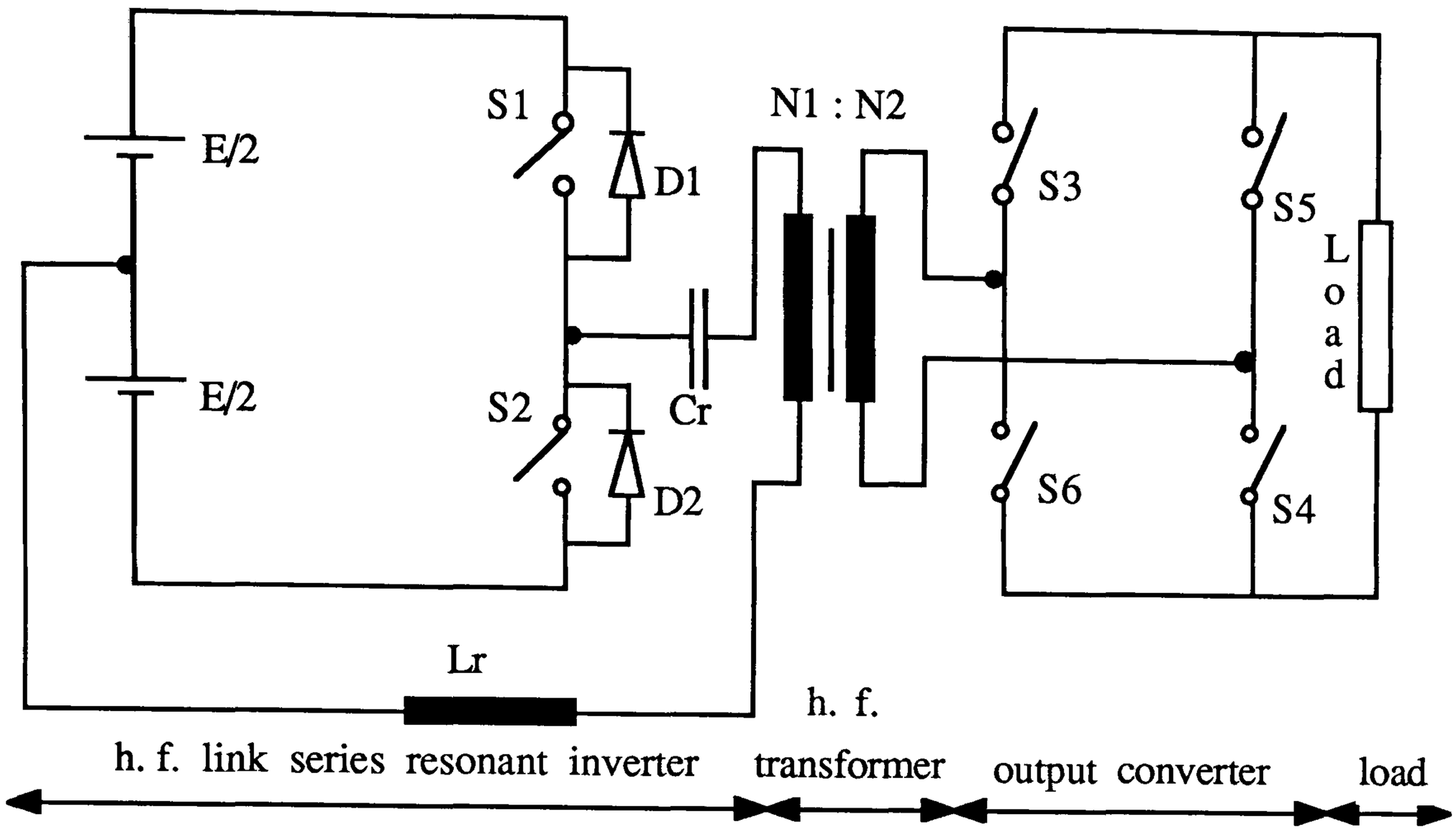

(a)

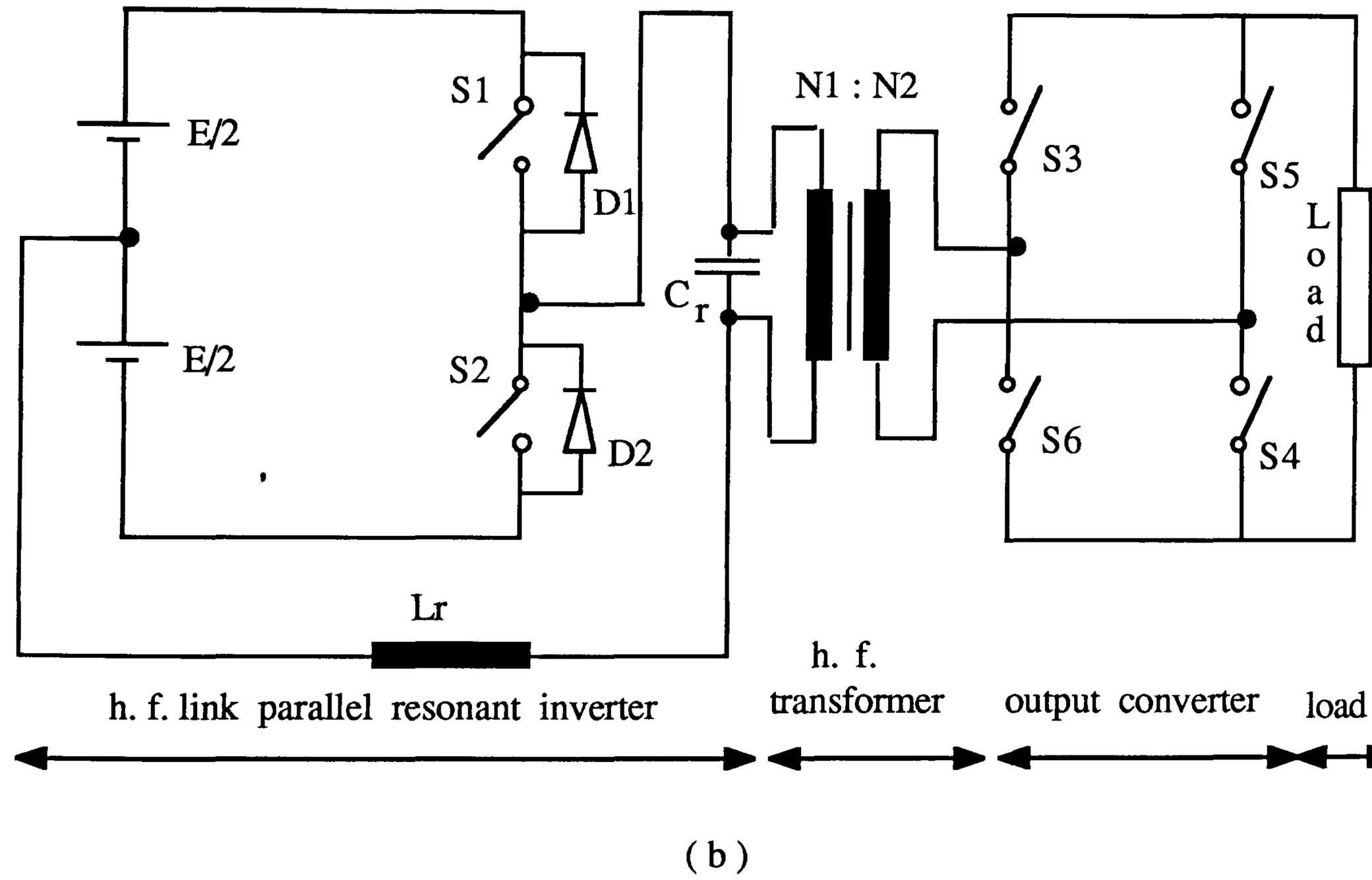

(b)

Fig. 2-29 (a) Series resonant inverter (b) Parallel resonant inverter

In the PRCs , Fig. 2-29(b) , the load (output converter) is connected to the h.f. link in parallel with the link capacitor in which the capacitor voltage is used to transfer energy from the source to the load. The steady-state analysis and performance of PRCs have been reported by [26] , [27] & [28] .

In both cases the h. f. feature of the link capacitor allows the use of a h. f. transformer to provide voltage transformation and isolation between the DC source and the load .

In Fig. 2-29 , the load on the inverter is the h. f. transformer and output converter consisting of the four bidirectional switches S3 , ... & S6 which can be turned ON and OFF as desired . In a DC-to-DC conversion scheme the output converter will be a rectifier(controlled or uncontrolled) where as for DC-to-AC conversion process , it will be a cycloconverter and firing angles is modulated .

In DC-to-AC conversion , the link inverter can encounter regenerative loads(power flow from the load to the link and thus from the link to the DC supply. But this condition can not be analysed by conventional methods .

The parallel resonant inverters can be operate either below resonance ($f_o < f_r$, leading power factor mode) or above resonance ($f_o > f_r$, lagging power factor mode) . Operation and analysis of PRC operating below resonance are presented in [27] , [29] . The operation , analysis and performance of operating above resonance are reported in [30] , [31] .

2.19 References :

1- N. Eguchi and T. Imura *" self commuted inverter for fuel cell power plant "* IEEE , IAS Annual meeting Conference Record , 1986 , pp.527-532 .

2- T. M. Jahns *" Improved reliability in solid state AC drives by means of multiple independent phase drive units "* IEEE Trans. Ind. Appl. , Vol. IA-16 , pp.321-331 , May/June 1980 .

3- K. N. pavithran , R. parimelalagan and M. R. Krishnamurthy *" Studies on inverter fed five phase induction motor drive "* IEEE Trans. on power Electronics , Vol. 3 , No. 2 , April 1988 , pp. 224-235 .

4- S. B. dewan and A. Straughen *" Power semicunductot circuits "* John Wiley & sons , 1975 .

5- S. R. Bowes and R. R. Clements*" Computer aided design of PWM inverter system "* IEE Proc. , Vol. 129 , Pt. B , No. 1 , Jan. 1982 , pp. 1-16 .

6- S. R. Bowes and M. J. Mount *" Microprocessor control of PWM inverters "* IEE Proc. , Vol. 128 , Pt. B , No. 6 , Nov. 1981 , pp. 293-305 .

7- M. H. Rashid *" Power Electronics-circuits , devices and application "* 1988 , prentice - Hall International Editions .

8- K. Thorborg *" Power Electronics "* 1988 , prentice Hall .

9- K. Thorborg *" Stair case PWM , an uncomplicated and efficient modulation technique for AC motor drivers "* IEEE , 17 th power electronics specialist conference , 1986 .

10- B. M. Bird & K. G. king *" An introduction to power Electronics "* 1985 , John Wiley & sons .

11- J. Zubek , A. Abondanti and C. J. Nordby *" Pulse width modulated inverter motor drives with improved modulation "* IEEE Trans. 1975 ,IA-11 , pp. 695-703 .

12- E. Y. Y. Ho and P. C. Sen *" Digital Simulation of PWM induction motor drivers for transient and steady state performance "* IEEE Trans. on Ind. Electronics , Vol. IE-33 , No. 1 , Feb 1986 , pp. 66-77 .

13- H. S. Patel and R. G. Hoft *" Generalized techniques of harmonic elimination and voltage control in thyristor inverters "* Part 1 , Harmonic elimination" IEEE , Vol. IA - 9 , No. 3 , May/June 1973 , pp. 310 - 317 .

14- J. E. Alexander and J. M. Bailey *" Systems Engineering Mathematics "* Englewood , N J : Prentice Hall , pp. 288 - 293 , 1962 .

15- G. S. Buja and G. B. Indri *" Optimal pulse width modulation for feeding AC motors "* IEEE , Vol. IA - 13 , pp. 38-44 , Jan. / Feb. 1977 .

16- R. W. Hamming *" Numerical Methods for Scientists and Engineers "* New York , Mcgraw - Hill , 1962 .

17- T. Kato *" Precise PWM wave form analysis of inverter for selected harmonic elimination "* IEEE IAS , Conf. Record , 1986 , pp. 611 - 616 .

18- A. Zuckerberger and A. Alexandrovitz *" Determination of commutation sequence with a view to eliminating harmonics in microprocessor controlled PWM voltage inverter "* IEEE , Industrial Electronics , Vol. IE - 33 , No. 3 , August 1986 , pp. 262 - 270 .

19- P. Enjeti , J. F. Lindsay , P. D. Ziogas and M. H. Rashid *" New current control scheme for PWM inverters "* IEE proc. , Vol. 135 , pt. B , No. 4 , July 1988 , pp. 172 - 179 .

20- R. G. Hoft *" Semiconductor Power Electronics "* 1986 , Van Nostrand Reinhold Company Inc. .

21- L. P. Huelsman *" Basic circuit theory with digital computer "* 1972 , Prentice Hall .

22- D. E. Johnson , J. R. Johnson and J. L. Hilburn *" Electric circuit analysis "* 1989 , Prentice Hall Inc. .

23- F. C. Schwarz *" An improved Method of resonant current pulse modulation for power converters "* IEEE Power Electronic Specialist Conference Record , 1975 , pp. 194 - 204 .

24- V. Vorperian and S. C'uk *" A complete DC analysis of the series resonant converters "* IEEE Power Electronic Specialist Conference Record 1982 , pp. 85 - 100 .

25- R. Oruganti and F. C. Lee *" resonant power processors : part 1-state plan analysis , pp. 860 - 867 , part 2 - method of control pp.868- 878 "* IEEE IAS - 1984 Annual meeting Conference Record .

26- V. T. Ranganathan , P. D. Ziogas , V. R. Stefanovic *" Performance characteristic of high frequency link under forward and regenerative power flow conditions "* IEEE IAS Annual meeting 1983 , pp. 831 - 839 .

27- N. Mapham*" An SCR inverter with good regulation and sine wave out put "* IEEE Trans. on Industry and general application , Vol. IGA - 3 , March/April 1967 , pp.176 - 187 .

28- V. T. Ranganathan , P. D. Ziogas and V. R. Stefanovic *" A regulated DC-to-DC voltage source converter using a high frequency link "* IEEE Trans. Ind. Appl. , Vol. IA - 18 , No. 3 , pp. 279-289 , May 1982 .

29- Y. G. Kang and A. K. Upadhyay *" Analysis and design of a half bridge parallel resonant convertr "* IEEE PESC Record , 1987 , pp. 23 -243 .

30- A. K. S. Bhat and M. M. Swamy *" Analysis and design of high frequency parallel resonant converter operating above resonance "* IEEE Applied power Electronic Confe. Record , 1988 , pp. 182 - 189 .

31- R. L. Steigewald*" High frequency resonant transistor DC-to-DC converters "* IEEE Trans. on Industrial Electronics , Vol. IE - 31 , No. 2 , May 1984 , pp.181 - 191 .

Chapter 3

The transformer in high frequency & switched mode operation

3.1 General

The conversion process in power Electronics (DC-to-DC , DC-to-AC , AC-to-DC , and AC-to-AC) requires the use of Transformers and Inductors . With the advent of Integrated Magnetics [1] and the increased use of Transformer leakage inductances as the resonant inductors in resonant circuits [2 & 3] , a crucial role in modern Power Electronics circuits is taken by these components .

An ideal transformer :

1- would pass all signal frequencies with no power loss .
2- provide any selected transformation ratio of voltage or current .
3- provide complete isolation between its input and its output .
4- process power in either direction with equal facility .
5- provide for additional inputs or outputs if are required .

Obviously , such a perfect transformation device does not exist physically .

Since the dramatic miniaturization of integrated logic circuits and power semi-conductor devices ; MOSFET , GTO & SIT (static induction transistor) , SITH (static induction thyristor) has not yet been matched by similar reduction in the size of transformers , so frequently they are the heaviest and bulkiest item in the conversion circuits . The use of high frequency switching on inverter-transformer circuitry , allows the design to reduce the size and weight of the transformer significantly .

The design of high frequency magnetic components is complicated as several considerations and constraints come in to effect , that are less important at low frequencies . Skin and proximity effects dominate copper losses , domain wall resonance phenomena raise hysteresis losses in the core magnetic materials . Parasitic inductance become as a proportion of total circuit inductance , and winding capacitance becomes considerable .

Transformers also have a significant effect upon the overall performance and efficiency of the power conversion system . Accordingly , the design of such transformers has an important influence on overall system weight , conversion efficiency and cost . Because of the interdependence and interaction of parameters , reasonable trade-offs are necessary to achieve design optimization , particularly if high frequency operation for conversion is wanted .

3.2 The design problems generally

The design process is faced with a set of constraints which must be observed in the design of any transformer , which are outlined as follows :

1- Efficiency in link with copper and core losses

2- Size and weight in connection with operating frequency

3- Maximum permissible temperature rise in link with core material

4- Cost effectiveness

Depending upon application , certain of these constraints will be dominant . It is not possible to optimize all parameters in a single design because of the interaction and interdependence of parameters . For example , if volume and weight are of great significance , reduction in both can be effected by operating the transformer at high frequency but at a penalty in efficiency and regulation . When the frequency can not be raised , reduction in weight and volume may still be possible by selecting a more efficient core material , but at a penalty of increased cost . Again necessary trade-offs should be made to achieve desirable design .

A detailed design procedure for different type of transformers may be found in [4 , 5 & 6]. Here those factors and topics which are in some way associated with the transformer design and operation at high frequency and switching circuitries (inverters and cycloconverters) are principally reviewed .

3.3 The core

In square-wave application (chopping by inverter) the core is rapidly switched from full magnetization in one direction to full magnetization in the opposite direction . Characteristic of such application is the large class of inverters and converters in which the power transformer is not operated in a saturated mode but is driven nearly to saturation by a transistor (MOSFET) or the thyristor (GTO) switching circuit having an independent drive-signal source .

Generally , the core material for the Inverter-transformer is selected for maximum flux density and maximum squareness . Fig. 3.1

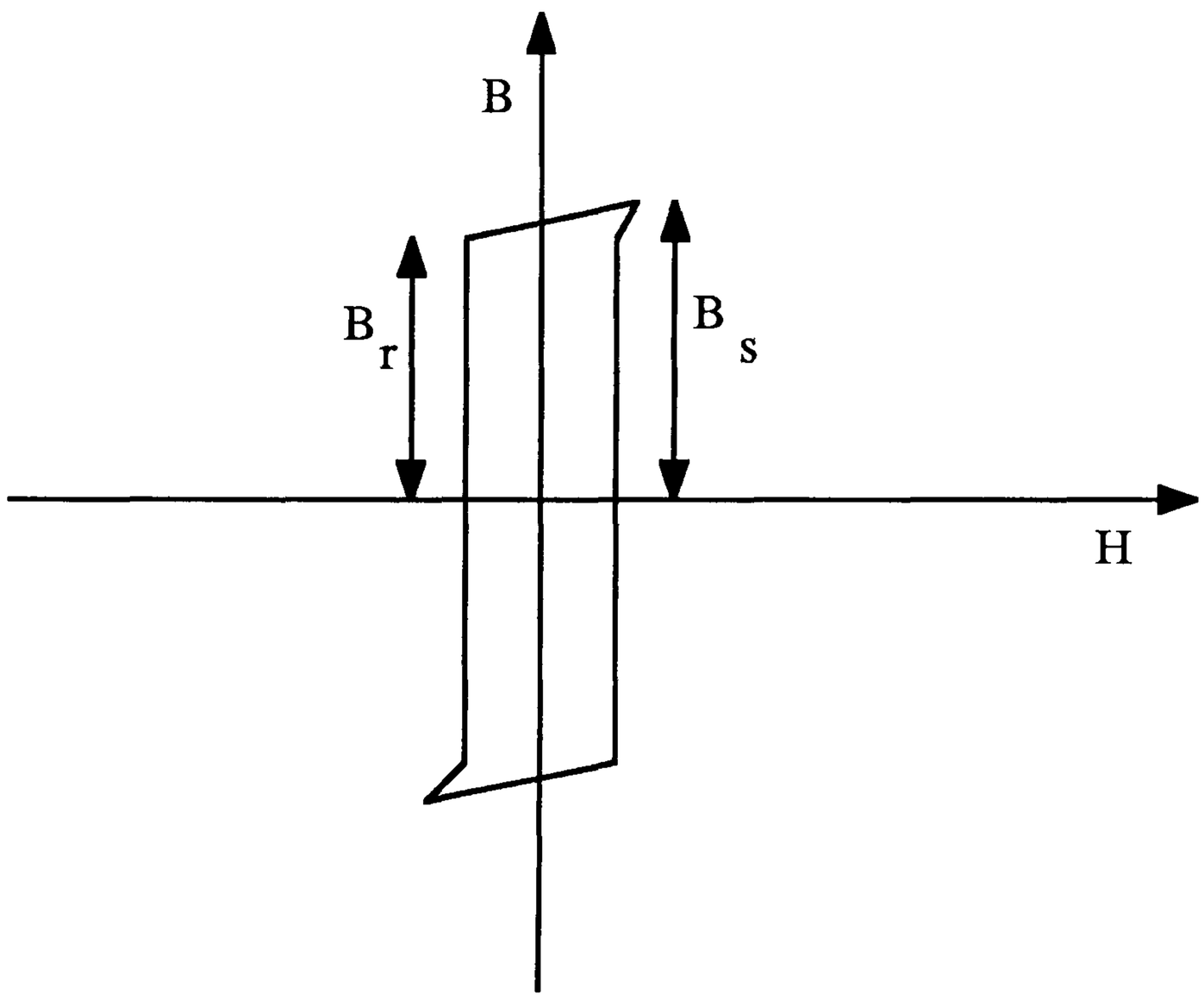

Fig. 3-1 square hysteresis loop

Cores with higher flux capabilities enable smaller transformers to be built . Maximum squareness is the more important characteristic , however , this must be tempered by the operating frequency , allowable temperature rise , maximum power output , as well as cost considerations .

A lack of a good B-H squareness results in spikes being generated on the out-put of the square wave which is potentially dangerous for the turned-off switch . Theoretically , when the core is saturated there is no flux change , however , in practice due to imperfect saturation when the squareness ratio (Br/Bs) is less than one , there is an unwanted flux change ($d\Phi/dt$). This flux change , in addition to other causes (stray inductance and capacitance) , generate a spike which , even though of short duration , causes heating of the semiconductor switch junctions , so the ideal inverter transformer should have a high squareness ratio to minimize the spike effect . Finally it should be added that square loop material has the steepest slope and thus the highest primary inductance .

3.4 Core materials and development

The first development from iron wire cores was around 1900 when non -oriented silicon-alloyed steel sheets were introduced for transformer use [7] . This new material was made by alloying 3% silicon to offer electrical steel with improved loss qualities and omnidirectional properties .

The next significant development was that in the late 1930s GOSS (Grain Oriented Silicon Steel) was invented . This was produced by adjusting the chemistry of previous steels , cold rolling the strip to the required thickness , followed by high temperature annealing at 1200 C° to induce secondary recrystallisation . This process produced large grains that were well oriented along the rolling direction of the steel sheet .

Then Hi-B steel was introduced , differing from GOSS in that improved grain orientation resulted in an improvement in magnetizing characteristics and a decrease in hysteresis loss . The loss in Hi-B steel sheets consists of hysteresis

loss which varies linearly with frequency :

$$p_h = k.B_{max}^{1.7}.f \quad \frac{watt}{m^3} \quad , \quad k= cons. \qquad (3\text{-}1)$$

and eddy current loss :

$$p_e = \frac{\pi^2.B_{max}^2.f^2.t^2}{6.\rho} \quad \frac{watt}{m^3} \qquad (3\text{-}2)$$

Where ρ is the resistivity and t is sheet thickness .

The total loss has traditionally consisted of hysteresis and eddy current loss . But , using improved measuring techniques it has been shown that the sum of hysteresis and classical eddy loss does not equate with the total loss in the steel . The term anomalous loss is used to describe the discrepancy . The anomalous loss is thought to be caused by domain wall movement and has been shown to be proportional to the distance between domain walls , hence any reduction in this distance will result in loss reduction[7] .

This fact is the basis of the second major development that of laser scribed , or surface scribed steels [7] . The laser surface treatment can reduce Hi-B type steel losses by a further 8% - 10% .

3.4.1 High frequency core material

For high frequency purposes , the four materials generally available for use in high frequency transformers are .

1- powdered iron .

2- powdered amorphous (not having crystalline structure) metal .

3- Manganese-Zinc Ferrite (Mn + Zn + Fe2 O4) .

4- Nikel-Zinc Ferrite (Ni + Zn + Fe2O4) .

The Ferromagnetic material like iron family generally have high electrical conductivity and must be laminated even at 50 Hz to prevent excessive eddy current loss . Since :

$$\delta = 0.5642\sqrt{\frac{\rho}{\mu.f}} \qquad (3\text{–}3)$$

Where :

δ is skin depth , ρ is resistivity , $\mu = \mu_0\mu_r$ is permeability (assumed constant) of the material and f is the frequency of the alternating field . To avoid high losses due to eddy currents , the iron would have to be laminated thinner than the skin depth . Lamination of much less than 2μm are quite impractical [8] .So , the amorphous metals which are prepared in the glassy state to lower their conductivity are employed . This process typically lowers the conductivity by a factor 3 at best , so the potential increase in skin depth is limited to a factor of 1.732 .

Ferrites are ferromagnetic iron oxides , prepared commercially as ceramics and distinguished by their high electrical resistivity compared to metals . (Mn + Zn) Ferrite typically displays a $\mu = 200\,\mu_0$ but a much lower conductivity $10^{-5}(\Omega.m)^{-1}$. So (Ni + Zn) Ferrite is an appropriate choice for transformers operating at MHz ranges for extremely low conductivity and its ignorable eddy current loss . A transformer computer design aid has been presented in ref. [9] on the basis of the total power loss minimization at f > 100 kHz .

3.5 Effect of high frequency on dielectric losses

Generally most of power losses constitutes Iron loss and Copper loss in commercial (50 , 60 Hz) transformers . By elevating operation frequency , some stray loss occurs which is not accounted for by Iron loss or Copper loss . The mechanism of generating such stray loss is not clear so far . The experimental

results have been demonstrated that the stray loss in high voltage / high frequency transformer [60 v / 1000 v , 30 kHz] is originated from the dielectric loss in the insulating materials of transformer as follow [10]

$$P_d = 2\pi . f . \varepsilon . E^2 .tang(\delta) \qquad (3\text{-}4)$$

Where :

P_d is dielectric loss per unit volume

f is frequency

ε is dielectric constant

$tang(\delta)$ is dielectric dissipation factor

E is electric field

The dielectric loss according to [10] arises from various portions of insulation :

1- between high voltage and low voltage windings

2- between high voltage winding and core

3- between insulating layer of high voltage winding

Moreover in some materials $tang(\delta)$ changes with temperature . The thermal stability of transformer in operation depends on the balance between the heat generation and heat dissipation to avoid pushing transformer operation toward the curie point . Curie temperature is the temperature at which a material changes it's ferromagnetic properties and become paramagnetic . For example Ferrites have a curie temperature about 200C° , which limits their operation core temperature to about 100C° [11] .

3.6 Effect of high frequency on size and output rating

Mathematical analysis indicate that the higher the power frequency , the smaller the size and weight of the transformer , motor or alternator . For

example a convectively cooled 4 kHz transformer has weight 28% less than its 400 Hz counter part [5] .

The basic relationship among the volt-amper rating (p_o) , volume (vol) , magnetic flux density (B) , operating frequency (f) , permissible temperature (θ , where $\theta = T_o - T_a$, T_o is the operating temperature of the winding hottest point and Ta is ambient temperature) is as follow [5] :

$$p_o = k\ (\text{vol})^{\frac{3}{4}}.\ f\ .\ B\ .\ (h.\theta)^{\frac{1}{2}} \qquad (3\text{-}5)$$

or

$$\text{vol} = k_1 \left(\frac{p_o}{f.B}\right)^{\frac{3}{4}} . \frac{1}{(h.\theta)^{\frac{3}{8}}} \qquad (3\text{-}6)$$

Where k , k_1 constants and h is coefficient of heat transfer .

From (3-5) , (3-6) , it is easy to say that the size and rating of a transformer are more responsive to a change in frequency and magnetic flux density than to a change in the temperature rise .

An increase in frequency more effectively reduces size(vol) .To evaluate the extent to which size may be reduced by increasing the frequency , we must first consider the relation among flux density , frequency , and core losses .

When the frequency of the input to a transformer is increased the flux density decreases , because B varies inversely with f :

$$E = 4.44\ f\ .\Phi_m\ N \qquad \text{or} \qquad E = 4.44\ f.B_m A.N \qquad (3\text{-}7)$$

In (3-7) if B_m be kept constant , any increasing of f , reduces A (core cross section) or N (number of turns) which in turn , cause more reduction in size and weight .

From (3-6) it can be inferred that by having fixed p_o , B , $h\theta$ if frequency increases m times , the vol. of transformer decreases with following multiple :

$$\frac{1}{(m)^{3/4}} = \frac{1}{m^{0.75}}$$

As has been stated in [12] for a fixed transformer configuration , and for a constant loss power , the volume is determined by the expression :

Vol. $= \left[\frac{1}{B_{max} f}\right]^{\frac{6}{7}}$, where B_{max} is the maximum flux density and f is the operating frequency .

For a wide range considering the dependency of total transformer weight from increased frequency may be referred to [13] . For a prototype rating pr for 60 Hz transformer with a 40° rise any increasing in f or / and θ will result increase p_r , which follows the formula [5] :

$$p_o = p_r \left(\frac{f}{60}\right)^{0.76} \cdot \left(\frac{\theta}{40}\right)^{0.63} \qquad (3\text{-}8)$$

3.7 Effect of high frequency on permeability (μ_r)

At high frequencies , eddy currents in the laminations may be great enough that the magnetic flux density will fall from a value B_o at the surface of core sheet to some lower value in the interior . The effect depends on the

properties of the material , the frequency of the alternating field and the dimensions of the sheet .

It is possible the magnetic flux density falls very rapidly in the interior of the sheet , so that most of the flux is confined to a thin layer or skin near the surface . This phenomenon is called eddy-current shielding or magnetic skin effect and is analogous to the more familiar Copper skin effect .

The variation of flux density with distance is given by [14] .

$$B = B_o (e)^{\frac{-x}{\delta}} \qquad (3\text{-}9)$$

Where , x is the distance in to the material from the surface . The δ is given by

$$\delta = \sqrt{\frac{2\rho}{\mu_o . \mu_r . \omega}} \qquad (3\text{–}10)$$

Where , ρ is the resistivity of the material , ω is the angular frequency of the alternating field . At a depth $x = \delta$ the $B = B_o e^{-1} = 0.3678 (B_o)$. So δ is known as the depth of penetration or magnetic skin depth .

The reduction in permeability from μ_r to μ'_r because of reduced flux penetration is described by [5] .

$$\frac{\mu_r}{\mu'_r} = \frac{1}{y}\left[\frac{\text{Sinh}(y) + \text{Sin}(y)}{\text{Cosh}(y) + \text{Cos}(y)}\right] \qquad (3\text{-}11)$$

Where $y = a / \delta$ and a is lamination sheet thickness (meters) , δ is from (3-10). Harmonic currents or voltages in transformer , result from the non linear relationship between flux and magnetizing current which is exemplified in the shape of the hysteresis loop , Fig. 3-2 , and the shape of the hysteresis curve depend on the properties of the core material .

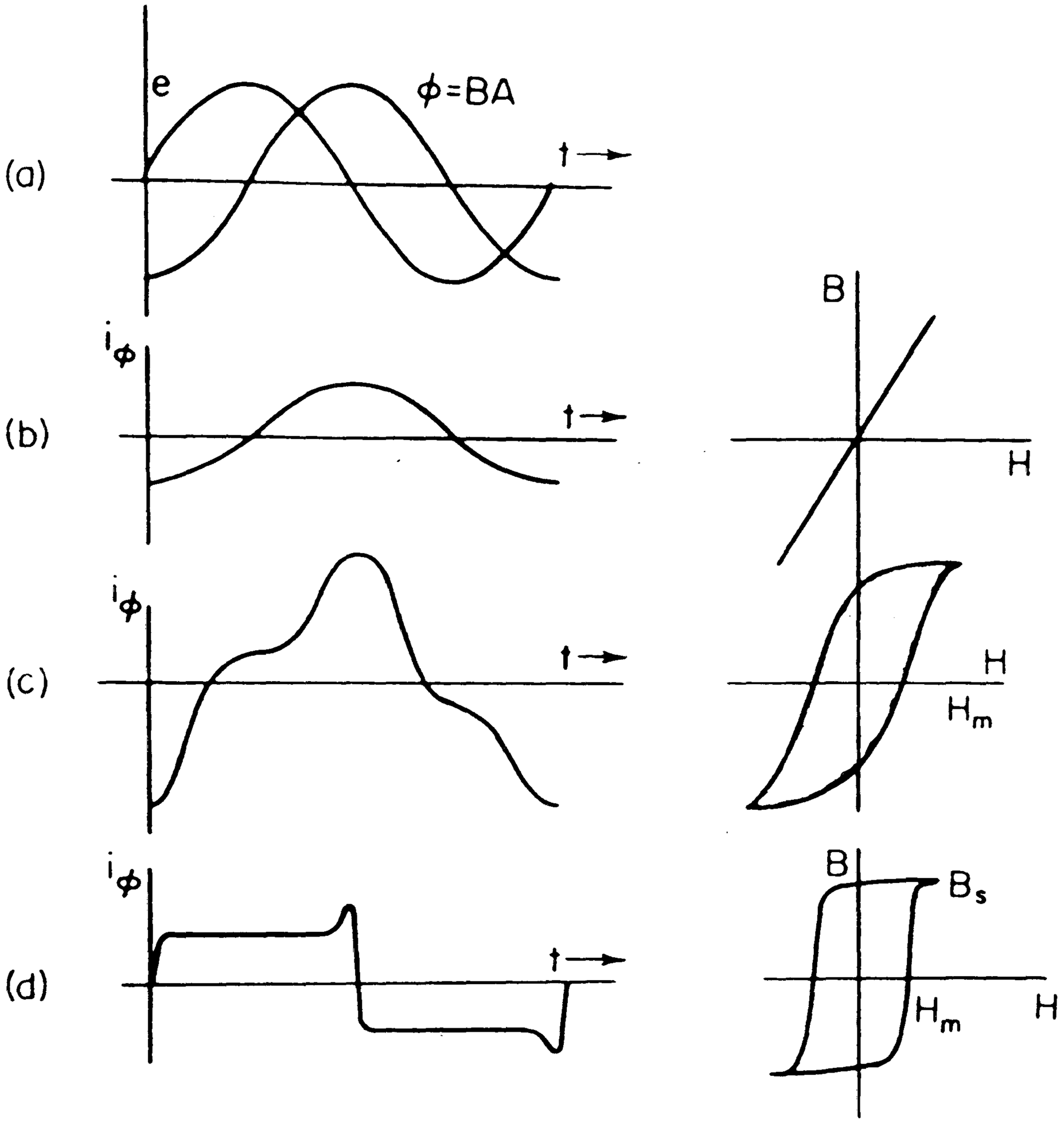

Fig. 3-2 dependency of magnetizing current (accordingly , voltage & current harmonics) in the transformer from the hysteresis loop :

(a) Sine flux and Cosine induced voltage

(b) Sine current with linear B-H curve

(c) Peak current with round B-H loop

(d) Square-wave current with square B-H loop

From equation (3-11) dependency of μ_r on frequency variation is realized , and since $\mu = \mu_o . \mu_r = \frac{dB}{dH}$, therefore any reformation of voltage or current harmonics due to variation on operation frequency are expected . Fig.3 - 3 shows the hysteresis loop / frequency variation for a typical transformer [4] .

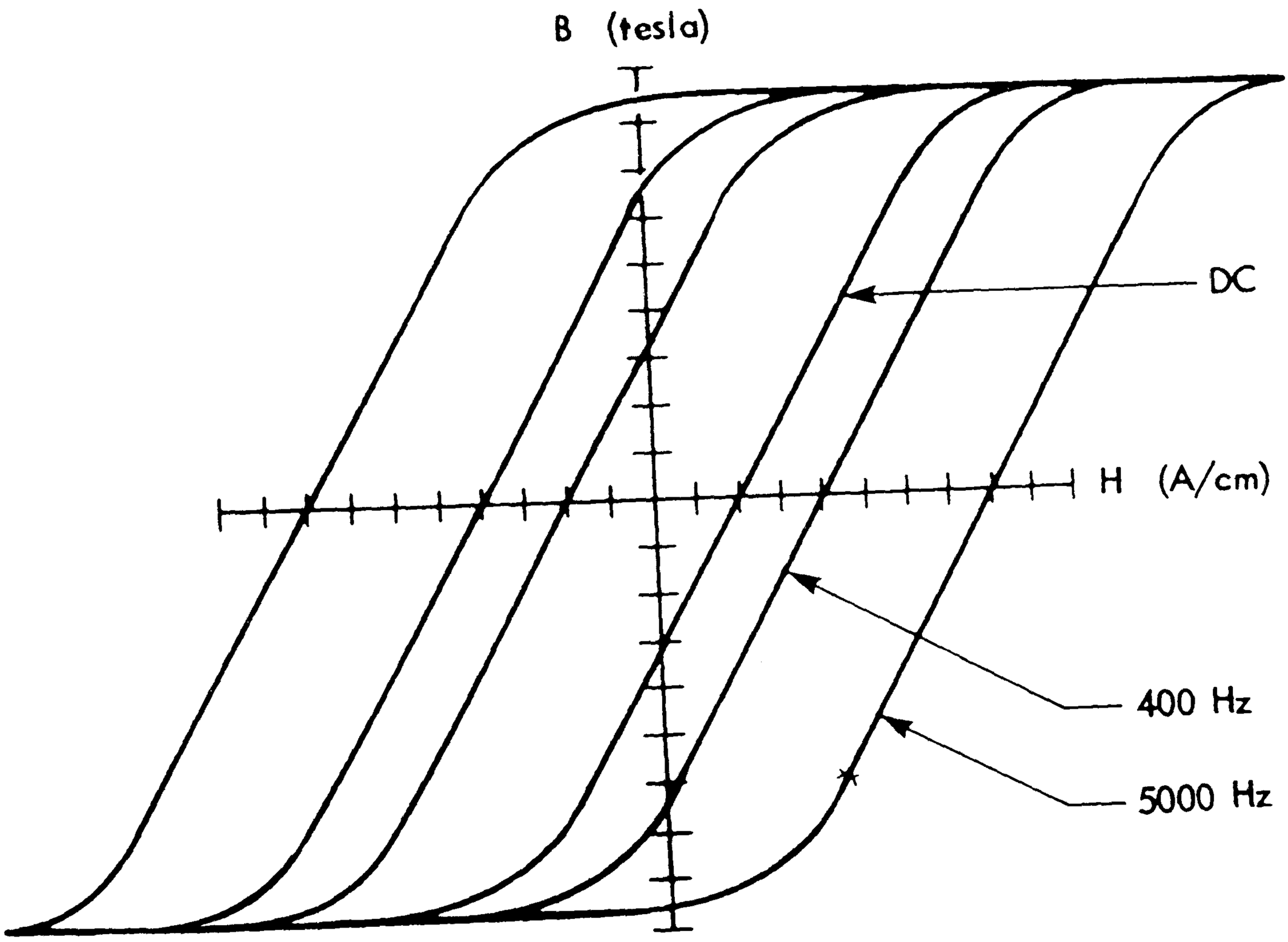

Fig. 3-3 variation of hysteresis loop with operating frequency

There is a critical frequency f_c at which y=2 and penetration is half the thickness of the sheet [5] .

$$f_c = 101.5\frac{\rho}{\mu r \,.\, a^2} \qquad (3-12)$$

Where ρ is in microhm-centimeters and a is in centimeters . For example for 4% Silicon , 50% Nickel and 80% Nickel sheet , with 14 mils thick is 12000 , 1300 , and 200 Hz respectively . It should be noted that these are audio frequencies , much lower than the radio frequencies associated with copper skin effect .

3.8 Effect of high frequency on magnetizing current

The equivalent circuit of a transformer with parameters as lumped constants is shown in Fig. 3-4 .

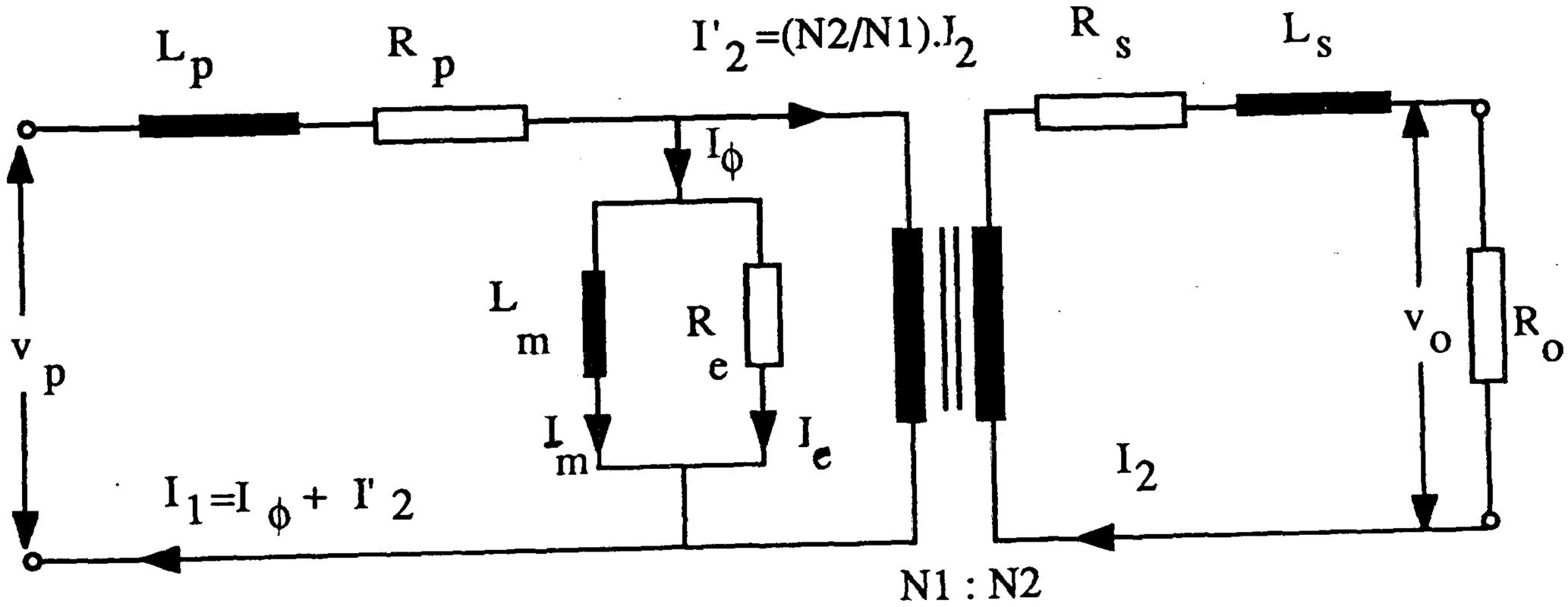

Fig. 3-4 transformer equivalent circuit

where :

L_m : the primary magnetizing inductance

L_p : the leakage inductance of primary

L_s : the leakage inductance of secondary

N_1 , N_2 are primary and secondary number of turns

R_e : the equivalent core loss shunt resistance

R_o : the load resistance

R_p : the equivalent D.C. primary resistance

R_s : the equivalent D.C. secondary resistance

V_p and V_o are the input and out-put voltages

Referring to Fig. 3-4 :

$$I_m = \frac{1}{L_m}\int_0^{T_{on}} v_p.dt \qquad (3\text{-}13)$$

$$L_m = KN_1^2 \quad , \quad K = \text{core constant} \qquad (3\text{-}14)$$

T_{on} = on time of Inverter switch , inversely proportional to frequency

I_m = primary magnetizing current .

From Fig. 3.5 , maximum magnetizing current is limited by the maximum useable flux density . The flux density also depends on the number of turns and core parameters :

$$B = \frac{\mu_o \mu_r N_1 I_m}{l_e} \qquad (3-15)$$

where , l_e is the equivalent magnetic path length

By substituting (3 - 13) , (3 - 14) in to (3 - 15)

$$B = \frac{\mu_o.\mu_r}{k.l_e.N_1}\int_o^{T_{on}} v_p.dt \qquad (3\text{-}16)$$

putting N_1 from (3-15) in to (3-14) yields :

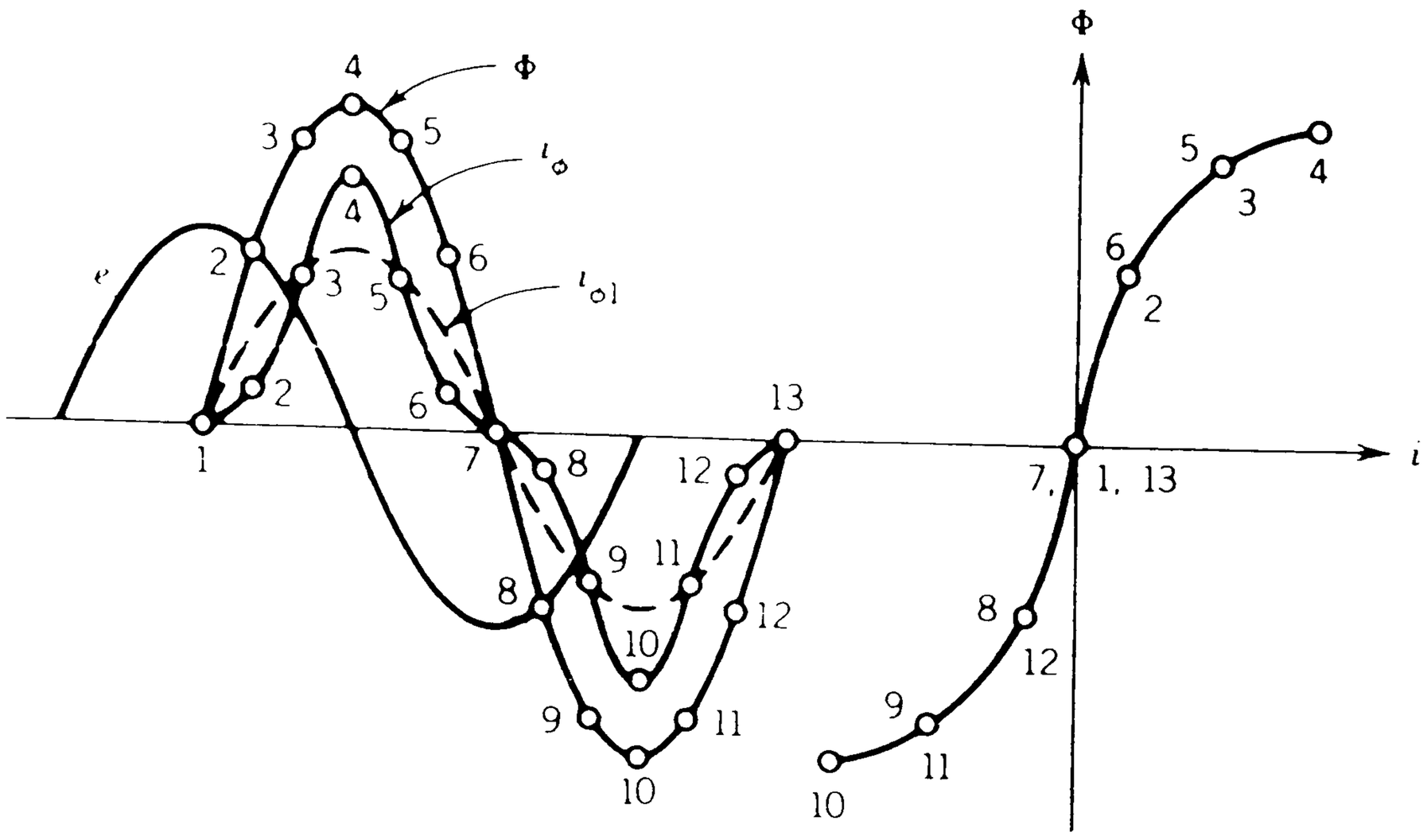

(a)

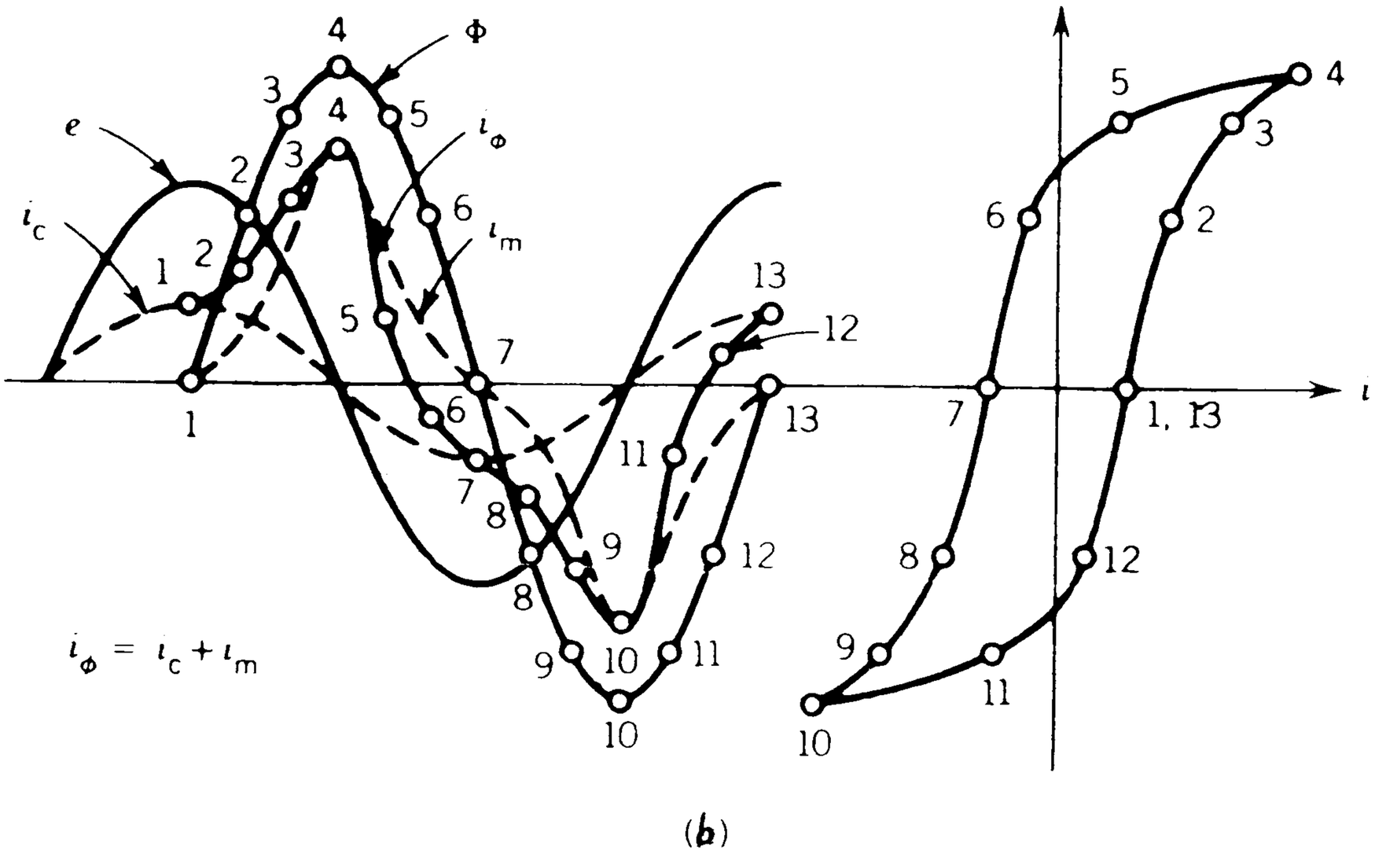

(b)

Fig. 3-5 magnetizing current waveform construction

(a) without hysteresis (b) with hysteresis

$$L_m = k\left[\frac{l_e.B}{\mu_o.\mu_r.I_m}\right]^2 \qquad (3\text{-}17)$$

by equating Lm from (3-17) and (3-13) we have :

$$\frac{1}{I_m}\int_0^{T_{on}} v_p.dt = k\left[\frac{l_e.B}{\mu_o.\mu_r.I_m}\right]^2$$

or :

$$I_m = \frac{k\left[\frac{l_e.B}{\mu_o.\mu_r}\right]^2}{\int_0^{T_{on}} v_p.dt} \qquad (3\text{-}18)$$

In (3-18) by increasing f (decreasing Ton) , I_m will be increased provided that all transformers parameters be kept constant . So very clearly , the magnetizing current I_m will generally increase with frequency if the high - frequency core material is fully utilized up to B_{max} . This is confirmed through Fig. 3-5

3.9 Transformer saturation on high-frequency switched mode power conversion

In practical magnetic component design , one of most important principles is that the magnetic flux is proportional to the volt-seconds applied to the winding :

$$v = N\frac{d\Phi}{dt} \quad , \quad d\Phi = \frac{1}{N}.v.dt \quad , \quad \Phi(t_1) - \Phi(t_o) = \frac{1}{N}\int_{t_o}^{t_1} v.dt \qquad (3\text{-}19)$$

The (3-19) shows that the change in flux during a time interval $t_1 - t_0$ is proportional to the integral of the voltage over the interval , or volt-seconds applied to the winding .

In push-pull type inverters (half-bridge , full-bridge) , it is clear that the volt.second unbalance can cause transformer saturation [15] , which can have harmful consequences :

1- increased conduction and switching losses

2- increased EMI (Electro Magnetic Interference)

3- decreased reliability and failure of the power transistors

So for these reasons , transformer saturation should be prevented , in a transformer , volt-second unbalance can originate from :

1- differences in the duty ratios of the "push" and "pull" switches .

2- differences in the positive and negative voltages of a center tap supply for half bridge converter .

3- differences in the voltage drops of the "push" and "pull" switches .

The voltage drop differences result from component tolerances , and duty ratio differences can result from differences in the time delays in the "push" and "pull" sections from load current pulsation . In association with PWM inverter operation , case 1(duty ratio differences) is the usual one .

Fig. 3-6 shows a full bridge inverter with duty ratio unbalance . If there is a duty ratio unbalance in a full-bridge inverter (Fig. 3-6 (a)) , which does not have capacitive coupling , the flux excursion in the core, equivalent magnetizing current and primary current become asymmetrical , Fig. 3-6(c) . As mentioned before this problem may cause saturation .

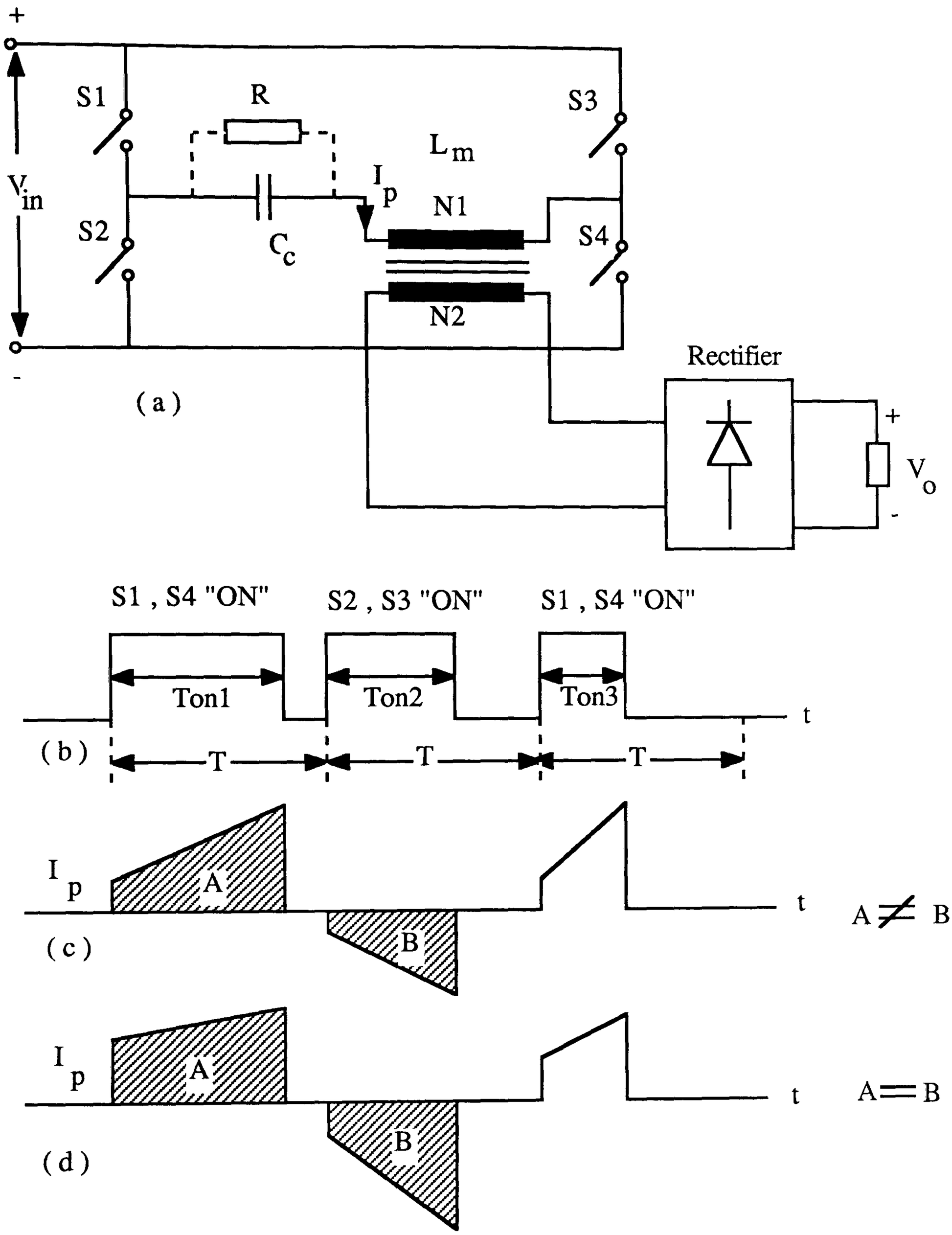

Fig. 3-6 Full bridge inverter (a) , switch status (b) , primary current without capacitor (c) , primary current with capacitor

One method to eliminate transformer saturation is to add a coupling capacitor in series with the transformer as shown in Fig. 3-6 (a) , for achieving $A \neq B$ becoming $A = B$, Fig. 3 - 6 (d) . In connection with Fig. 3 - 6 (a) , it has been discovered recently [16] that a low frequently oscillation can develope in the primary side of transformer , resulting from the change of the transistor Bipolar storage time in response to change in the collector current . This oscillation is a periodic exchange of energy between the coupling capacitor C_c and primary magnetizing inductance Lm . The oscillation can produce a large enough magnetizing current to drive the transformer in to severe saturation and can also cause excessive low - frequency EMI .

The above mentioned oscillation takes place only in the primary side of power circuit , therefore it is not detectable by observing only the inverter out put voltage . It has been shown in [16] that a resistor shunting the coupling capacitor Fig. 3-6 (a) provides a simple but effective method for preventing both system oscillation caused by the storage time modulation [17] and transformer saturation caused by duty-ratio unbalance . For more detailed discussion about oscillation frequency and cure for that oscillation refer to [16] .

3.10 Leakage Inductance

The existence of leakage inductance lies in the fact that part of the primary magnetic flux is not coupled to the secondary winding and vice versa , in result , gives rise to leakage inductance in each winding without contributing to the mutual flux . Leakage inductance is actually distributed throughout the winding in a transformer . However , for simplicity , this inductance is shown as a lumped constant Lp in Fig. 3-4 .

The leakage inductance depends very little on the core material , and strongly depends on number of turns . This inductance can be reduced drastically by bifilar winding . A pair of insulated wires are wound simultaneously and contiguously (close enough to tough each other) . Each wire constitutes a winding ; this very close proximity to its neighbour reduces leakage inductance by several orders of magnitude more than does ordinary inter leaving. Therefore , by this method , toroid transformers provide negligible leakage inductance .

By the following means leakage inductance can be reduced :

1- minimizing turns (will be discussed later on)
2- increasing winding width (windings cover the magnetic path as far as possible)
3- minimizing isolation between primary and secondary
4- using bifilar windings
5- inter weaving the primary and secondary windings , more detailed in [4]

It should be emphasized that reduction of leakage inductance usually increases transformer capacitances [5] .

3.11 Transformer capacitances

When the transformer is energized , different voltage gradients arise almost everywhere and consequently there are a large variety of capacitance which correspond to each of these gradients .

1- turn -to- turn
2- layer -to- layer
3- winding -to- winding
4- winding -to- core
5- terminal -to- terminal

The turn-to-turn capacitance is so small because they are in series when referred the whole winding . The effect of these capacities on transformer varies with the application , particularly they emerge in high frequency operation .

They are considered as a combined lumped capacitance of the primary and the secondary windings Fig. 3-7 .

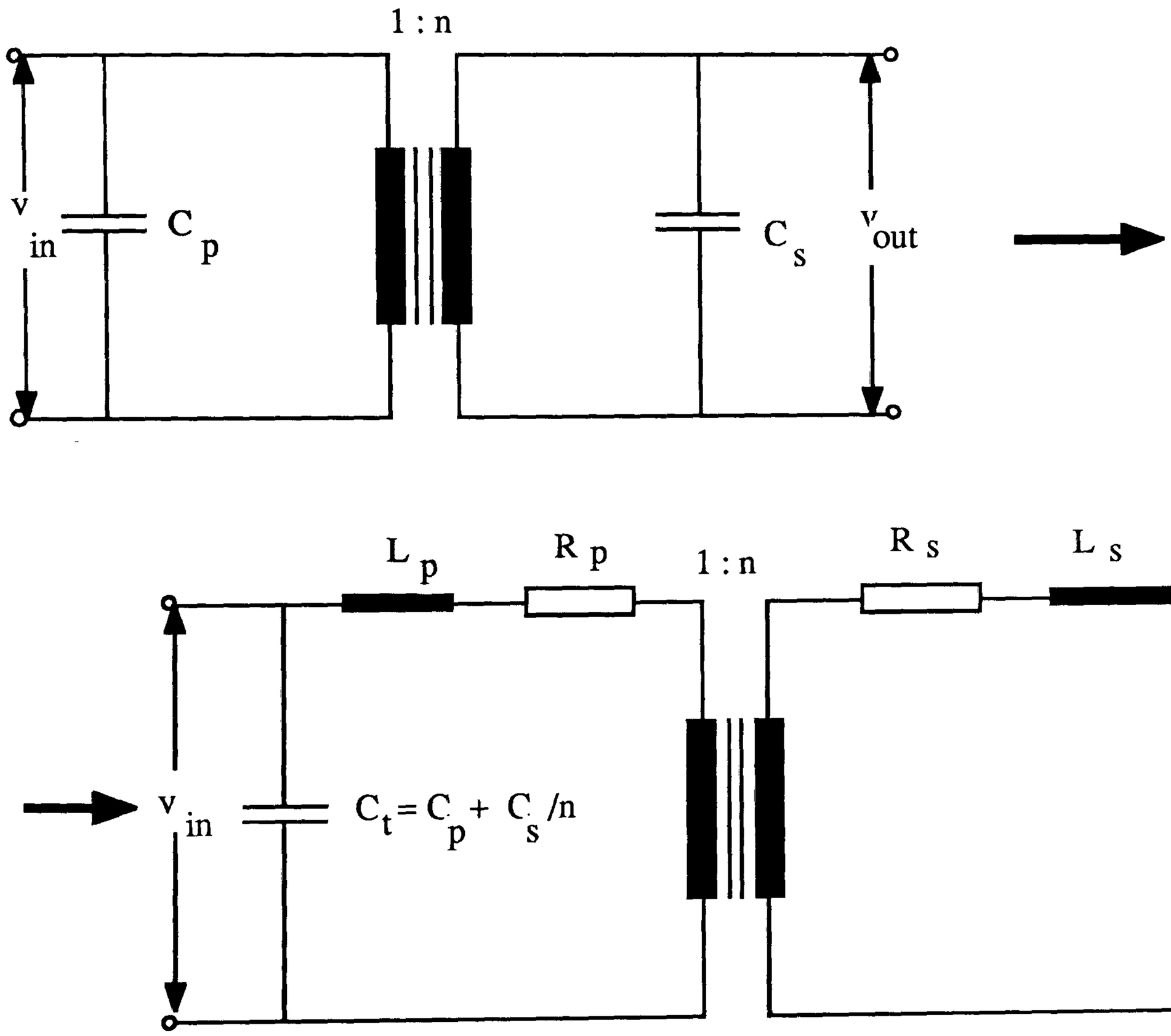

Fig. 3-7 transformer capacitances

By following means transformer capacitances can be reduced :

1- increased dielectric thickness between layer , turns , and windings

2- reduce winding width

3- increase number of layers

4- avoid bifilar winding

Since the corrective measures work in opposite directions for minimizing transformer capacitance and leakage inductance , a trade off has to be made between them .

3.12 Effect of frequency on leakage inductance

It is difficult to scale transformer design over a wide frequency range , since materials characteristics and design criteria changes . It is important to know how the leakage inductance changes with frequency to obtain an idea how overlap might affect output waveform if the system was designed to operate at much higher frequencies .

Here investigation is based on two mode of operation

I - $f.\Phi = \text{const.}$, $(\Phi = A.B_{max})$ (3-20)

Where f is frequency and Φ is the core flux . This means that the benefits of increasing the transformer frequency are absorbed by reducing the core size which is accompany with weight reduction of windings , but number of turns is unchanged . The leakage inductance of primary and secondary windings for concentric cylindrical coils are described in [18] :

$$L_p = K_p N_1^2 \frac{L_{mt}}{L_c} \qquad (3-21)$$

$$L_s = K_s N_2^2 \frac{L_{mt}}{L_c} \qquad (3-22)$$

$$L_t = L_p + \left(\frac{N_1}{N_2}\right)^2 Ls \qquad (3-23)$$

Where :

L_t : total transformer leakage inductance in primary terms

K_p , K_s : constants (irrelevant to this study)

N_1 , N_2 : number of primary and secondary turns

L_{mt} : the mean turn length

L_c : winding length

Since :

$$E_1 = 4.44 f \Phi_m N_1$$
$$E_2 = 4.44 f \Phi_m N_2 \qquad (3-24)$$
$$f \Phi_m = cte$$

Hence for constant terminal voltages , N does not change with frequency as the core area is inversely proportional to frequency , then the dependency of L_{mt} from frequency is :

$$L_{mt} \Delta \frac{1}{\sqrt{f}} \qquad (3-25)$$

L_c can be assumed to be independent of frequency (since N = const.) . The above conditions lead to the overall result that :

$$L_p \Delta \frac{1}{\sqrt{f}} \qquad (3-26)$$

II - $\Phi = \text{const.}$ (3-27)

From equations (3 - 24) , with constant E_1 , Φ_m , the following proportions can be drived :

$N_1 \Delta \frac{1}{f}$ or : $N_1^2 \Delta \frac{1}{f^2}$ (3-28)

$L_c \Delta N$ or : $L_c \Delta \frac{1}{f}$ (3-29)

Therefore :

$L_p \Delta \frac{1}{f^3}$ (3 - 30)

3.13 Effect of leakage inductance on overlap and converter operation

In phase controlled converter and cycloconverters , the transfer or commutation of the current from one switch (MOSFET) to the next does not take place instantaneously . Due to existence of resistance and inductance in the supply source (transformer here) it takes a finite time (called overlap period) for the current to decay to zero in the out going switch , whilst the current will rise at the same rate in incoming switch . Consequently , on the output of cycloconverter , which is theoretically designed for maximum fundamental output voltage and clean harmonic spectra , there will be loss of voltage and a modification of the harmonic distortion . This deterioration will be higher as long as the system operation frequency is increasing .

In transformer feeding the cycloconverter each phase may be represented by its Thevenin equivalent circuit consist of a voltage source in series with its inductance . The major contributer to the supply impedance here , is the transformer leakage reactance .

In ref.[19] it can be seen that the overlap period(angle) :

1- increases with load current increasing

2- increases with supply frequency increasing

3- decreases with supply voltage wave amplitude increasing

4- increases with supply reactance (leakage inductance) increasing

A further effect of the transformer leakage inductance is to produce commutation notches in the waveforms of the voltages appearing at the cycloconverter output terminals Fig. 3-8 .

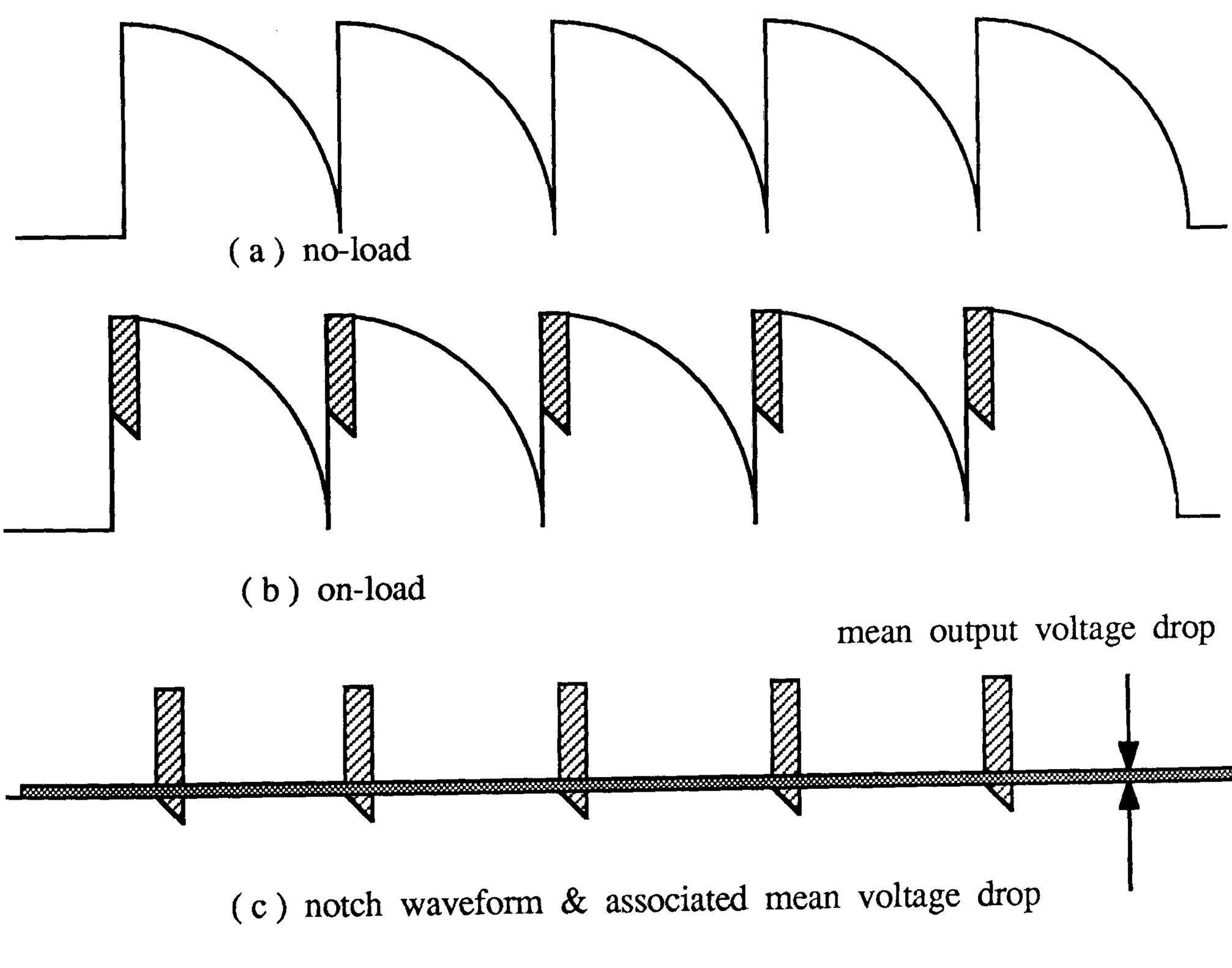

Fig. 3-8 (a) no-load converter output (b) on-load converter output
(c) voltage loss due to overlap due to leakage inductance

If the proper precautions are not taken , the presence of these notches can lead to some harmful effects [20] :

1- to influence the firing angles limit .

2- due to overlap period the fundamental component of cycloconverter input current will have a slight lagging phase shift with respect to input source voltage and consequently affects the input displacement factor and cycloconverter input power factor [19] .

Of course this lagging phase shift and mean voltage reduction is consistent with presence of transformer leakage inductance .

For a more detailed discussion on leakage inductance and over lap problems , such as mean voltage reduction calculation for different configurations see ref.s[19] , [20] & [21] .

3.14 Study of interaction between transformer inductances and snubber circuits

As it was outlined in chapter 1 , in the proposed DC -to- 3 phase AC multistage conversion system , the transformer operates between inverter and cycloconverter on basis of storage / transfer of energy with two purposes :

1- making isolating AC output from DC input .

2- any desired voltage / current level transformation .

Since the transformer inductances have key role in power conversion circuits , hence it is important to know the behaviour of these inductances with regard to "over lap" problem and "snubber circuit design" for the inverter on the primary side , and the cycloconverter on the secondary side .

It is quite difficult and far beyond the scope of this chapter to show analytically the details of interaction between the inverter and its snubber circuits , the transformer and its inductances (magnetizing & leakage) , the cycloconverter and its snubbers , output filter elements and the load .

For overall prototype system operation and interactions investigation , the computer base circuit simulation packages , for example , **SPICE**(**S**imulation **P**rogram with **I**ntegrated **C**ircuit **E**mphasis) can be employed[22] .

In single capacitor snubber arrangement (no R_1 , D_{11} , R_2 , D_{22} in Fig. 3-9) the energy stored in the capacitors is returned to the load via transformer leakage inductance and causes ringing effects . In other words there is a natural frequency , $f_r = \frac{1}{2\pi\sqrt{2LC}}$, in the system which is not in connection with inverter operation frequency(inverter with single capacitor snubbers can be analyzed) . This is the interaction between the total inductance (primary leakage and magnetizing inductance) of transformer and the snubber capacitors .

The employing of CRD snubber arrangements , Fig. 3 - 9 , overcome this problem . Here the capacitor acts in the same way to control the rate of rise of voltage across its associated switch at turn-OFF . At switch turn-ON , the capacitor discharges through the resistor (R_1 & R_2) in which it's stored energy is dissipated .

As Fig. 3-10 shows there are 3 distinct transient mechanisms during **T_1-OFF & T_2-ON** period .

1- At **t = t'** MOSFET T_1 turn-OFF ; the associated equivalent circuit is shown in Fig. 3 - 10 (a) . It has been assumed that the MOSFETs and Diodes are ideal , so the switching-ON and switching-OFF times of transistors , also recovery time for diodes are neglected. In consequence i_1 immediately is transfered to snubber circuit and goes through C_1 , D_{11}. The capacitor C_1 starts charging , so v_{T_1} increases , consequently i_1 and v_L decrease . At the same time i_2 starts increasing through C_2 and R_2 . C_2 starts discharging and v_{T2} falls from 2E .

During this transient period changes on i_L are insignificant ($\frac{d_{iL}}{d_t} = 0$), due to this fact that the rate of change of i1 and i_2 approximately equal ($\frac{d_{i_1}}{d_t} = \frac{d_{i_2}}{d_t}$) · This stage would last unitil v_{T2} approaches to zero , so that D_2 becomes forward biased and start to conduct i_2 current . The duration t''-t', $\frac{d_{i_1}}{d_t}$ and $\frac{d_{i_2}}{d_t}$ are affected by the size of snubber's capacitor and resistor (shown in Fig. 3 - 10) .

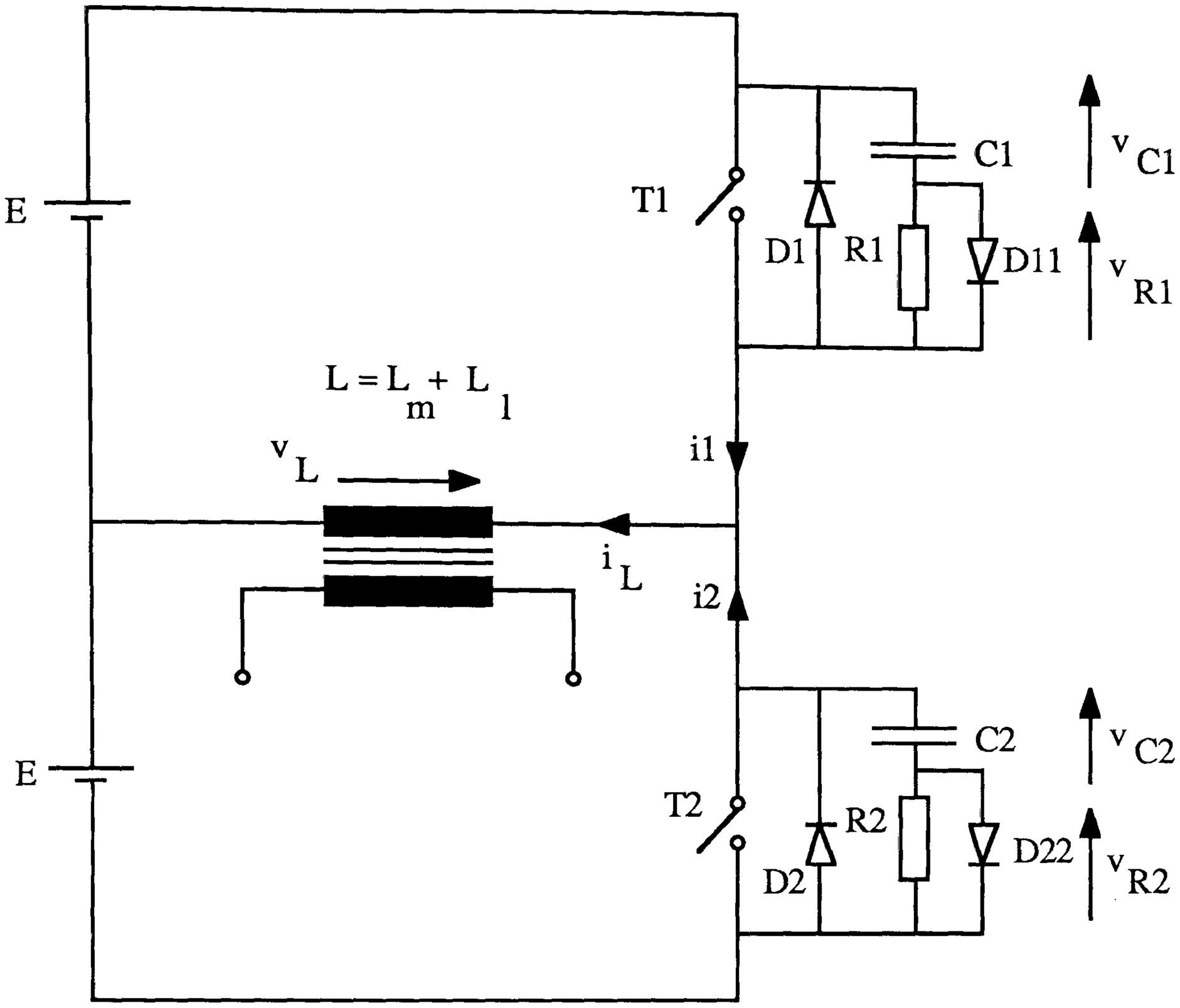

Fig. 3-9 single phase , half bridge inverter with C-R-D snubbers and transformer with open circuit secondary winding

(L_m is the primary magnetizing inductance & L_l is the primary leakage inductance)

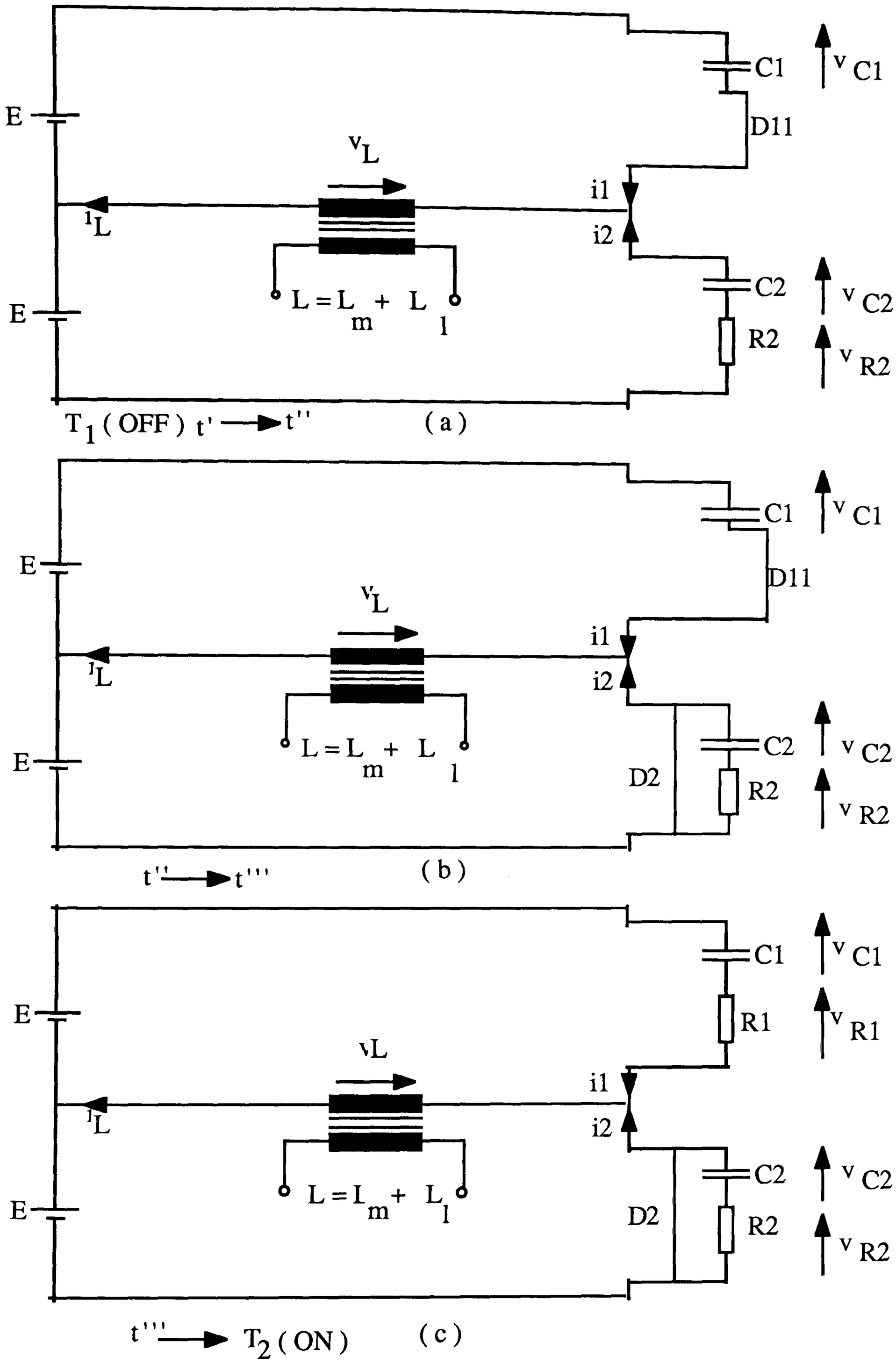

Fig. 3-10 3-occurance circuit diagram between T1 turn-OFF and T2 turn-ON in inverter circuit of Fig. 3-9

2- at $t = t''$, when v_{T_2} reaches to zero and D_2 starts to conduct i_2 , Fig. 3 -10 (b) . Since i_2 is no longer limited by R_2 , it increases sudenly up to the load current , whereas i_1 decreases accordingly . Due to this rapid change in i_1 and i_2 , presence of any inductance in the way of snubber to transformer , will produce a voltage spike equal to 2E + induced voltage across the T_1 which may be harmfull for switch T_1 .

The voltage spike can be reduced by increasing snubber circuit capacitors :

$$\frac{1}{2} C V_{spike}^2 = \frac{1}{2} L_{(leakage + stray)} I^2$$

$$V_{spike} = I \sqrt{\frac{L_{(leakage + stray)}}{C}} \qquad (3\text{-}31)$$

This interval ends when $i_1 = 0$, $v_{T_1} = v_{C_1} = 2E$, and $i_2 = i_L$.

3- At $t = t'''$, when $i_1 = 0$, $v_{C_1} = 2E$ the related circuit becomes as shown in Fig. 3 - 10 (c) . Now any current because of voltage spikes , can flow through R_1 , C_1 to the supply .

At this moment $v_{T_2} = 0$ (D_2 conducts) , therefore v_L approaches to - E consequently i_2 decreases and when it reaches zero MOSFET T_2 can be triggered . Therefore the under investigation period between T_1-OFF & T_2-ON is ended .

3.15 References :

1- S. C'uk *" New magnetic structures for switching converters "* IEEE Trans. on Magnetics , Vol. MAG - 19 , No. 2 , pp. 75 - 83 ,march 1983 .

2- K. H. Liu and F. C. Lee *" Zero voltage switching technique in DC-to-DC converters "* IEEE Power Electronics Specialist Conference 1986 Record , Vancouver , BC , June 1986 , pp. 58 - 70 .

3- R. A. Fisher , K. D. T. Ngo and M. H. Kuo *" A 500 Khz , 250 w DC-to-DC converter with multiple out-puts controlled by phase shifted PWM and Magnetic Amplifier"* High Frequency Power Conversion Conference Record , Sandiego , Ca , May 1988 , pp. 100 - 110 .

4- W. T. McLyman *" Transformer and Inductor Design Handbook "* New York : Marcel Dekker , Inc. 1988 .

5- N. R. Grossner *" Transformer for Electronic circuits "* Magraw - Hill Book company , 1967 .

6- M. G. Say" *The performance and design of alternating current machines "* 1949 , Pitman , London .

7- Brain Richardson *" Transformer core losses "* IEE Electronics and power , May 1986 , pp. 365-368

8- A. F. Goldberg , J. G. Kassakian and M. F. Schlecht *" Issues Related to 1-10 Mhz Transformer design "* IEEE Trans. on Power Electronics , Vol. 4 , No. 1 , Jan. 1989 , pp. 113 - 123 .

9- N. R. Coonrod *" Transformer computer design aid for high frequency switching power supplies "* IEEE Trans. on Power Electronics , Vol. PE - 1 , No. 4 , Oct. 1986 , pp. 248 - 256 .

10- H. Kurita , T. Hasegava , Y. Shibuya , T. Gohnai , H. Ohsuga and Y. Honda *" Dielectric loss of high voltage/high frequency transformer used in switching power supply for space "* IEEE , PESC 1988 Record , pp. 1120 - 1126 .

11- G. Chryssis *" High frequency switching power supply , theory and design "* 1984 , McGraw - Hill Book Company .

12- O. Ferenczi **" Power supplies Part B Switched-Mode Power Supplies "** 1987 , ELSEVIER , Budapest , Hunngry

13- R. L. Steigerwald and R. E. Tompkins *" A comparison of high frequency link schems for interfacing a DC source to a utility grid "* IEEE , 1982 , pp. 759 - 766 .

14- J. D. Edwards *" Electrical Machines-an introduction to principles and characteristics "* 1982 , International text Book Company .

15- R. Redl , M. Domb and N. O. Sokal *" How to predict and limit volt-second unbalance in voltag-fed push-pull converters "* PCI April 1983 Proc. , pp. 314 - 330 .

16- R. Redl , N. O. Sokal and C. W. Schaefer *" Transformer saturation and unusual system oscillation in capacitively coupled half bridge or full bridge power converters : causes , analysis , and cures "* IEEE , Power Electronics Specialist Conference Record , 1988 , pp. 820 - 829 .

17- W. M. Polivka , P. R. K. Chetty and R. D. Middlebrook *" State-space aveage modelling of converters with parasitics and storage-time modulation "* IEEE , Power Electronics Specialist Conference Record , 1980 , pp. 119 - 143 .

18. M. G. Say *" Alternating Current Machines "* fifth edition , logman , 1986 .

19- C. W. Lander *" Power Electronics "* second edition , Mcgraw - Hill Book Company (U. K. limited) , 1987 .

20- B. R. Pelly*"Thyristor phase controlled converters & cycloconveters "* john wiley & sons , Inc. , 1971 .

21- D. O'Kelly " **Performance and control of Elecrical Machines** " 1991 , McGraw-Hill Book Company , London

22- W. Banzhaf *" Computer aided circuit analysis using SPICE "* Prentice - Hall International Editions , 1989 .

Chapter 4

Cycloconverters & the Prototype System Cycloconverter (Proposed Modulation Strategy)

4.1 Two quadrant operation

In phase controlled converters the output DC voltage of either polarity , can be controlled continously by varing α , delaying firing angles [1 , 2 & 3] . For example in Fig. 4-1 (a) for :

$\alpha = 0°$ V_{DC} = Maximum

$\alpha = 90°$ $V_{DC} = 0$

$\alpha = 180°$ V_{DC} = Minimum

And because of the unidirectional current carrying property of the semiconductor switches with in the converter , the current at the DC terminals can flow in only one direction (2-quadrant operation) as shown in Fig . 4-1 (b) .

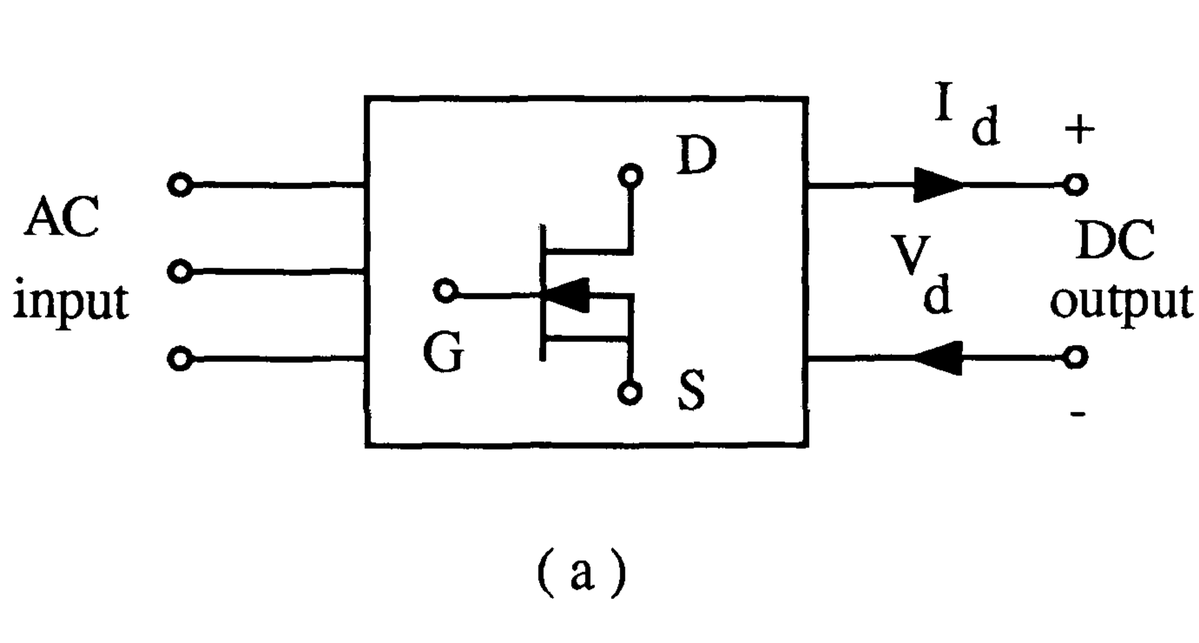

Fig. 4-1 2-quadrant operation

4.2 Four quadrant operation and dual converters

By connecting the DC terminals of two phase controlled converters in parallel and oppositely poled with one another , the resultant system is called dual converter Fig. 4-2 (a) , which can operate with both polarities of voltage

and current at its DC terminals(4-quadrant operation) as shown in Fig. 4-2 (b) .

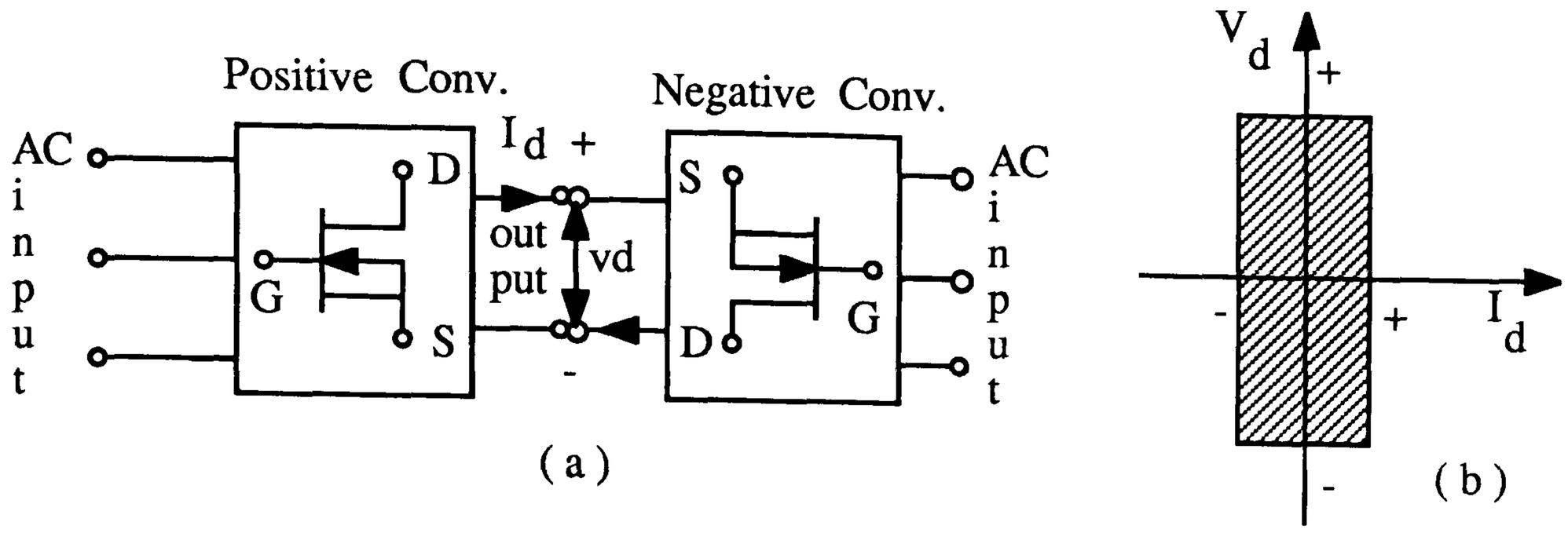

Fig. 4-2 4-quadrant operation

If α_p is the firing angle for positive converter and α_N is the firing angle of the Negative converter , in order to producing the exactly equal voltages and the same circuit polarity at the DC terminal of dual converter the following relationship should be satisfied .

$$\widehat{\alpha_p} + \widehat{\alpha_N} = 180^\circ \qquad (4-1)$$

It means when one converter operates as a rectifier ($0^\circ \le \alpha \le 90^\circ$) , the other operates as an inverter ($90^\circ \le \alpha \le 180^\circ$) [1] .

If (4-1) is not be satisfied , due to inequality between DC voltages of two groups , there will be a circulating current , flowing through converters which in many cases is harmful and unwanted .

It is possible that by a process of continuous phase modulation of the converter firing angles such that the output voltage in Fig. 4-2(a) is varied continuously with a sinusoidal mode and with frequency different from input

source frequency . Now this dual converter is called " cycloconverter " or " frequency changer " [2] .

4.3 Power frequency changers (cycloconverters)

The " power frequency changer " term , in general can apply to any electrical system that converts AC power of a given frequency to AC power with another chosen frequency . Such a system can employ static systems using solid-state and controllable switching devices or rotating electrical machinery :

$$f_{rotor} = S \cdot f_{stator}$$

$$S = \frac{N_s - N_r}{N_s} \qquad (4\text{-}2)$$

$$N_s = 120 \frac{f_{stator}}{p} \qquad \text{(synchronous speed)}$$

where ; f_{stator} is supply frequency and p is number of stator pole pairs . It is clear that any change in N_r will be reflected on f_{rotor} .

4.4 Static power frequency changers

There are two categories of static system . In the first type , the power is converted in two stages with an intermediate DC link (AC- to -DC- to -AC) . This type is called indirect " AC- to -AC " power conversion or " Rectifier - inverter type " frequency conversion . In the second type , the power is converted in one stage (AC- to -AC) , which is termed "direct AC- to -AC power converters " or " cycloconverters " , devised in the early 1930s . Recently many circuit configurations for static frequency changers have been designed .

The frequency changers are closely related to conventional rectifiers or AC- to -DC converter circuits . In fact , for any given AC- to -DC converter circuit , there is a corresponding AC- to -AC frequency changer circuit .

As has been outlined in chapter one , for a multistage DC- to -3 phase AC power conversion , different inverter-cycloconverter circuit configurations have been proposed (Fig. 1-15) . From cycloconverter operation points of view and on the basis of direct and indirect conversion modes , these configurations can be classified :

i - Direct conversion

1- Single phase (1000 Hz)- to -single phase (50 Hz) , Fig. 1-15 (a)

2- Single phase (50 Hz)- to -3 phase (50 Hz) , Fig. 1-15 (b)

3- 3 phase (1000 Hz)- to -3 phase (50 Hz) , Fig. 1-15 (d)

ii - Indirect conversion

1- Single phase (1000 Hz)- to -DC- to 3 phase (50 Hz) , Fig. 1-15 (c)

2- 3 phase (1000 Hz)- to -DC- to -3 phase (50 Hz) , expansion of Fig.1-15 (c)

Here , first the general theoretical principle of operation for different modes are discussed and at the end , the proposed technique for direct single phase (1000 Hz)- to -single phase (50 Hz) in comparison with the conventional method will be studied .

4.5 Direct AC- to -AC conversion(general discussion)

The direct AC - to - AC power frequency changer , consists of arrays of solid-state and bidirectional controllable switches , connected directly between the

input and output terminals . Operationally , it is a wave synthesizer ; output voltage waves of the desired amplitude and frequency are produced by sequentially switching chosen segments of the voltage waves of the AC input source to the output terminals . The resulting waveforms of current flowing at the input terminals are built up of segments of the current waves flowing at the output terminals .

The basic principle of operation of the cycloconverter is based on the fact that , the multiplication of a set of **n . 1** sinusoidal quantities (input voltage matrix) by a set of **m . n** balanced sinusoidal quantities (cycloconverter switching functions) yields a third set of **m . 1** sinusoidal quantities (output voltage matrix) , whose frequency can be varied by varying the frequency of the second set . The graphical representation of the direct AC- to -AC power conversion is shown in Fig. 4-3 [4] .

We can write :

$$\text{Matrix}\,(\,\mathbf{m\,.\,1}\,) = \text{Matrix}\,(\,\mathbf{m\,.\,n}\,)\,.\,\text{Matrix}\,(\,\mathbf{n\,.\,1}\,) \qquad (4-3)$$

or :

$$\left[v_o(\omega_o t)\right] = \left[s_f(\omega_s t)\right].\left[v_i(\omega_i t)\right] \qquad (4-4)$$

Referring to Fig. 4 - 3 , the equation (4 - 4) can be expanded :

$$\begin{bmatrix} v_{o1} \\ . \\ . \\ v_{ol} \\ . \\ . \\ v_{om} \end{bmatrix} = A \begin{bmatrix} f_{11} \ldots f_{1k} \ldots f_{1n} \\ \ldots\ldots\ldots\ldots\ldots \\ \ldots\ldots\ldots\ldots\ldots \\ f_{l1} \ldots f_{lk} \ldots f_{ln} \\ \ldots\ldots\ldots\ldots\ldots \\ \ldots\ldots\ldots\ldots\ldots \\ f_{m1} \ldots f_{mk} \ldots f_{mn} \end{bmatrix} . V_i(\max) \begin{bmatrix} v_{i1} \\ \ldots \\ \ldots \\ v_{ik} \\ \ldots \\ \ldots \\ v_{in} \end{bmatrix} \qquad (4-5)$$

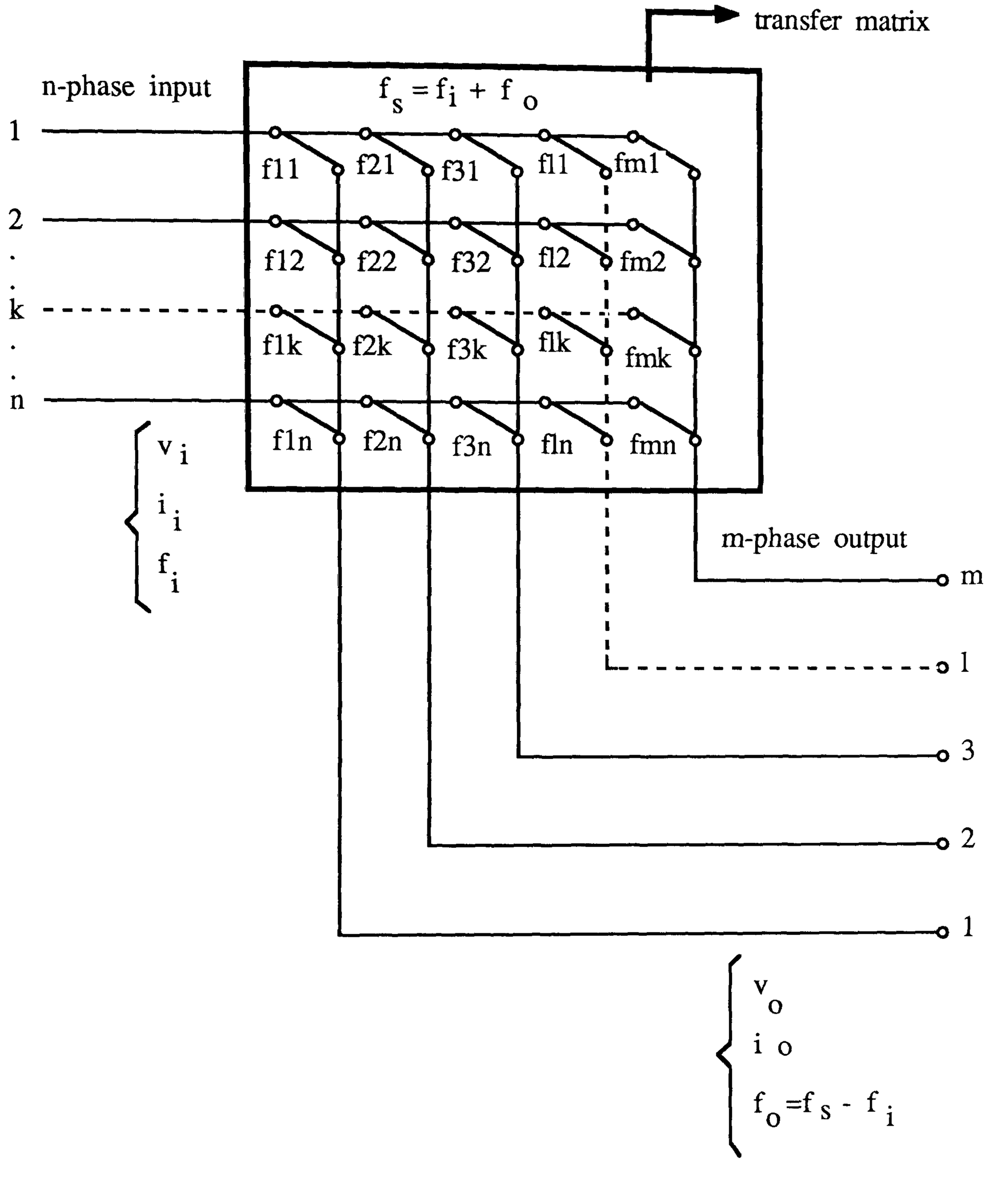

Fig. 4-3 Generalized cycloconverter topology for :

(**n-phase** input with $\mathbf{f_i}$ Hz)- to -(**m-phase** output with $\mathbf{f_o}$ Hz)

For input current the following matrix can be derived .

$$\text{Matrix}\,(\,\mathbf{n}\,.\,\mathbf{1}\,) = \text{Matrix}\,(\,\mathbf{n}\,.\,\mathbf{m}\,)\,.\,\text{Matrix}\,(\,\mathbf{m}\,.\,\mathbf{1}\,) \qquad (4-6)$$

Comparing (4 - 6) with (4 - 3) , it results:

$$\left[I_i\,(\,\omega_i t\,)\right] = \left[S_f(\omega_s t)\right]^T \left[I_o\,(\omega_o t\,)\right] \qquad (4-7)$$

With reference to Fig. 4-3 , the equation (4 - 7) can be expanded :

$$\begin{bmatrix} I_{i1} \\ \cdots \\ \cdots \\ I_{ik} \\ \cdots \\ \cdots \\ I_{in} \end{bmatrix} = A \begin{bmatrix} f_{11} \cdots f_{l1} \cdots f_{m1} \\ \cdots\cdots\cdots\cdots\cdots \\ \cdots\cdots\cdots\cdots\cdots \\ f_{1k} \cdots f_{lk} \cdots f_{mk} \\ \cdots\cdots\cdots\cdots\cdots \\ \cdots\cdots\cdots\cdots\cdots \\ f_{1n} \cdots f_{ln} \cdots f_{mn} \end{bmatrix} . I_o \begin{bmatrix} I_{o1} \\ \cdots \\ \cdots \\ I_{ol} \\ \cdots \\ \cdots \\ I_{om} \end{bmatrix} \qquad (4-8)$$

It should be noted again , all elements in (4 - 5) and (4 - 8) are sinusoidul time functions. In Fig. 4-3 , the input is a system of n balanced and symmetric phases , in which each phase is related by $\frac{1}{n}360°$ with respect to the one ahead and similarly the output is a system of m balanced and symmetric phases , in which each phase is related by $\frac{1}{m}360°$ with respect to the one ahead . Therefore the general term of the transform matrix of $S_f(\,\omega_s t\,)$ can be written :

$$f_{l,k}(\,t\,) = A\,\text{Cos}\left[\omega_s t - \frac{k-1}{n}360° + \frac{l-1}{m}360°\right] \qquad (4-9)$$

$$k = 1\,,\,2\,,\,\ldots\,,\,n$$
$$l = 1\,,\,2\,,\,\ldots\,,\,m$$

More details may be found in [5] .

4.5.1 Direct 3 phase- to -3 phase conversion

For $n = m = 3$ the common and practical case , (3-phase)- to -(3-phase) is yielded [6], Fig. 4-4 and part of Fig. 1-14 (d) .

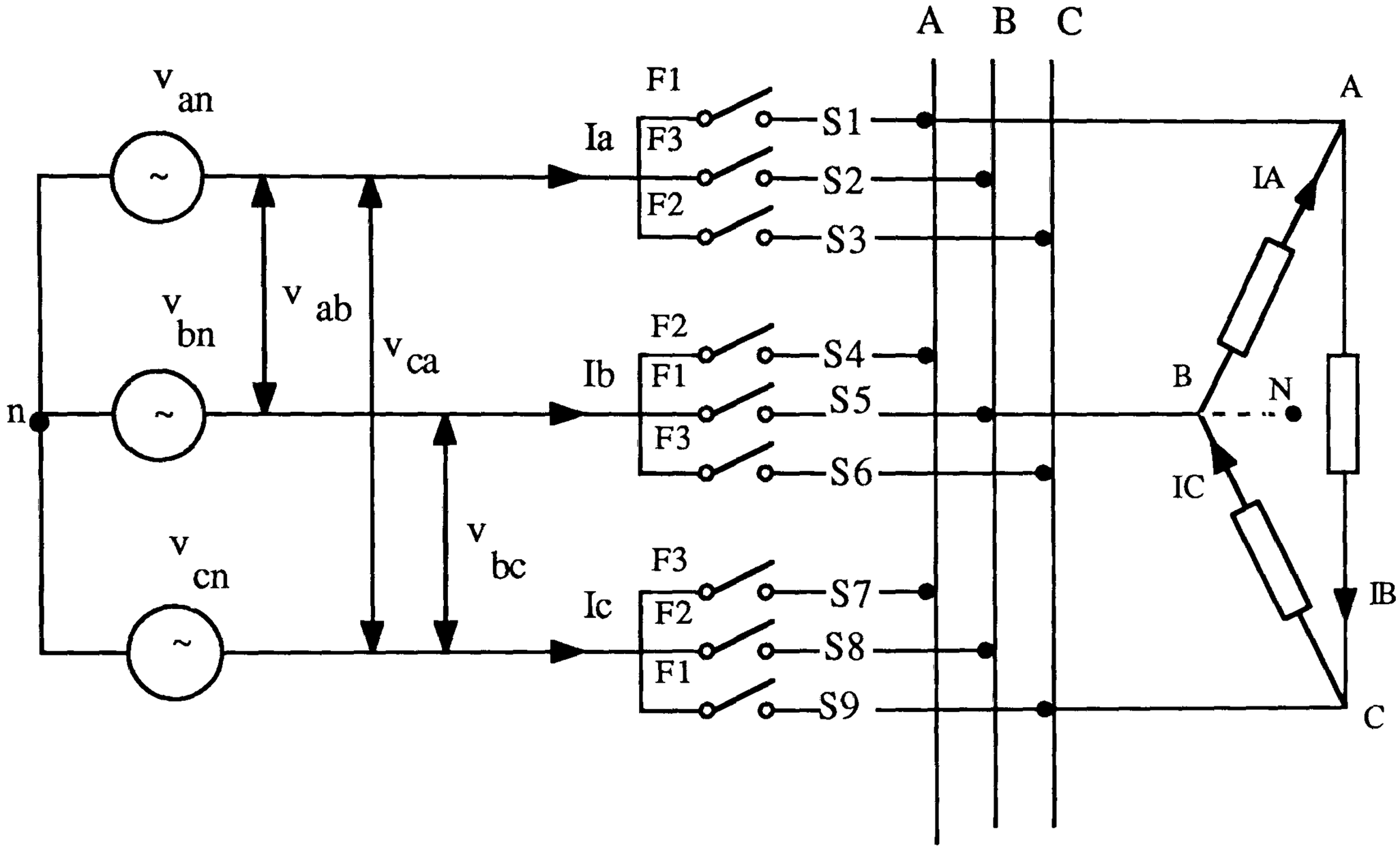

Fig. 4-4 direct 3-phase - to - 3-phase conversion

With reference to Fig. 4 - 4 and following assumptions :

$$\begin{bmatrix} v_{an} \\ v_{bn} \\ v_{cn} \end{bmatrix} = V_i\,(\max) \begin{bmatrix} \cos(\omega_i t) \\ \cos(\omega_i t - 120^\circ) \\ \cos(\omega_i t + 120^\circ) \end{bmatrix} \qquad (4\text{-}10)$$

$$\begin{bmatrix} I_A \\ I_B \\ I_C \end{bmatrix} = I_o\,(\max) \begin{bmatrix} \cos(\omega_o t) \\ \cos(\omega_o t - 120^\circ) \\ \cos\omega_o t + 120^\circ \end{bmatrix} \qquad (4\text{-}11)$$

$$\begin{bmatrix} F_1 \\ F_2 \\ F_3 \end{bmatrix} = A \begin{bmatrix} \cos(\omega_s t) \\ \cos(\omega_s t - 120^\circ) \\ \cos(\omega_s t + 120^\circ) \end{bmatrix} \qquad (4-12)$$

The equations (4 - 5) , (4 - 8) become :

$$\begin{bmatrix} V_{AN} \\ V_{BN} \\ V_{CN} \end{bmatrix} = \begin{bmatrix} F_1 & F_2 & F_3 \\ F_3 & F_1 & F_2 \\ F_2 & F_3 & F_1 \end{bmatrix} \cdot \begin{bmatrix} V_{an} \\ V_{bn} \\ V_{cn} \end{bmatrix} \qquad (4-13)$$

$$\begin{bmatrix} I_a \\ I_b \\ I_c \end{bmatrix} = \begin{bmatrix} F_1 & F_3 & F_2 \\ F_2 & F_1 & F_3 \\ F_3 & F_2 & F_1 \end{bmatrix} \cdot \begin{bmatrix} I_A \\ I_B \\ I_C \end{bmatrix} \qquad (4-14)$$

Putting(4-10) , (4-11) , (4-12) in the (4-13) and (4-14) yields :

$$\begin{bmatrix} V_{AN} \\ V_{BN} \\ V_{CN} \end{bmatrix} = A \begin{bmatrix} \cos(\omega_s t) & \cos(\omega_s t - 120^\circ) & \cos(\omega_s t + 120^\circ) \\ \cos(\omega_s t + 120^\circ) & \cos(\omega_s t) & \cos(\omega_s t - 120^\circ) \\ \cos(\omega_s t - 120^\circ) & \cos(\omega_s t + 120^\circ) & \cos(\omega_s t) \end{bmatrix} . V_i(\max) \begin{bmatrix} \cos(\omega_i t) \\ \cos(\omega_i t - 120^\circ) \\ \cos(\omega_i t + 120^\circ) \end{bmatrix}$$

(4 -15)

$$\begin{bmatrix} I_a \\ I_b \\ I_c \end{bmatrix} = A \begin{bmatrix} \cos(\omega_s t) & \cos(\omega_s t + 120^\circ) & \cos(\omega_s t - 120^\circ) \\ \cos(\omega_s t - 120^\circ) & \cos(\omega_s t) & \cos(\omega_s t + 120^\circ) \\ \cos(\omega_s t + 120^\circ) & \cos(\omega_s t - 120^\circ) & \cos(\omega_s t) \end{bmatrix} . I_o(\max) \begin{bmatrix} \cos\omega_o t \\ \cos(\omega_o t - 120^\circ) \\ \cos(\omega_o t + 120^\circ) \end{bmatrix}$$

(4 -16)

Noting that :

$$\text{Cos}(P).\text{Cos}(Q) = \frac{1}{2}\left[\cos(P+Q) + \cos(P-Q)\right]$$

And :

$$\omega_o = \omega_s - \omega_i$$

After trigonometric manipulation , the (4 - 15) and (4 - 16) become :

$$\begin{bmatrix} V_{AN} \\ V_{BN} \\ V_{CN} \end{bmatrix} = \frac{3}{2} AV_i\,(max) \begin{bmatrix} \cos\left[(\omega_s - \omega_i)t\right] \\ \cos\left[(\omega_s - \omega_i)t\text{-}120^\circ\right] \\ \cos\left[(\omega_s - \omega_i)t + 120^\circ\right] \end{bmatrix} = \frac{3}{2} AV_i\,(max) \begin{bmatrix} \cos(\omega_o t) \\ \cos(\omega_o t\text{-}120^\circ) \\ \cos(\omega_o t + 120^\circ) \end{bmatrix}$$

(4 - 17)

$$\begin{bmatrix} I_a \\ I_b \\ I_c \end{bmatrix} = \frac{3}{2} AI_o(max) \begin{bmatrix} \cos\left[(\omega_s - \omega_o)t\right] \\ \cos\left[(\omega_s - \omega_o)t\text{-}120^\circ\right] \\ \cos\left[(\omega_s - \omega_o)t + 120^\circ\right] \end{bmatrix} = \frac{3}{2} AI_o(max) \begin{bmatrix} \cos(\omega_i t) \\ \cos(\omega_i t\text{-}120^\circ) \\ \cos(\omega_i t + 120^\circ) \end{bmatrix}$$

(4 - 18)

4.5.2 Harmonic studies in 3 phase- to -3 phase conversion

The coefficient of the input voltages in (4 - 5) and (4 - 13) are termed cycloconverter " transfer matrix " or in terms of switch operation they are called cycloconverter " existence function " or " switching pattern " .

In practice the switching patterns , $f_{l,k}$, represent the ON/OFF states of the power switches , resulting in a train of rectangular pulses with unity amplitude .

They can be expressed mathematically as follow :

$$f_{l\,,\,k}(t) = A_0 + A_1 \cos\left[\omega_s t - \frac{k\text{-}1}{n} 360^\circ + \frac{l\text{-}1}{m} 360^\circ\right] + \sum_{n=2,3,4}^{\infty} A_n \cos\left\{ n\left[\omega_s t - \frac{k\text{-}1}{n} 360^\circ + \frac{l\text{-}1}{m} 360^\circ\right]\right\}$$

$$k = 1\,,\,2\,,\,\ldots\,,\,n$$
$$l = 1\,,\,2\,,\,\ldots\,,\,m$$

(4-19)

For $n = m = 3$ case :

$$\begin{bmatrix} F_1 \\ F_2 \\ F_3 \end{bmatrix} = \begin{bmatrix} (A_0+A_1\cos\omega_s t)+\sum_{n=2.3,4}^{\infty} A_n\cos(n\omega_s t) \\ A_0+A_1\cos(\omega_s t-120^\circ)+\sum_{n=2,3,4}^{\infty} A_n\cos\left[n(\omega_s t-120^\circ)\right] \\ (A_0+A_1\cos(\omega_s t+120^\circ)+\sum_{n=2,3,4}^{\infty} A_n\cos\left[n(\omega_s t+120^\circ)\right] \end{bmatrix} \qquad (4\text{-}20)$$

Comparing(4 - 12) and (4 - 20) reveals the harmonic components in the switching patterns as follow :

$$F_h = \begin{bmatrix} F_1h \\ F_2h \\ F_3h \end{bmatrix} = \begin{bmatrix} \sum_{n=2,3,4}^{\infty} A_n\cos(n\omega_s t) \\ \sum_{n=2,3,4}^{\infty} A_n\cos\left[n(\omega_s t-120^\circ)\right] \\ \sum_{n=2,3,4}^{\infty} A_n\cos\left[n(\omega_s t+120^\circ)\right] \end{bmatrix} \qquad (4\text{-}21)$$

The infinite series of harmonics present in the cycloconverter output voltage and input current yields from :

$$\begin{bmatrix} V_{ANh} \\ V_{BNh} \\ V_{CNh} \end{bmatrix} = \begin{bmatrix} F_{1h} & F_{2h} & F_{3h} \\ F_{3h} & F_{1h} & F_{2h} \\ F_{2h} & F_{3h} & F_{1h} \end{bmatrix} \begin{bmatrix} V_{an} \\ V_{bn} \\ V_{cn} \end{bmatrix} \qquad (4\text{-}22)$$

and :

$$\begin{bmatrix} I_{ah} \\ I_{bh} \\ I_{ch} \end{bmatrix} = \begin{bmatrix} F_{1h} & F_{3h} & F_{2h} \\ F_{2h} & F_{1h} & F_{3h} \\ F_{3h} & F_{2h} & F_{1h} \end{bmatrix} \begin{bmatrix} I_A \\ I_B \\ I_C \end{bmatrix} \qquad (4-23)$$

By substituting (4 - 10) , (4 - 11) , (4 - 21) in to (4 - 22) and (4 - 23) , after some trigonometric manipulation the first term of output voltage and input current can be expressed : [7]

$$V_{ANh}(\omega_o t) = \sum_{k=1}^{\infty} \frac{3(A_{3k\pm1}).v_i(max)}{2} \cos\left[3k\omega_i + (3k \pm 1)\omega_0\right] t \qquad (4-24)$$

$$I_{ah}(\omega_i t) = \sum_{k=1}^{\infty} \frac{3(A_{3k\pm1}).I_o(max)}{2} \cos\left[\left[3k\omega_o + (3k\pm1)\,\omega_i\right] t\right] \qquad (4-25)$$

From (4 - 24) the harmonic frequencies of the output voltage are :

$$3k\omega_i + (3k \pm 1)\,\omega_o$$

$$(2\omega_o + 3\omega_i)\,,\ (4\omega_o + 3\omega_i)\,,\ (5\omega_o + 6\omega_i)\,,\ (7\omega_o + 6\omega_i)\,,\ \ldots\ldots \qquad (4-26)$$

$$k = 1,2,3,\ldots\ldots$$

and from the (4 - 25) the harmonic frequencies of the input current are :

$$3k\omega_o + (3k \pm 1)\,\omega_i \qquad (4-27)$$

$$(2\omega_i + 3\omega_o)\,,\ (4\omega_i + 3\omega_o)\,,\ (5\omega_i + 6\omega_o)\,,\ (7\omega_i + 6\omega_o)\,,\ \ldots$$

$$k = 1,2,3,\ldots.$$

by assuming :

$$R = \frac{\omega_i}{\omega_o} > 1 \text{ and integer .}$$

the output voltage harmonic frequencies = $\omega_o[3k(R+1)\pm 1]$ k=1,2,3,...

the input current harmonic frequencies = $\omega_o[3k(R+1)\pm R]$ k=1,2,3,....

(4 - 28)

From (4 - 28) it is obvious that harmonic spectrum will be free from low order harmonics if R be chosen higher regardless of its side effects .

4.6 More discussion about cycloconverter switching pattern

From (4 - 5) and (4 - 20) it can be realized that each element of transform matrix , $f_{l,k}(t)$, describes the operation of one switch in the power circuit such that $f_{l,k}(t) = 0$ when switch is open and $f_{l,k}(t) = 1$ when switch is conducting and connecting output terminal l to input terminal k (Fig. 4 - 3) .

Generally each element is a function of f_i , f_o , v_o/v_i , and t [8]

$$f_{l,k}(t) = f_{l,k}\left(f_i, f_o, \frac{v_o}{v_i}, t\right) \qquad (4-29)$$

l = 1 , 2 , ...m

k = 1 , 2 , ... n

From (4 - 24) and (4 - 25) it can be understood that the quality of the input current waveform and output voltage waveform is greatly dependent upon the character of the switching pattern . The various character of $f_{l,k}(t)$ (pulse position , width , and repetition rate) , represent different modulation techniques , which may produce wave forms with identical wanted components but widely differing spectral characteristics . So it is important to find the optimal cycloconverter switching pattern for specific application requirements (minimum total harmonic distortion and maximum fundamental component) . This problem will be considered in indirect AC- to -AC power conversion .

4.7 Some important conclusion about direct 3 phase- to - 3 phase conversion

1- In Fig. 4 - 4 , it is assumed that the 3 phase- to - 3 phase cycloconverter feeds a 3 phase inductive load with cosΦ power factor , therefore (4 - 11) becomes :

$$\begin{bmatrix} I_A \\ I_B \\ I_C \end{bmatrix} = I_o\,(\max) \begin{bmatrix} \cos(\omega_o t - \Phi) \\ \cos(\omega_o t - \Phi - 120^\circ) \\ \cos(\omega_o t - \Phi + 120^\circ) \end{bmatrix} \qquad (4 - 30)$$

by substituting (4 - 30) in to (4 - 23) and doing trigonometric manipulation , the first term of the input current matrix is expressed . [7]

$$I_{ah}(\omega_i t) = \sum_{k=1}^{\infty} \frac{3(A_{3k \pm 1}) I_{o\text{-}max}}{2} \cos\left\{\left[3k\omega_o + (3k \pm 1)\omega_i\right] t + \Phi\right\} \qquad (4 - 31)$$

considering the sign of Φ in (4 - 30) and (4 - 31) shows the input power factor appears as the inverse of the output power factor , that is an inductive load at the output of cycloconverter is seen by the source as a capacitive load , and vice versa . This is a welcome side benefit for a direct AC- to -AC frequency changer which it may operate as a VAR compensator [8] .

2- As (4 - 28) shows , there is no subharmonic below the fundamental components in the output voltage .

3- The 3 phase- to - 3 phase cycloconverter can be viewed as a generalized solid-state transformer with turn ratio of :

$$\frac{N_s}{N_p}=\frac{V_{out}}{V_{in}}=\frac{\frac{3}{2}A_1V_{in}(max)}{V_{in}(max)}=\frac{3}{2}A_1 \qquad (4-32)$$

As has been shown in [6] and [8-Chap. 3]

$$A_{1max}=\frac{\sqrt{3}}{\pi} \qquad (4-33)$$

therefore :

$$\frac{N_s}{N_p}(max)=\frac{3}{2}\cdot\frac{\sqrt{3}}{\pi}=0.827\ (step\ down) \qquad (4-34)$$

equation(4-34) demonstrates that 3 phase- to - 3 phase cycloconverter of Fig. 4 - 4 operates as a step down transformer .

4.8 Indirect AC- to -AC conversion(AC-to-DC- to AC)

Generally this mode of operation is based on that :

$$\text{Matrix}(\mathbf{m}.1).\left[\text{Matrix}(1.\mathbf{n}).\text{Matrix}(\mathbf{n}.1)\right]=\text{Matrix}(\mathbf{m}.1) \qquad (4-35)$$

The multiplication of a set of (**1 . n**) balanced sinusoidal quantities (rectifier switching matrix , $f_r(\omega_i t)$) by a set of (**n . 1**) sinusoidal quantities (input voltage matrix , $V_i(\omega_i t)$) results in a DC quantity free of harmonics , then multiplication of DC quantity (rectifier output voltage) by a set of (**m . 1**) balanced sinusoidal quantities (inverter switching matrix $f_i(\omega_o t)$) results in a set of (**m . 1**) balanced sinusoidal quantities (output voltage matrix , $V_o(\omega_o t)$) . This process is shown in Fig. 4-5 . Referring to Fig. 4 - 5 and (4 - 35) :

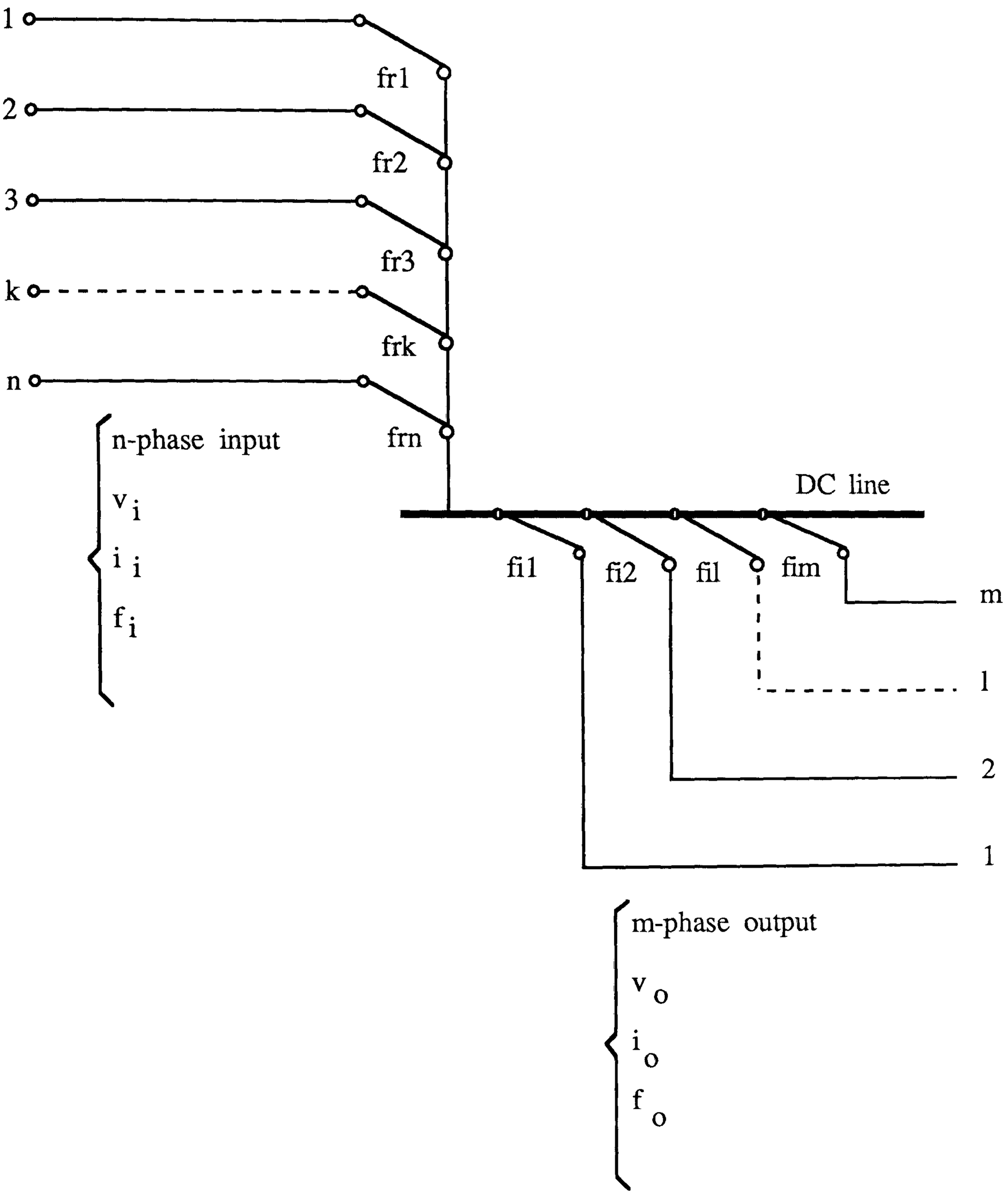

Fig 4-5 Generalized indirect :

(**n-phase** input with $\mathbf{f_i}$ Hz)- to -(**m-phase** output with $\mathbf{f_o}$ Hz)

$$\begin{bmatrix}\text{inverter}\\ F_i(\omega_o t)\end{bmatrix}\left[\begin{bmatrix}\text{rectifier}\\ F_r(\omega_i t)\end{bmatrix}\cdot\begin{bmatrix}\text{input}\\ V_i(\omega_i t)\end{bmatrix}\right]=\begin{bmatrix}\text{output}\\ V_o(\omega_o t)\end{bmatrix} \qquad (4-36)$$

or :

$$A\begin{bmatrix}f_{i1}\\ \cdot\\ \cdot\\ f_{il}\\ \cdot\\ \cdot\\ f_{im}\end{bmatrix}\left[B\left[f_{r1}.....f_{rk}.....f_{rn}\right]\cdot V_i\begin{bmatrix}V_{i1}\\ \cdot\\ \cdot\\ V_{ik}\\ \cdot\\ \cdot\\ V_{in}\end{bmatrix}\right]=\frac{mABV_i}{2}\cdot\begin{bmatrix}V_{o1}\\ \cdot\\ \cdot\\ V_{ol}\\ \cdot\\ \cdot\\ V_{om}\end{bmatrix} \qquad (4-37)$$

The all matrix elements in (4 - 37) are sinusoidal and function of time .

The general term of the different matrixes are :

1- Input voltage matrix :

$$V_{ik}=V_i\cos\left[\omega_i t-\frac{k-1}{n}360^\circ\right] \qquad k=1,2,3,....,n$$

2- Input rectification matrix :

$$f_{rk}=B\cos\left[\omega_i t-\frac{k-1}{n}360^\circ\right] \qquad k=1,2,3,.....,n$$

3- Inversion matrix :

$$f_{il}=A\cos\left[\omega_o t-\frac{1-1}{m}360^\circ\right] \qquad l=1,2,3,.....,m$$

4- Output voltage matrix :

$$f_{il}=A\cos\left[\omega_o t-\frac{1-1}{m}360^\circ\right] \quad l=1,2,3,.....,m \qquad (4-38)$$

Where :

n is the input phase number

m is the output phase number

ω_i is the cycloconverter input angular frequency rad/sec

ω_o is the cycloconverter output angular frequency rad/sec

similar to (4 - 6) the input current matrix can be derived as follow :

$$\left[F_r(\omega_i t)\right]^T . \left[F_i(\omega_o t)\right]^T . \left[I_o(\omega_o t)\right] = \left[I_i(\omega_i t)\right] \qquad (4-39)$$

(4 - 39) can be expanded in terms of matrix elements :

$$B\begin{bmatrix} f_{r1} \\ \cdot \\ \cdot \\ \cdot \\ f_{rk} \\ \cdot \\ \cdot \\ \cdot \\ f_{rm} \end{bmatrix}\left[A\left[f_{i1}.....f_{il}.....f_{im}\right] . I_o\begin{bmatrix} I_{o1} \\ \cdot \\ \cdot \\ \cdot \\ I_{om} \end{bmatrix}\right] = \frac{mABI_o}{2}.\begin{bmatrix} \cdot \\ \cdot \\ \cdot \\ I_{ik} \\ \cdot \\ \cdot \\ \cdot \\ I_{in} \end{bmatrix} \qquad (4-40)$$

the general terms in (4 - 40) for the input and output currents are :

1- input current :

$$I_{i\,k} = \frac{mABI_o}{2}\cos\left[\omega_i t - \frac{k-1}{n}360^\circ\right],\ k = 1\ ,\ 2\ ,\ .....\ ,\ n \qquad (4-41)$$

2- output current :

$$I_{ol} = I_o \cos\left[\omega_o t - \frac{1-1}{m}360^\circ\right], 1 = 1\ ,\ 2\ ,\ .....\ ,\ m$$

4.8.1 Indirect 3 phase- to - 3 phase conversion

For $m = n = 3$, the known and practical configuration (3 phase- to -DC - to - 3 phase) is achieved(Fig. 4-6) . For $n = 1$, $m = 3$ part of Fig. 1-15 (b) is resulted .

Referring to Fig. 4-6 , (4 - 37) and (4 - 40) the output voltage and input current matrixes can be derived as follows .

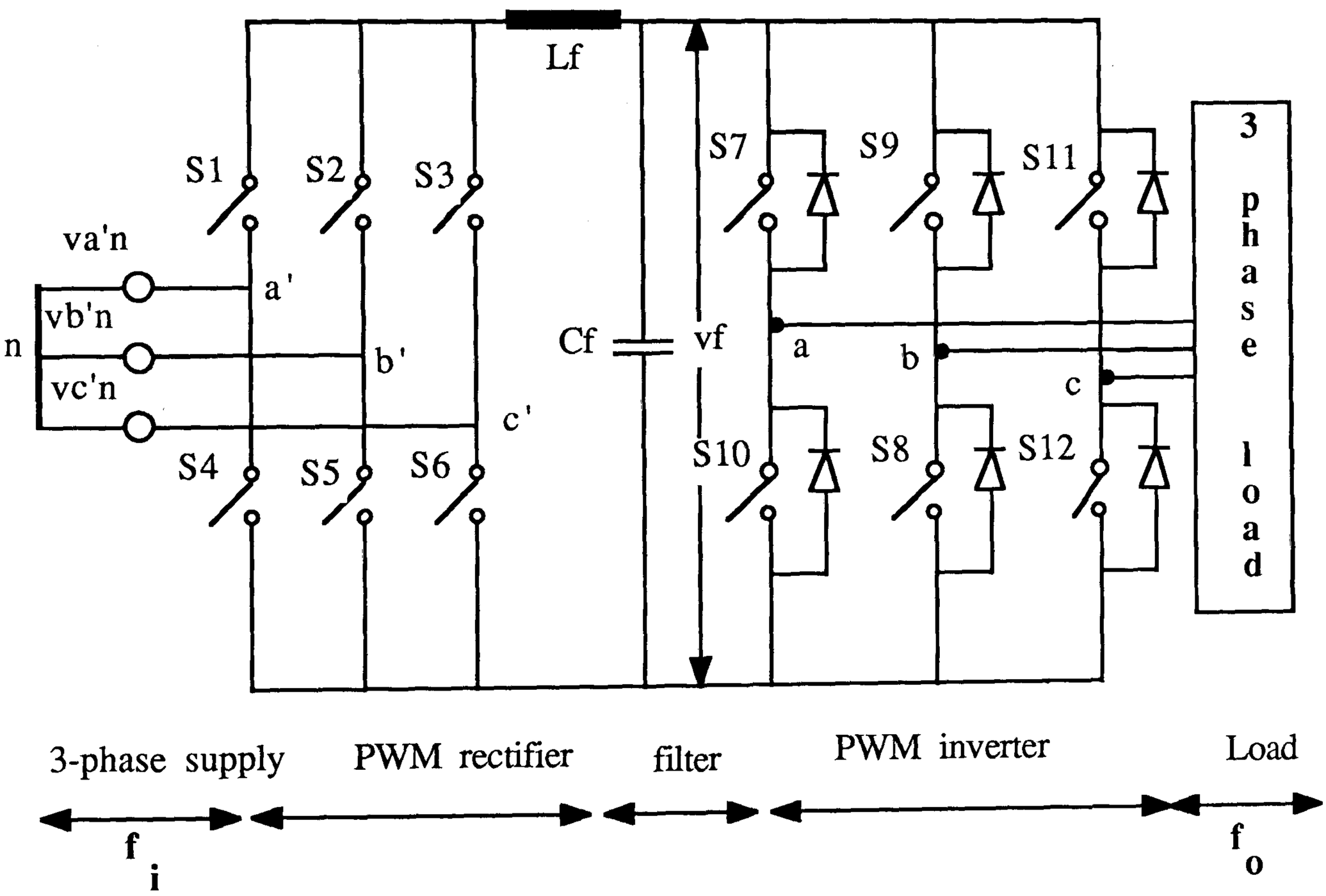

S1 - S6 bidirectional Switches

Fig. 4-6 Indirect 3-phase(f_i) - to - 3-phase (f_o) power conversion

output voltages :

$$A\begin{bmatrix}\text{inversion of DC link voltage}\\ \cos(\omega_o t)\\ \cos(\omega_o t - 120^\circ)\\ \cos(\omega_o t + 120^\circ)\end{bmatrix}.B\begin{bmatrix}\text{input rectification}\\ \cos(\omega_i t) & \cos(\omega_i t - 120^\circ) & \cos(\omega_i t + 120^\circ)\end{bmatrix}.$$

$$.V_i\begin{bmatrix}\text{3 phase input } (f_i)\\ \cos(\omega_i t)\\ \cos(\omega_i t - 120^\circ)\\ \cos(\omega_i t + 120^\circ)\end{bmatrix} = \frac{3}{2}B.A.V_i\begin{bmatrix}\text{output voltage } (f_o)\\ \cos(\omega_o t)\\ \cos(\omega_o t - 120^\circ)\\ \cos(\omega_o t + 120^\circ)\end{bmatrix} \qquad (4-42)$$

Input current :

$$B\begin{bmatrix}\text{inversion}\\ \cos(\omega_i t)\\ \cos(\omega_i t - 120^\circ)\\ \cos(\omega_i t + 120^\circ)\end{bmatrix}.A\begin{bmatrix}\text{output current rectification}\\ \cos(\omega_o t) & \cos(\omega_o t - 120^\circ) & \cos(\omega_o t + 120^\circ)\end{bmatrix}.$$

$$.I_o\begin{bmatrix}\text{3 phase output } (f_o)\\ \cos(\omega_o t)\\ \cos(\omega_o t - 120^\circ)\\ \cos(\omega_o t + 120^\circ)\end{bmatrix} = \frac{3}{2}B.A.I_o\begin{bmatrix}\text{Input current } (f_i)\\ \cos(\omega_i t)\\ \cos(\omega_i t - 120^\circ)\\ \cos(\omega_i t + 120^\circ)\end{bmatrix} \qquad (4-43)$$

As (4 - 42) and (4 - 43) shows , the output of rectifier is pure DC voltage ($3/2\,BV_i$) , that is , a filter is not needed. Also , since the semiconductor switches , operate in the ON/OFF mode and switching patterns for inversion , rectification stages are train of pulses with unity amplitude and different ON/OFF durations. As a result these switching patterns can be expressed mathematically similar to (4 - 20) and in order to feeding the inverter without any ripple , the filtering components C_f and L_f in Fig. 4-6 are employed . Here the output waveforms are obtained with selective PWM technique and associated harmonic elimination , voltage control strategy .

4.8.2 Indirect 3 phase- to - 3 phase conversion with removed DC link components

In Fig. 4-6 the filter components fulfil the following duties :

Link inductor L_f is used to smooth the DC link current and suppress link current discontinuities . The capacitor C_f is mainly employed to store the energy flowing back the inverter (due to inductance of the load) . In other words capacitor C_f , plays the role of regenerative and flow back energy sink . In addition these components have the following disadvantages :

1- are heavy and bulky

2- slow down system response

3- limit future load development

As it has been explained in [9] , it is possible to remove the DC link components provided that an approach for the release of trapped and regenerative energy should be implemented . To satisfy that in Fig. 4-6 , the regenerative PWM rectifier , comprised of bidirectional switches is selected . The power flow in new structure is controlled by varying the modulation index of the corresponding inverter , therefore an optimized switching pattern may be applied to the rectifier .

4.8.3 Harmonic studies in indirect 3 phase- to -3 phase conversion with suppressed DC link

Since filter components are not employed , the harmonic components of the rectifier output voltage have a direct effect on the inverter operation . Similarly , the harmonic components of the inverter input current have a direct effect on the input line current of the rectifier . This design of the switching pattern for both inverter and rectifier has significant importance .

The output of rectifier of Fig. 4-6 with removed DC link can be expressed by [9] :

$$v_r(\omega_i t) = E + \sum_{k=6,12}^{\infty} v_{r,k} \sin(k\omega_i t + \Phi_{r,k}) \qquad (4\text{–}44)$$

where :

E is the DC component of rectifier output voltage

$v_{r,k}$ is the amplitude of k-th unwanted component of v_r

$\Phi_{r,k}$ is the phase displacement of k-th unwanted component of v_r

$\omega_i = 2\pi f_i$, f_i is the frequency changer input frequency

If the switching pattern of the inverter be assumed as follows :

$$S_I(\omega_o t) = \begin{bmatrix} f_{i1} \\ f_{i2} \\ f_{i3} \end{bmatrix} = \begin{bmatrix} A_1 \sin \omega_o t + \sum_{n=5,7}^{\infty} A_n \sin n\, \omega_o t \\ A_1 \sin (\omega_o t - 120^\circ) + \sum_{n=5,7}^{\infty} A_n \sin n (\omega_o t - 120^\circ) \\ A_1 \sin (\omega_o t + 120^\circ) + \sum_{n=5,7}^{\infty} A_n \sin n (\omega_o t + 120^\circ) \end{bmatrix}$$

(4-45

Then the output voltage of inverter $v_o = (\omega_o t)$ or across the load can be expressed by :

$$v_o(\omega_o t) = \begin{bmatrix} v_{ab}(\omega_o t) \\ v_{bc}(\omega_o t) \\ v_{ca}(\omega_o t) \end{bmatrix} = v_r(\omega_i t) \,.\, S_I(\omega_o t) \qquad (4 - 46)$$

The (4 - 46) can be expanded by substituting (4 - 44) and (4 - 45)

$$\begin{bmatrix} v_{ab}(\omega_o t) \\ v_{bc}(\omega_o t) \\ v_{ca}(\omega_o t) \end{bmatrix} = \left[E + \sum_{k=6,12}^{\infty} v_{r,k} \mathrm{Sin}(k\omega_i t + \Phi_{r,k}) \right] . \begin{bmatrix} A_1 \mathrm{Sin}\omega_o t + \sum_{n=5,7}^{\infty} A_n \mathrm{Sin}(n\omega_o t) \\ A_1 \mathrm{Sin}(\omega_o t - 120^\circ) + \sum_{n=5,7}^{\infty} A_n \mathrm{Sin}(n\omega_o t - 120^\circ) \\ A_1 \mathrm{Sin}(\omega_o t + 120^\circ) + \sum_{n=5,7}^{\infty} A_n \mathrm{Sin}(n\omega_o t + 120^\circ) \end{bmatrix}$$

$$= EA_1 \begin{bmatrix} \text{output} \\ \mathrm{Sin}\omega_o t \\ \mathrm{Sin}(\omega_o t - 120^\circ) \\ \mathrm{Sin}(\omega_o t + 120^\circ) \end{bmatrix} + E . \begin{bmatrix} \text{class 1 output harmonics} \\ \sum_{n=5,7}^{\infty} A_n \mathrm{Sin}[n(\omega_o t)] \\ \sum_{n=5,7}^{\infty} A_n \mathrm{Sin}[n(\omega_o t - 120^\circ)] \\ \sum_{n=5,7}^{\infty} A_n \mathrm{Sin}[n(\omega_o t + 120^\circ)] \end{bmatrix}$$

$$+ \begin{bmatrix} \text{class 2 output harmonics} \\ \sum_{k=6,12}^{\infty} \sum_{n=1,5,7}^{\infty} v_{r,k} A_n \mathrm{Sin}\,(k\,\omega_i t + \Phi_{r,k})\,[n\,(\omega_o t)] \\ \sum_{k=6,12}^{\infty} \sum_{n=1,5,7}^{\infty} v_{r,k} A_n \mathrm{Sin}\,(k\,\omega_i t + \Phi_{r,k})\,[n\,(\omega_o t - 120^\circ)] \\ \sum_{k=6,12}^{\infty} \sum_{n=1,5,7}^{\infty} v_{r,k} A_n \mathrm{Sin}\,(k\,\omega_i t + \Phi_{r,k})\,[n\,(\omega_o t + 120^\circ)] \end{bmatrix}$$

For one phase : (4-47)

$$v_{ab}(\omega_o t) = EA_1 \mathrm{Sin}\,\omega_o t + E \sum_{n=5,7}^{\infty} A_n \mathrm{Sin}[n(\omega_o t)] +$$

$$\sum_{k=6,12}^{\infty} \sum_{n=1,5,7}^{\infty} v_{r,k} A_n \mathrm{Sin}(k\omega_i t + \Phi_{r,k}) \mathrm{Sin}\left[n(\omega_o t)\right] \qquad (4\text{-}48)$$

Since :

$\text{Sin}(P).\text{Sin}(Q) = \frac{1}{2}[\cos(P-Q) - \cos(P+Q)]$, the (4-48) can be rewritten :

$$v_{ab}(\omega_o t) = EA_1 \text{Sin}\omega_o t + E\sum_{n=5,7}^{\infty} A_n \text{Sin}\omega_o t + \sum_{k=6,12}^{\infty}\sum_{n=1,5,7}^{\infty} \frac{1}{2} v_{r,k} A_n \cos\left[(k\omega_i - m\omega_o)t + \Phi_{r,k}\right]$$
$$- \sum_{k=6,12}^{\infty}\sum_{1,5,7}^{\infty} \frac{1}{2} v_{r,k} A_n \cos\left[(k\omega_i + m\omega_o) + \Phi_{r,k}\right]$$

(4 - 49)

In (4 - 49) there are 4 group of frequencies :

1- f_o fundamental

2- $n.f_o$ $n = 5, 7, \ldots\ldots$

3- $k.f_i - nf_o$ $k = 6, 12, \ldots$ & $n = 1, 3, 5, \ldots\ldots$ (4 - 50)

4- $kf_i + nf_o$ $k = 6, 12, \ldots$ & $n = 1, 5, 7, \ldots\ldots\ldots$

4.8.4 Subharmonics and their effects

As (4-50) shows , in group 3 , there are harmonic components which have frequency lower than the fundamental frequency (f_o) . They are called subharmonics . In induction motor applications these subharmonics can cause a number of problems such as torque pulsations , energy losses , light flickering and magnetic saturation (the amplitude of flux wave produced in the AC machine by a harmonic component is inversely proportional to its frequency) .The presence of subharmonics in the inverter output voltage , is the main disadvantage for indirect AC- to -AC conversion with removed DC link components . In (4 - 49) the subharmonics will appear when :

$$kf_i - mf_o < f_o \qquad \text{or} \qquad kf_i < (m+1) f_o \qquad (4-51)$$

to avoid the creation of subharmonics always :

$$kf_i - mf_o > f_o \text{ or } kf_i > (m+1) f_o \quad k = 6, 12, \ldots m = 1, 5, 7, \ldots \quad (4-52)$$

in (4 - 52) the simultaneous values for k and m should be considered .

In reference [9] & [10] the method in which the generation of low frequency components in the inverter output voltage can be avoided has been discussed .

4.9 phase conversion

In order to reduce the size and maintenance problems in conventional rotary phase conversion systems [11] , several types of static phase converter circuits have been developed with varing performance and circuit complexities . Three-phase electrical equipments such as three-phase induction motors are significantly more efficient and economical than their single-phase counter parts . In addition in many cases the extension of three phase power lines to rural and light industrial areas is not economical , and also other applications such as , operation of the 3-phase auxiliary pumps and fans (from single-phase traction supply) in electric locomotives , necessitate single-phase to three-phase power conversion process .

4.9.1 General approach for single phase-to-three phase power conversion

This approach is based on the principle of direct cycloconversion which was discussed in section (4 - 5). In equations (4 - 5) , (4 - 8) by setting n = 1 and m = 3 , the single phase- to -three phase configuration will be resulted as shown in Fig. 4-7 and also Fig. 1-15 (b) .

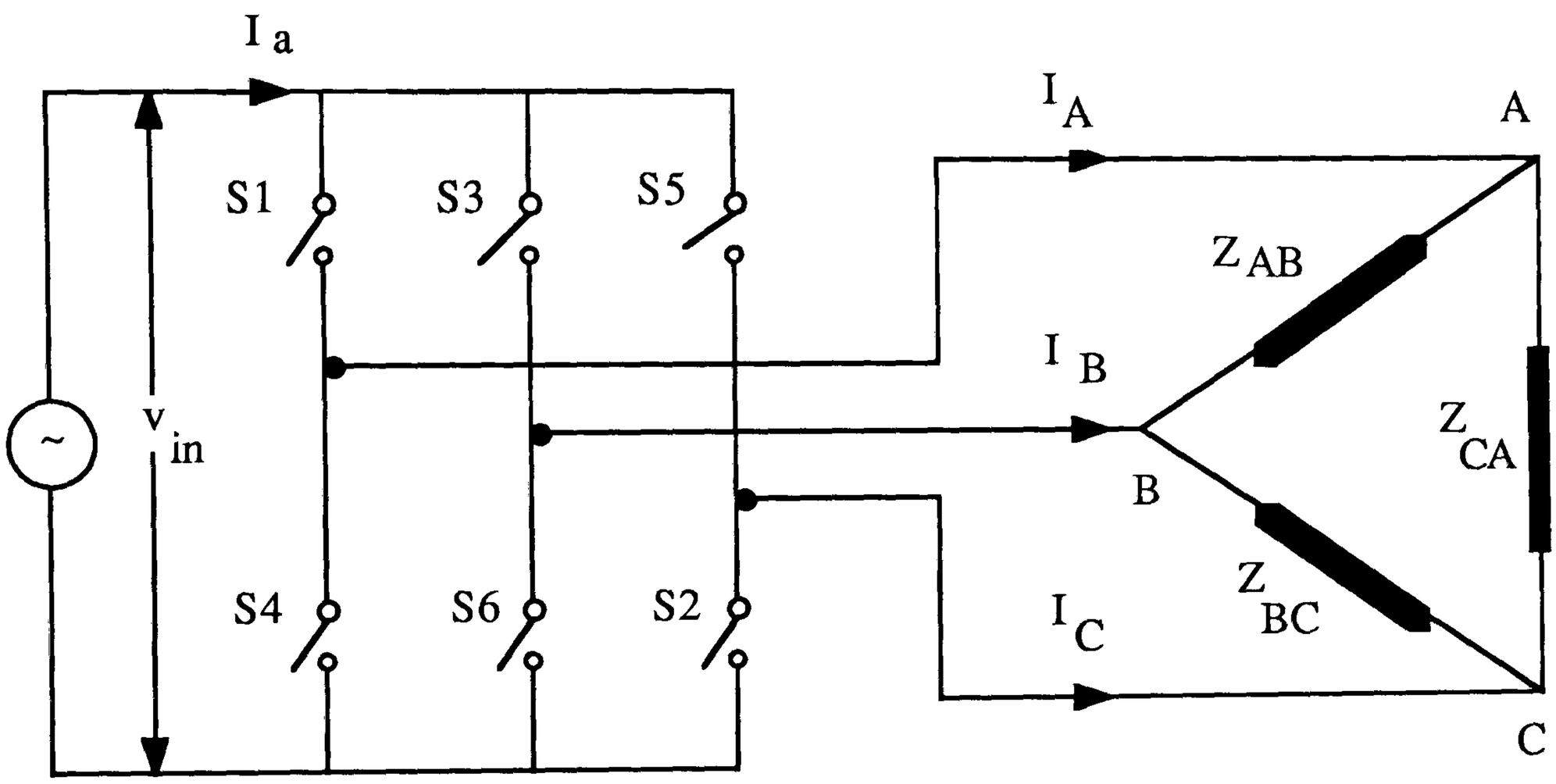

Fig. 4-7 direct single phase -to- 3-phase cycloconversion

According to (4 - 5) , (4 - 8) and n = 1 , m = 3 the general relationship for cycloconverter input / output voltage and currents can be derived .

$$\begin{bmatrix} v_{o1} \\ v_{o2} \\ v_{o3} \end{bmatrix} = A \begin{bmatrix} f_{11} \\ f_{12} \\ f_{13} \end{bmatrix} . \, v_i [v_{i1}] \qquad (4 - 53)$$

$$[I_i] = A \begin{bmatrix} f_{11} & f_{12} & f_{13} \end{bmatrix} I_o \begin{bmatrix} I_{o1} \\ I_{o2} \\ I_{o3} \end{bmatrix} \qquad (4 - 54)$$

Referring to relationships (4 - 10) , (4 - 12) the (4 - 53) and (4 - 54) becomes :

$$\begin{bmatrix} v_{AB} \\ v_{BC} \\ v_{CA} \end{bmatrix} = A \begin{bmatrix} \cos(\omega_s t) \\ \cos(\omega_s t - 120^\circ) \\ \cos(\omega_s t + 120^\circ) \end{bmatrix} . v_i \left[\cos\omega_i t\right] = \frac{A v_i}{2} \begin{bmatrix} \cos(\omega_o t) + \cos(\omega_s + \omega_i) t \\ \cos(\omega_o t - 120^\circ) + \cos\left[(\omega_s + \omega_i) t - 120^\circ\right] \\ \cos(\omega_o t + 120^\circ) + \cos\left[(\omega_s + \omega_i) t + 120^\circ\right] \end{bmatrix}$$

(4 - 55)

$$\left[I_a\right] = A \left[\cos(\omega_s t) \quad \cos(\omega_s t - 120^\circ) \quad \cos(\omega_s t + 120^\circ)\right] . I_o \begin{bmatrix} \cos(\omega_o t) \\ \cos(\omega_o t - 120^\circ) \\ \cos(\omega_o t + 120^\circ) \end{bmatrix}$$

$$= \frac{3AI_o}{2} \cos(\omega_s - \omega_o) t = \frac{3AI_o}{2} \cos(\omega_i t)$$

(4 - 56)

The (4 - 55) and (4 - 56) are based on the ideal phase converter . For the actual converter the switching pattern is comprised of the ON/OFF states of switches S_1 , S_2 , ...S_6 in Fig. 4 - 7 , consequently a train of rectangular pulses with unity amplitude and different ON/OFF durations , which their Fourier Series expansions can be written as follows [12] .

$$\begin{bmatrix} F_1 \\ F_2 \\ F_3 \end{bmatrix} = \begin{bmatrix} A_1 \cos(\omega_s t) + \sum_{n=3,5,7}^{\infty} A_n \cos(n \omega_s t) \\ A_1 \cos(\omega_s t - 120^\circ) + \sum_{n=3,5,7}^{\infty} A_n \cos\left[n (\omega_s t - 120^\circ)\right] \\ A_1 \cos(\omega_s t + 120^\circ) + \sum_{n=3,5,7}^{\infty} A_n \cos\left[n (\omega_s t + 120^\circ)\right] \end{bmatrix} \qquad (4 - 57)$$

Therefore (4 - 53) becomes :

$$\begin{bmatrix} v_{AB} \\ v_{BC} \\ v_{CA} \end{bmatrix} = \begin{bmatrix} A_1 \text{Cos}\,(\omega_s t) + \sum_{n=3,5,7}^{\infty} A_n \text{Cos}(n\omega_s t) \\ A_1 \text{Cos}\,(\omega_s t - 120^\circ) + \sum_{n=3,5,7}^{\infty} A_n \text{Cos}[n\,(\omega_s t - 120^\circ) \\ A_1 \text{Cos}\,(\omega_s t + 120^\circ) + \sum_{n=3,5,7}^{\infty} A_n \text{Cos}[n\,(\omega_s t + 120^\circ) \end{bmatrix} . \; v_I \Big[\text{Cos}\,(\omega_o t)\Big]$$

(4 - 58)

Since :

$$\text{Cos}(P).\text{Cos}(Q) = \frac{1}{2}\Big[\text{Cos}(P+Q) + \text{Cos}(P-Q)\Big]$$

$\omega_s = \omega_o + \omega_i$ and for single phase (50 Hz) - to - three phase (50 Hz) purpose

$\omega_o = \omega_i$, so $\omega_s = 2\omega_o$

and :

$\omega_s + \omega_o = 3\omega_o$

Thus :

$$\begin{bmatrix} v_{AB} \\ v_{BC} \\ v_{CA} \end{bmatrix} = \frac{A_1 v_i}{2} \begin{bmatrix} \text{Cos}\,(\omega_o t) \\ \text{Cos}\,(\omega_o t - 120^\circ) \\ \text{Cos}\,(\omega_o t + 120^\circ) \end{bmatrix} + \frac{A_1 v_i}{2} \begin{bmatrix} \text{Cos}\,3\,(\omega_o t) \\ \text{Cos}\,3\,(\omega_o t - 120^\circ) \\ \text{Cos}\,3\,(\omega_o t + 120^\circ) \end{bmatrix}$$

$$+ \sum_{n=3,5,7}^{\infty} \frac{A_n v_i}{2} \begin{bmatrix} \text{Cos}\,(n\omega_s - \omega_i)\,t + \text{Cos}\,(n\omega_s + \omega_i)t \\ \text{Cos}\,[(n\omega_s - \omega_i)\,t - n\,120^\circ] + \text{Cos}\,[(n\omega_s + \omega_i)t - n\,120^\circ] \\ \text{Cos}\,[(n\omega_s - \omega_i)\,t + n\,120^\circ] + \text{Cos}\,[(n\omega_s + \omega_i)t + n\,120^\circ] \end{bmatrix}$$

(4 - 59)

in the same way :

$$[I_a]=[F_1\ F_2\ F_3].I_o\begin{bmatrix}\text{Cos}(\omega_o t)\\ \text{Cos}(\omega_o t-120^\circ)\\ \text{Cos}(\omega_o t+120^\circ)\end{bmatrix}=\frac{3A_1 I_o}{2}\text{Cos}(\omega_i t)+\sum_{n=5,11}^{\infty}\frac{3A_n I_o}{2}\text{Cos}(n\omega_s+\omega_o)t$$

$$+\sum_{n=7,13}^{\infty}\frac{3A_n I_o}{2}\text{Cos}(n\omega_s-\omega_o)t \qquad (4-60)$$

As (4 - 59) shows the output line voltage contain third harmonics , whose amplitude is equal to the amplitude of the respective fundamental component , these component are inherent with the proposed general approach and independent of the PWM strategy employed . More details and practical example may be found in [12] .

4.10 Single phase- to -single phase cycloconverters

The main power circuits of single phase -to- single phase cycloconverters are shown in Fig. 4-8 .

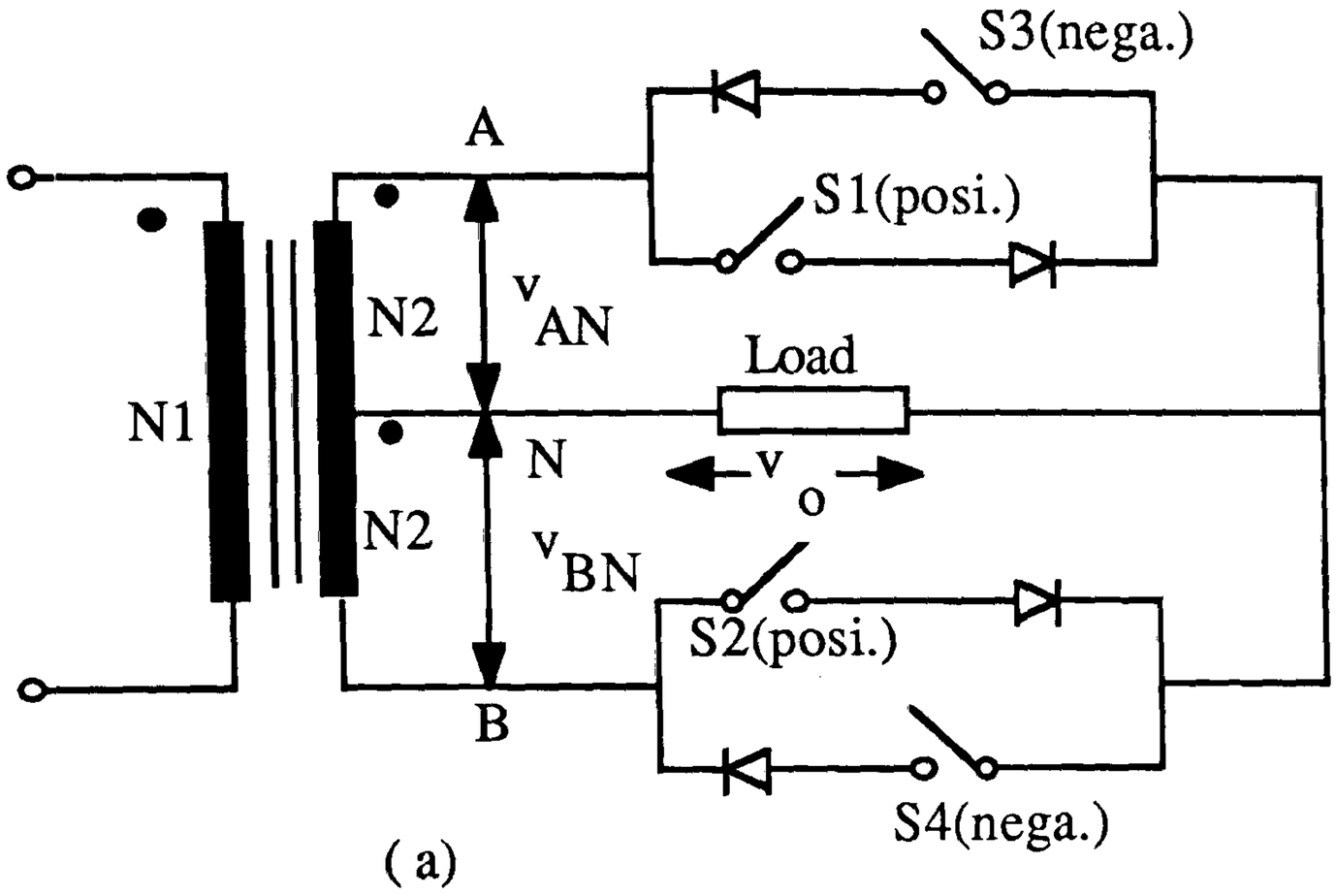

(a)

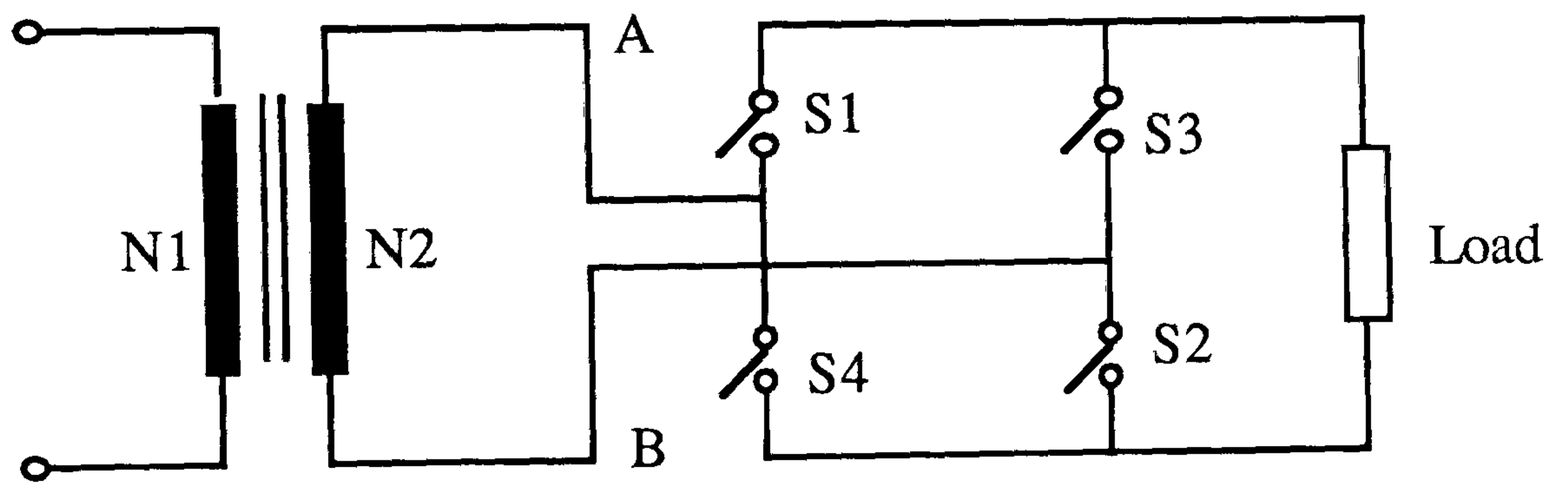

S1 to S4 are bilateral switches 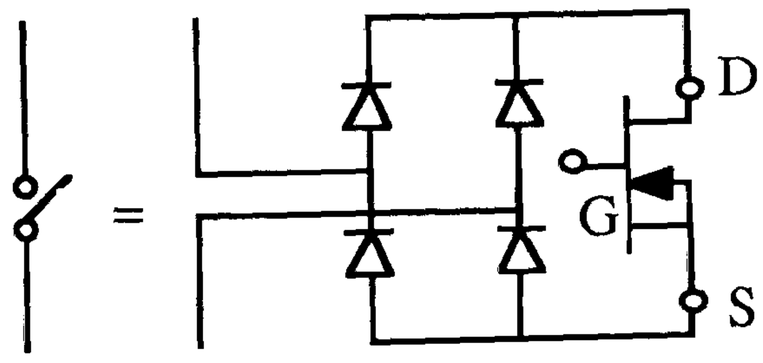

(b)

Fig. 4-8 single-phase cycloconverter circuit configuration :

(a) for conventional modulation technique

(b) for proposed modulation stategy

In fig. 4-8 , the (single-phase) -to- (single-phase) cycloconverter configurations are:

(a) with centre tapped transformer and unidirectional switching devices (with conventional modulation technique) .

(b) bridge connection with bidirectional switches and full voltage utilization (with proposed modulation strategy).

The principle of operation of the single phase -to- single phase cycloconverter[13] can be explained with the help of Fig. 4 - 8 (a) & (b) . The two phase controlled converter (positive and negative groups) are operated as bridge rectifiers . Their delay angles are such that the output voltage of positive group is equal and opposite to the negative group . For satisfying this requirement , as indicated in section 4 - 2 , if α_p is the delay angle of positive group , then the delay angle of negative group should be :

$$\alpha_n = 180^\circ - \alpha_p \qquad (4-61)$$

consequently the average output voltage of the positive converter is equal and opposite of the negative converter (output is alternative with any frequency of $f_o < f_i$) .

In cycloconverter operation with continuously variable output frequency and increasing capability of cycloconverter to produce sinusoidal output voltage (to reduce torque pulsation in AC drives) any effort should be taken in to effect . Since in all cases the output voltage waveform is necessarily made up of segments of the source voltage waveforms (Fig. 4-9(d)), so it is possible to arrange that these segments such as to contain the minimum output voltage (**proposed strategy**) , or input current harmonics . Here , two different strategies for cycloconverter control are presented .

4.10.1 Conventional modulation strategy for sinusoidal cycloconverter

This modulation strategy which is based on cosine wave crossing method [2 , 13] is applied for determining the timing of the firing pulses for cycloconverter switches . Referring to Fig. 4-9 (a) and assuming :

$$v_{AN} = V_m \mathrm{Sin}(\omega_i t) \qquad (4-62)$$

$$u_{AN} = \frac{2}{\pi}.V_m \mathrm{Cos}(\omega_i t) \qquad (4-63)$$

$$v_{BN} = V_m \mathrm{Sin}(\omega_i t - \pi) = -V_m \mathrm{Sin}(\omega_i t) \qquad (4-64)$$

$$u_{BN} = -(\frac{2}{\pi}).\mathrm{Cos}(\omega_i t) \qquad (4-65)$$

$$v_o = M.V_m \mathrm{Sin}(\omega_o t) = MV_m \mathrm{Sin}\frac{1}{R}(\omega_i t) \qquad (4-66)$$

Where :

v_o is the cycloconverter output voltage

M is the depth of modulation for out-put voltage and $0.0 \leq M < 2/\pi$

$$\omega_o = 2.\pi.f_o \qquad (4-67)$$

f_o is the cycloconverter output frequency

$R = \frac{f_i}{f_o}$ is the input /output frequency ratio

A few cycles of the anti-phase sinusoidal source voltages v_{AN} and v_{BN} and also u_{AN}, u_{BN}, and v_o are shown in Fig. 4 - 9 .

The firing angles are determined so that the average out-put voltage , produced across the load by the conducting switch , is equal to the instantaneous value of the required out-put voltage at the firing instant .

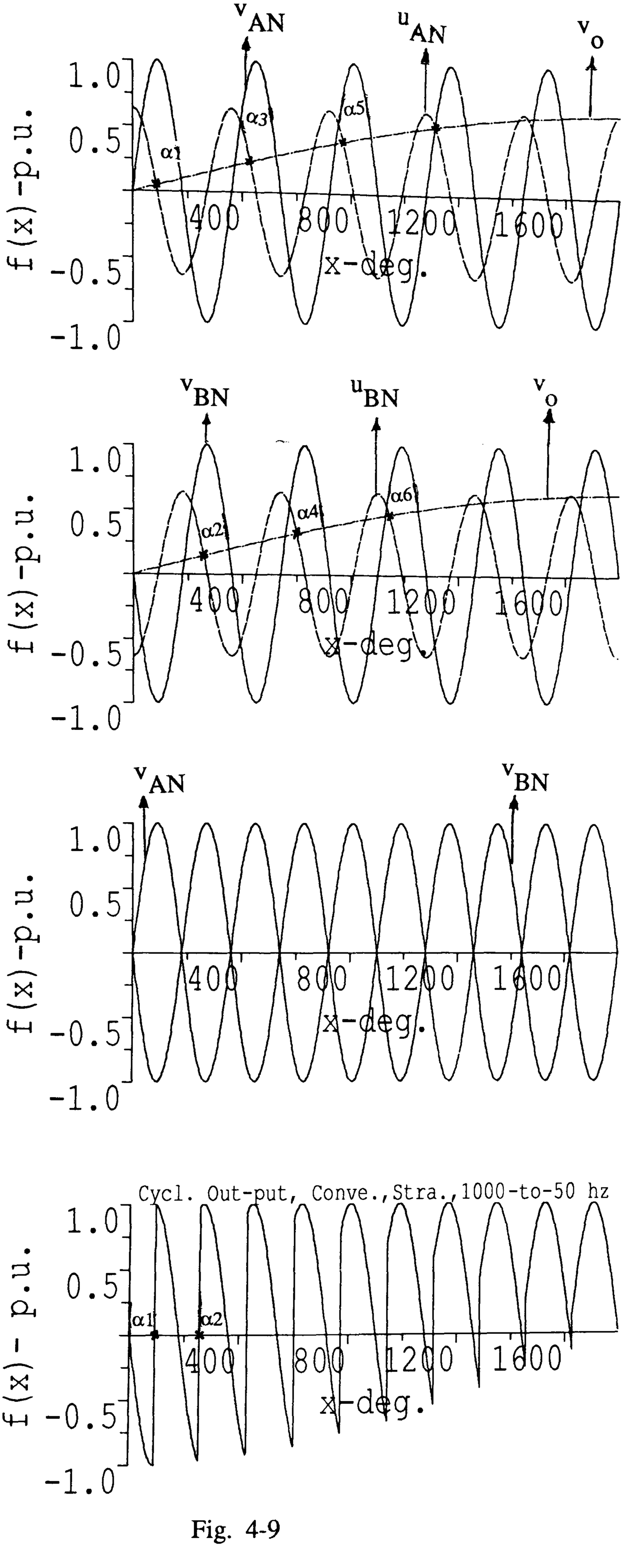
v_{AN}
u_{AN}
v_o
1.0
0.5
-0.5
-1.0
f(x)-p.u.
α1
α3
α5
400
800
1200
1600
x-deg.
(a)
v_{BN}
u_{BN}
v_o
α2
α4
α6
(b)
v_{AN}
v_{BN}
(c)
Cycl. Out-put, Conve.,Stra.,1000-to-50 hz
f(x)- p.u.
(d)

Fig. 4-9

From Fig. 4 - 10 (a) , for firing angle α , the average value of the out-put is

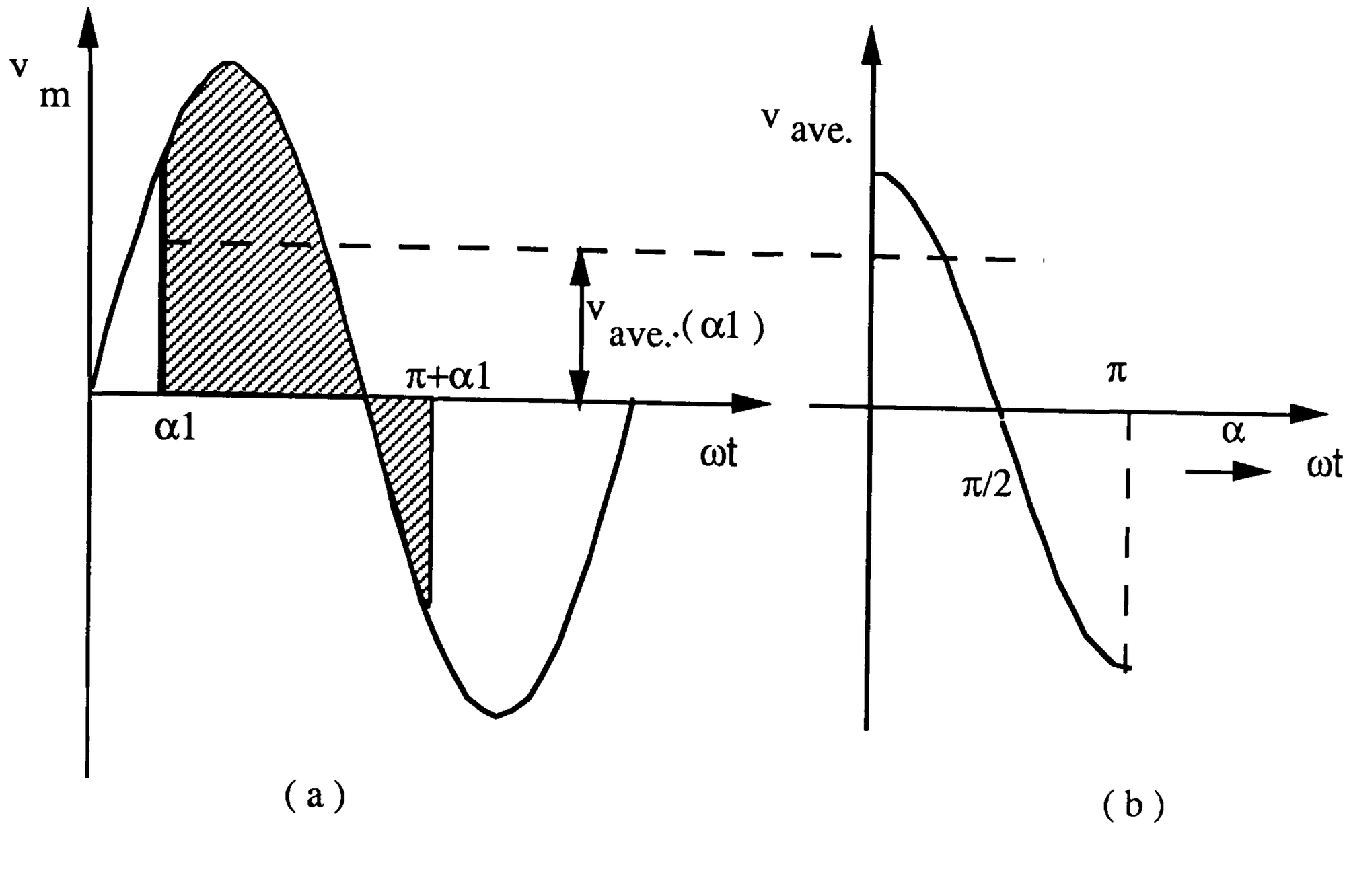

Fig. 4-10 (a) firing delay angle (b) average out-put voltage

$$v_{ave.} = \frac{1}{\pi}\int_{\alpha}^{\pi+\alpha} V_m \mathrm{Sin}(\omega_i t).d(\omega_i t) = \frac{2}{\pi}.V_m \mathrm{Cos}(\alpha) \quad , \quad \alpha=\omega_i t = 2\pi f_i t \qquad (4 - 68)$$

therefore :

$$\frac{2}{\pi}.V_m.\mathrm{Cos}(\alpha) = M.V_m.\mathrm{Sin}(\frac{\alpha}{R}) \qquad (4 - 69)$$

(4 - 69) implies that the intersection points of a sinusoidal reference voltage , $M.\mathrm{Sin}(\frac{1}{R}\omega_i t)$, with a series of cosine timing waves are the required switching points of the MOSFETs . The cosine timing waves are derived from , and synchronized to the AC input voltage (4-63) , (4-65) , and it's phase is such that it's peak occurs at the earliest possible commutation angle ($\alpha = 0$) of the associated MOSFET.

In Fig. 4 - 9 the switching points for a few cycles have been identified . Switch S1 of positive group is triggered at $\alpha 1$, $\alpha 3$, $\alpha 5$, ..when v_{AN} is positive and switch S_2 of positive group is triggered at $\alpha 2$, $\alpha 4$, $\alpha 6$, ..when v_{BN} is positive . The resulting output modulated voltage wave form of the positive group $v_{o\text{-}p}$ is also shown in Fig. 4 - 9 (d) .

In a similar way , the next half of output modulated voltage wave form of the negative group can be sketched . More details are given in [2 & 13] . It should be noted that in Fig. 4 - 9 the current is positive and continuous .

The theoretical results of switching angles (table 4-1) and modulated output voltage and its harmonic spectrum are presented in Fig.s 11 , 12 , 13 for this modulation strategy(**4.10.1**) with $\mathbf{f_i = 1\ kHz}$, $\mathbf{f_o = 50\ Hz}$, **R = 20** , and **M=0.63** .

Table 4-1

Stage	OFF(deg.)	ON(deg.)	ON + OFF
1	94.7997	85.2003	180.0
2	77.1970	102.803	180.0
3	68.6080	111.392	180.0
4	60.0180	119.982	180.0
5	51.4290	128.571	180.0
6	42.8390	137.161	180.0
7	34.2200	145.780	180.0
8	25.5800	154.420	180.0
9	16.9399	163.060	180.0
10	8.09998	171.900	180.0
11	3.05005	176.950	180.0
12	9.41003	170.590	180.0
13	18.7600	161.240	180.0
14	28.5200	151.480	180.0
15	37.8701	142.130	180.0
16	47.4199	132.580	180.0
17	56.9800	123.020	180.0
18	66.3301	113.670	180.0
19	75.8799	104.120	180.0
20	94.4399	85.5601	180.0
21	94.7900	85.2100	180.0
22	77.1899	102.810	180.0
23	68.7100	111.290	180.0
24	60.2002	119.800	180.0
25	51.5601	128.440	180.0
26	42.9302	137.070	180.0
27	34.5000	145.500	180.0
28	25.8599	154.140	180.0
29	16.2002	163.800	180.0
30	8.39990	171.600	180.0
31	3.16992	176.830	180.0
32	9.14990	170.850	180.0
33	18.9399	161.060	180.0
34	28.5200	151.480	180.0
35	38.1099	141.890	180.0
36	47.4902	132.510	180.0
37	57.0801	122.920	180.0
38	66.4600	113.540	180.0
39	76.0498	103.950	180.0
40	94.4399	85.5601	180.0

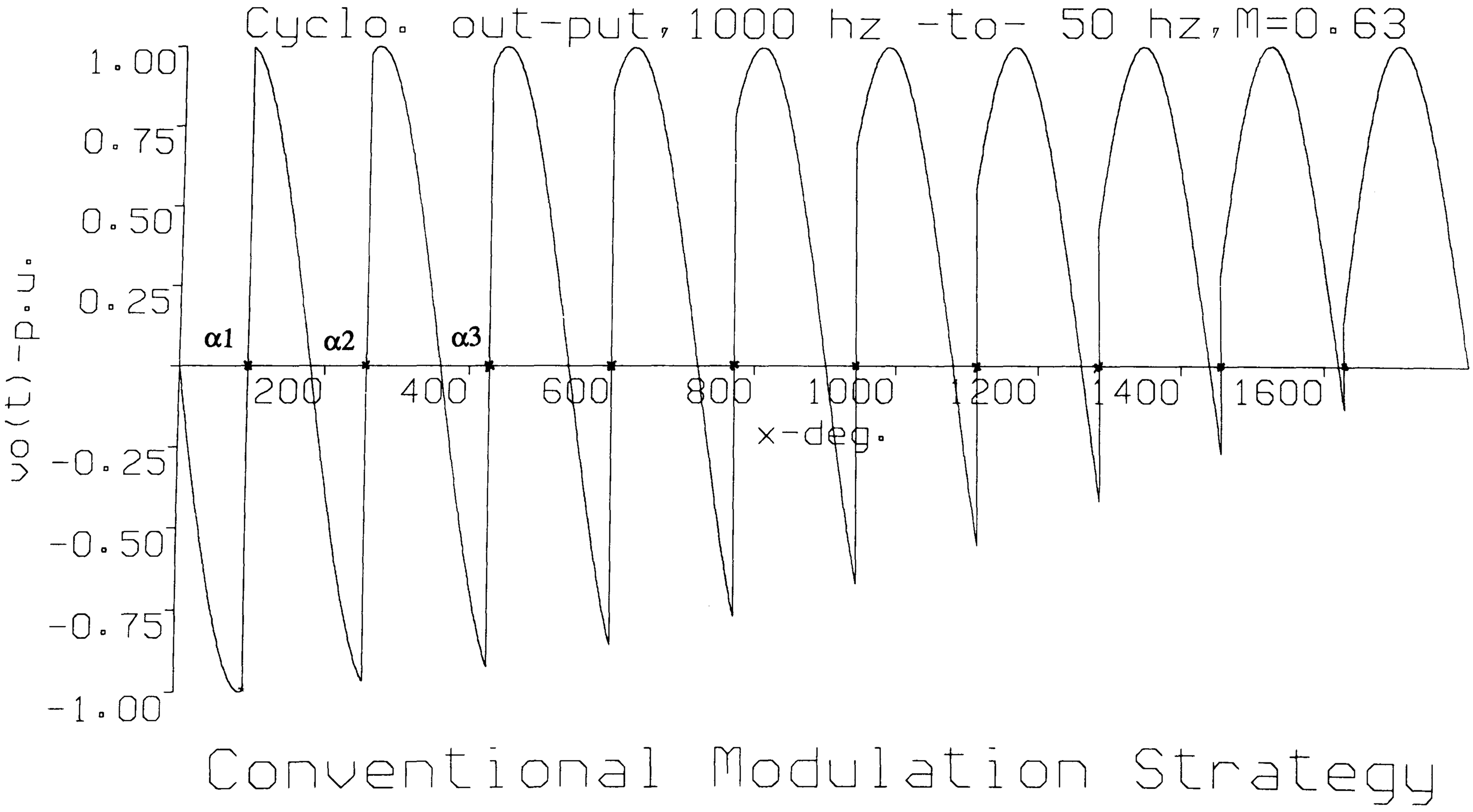
Cyclo. out-put, 1000 hz -to- 50 hz, M=0.63
1.00
0.75
0.50
0.25
-0.25
-0.50
-0.75
-1.00
vo(t)-p.u.
α1
α2
α3
200
400
600
800
1000
1200
1400
1600
x-deg.
Conventional Modulation Strategy

Fig. 4-11

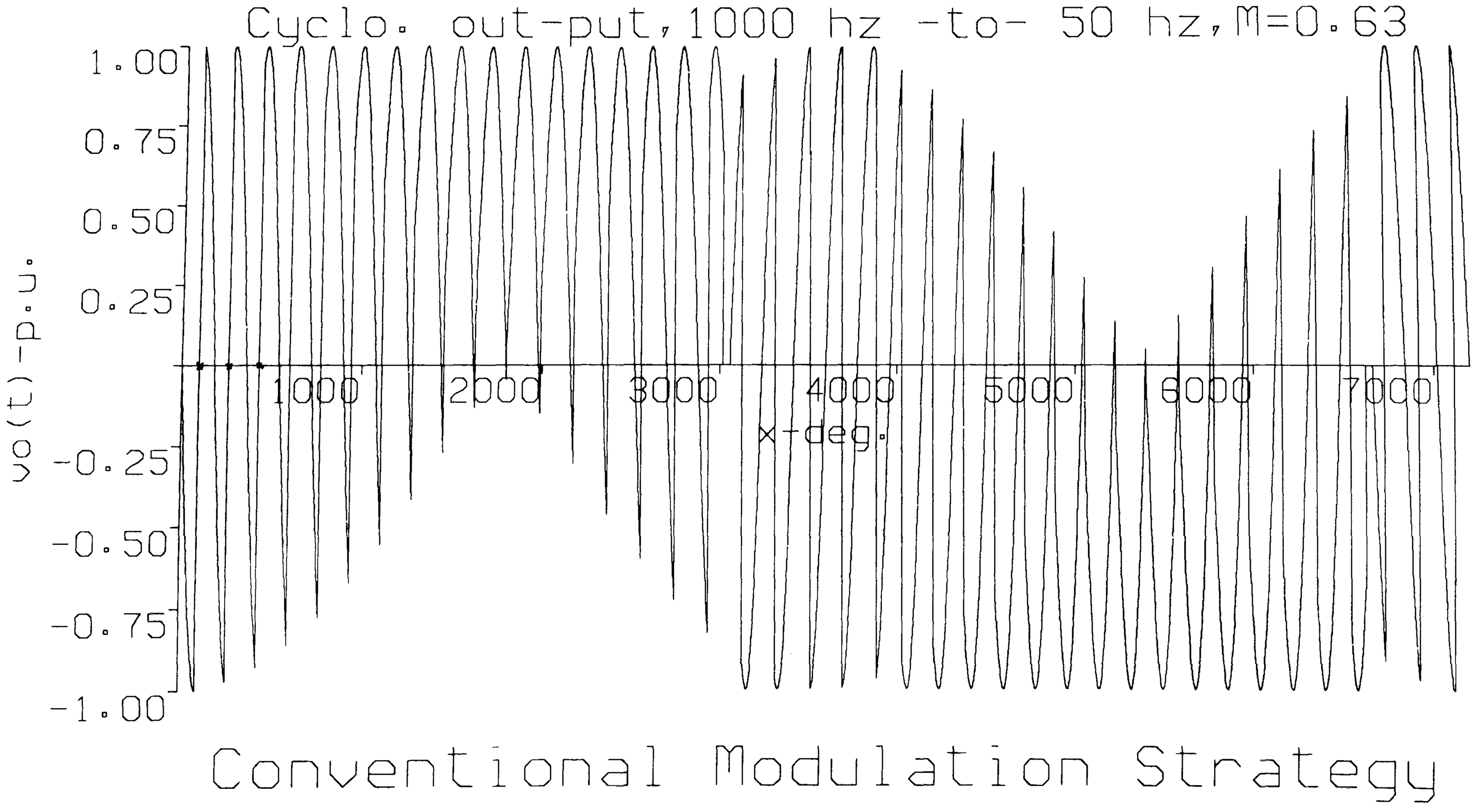
Cyclo. out-put,1000 hz -to- 50 hz,M=0.63
1.00
0.75
0.50
0.25
-0.25
-0.50
-0.75
-1.00
vo(t)-p.u.
1000
2000
3000
4000
5000
6000
7000
x-deg.
Conventional Modulation Strategy

Fig. 4-12

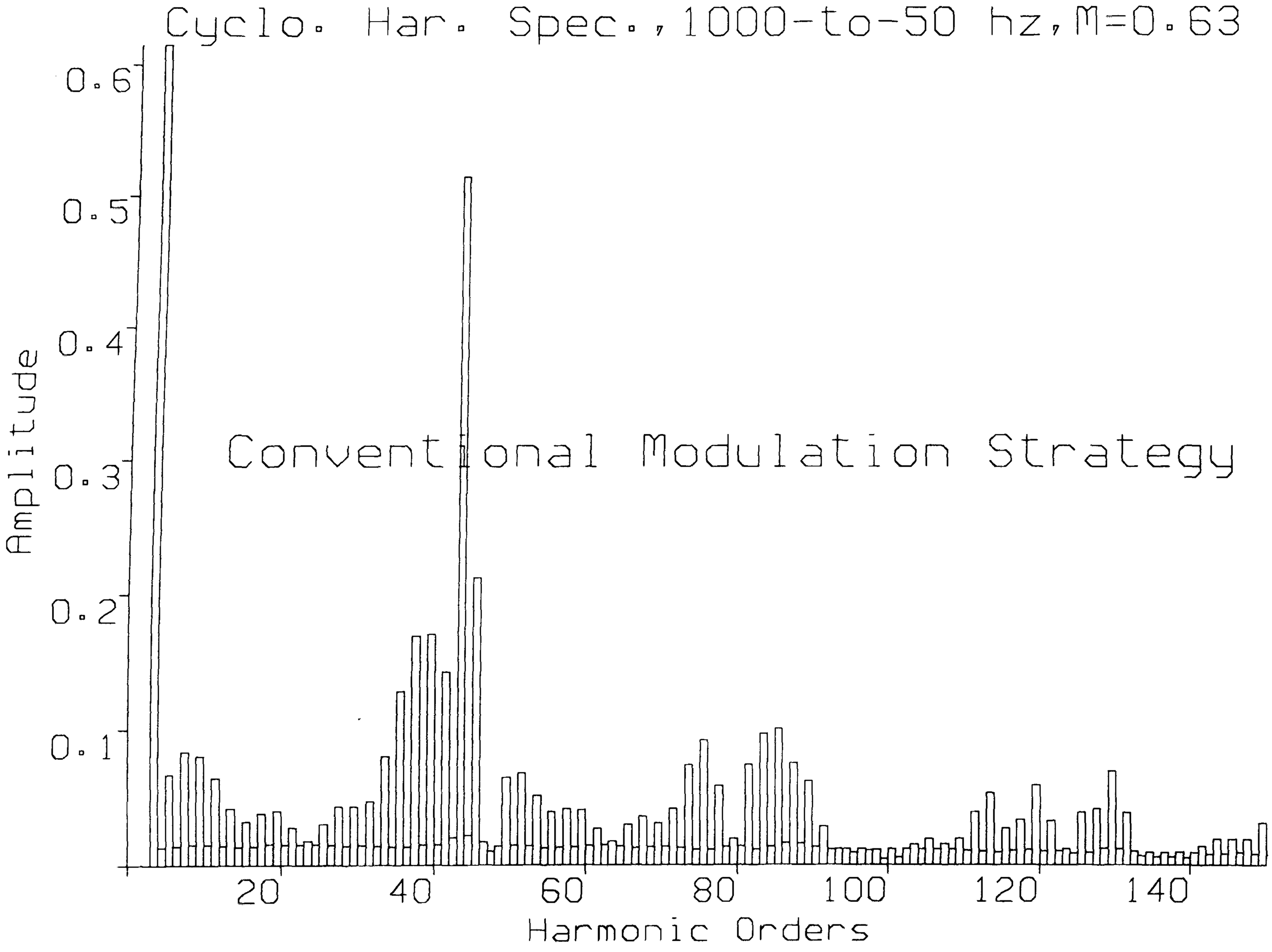
Cyclo. Har. Spec.,1000-to-50 hz,M=0.63
Conventional Modulation Strategy
Amplitude
0.6
0.5
0.4
0.3
0.2
0.1
20
40
60
80
100
120
140
Harmonic Orders

Fig. 4-13

4.11 proposed modulation strategy for sinusoidal cycloconverter

This strategy is based on the" **equal area criterion** " . Referring to Fig. 4 - 8(b) , in Fig. 4-14 the two dotted and hatched areas are equated :

4.11.1- equivalent hatched area is built symmetrically on the both sides of 90° line .

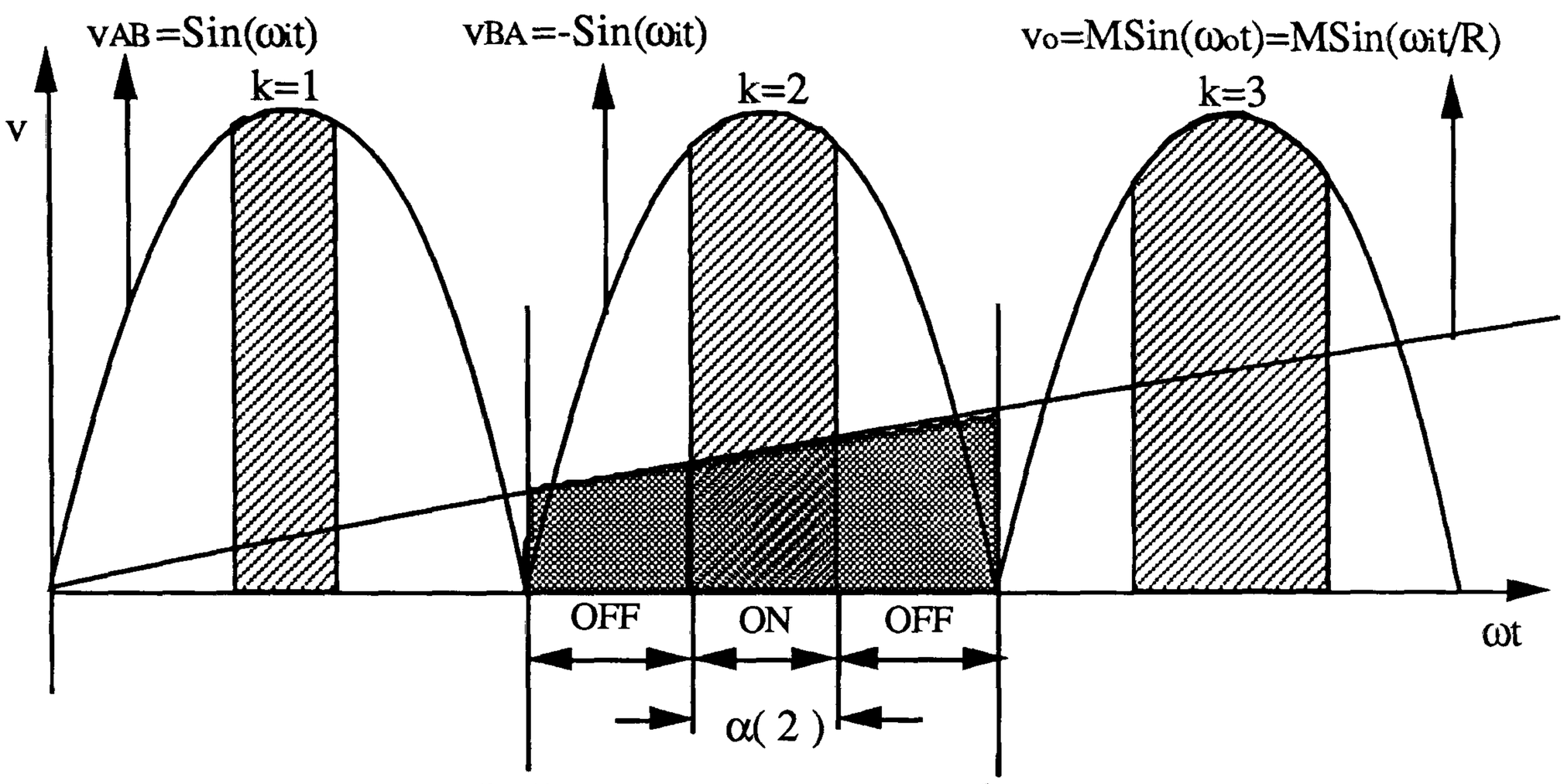

Fig. 4-14 equivalent hatched area is built symmetrically around the 90° line

$$t = \frac{T_o}{2R\pi} = \frac{\frac{1}{f_o}}{2R\pi} = \frac{\frac{R}{f}}{2R\pi} = \frac{R}{2R\pi f_i} = \frac{1}{\omega_i}\ \frac{\text{sec}}{\text{rad}} \quad \text{(time unit for X axis)} \qquad (4-70)$$

$$A_{dot.} = \int_{\frac{(k-1)\pi}{\omega_i}}^{\frac{k\pi}{\omega_i}} MSin(\omega_o t)dt = \frac{M}{\omega_o}\left\{ -Cos\left[\omega_o\left(\frac{k\pi}{\omega_i}\right)\right] + Cos\left[\omega_o\left(\frac{k-1}{\omega_i}\right)\pi\right]\right\} \qquad (4-71)$$

or :

$$A_{dot.} = = \frac{M}{\omega_o}\left[\text{Cos}(k\text{-}1)\frac{\pi}{R} - \text{Cos}(k\frac{\pi}{R})\right] \qquad (4\text{-}72)$$

and :

$$A_{hatch.} = \int_{\frac{(k-1)\pi + \frac{\pi}{2} - \frac{\alpha}{2}}{\omega_i}}^{\frac{(k-1)\pi + \frac{\pi}{2} + \frac{\alpha}{2}}{\omega_i}} \text{Sin}(R\omega_o t)dt =$$

$$= \frac{1}{R\omega_o}\left\{ - \text{Cos } R\omega_o\left[\frac{(k-1)\pi + \frac{\pi}{2} + \frac{\alpha}{2}}{\omega_i}\right] + \text{Cos } R\omega_o\left[\frac{(k-1)\pi + \frac{\pi}{2} - \frac{\alpha}{2}}{\omega_i}\right]\right\} \qquad (4\text{-}73)$$

or :

$$A_{hatch.} = \frac{1}{R\omega_o}\left\{ \text{Cos}\left[(k\text{-}0.5)\pi - \frac{\alpha}{2}\right] - \text{Cos}\left[(k\text{-}0.5)\pi + \frac{\alpha}{2}\right]\right\} \qquad (4\text{-}74)$$

Since :

$$\text{Cos}(Q) - \text{Cos}(P) = 2\text{Sin}(\frac{P+Q}{2})\text{Sin}(\frac{P-Q}{2}) \qquad (4\text{-}75)$$

then :

$$A_{hatch.} = \frac{2}{R\omega_o}\text{Sin}(k\text{-}0.5)\pi.\text{Sin}(\frac{\alpha}{2}) \qquad (4\text{-}76)$$

by equating (4 - 72) with (4 - 76) yields :

$$A_{\text{dot .}} = A_{\text{hatch.}} \qquad (4 - 77)$$

$$\frac{M}{\omega_o}\left[\text{Cos}\,(k-1)\frac{\pi}{R} - \text{Cos}\,k\frac{\pi}{R}\right] = \frac{2}{R\omega_o}\,\text{Sin}\,(k-\frac{1}{2})\,\pi\,\text{Sin}\frac{\alpha}{2} \qquad (4-78)$$

The amount of $\alpha(k)$ can be determined :

$$\alpha(k) = 2\,\text{Sin}^{-1}\left[\frac{RM\left[\text{Cos}\,(k-1)\frac{\pi}{2} - \text{Cos}k\frac{\pi}{2}\right]}{2\,(-1)^{k+1}\,\text{Sin}\,(k-\frac{1}{2})\pi}\right]\cdot\frac{180^\circ}{\pi} \qquad (4-79)$$

$$k = 1\,,\,2\,,\,3\,,\,\ldots\ldots\,,\,2R$$
$$M = 0.0\,,\,\ldots\ldots\,,\,0.636$$

For $\mathbf{f_i = 1\ kHz}$, $\mathbf{f_o = 50\ Hz}$, $\mathbf{R = 20}$ and $\mathbf{M = 0.63}$ the **OFF** and **ON** $= \alpha(k)$ durations for this mode are given in table 4-2 . The simulation of cycloconverter modulated output voltage is presented in Fig.4-15 and modulated output voltage harmonic spectrum is shown in Fig. 4-16 .

Table 4-2

Stage	OFF (deg.)	ON (deg.)	OFF (deg.)	ON + OFF
1	85.5090	8.98199	85.5090	180.0
2	76.5275	26.9449	76.5275	180.0
3	67.5475	44.9051	67.5275	180.0
4	58.5702	62.8596	58.5702	180.0
5	49.5978	80.8044	49.5978	180.0
6	40.6340	98.7319	40.6340	180.0
7	31.6865	116.627	31.6865	180.0
8	22.7751	134.450	22.7751	180.0
9	13.9694	152.061	13.9694	180.0
10	5.77566	168.449	5.77566	180.0
11	5.77566	168.449	5.77566	180.0
12	13.9694	152.061	13.9694	180.0
13	22.7751	134.450	22.7751	180.0
14	31.6865	116.627	31.6865	180.0
15	40.6340	98.7319	40.6340	180.0
16	49.5978	80.8044	49.5978	180.0
17	58.5702	62.8596	58.5702	180.0
18	67.5475	44.9051	67.5275	180.0
19	76.5275	26.9449	76.5275	180.0
20	85.5090	8.98199	85.5090	180.0
21	85.5090	8.98199	85.5090	180.0
22	76.5275	26.9449	76.5275	180.0
23	67.5475	44.9051	67.5275	180.0
24	58.5702	62.8596	58.5702	180.0
25	49.5978	80.8044	49.5978	180.0
26	40.6340	98.7319	40.6340	180.0
27	31.6865	116.627	31.6865	180.0
28	22.7751	134.450	22.7751	180.0
29	13.9694	152.061	13.9694	180.0
30	5.77566	168.449	5.77566	180.0
31	5.77566	168.449	5.77566	180.0
32	13.9694	152.061	13.9694	180.0
33	22.7751	134.450	22.7751	180.0
34	31.6865	116.627	31.6865	180.0
35	40.6340	98.7319	40.6340	180.0
36	49.5978	80.8044	49.5978	180.0
37	58.5702	62.8596	58.5702	180.0
38	67.5475	44.9051	67.5275	180.0
39	76.5275	26.9449	76.5275	180.0
40	85.5090	8.98199	85.5090	180.0

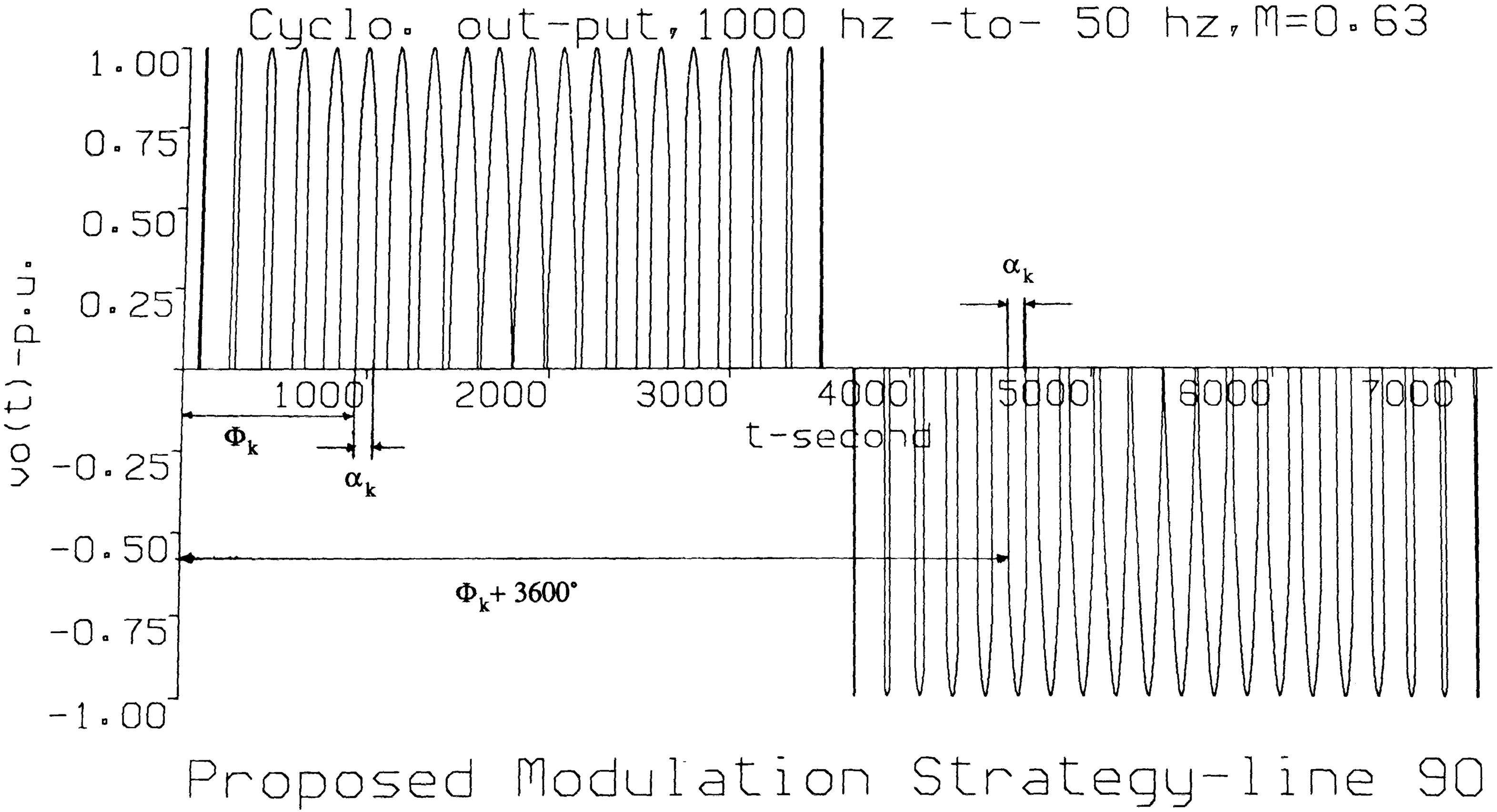
Cyclo. out-put, 1000 hz -to- 50 hz, M=0.63
1.00
0.75
0.50
0.25
-0.25
-0.50
-0.75
-1.00
vo(t) -p.u.
1000
2000
3000
4000
5000
6000
7000
t-second
α_k
Φ_k
α_k
Φ_k+ 3600°
Proposed Modulation Strategy-line 90

Fig. 4-15

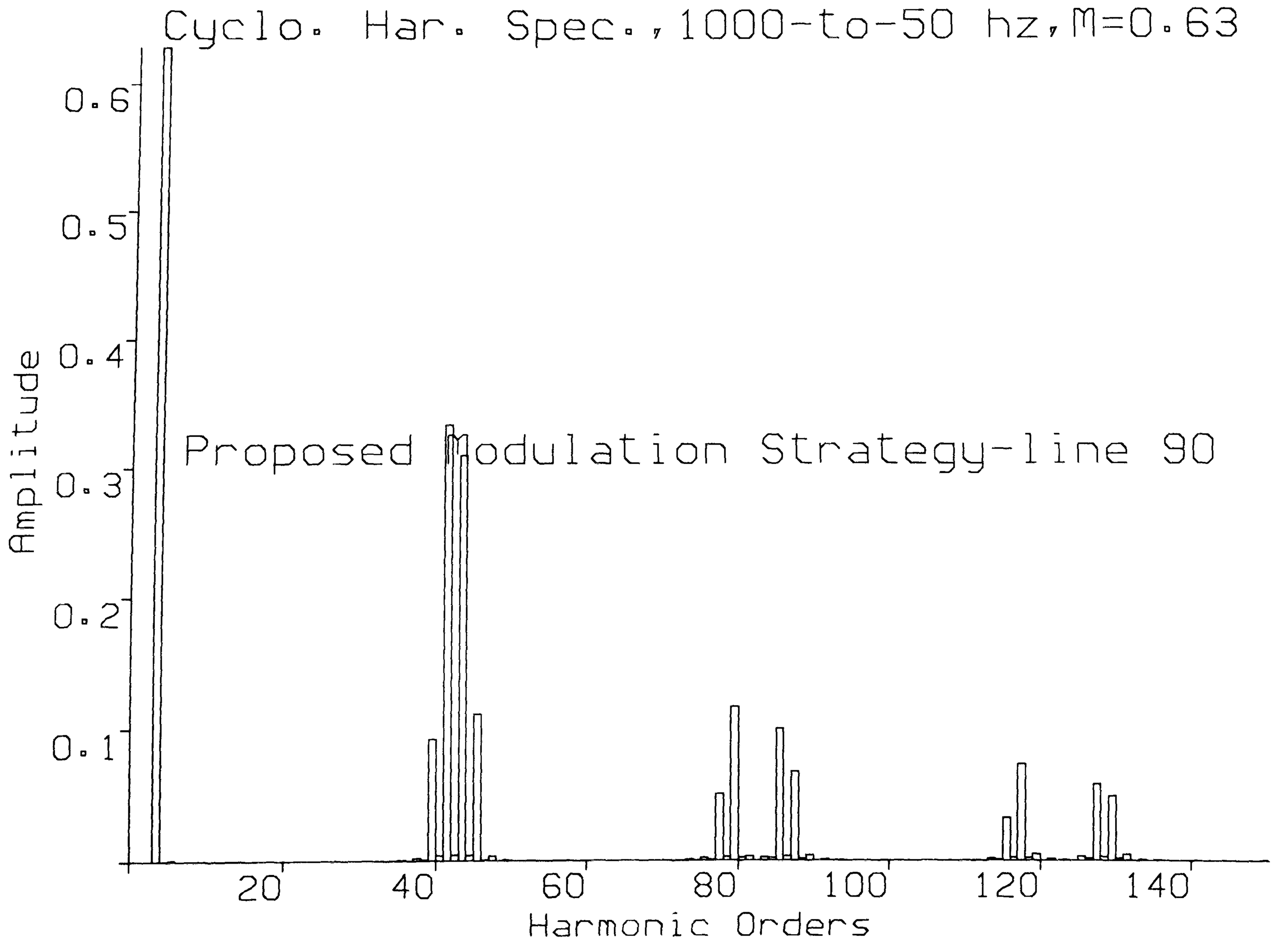
Cyclo. Har. Spec.,1000-to-50 hz,M=0.63
Proposed Modulation Strategy-line 90
Amplitude
0.6
0.5
0.4
0.3
0.2
0.1
20
40
60
80
100
120
140
Harmonic Orders

Fig. 4-16

4.11.2 The equivalent areas are built equally around the 45° and 135° lines as shown in Fig.4-17 .

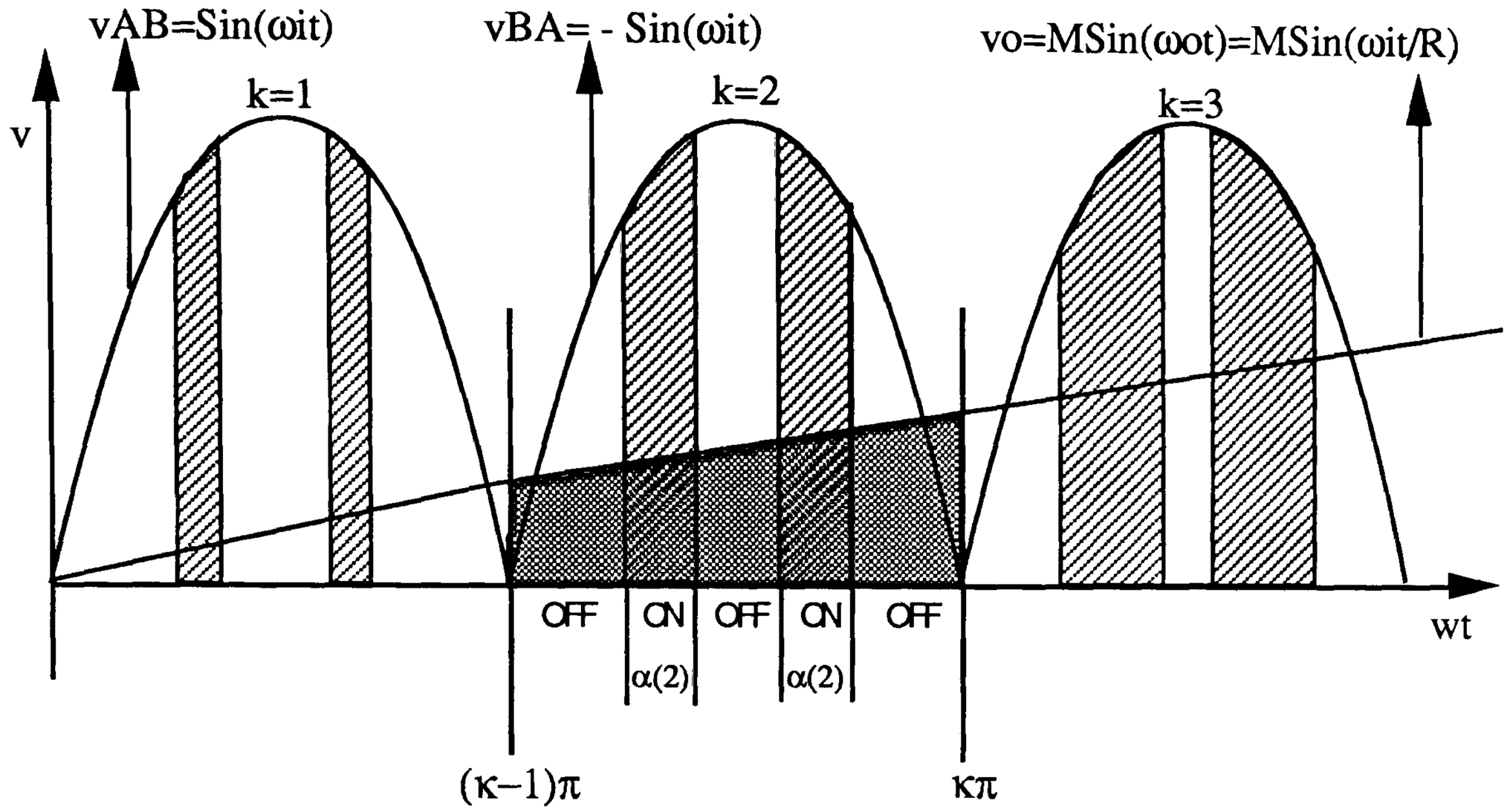

Fig. 4-17 dotted area = Σ hatched areas

By equating the dotted area with the sum of the two hatched areas the following expression for ON durations can be derived :

$$\alpha(k) = 2\,\mathrm{Sin}^{-1}\left[\frac{RM\left[\mathrm{Cos}\,(k-1)\frac{\pi}{R} - \mathrm{Cos}\,k\frac{\pi}{R}\right]}{2\sqrt{2}\,\mathrm{Sin}\,(k-\frac{1}{2})\pi}\right]\cdot\frac{180^\circ}{\pi} \qquad (4-80)$$

$k = 1\ ,\ 2\ ,\ 3\ ,\ .....\ ,\ 2R$

$M = 0.0\ ,\ .....\ ,\ 0.63$

Table 4-3 presents the **ON** = $\alpha(\mathbf{k})$ and **OFF** durations and Fig. 4-18 shows the modulated output voltage harmonic spectrum .

Table 4-3

Stage	OFF	ON	OFF	ON	OFF	ON+OFF
1	41.8560	6.28803	83.7120	6.28803	41.8560	180.0
2	35.6081	18.7838	71.2162	18.7838	35.6081	180.0
3	29.4839	31.0322	58.9678	31.0322	29.4839	180.0
4	23.5773	42.8453	47.1547	42.8453	23.5773	180.0
5	18.0002	53.9996	36.0004	53.9996	18.0002	180.0
6	12.8897	64.2205	25.7795	64.2205	12.8897	180.0
7	8.41423	73.1715	16.8285	73.1715	8.41423	180.0
8	4.77250	80.4550	9.54500	80.4550	4.77250	180.0
9	2.17818	85.6436	4.35635	85.6436	2.17818	180.0
10	0.82273	88.3545	1.64546	88.3545	0.82273	180.0
11	0.82273	88.3545	1.64546	88.3545	0.82273	180.0
12	2.17818	85.6436	4.35635	85.6436	2.17818	180.0
13	4.77250	80.4550	9.54500	80.4550	4.77250	180.0
14	8.41423	73.1715	16.8285	73.1715	8.41423	180.0
15	12.8897	64.2205	25.7795	64.2205	12.8897	180.0
16	18.0002	53.9996	36.0004	53.9996	18.0002	180.0
17	23.5773	42.8453	47.1547	42.8453	23.5773	180.0
18	29.4839	31.0322	58.9678	31.0322	29.4839	180.0
19	35.6081	18.7838	71.2162	18.7838	35.6081	180.0
20	41.8560	6.28803	83.7120	6.28803	41.8560	180.0
21	41.8560	6.28803	83.7120	6.28803	41.8560	180.0
22	35.6081	18.7838	71.2162	18.7838	35.6081	180.0
23	29.4839	31.0322	58.9678	31.0322	29.4839	180.0
24	23.5773	42.8453	47.1547	42.8453	23.5773	180.0
25	18.0002	53.9996	36.0004	53.9996	18.0002	180.0
26	12.8897	64.2205	25.7795	64.2205	12.8897	180.0
27	8.41423	73.1715	16.8285	73.1715	8.41423	180.0
28	4.77250	80.4550	9.54500	80.4550	4.77250	180.0
29	2.17818	85.6436	4.35635	85.6436	2.17818	180.0
30	0.82273	88.3545	1.64546	88.3545	0.82273	180.0
31	0.82273	88.3545	1.64546	88.3545	0.82273	180.0
32	2.17818	85.6436	4.35635	85.6436	2.17818	180.0
33	4.77250	80.4550	9.54500	80.4550	4.77250	180.0
34	8.41423	73.1715	16.8285	73.1715	8.41423	180.0
35	12.8897	64.2205	25.7795	64.2205	12.8897	180.0
36	18.0002	53.9996	36.0004	53.9996	18.0002	180.0
37	23.5773	42.8453	47.1547	42.8453	23.5773	180.0
38	29.4839	31.0322	58.9678	31.0322	29.4839	180.0
39	35.6081	18.7838	71.2162	18.7838	35.6081	180.0
40	41.8560	6.28803	83.7120	6.28803	41.8560	180.0

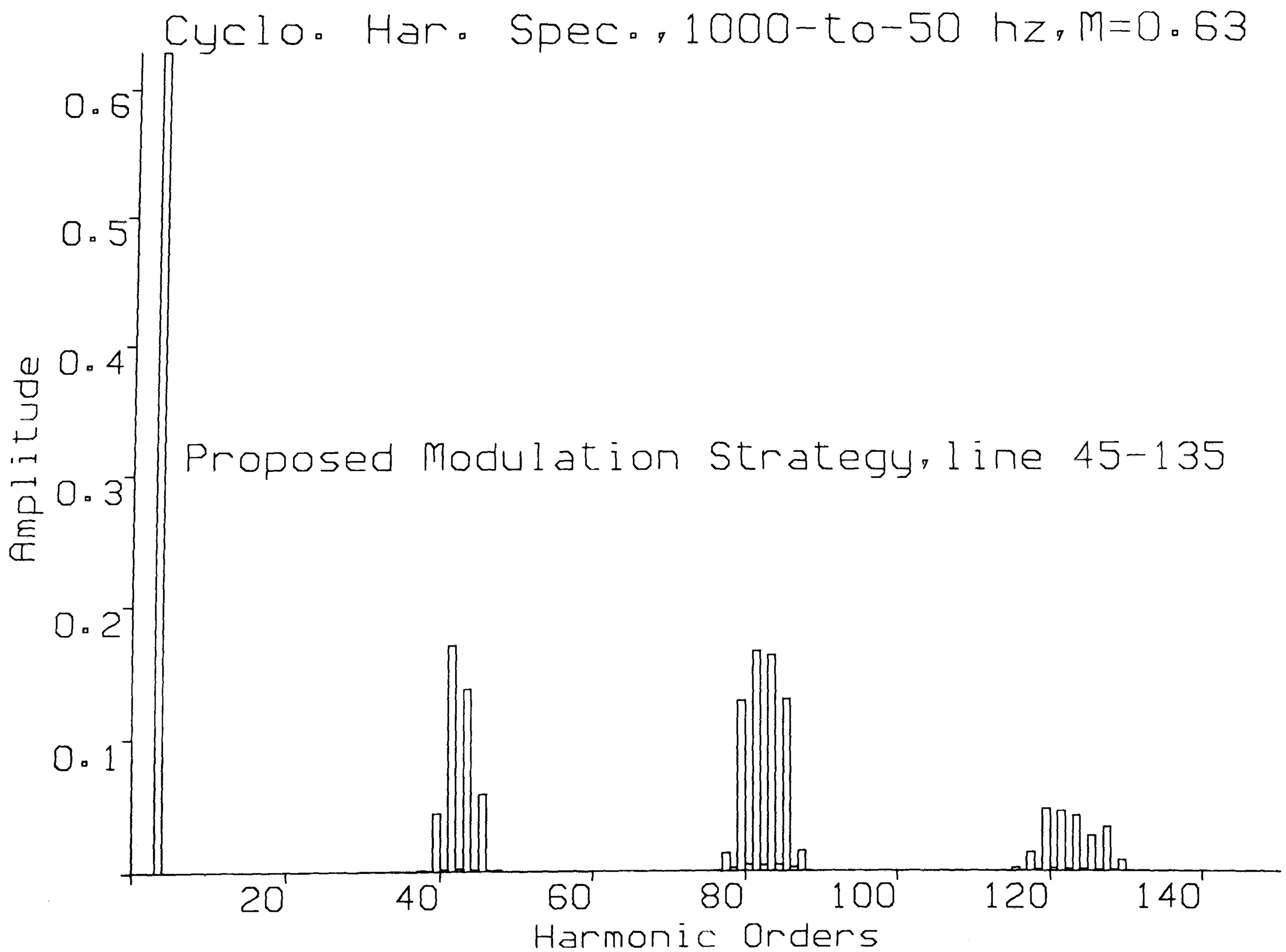
Cyclo. Har. Spec.,1000-to-50 hz,M=0.63
Proposed Modulation Strategy,line 45-135
Amplitude
0.6
0.5
0.4
0.3
0.2
0.1
20
40
60
80
100
120
140
Harmonic Orders

Fig. 4-18

4.11.3 The equivalent areas are built equally around the 45° , 90° and 135° lines as shown in Fig.4-19 .

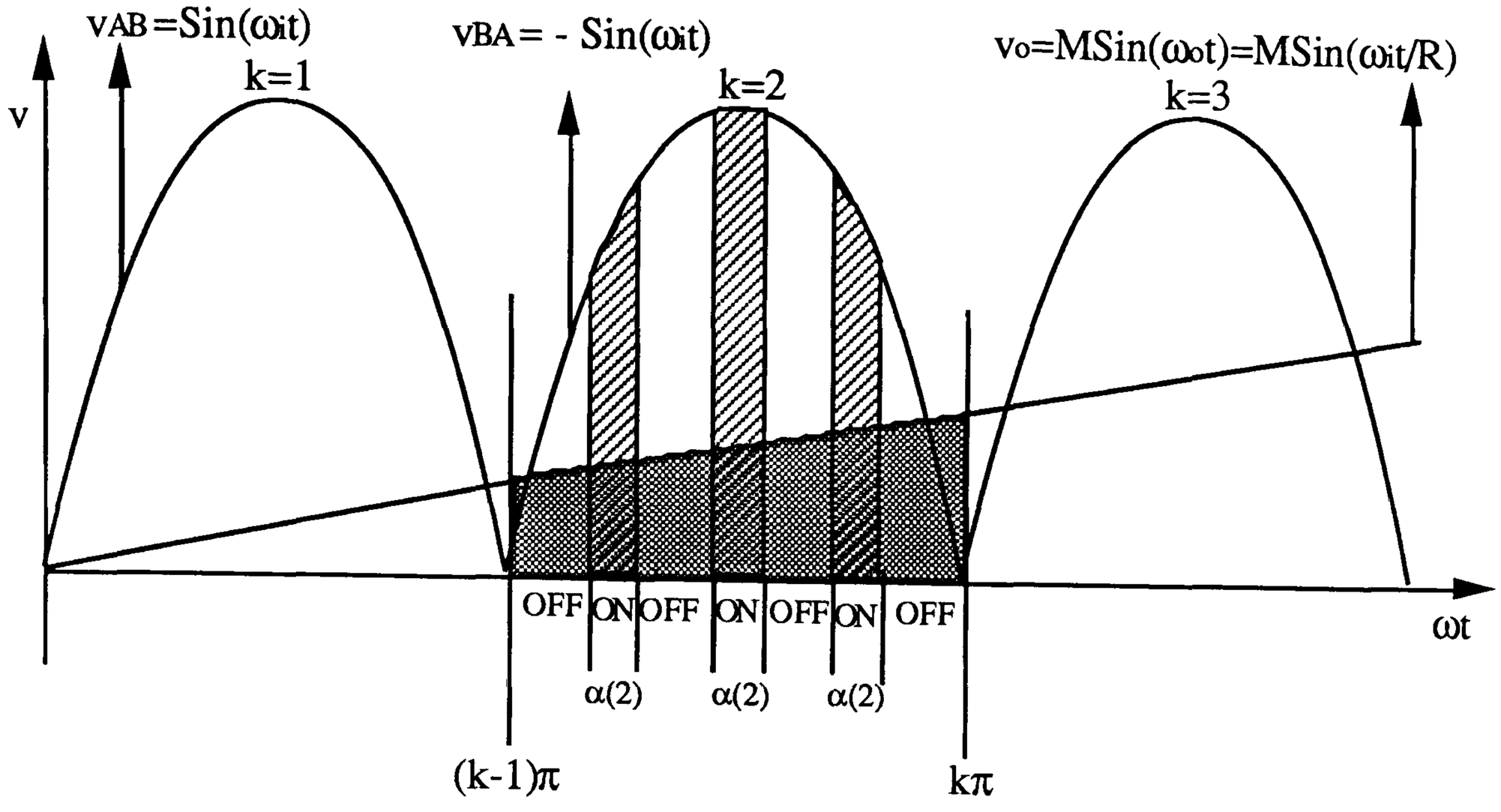

Fig. 4- 19 dotted area = Σ hatched areas

By equating the dotted area with the sum of the three hatched areas the ON durations , α (**k**) , is determined from :

$$\alpha(\mathbf{k}) = 2\,\mathrm{Sin}^{-1}\left[\frac{RM\left[\mathrm{Cos}\,(k-1)\frac{\pi}{R} - \mathrm{Cos}\,k\frac{\pi}{R}\right]}{2\,(\sqrt{2}+1)\,\mathrm{Sin}\,(k-\frac{1}{2})^{\pi}}\right].\frac{180^{\circ}}{\pi} \qquad (4-81)$$

$k = 1 , 2, 3 , ... , 2R$

$R = \frac{f_i}{f_o}$

$M = 0.0 , ... , 0.63$

Table 4-4 gives the ON durations and Fig. 4-20 shows the harmonic component spectrum for this mode .

Table 4-4

Stage	OFF	ON	OFF	ON	OFF	ON	OFF	ON+OFF
1	43.305	3.3899	41.610	3.3899	41.610	3.3899	43.30	180.0
2	39.951	10.097	34.902	10.097	34.902	10.097	39.951	180.0
3	36.705	16.589	28.410	16.589	28.410	16.589	36.705	180.0
4	33.639	22.720	22.279	22.720	22.279	22.720	33.639	180.0
5	30.828	28.344	16.656	28.344	16.656	28.344	30.828	180.0
6	28.341	33.316	11.683	33.316	11.683	33.316	28.828	180.0
7	26.250	37.499	7.5006	37.499	7.5006	37.499	26.250	180.0
8	24.617	40.765	4.2344	40.765	4.2344	40.765	24.617	180.0
9	23.495	43.008	1.9915	43.008	1.9915	43.008	23.495	180.0
10	22.924	44.150	0.8494	44.150	0.8494	44.150	22.924	180.0
11	22.924	44.150	0.8494	44.150	0.8494	44.150	22.924	180.0
12	23.495	43.008	1.9915	43.008	1.9915	43.008	23.495	180.0
13	24.617	40.765	4.2344	40.765	4.2344	40.765	24.617	180.0
14	26.250	37.499	7.5006	37.499	7.5006	37.499	26.250	180.0
15	28.341	33.316	11.683	33.316	11.683	33.316	28.828	180.0
16	30.828	28.344	16.656	28.344	16.656	28.344	30.828	180.0
17	33.639	22.720	22.279	22.720	22.279	22.720	33.639	180.0
18	36.705	16.589	28.410	16.589	28.410	16.589	36.705	180.0
19	39.951	10.097	34.902	10.097	34.902	10.097	39.951	180.0
20	43.305	3.3899	41.610	3.3899	41.610	3.3899	43.30	180.0
21	43.305	3.3899	41.610	3.3899	41.610	3.3899	43.30	180.0
22	39.951	10.097	34.902	10.097	34.902	10.097	39.951	180.0
23	36.705	16.589	28.410	16.589	28.410	16.589	36.705	180.0
24	33.639	22.720	22.279	22.720	22.279	22.720	33.639	180.0
25	30.828	28.344	16.656	28.344	16.656	28.344	30.828	180.0
26	28.341	33.316	11.683	33.316	11.683	33.316	28.828	180.0
27	26.250	37.499	7.5006	37.499	7.5006	37.499	26.250	180.0
28	24.617	40.765	4.2344	40.765	4.2344	40.765	24.617	180.0
29	23.495	43.008	1.9915	43.008	1.9915	43.008	23.495	180.0
30	22.924	44.150	0.8494	44.150	0.8494	44.150	22.924	180.0
31	22.924	44.150	0.8494	44.150	0.8494	44.150	22.924	180.0
32	23.495	43.008	1.9915	43.008	1.9915	43.008	23.495	180.0
33	24.617	40.765	4.2344	40.765	4.2344	40.765	24.617	180.0
34	26.250	37.499	7.5006	37.499	7.5006	37.499	26.250	180.0
35	28.341	33.316	11.683	33.316	11.683	33.316	28.828	180.0
36	30.828	28.344	16.656	28.344	16.656	28.344	30.828	180.0
37	33.639	22.720	22.279	22.720	22.279	22.720	33.639	180.0
38	36.705	16.589	28.410	16.589	28.410	16.589	36.705	180.0
39	39.951	10.097	34.902	10.097	34.902	10.097	39.951	180.0
40	43.305	3.3899	41.610	3.3899	41.610	3.3899	43.30	180.0

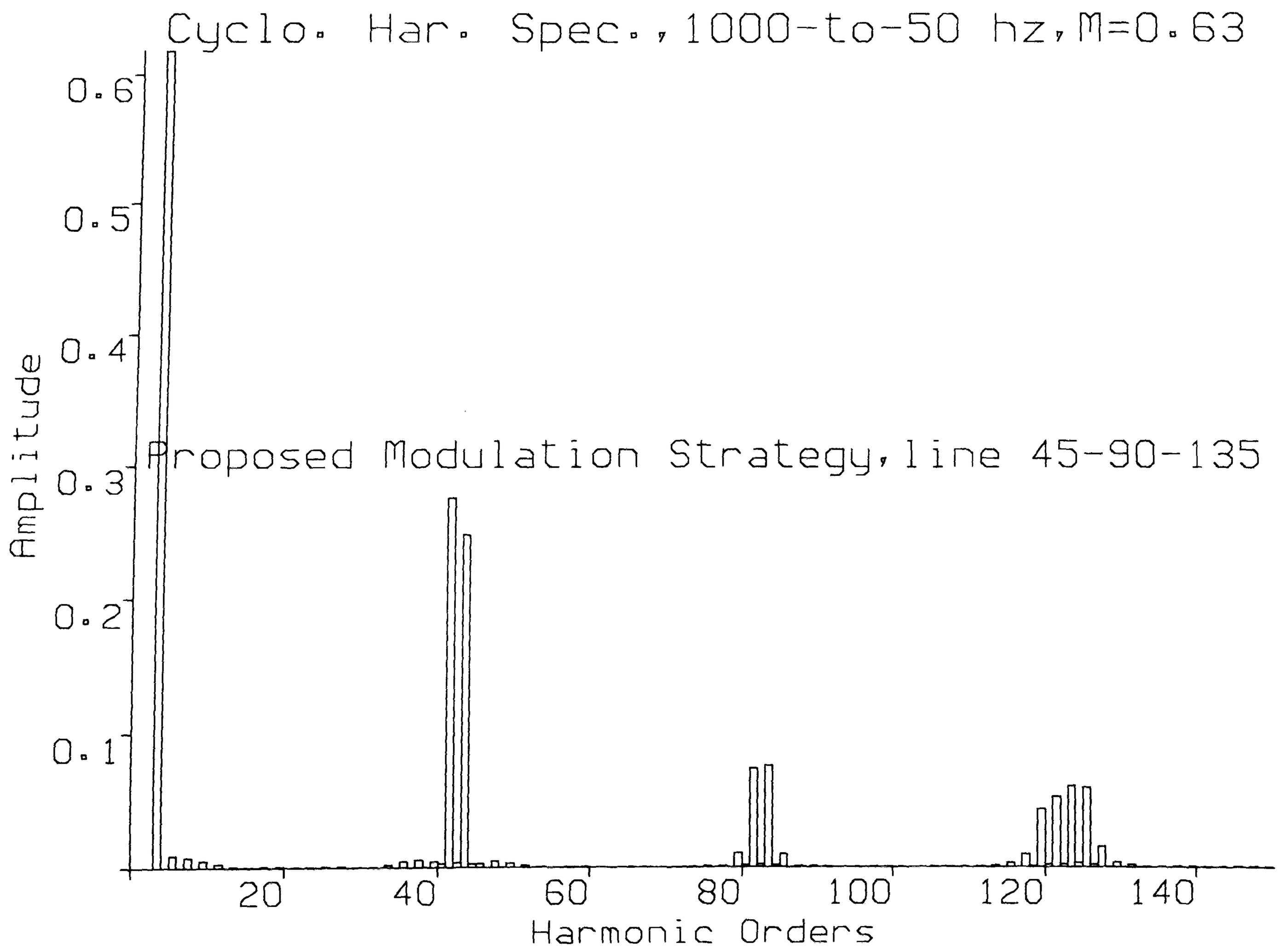
Cyclo. Har. Spec., 1000-to-50 hz, M=0.63
Proposed Modulation Strategy, line 45-90-135
Amplitude
0.6
0.5
0.4
0.3
0.2
0.1
20
40
60
80
100
120
140
Harmonic Orders

Fig. 4-20

4.11.4 The equivalent area is built as shown in Fig . 4 - 21

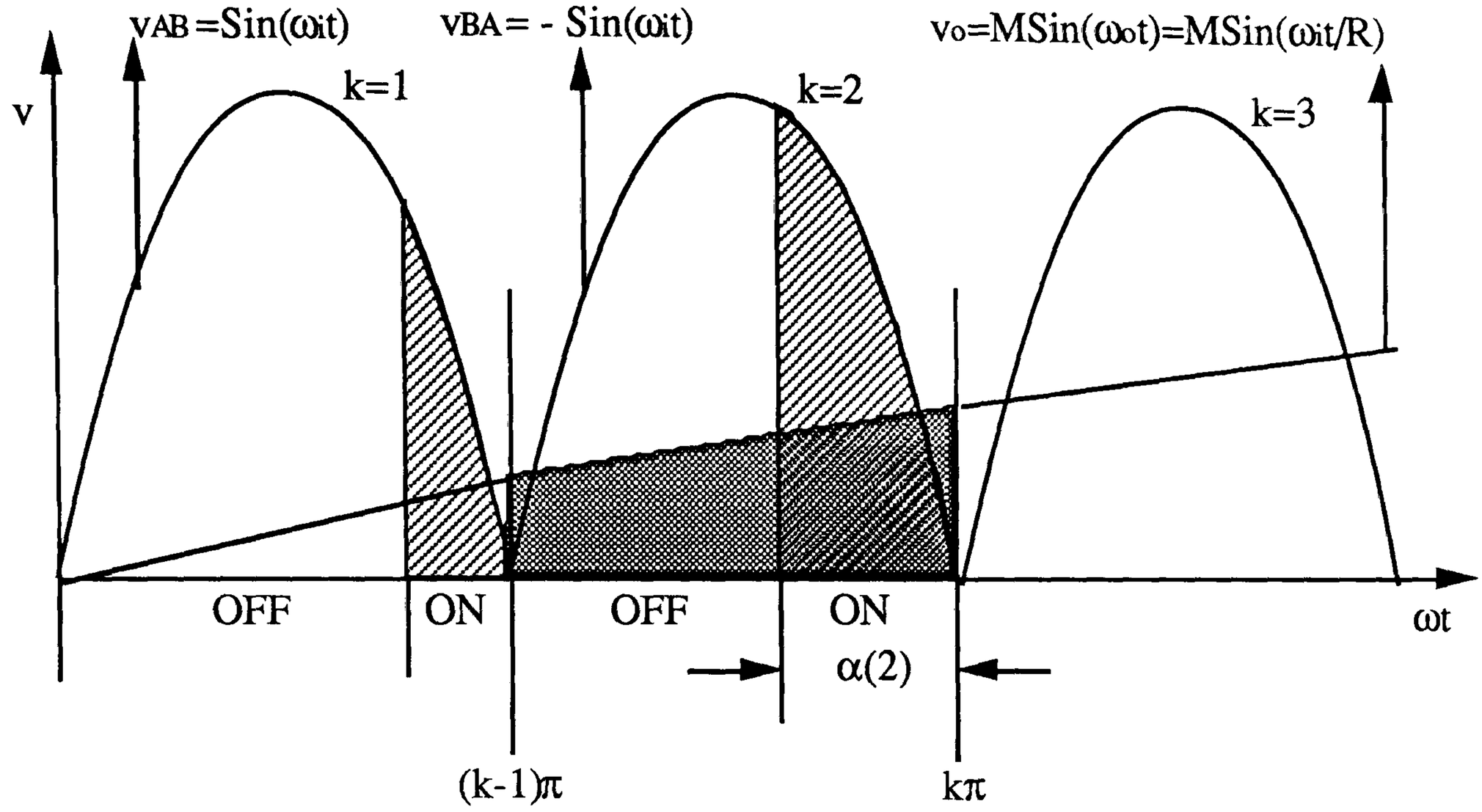

Fig. 4-21 equivalent hatched area is built on the right side of input half cycles

From the equality of two areas following expression for this mode can be derived :

$$\alpha(k) = \left\{\left[1 - (-1)^{k+1}\right]\frac{\pi}{2} - (-1)^{k}\right\}\left\{\cos^{-1}\left[\frac{RM\left[\cos(k-1)\frac{\pi}{R} - \cos k\frac{\pi}{R}\right] - (-1)^{k}\cos k\pi}{(-1)^{k+1}}\right]\right\}$$

$$k = 1, 2, 3, \ldots\ldots, 2R \qquad (4-82)$$

$$R = \frac{f_i}{f_o}$$

$$M = 0.0, \ldots\ldots, 0.63$$

The related results and harmonic spectrum are shown in table 4-5 and Fig. 4-22 respectively .

Table 4-5

Stage	OFF(deg.)	ON(deg.)	ON + OFF
1	147.658	32.3417	180.0
2	122.577	57.4225	180.0
3	104.086	75.9145	180.0
4	88.1050	91.8950	180.0
5	73.4968	106.503	180.0
6	59.7714	120.229	180.0
7	46.7004	133.300	180.0
8	34.2423	145.758	180.0
9	22.6998	157.300	180.0
10	13.8142	166.186	180.0
11	13.8142	166.186	180.0
12	22.6998	157.300	180.0
13	34.2423	145.758	180.0
14	46.7004	133.300	180.0
15	59.7714	120.229	180.0
16	73.4968	106.503	180.0
17	88.1050	91.8950	180.0
18	104.086	75.9145	180.0
19	122.577	57.4225	180.0
20	147.658	32.3417	180.0
21	147.658	32.3417	180.0
22	122.577	57.4225	180.0
23	104.086	75.9145	180.0
24	88.1050	91.8950	180.0
25	73.4968	106.503	180.0
26	59.7714	120.229	180.0
27	46.7004	133.300	180.0
28	34.2423	145.758	180.0
29	22.6998	157.300	180.0
30	13.8142	166.186	180.0
31	13.8142	166.186	180.0
31	22.6998	157.300	180.0
32	34.2423	145.758	180.0
34	46.7004	133.300	180.0
35	59.7714	120.229	180.0
36	73.4968	106.503	180.0
37	88.1050	91.8950	180.0
38	104.086	75.9145	180.0
39	122.577	57.4225	180.0
40	147.658	32.3417	180.0

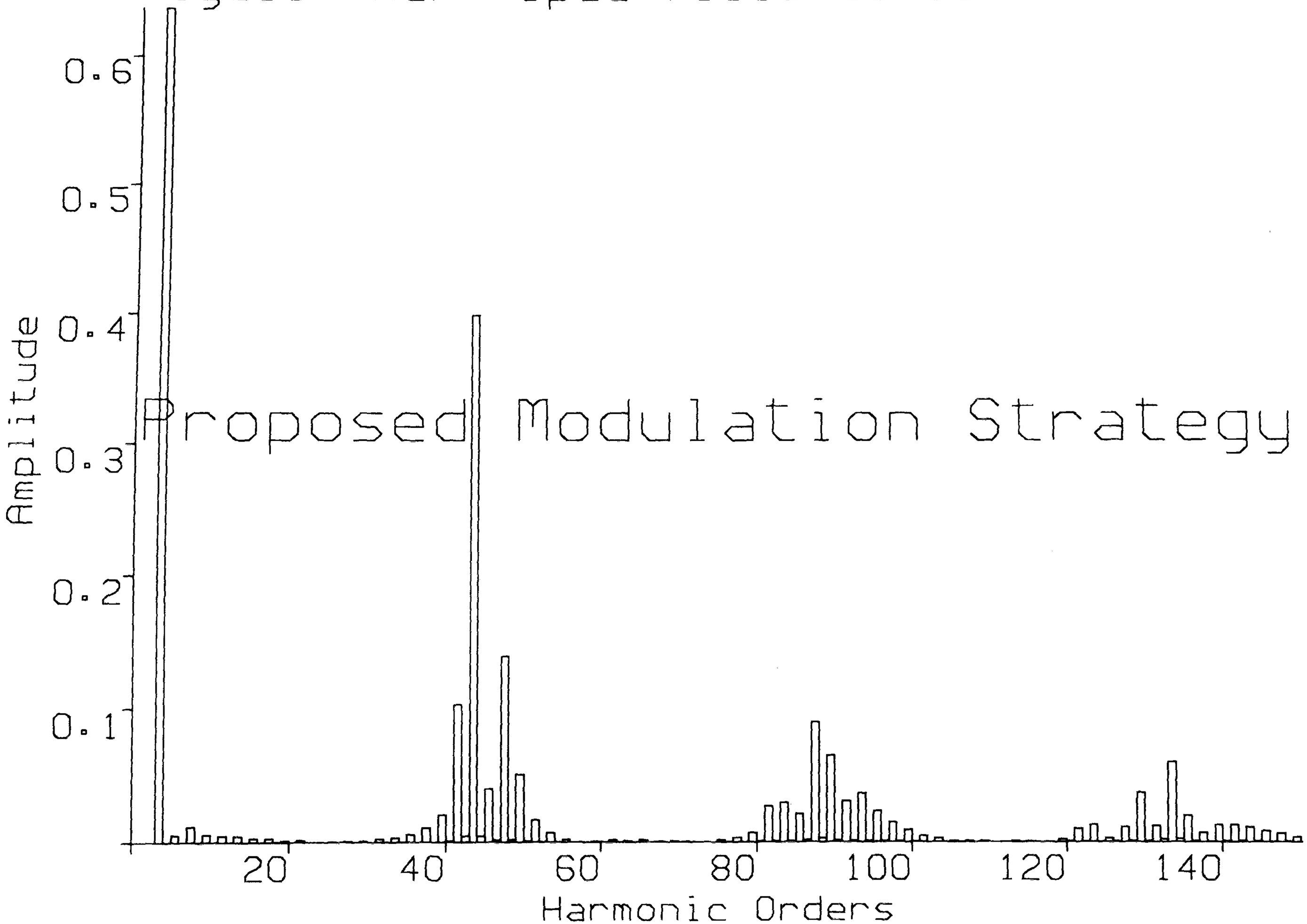
Cyclo. Har. Spec.,1000-to-50 hz,M=0.63
Amplitude
0.6
0.5
0.4
0.3
0.2
0.1
Proposed Modulation Strategy
20
40
60
80
100
120
140
Harmonic Orders

Fig. 4-22

4.12 *Harmonic Analysis for proposed modulation strategy "General mathematical expression"*

Due to absence of low order harmonics and decreased device switching among the four " equal area criterion " modes , those were discussed in section 4 - 11 . Mode number 1 is selected for microprocessor implementation .

Although the harmonic spectra of the modes are to some extent close to each other , mode number 1 has a clearer spectrum and is easier to implement than the others .

Referring to Fig. 4 - 15 , the general expression of a Fourier Series for the instantaneous output voltage in Fig. 4 - 8(b) is :

$$\mathbf{v_o}(\omega t) = \sum_{n=1,3,5,\ldots}^{\infty} (\mathbf{A_n} \operatorname{Cos} n\omega t + \mathbf{B_n} \operatorname{Sin} n\omega t) \qquad (4 - 83)$$

The coefficients $\mathbf{A_n}$ and $\mathbf{B_n}$ are determined by considering a pair of pulses such that the positive pulse of duration α°_k starts at $\omega t = \Phi^\circ_k$ and the negative one of the same width starts at $\omega t' = 3600^\circ + \Phi^\circ_k$ (Fig. 4 - 15) . The effects of all pulses can be combined together to obtain the effective out-put voltage . If the positive pulse of kth pair starts at $\omega t = \Phi^\circ_k$ and ends at :

$\omega t' = 3600^\circ + \Phi^\circ_k$

or :

$\omega t' = R\pi + \Phi_k$ (rad.)

the Fourier coefficients for this pair of pulses are :

$$a_n = \frac{2}{R\pi}\int_{\Phi_k}^{\Phi_k+\alpha_k} V_m \mathrm{Sin}(R\omega_o t)\,.\,\mathrm{Cos}\,(n\omega_o t)\,d(\omega_o t) \qquad (4-84)$$

Since :

$$\mathrm{Sin}\left(\frac{P+Q}{2}\right)\mathrm{Cos}\left(\frac{P-Q}{2}\right)\frac{1}{2}[\mathrm{SinP} + \mathrm{SinQ}]$$

Then :

$$\mathrm{Sin}\,(R\omega_o t)\,.\,\mathrm{Cos}\,(n\omega_o t) = \frac{1}{2}\left[\mathrm{Sin}\,(R+n)\,\omega_o t + \mathrm{Sin}\,(R-n)\,\omega_o t\right]$$

and (4 - 84) becomes :

$$a_n = \frac{2}{R\pi}\cdot\frac{v_m}{2}\left\{\int_{\Phi_k}^{\Phi_k+\alpha_k} \mathrm{Sin}\,(R+n)\omega_o t\;d(\omega_o t) + \int_{\Phi_k}^{\Phi_k+\alpha_k} \mathrm{Sin}\,(R-n)\omega_o t\;d(\omega_o t)\right\}$$

(4 - 85)

$$a_n = \frac{v_m}{R\pi}\left\{\frac{1}{R+n}\left[\mathrm{Cos}(R+n)\Phi_k - \mathrm{Cos}\left[(R+n)(\Phi_k+\alpha_k)\right]\right] + \frac{1}{(R-n)}\left[\mathrm{Cos}(R-n)\Phi_k - \mathrm{Cos}\left[(R-n)(\Phi_k+\alpha_k)\right]\right]\right\}$$

(4 - 86)

and:

$$b_n = \frac{2}{R\pi}\int_{\Phi_k}^{\Phi_k+\alpha_k} V_m \mathrm{Sin}(R\omega_o t)\,.\,\mathrm{Sin}\,(n\omega_o t)\,d(\omega_o t) \qquad (4-87)$$

since :

$$\text{Sin}\left(\frac{P+Q}{2}\right)\text{Sin}\left(\frac{P-Q}{2}\right)=\frac{1}{2}\left[\text{Cos}(P)-\text{Cos}(Q)\right]$$

Then :

$$\text{Sin}\left(R\omega_o t\right).\ \text{Sin}\left(n\omega_o t\right)=\frac{1}{2}\left[\text{Cos}\left(R+n\right)\omega_o t-\text{Cos}\left(R-n\right)\omega_o t\right]$$

and (4-87) becomes :

$$b_n=\frac{2}{R\pi}\cdot\frac{v_m}{2}\left\{\int_{\Phi_k}^{\Phi_k+\alpha_k}\text{Cos}\left(R+n\right)\omega_o t\ d\left(\omega_o t\right)-\int_{\Phi_k}^{\Phi_k+\alpha_k}\text{Cos}\left(R-n\right)\omega_o t\ d\left(\omega_o t\right)\right\}$$

(4 - 88)

$$b_n=\frac{v_m}{R\pi}\left\{\frac{1}{R+n}\left[\text{Sin}\left[\left(R+n\right)\left(\Phi_k+\alpha_k\right)\right]-\text{Sin}\left(R+n\right)\Phi_k\right]-\frac{1}{R-n}\left[\text{Sin}\left(R-n\right)\left(\Phi_k+\alpha_k\right)-\text{Sin}\left(R-n\right)\Phi_k\right]\right\}$$

(4 - 89)

Where :

$$R=\frac{f_i}{f_o}$$

$n = 1\ ,\ 3\ ,\ 5\ ,\ .....$

$$\alpha_k=\left(k-\frac{1}{2}\right)\pi-\frac{1}{2}\alpha_k \quad (\text{in Fig.4 - 15})$$

$k = 1\ ,\ 2\ ,\ 3\ ,\ .....\ ,\ R$ (number of pulses per cycloconverter out-put voltage half cycle)

V_m = amplitude of cycloconverter input voltage in Fig. 4 - 8(b)

Therefore the $\mathbf{A_n}$ and $\mathbf{B_n}$ can be expressed as follows :

$$\mathbf{A_n} = \sum_{k=1}^{R} \frac{V_m}{R\pi} \left\{ \begin{array}{l} \frac{1}{(R+n)}\left[\mathrm{Cos}(R+n)\Phi_k - \mathrm{Cos}\left[(R+n)(\Phi_k+\alpha_k)\right]\right] + \\ \qquad + \frac{1}{(R-n)}\left[\mathrm{Cos}(R-n)\Phi_k - \mathrm{Cos}\left[(R-n)(\Phi_k+\alpha_k)\right]\right] \end{array} \right\}$$

(4-90)

$$\mathbf{B_n} = \sum_{k=1}^{R} \frac{V_m}{R\pi} \left\{ \begin{array}{l} \frac{1}{(R+n)}\left[\mathrm{Sin}\left[(R+n)(\Phi_k+\alpha_k)\right] - \mathrm{Sin}(R+n)\Phi_k\right] - \\ \qquad - \frac{1}{(R-n)}\left[\mathrm{Sin}\left[(R-n)(\Phi_k+\alpha_k)\right] - \mathrm{Sin}(R-n)\Phi_k\right] \end{array} \right\}$$

(4-91)

By substituting (4-90) and (4-91) in to following equation :

$$\mathbf{v_o}(\omega t) = \sum_{n=1,3,5,\ldots}^{\infty} \left[\mathbf{A_n} \mathrm{Cos}\, n\omega t + \mathbf{B_n} \mathrm{Sin}\, n\omega t \right] \qquad (4\text{-}92)$$

The general expression of the cycloconverter out-put voltage will be resulted .

It should be emphasized that if the $R = \frac{f_i}{f_o}$ is not integral , the positive and negative half-cycle waveforms may have different voltage profiles. As a result the output voltage may have even harmonics and subharmonics in addition to the ordinary odd harmonics[14] . The effects of the subharmonics on the induction motor operation was discussed in this chapter.

4.13 References :

1- C. W. Lander *" Power Electronics "* Second edition . 1987 , McGraw - Hill Book Company , Chap. 3 & 5 .

2- B. R. Pelly *" Thyristor phase-controlled converter & cycloconverter "* 1971 , John Wiley & Sons , Inc. .

3- M . H . Rashid *" Power electronics circuits , Devices and applications"* 1988 , Prentice - Hall International Editions .

4- P . Wood *" Switching Power Converters "* 1981 , VAN NostrandReinhold.

5- S . I . Khan , P . D . Ziogas , & M . H . Rashid *" Forced commutated cycloconverter for High Frequency link application "* 1986 , IEEE , pp. 476 - 487 .

6- P . D . Ziogas , S . I . Khan , & M . Rashid *" Analysis and design of forced commutated cycloconverter structures with improved transfer characteristics "* August 1986 , IEEE , trans. on Industrial Electronics , Vol. IE - 33 , No. 3 pp. 271 - 280 .

7- D . H . Shin , G . Cho , S . B . Park . *" Improved PWM method of forced commutated cycloconverters "* May 1989 , IEE proc. , Vol. 136 , pt. B , pp.121 - 126 .

8- L . Gyugyi & B . R . Pelly *" Static power frequency changers "* 1976 - John Wiley & Sons .

9- P . D . Ziogas , Y . G . Kang , & V . R . Stafanovic *" Rectifier-Inverter frequency changers with suppressed DC link components "* Nov. / Dec. 1986 , IEEE Trans. on industry application , Vol. IA-22 , No.6 , pp. 1027 - 1036.

10- J . A . Houldsworth & F . J . Burgum *" Induction motor drives using new digital sine - wave pwm system "* 1979 , in IEE conf. publication . 179 , pp. 11 - 14 .

11- T . R . Mukunda , B.G . Desai*" Analysis and performance of the ARNO converter "* May / June 1972 , IEEE , Vol. IA - 8 , No. 3 , pp. 283 - 288 .

12- S . I . Khan , P . D . Ziogas , & M . H . Rashid *" A novel single - to three phase static converter "* Jan. / Feb. 1989 , IEEE Trans. on industry applications , Vol. 25 , No. 1 .

13- S. B. Dewan and A. Straughen " **Power semiconductor circuits** " Wiley , 1975

14- D. O'Kelly " **Performance and control of ELECTRICAL MACHINES**" McGraw-Hill Book Company (UK) , 1991

Chapter 5

Design & performance of the prototype system

5.1 Introduction

This chapter deals with the design and performance of the prototype **DC**-to-**AC**(3-phase & 1 k Hz)-to-**AC**(3-phase & 50 Hz) power conversion through the **Inverter-Transformer-Cycloconverter** system . The block diagram for this system is shown in Fig. 5-1 . The chapter contains six main sections :

1- the 3-phase inverter

2- the high frequency transformer

3- the 3-phase cycloconverter

4- the control circuits

5- the phase shifters

6- the experimental results of the prototype system

5.2 The 3-phase inverter

There are three inverter circuit configurations :

5.2.1 Push-pull inverter(with center tapped transformer)

The push-pull type inverter shown in Fig. 5-2 has two disadvantages . First , in this type the peak value of the Drain-to-source voltage of each MOSFET is equal to twice the supply voltage plus the amplitude of the voltage spike generated by transformer leakage inductance and stray inductances in series with the MOSFET [1] . Their associated energy is suppressed by the snubber capacitors . This can be consider as a limitation for the high power inverters energized from high DC source voltages , but less likely for battery fed inverters.

Secondly , in PWM application due to a small difference in the switching times of the transistors , or in other words , as a result of unsymmetrical switching of the transistors a net DC voltage component is applied .

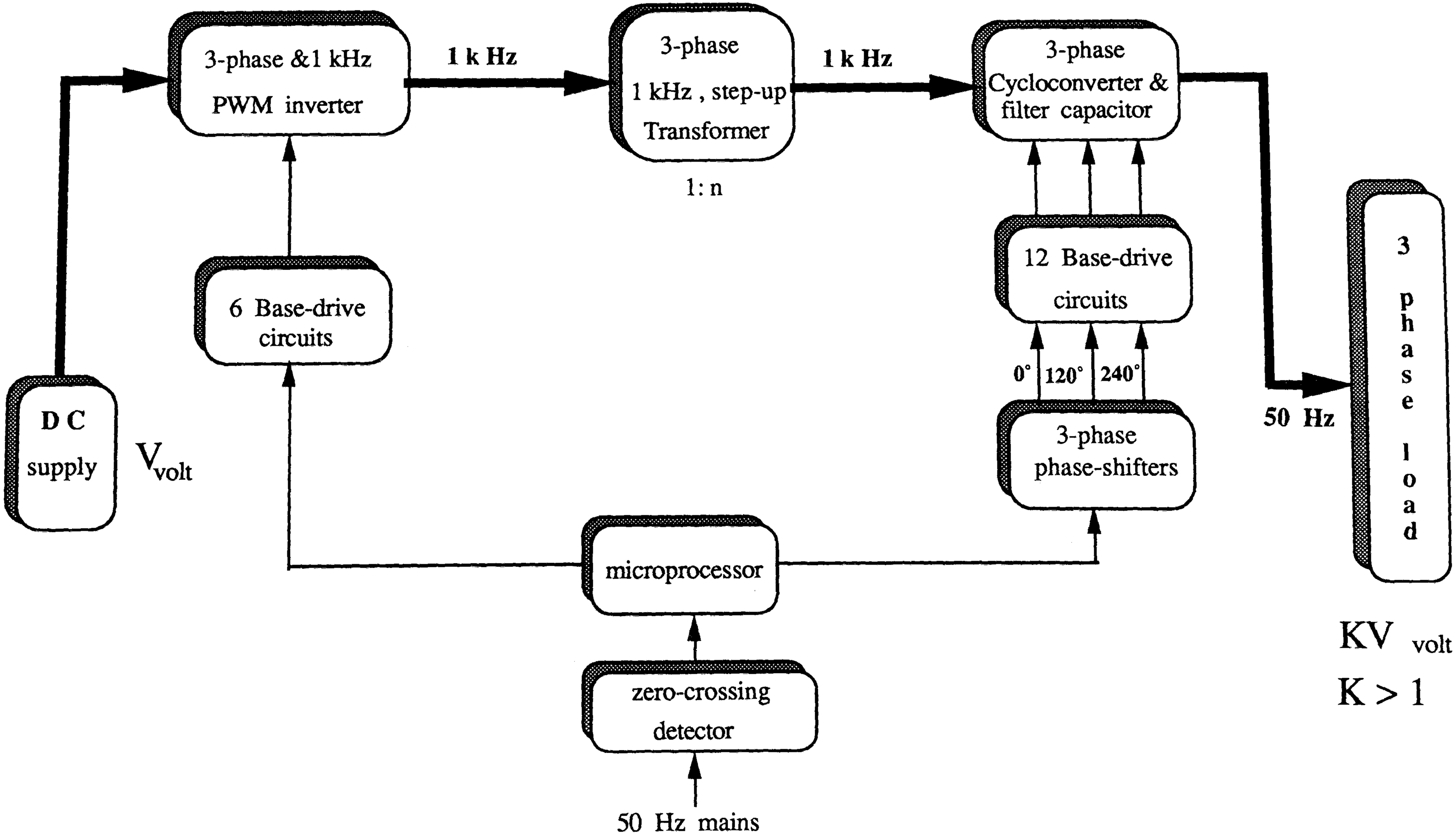

Fig. 5-1 The block diagram of DC -to- AC(1kHz) -to- AC(50 Hz) power conversion system

to the transformer and consequently the core enters saturation in one direction as a result of the magnetizing current spike . Therefore in core materials like Ferrite the saturation flux is lower than that of laminated core materials and this problem will be more apparent [1] & [2] .

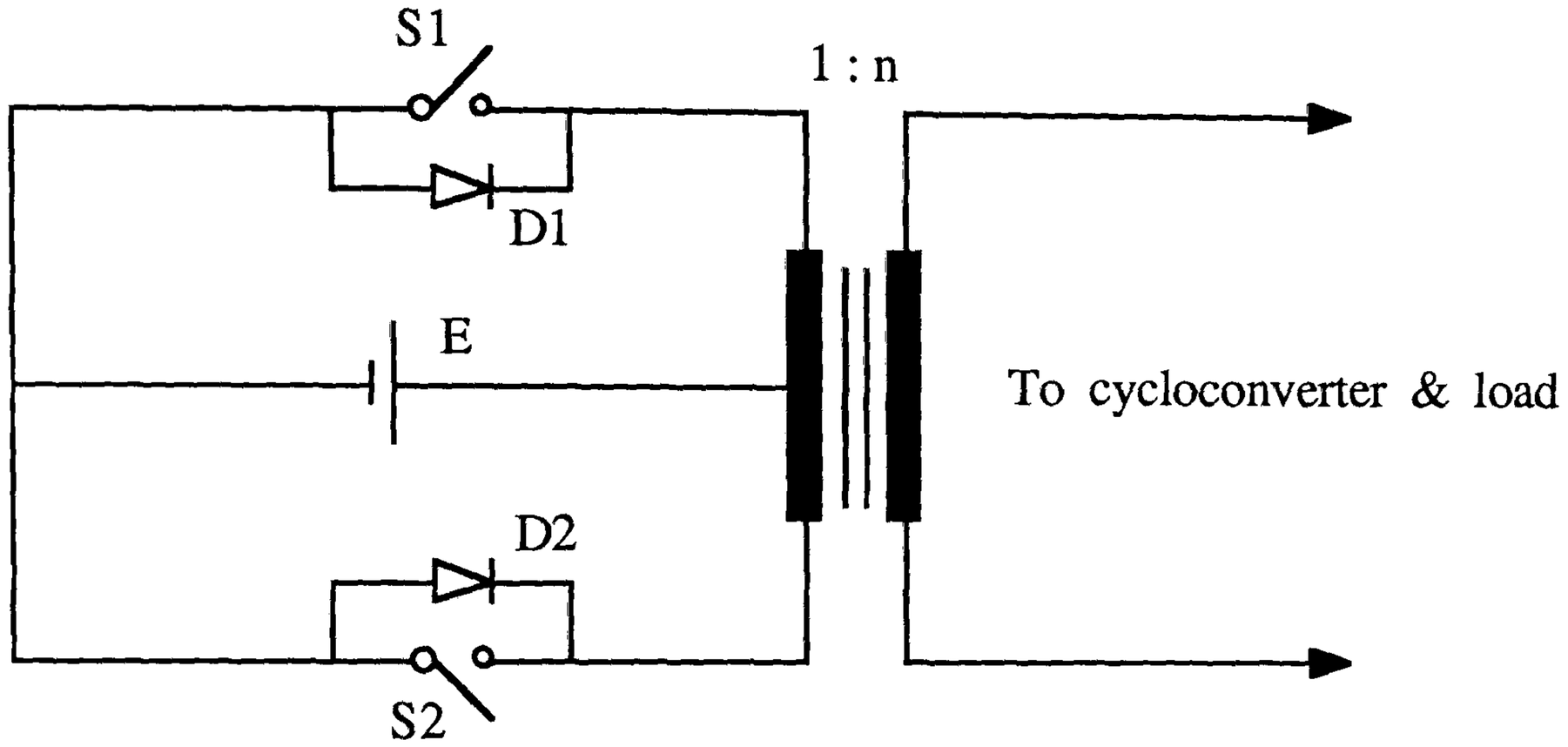

Fig. 5-2 push-pull inverter

For handling the same load power , this problem relatively can be solved by inserting an air gap in the transformer magnetic circuit but at the cost of higher magnetizing current , greater losses & increased leakage flux which increases the voltage spike across the MOSFET at switch off . In reference [3] symmetry correction circuit on basis of feed back from the two primary current difference has been suggested but at the cost of circuit complexity . As an advantage for this type of inverter , the MOSFET base drive circuits may be left non-isolated from each other .

5.2.2 Half bridge inverter(with center tapped power supply)

This type is shown in Fig. 5-3 . Here the peak value of Drain-to Source voltage of each MOSFET is equal to the supply voltage (E) plus the amplitude of the voltage spike , and therefore suitable for higher supply voltages (advantage) . This type offers two disadvantages .

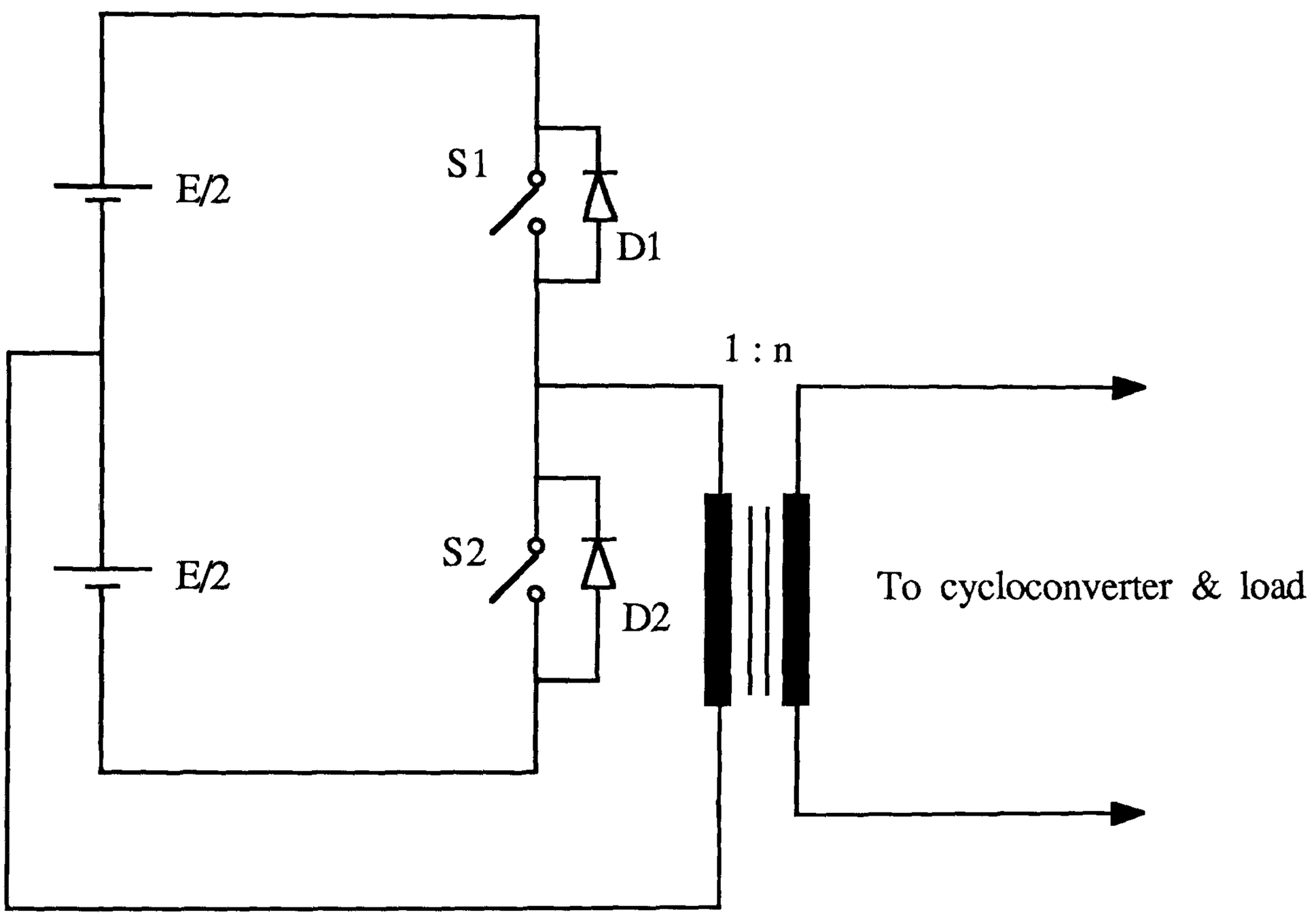

Fig. 5-3 half-bridge inverter (with center tapped power supply)

Firstly for handling the same load power the current will be doubled which causes limitations for high power circuit configurations and secondly for avoiding any supply short circuit isolated gate drive circuits for each MOSFET are required .

5.2.3 The full bridge inverter

As Fig. 5-4 shows , in this inverter , the push-pull and half bridge advantages are combined , that is the MOSFET voltage rating is E and the current through it is half of the half bridge inverter for the same load power , but in contrast four MOSFET have to be used and isolated base drive circuits are required .

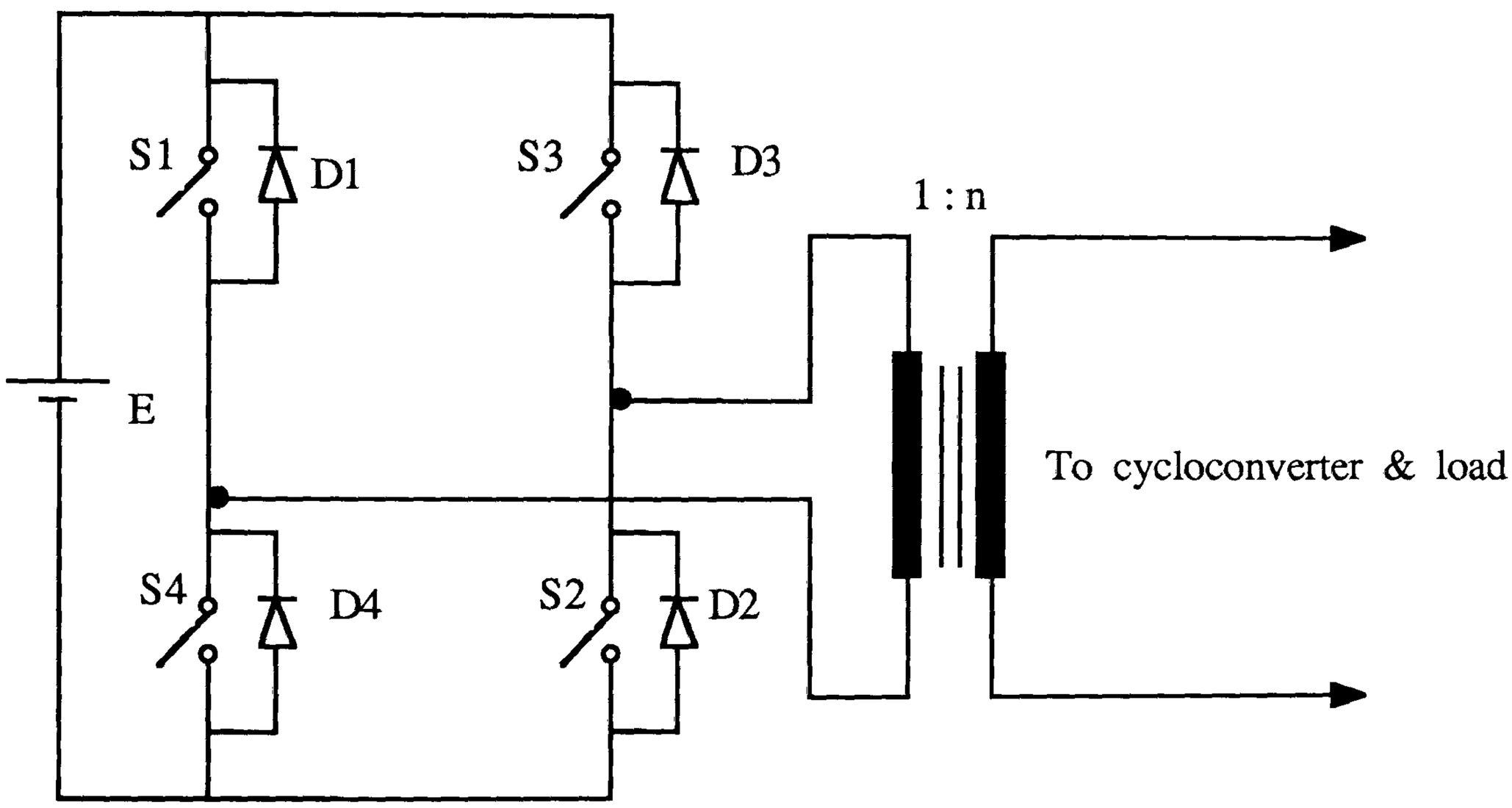

Fig. 5-4 full-bridge inverter

5.2.4 prototype system inverter

By review of the merits and short comings of three explained types , the 3-phase version of half bridge inverter shown in Fig. 5-5 is chosen for the prototype system to generate 3-phase symmetric and 1000 Hz sinusoidal waveforms (all details have been presented in chapter 2) for applying to the cycloconverter through the step-up transformer .

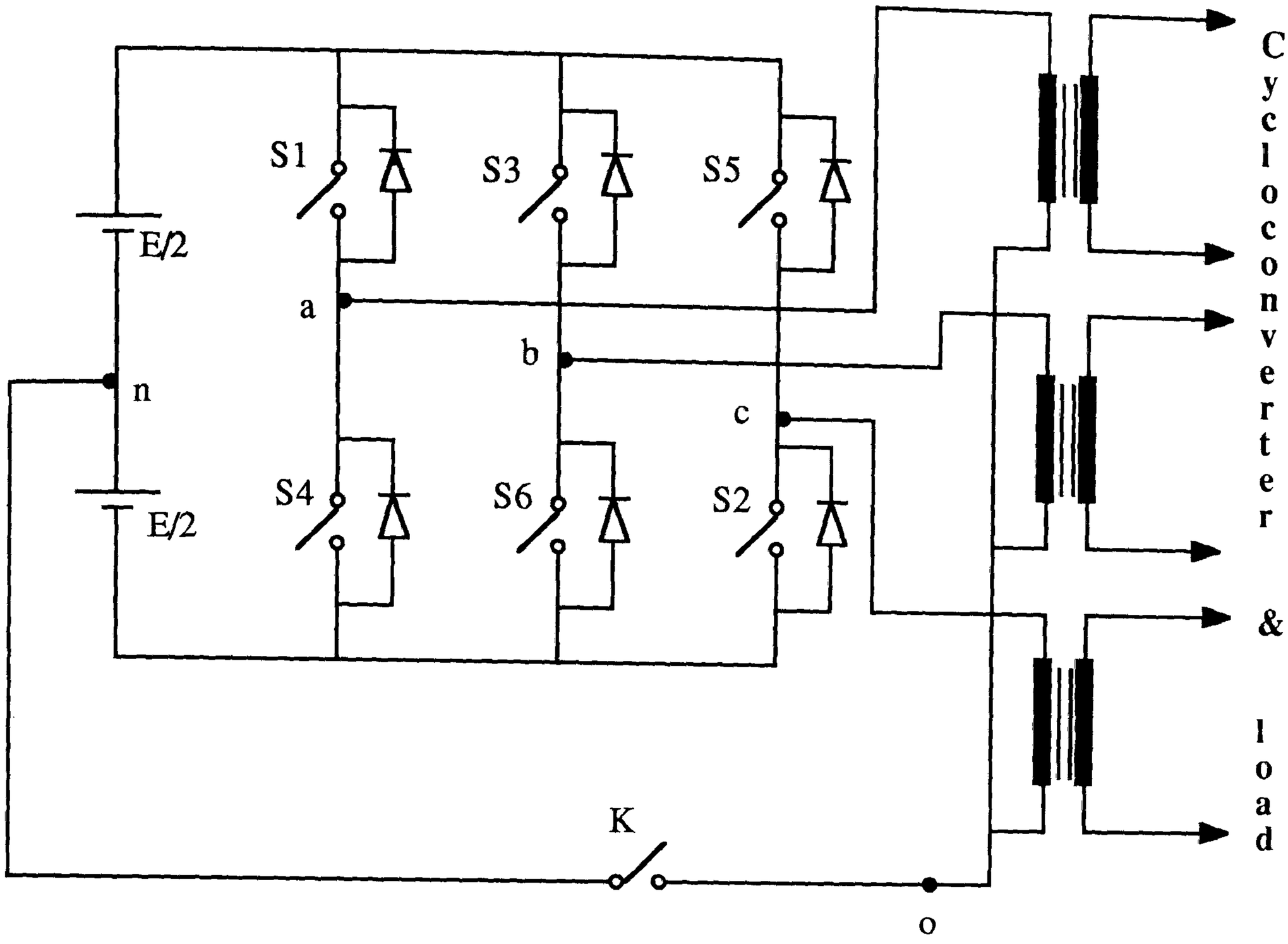

Fig. 5-5 3-phase , half-bridge inverter with isolating & stepping-up transformer for prototype system

5.2.5 Selection of power semiconductor switches for the inverter

The selection of a switch for use in a high-speed inverter is dictated by the following conditions :

1- the peak value of the Drain- to -Source voltage of each MOSFET during turn off should be equal to or greater than the total applied Electric pressure across it due to supply voltage plus voltage spikes caused by transformer leakage inductance and stray inductances .

2- the frequency cut-off characteristics of the switch must be high compared to the actual switching frequency . If the transistor can not switch rapidly between the states of saturation and cut–off , excessive junction heating results . When the transistor frequency cut-off characteristic is several times that of the switching devive the output waveform would be more nearly a square wave (free of pulse corner oscillation)

3- the transistor must be able to handle the currents that are necessary to produce the required output power at the given source voltage , moreover in order to achieve the wanted efficiency the switch saturation voltage at rated currents should be low enough .

4- as was mentioned in chapter 2 , when the inverter is running an inductive load , for keeping voltage stability and releasing the trapped energy (feed back from load to supply source) , antiparallel diodes (feed back diodes) are necessary (Fig. 5-5) .

In modern power MOSFET transistors a parasitic anti-parallel diode is inherently built in the process of device fabricating . The voltage and current ratings are equal to the MOSFET values , but there is in general , a slow reverse recovery [4] .

For the prototype system inverter , by considering the above mentioned conditions and the fact that the maximum DC input voltage used at the primary side of the transformer will be 110 V and give application flexibility for MOSFETS to be employed in different inverter configurations , it was decided to work at maximum primary current 10A . So the **SILICONIX** power **MOSFET** " **SMM 20N 50 , N -** chanel , **Enhancement** Mode transistor " is selected . More information and data sheets for this MOSFET and associated antiparallel diode are given in Apendix B .

5.2.6 The base drive circuit

The base drive circuit shown in Fig. 5-6 was developed successfully . This drive circuit mainly includes the Optocoupler **6N137** and newly developed power MOSFET drive **ICL7667 CPA** by Harris semiconductor .

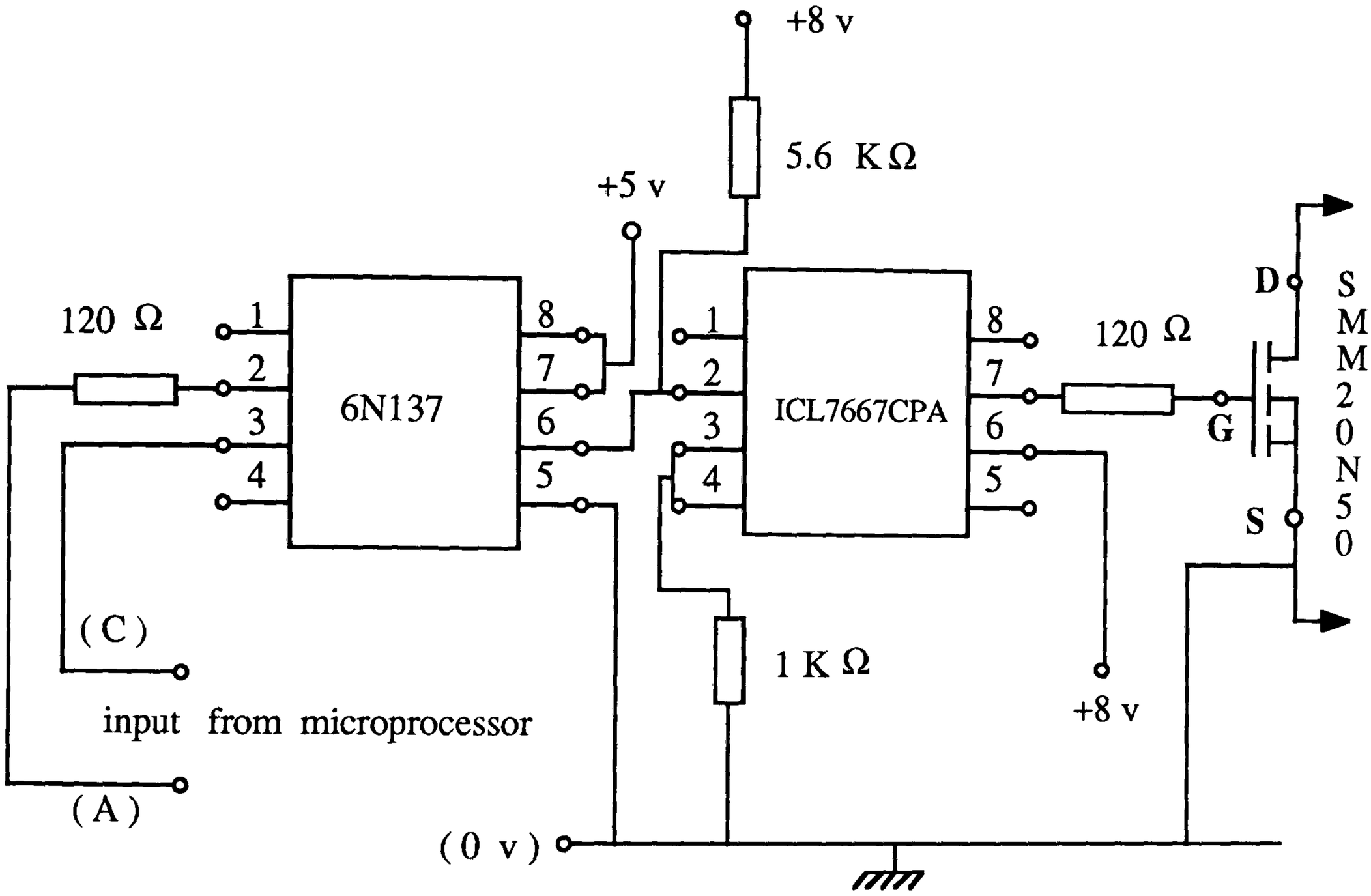

Fig. 5-6 The base drive circuit for (**SMM20N50**) MOSFET

5.2.6.1 Optocouplers and isolation of gatecontrolling signals from power circuits(MOSFETs)

The power circuits (inverters) are generally multiple transistors and each transistor must be gated individually . The gate signals should be applied between gate and source terminals . This gate signals can be isolated from the

power circuit (MOSFETS) by employing pulse transformers or optocouplers . The pulse transformer is simple . It has one primary and one or more secondary windings for simultaneous gating signals to series or parallel MOSFETs . But they have the leakage inductance , rise time of the output pulse and saturation problems [5] . Therefore optocouplers are preferable in spite of the requirement for a separate power supply .

The optocoupler (optical isolator) is comprised of an infrared light - emitting diode (ILED) and a silicon phototransistor , Fig. 5-7 .

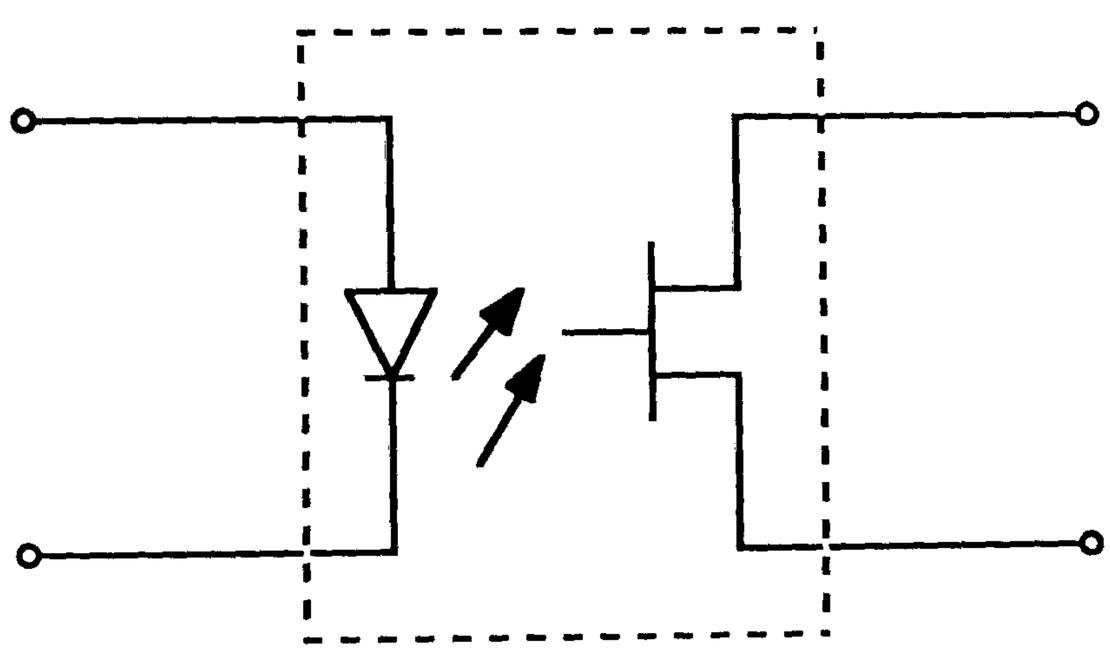

Fig. 5-7 The basic optocoupler structure

The input signal (from microprocessor) is applied to the ILED and the output is taken from phototransistor . This phototransistor has rapid rise and fall times , for example 25 nsec. for optocoupler **6N137** which was employed for gate drive circuits of prototype system inverter MOSFETs . The data sheets are given in Appendix B .

5.2.6.2 The ICL7667 CPA Chip

The **ICL7667CPA** is a high speed driver designed to convert T.T.L level signal (from microprocessor) in to high current outputs at voltages up to 15v. This chip is ideal for driving power MOSFETs in high frequency switched mode power converters . It has rise and fall time about 30 nsec quite compatible with optocoupler 6N 137 and MOSFET of **SMM20N50** . The respective data sheets are included in Appendix B .

5.2.7 The snubber circuits design

The protection of the power semiconductor devices , here , MOSFETs are accomplished by turn-ON and turn-OFF snubbers against excessive di/dt and dv/dt respectively , shown in Fig. 5-8 .

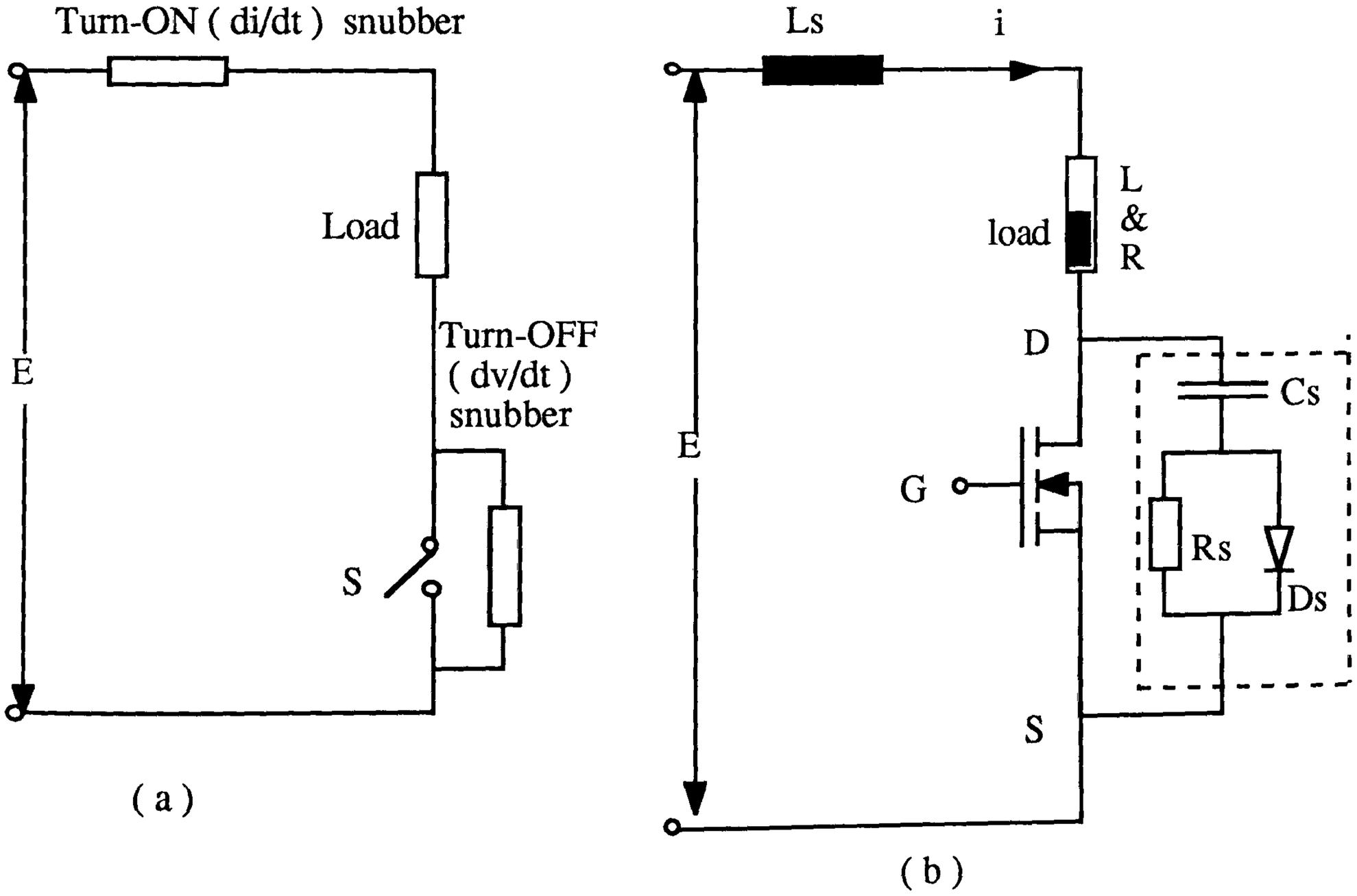

Fig. 5-8 Turn-ON & Turn-OFF snubbers :

(a) schematic (b) with circuit elements

5.2.7.1 The MOSFET equivalent circuit

The switching equivalent circuit of a power MOSFET is shown in Fig. 5-9 [6] .

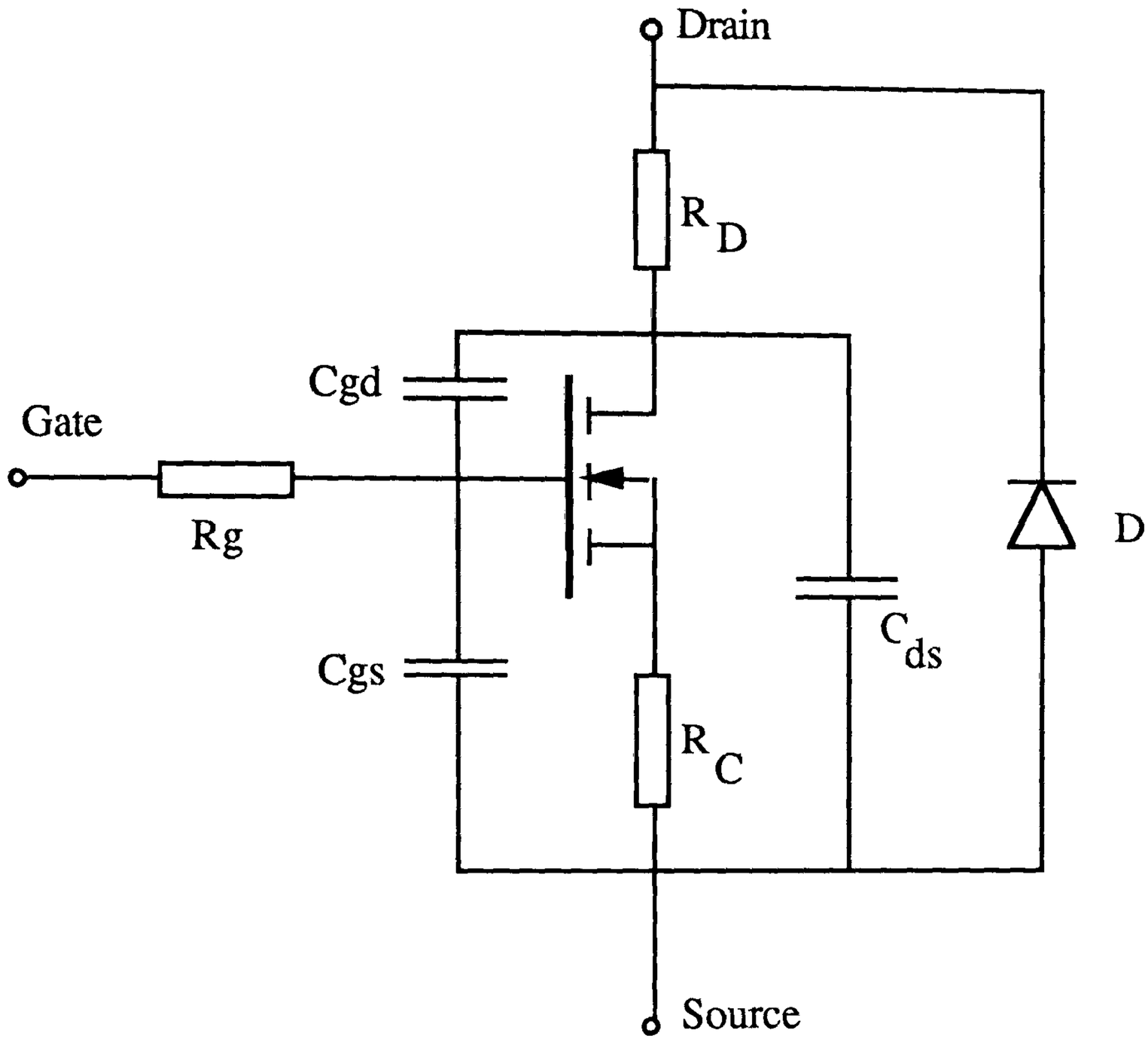

Fig. 5-9 The MOSFET equivalent

Where :

R_g gate resistance

R_D epitaxial layer resistance

R_C channel resistance

$R_{DS\,(on)} = R_D + R_C$ Drain-Source resistance at turn-on

D parasitic anti - parallel diode (MOSFET body diode)

$C_{input} = C_{gd} + C_{gs}$ (with the source ac shorted to the drain)

$C_{output} = C_{gd} + C_{ds}$ (with the gate ac shorted to the source)

these quantities of the **MOSFET-SMM 20N50** may be found in Appendix B .

5.2.7.2 MOSFET switching waveforms and times

General switching waveforms and times are shown in Fig. 5-10 [7] .

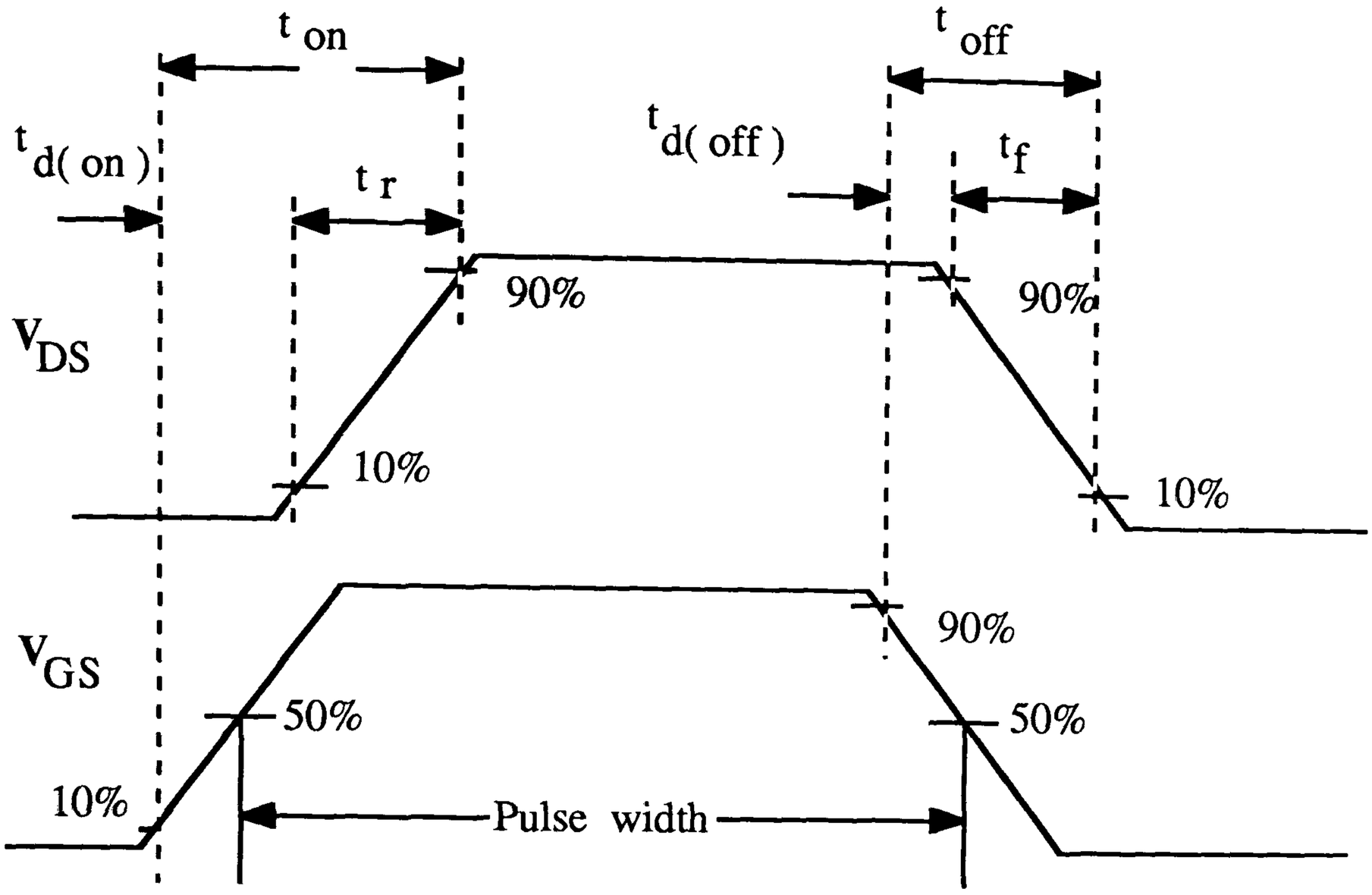

$t_{on} = t_{d(on)} + t_r$ $\qquad$ $t_{off} = t_{d(off)} + t_f$

Fig. 5-10 General MOSFET switching waveforms

The switching times[t_d(on) , t_r , t_d(off) & t_f] for **SMM20N50** MOSFET can be found in related data sheets (Appendix B) .

i- Turn-on period

In Fig. 5-10 the timing relationship between the gate-source voltage and the drain-source voltage for a complete (ON and OFF) drive pulse applied to the gate is presented . During the turn-on period a delay occurs (turn-on delay) . This delay , t_d (on) is the time that is required to charge the input capacitance (C_{input}) to gate threshold voltage level . This duration , t_d (on)

is determined by the gate-to-source (c_{gs}) and drain -to- source (c_{ds})capacitances. After the delay , the drain current rises as the drain-to-source voltage falls . The rise time , t_r , is the gate charging time from the threshold level to the full - gate voltage , which is required to drive the MOSFET in to the linear region . This time (t_r) is measured using the 10% and 90% points on the rising waveform . The sum of turn-on delay time and rise time is known as turn-on time :

$$t_{on} = t_{d(on)} + t_r \qquad (5-1)$$

ii- Turn-off period

During the turn-off period , another delay occurs (turn-off delay , $t_{d\text{-}off}$). This delay , which is followed by a fall in drain current as the drain-source voltage rises , is the time required for the input capacitance (C_{input}) to discharge from the full gate voltage to the 90% falling waveform point . The V_{gs} must decrease significantly before V_{ds} begins to rise . The fall time , t_f , is the time that is required for the input capacitance to discharge from the 90% falling waveform point to threshold voltage and if $V_{gs} < V_{threshold}$ the transistor turns off . The sum of turn-off delay time $t_{d(off)}$ and fall time is known as turn-off time .

$$t_{off} = t_{d(off)} + t_f \qquad (5-2)$$

Switching-time calculations , and further information about switching characteristics , may be found on section 2.2.1 and 3.2 in reference [4] .

5.2.7.3 di/dt protection or turn-on snubber design

The typical voltage and current waveforms of a MOSFET switch during turn-on and turn-off are shown in Fig. 5 - 11 .

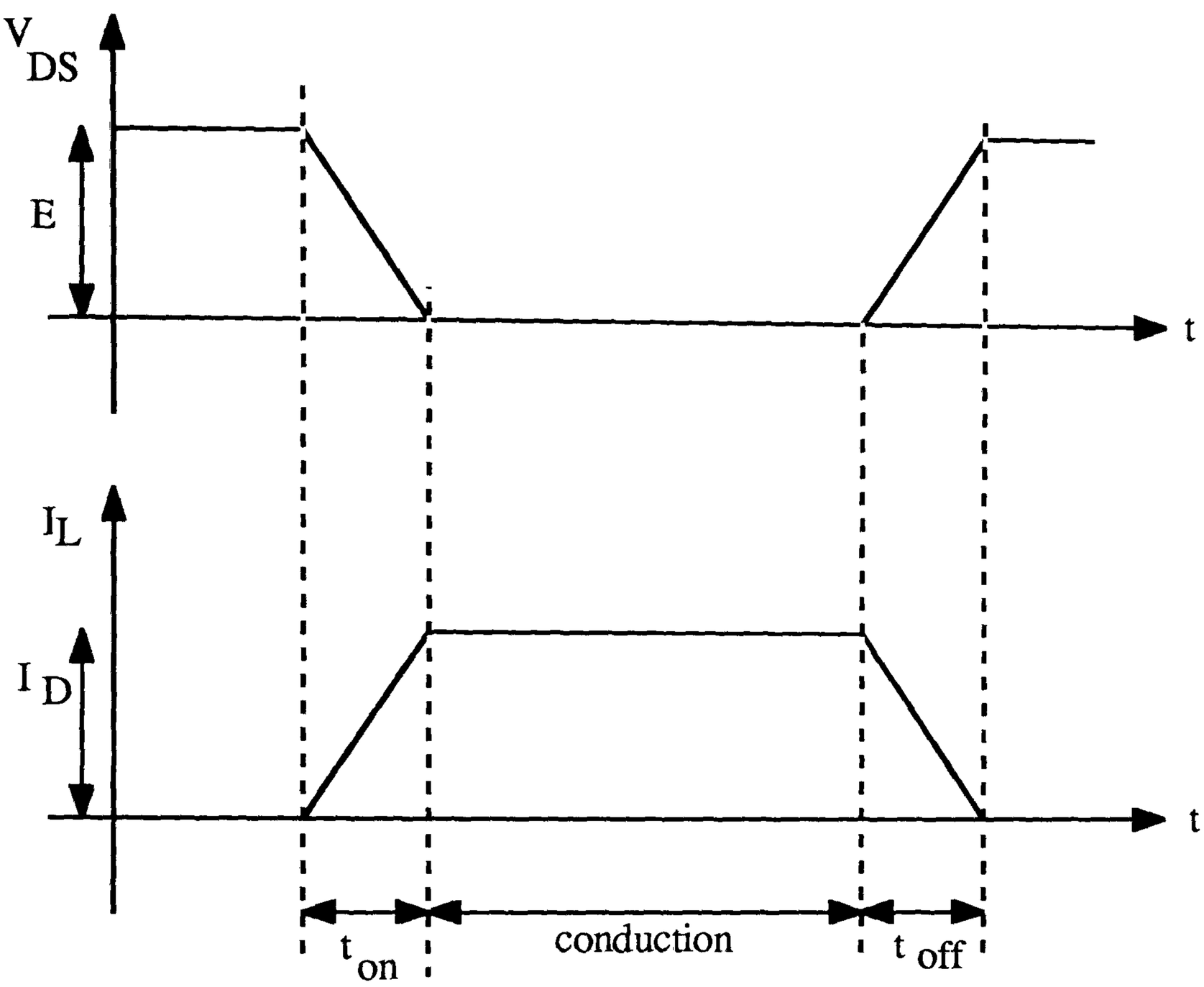

Fig. 5-11 The typical MOSFET voltage & current waveforms

During turn-on , the drain current (I_D) rises and from Fig. 5-11 di / dt is :

$$\frac{di}{dt} = \frac{I_L}{t_{on}} = \frac{I_D}{t_{on}} \qquad (5-3)$$

If the rate of rise of drain current (di /dt) is greater than the allowable limit , due to high current density switch failure may be inevitable . The di/dt

may be held down to an acceptable value by including a small amount of inductance (turn-on snubber) in the drain circuit . The amount of this inductance is calculated such that after elapsed specified t_{on} time , the switch will turn-to full conduction . In Fig. 5-8 (b) immediately after voltage E being applied :

$$E = R.i + (L_s + L) \frac{di}{dt} \qquad (5\text{-}4)$$

If (5-4) be solved for i (t) :

$$i(t) = \frac{E}{R} \left\{ 1 - [e]^{\frac{-R}{(L+L_s)}t} \right\} \qquad (5\text{-}5)$$

$$\frac{di(t)}{dt} = \frac{-E}{R} \cdot \frac{-R}{L+L_s} e^{\frac{-tR}{L+L_s}} = \frac{E}{L+L_s} e^{-\frac{R}{(L+L_s)}t} \qquad (5\text{-}6)$$

$$\left[\frac{di(t)}{dt}\right]_{max(t=0)} = \frac{E}{L+L_s} \qquad (5\text{-}7)$$

and :

By equating (5 - 3) with (5 - 7) :

$$\frac{I_D}{t_{on}} = \frac{E}{L+L_s} \qquad (5\text{-}8)$$

From (5 - 8) :

$$L + L_s = \frac{E \,.\, t_{on}}{I_D} \qquad (5\text{-}9)$$

Since the t_{on} for power MOSFETs (like **SMM20N50**) is very short (120nsec) , by referring to (5 - 9) , the presence of any load inductance and even any stray inductance will be sufficient for di / dt protection .

5.2.7.4 dv/dt protection or turn-off snubber design

During turn-off , the drain-to-source voltage rise in relation to the fall of drain current . From Fig. 5 - 11 :

$$\frac{dv}{dt} = \frac{v_{DS}}{dt} = \frac{E}{t_{off}} \qquad (5\text{-}10)$$

Referring to Fig. 5-8 (b) at the instant that the MOSFET carring I_D (amp.) , the switch is turned-off the current will divert and pass through the turn-off snubber circuit . Here the size of the capacitor can be determined such that :

$$I_D = C_S \frac{dv}{dt} \quad \text{or} \quad \frac{dv}{dt} = \frac{I_D}{C_S} \qquad (5\text{-}11)$$

Where I_D is maximum drain current and dv/dt is the allowable rate of drain - to-source voltage . By equating (5-10) with (5-11) yields :

$$\frac{E}{t_{off}} = \frac{I_D}{C_S} \qquad (5\text{-}12)$$

$$C_S = \frac{I_D t_{off}}{E}$$

During turn-on the capacitor C_S has to discharge through the transistor and this increases the peak current rating of the transistor .The discharge through the transistor can be avoid by placing R_S across C_S instead of placing R_S across D_S .

5.2.7.5 Discussion about R_S determination

The resistor R_S is presented to prevent the immediate discharge of the capacitor-stored energy in to the switch at turn-on . This resistor must be capable of dissipating a power of :

$$P = \frac{1}{2} C_S E^2 f_{switching} \qquad (5\text{-}13)$$

In choosing the value of R_S , taking the time constant $R_S.C_S$ as one-fifth of the switching period (before the switch turn-off , the capacitor has completely been discharged) :

$$5 R_S .C_S = T_{on} \text{ (the shortest one in PWM operation)} \qquad (5\text{-}14)$$

$$R_S = \frac{1}{5} \frac{T_{on}}{C_S} \qquad (5\text{-}15)$$

From other hand , as has been discussed in Chap. 2 , resonant inverter section , due to the energy stored in L_S , there will be a formation of damped resonant circuit between turn-on and turn-off snubber elements . The R_S - L_S - C_S circuit is normally designed critically damped to avoid oscillations .

Thus :

$$R_S > 2 \sqrt{\frac{(L + L_S)}{C_S}} \qquad (5\text{-}16)$$

Therefore R_S is chosen such that the (5-13) , (5-15) and (5-16) should be satisfied .

The diode D_S in Fig. 5-8 (b) is presented to eliminate the delay that the resistor introduces in protecting against rapid dv/dt (rapid charging) . It should be emphasized that the snubber circuits must be located physically as near as possible to the device in order to minimize stray inductance effects .

For the prototype system the snubber circuit shown in Fig. 5-8 (b) with $C_S = 0.1\,\mu F$ and $R_S = 15\,\Omega$ was employed with satisfactory operation .

5.3 High-Frequency Transformer

In DC -to- AC (1 kHz) -to- AC (50 Hz) power conversion system the high-frequency transformer plays a crucial role . The power conversion with high-frequency link and the transformer behavior in high-frequency & switched mode operation have been discussed in **Chapter-1** and **Chapter-3** respectively , where the inter-effect of leakage inductance on system (in connection with the snubber capacitance & generation of the harmful voltage spikes) was discussed .

For the prototype system , 3 units of the single-phase transformer were ordered & manufactured externally with following specifications :

High-frequency transformer

1- operating frequency , **1** kHz

2 - power rating , **800** w

3- winding configurations :

The **P1** , **P2** and **P3** windings also **S1** and **S2** windings are bifilar wound to minimize leakage inductance . The secondary parts should be sandwiched between the parts of primary sections as shown in Fig. 5-12 . A very tiny air gap is left between **E** & **I** parts of the core .

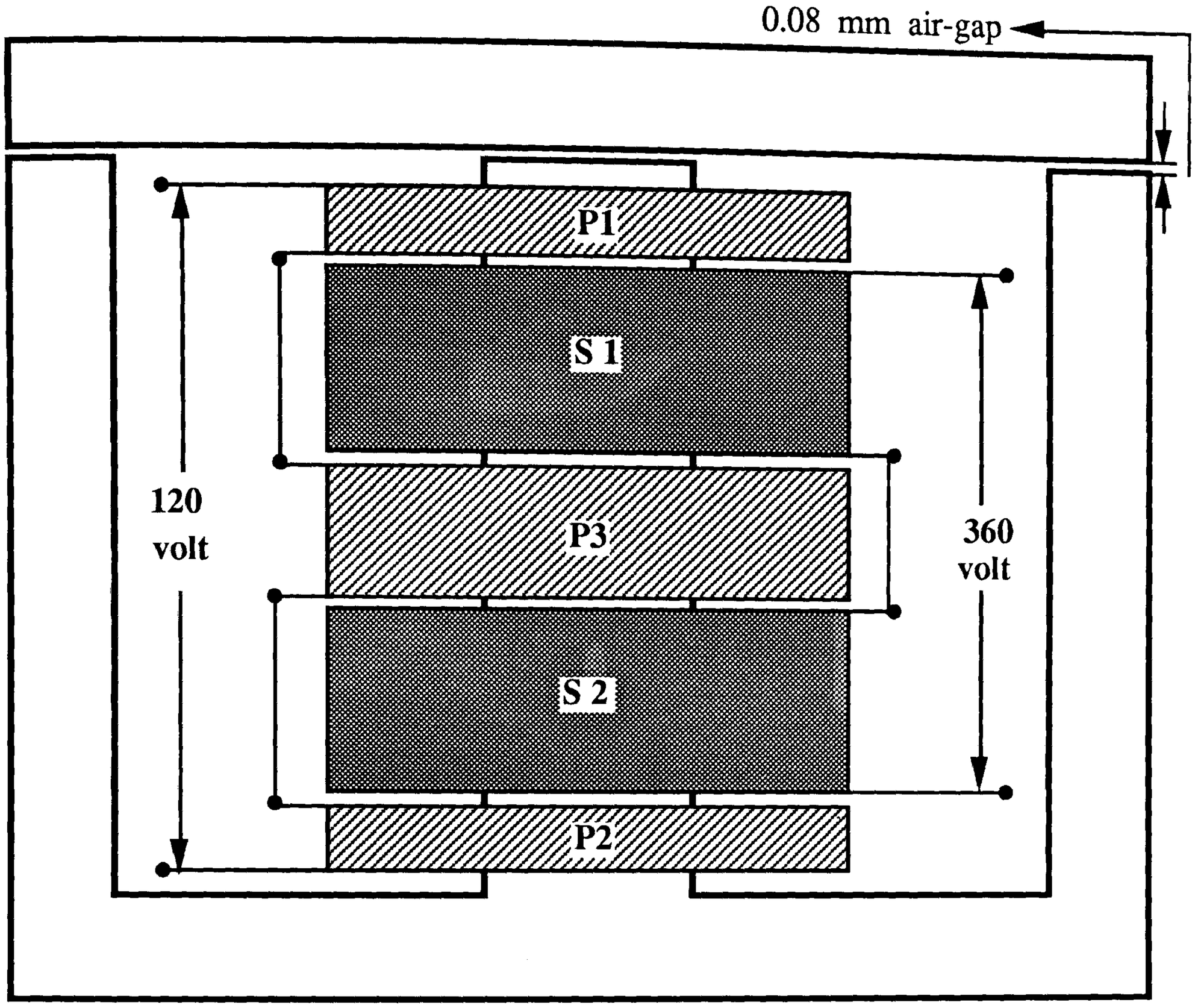

Fig.5-12 **1 kHz** transformer winding configuration (operating in prototype system)

4 - voltage rating:

As can be seen from Fig. 5-3 & Fig. 5.5 the each primary winding will be supplied by two MOSFETs and centre-tapped DC source of **60** v ($\frac{\mathbf{E}}{\mathbf{2}} = \mathbf{60}$ v) . The turn ratio of this transformer is **1 : 3** , that is the secondary output voltage is **360** v .

5 - current rating :

The primary winding is to be designed for maximum **7** amp. and secondary winding is to be designed for maximum **2.5** amp. . The 3-phase connection of this transformer will be feeding an induction motor . A very tiny air-gap (0.08 mm) was left because of reasons explained in section 5.2.1 .

This transformer was supplied by width modulated pulses with **1 kHz** fundamental [according to Figs. 2-(20 , 21 & 22)] by connecting the primary windings to the DC source through the inverter . To avoid any saturation associated problem , the conversion system was operated at **60-80** v of DC supply .

5.4 3-Phase Cycloconverter For Prototype System

The comprehensive discussions on power frequency changers (cycloconverters) have been presented in chapter 4 , including :

1- Direct frequency conversion :

i - generalized **m**-phase input with $\mathbf{f_i}$ frequency -to- **n**-phase output with $\mathbf{f_o}$ frequency

ii - **3**-phase with $\mathbf{f_i}$ frequency -to- **3**-phase with $\mathbf{f_o}$ frequency

iii - **single**-phase with $\mathbf{f_i}$ frequency -to- **single**-phase with $\mathbf{f_o}$ frequency

iv - **single**-phase with **f** frequency -to- **3**-phase with **f** frequency (**phase-conversion**)

2 - Indirect frequency conversion :

i - generalized **m**-phase with $\mathbf{f_i}$ frequency -to- **DC** -to- **n**-phase with $\mathbf{f_o}$ frequency

ii - **3**-phase with $\mathbf{f_i}$ frequency -to- **DC** -to- **3**-phase with $\mathbf{f_o}$ frequency

The suggested technique (demonstrated in chapter 4) for cycloconverter operation was implemented on prototype system . The same switching devices (used in inverter) are employed for the prototype system force commutated cycloconverter , shown in Fig. 5-13 .

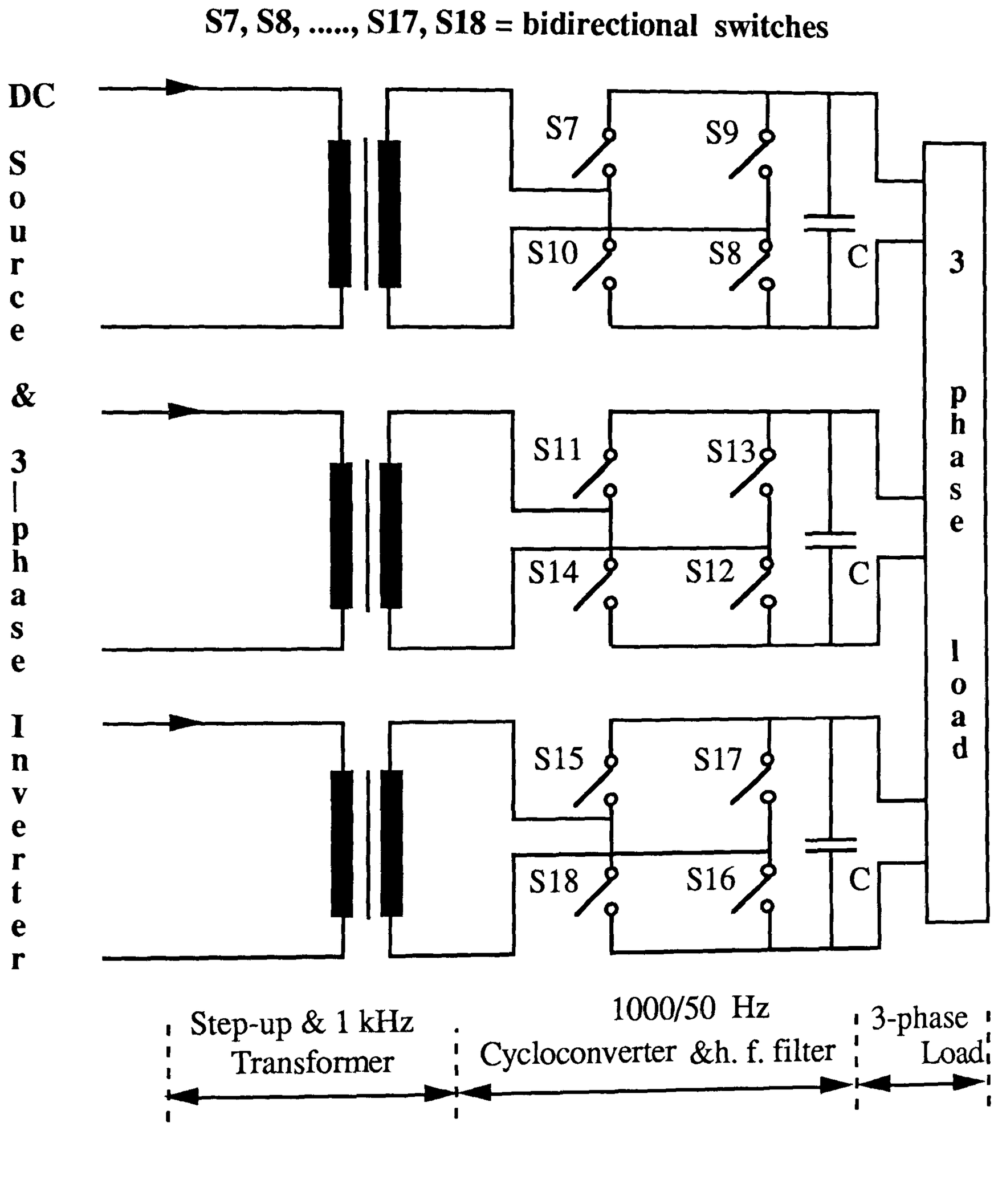

Fig. 5-13 3-phase force commutated cycloconverter for prototype system

5.5 The control circuits

This section deals with the those components that take part in control of the prototype system operation .

5.5.1 Microprocessor for prototype system control

The existing **INTEL-8085** microprocessor system was used to generate :

I- gate signals for 3-phase , half bridge inverter MOSFETs for formation of 3-phase symmetric and 1000 Hz sinusoidal waveforms from DC supply on basis of optimized PWM strategy which have been fully discussed in chapter 2 . The prospective switching pattern are shown in Fig. 5-14 (referring to Fig. 5-5).

II- gate signals for three signal phase -to- signal phase cycloconverter MOSFETs for converting 1000 Hz- to -50 Hz loading power .

The switching pattern for one phase of the cycloconverter MOSFETs are presented in Fig. 5-15 (referring to Fig. 5-13)

Fig. 5-14 Switching patterns for one cycle of 3-phase & 1 kHz prototype system inverter in Fig. 5-5

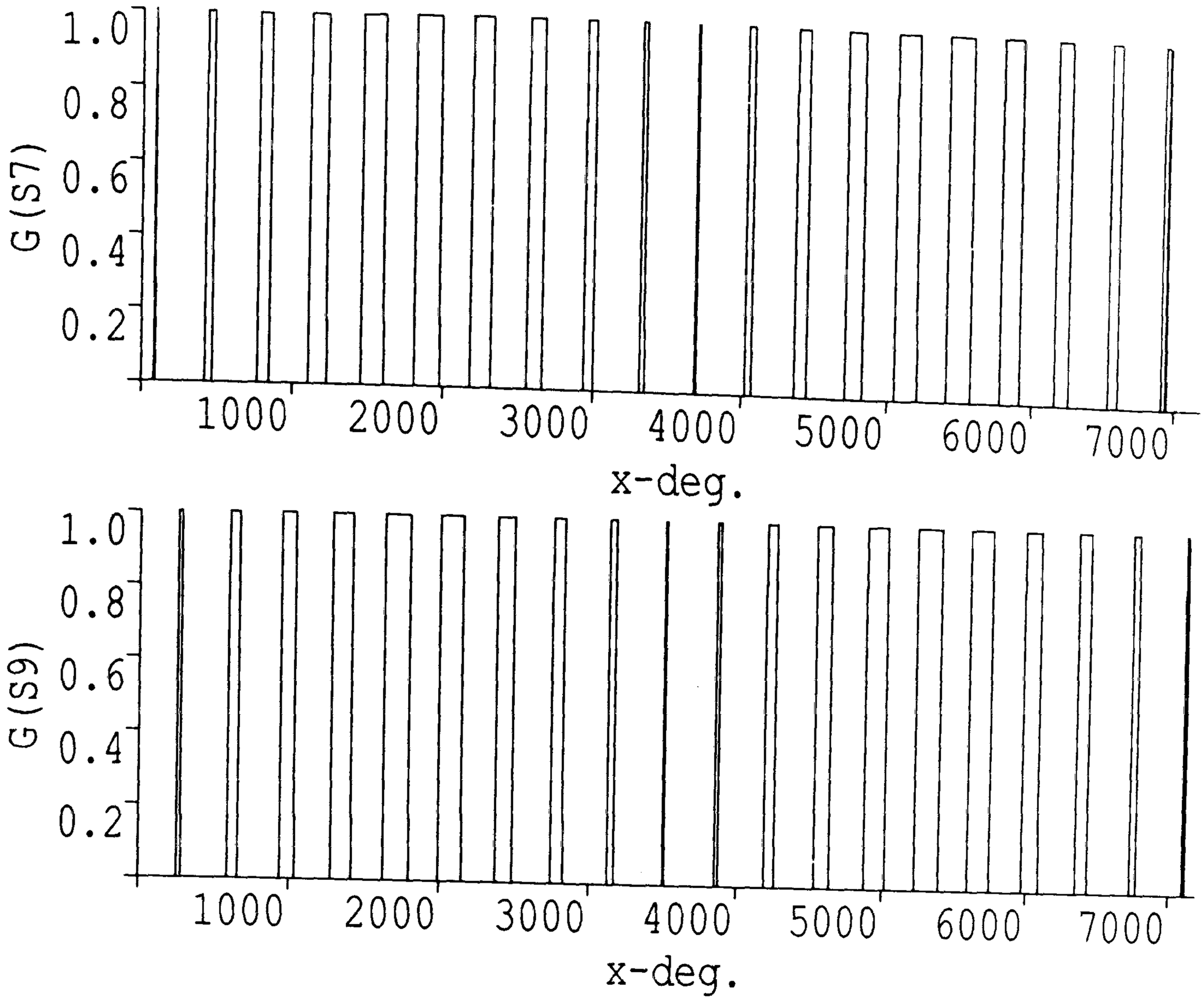

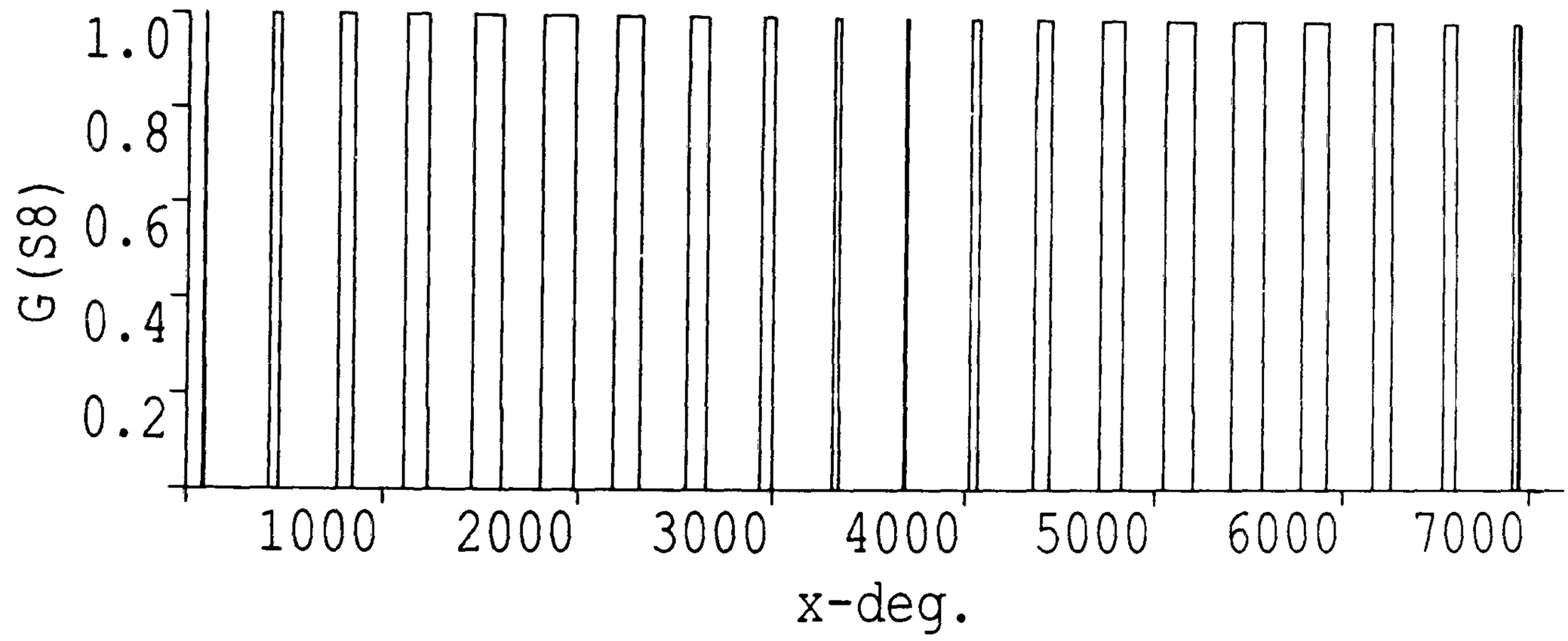

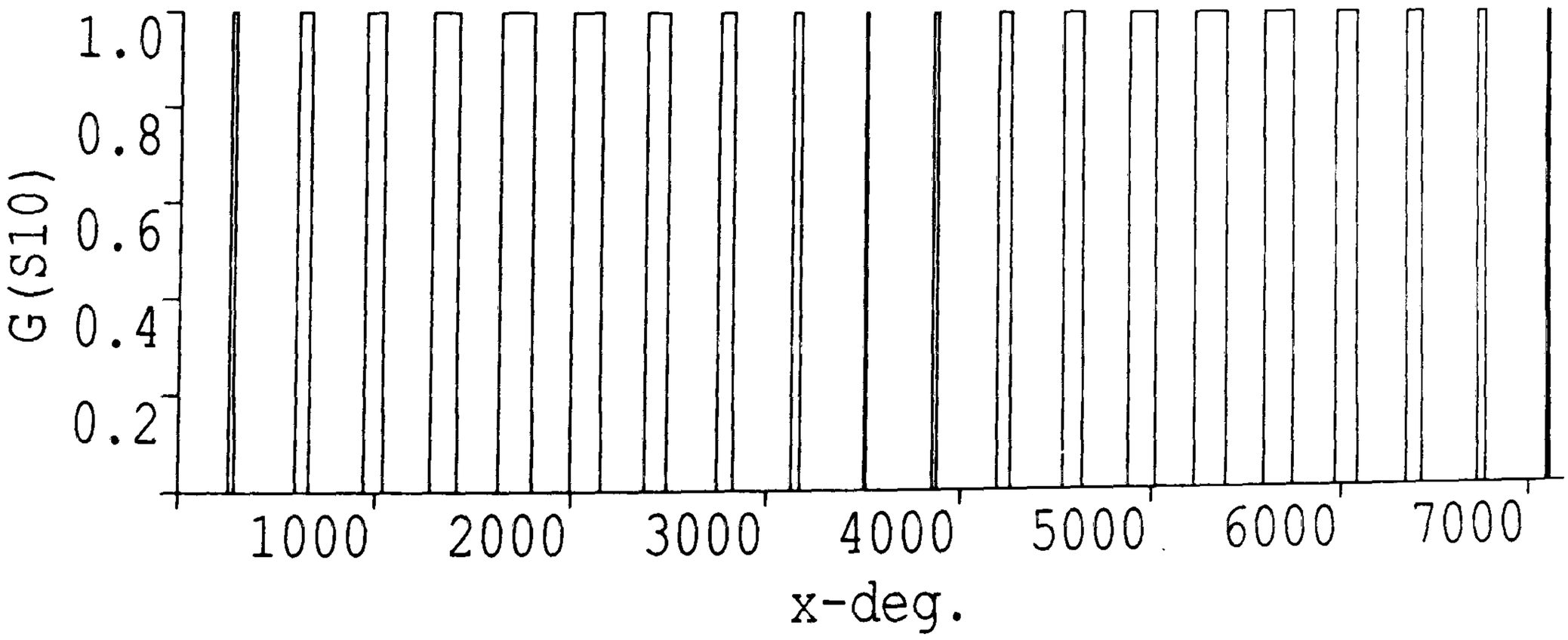

Fig. 5-15 Switching patterns for one cycle of the 1000-to-50 Hz prototype system cycloconverter (in Fig.5-13)

The basic clock frequency of the **INTEL-8085** is **3.072** MHz (internally divided by 2 from the **6.144** MHz quartz crystal input) or state duration = **325.6** nsec [8] & [9] .

The gate triggering angles for both inverter (**table2-10**) and cycloconverter (**table 4-2**) are stored in suitable adresses in the microprocessor **EPROM** . The program starts to execute when zero crossing pulse arrives through the interrupt . Then the required control pulses are transmitted to the drive circuits through the output port .

5.5.2 The zero crossing detector

The prospective application of minicomputers and microprocessors to the control of static converters can only materialize with development of suitable transducers to extract the required informations from the operating converter circuit . For example the zero point detection of current or voltage waveforms .

Since , the cycloconverter in the prototype system , converts the 1000 Hz to 50 Hz and by reconsidering the proposed strategy for cycloconverter switching pattern structure it will be clear that the generation of 1000 Hz by 3 phase inverter should be synchronized by generation of the modulated and 50 Hz cycloconverter output . In other words all the timing circuitry for both inverter and cycloconverter will be referenced to the same point (the mains supply) . A convenient way of this implementation is to use a zero crossing detector which gives a pulse every time the A.C. voltage passed through the zero point . The circuit diagram of the zero-crossing detector is shown in Fig. 5-16 .

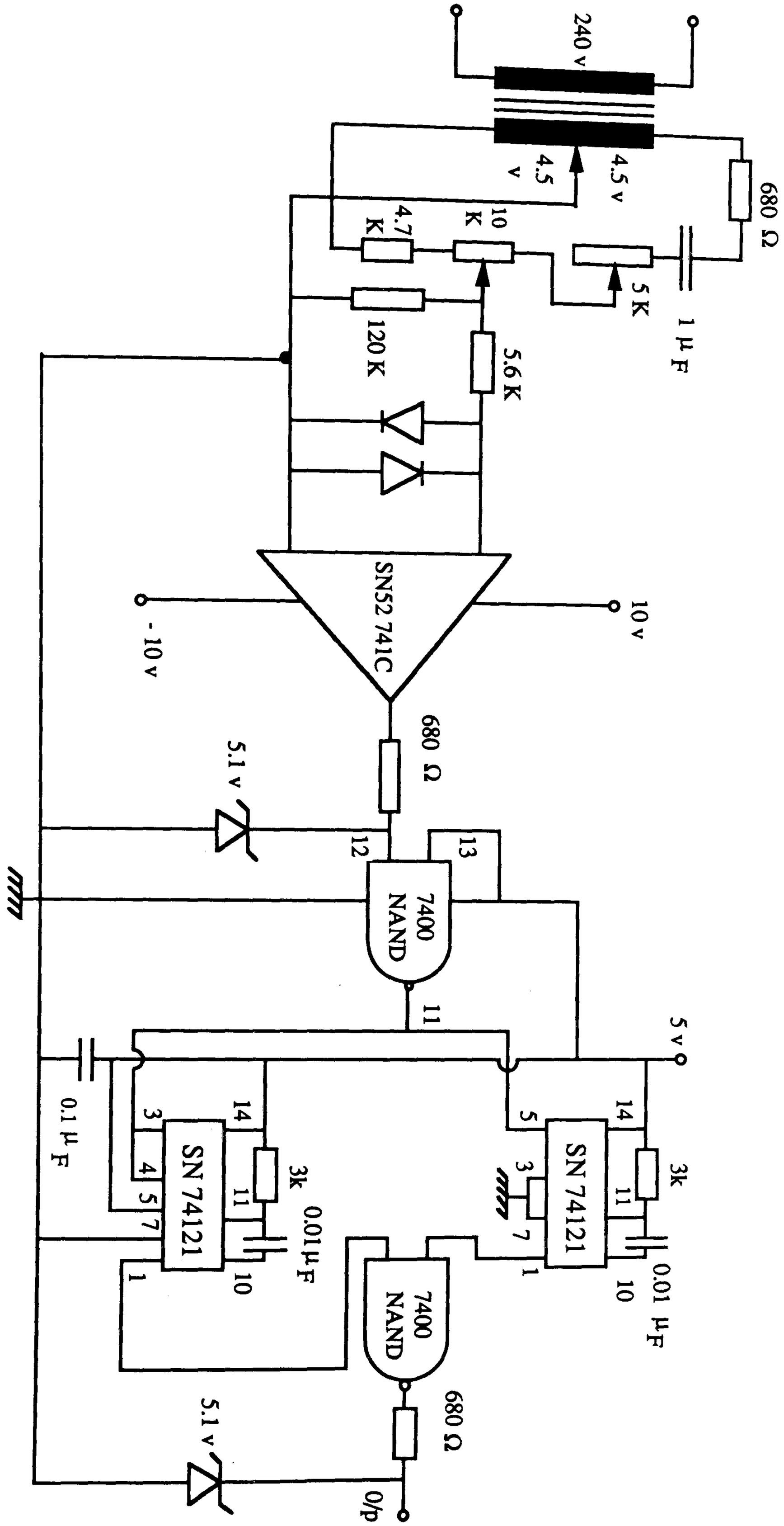

Fig. 5-16 zero crossing detector circuit configuration

A miniature transformer provides isolated low voltage to the circuit. One end of the secondary is grounded to the reset of the system while the other is connected to the inverting input of a **differential voltage comparator** (**SN 52-741 C**) . The non-inverting input is held at 0.0V. The back -to- back diodes across the inputs of the comparator and in series with a resistor ensure that both the current and the voltage ratings of it are never exceeded .

5.5.3 The phase shifter

Referring to Fig. 5-13 , for 3-phase cycloconverter MOSFETs , 12 gating signals are required. Although the microprocessor is capable of generating 12 switching pulses , but it is more efficient (from the software design points of view and avoiding excessive device switching) if the microprocessor generates only gating signals for **No. 1** single phase cycloconverter and then by using appropriate logic circuit converters (**phase-shifters**) for generating **120°** and **240°** delayed pulses , the **No. 2** and **No. 3** single-phase cycloconverters will efficiently be gated and finally the 3-phase cycloconverter will be ready to convert the **1000** Hz to **50** Hz according to suggested modulation strategy .

Fig. 5-17 shows a **0°** , **120°** and **240°** phase shifter circuit diagram . Where two **4-bit down counter** (741 S193) , **monostable** (74121) , **D-Flip-Flop** (7474) and 25 **8-bit Registers** (741 S164) , and **NAND gate** (74000) are taken part to generate **120°** and **240°** delayed pulses . The **4** units of this phase shifters are needed for prototype system .

5-6 Experimental results taken from the prototype system

The prototype system , shown in Fig. 1-18 , was designed and performed based on the circuit diagram of Fig. 5-1. The different practical results of the normal system operation is presented in coming pages .

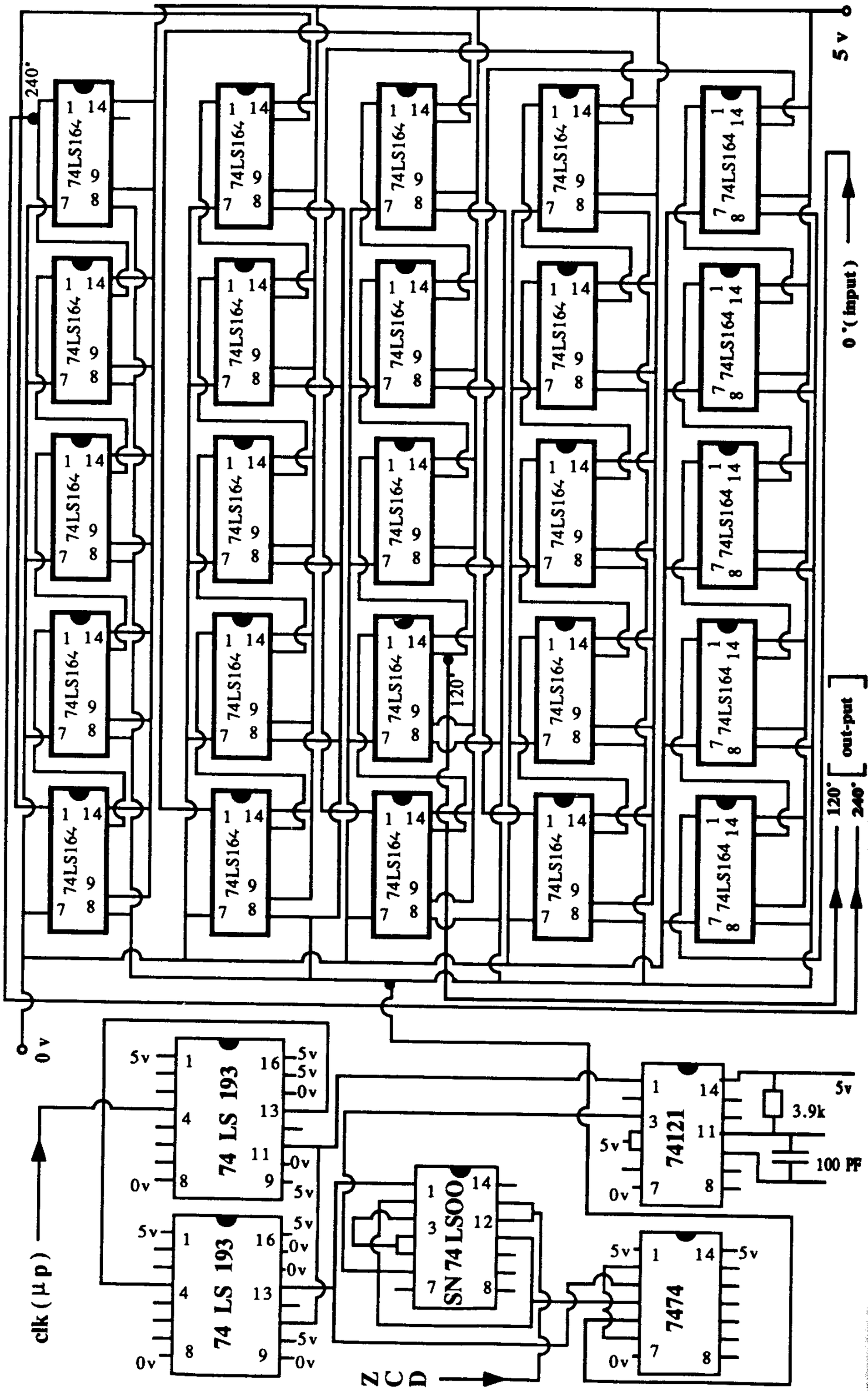

Fig. 5-17 The phase shifter circuit diagram , employed for gating of the cycloconverter MOSFETs(S11 , S12 , ... , S18)

S7 , S8 , ..., S17 , S18 = bidirectional switches

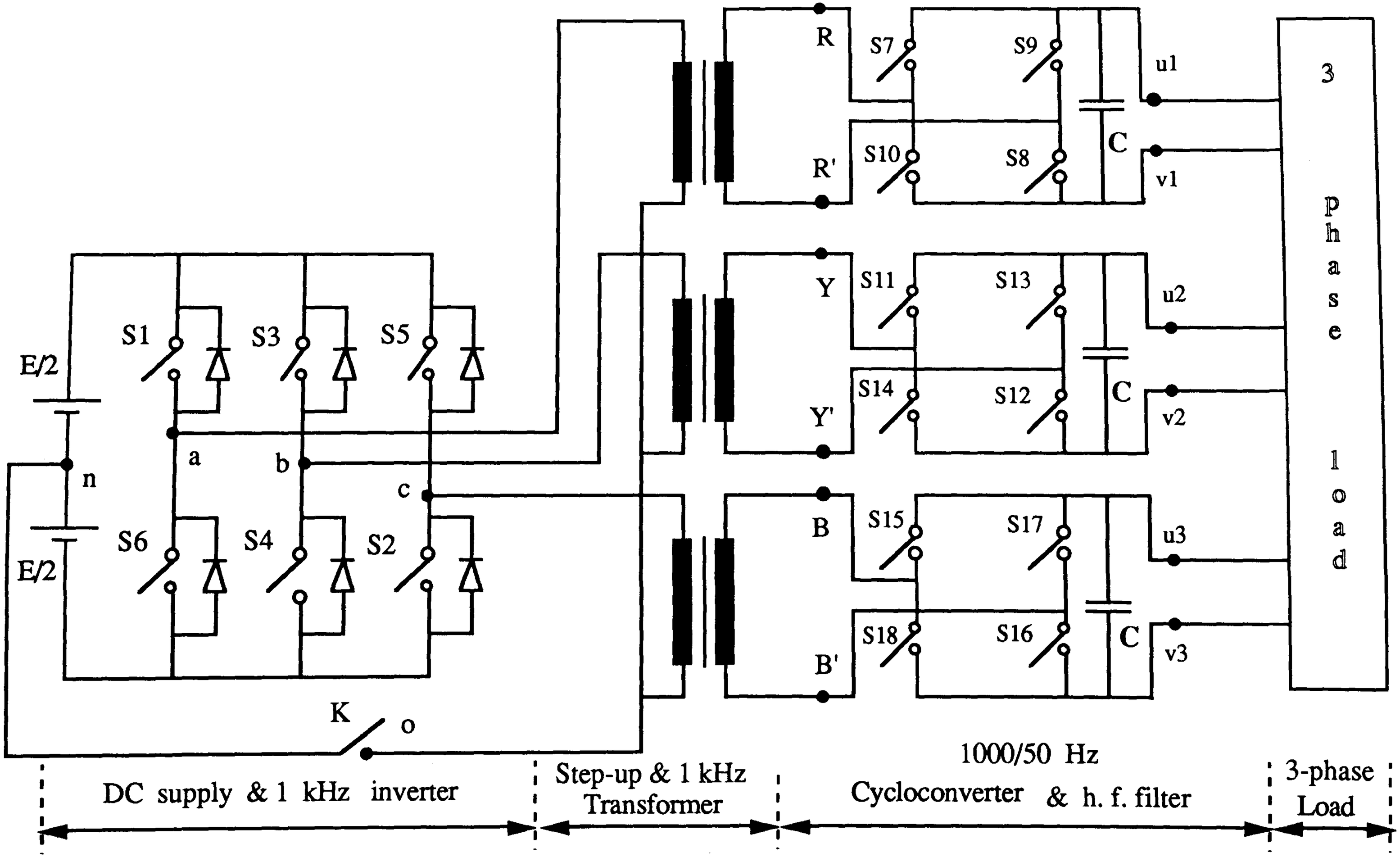

Fig. 5-18 Prototype system circuit configuration for DC-to-AC(3-phase,1 kHz)-to-AC(3-phase,50 Hz) conversion

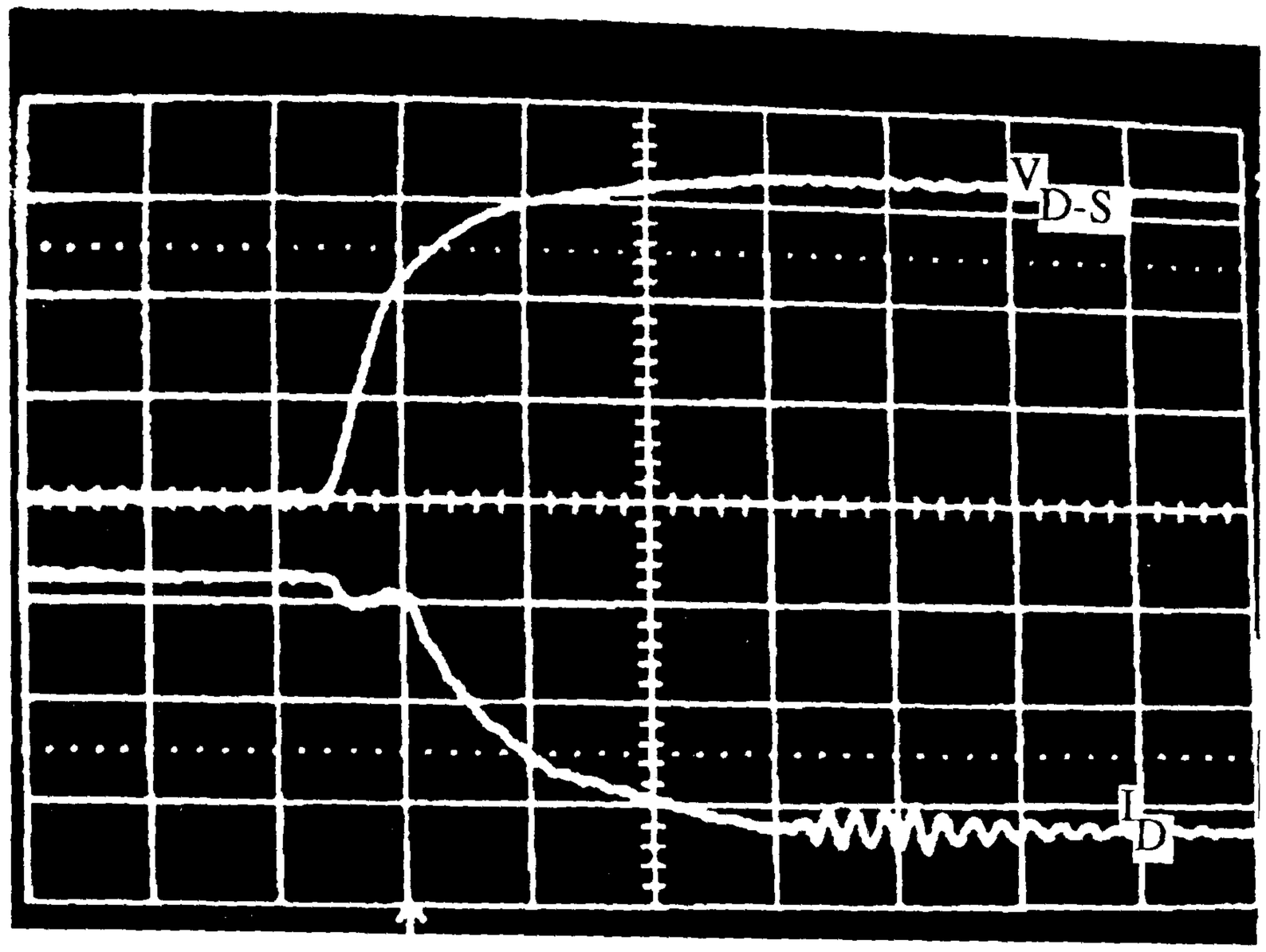

Fig. 5-19 Typical switching waveforms (turn-off) of resistive load for Siliconix **SMM20N50** power MOSFET employed in prototype system inverter & cycloconverter

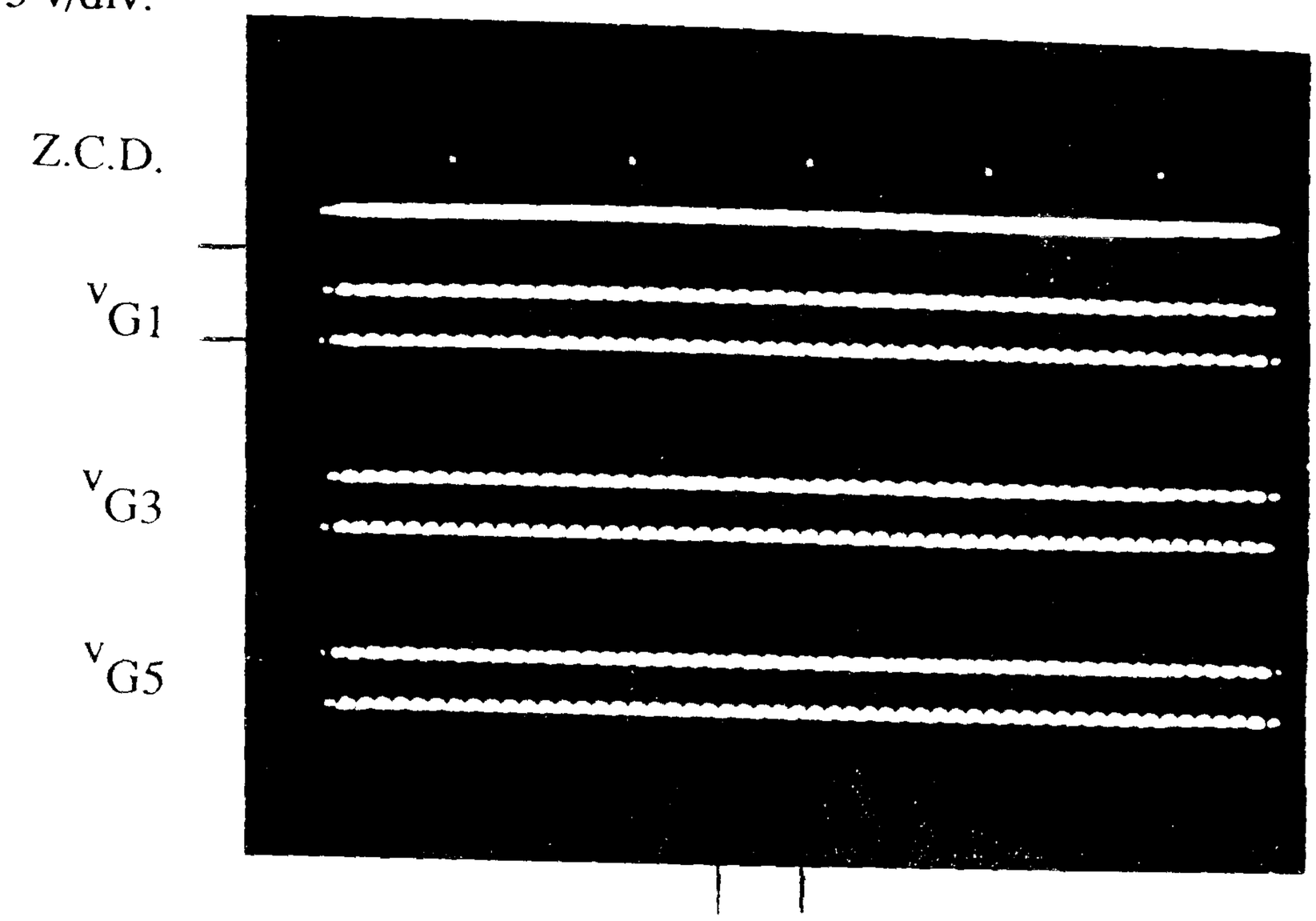

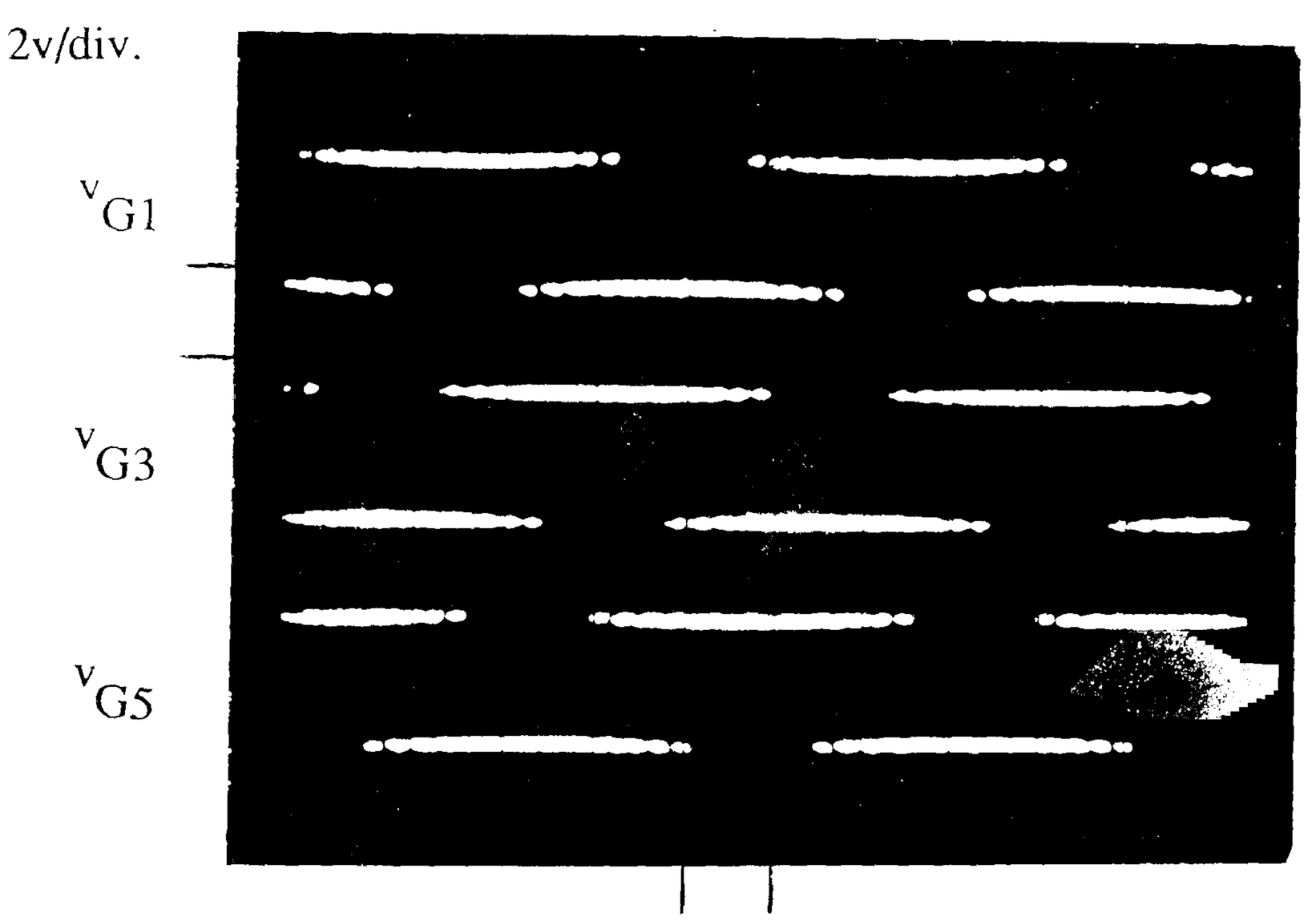

Fig. 5-20 (**a**) Control signals generated by microprocessor for the base drive circuits of **S1** , **S3** and **S5** MOSFETs in inverter of Fig. 5.18 (**b**) Expansion of (**a**) in time domain

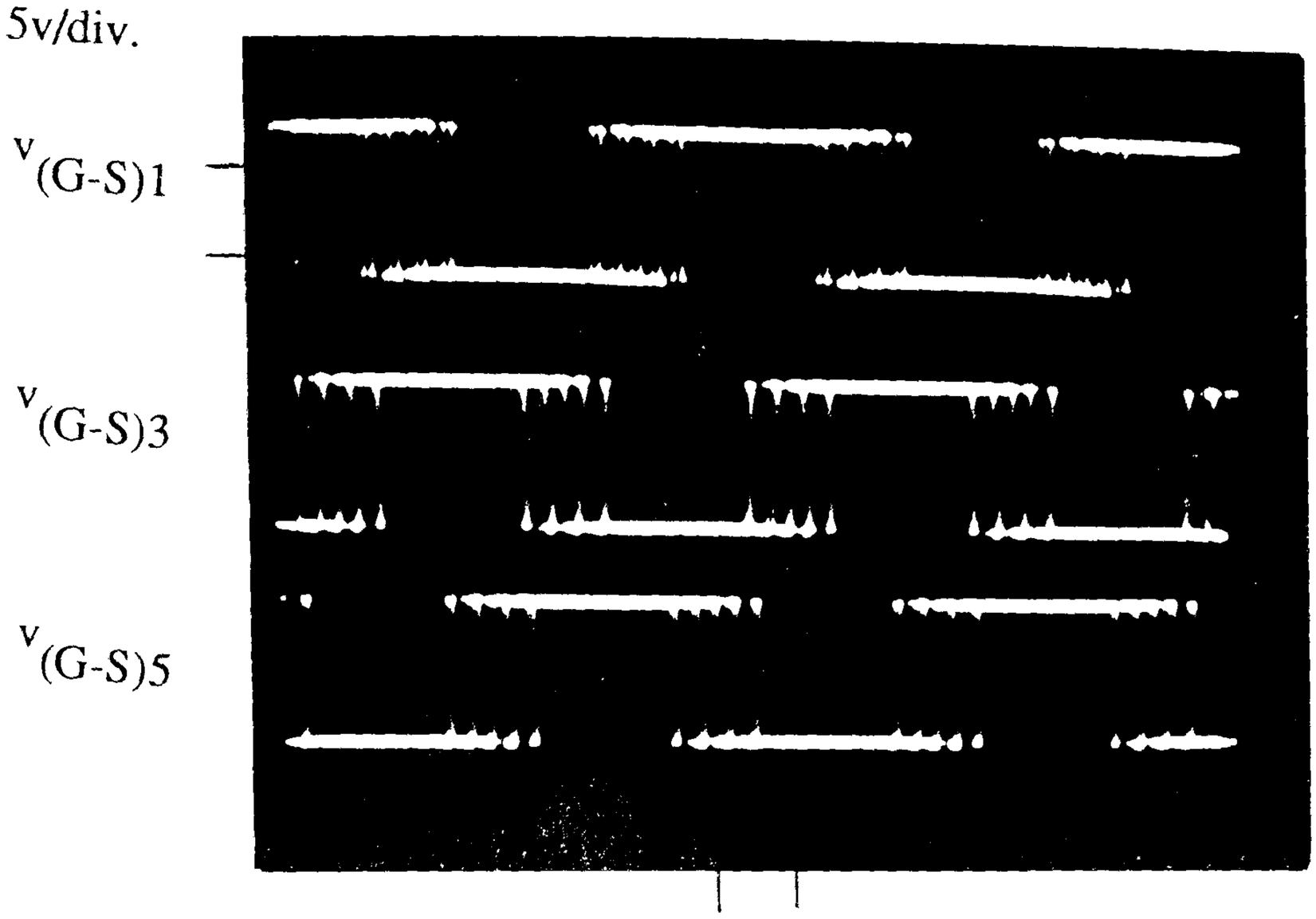

(a) 0.2 msec./div.

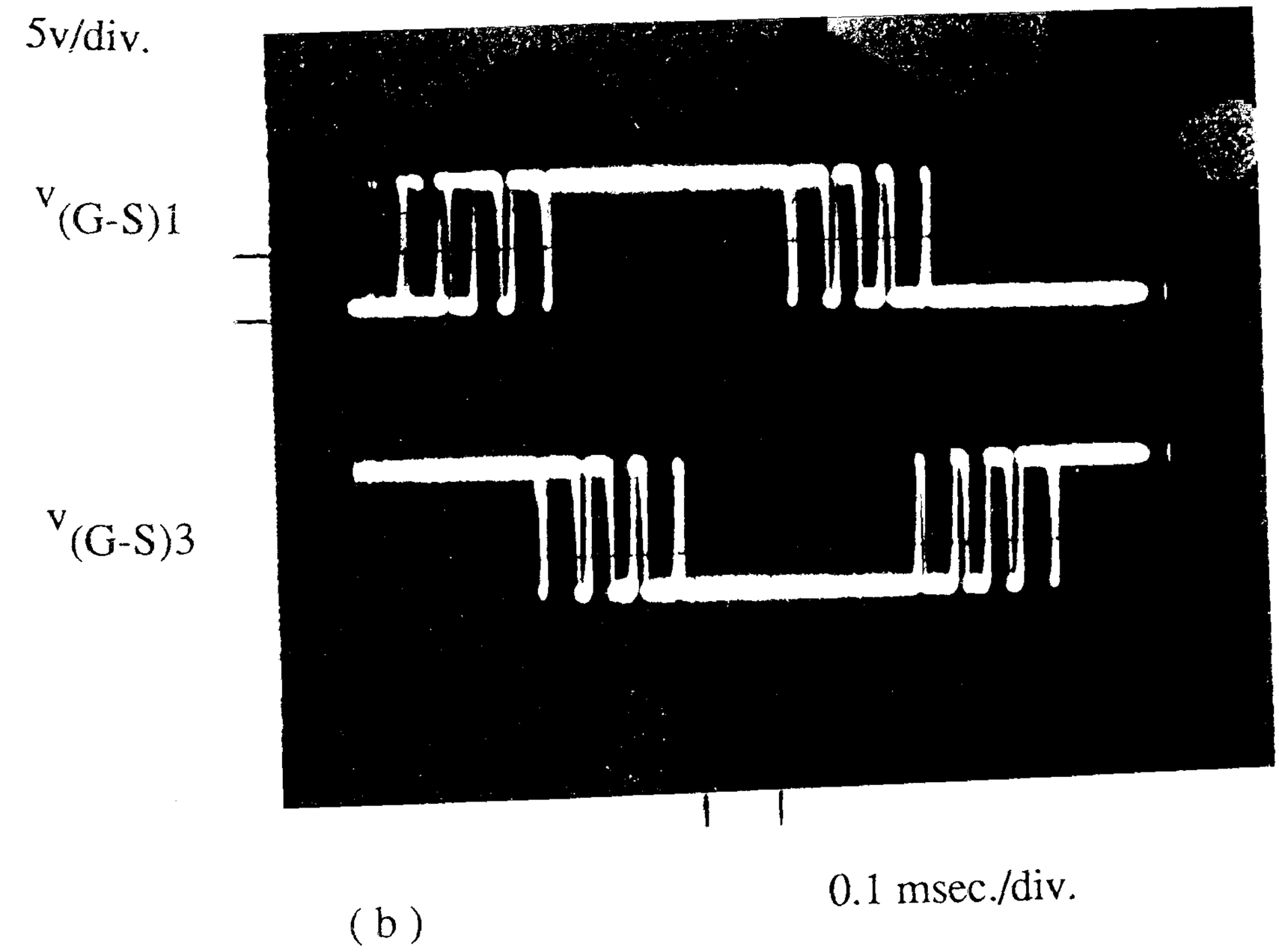

(b) 0.1 msec./div.

Fig. 5-21 (**a**) Triggering signals measured at the **Gate-Source** of **S1** , S3 and **S5** MOSFETs in inverter of Fig. 5-18

(**b**) Expansion of (**a**) in time domain for **S1** & **S3**

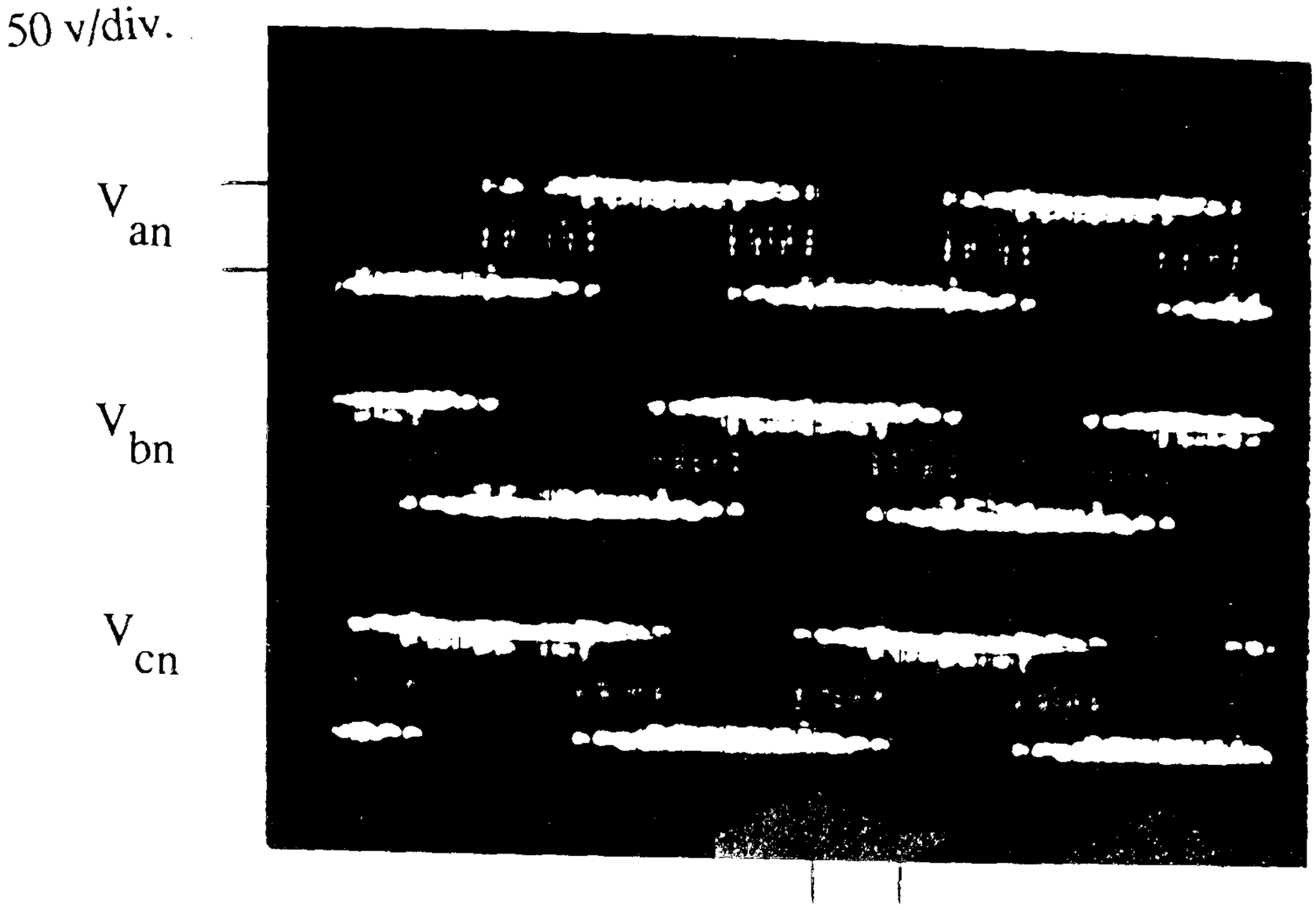

(a)

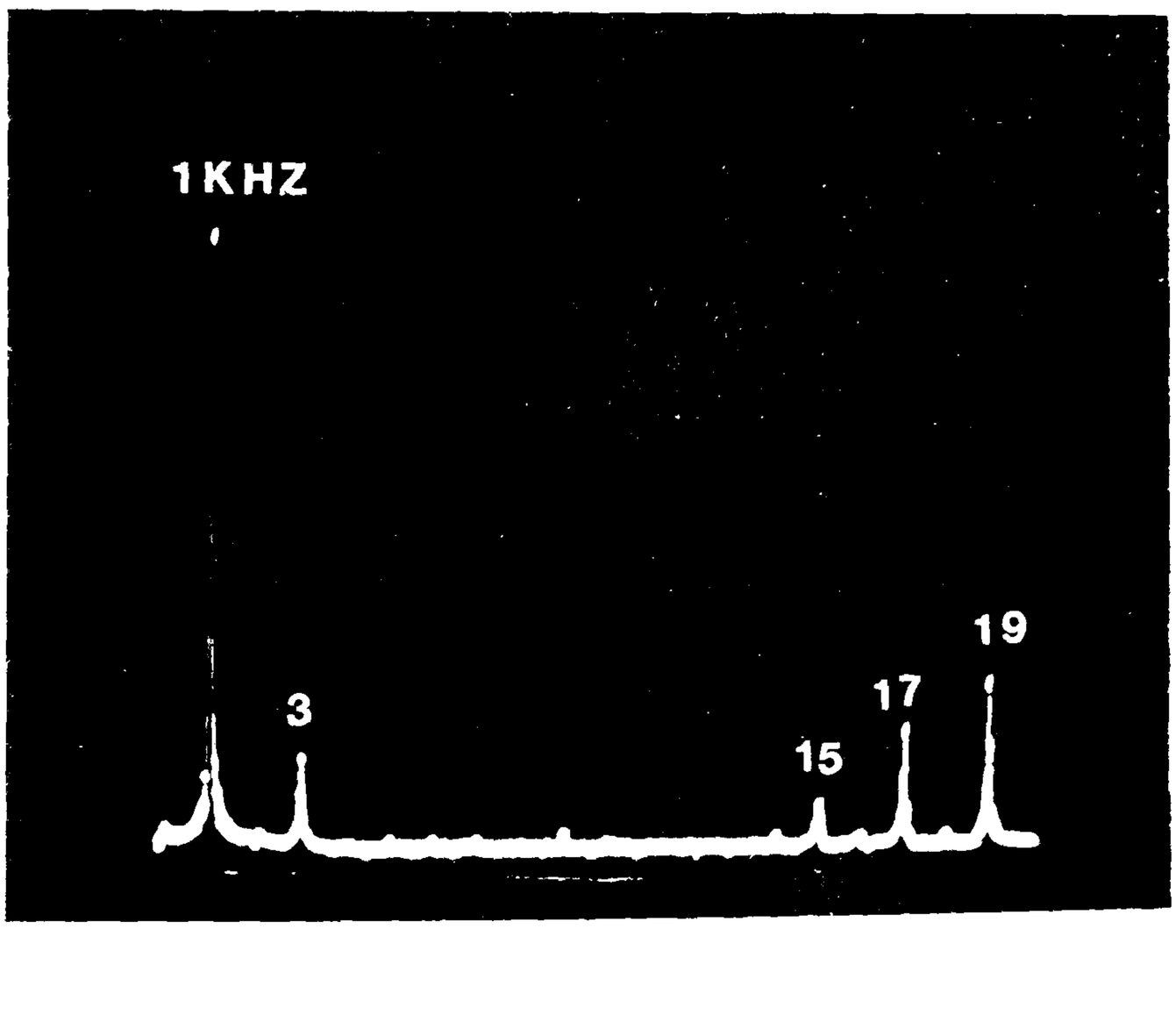

(b)

Fig. 5-22 (**a**) Inverter output (transformer primary) voltage waveforms with secondary open circuit in Fig. 5-18

(**b**) Harmonic spectrum of $\mathbf{V_{an}}$ (K is closed)

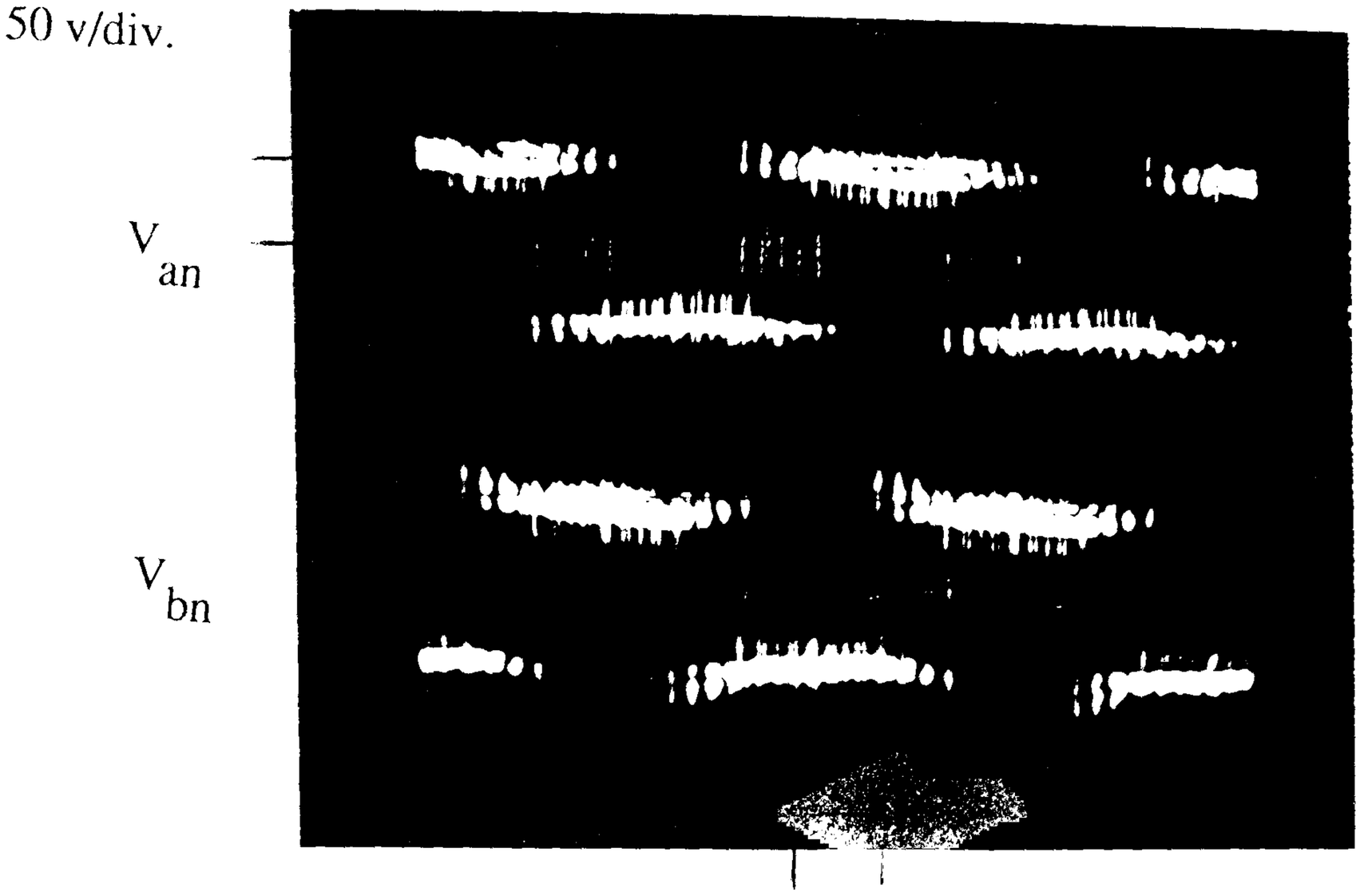

(a) 0.2 msec./div.

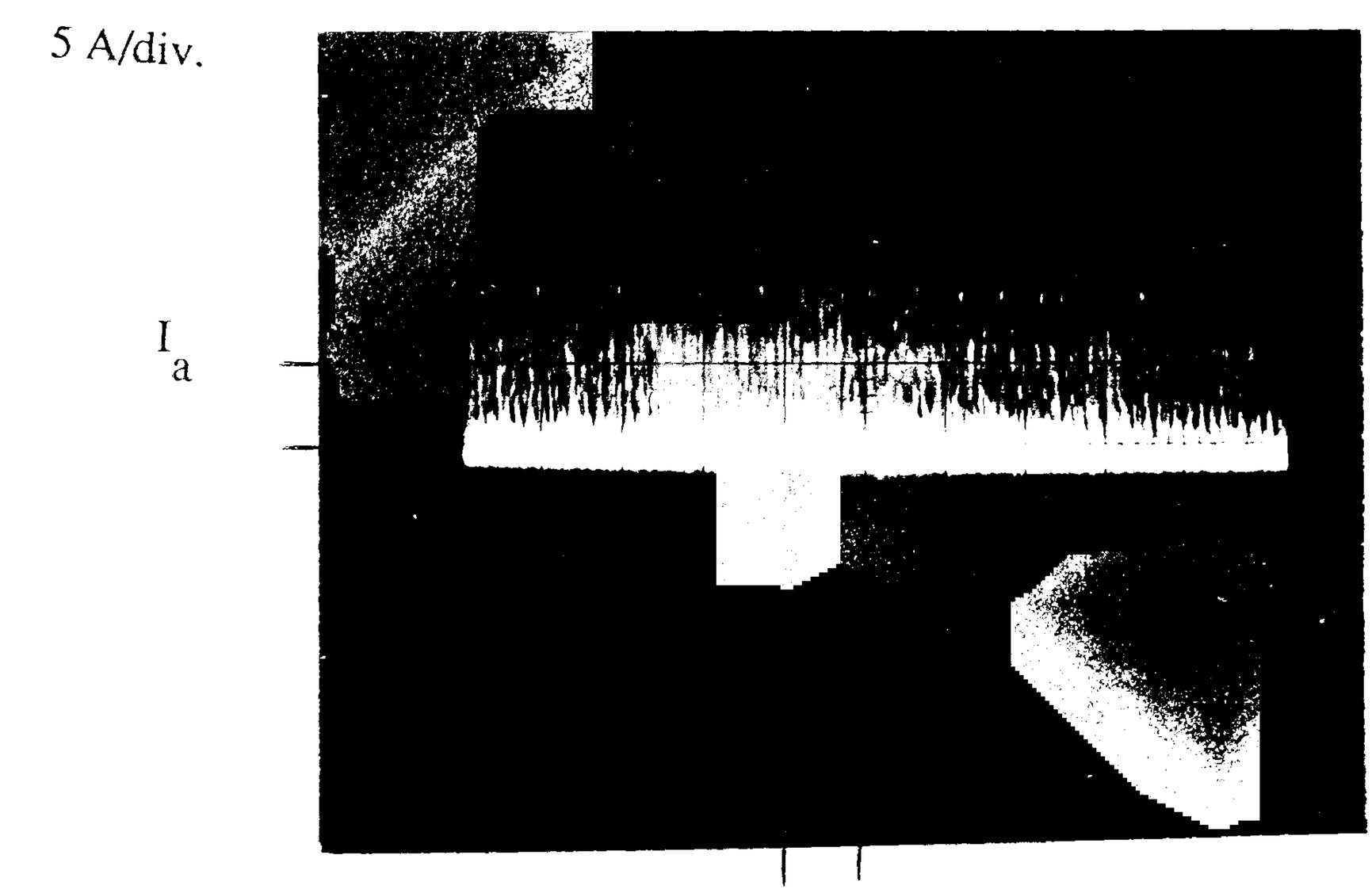

(b) 2 msec./div.

Fig. 5-23 (**a**) Inverter output (transformer primary) voltage waveforms with secondary connected to the set of **Cycloconverter+Filter+Induction motor** (**b**) Primary current waveform

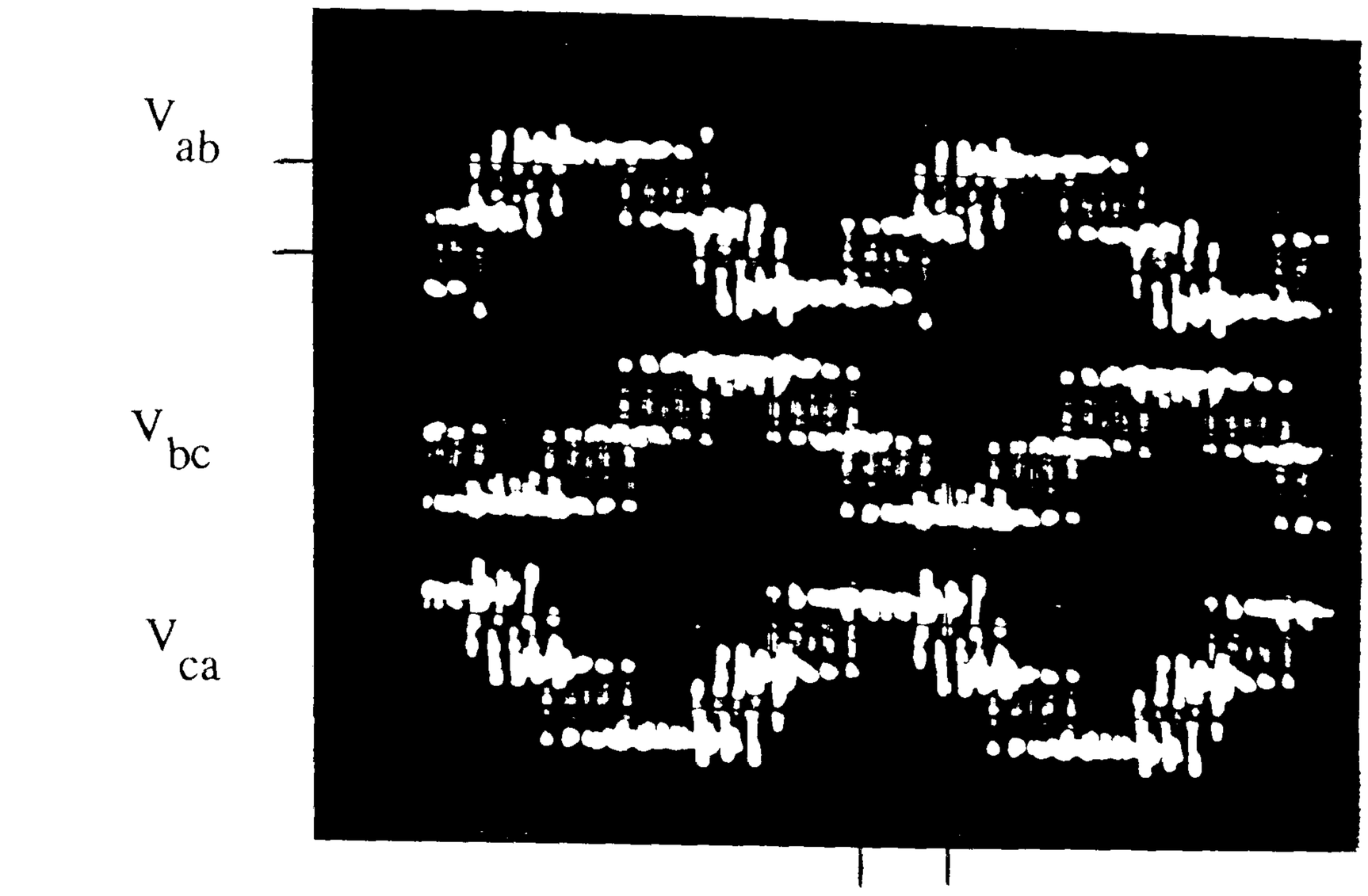

(a)

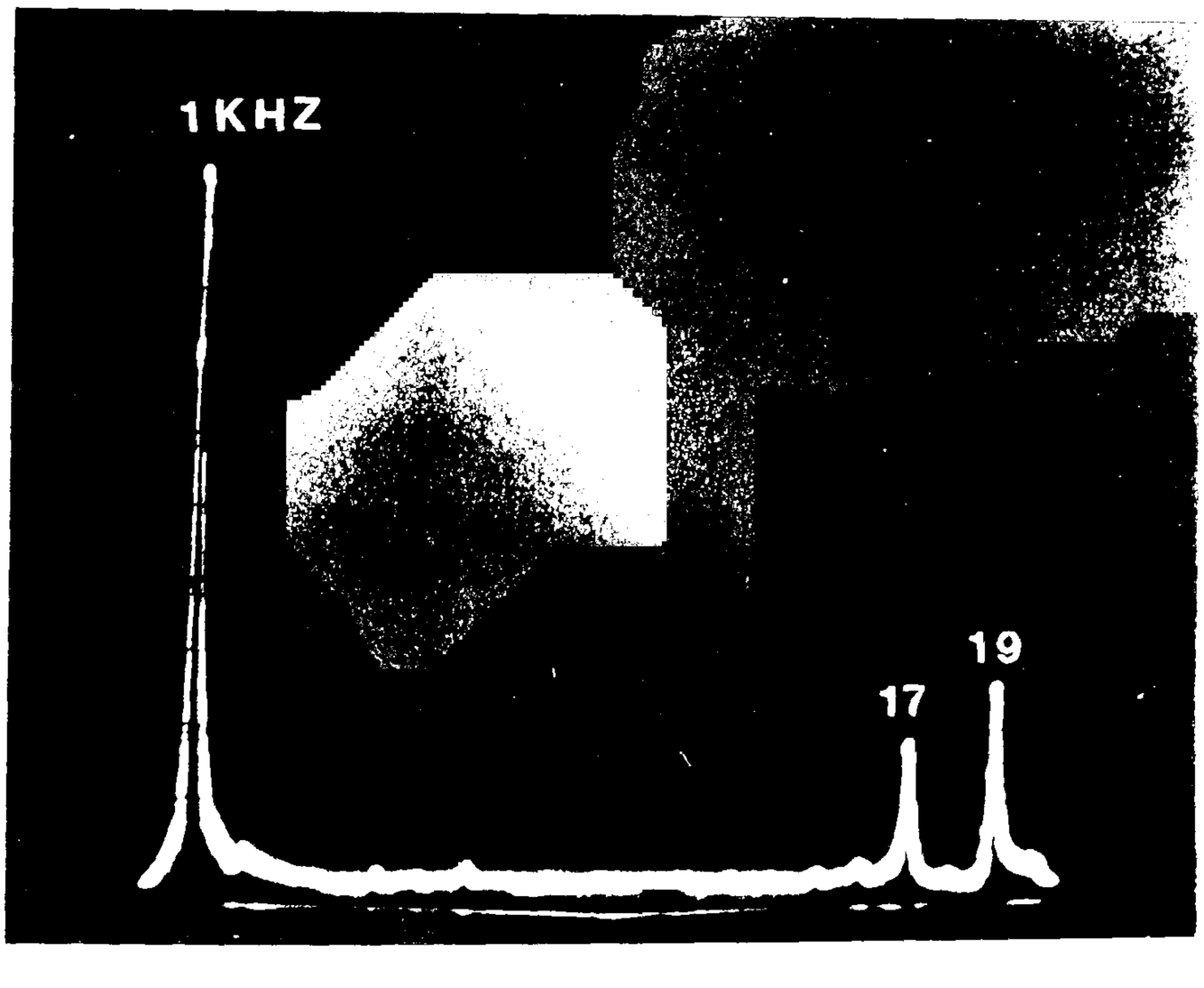

(b)

Fig. 5-24 (**a**) Inverter (primary) line voltage waveforms with secondary open circuit .

(**b**) Harmonic spectrum of the V_{ab}

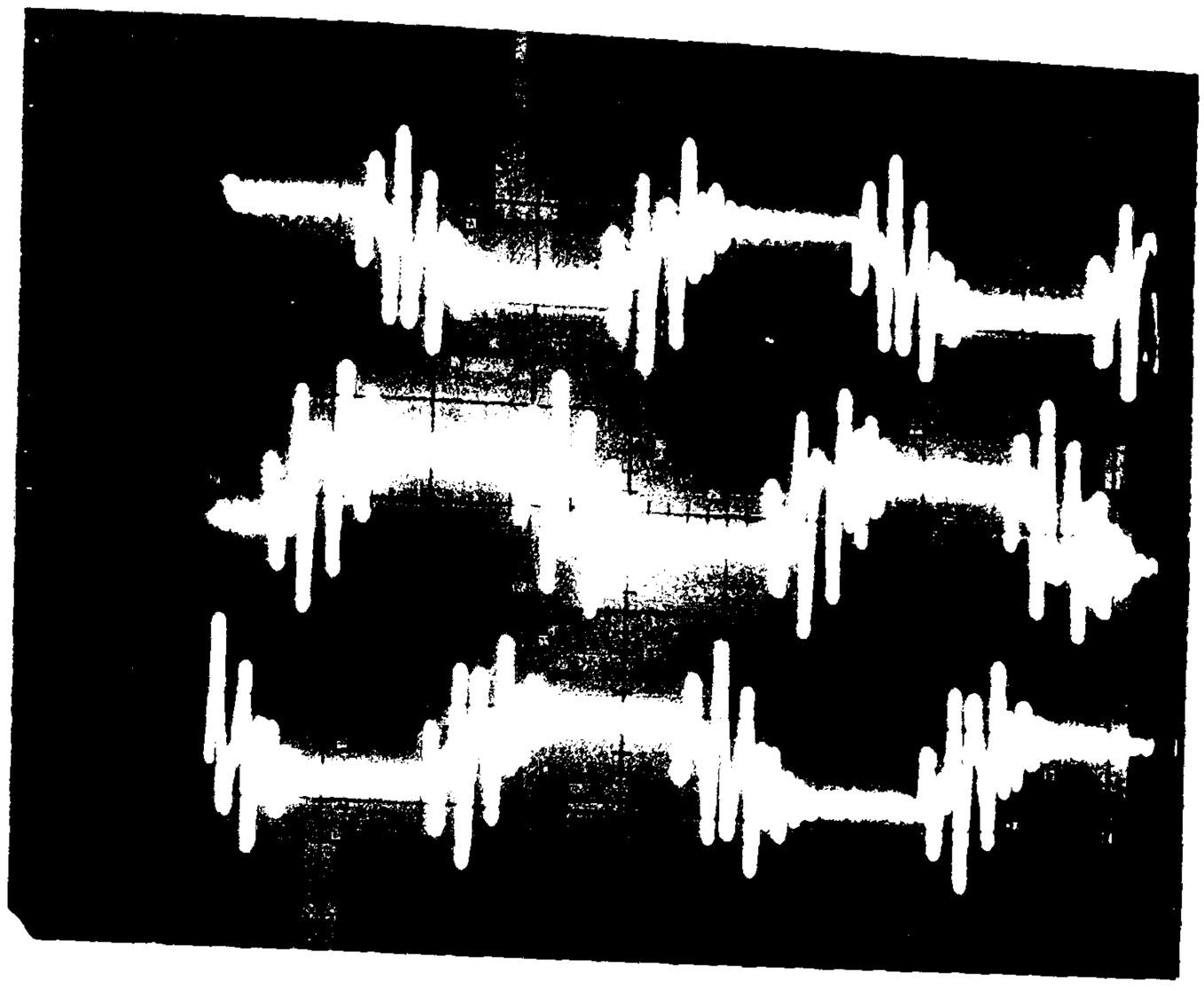

(a) 0.2 msec./div.

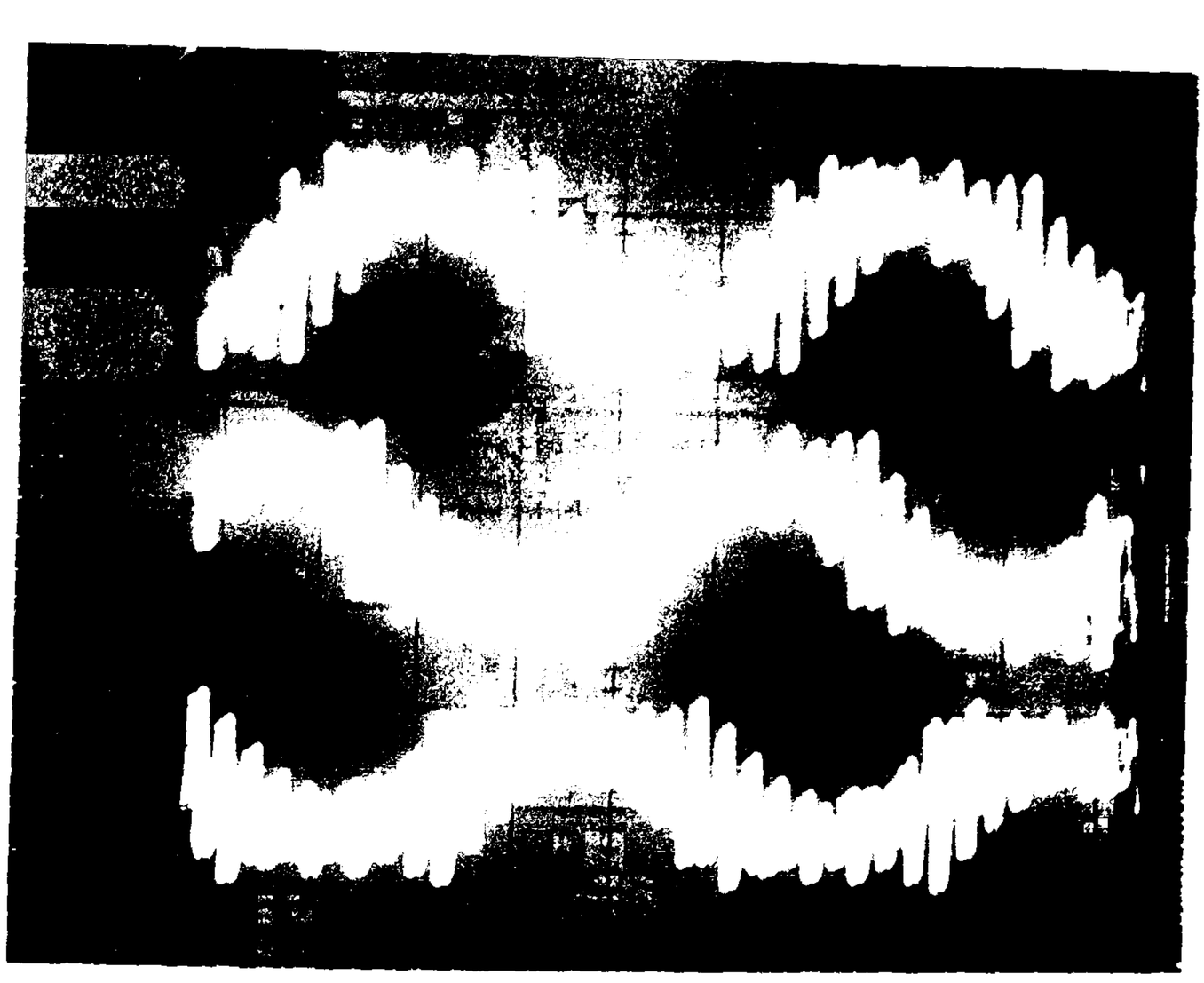

(b) 0.2 msec./div.

Fig. 5-25 Secondary open circuit waveforms (in Fig. 5-18)

(**a**) **n** to **o** is closed

(**b**) **n** to **o** is open

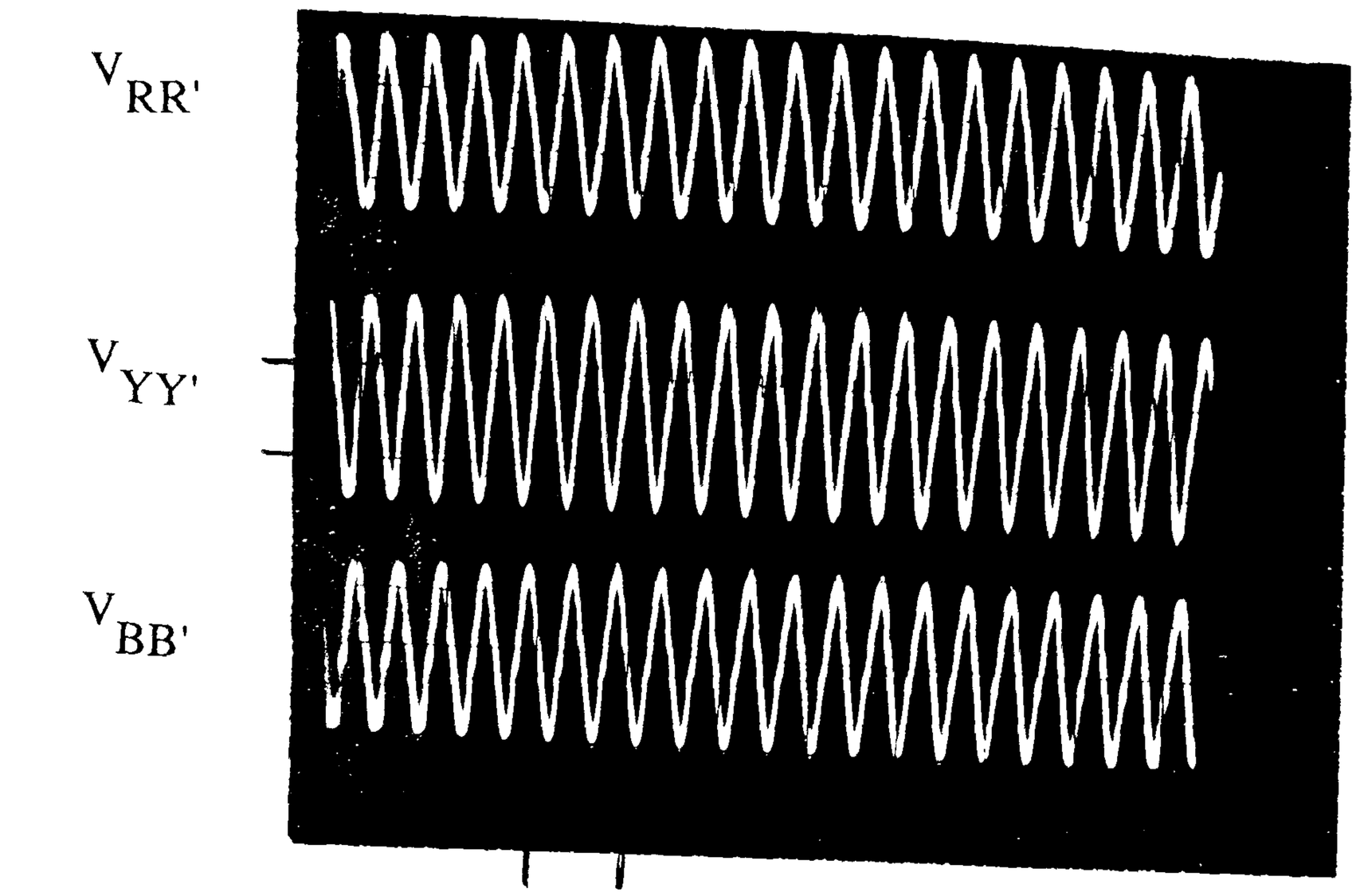

(a)

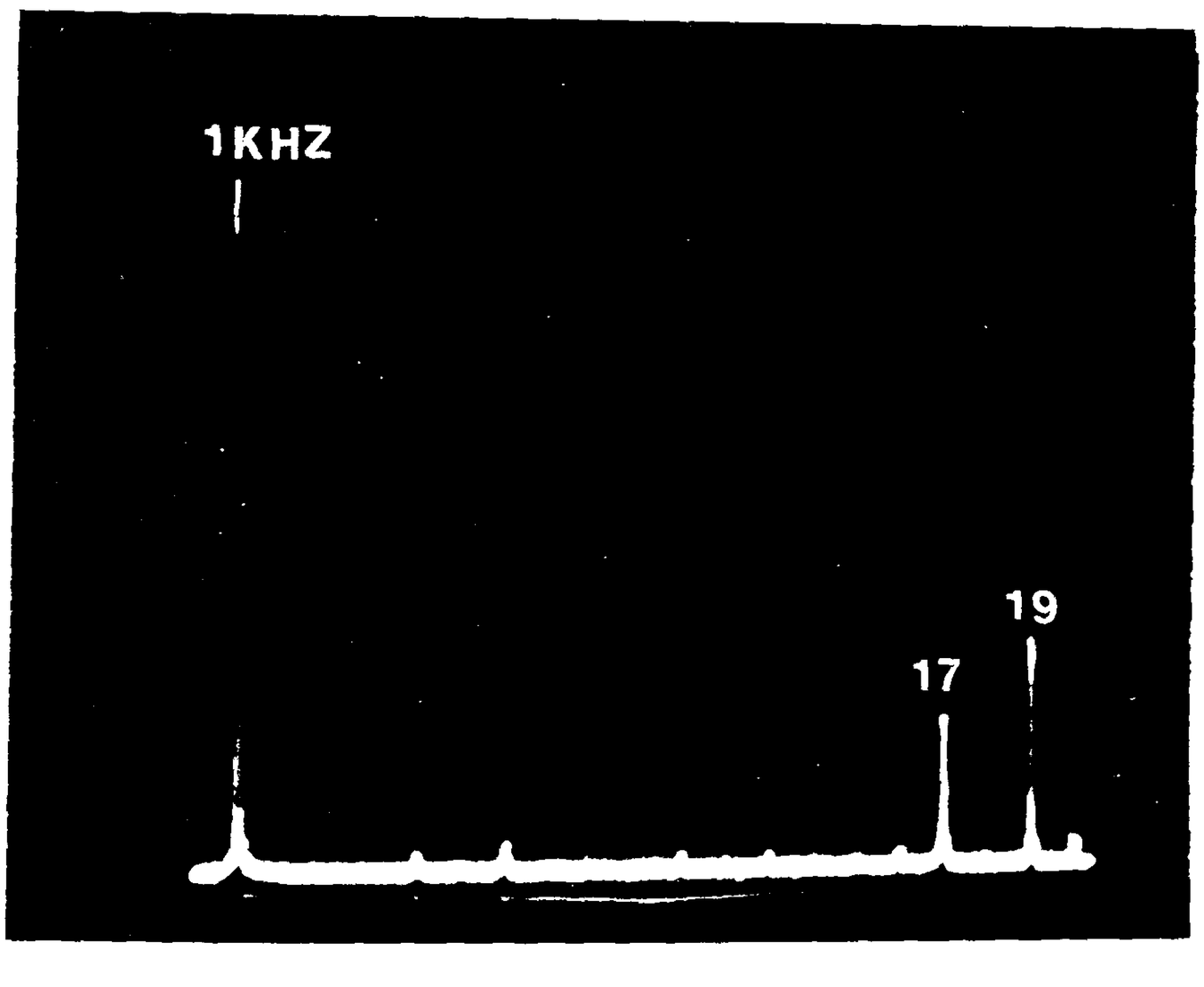

(b)

Fig. 5-26 (**a**) Secondary open circuit wavforms with **L-C series filter** connected between inverter & primary , tuned for **1 kHz** (may be compared with Fig 5-25) (**b**) Harmonic spectrum of $\mathbf{v_{RR}}$, in Fig. 5-25 (b)

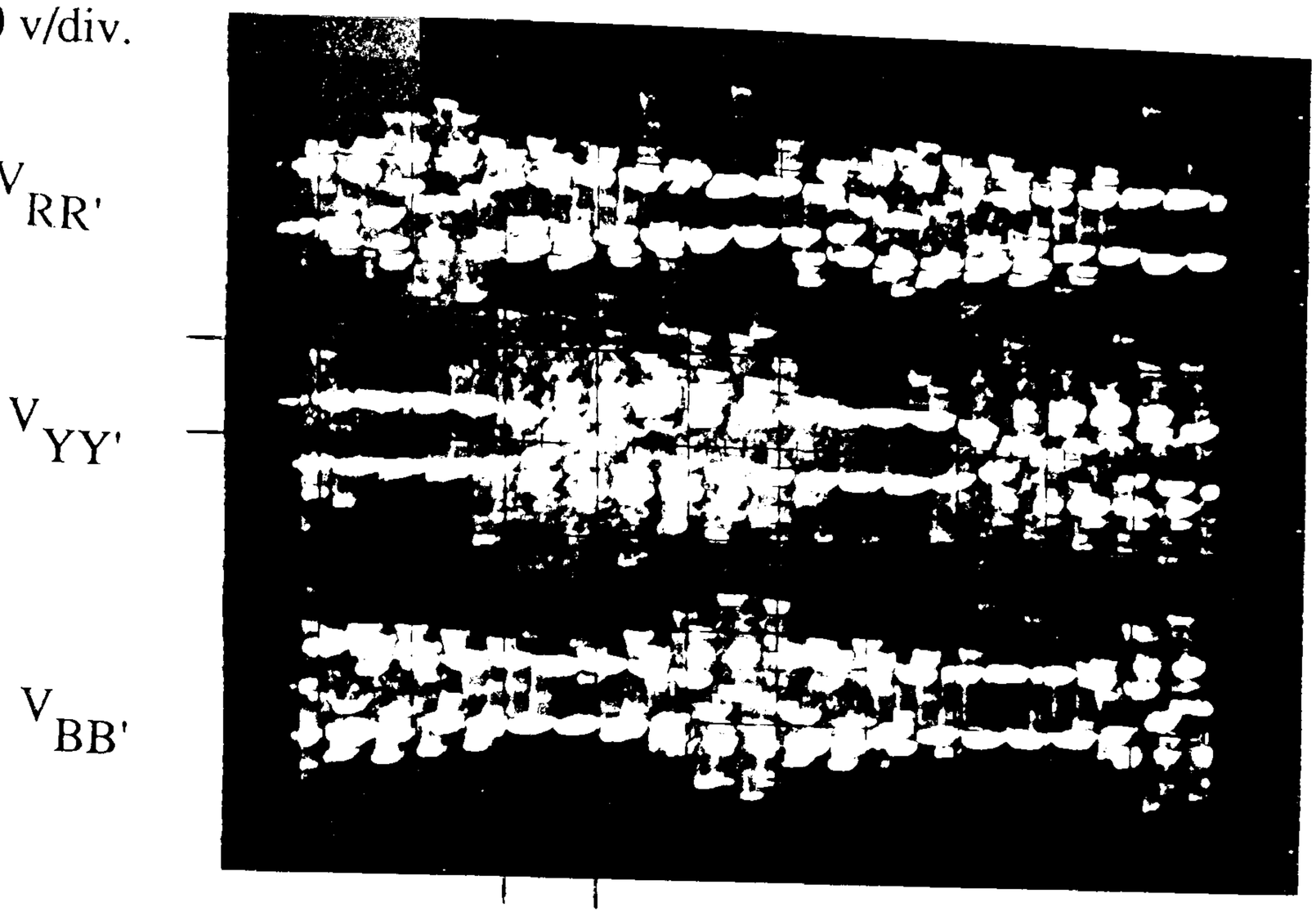

(a)

0.2 msec./div.

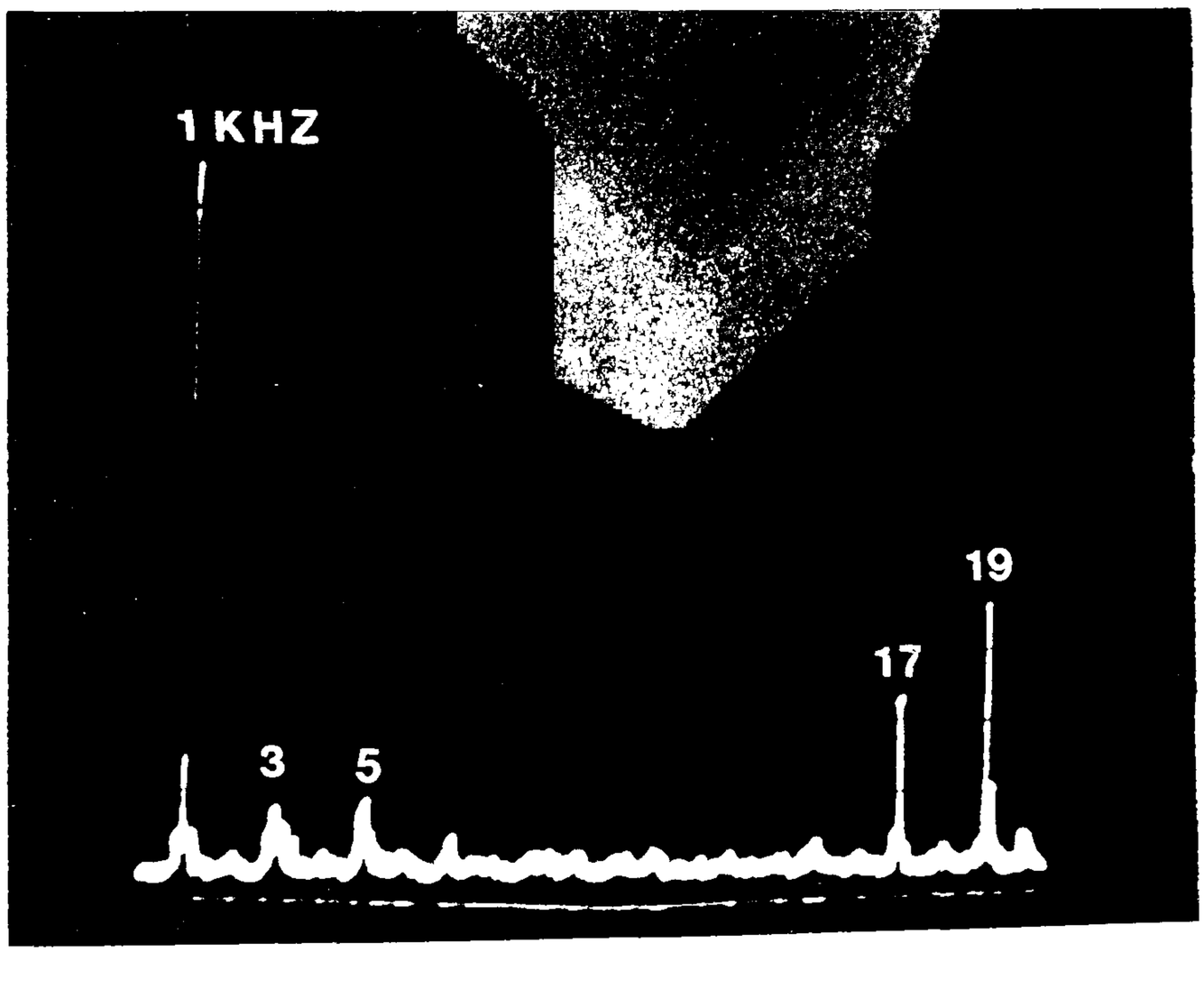

(b)

Fig. 5-27 (**a**) Secondary waveforms during load (induction motor)operation

(**b**) Harmonic spectrum of $\mathbf{V_{RR'}}$

100 v/div.

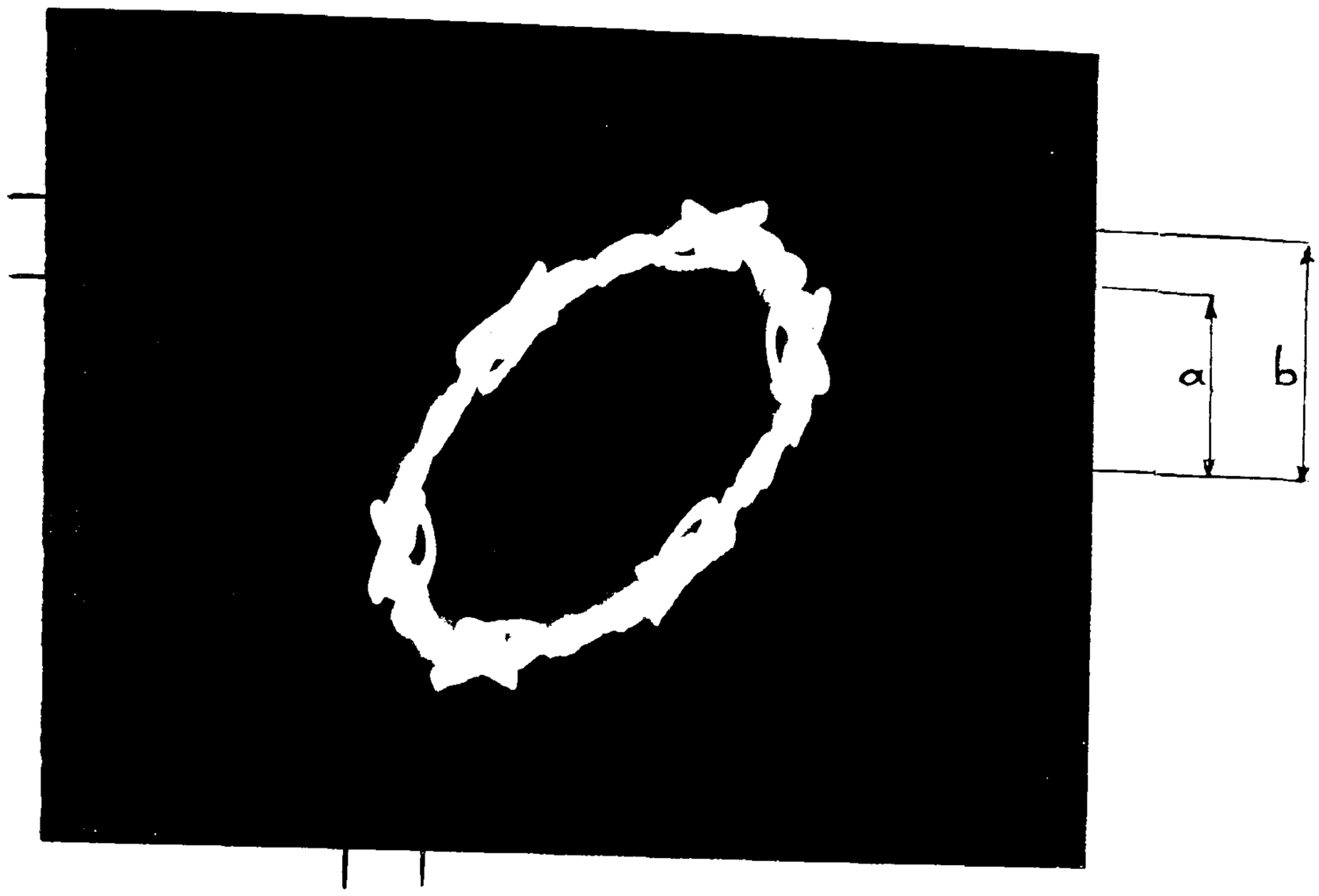

$v_{RR'}$ with $v_{YY'}$

(a) 0.5 msec./div.

$$\Phi(\overset{\frown}{v_{RR'}, v_{YY'}}) = \sin^{-1}(\frac{a}{b}) = \sin^{-1}(\frac{2.2}{2.6}) = 117.85°$$

100 v/div.

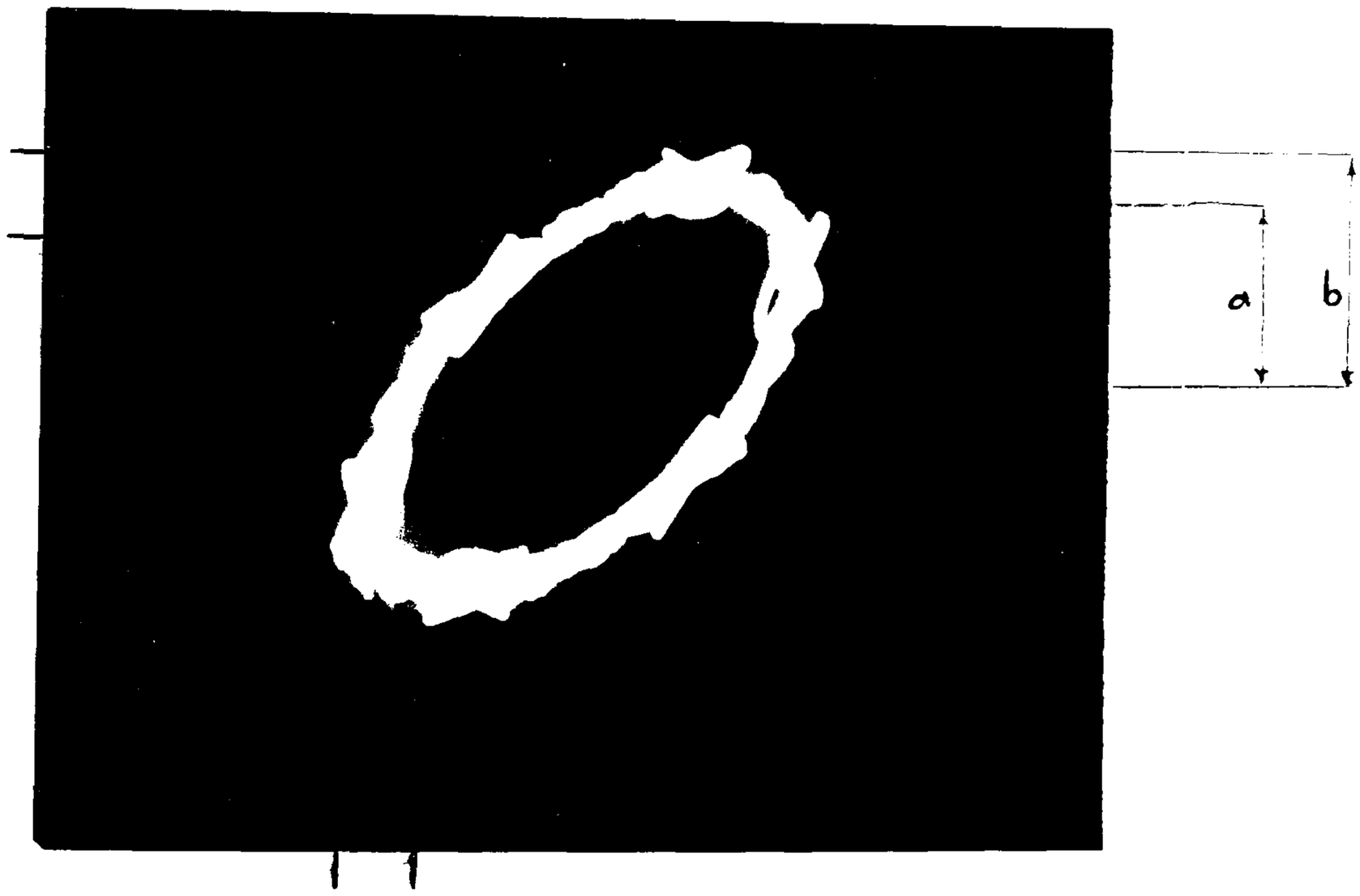

$v_{YY'}$ with $v_{BB'}$

(b) 0.5 msec./div.

$$\Phi(\overset{\frown}{v_{YY'}, v_{BB'}}) = \sin^{-1}(\frac{a}{b}) = \sin^{-1}(\frac{2.2}{2.6}) = 117.85°$$

Fig. 5-28 Secondary voltage waveforms combination for phase angle determination

(**a**) $v_{RR'}$ with $v_{YY'}$ (**b**) $v_{YY'}$ with $v_{BB'}$

100 v/div.

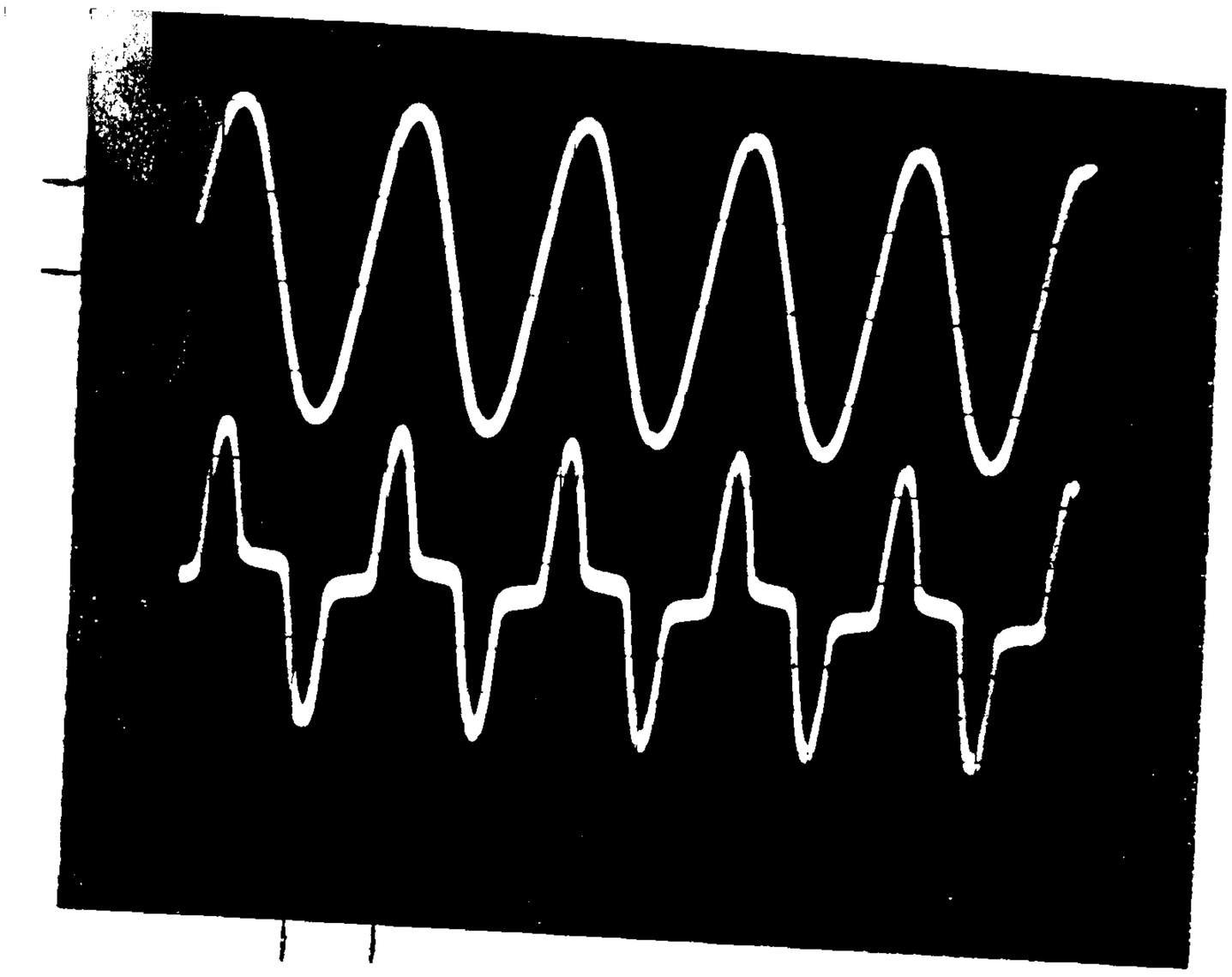

(a)

0.5 msec./div.

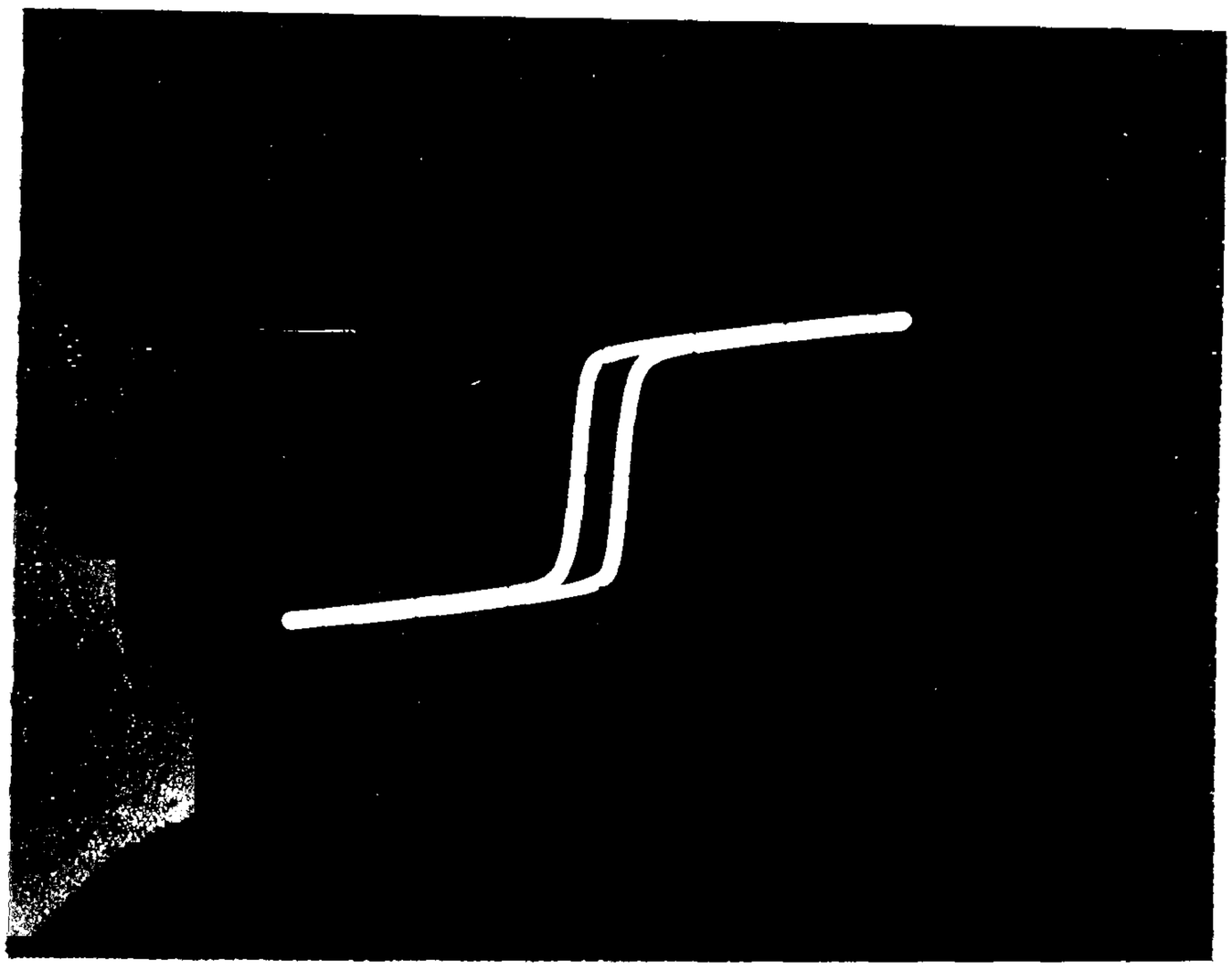

(b) I_ϕ

Fig. 5-29 Prototype system transformer characteristics at **1 kHz** (in Fig. 5-18)

(**a**) Flux and magnetizing current

(**b**) Hysteresis loop

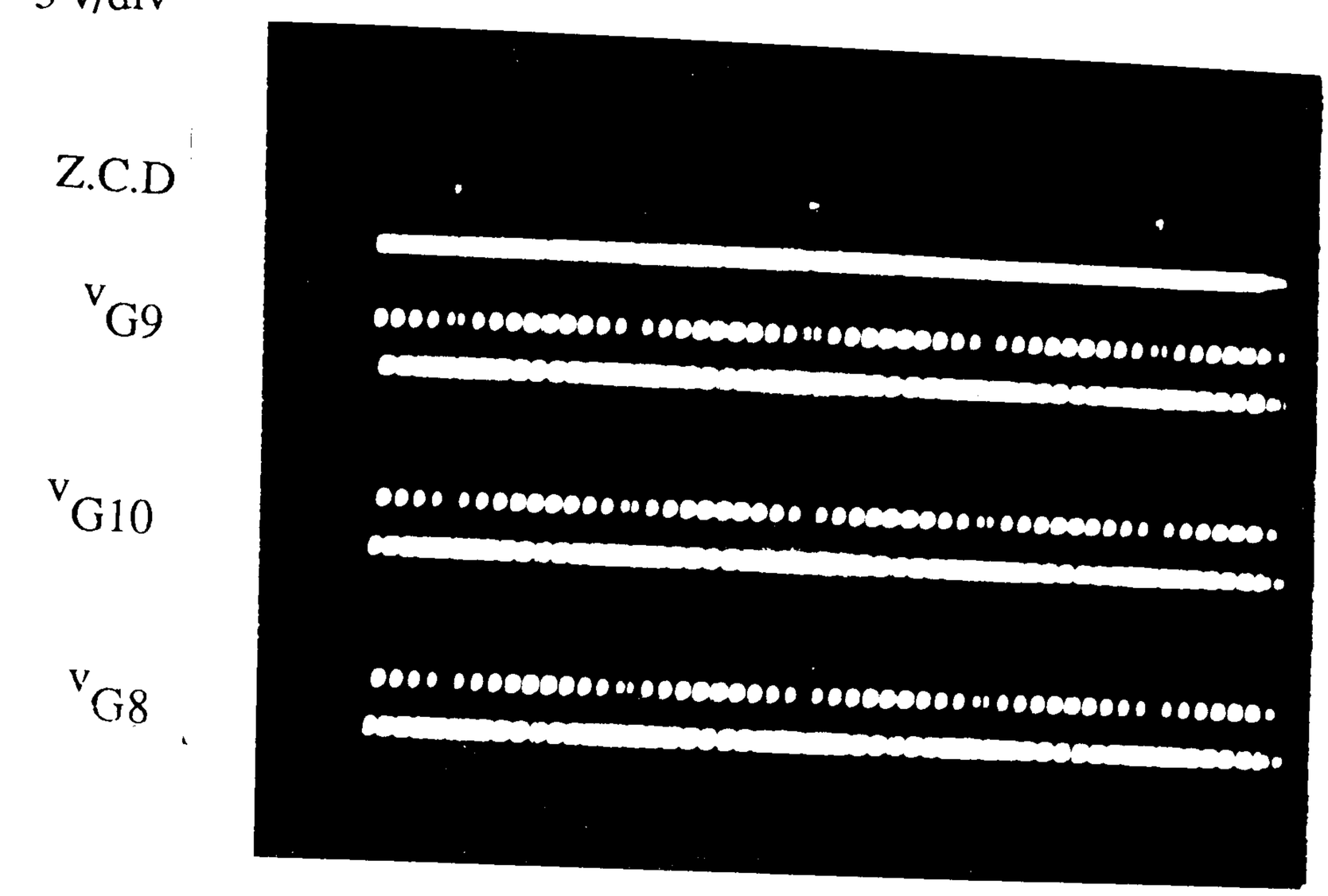

(a) 5 msec/div.

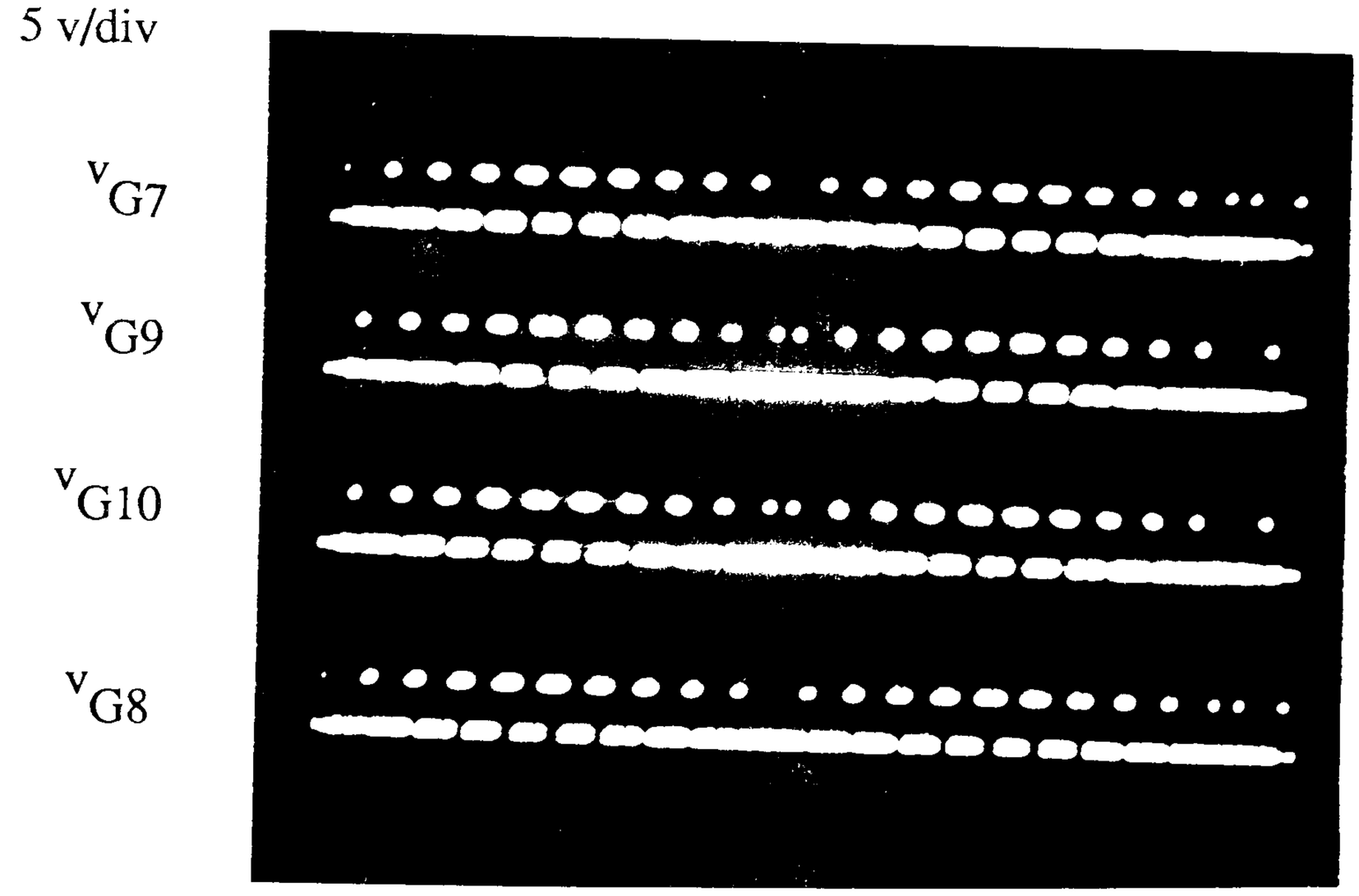

(b) 2 msec/div.

Fig. 5-30 (**a**) Control signals generated by microprocessor for the base drive circuits of **S7** , **S8** , **S9** and **S10** MOSFETs in fig. 5-18
(**b**) Expansion of (**a**) in the time domain

10 v/div

$v_{(G-S)7}$

$v_{(G-S)9}$

$v_{(G-S)10}$

$v_{(G-S)8}$

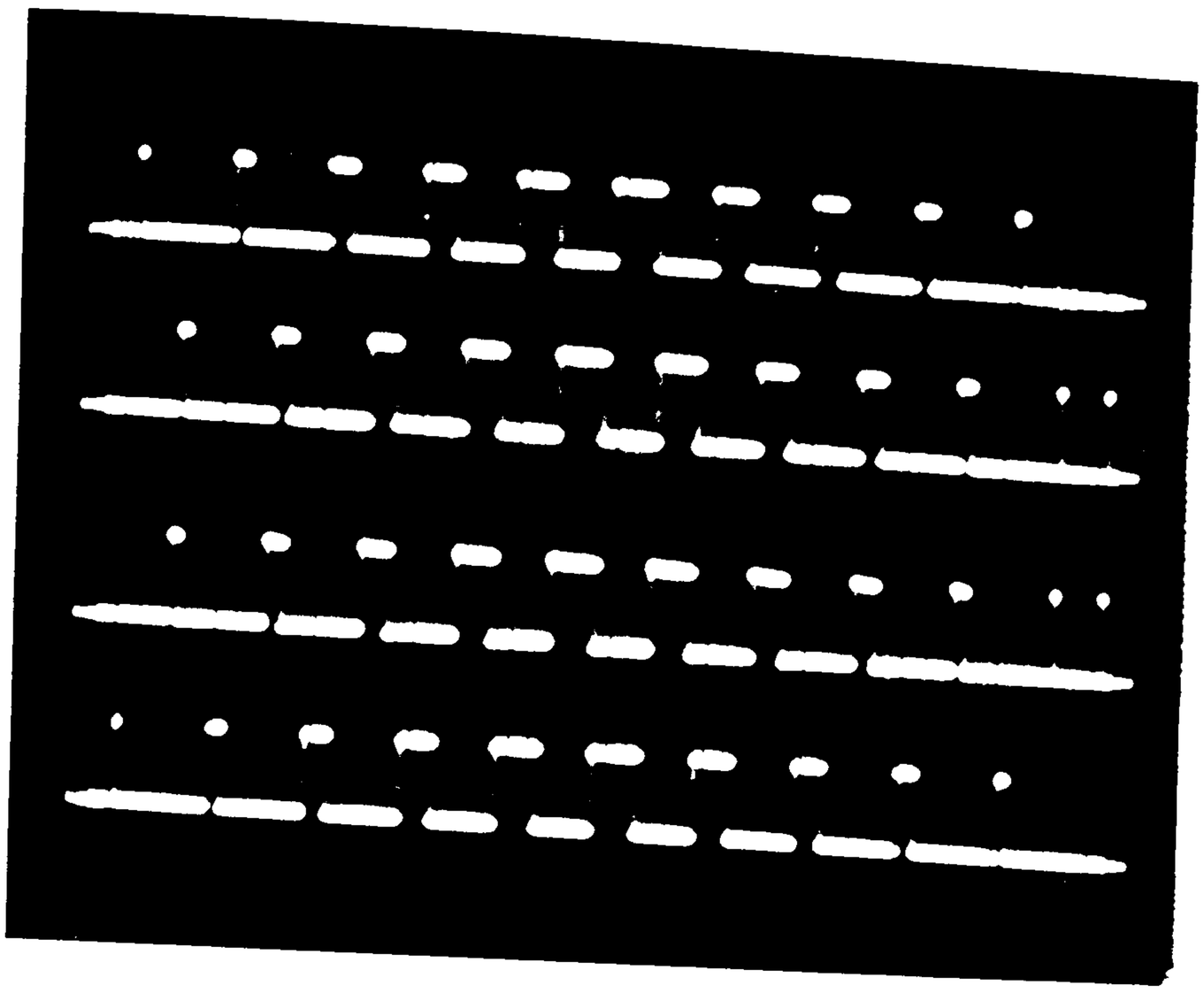

(a) 1 msec/div.

200 v/div.

$v_{(u1-v1)}$

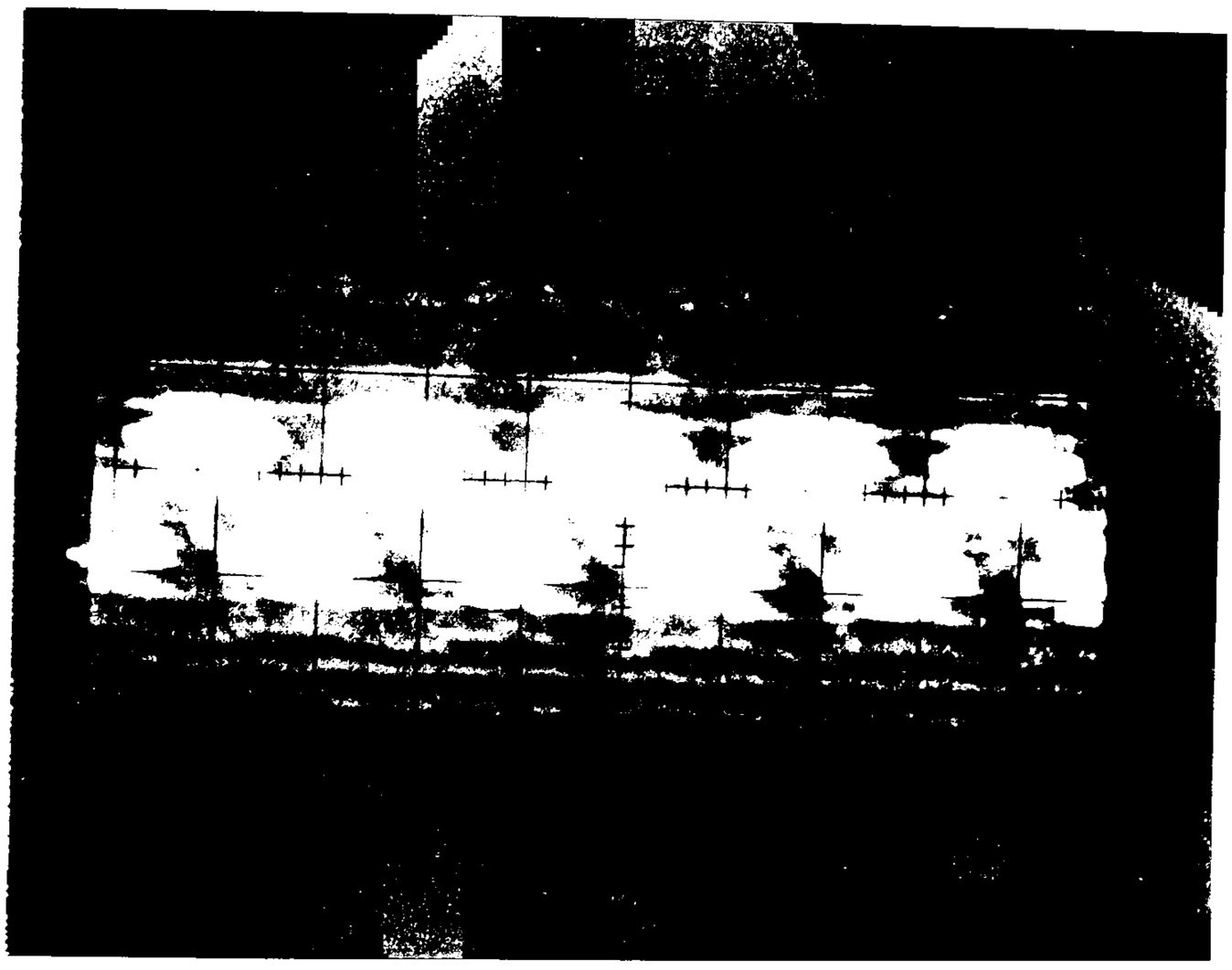

(b) 10 msec./div.

Fig. 5-31 (**a**) Triggering signals measured at the Gate-Source of **S7** , **S8** , **S9** and **S10** MOSFETs in Cycloconverter of Fig 5-18

(**b**) Cycloconverter output voltage ($\mathbf{v_{u1-v1}}$) in Fig. 5-18 (no filter , no load)

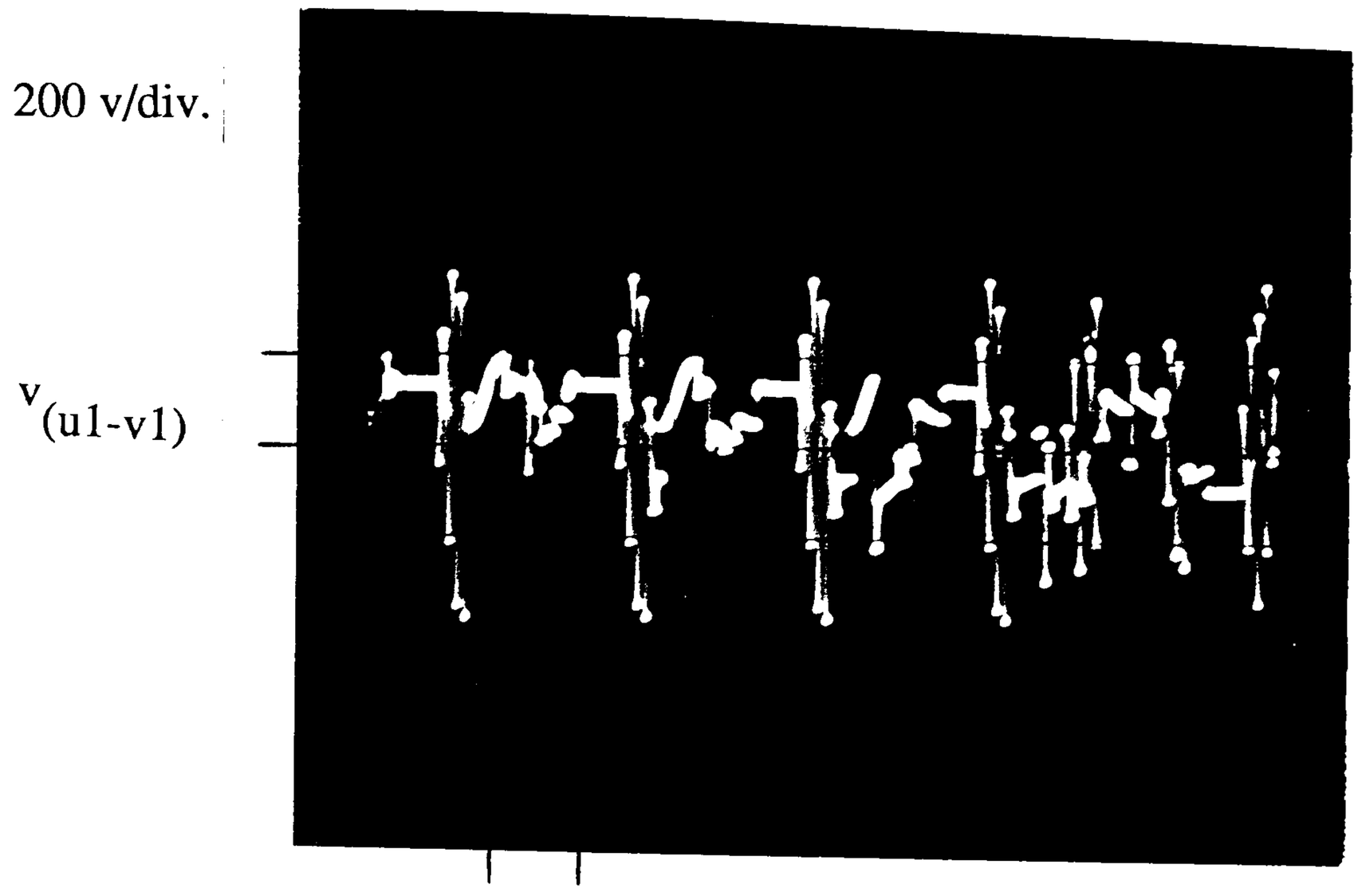

(a) 0.5 msec./div.

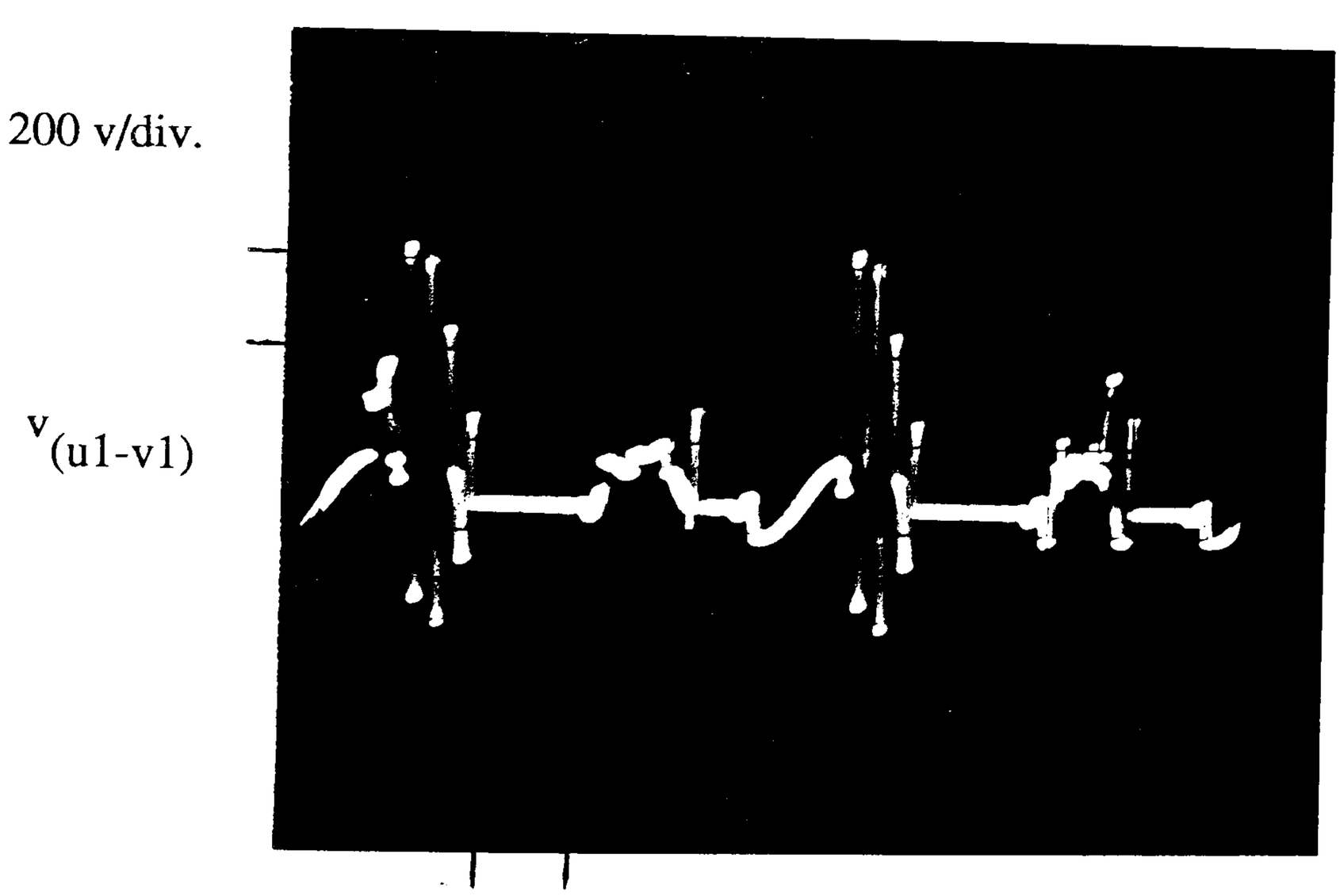

(b) 0.2 msec./div.

Fig. 5-32 (**a**) & (**b**) Expansion of Fig. 5-31(b) to show intereffect of transformer **leakage reactance** with **snubber circuit capacitance** (which was not established in this thesis)

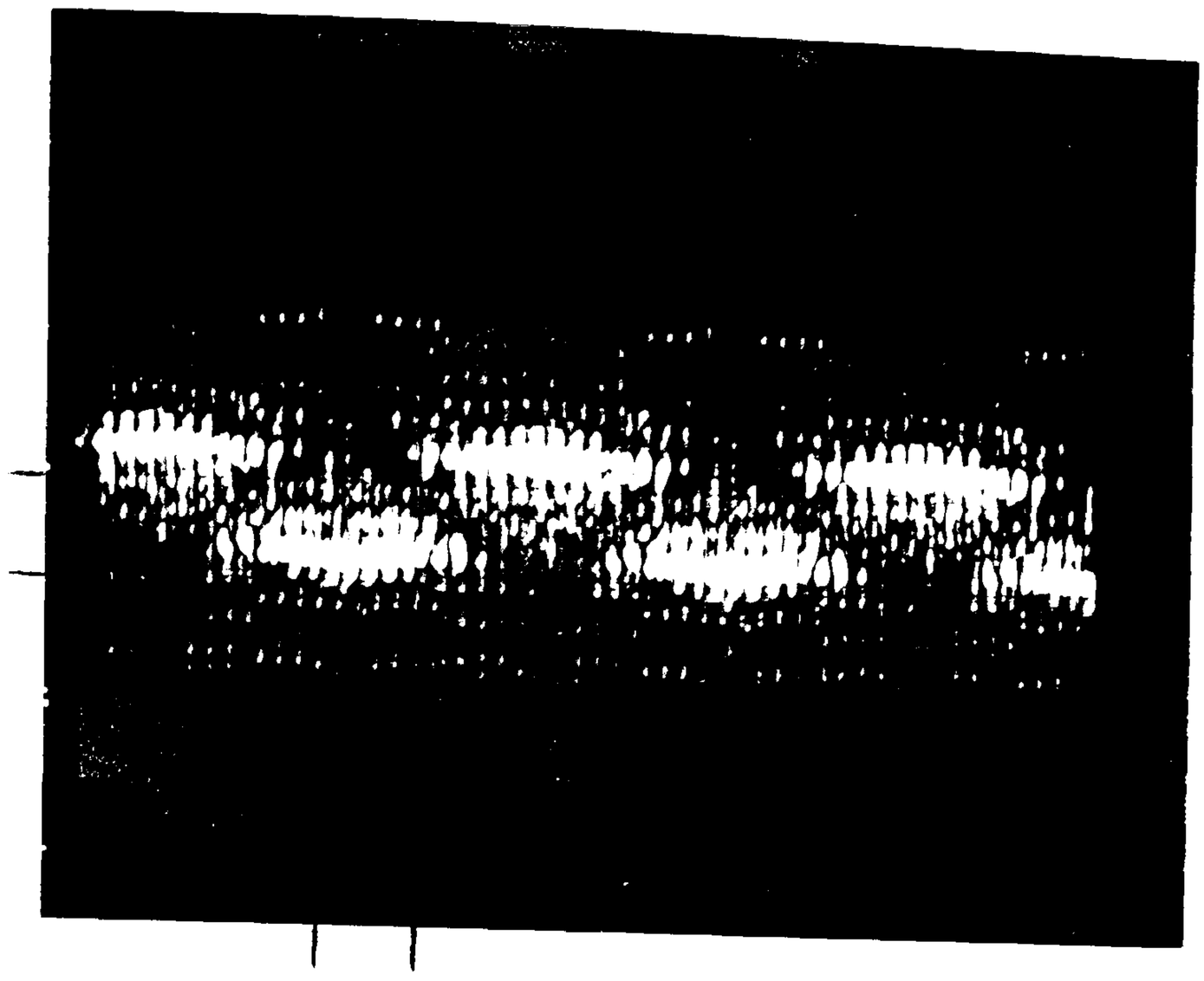

(a)

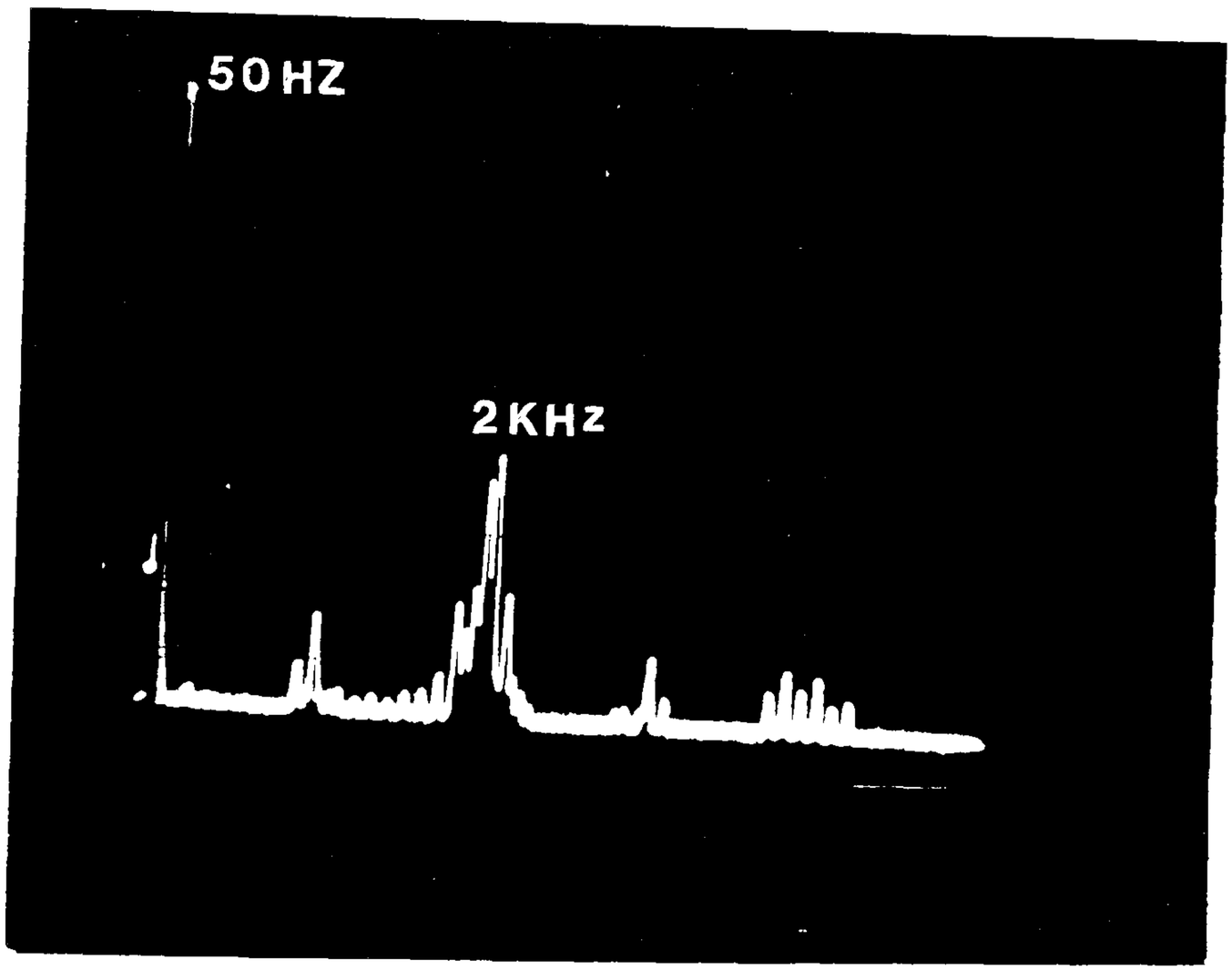

(b)

Fig. 5-33 (**a**) Cycloconverter crude output voltage v_{u1-v1} in Fig. 5-18 (no filter , no load)

(**b**) Harmonic spectrum of (**a**)

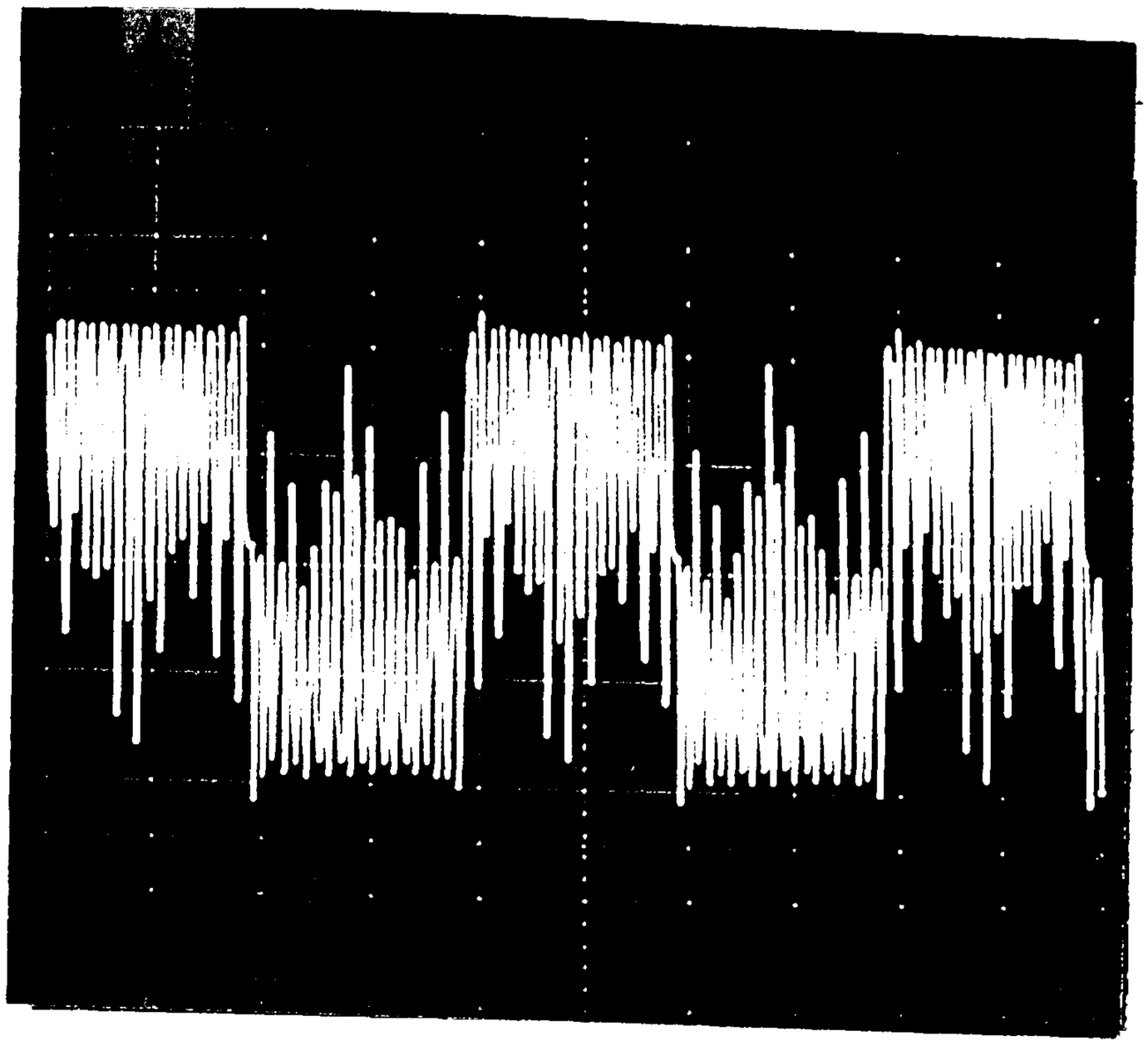

(a) 5 msec./div.

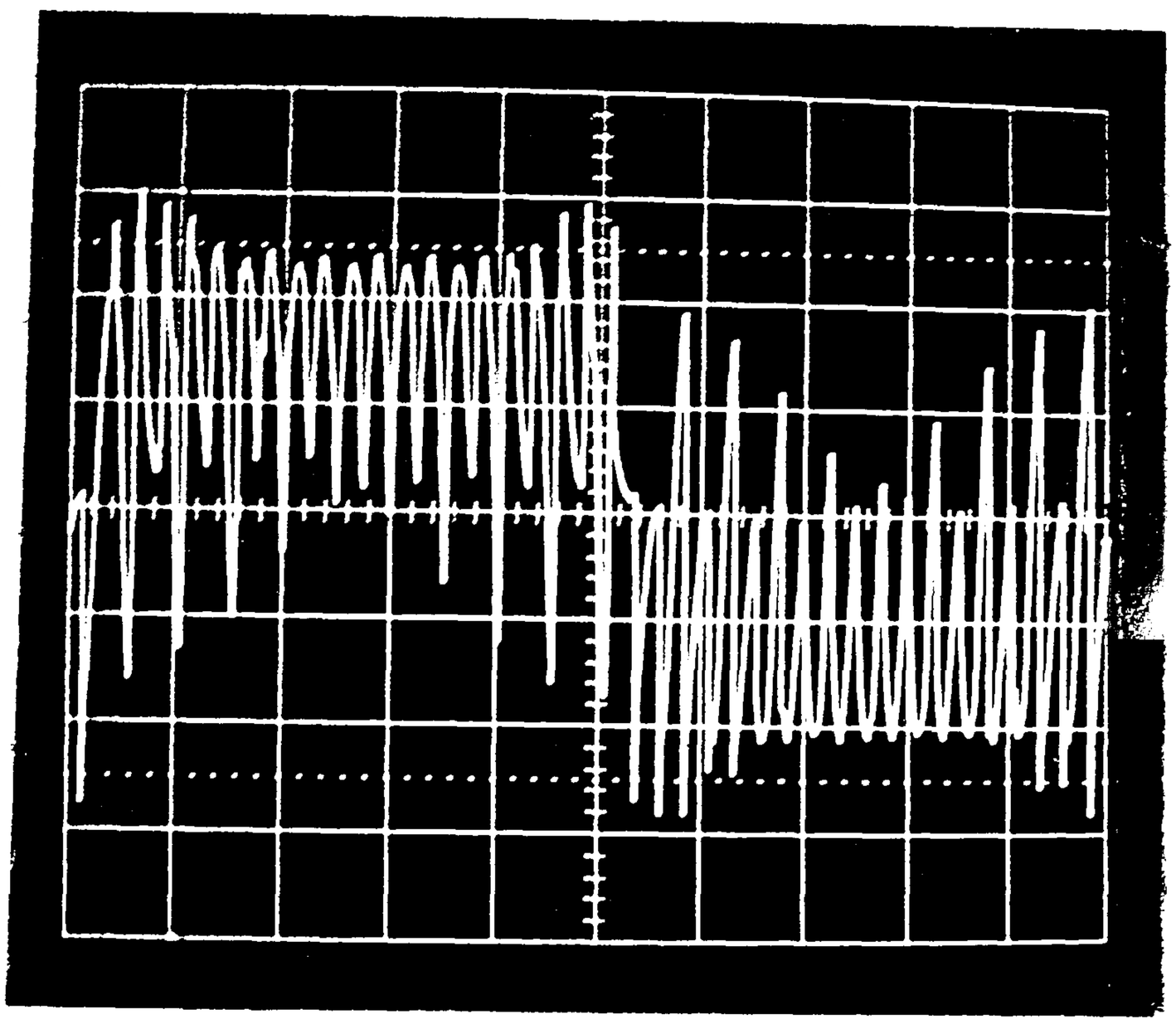

(b) 2 msec./div.

Fig. 5-34 (**a**) Cycloconverter output voltage waveform , the cycloconverter input was supplied by 1 kHz sinusoidal waveforms , generated by power amplifier rather than by inverter & transformer for spectrum comparison (**b**) Expansion of (**a**) in time domain

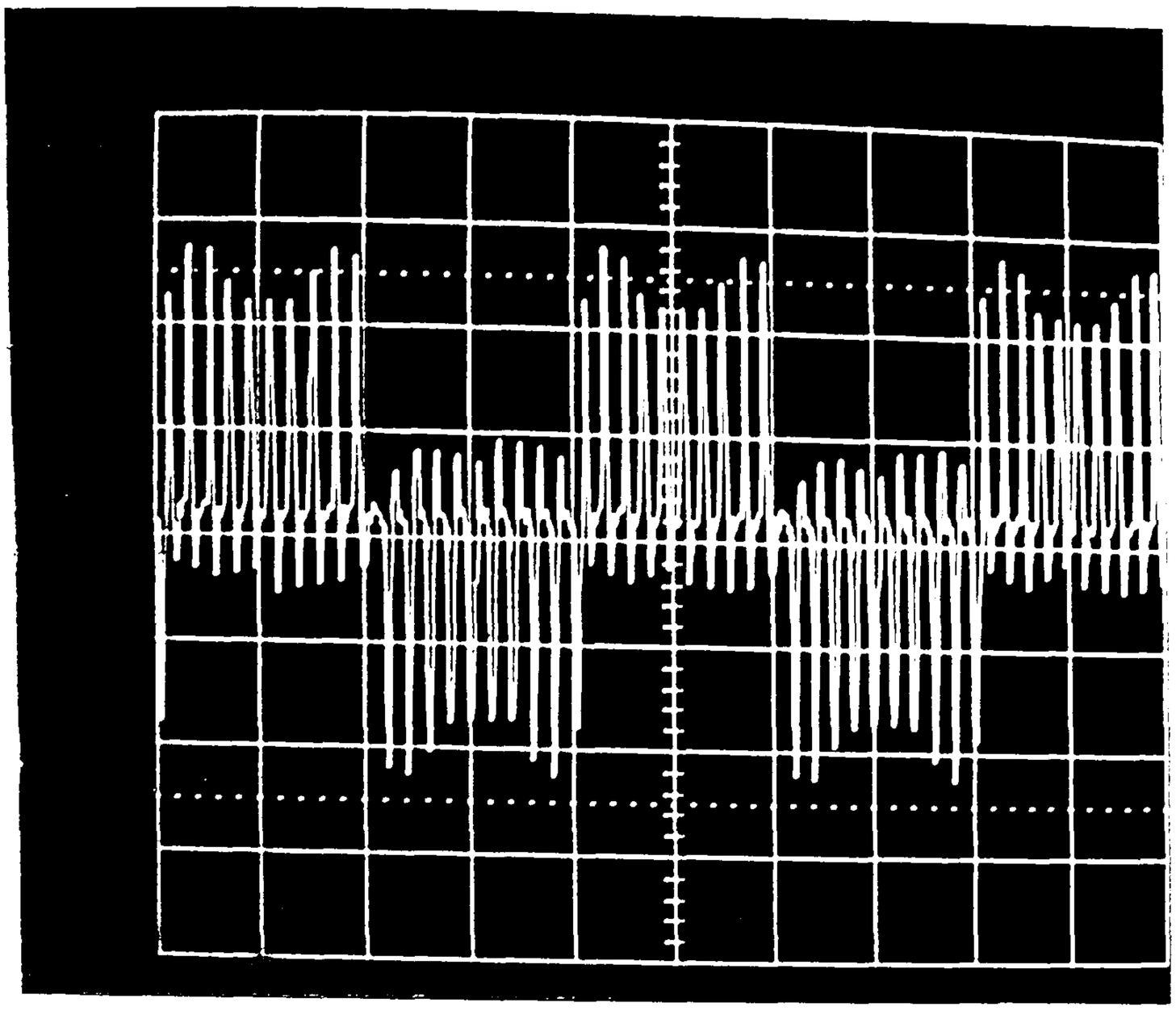

(a) 5 msec./div.

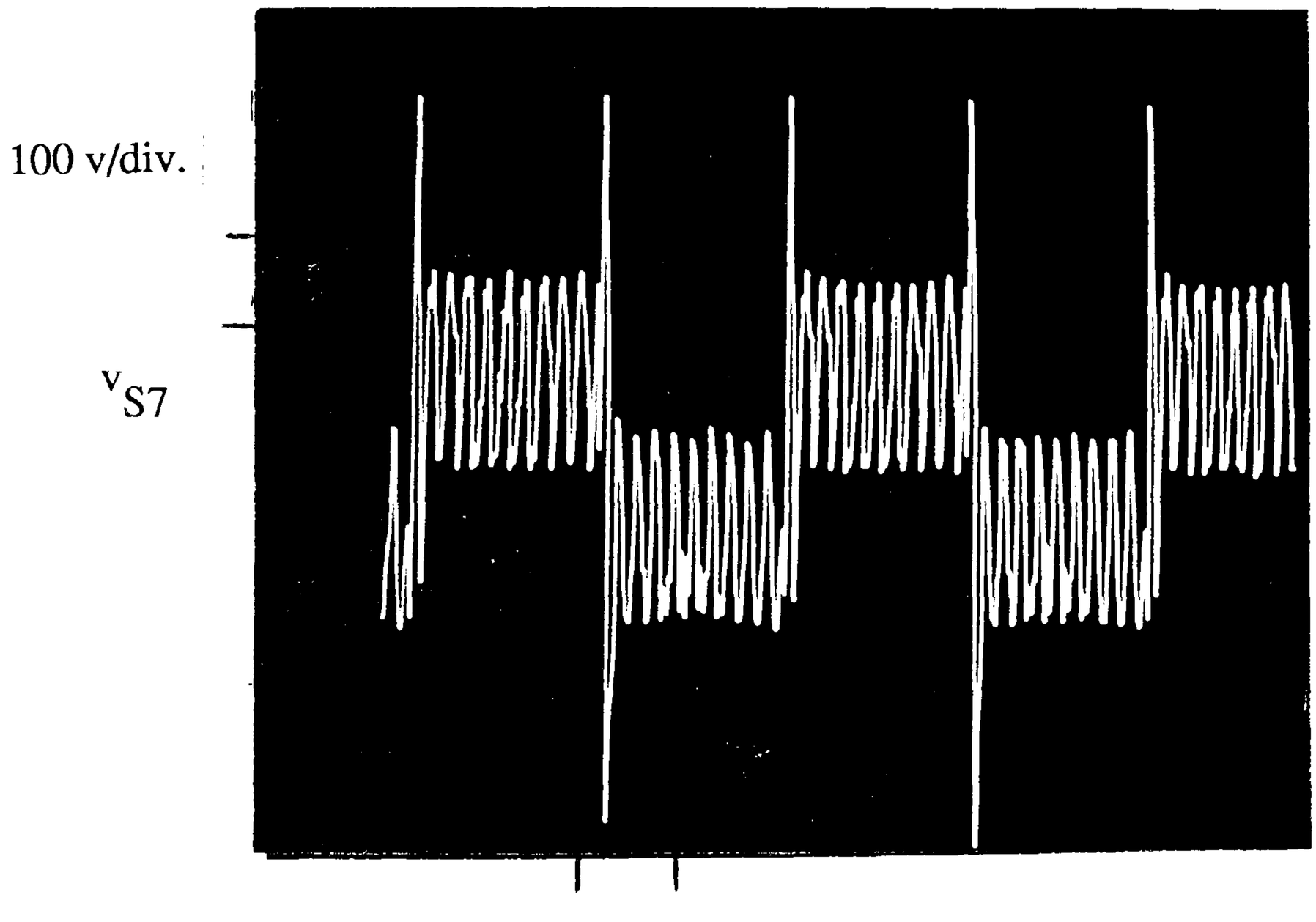

(b) 5 msec./div.

Fig. 5-35 (**a**) Voltage waveforms across **S7** or **S8** MOSFET in Fig. 5-18
(**b**) Effect of **4** μ**F** filtering capacitor on (**a**)

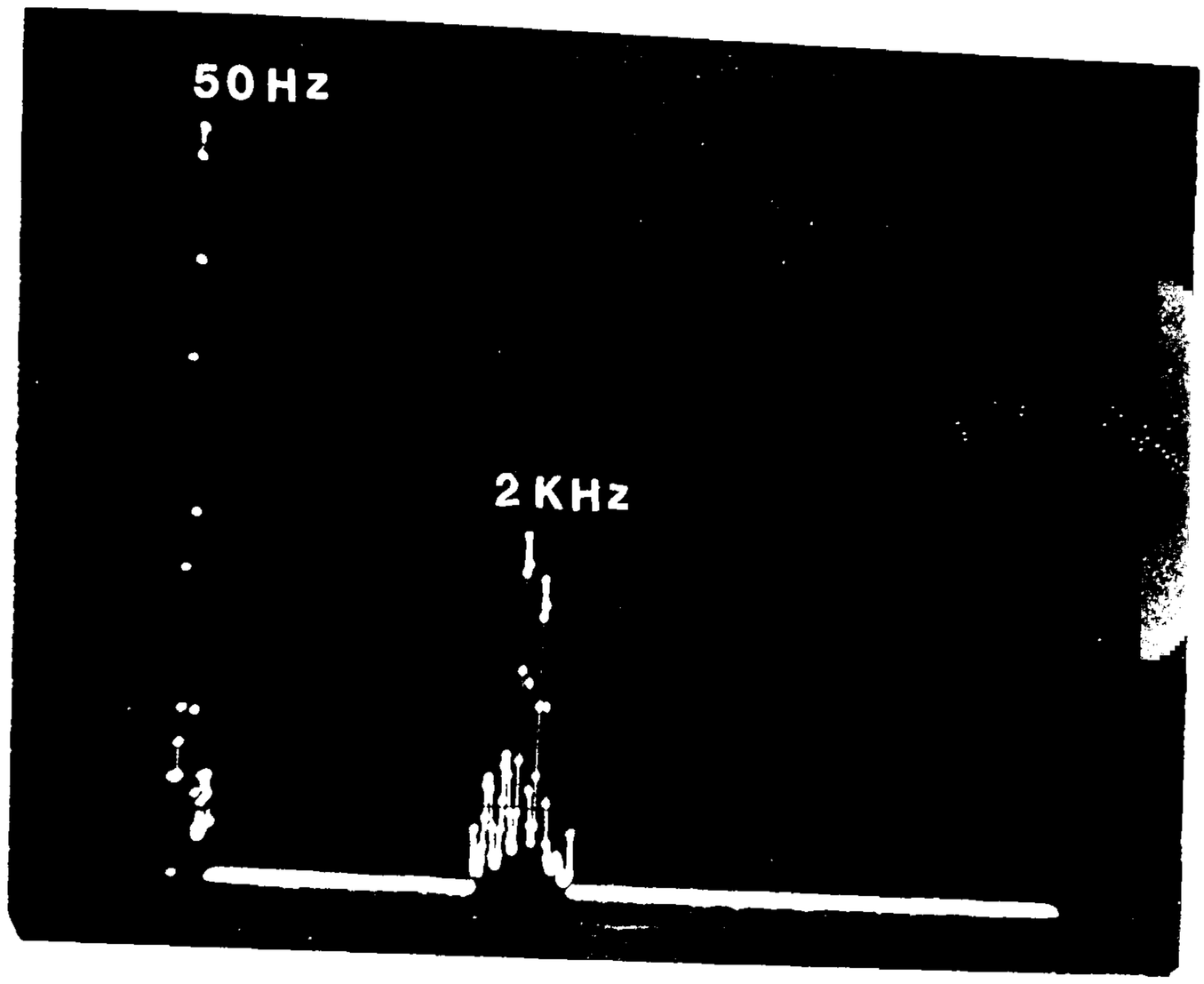

(a)

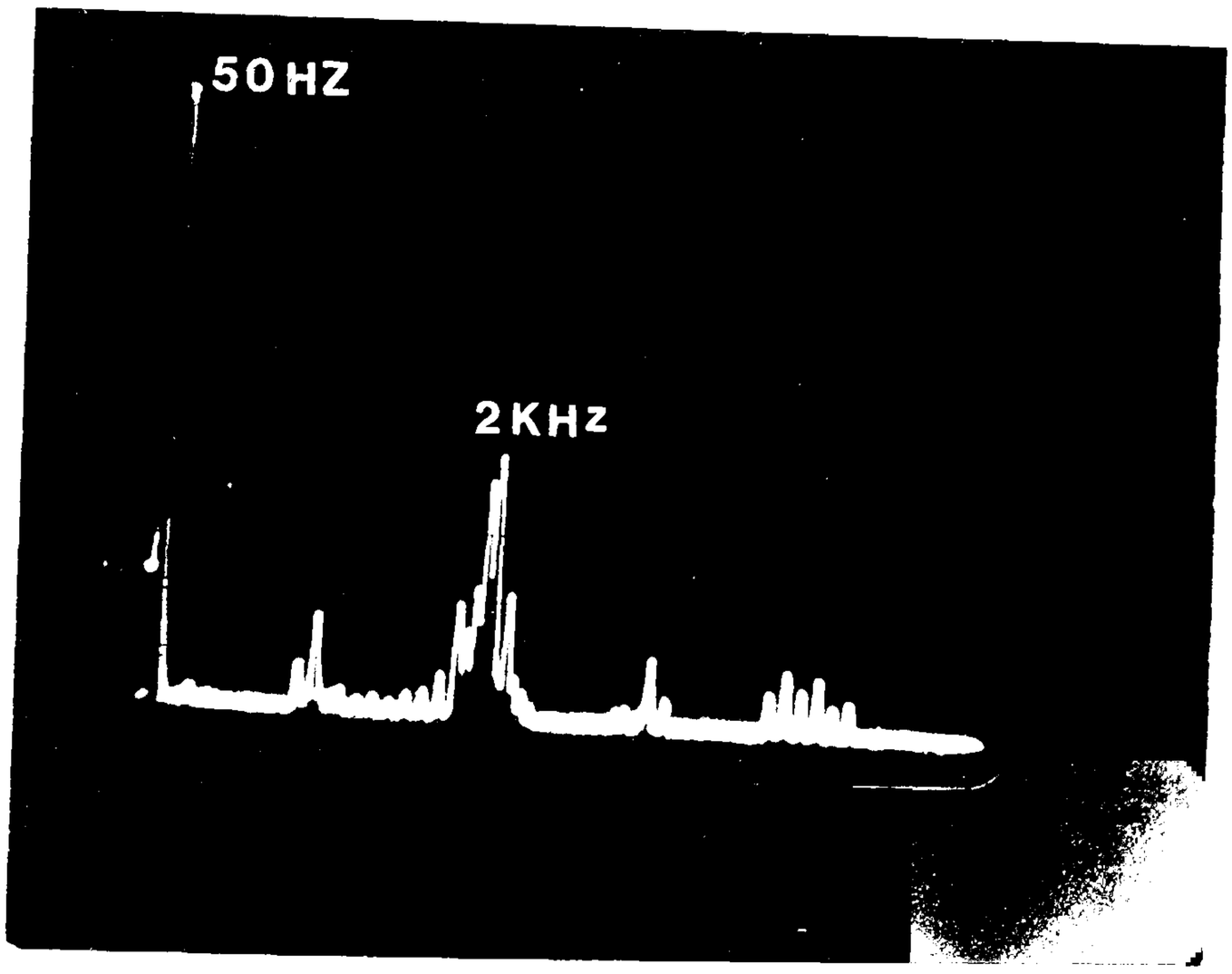

(b)

Fig. 5-36 (**a**) Harmonic spectrum of Fig. 5-34(**a**) which may be compared and verified with Fig. 4-16

(**b**) Harmonic spectrum of the waveform shown in Fig. 5-33 (**a**)

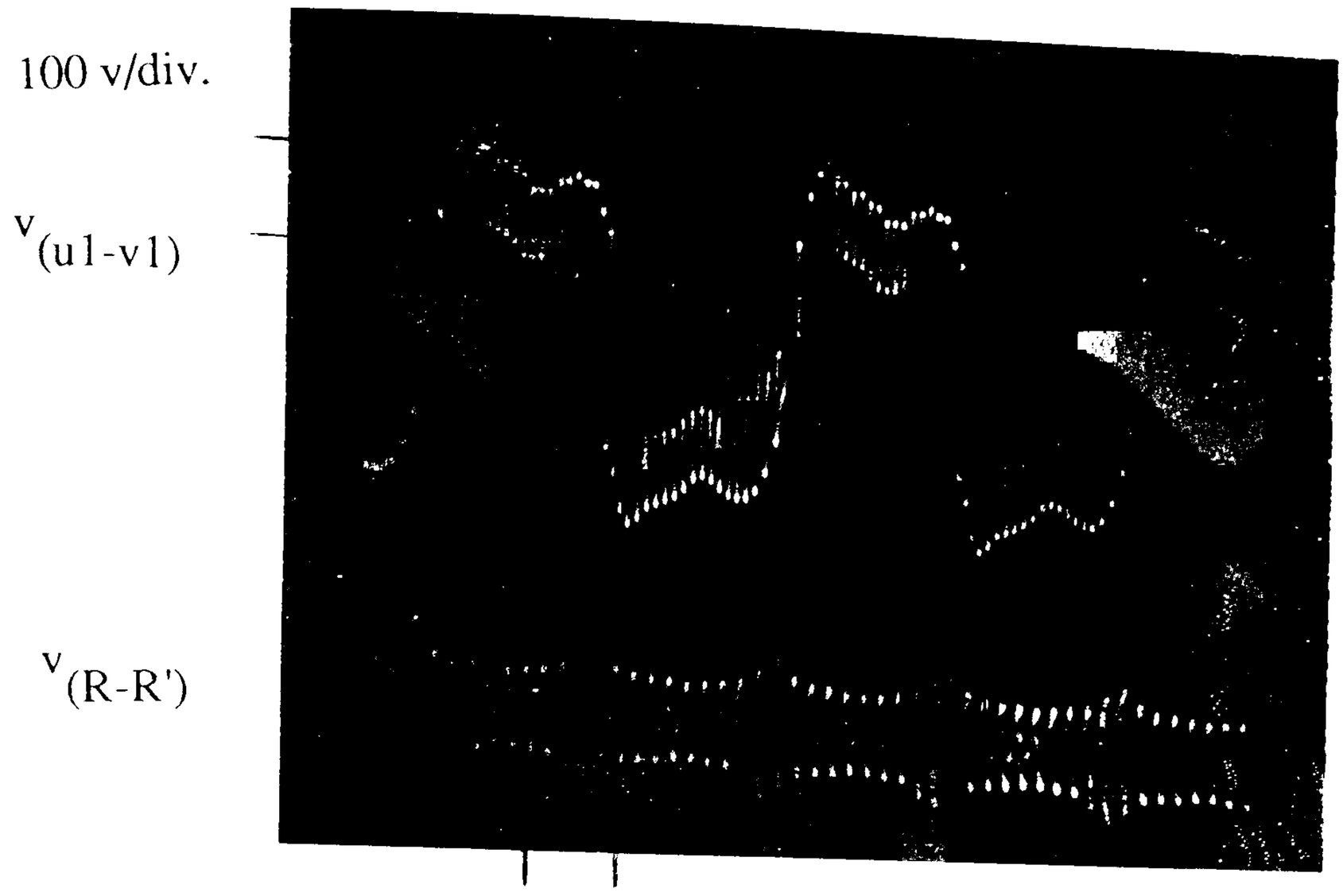

(a) 5 msec./div.

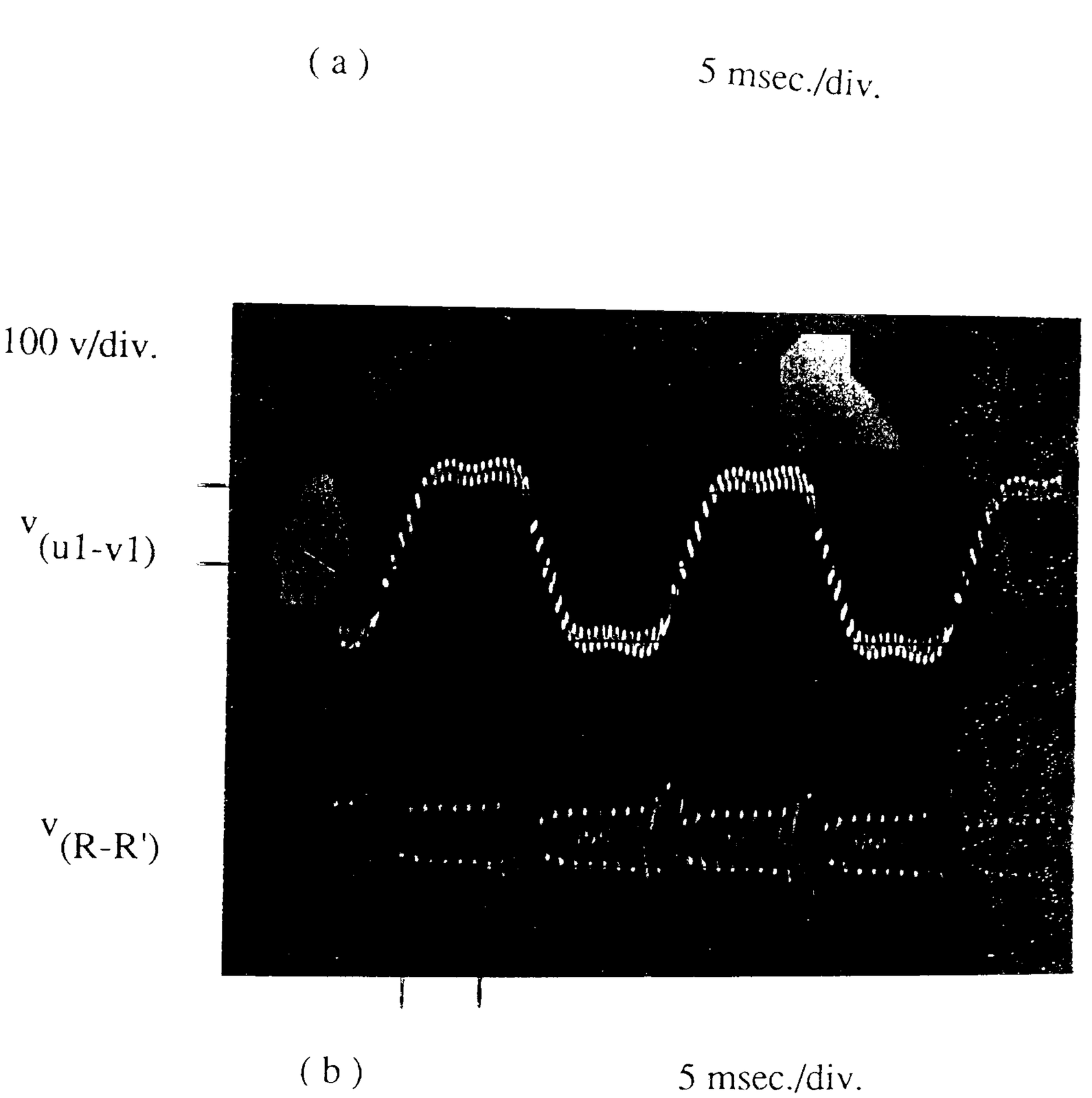

(b) 5 msec./div.

Fig. 5-37 (**a**) Cycloconverter output voltage (Fig. 5-33(a)) after filtering with **C = 0.1 μF**

(**b**) Filtering with **C = 1 μF**

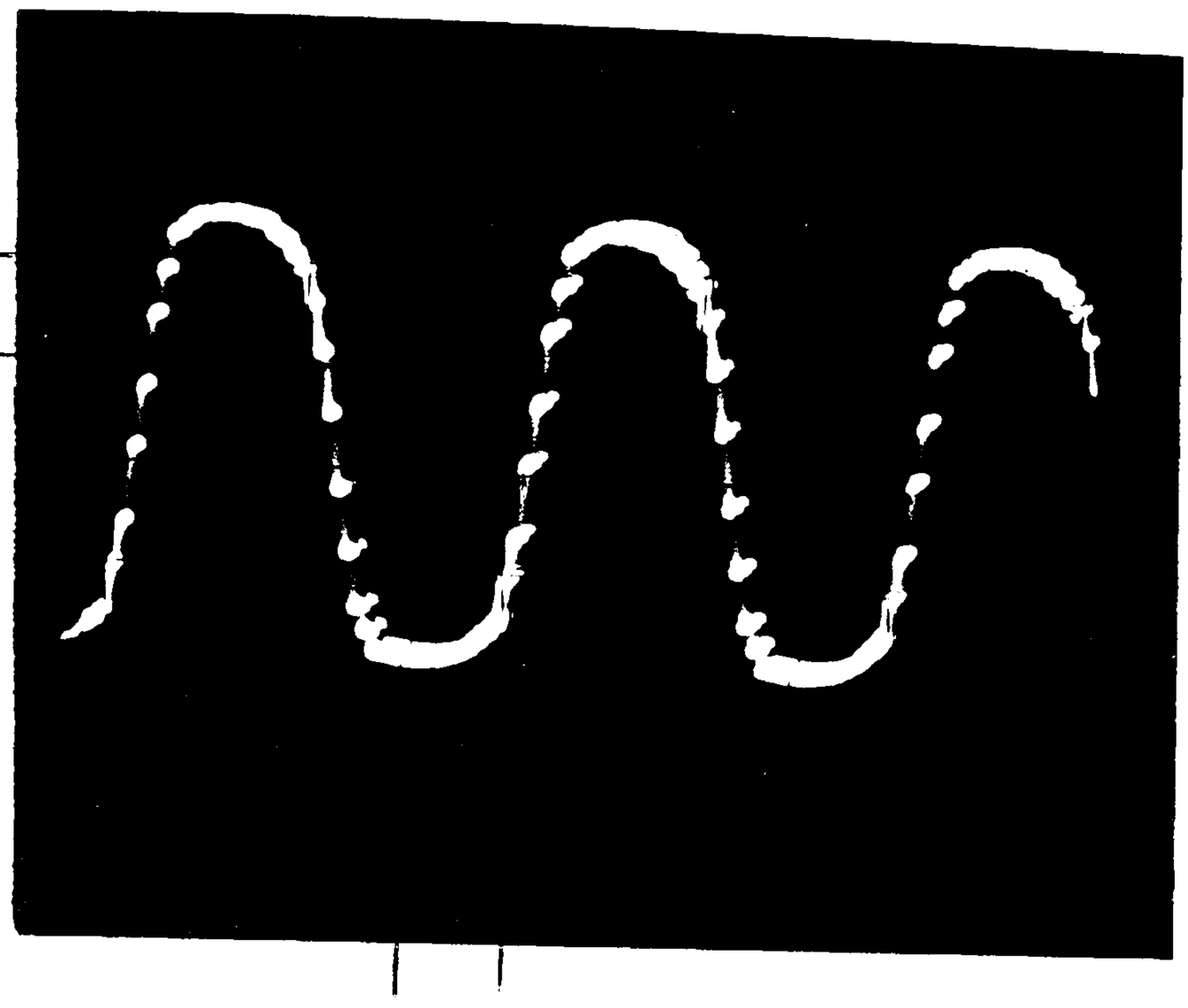

(a)

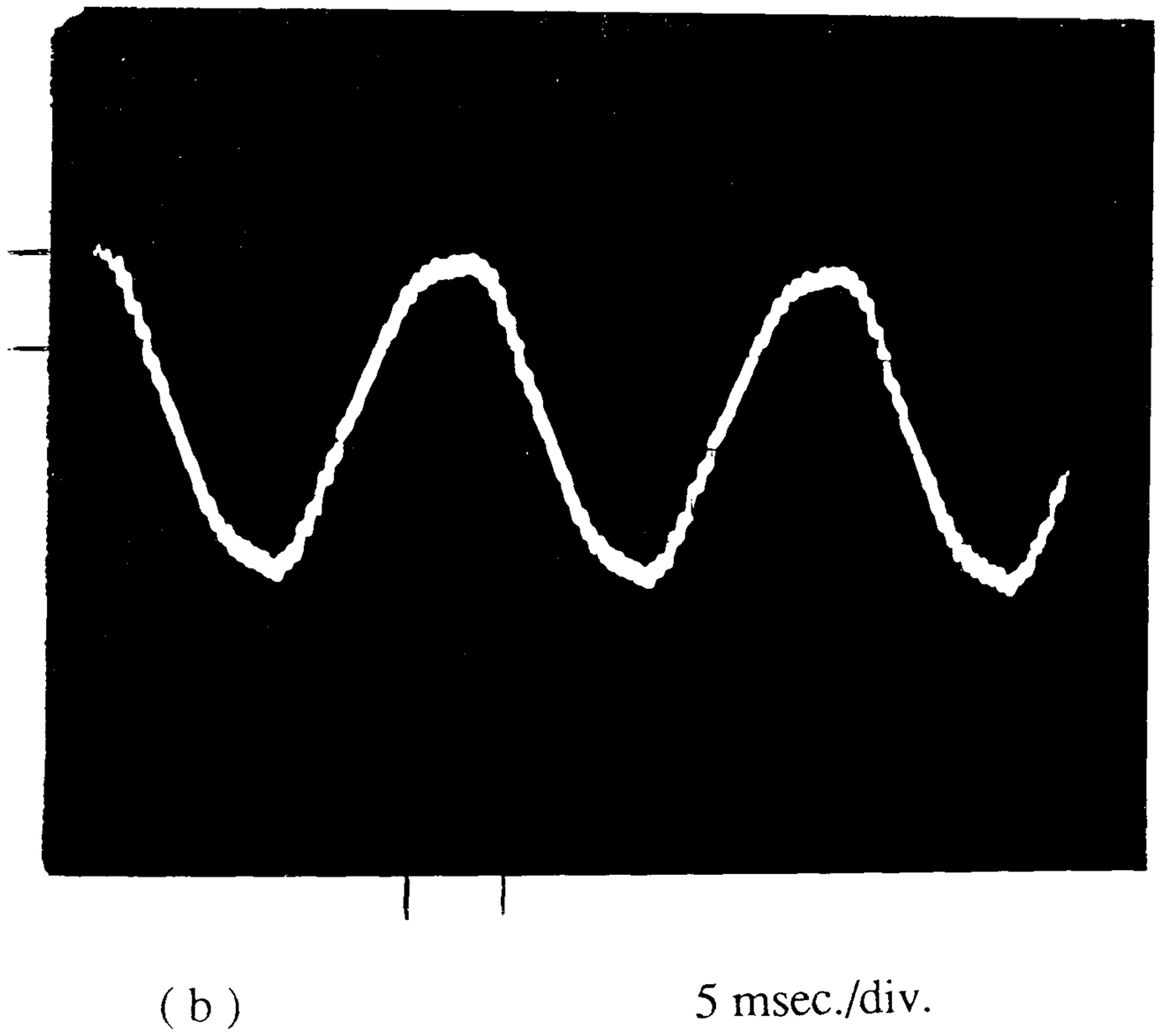

(b)

Fig. 5-38 (**a**) Cycloconverter output voltage (Fig. 5-33 (a)) after filtering with **C = 4** μF

(**b**) Voltage waveform across inductive load (**Cos Φ = 0.716**)

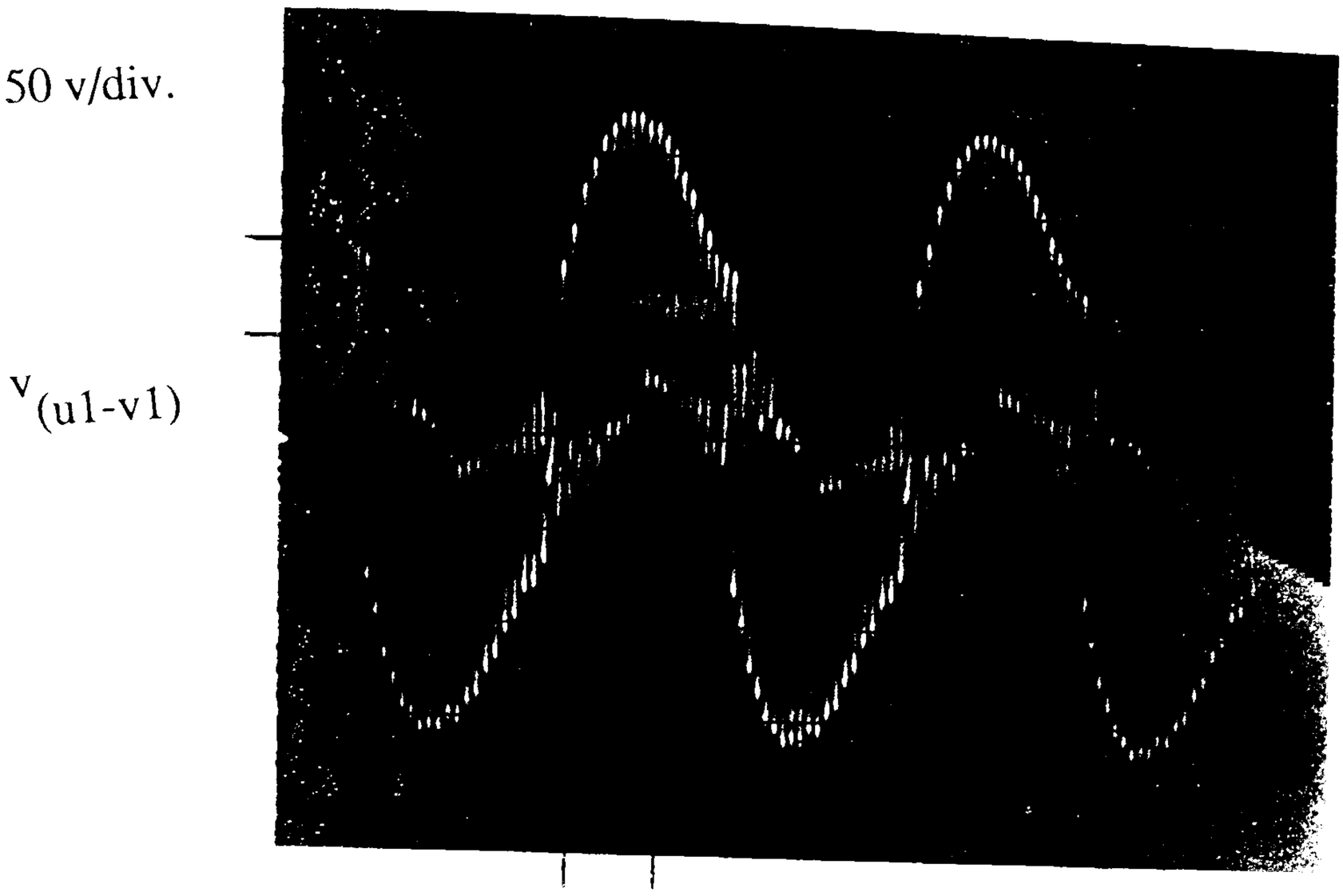

(a)

5 msec./div.

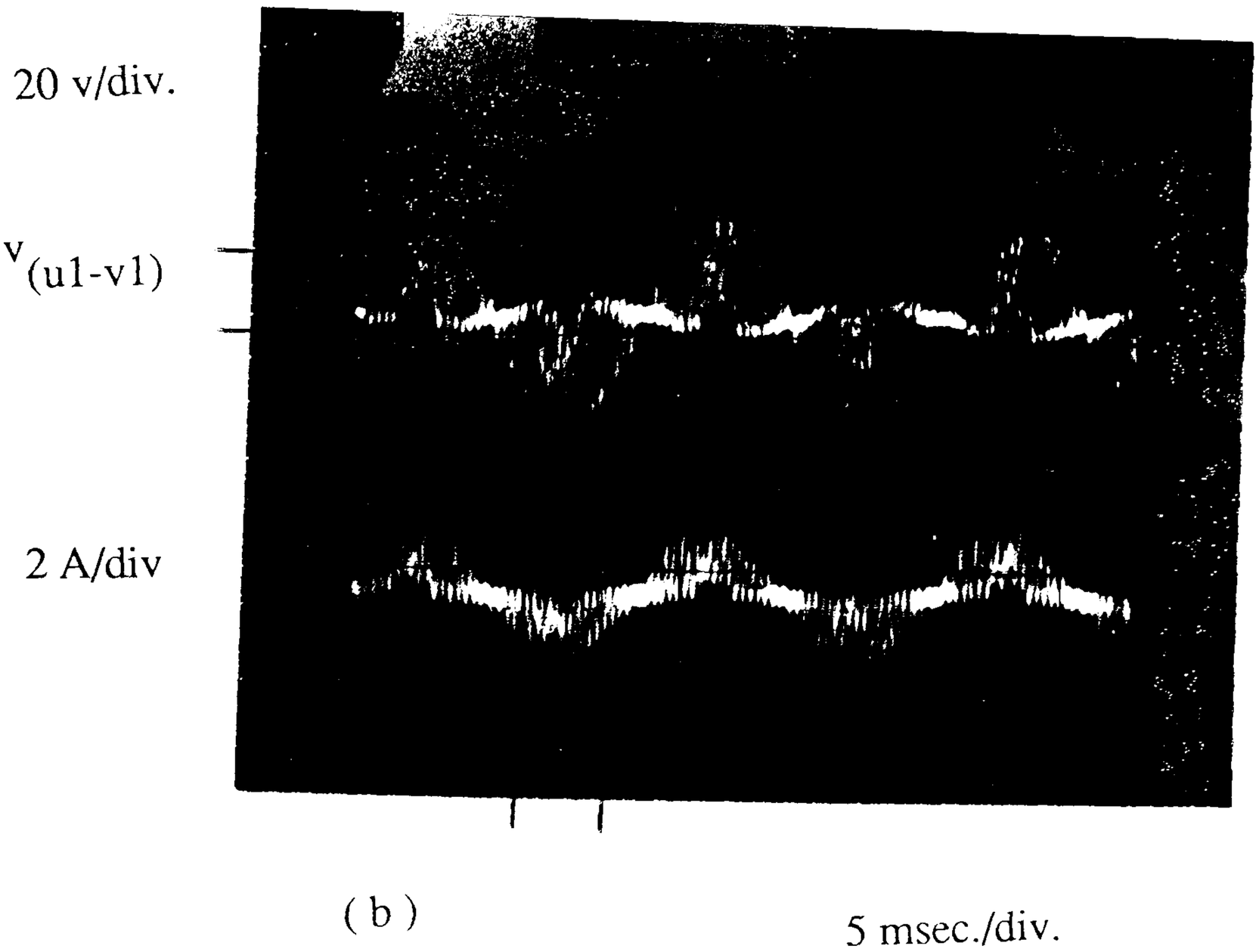

(b)

5 msec./div.

Fig. 5-39 (**a**) Voltagewaveform across resistive load (**10** Ω , CosΦ =**1**)

(**b**) Voltage & current waveforms of resistive load (**15** Ω , Cos Φ =**1**)

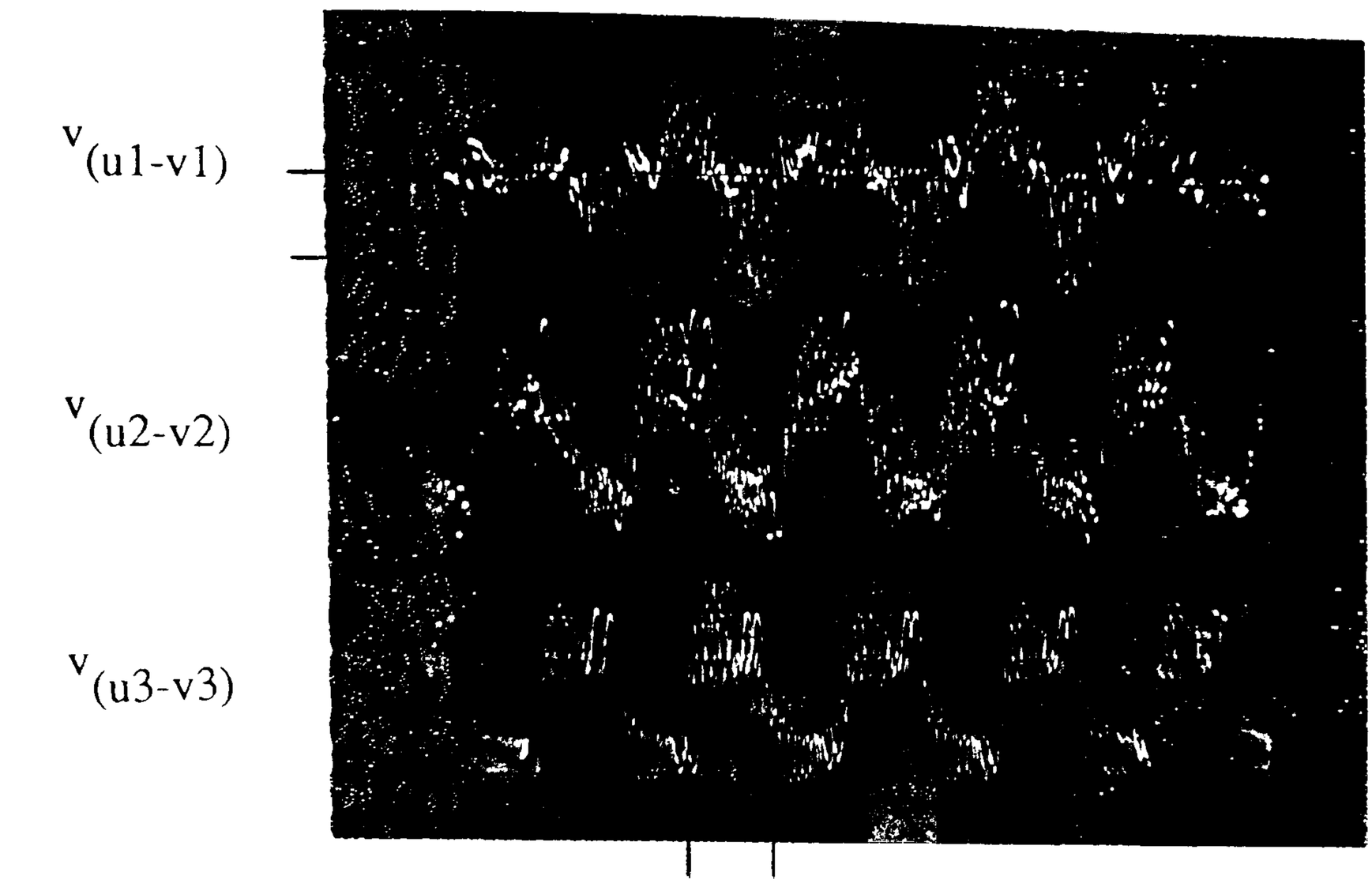

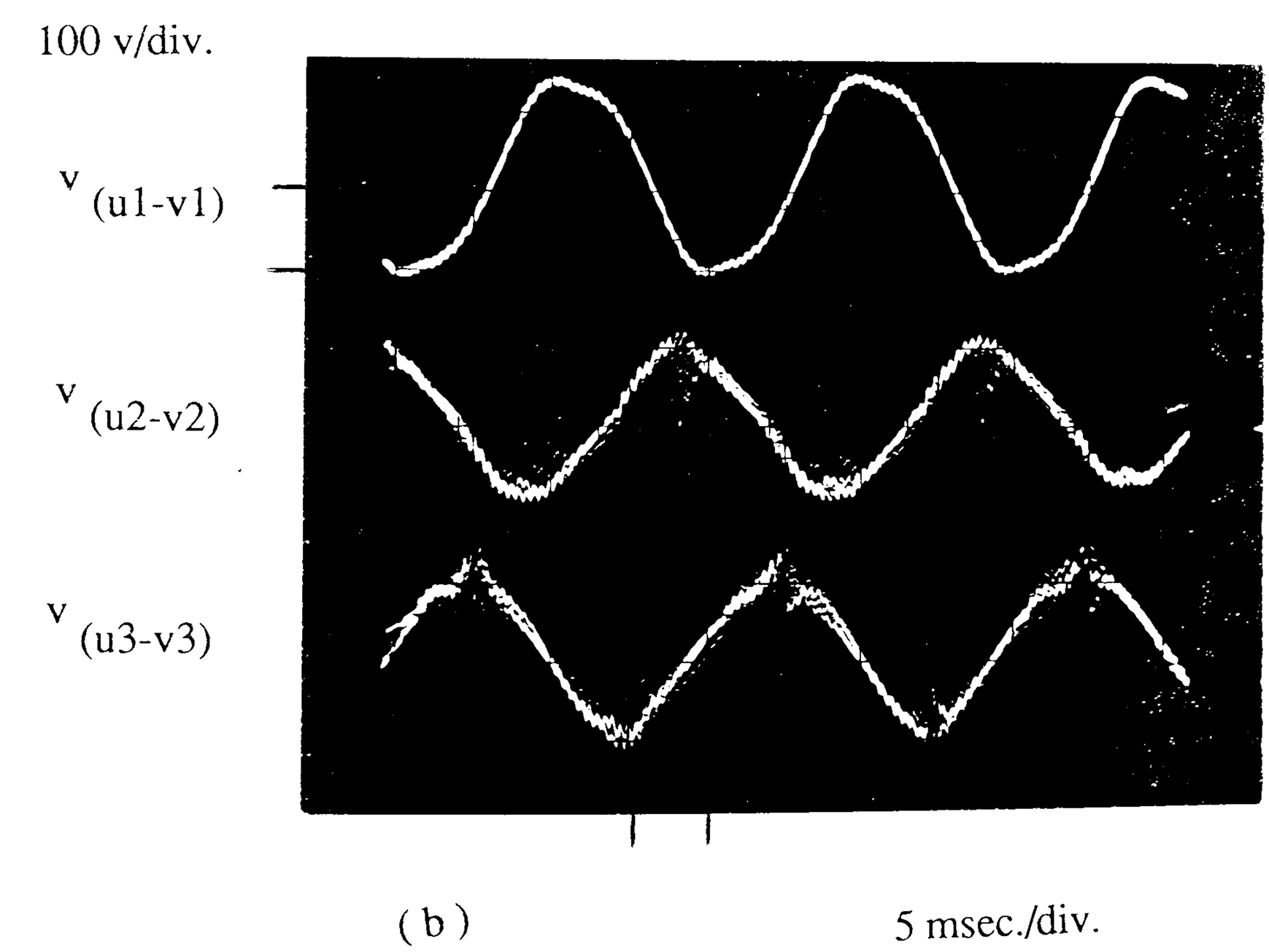

Fig. 5-40 (**a**) Voltage waveforms across 3-phase induction motor load with

Cos Φ = 0.716

(**b**) waveforms in (**a**) after filtering with 4 μF connected across the output

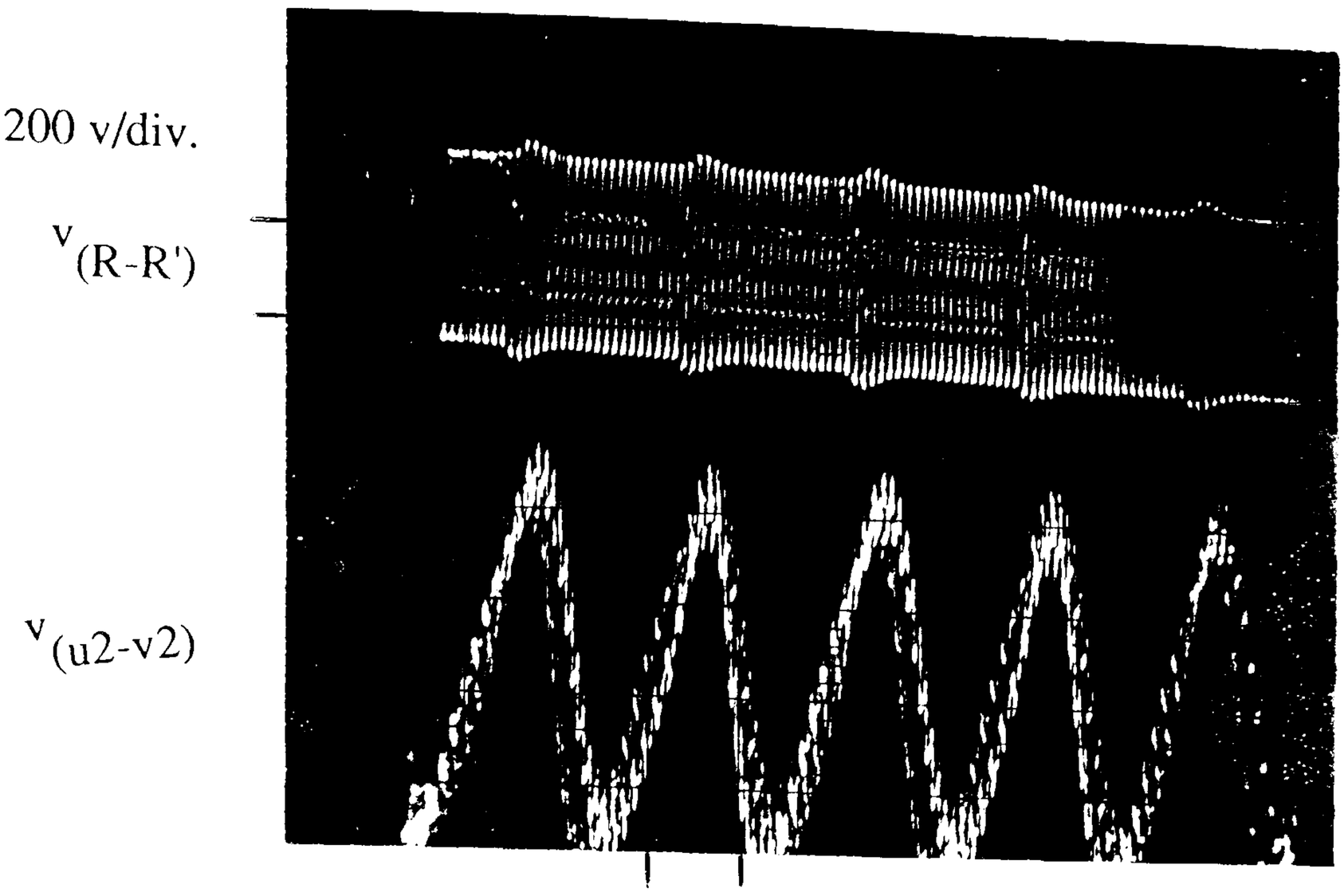

(a) 10 msec./div.

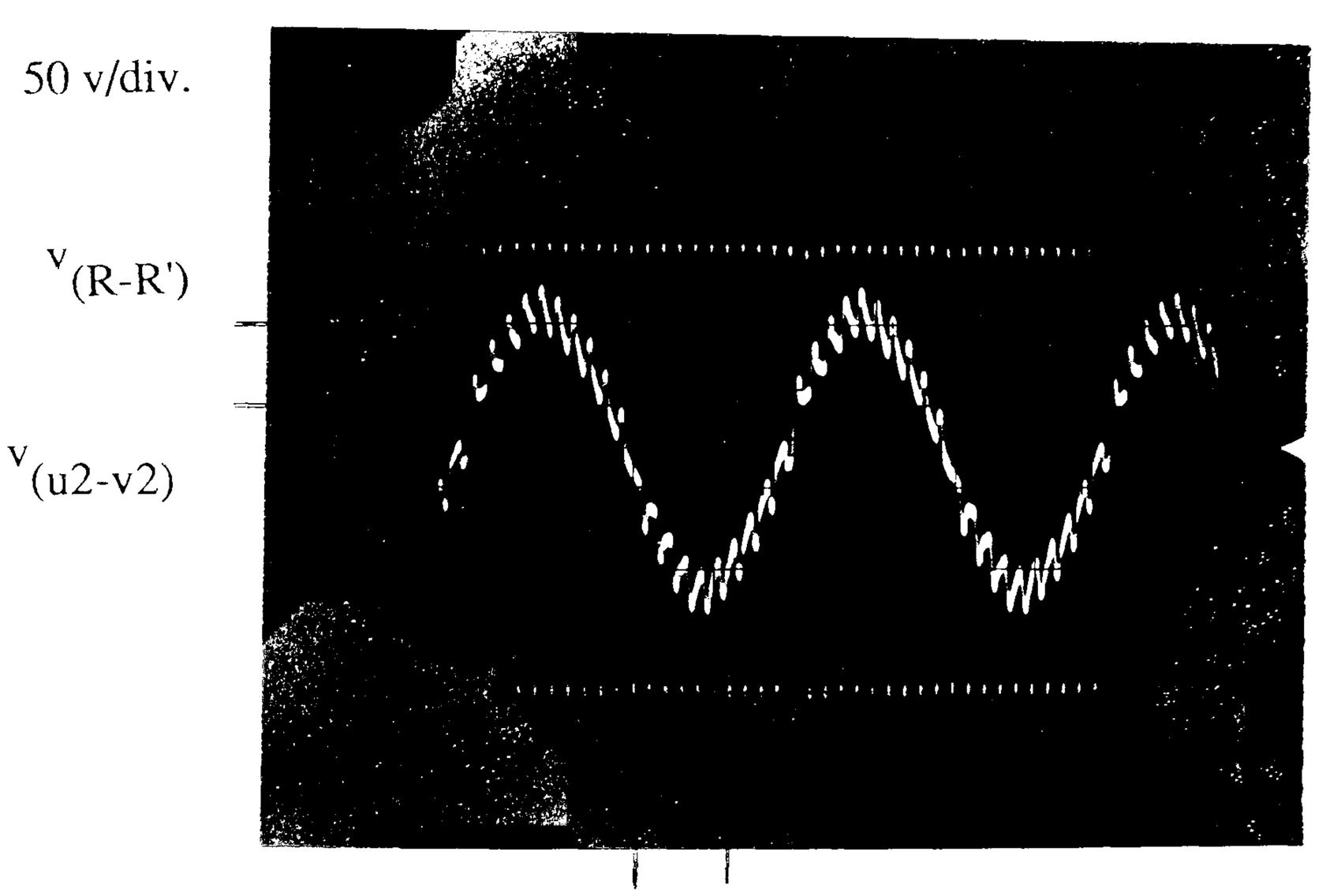

(b) 5 msec./div.

Fig. 5-41 (**a**) Cycloconverter input voltage($\mathbf{v_{RR'}}$, **1000 Hz**) and output($\mathbf{v_{u2\text{-}v2}}$, **50 Hz**) voltage(inductive load) waveforms (**b**) waveforms of (**a**) for reverification of proposed modulation strategy

5-7 References :

1- E . R . Hnatek *" Design of solid-state power supplies "* 1981 , Van Nostrand Reinhold Company .

2- G . Chryssis *" High frequency switching power supplies :Theory and design "*1984 , Mcgrow - Hill Book Company .

3- H . R . Weischedel & G . R . Westerman *" A symmetry correction pulse width modulator for power conditioning applications "* May / June 1973, pp. 318 - 322 IEEE Trans ; Vol. IA - 9 , No. 3

4- R . Severns & S . Armijos *" Mospower Application Handbook "* 1984 , Siliconix incorporated .

5- M. H. Rashid*"Power Electronics : circuits, Devices , and applications"* 1988 , Prentice - Hall international Editions .

6- T . Kalker , Dipl . Ing .*"Over current protection of power MOSFET "* EPE , 1989 , Aachen , pp. 181 - 183 .

7- **" siliconix MOSPOWER application handbook "** Siliconix incorporated 1986

9- **" 8085 Assembly language programming manual "** Intel corporation - 1981

10 - **"SDK-85 system design kit user's manual"** Intel corporation - 1978 " .

Chapter 6

Results , Discussions , Conclusion & Future Work

6.1 General

The work which has been presented here is an investigation of a high frequency link multistage power conditioning system for DC-to-3 phase (1 kHz)-to-3 phase (50 Hz) power processing .

System operation is based on the high-frequency inverter , high-frequency transformer and cycloconverter circuitry with the following objectives :

1- conversion of DC Power to AC form with higher voltage level than the DC source , which necessitate that a power transformer should be employed for both voltage transformation and system input from output isolation purposes .

2- transfer of power by high-frequency link for size reduction of transformer and energy store/transfer elements (inductors and capacitors) .

A detailed investigation on such a system(high-frequency and multistage) presents a formidable array of problems that could be tackled. For example the cause and side effects of input current & output voltage harmonics(also in some applications subharmonics) and crucial role of the transformer on overall conversion system design and operation may be future research targets .

6.2 Results and discussions

6.2.1 Inverter connected to the primary and secondary is open circuit

The inverter phase voltages (V_{an} , V_{bn} , V_{cn}) , inverter line voltages (V_{ab} , V_{bc} , V_{ca}), V_{no} and V_{an} harmonic spectrum , those presented in chapter 5, were in very good agreement with those have shown in chapter 2 with computer simulation . Any slight discrepancy on the waveforms is due to the tiny distortion of microprocessor output signals caused by the MOSFET base drive circuits ,

Fig. 5-20(b) and Fig. 5-21(b) may be compared .

The inverter fundamental frequency is **1 kHz** and each cycle is modulated by **R=9** pulses with different widths(according to **table 2-10**) , and from other hand there is oscillatory tendency between transformer inductances and snubber capacitors during switch turn-off (**chapter 3**) , so attribution of any discrepancy in practical waveforms to these problems is quite recognizable .

From chapter 3 , resonance frequency between snubber capacitors (C) and transformer inductances (L = magnetizing + leakage) is :

$$f_r = \frac{1}{2\pi\sqrt{2LC}}$$

and developed spike voltage across switch during turn-off is :

$$v_{spike} = I(\text{ primary current })\sqrt{\frac{L}{C}}$$

Therefore any attempt to increase C to lower v_{spike} will decrease f_r which is undesirable for inverter output . By significantly reduced leakage inductance and using high quality core material the effect on both f_r and v_{spike} will be more desirable. It should be reminded this conclusion is concerned with the case with open circuit secondary .

The primary and secondary voltages were measured **1 kHz** sinewave (Fig. 5-25(b)) which is expected , because up to order of **17 th (17 kHz**) , the harmonic components theoretically and practically are eliminated and the rest have insignificant effect on the fundamental .

6.2.2 Inverter connected to the primary through filtering elements and secondary is open circuit

By connecting L-C series filter between primary and inverter and tuned for **1 kHz** the secondary voltages will be a pure sinewave (Fig.5-26(a)). But adding parallel L-C across primary did not make any change which means that effects of high order harmonics is negligible .

6.2.3 Unloaded cycloconverter is connected to the secondary

With rated voltage transformer operation , the cycloconverter sinusoidally modulated output voltage (Fig.5-33 (a)) and it's harmonic spectrum (Fig.5-33 (b)) are satisfactory , but different slightly from those shown in Fig.s (4-15) & (4-16). The possible unwanted distortion factors are :

1- distortion on conducted input half-cycle segments (pulse durations from 4-79) is mainly due to transformer leakage inductance acting as a source impedance causing overlap between switches . By considering both conventional and proposed modulation strategies , it is clear that in proposed technique any possibility of source short circuit via in-coming and out-going MOSFETs is eliminated.

2- interaction between snubber capacitors of the cycloconverter and transformer inductances (Fig. 5-32).

3- effect of filtering capacitor on output voltage(Fig.5-35(b)).

Since a study of these interactions on overall conversion system using classical analysis is very complex , they were not discussed in this thesis in detail(simulation packages , for example **SPICE** , may be used) .

6.2.4 Cycloconverter output filtering

Since system operating link frequency is **1 kHz** , the transformer offers some leakage reactance . In addition some stray inductances are present , so by connecting filtering capacitor of **2-4** μF across the cycloconverter output , the overall system output is a **50 Hz** sinusoidal wave , Figures 5(37-41) .

6.2.5 System loading

A three-phase induction motor was connected to the cycloconverter output . It's starting and unloaded performance was normal , but further motor load caused excessive voltage drop across secondary. The cycloconverter measured output voltage verifies the theoretical value , **64%** of secondary voltage , Fig.s 4-16 and 5-41(b) may be compared . But in load condition , as long as load current increases the transformer regulation gets worse .The same problem occurred with the resistive load .

By considering all facts and explanations about overall system operation the following points are made :

1- the 3-phase inverter operation under the **suggested optimized PWM strategy** was well satisfied. The low order harmonics up to **17th(17 kHz)** are eliminated and output voltage fundamental is achieved by **1.17 p.u.** of DC source voltage(table 2-9) .

2- the cycloconverter operation (**1 kHz-to-50 Hz**) under implementation of **proposed modulation strategy** results **50 Hz** sinusoidal output with **64%** of input or secondary voltage (Fig.5-41(b)) , which is satisfactory in compare with conventional and other methods demonstrated in chapter 4 .

3- no need for bulky filtering elements except a small capacitor (**2-4** μF) across cycloconverter output .

Therefore the prototype system operation for **DC-to-3 phase (1kHz)-to-3 phase (50 Hz)** power conversion and 3-phase induction motor application purposes is well approved provided that the high-frequency transformer should meet all appropriate requirements dictated by conversion system such as minimized and optimized leakage inductance , interwinding capacitance and design recommendation core material which in turn require another research period itself .

6.3 Future Work

There are different aspects of the system raised as a result of this research work which could be given more attention . These aspects can be summarized as follows :

1- it is possible to provide closed loop control such that the constant output voltage is maintained as the load varies . The existing microprocessor based waveform generating system could be incorporated in the loop .

2- referring to Fig. 2-19 , by controlling of the inverter fundamental output voltage (in terms of $\alpha 1$, $\alpha 2$, $\alpha 3$, $\alpha 4$ variation which is accomplished with the elimination of **5**th , **7**th and **11**th components) accordingly the output of cycloconverter can be controlled either by open loop or close loop . The aspect seems very attractive especially in induction motor application with constant maximum torque and variable speed by high frequency inverter-transformer-cycloconverter configuration . Because in this mode , in the inverter side components up-to **13th** (**13 kHz**) and in cycloconverter output the components up-to **39th**(**1.8 kHz**) will be eliminated .

3- microprocessor implementation for variable cycloconverter output voltage and frequency based on relationships of (**4-79**) & (**4-82**) which produce predictable no load output voltage harmonics .

4- if system load is a slip ring induction motor , the rotor energy recovery and injection of this energy to the system as a close loop .

5- for the prototype system the transformer was designed and manufactured externally but it was not sought after one . The exact transformer design to predict the leakage inductance and inter-winding capacitances reliably would help in the overall system performance . For precise system efficiency assessment , the calculation of transformer losses under non-sinusoidal operation conditions is necessary . Therefore for switched mode and high-frequency operation , the transformer is worth much further study , though this is beyond of the scope of this thesis and itself is a major project in its own right , especially for following targets :

1- high-frequency and high-power handling capability

2- low cost & high efficiency design

Appendix A (Computer programs)

```
c     ***************************************************
c     yy.f   program  for  3-Dimension  plotting of  T.H.D=f(R,M)
c     R=fc/fm
c     fc is carrier wave frequency
c     fm is modulating wave frequency
c     M is dept of modulation
c     T.H.D is total harmonic distortion factor on inverter out-put
c     ***************************************************

      INTEGER NUMX,NUMY,NP,NW,NCONT,ISM,I,IVIEW
      REAL XLOW,XHIGH,YLOW,YHIGH,PI,XAV,YAV,SCALE,ZANGLE,
     1     X1,Y1,X2,Y2,X3,Y3,X4,Y4
      REAL X(25),Y(25),Z(25),GRIDZ(60,60),W(15000)
      NUMX=60
      NUMY=60
      NW=15000
      XLOW=3.0
      XHIGH=11.0
      YLOW=0.2
      YHIGH=1.0
      read(*,*)id,un,iv
      ISM=0
      READ (70,*) NP
      DO 10 I=1,NP
      READ (70,*) X(I),Y(I),Z(I)
10    CONTINUE
      CALL GINO
      if(id.eq.1) call t4107
      if(id.eq.2) call laserw
      CALL UNITS(un)
      CALL RANGRD(NP,X,Y,Z,NUMX,XLOW,XHIGH,NUMY,YLOW,YHIGH,GRIDZ,NW,W)
      call isoprj(numx,xlow,xhigh,numy,ylow,yhigh,gridz,iv,nw,w)
      call ginend
      CLOSE (UNIT=5)
      STOP
      END
```

```
C     ***************************************************************
C     SET OF NONLINEAR EQUATION SOLUTION , NAG-(c05nbf)ROUTINE
C     nag4.f,harmonic elimination(5,7,11,13th)and v1(max)=1.17E
C     alfa1=10.548153,alfa2=16.094384,alfa3=30.905343,alfa4=32.864859
C     20/SEP/1989 , LIB.-TERMINAL , 4 PM
C     ***************************************************************
      DOUBLE PRECISION  FNORM, TOL
      IMPLICIT DOUBLE PRECISION (A-H,O-Z)
      INTEGER IFAIL, J, NOUT
      DOUBLE PRECISION FVEC(4), WA(54), X(4)
      DOUBLE PRECISION F05ABF, DSQRT, X02AAF
      EXTERNAL FCN
      DATA NOUT /6/
      WRITE (NOUT,99999)
      DO 20 J=1,4
      X(J)=49813000.E-08
   20 CONTINUE
      TOL = DSQRT(X02AAF(0.0))
      IFAIL = 1
      N1=1
    8 CALL C05NBF(FCN, 4, X, FVEC, TOL, WA, 54, IFAIL)
      N2=N1+1
      FNORM = F05ABF(FVEC,4)
      PI=3.1415926
      Y=(PI/2)
      IF(X(2)-X(1))8,8,9
    9 IF(X(3)-X(2))8,8,7
    7 IF(X(4)-X(3))8,8,6
    6 IF(x(4)-Y)5,8,8
    5 WRITE (NOUT,99998) FNORM, IFAIL, (X(J),J=1,4)
      STOP
99999 FORMAT (4(1X/), 31H C05NBF EXAMPLE PROGRAM RESULTS/1X)
99998 FORMAT (5X, 31H FINAL L2 NORM OF THE RESIDUALS, E12.4//5X,
     * 15H EXIT PARAMETER, I10//5X, 27H FINAL APPROXIMATE SOLUTION//
     * (5X, 3E12.4))
      END
      SUBROUTINE FCN(N, X, FVEC, IFLAG)
      INTEGER IFLAG, N
      DOUBLE PRECISION FVEC(N), X(N)
      INTEGER K
      I=1
      DO 30 M=5,13,2
      K=1
      IF(M-9)11,30,11
      WRITE(6,*)M
   11 TEMP=COS(M*X(K))-COS(M*X(K+1))+COS(M*X(K+2))-COS(M*X(K+3))-0.5
      K=I
      FVEC(K) =TEMP
      I=1+K
   30 CONTINUE
      RETURN
      END
```

```
c       ************************************************************
c       kar.f , fi=1000 hz , fo=50 hz , R=fi/fo=20 , M=0.63
c       proposed modulation strategy , equal area , 90 deg. line
c       ************************************************************
        pi=3.1415926
        z=0.6360
        r=20.
        do  14 k=1,40
        a1=pi/r
        a2=k*a1
        a3=cos(a2)
        j=k-1
        a4=j*a1
        a5=cos(a4)
        a6=a5-a3
        a7=a6*r*z
        a8=k-0.5
        a9=a8*pi
        a10=sin(a9)
        l=k+1
        a11=(-1)**l
        a12=2*a11*a10
        a13=a7/a12
        if(k-20)1,1,2
1       a14=asin(a13)
3        beta=a14*(180./pi)
        alfa1=2*beta
        n=k-1
        x1=90.-beta
        x2=x1+alfa1
        x3=x1+x2
        landa=180*n
        x4=x1+landa
        x5=x2+landa
        x6=x3+landa
        write(50,*)x4,x5,x6
        alfa2=90.-beta
        alfa3=90.+beta
        alfoff=90.-beta
        toff=alfoff*(20000./7200)
        alfaon=2*beta
        ton=alfaon*(20000./7200)
        write(71,*)alfoff,alfaon,alfoff
        ttotal=toff+ton+toff
        write(72,*)toff,ton,toff,ttotal
        write(46,*)k,alfa2,alfaon,alfa3
        write(47,*)k,toff,ton,toff
        write(48,*)k,alfoff,alfaon,alfoff
        write(49,*)alfoff,alfaon,alfoff
        write(6,*)k
        go to 14
 2      a14=(-1)*asin(a13)
        go to 3
14      continue
        stop
        end
```

Appendix B (SMM20N50 Power MOSFET data sheets)

Siliconix
incorporated

MOSPOWER

SMM20N50

N-Channel Enhancement Mode Transistor

PRODUCT SUMMARY

PART NUMBER	$V_{(BR)DSS}$ (VOLTS)	$r_{DS(on)}$ (OHMS)	I_D (AMPS)
SMM20N50	500	0.30	20

BOTTOM VIEW

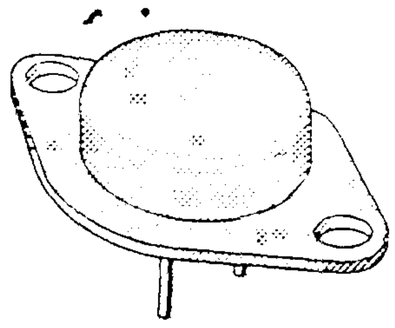

TO-204AE (TO-3)

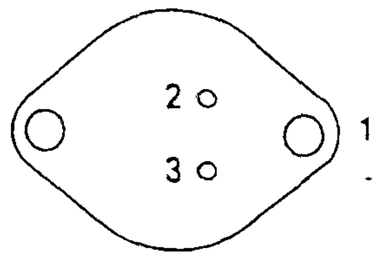

1 DRAIN (CASE)
2 GATE
3 SOURCE

ABSOLUTE MAXIMUM RATINGS (T_C= 25°C unless otherwise noted)

PARAMETERS/TEST CONDITIONS		Symbol	SMM20N50	Units
Drain-Source Voltage		V_{DS}	500	V
Gate-Source Voltage		V_{GS}	± 40	
Continuous Drain Current	T_C = 25°C	I_D	20	A
	T_C = 100°C		12.5	
Pulsed Drain Current[1]		I_{DM}	80	
Avalanche Current (see figure 9)		I_A	20	
Power Dissipation	T_C = 25°C	P_D	250	W
	T_C = 100°C		100	
Operating Junction & Storage Temperature Range		T_J, T_{stg}	-55 to 150	°C
Lead Temperature (1/16" from case for 10 secs.)		T_L	300	

THERMAL RESISTANCE RATINGS

THERMAL RESISTANCE	Symbol	Typ.	Max.	Units
Junction-to-Case	R_{thJC}	-	0.50	K/W
Junction-to-Ambient	R_{thJA}	-	30	
Case-to-Sink	R_{thCS}	0.1	-	

[1]Pulse width limited by maximum junction temperature (refer to transient thermal impedance data, figure 11)

4

Siliconix incorporated

ELECTRICAL CHARACTERISTICS (T_J = 25°C unless otherwise noted)

PARAMETERS/TEST CONDITIONS		Symbol	Min.	Typ.	Max.	Units
Drain-Source Breakdown Voltage V_{GS} = 0, I_D = 250 µA		$V_{(BR)DSS}$	500	–	–	V
Gate Threshold Voltage V_{DS} = V_{GS}, I_D = 1000 µA		$V_{GS(th)}$	2.0	2.6	4.0	
Gate-Body Leakage V_{DS} = 0, V_{GS} = ±20 V		I_{GSS}	–	–	100	nA
Zero Gate Voltage Drain Current V_{DS} = $V_{(BR)DSS}$, V_{GS} = 0		I_{DSS}	–	–	250	µA
Zero Gate Voltage Drain Current V_{DS} = 0.8 × $V_{(BR)DSS}$, V_{GS} = 0, T_J = 125°C		I_{DSS}	–	–	1000	
On-State Drain Current[2] V_{DS} = 10 V, V_{GS} = 10 V		$I_{D(on)}$	20	–	–	A
Drain-Source On-State Resistance[2] V_{GS} = 10 V, I_D = 10 A		$r_{DS(on)}$	–	0.26	0.30	Ω
Drain-Source On-State Resistance[2] V_{GS} = 10 V, I_D = 10 A, T_J = 125°C		$r_{DS(on)}$	–	0.52	0.70	
Forward Transconductance[2] V_{DS} = 15 V, I_D = 10 A		g_{fs}	8.0	11	–	S(℧)
Input Capacitance	V_{GS} = 0 V_{DS} = 25 V f = 1 MHz	C_{iss}	–	3800	4500	pF
Output Capacitance		C_{oss}	–	750	1000	
Reverse Transfer Capacitance		C_{rss}	–	350	500	
Total Gate Charge	V_{DS} = 0.5 × $V_{(BR)DSS}$, V_{GS} = 10 V, I_D = 20 A (Gate charge is essentially independent of operating temperature)	Q_g	–	70	100	nC
Gate-Source Charge		Q_{gs}	–	15	–	
Gate-Drain Charge		Q_{gd}	–	34	–	
Turn-On Delay Time	V_{DD} = 250 V, R_L = 25 Ω I_D = 10 A, V_{GEN} = 10 V R_G = 4.7 Ω (Switching time is essentially independent of operating temperature)	$t_{d(on)}$	–	34	45	ns
Rise Time		t_r	–	57	70	
Turn-Off Delay Time		$t_{d(off)}$	–	120	150	
Fall Time		t_f	–	62	75	

SOURCE-DRAIN DIODE RATINGS & CHARACTERISTICS (T_J = 25°C unless otherwise noted)

PARAMETERS/TEST CONDITIONS	Symbol	Min.	Typ.	Max.	Units
Continuous Current	I_S	–	–	20	A
Pulsed Current[1]	I_{SM}	–	–	110	
Forward Voltage[2] I_F = I_S, V_{GS} = 0	V_{SD}	–	–	1.6	V
Reverse Recovery Time I_F = I_S, dI_F/dt = 100 A/µS	t_{rr}	–	300	650	ns
Reverse Recovered Charge I_F = I_S, dI_F/dt = 100 A/µS	Q_{rr}	–	2.0	–	µC

[1] Pulse width limited by maximum junction temperature (refer to transient thermal impedance data, figure 11)
[2] Pulse test: Pulse width ≤ 300 µsec, Duty Cycle ≤ 2%

PERFORMANCE CURVES (25°C Unless otherwise noted)

FIGURE 1: Typical Output Characteristics

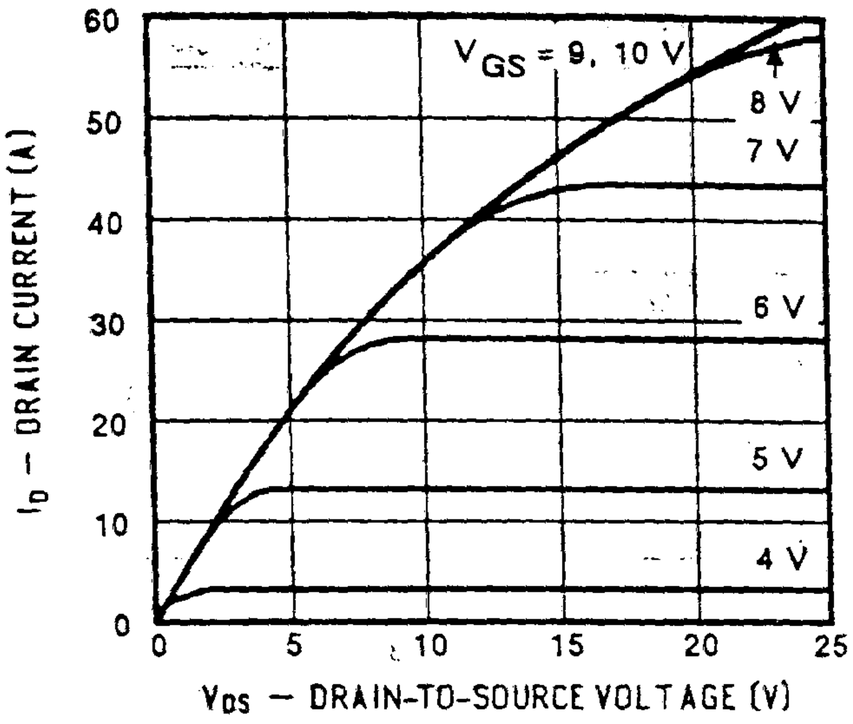

FIGURE 2: Typical Transfer Characteristics

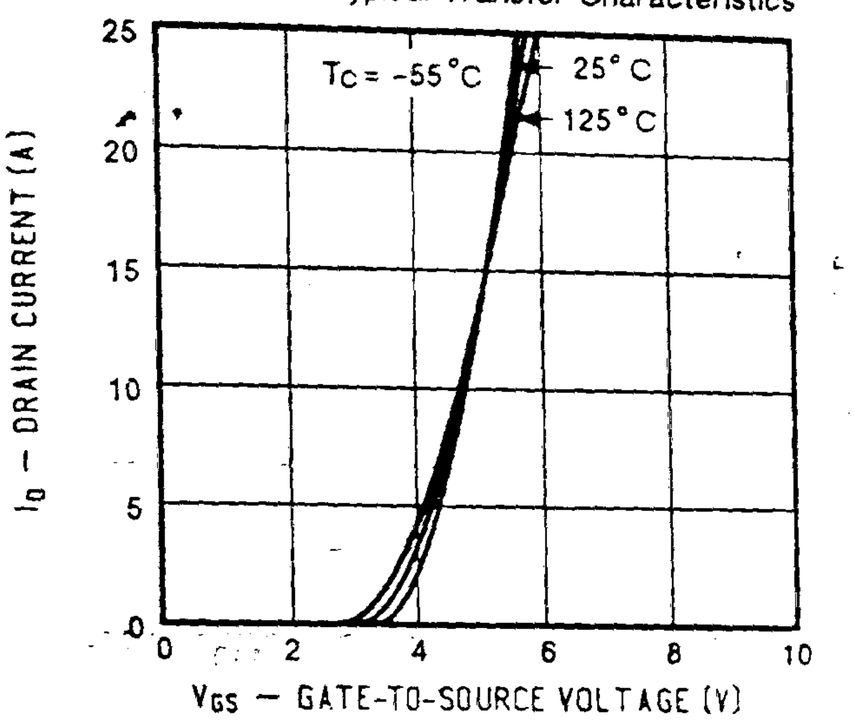

FIGURE 3: Typical Transconductance

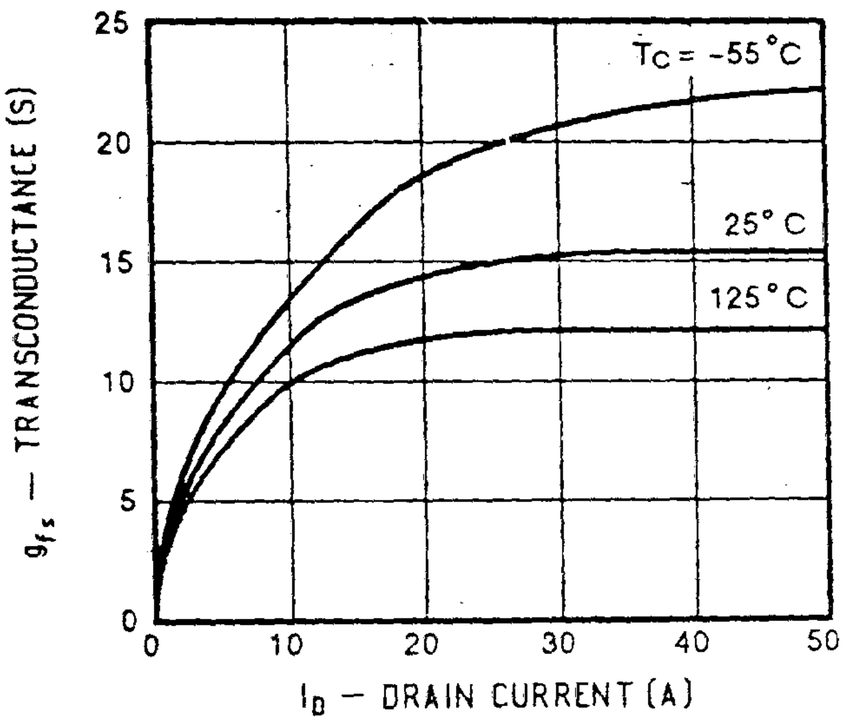

FIGURE 4: Typical On-Resistance

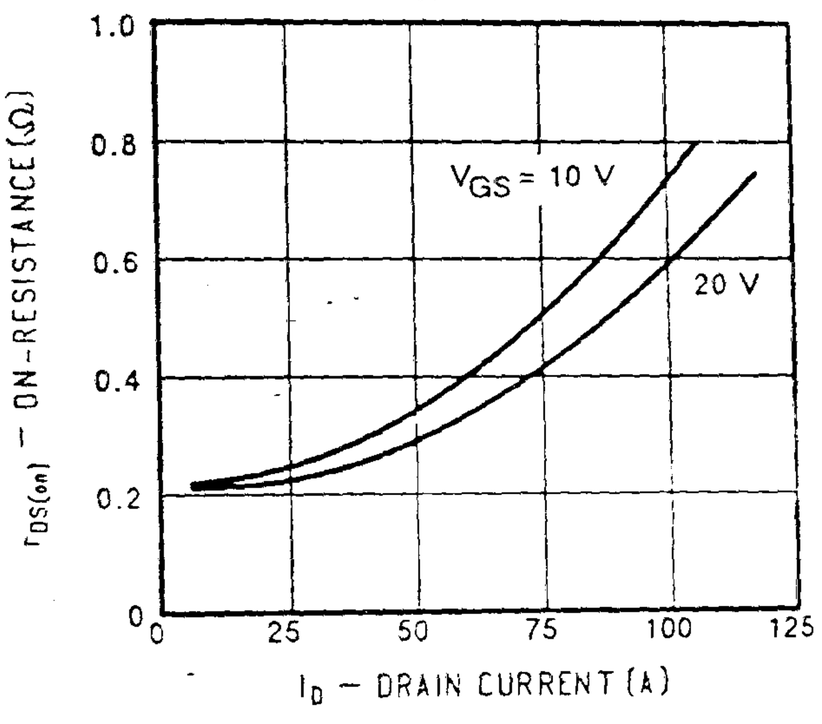

FIGURE 5: Typical Capacitance

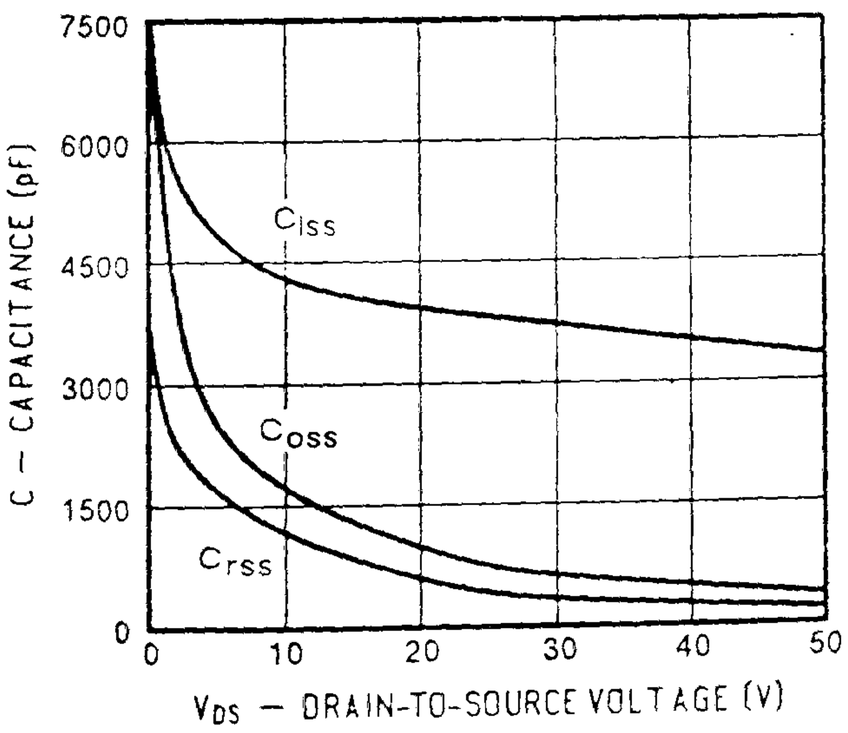

FIGURE 6. Typical Gate Charge

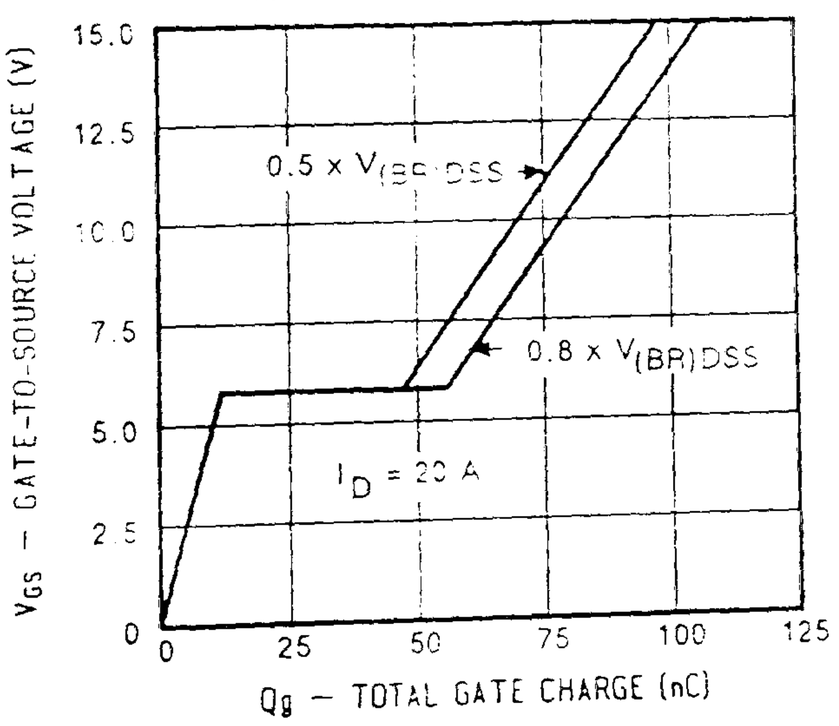

Siliconix incorporated

PERFORMANCE CURVES (25°C Unless otherwise noted)

FIGURE 7: On-Resistance vs. Junction Temperature

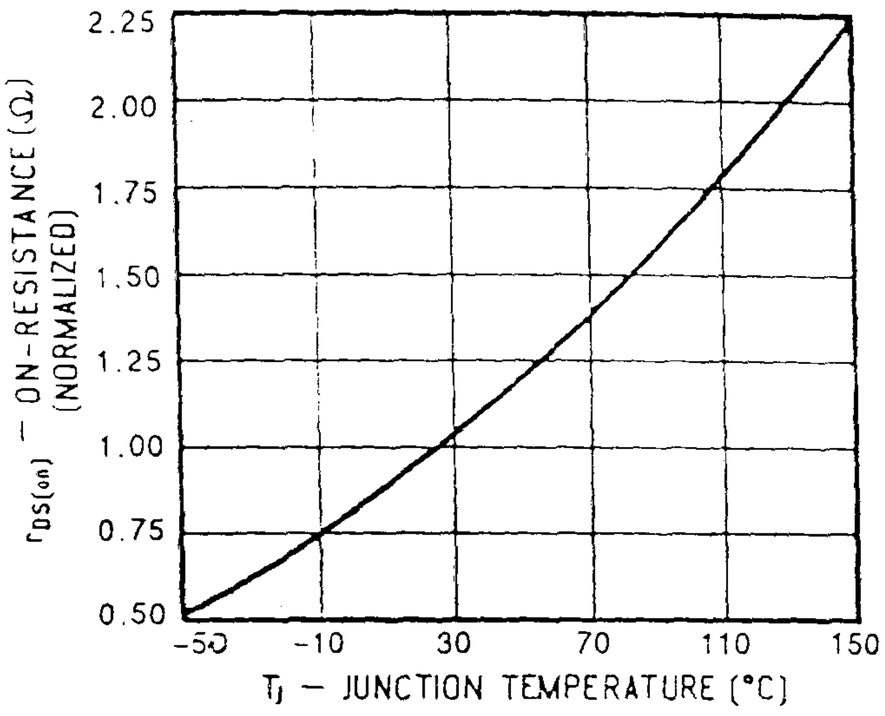

FIGURE 8: Typical Source-Drain Diode Forward Voltage

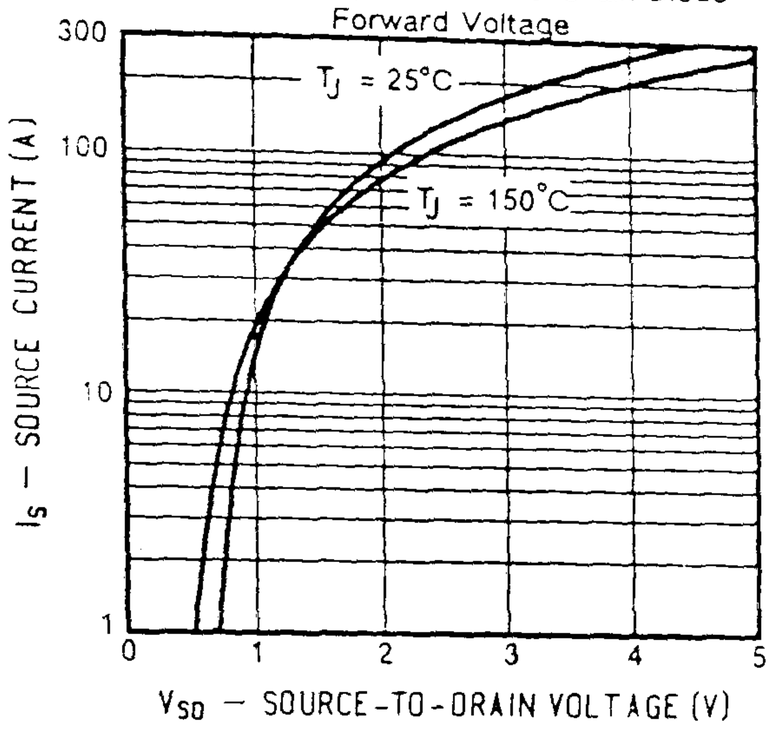

FIGURE 9: Maximum Avalanche and Drain Current vs. Case Temperature

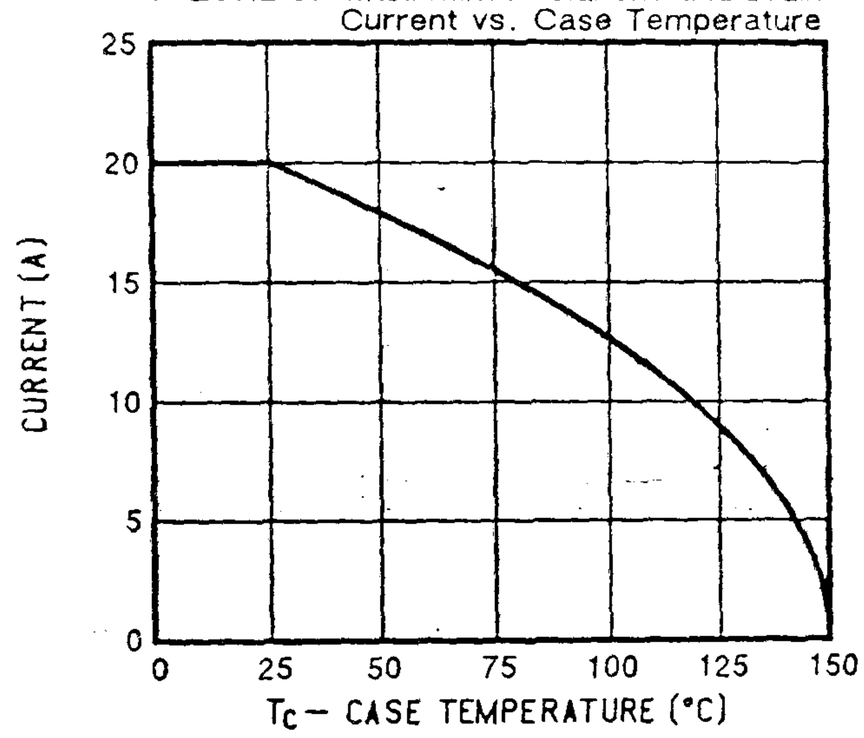

FIGURE 10: Safe Operating Area

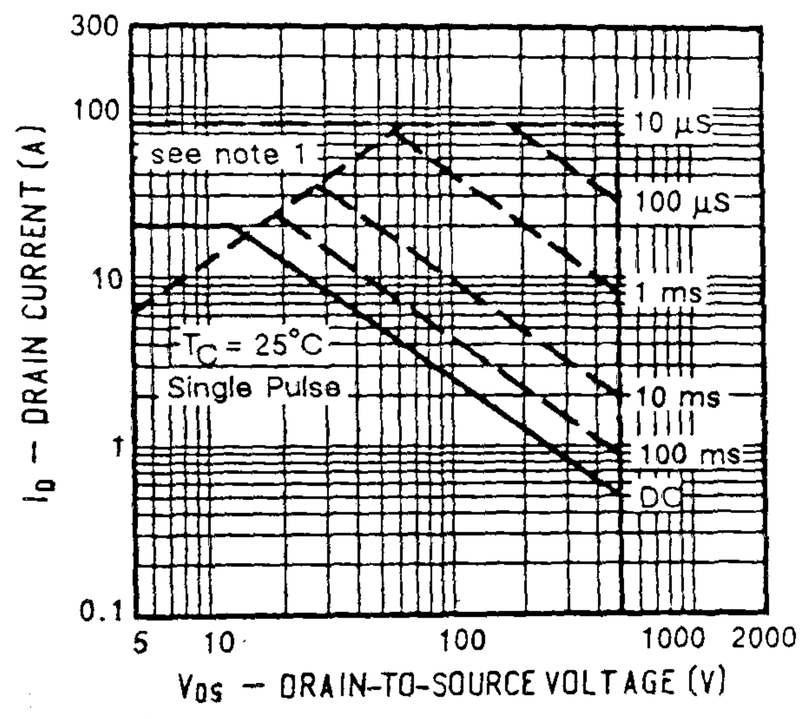

[1]Operation in this area may be limited by $r_{DS(on)}$

FIGURE 11: Normalized Effective Transient Thermal Impedance, Junction-to-Case

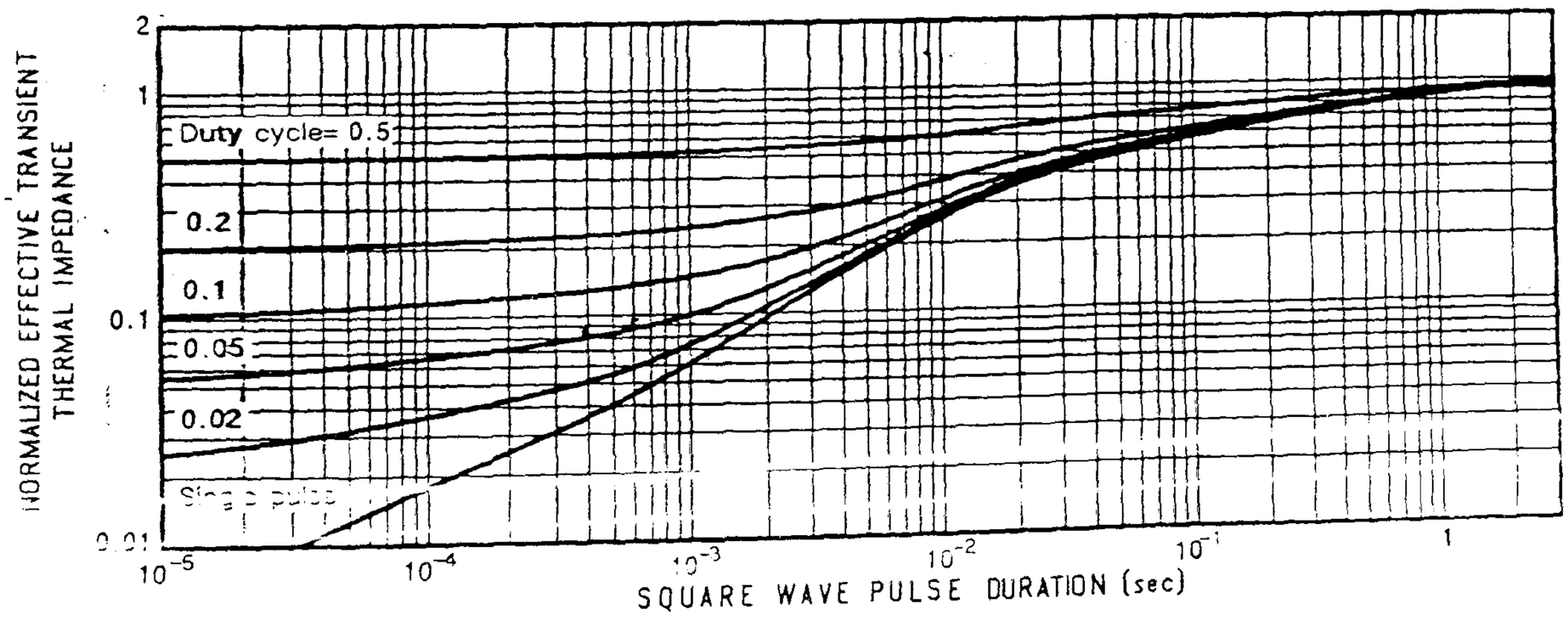

Appendix C

1 - Semi-Graphic & Semi-Numerical Analysis

2 - Effect of the load power factor on the Inverter-Transformer operation

Semi-Graphical & Semi-Numerical Analysis

Any periodic and non-sinusoidal function may be expressed by a Fourier Series :

$$y = f(x) = \frac{a_0}{2} + \sum_{n=1}^{\infty} \left[a_n \sin(nx) + b_n \cos(nx) \right] \qquad (1)$$

Where

$$a_0 = \frac{1}{\pi}\int_0^{2\pi} y\,dx \quad , \quad a_n = \frac{1}{\pi}\int_0^{2\pi} y\sin(nx)\,dx \quad , \quad b_n = \frac{1}{\pi}\int_0^{2\pi} y\cos(nx)\,dx \qquad (2)$$

The following cases may occur :

1- if the areas of the positive and negative half cycles are equal , then $a_0 = 0$

2- if $f(x + \pi) = -f(x)$, then odd harmonics only are present

3- if $f(-x) = -f(x)$, then $b_n = 0$

4- if $f(-x) = f(x)$, then $a_n = 0$

If it is difficult to find a manageable mathematical expression to $f(x)$, the "**semi-Graphical , semi-Numerical**" method can be applied[1 , 2]. Here , one cycle of the curve is divided into **m** vertical strips of equal width(the **m** an even number) . If y_k is the ordinate of **k-th** strip , then the coefficients of the **n-th** harmonic are

$$a_n = \frac{2}{m} \sum_{k=1}^{k=m} \left[y_k \sin(n x_k) \right] \qquad (3)$$

$$b_n = \frac{2}{m} \sum_{k=1}^{k=m} \left[y_k \cos(n x_k) \right] \qquad (4)$$

or

$$a_n = \frac{2}{m} \sum_{k=1}^{k=m} \left\{ y_k \sin\left[k\frac{2\pi}{m}\right]n \right\} \qquad (5)$$

$$b_n = \frac{2}{m} \sum_{k=1}^{k=m} \left\{ y_k \cos\left[k\frac{2\pi}{m}\right]n \right\} \qquad (6)$$

For the greater accuracy , **m**(the number of ordinate) >> **n**(the harmonic order) shoud be considered .

1- Bela E.F. Karsa " **Electrical measuring instruments and measurements** " Budapest , 1967

2- Cyril W.Lander " **Power Electronics** " second edition , Mc Graw.Hill Book company (UK) limited , 1987

Effect of the load power factor on the Inverter-Transformer operation

Refferring to the Figs. 2-2 & 2-3 of the chapter 2 :

1- when the load is a pure resistive($\cos \Phi = 1$) , the current waveform will be identical to the voltage waveform. So the power delivered to the load via the switches is proportional to the dotted areas in the current waveforms , shown in Fig.2-2(a) .

2- when the load is completely inductive($\cos \Phi = 0$ lagging) the current waveform is semilar to the Fig. 2-2(b) , $i = \frac{1}{L}\int_{t1}^{t2} Edt$. When the power(trapped in the inductive load) is feed backed in to the source(hatched areas in the current waveform), at the same time power is pushed into the load by the source. Because of the unidirectional cuuernt carring property of the simiconductor switches the reverse current is blocked by the switch , in result causes a reverse voltage spike at the primary . By connecting the anti-parallel diodes across the MOSFETs this problem can be avoided . when the load is a pure inductive , the diode conduction duration is 90° .

3- when the load is comletely capacitive($\cos \Phi = 0$ leading) , in the beginning of any MOSFET conduction the power is supplied to the reverse charged capacitor through a very low impedance(transformer impedance + switch saturation resistance) and the current rises to extremely high levels until the capacitor begins to represent a rising impedance(charging to source voltage). A general current waveform for this mode of operation is shown in Fig. 2-2(c) .

Published papers

These papers have been accepted for presentation at the :

1. 22-th annual Power Electronics Specialists conference , Texas , U.S.A , (24-28)-June-1991

2. 26-th Universities Power Engineering conference(UPEC) , Brighton , U.K. (18-20)-September-1991

A NOVEL STRATEGY FOR CONTROL OF CYCLOCONVERTERS

Asghar Karamat Tom Thomson Pratap Mehta

Brunel University UK

ABSTRACT

This paper presents a novel technique for controlling cycloconverters. The main advantages claimed are (i) much improved harmonic spectrum in the output voltage, (ii) the proposed strategy allows much easier implementation using microprocessors and (iii) it reduces the possibility of short-circuit between the positive and the negative groups of converters.

INTRODUCTION

Multi-stage power conversion from dc to ac with high frequency-links and inverter-transformer-phase controlled cycloconverter topologies have been of growing interest for uninterruptible power supplies and solar converters. During the last decade, there have been a number of suggestions for dc to ac systems (1,2,3). For a required voltage transformation and/or electrical isolation between the dc input and ac output conventionally a transformer is employed. In the new generation of lighter power converters these demands are met by small transformers operating at high frequency. The relative merits and shortcomings of these new systems, however, have not all been fully explored, but eventually are dependent to some extent on the application and power and voltage levels for which these systems are designed.

CONVENTIONAL MODULATION STRATEGY

Conventional control strategy is based on the cosine-wave crossing method (4,5) for determining the timing of the triggering pulses for cycloconverter switches. Referring to Figure 1 the voltage equations for this configuration are:

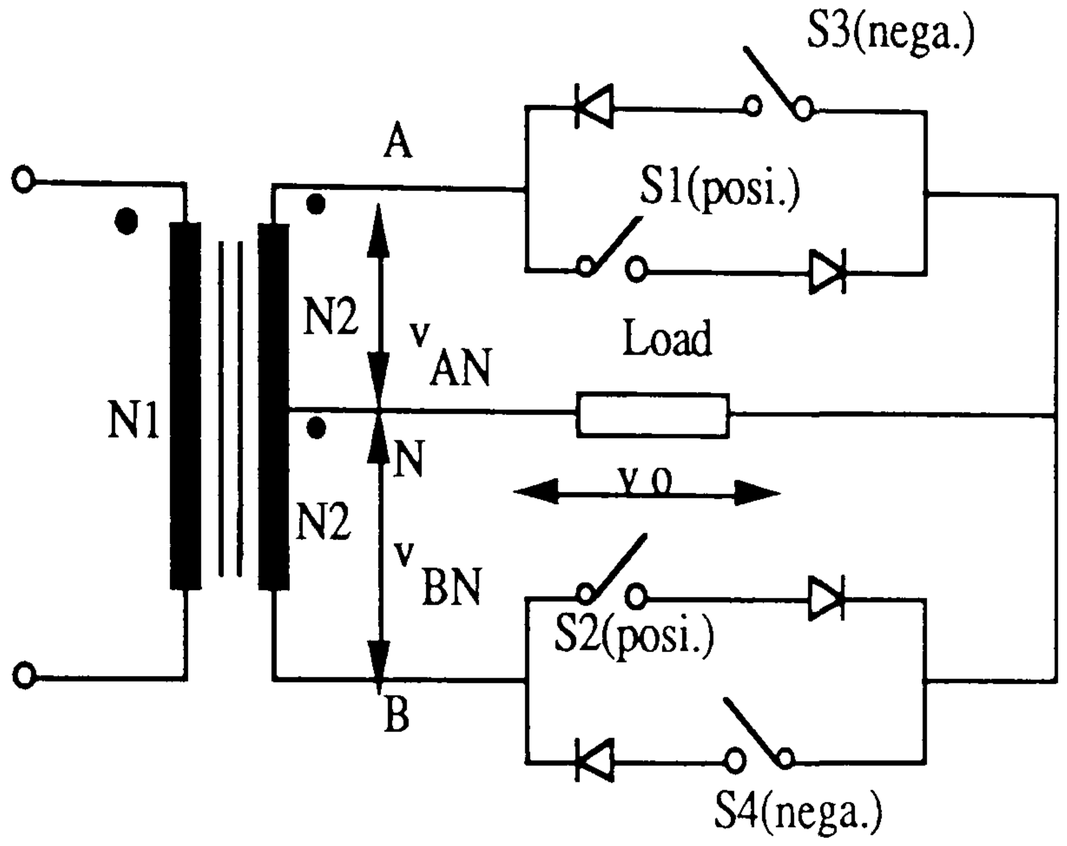

Figure 1 Circuit configuration for conventional modulation strategy

$$v_{AN} = V_m \sin(\omega_i t) \qquad (1)$$

$$u_{AN} = \frac{2}{\pi} V_m \cos(\omega_i t) \qquad (2)$$

$$v_{BN} = V_m \sin(\omega_i t - \pi) = -V_m \sin(\omega_i t) \qquad (3)$$

$$u_{BN} = -\frac{2}{\pi} V_m \cos(\omega_i t) \qquad (4)$$

$$v_o = M.V_m \sin(\omega_o t) \qquad (5)$$

v_o is the cycloconverter output voltage
M is the depth of modulation for output voltage and $0.1 < M < 2/\pi$
$\omega_o = 2\pi f_c$
f_o is the cycloconverter output frequency

R = fi/fo is the input/output frequency ratio. Refering to equations (1) to (5) it is clear that the firing angles are determined so that the average output voltage , produced across the load by a conducting switch , is equal to the instantaneous value of the required output voltage at that firing instant .

From equation (1), for triggering angle α , the average value of the output voltage is

$$v_{ave.} = \frac{1}{\pi}\int_{\alpha}^{\pi+\alpha} V_m \sin(\omega_i t)\, d(\omega_i t) = \frac{2}{\pi} V_m \cos(\alpha) \qquad (6)$$

$$\alpha = \omega_i t = 2\pi f_i t$$

Therefore the (5) and (6) values should be equal at any instant of conduction , so

$$\frac{2}{\pi} V_m \cos(\alpha) = M V_m \sin(\frac{\alpha}{R}) \qquad (7)$$

Equation (7) implies that the intersecting points of a sinusoidal reference voltage with a series of cosine timing waves[(2) and (4)] , which are derived from and synchronized to the ac input voltage , are the required switching points of the switches .

Depending on M, R and fi, equation (7) may be applied by appropriate implementation . For M = 0.63 , R = 20 , fi = 1 kHz and resistive load the full output modulated voltage and associated harmonic spectrum are presented in Figure 2.

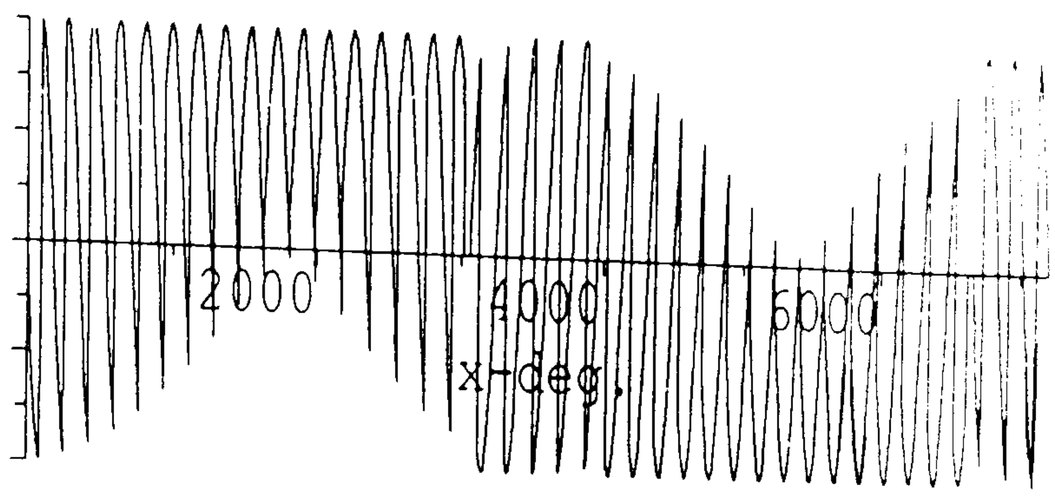

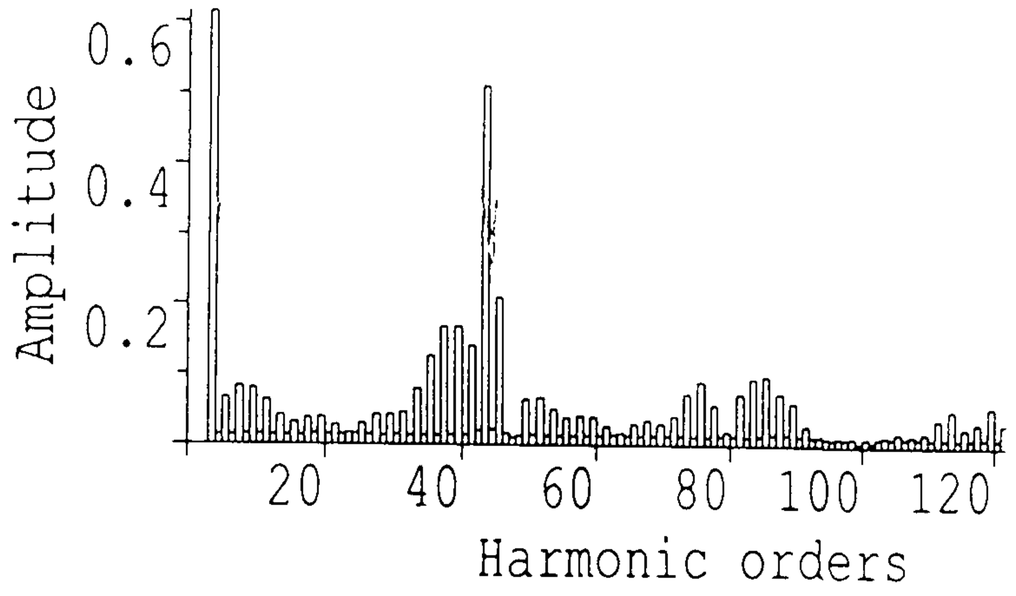

Figure 2 cycloconverter modulated output voltage and associated harmonic spectrum with conventional strategy

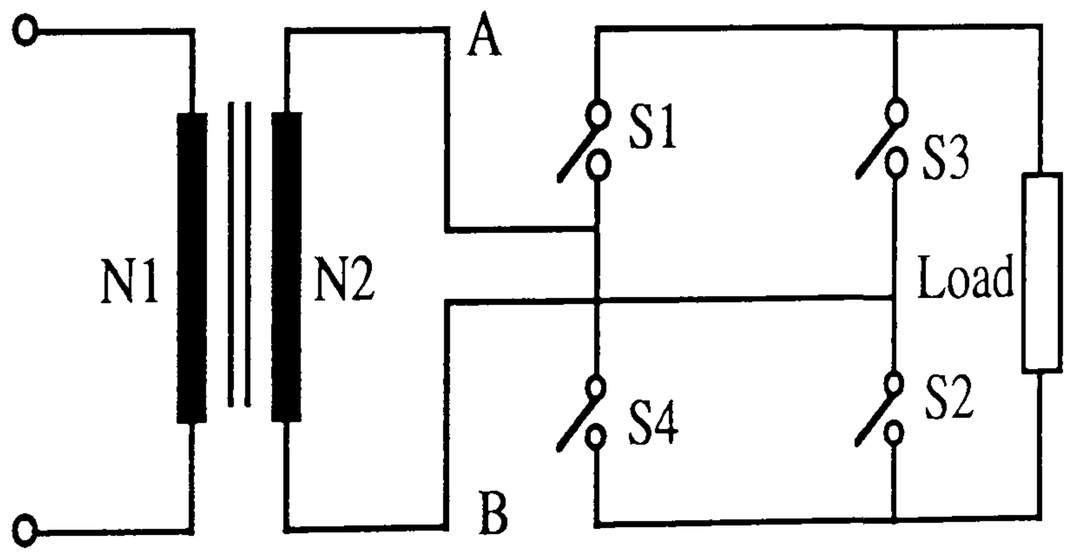

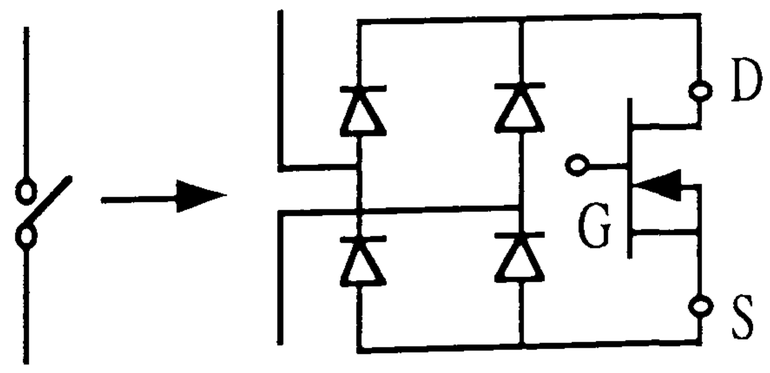

Figure 3 circuit configuration for proposed modulation strategy

Proposed modulation strategy

Figure 3 shows the configuration suitable for implementing the new strategy. S1 to S4 are biletral switches as shown. S1 and S2 conduct when point A is positive with respect to B and similarly S3 and S4 conduct when point B is positive with respect to A, thereby producing the positive half-cycle of the cycloconverter

output. The negative half-cycle of the output is produced in a similar fashion. Figure 4 illustrates the strategy for deriving the triggering angles of the switches which uses the "equal area crierion" i.e. the hatched area being equal to the dotted area. The two ares are given by the following expressions.

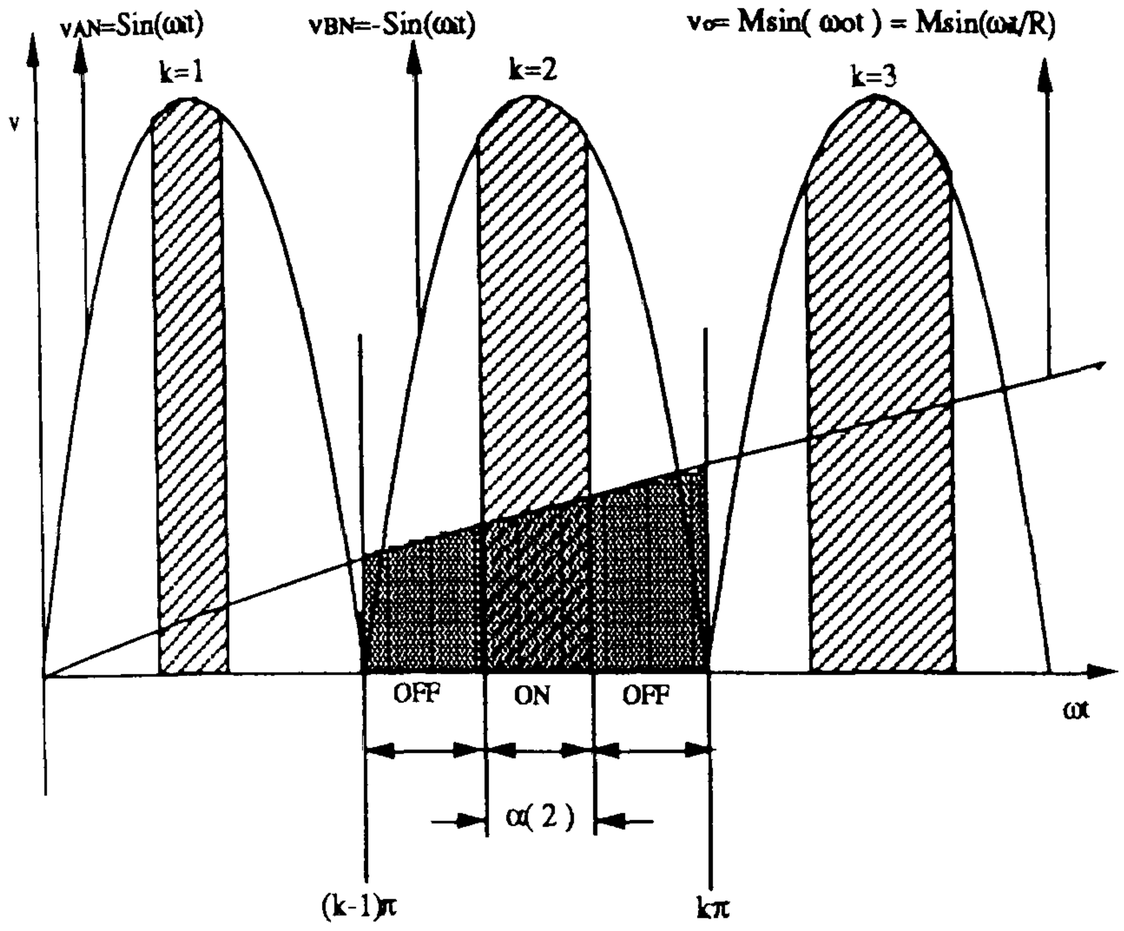

Figure 4 Equal area criterion for proposed modulation strategy

$$A_{dot} = \int_{\frac{(k-1)\pi}{\omega_i}}^{\omega_i} MSin(\omega_o t)dt \qquad (8)$$

$$= \frac{M}{R}\left[Cos(k-1)\frac{\pi}{R} - Cos(k\frac{\pi}{R})\right]$$

$$A_{hatch.} = \int_{\frac{(k-1)\pi+\frac{\pi}{2}-\frac{\alpha}{2}}{\omega_i}}^{\frac{(k-1)\pi+\frac{\pi}{2}+\frac{\alpha}{2}}{\omega_i}} Sin(R\omega_o t)\,dt \qquad (9)$$

$$A_{hatch.} = \frac{1}{R\omega_o}\left\{ Cos\left[(k-0.5)\pi - \frac{\alpha}{2}\right] - Cos\left[(k-0.5)\pi + \frac{\alpha}{2}\right] \right\} \qquad (10)$$

Since :

$$Cos(Q) - Cos(P) = 2Sin(\frac{P+Q}{2})Sin(\frac{P-Q}{2}) \qquad (11)$$

Then :

$$A_{hatch.} = 2Sin(k-0.5)\pi.Sin(\frac{\alpha}{2}) \qquad (12)$$

By equating (8) with (12) :

$$A_{dot.} = A_{hatch}$$

or

$$\frac{M}{\omega_o}\left[Cos(k-1)\frac{\pi}{R} - Cos(k\frac{\pi}{R})\right] = \qquad (13)$$

$$= \frac{2}{R\omega_o}.Sin(k-0.5)\pi.Sin(\frac{\alpha}{2})$$

From equation (13) the value of $\alpha(k)$ can be determined from:

$$\alpha(k) = Sin^{-1}\left[\frac{X}{Y}\right].\frac{360}{\pi} \qquad (14)$$

Where

$$X = RM\left[Cos(k-1)\frac{\pi}{R} - Cos(k\frac{\pi}{R})\right] \qquad (15)$$

$$Y = 2(-1)^{k+1}Sin(k-0.5)\pi$$

Where

k = 1,2,3,.....2R

M = 0, ...$2/\pi$

For M = 0.63, R = 20 and fi = 1 kHz, the modulated output voltage and associated harmonic spectrum are presented in Figure 5.

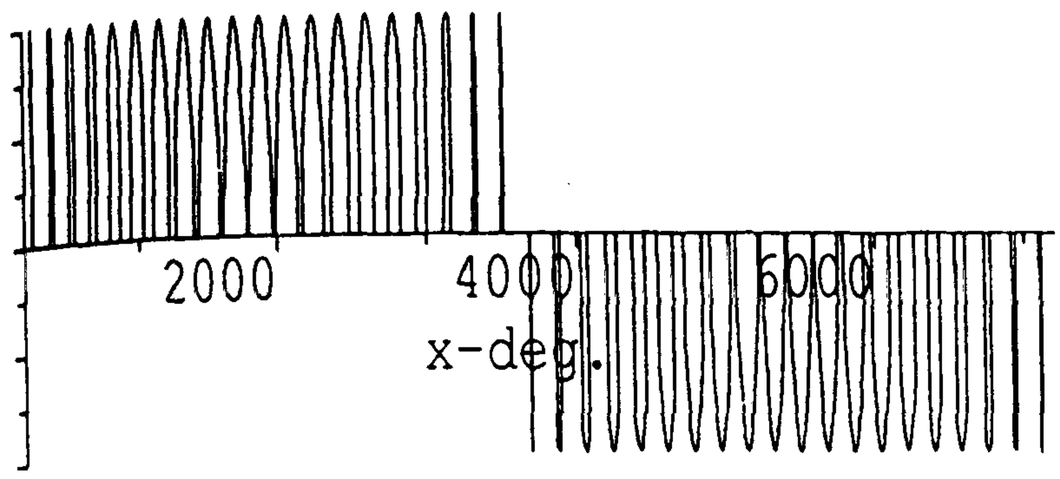

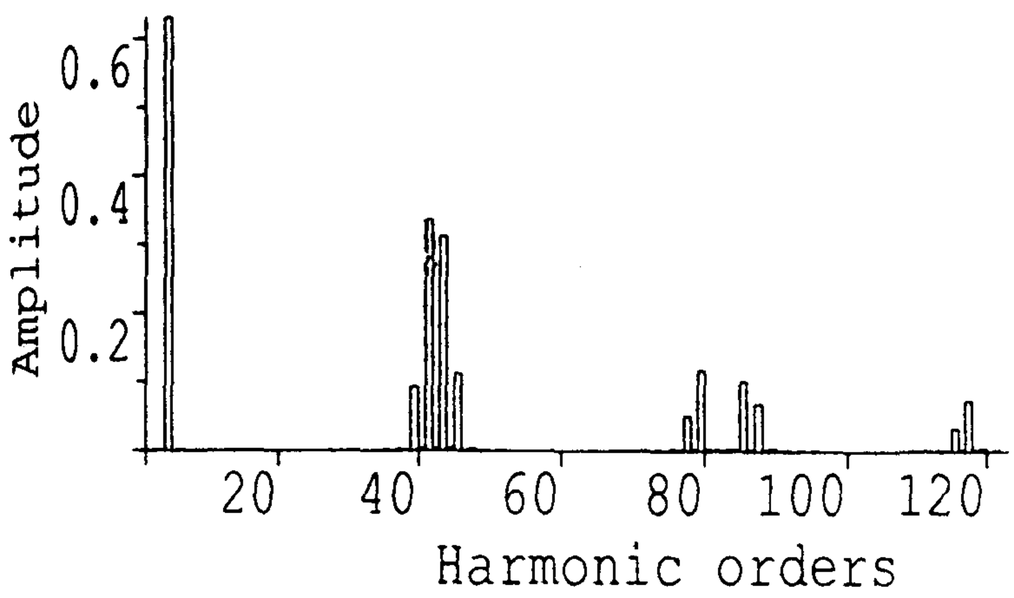

Figure 5 cycloconverter modulated output voltage and associated hamonic spectrum with proposed strategy

EXPERIMENTAL RESULTS

The proposed control strategy was verified on a three-phase cycloconverter supplied at lkHz from a dc source via a 1kHz inverter-transformer system.

Figure 6 shows the output voltage harmonic spectrum of the 50Hz output cycloconverter. As can be seen there are no significant harmonics below 2kHz for the input frequency of lkHz. Also this results compare very favourably with the predicted spectrum shown in Figure 5.

Figure 7 shows the three-phase voltage waveforms. For measurement purposes these oscillograms were obtained with a 2 microfarad capacitor connected across the output to filter out harmonics in excess of 1.8 kHz.

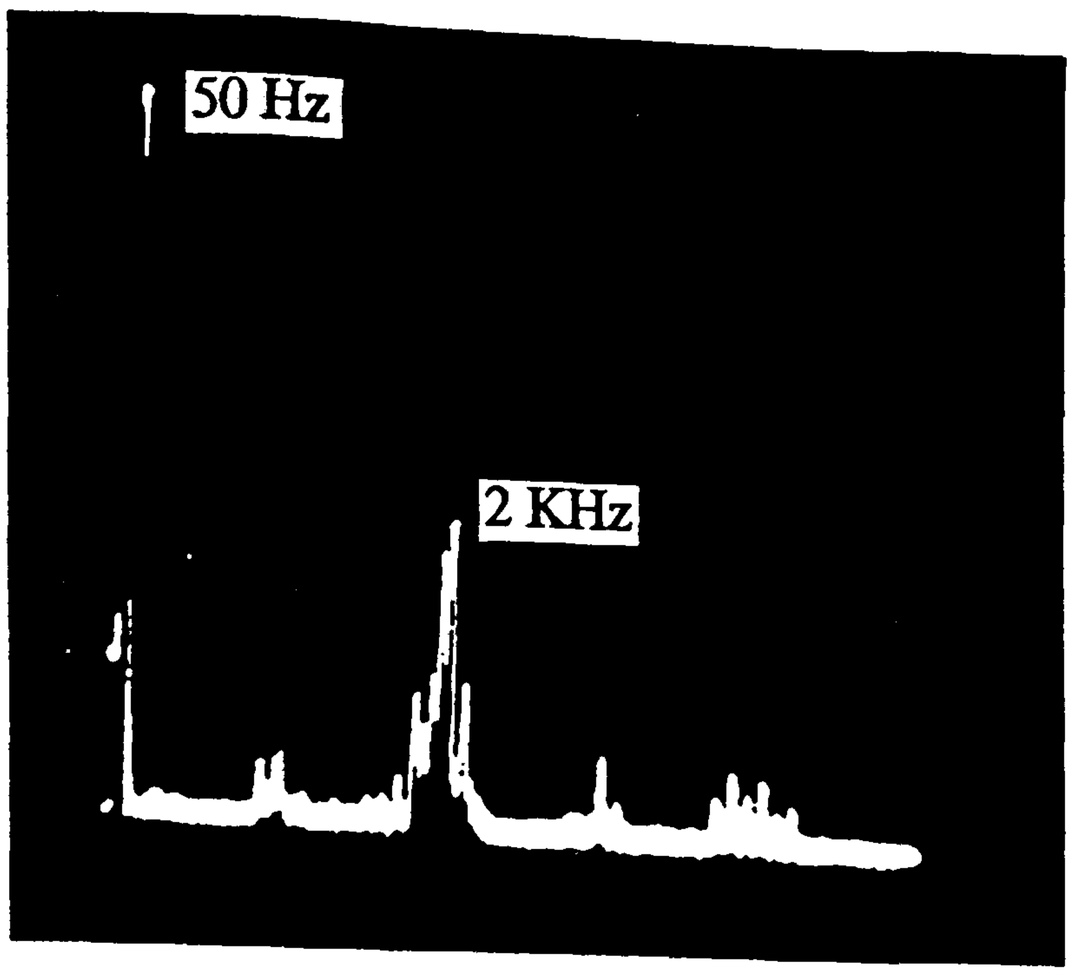

Figure 6 Output voltage harmonic spectrum

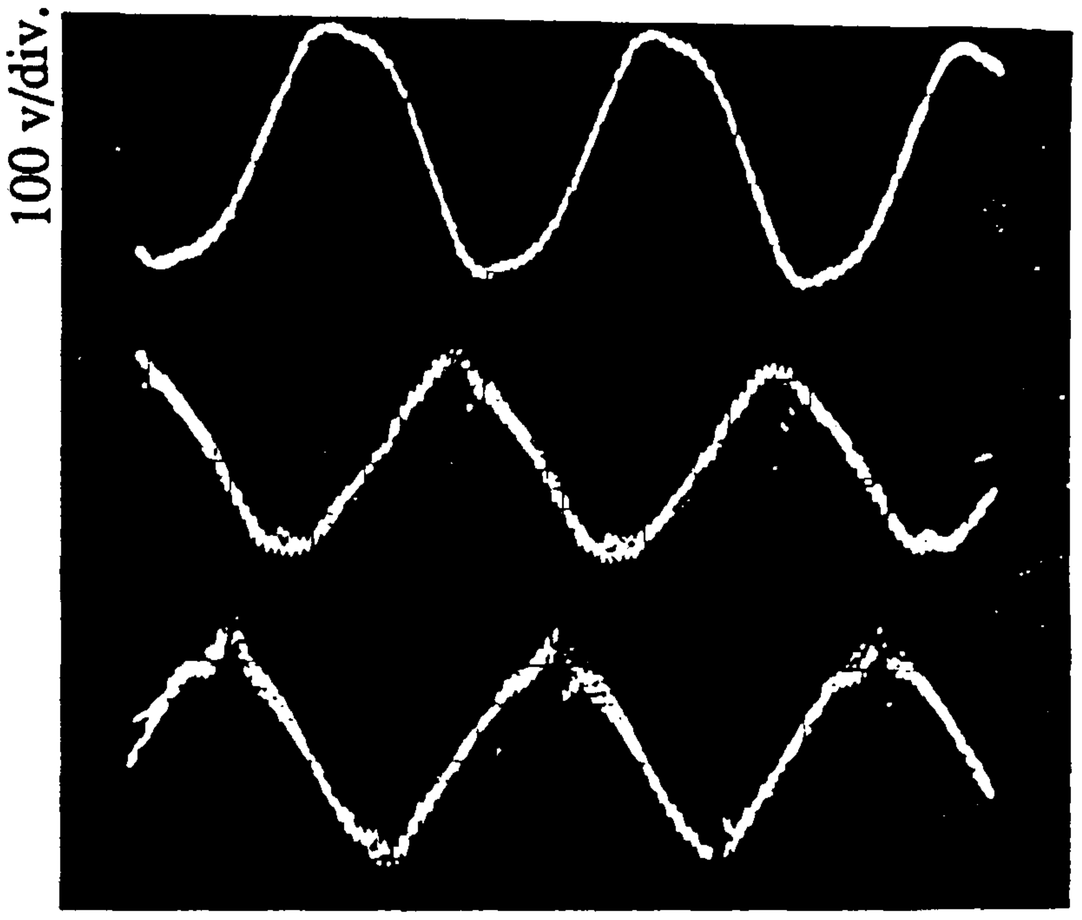

Figure 7 Three-phase output voltage waveforms

CONCLUSIONS

The proposed control strtategy for a non-circulating current cycloconverter offers the following advantages:

1 Typically for a 1kHz input system the control strategy assures that there are no significant harmonics below 2kHz.

2 The strategy is amenable to implementation using on-line microprocessor control i.e. equation (14) can be programmed into the system.

3 Unlike conventional cycloconverter the proposed configuration does not require any centre-tapped windings.

APPENDIX

Harmonic analysis for the psoposed modulation strategy

Refering to Fig. (8), the general expression of a Fourier Series for the instantaneous out-put voltage is

$$v_o(\omega_o t) = \sum_{1,3,5}^{\infty} (A_n \operatorname{Cos} n\omega_o t + B_n \operatorname{Sin} n\omega_o t)$$

(16)

The coefficients An and Bn are determined by considering a pair of pulses such that the positive pulse of duration α°_k starts at $\omega t = \Phi^\circ_k$ and the negative one of the same width starts at $\omega t' = 3600^\circ + \Phi^\circ_k$ (Fig.8) . The effects of all pulses can be combined together to obtain the effective out-put voltage. If the positive pulse of kth pair starts at $\omega t = \Phi^\circ_k$ and ends at :

$\omega t' = 3600^\circ + \Phi^\circ_k$

or :

$\omega t' = R\pi + \Phi^\circ_k$ (rad.)

The Fourier coefficients for this pair of pulses are :

$$a_n = \frac{2}{R\pi} \int_{\Phi_k}^{\Phi_k+\alpha_k} V_m \operatorname{Sin}(R\omega_o t) \,.\, \operatorname{Cos}(n\omega_o t)\, d(\omega_o t)$$

(17)

Since

$$\operatorname{Sin}(R\omega_o t).\ \operatorname{Cos}(n\omega_o t) = \frac{1}{2}\left[\operatorname{Sin}(R+n)\omega_o t + \operatorname{Sin}(R-n)\omega_o t\right]$$

(18)

then (17) becomes

$$a_n = \frac{2}{R\pi} \cdot \frac{V_m}{2} \left\{ \int_{\Phi_k}^{\Phi_k+\alpha_k} \sin(R+n)\omega_o t \,.d(\omega_o t) + \int_{\Phi_k}^{\Phi_k+\alpha_k} \sin(R-n)\omega_o t \,.d(\omega_o t) \right\}$$

(19)

or

$$a_n = \frac{v_m}{R\pi} \left\{ \frac{1}{R+n}\left[\cos(R+n)\Phi_k - \cos\left[(R+n)(\Phi_k+\alpha_k)\right]\right] + \frac{1}{R-n}\left[\cos(R-n)\Phi_k - \cos\left[(R-n)(\Phi_k+\alpha_k)\right]\right] \right\}$$

and (20)

$$b_n = \frac{2}{R\pi} \int_{\Phi_k}^{\Phi_k+\alpha_k} V_m \sin(R\omega_o t).\sin(n\omega_o t).d(\omega_o t)$$

since (21)

$$\sin(R\omega_o t).\ \sin(n\omega_o t) = \frac{1}{2}\left[\cos(R+n)\omega_o t - \cos(R-n)\omega_o t\right]$$

(22)

then (21) becomes

$$b_n = \frac{2}{R\pi} \cdot \frac{V_m}{2} \left\{ \int_{\Phi_k}^{\Phi_k+\alpha_k} \cos(R+n)\omega_o t \,.d(\omega_o t) - \int_{\Phi_k}^{\Phi_k+\alpha_k} \cos(R-n)\omega_o t \,.d(\omega_o t) \right\}$$

(23)

or

$$b_n = \frac{v_m}{R\pi} \left\{ \frac{1}{R+n}\left[\sin\left[(R+n)(\Phi_k+\alpha_k)\right] - \sin(R+n)\Phi_k\right] - \frac{1}{R-n}\left[\sin(R-n)(\Phi_k+\alpha_k) - \sin(R-n)\Phi_k\right] \right\}$$

Where (24)

$R = \frac{f_i}{f_o}$

Vm = cycloconverter input voltage amplitude as shown in Figure 3

n = 1 , 2 , 3 , 5 , ...

α°_k = ON durations for kth pulse pair(Fig. 8) , resulting from (14)

k = 1 , 2 , 3 , ... , R (number of pulses per cycloconverter output voltage half cycle

$$\Phi_k = (k - \frac{1}{2}).\ \pi \ - \ \frac{1}{2}\alpha_k$$

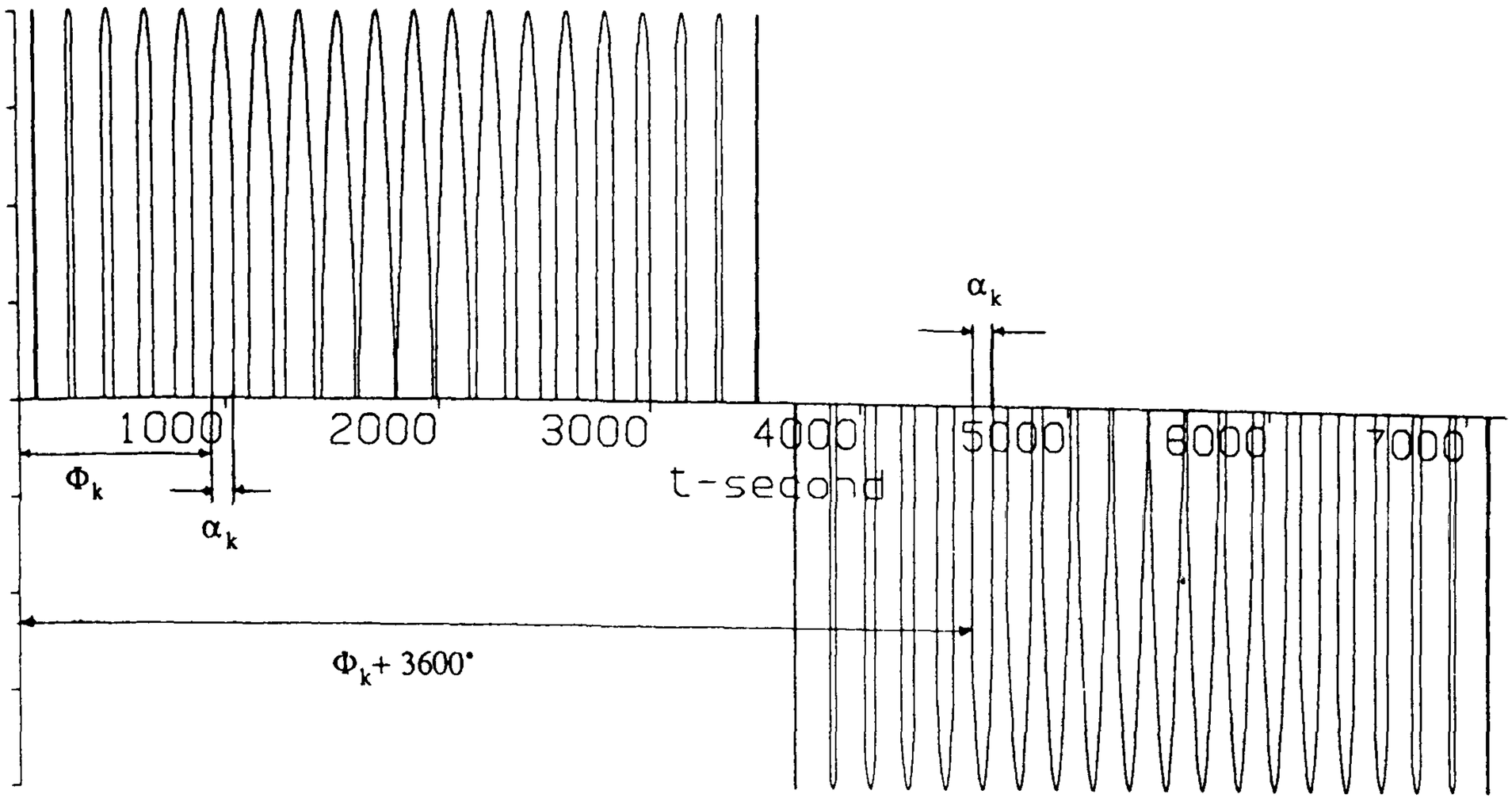

Figure 8 Output voltage of the cycloconverter

Therefore A_n and B_n can be expressed as follows :

$$A_n = \sum_{k=1}^{R} \frac{V_m}{R\pi} \left\{ \frac{1}{R+n}\left[\cos(R+n)\Phi_k - \cos\left[(R+n)(\Phi_k+\alpha_k)\right]\right] + \frac{1}{R-n}\left[\cos(R-n)\Phi_k - \cos\left[(R-n)(\Phi_k+\alpha_k)\right]\right] \right\} \quad (25)$$

$$B_n = \sum_{k=1}^{R} \frac{V_m}{R\pi} \left\{ \frac{1}{R+n}\left[\sin\left[(R+n)(\Phi_k+\alpha_k)\right] - \sin(R+n)\Phi_k\right] - \frac{1}{R-n}\left[\sin\left[(R-n)(\Phi_k+\alpha_k)\right] - \sin(R-n)\Phi_k\right] \right\} \quad (26)$$

By substituting (25) and (26) in to following expression

$$v_0(\omega_o t) = \sum_{n=1,3,5}^{\infty} \left[A_n \cos(n\omega_o t) + B_n \sin(n\omega_o t)\right] \quad (27)$$

The general expression of the cycloconverter output voltage will can be obtained.

REFERENCES

1 I. Yamato , N. Tokunaga , Y. Matsuda , H. Amano , and Y. Suzuki "New conversion system for UPS using high frequency link" IEEE , PESC 1988 , pp.658-663 .

2 V.T. Ranganathan , P.D. Ziogas and U.R. Stefanovic "A DC-to-AC power conversion technique using twin resonant high freuency links" IEEE ,IA-19,No. 3,1983 ,pp.393-400

3 A.K.S Bhat , S.B. Dewan "DC to Utility interface using sinewave resonant inverter" IEE,Vol.135,pt. B,No. 5,sep. 88,pp.193-201

4 B.R. Pelly "Thyristor phase-controlled converters and cycloconverters,Wiley 1971

5 S. B. Dewan, A. Straughen "Power semiconductor circuits" Wiley 1975

A NOVEL STRATEGY FOR CONTROL OF CYCLOCONVERTERS

Asghar Karamat Tom Thomson Pratap Mehta

Brunel University UK

ABSTRACT

This paper presents a novel technique for controlling cycloconverters. The main advantages claimed are (i) much improved harmonic spectrum in the output voltage, (ii) the proposed strategy allows much easier implementation using microprocessors and (iii) it reduces the possibility of short-circuit between the positive and the negative groups of converters.

INTRODUCTION

Multi-stage power conversion from dc to ac with high frequency-links and inverter-transformer-phase controlled cycloconverter topologies have been of growing interest for uninterruptible power supplies and solar converters. During the last decade, there have been a number of suggestions for dc to ac systems (1,2,3). For a required voltage transformation and/or electrical isolation between the dc input and ac output conventionally a transformer is employed. In the new generation of lighter power converters these demands are met by small transformers operating at high frequency. The relative merits and shortcomings of these new systems, however, have not all been fully explored, but eventually are dependent to some extent on the application and power and voltage levels for which these systems are designed.

CONVENTIONAL MODULATION STRATEGY

Conventional control strategy is based on the cosine-wave crossing method (4,5) for determining the timing of the triggering pulses for cycloconverter switches. Referring to Figure 1 the voltage equations for this configuration are:

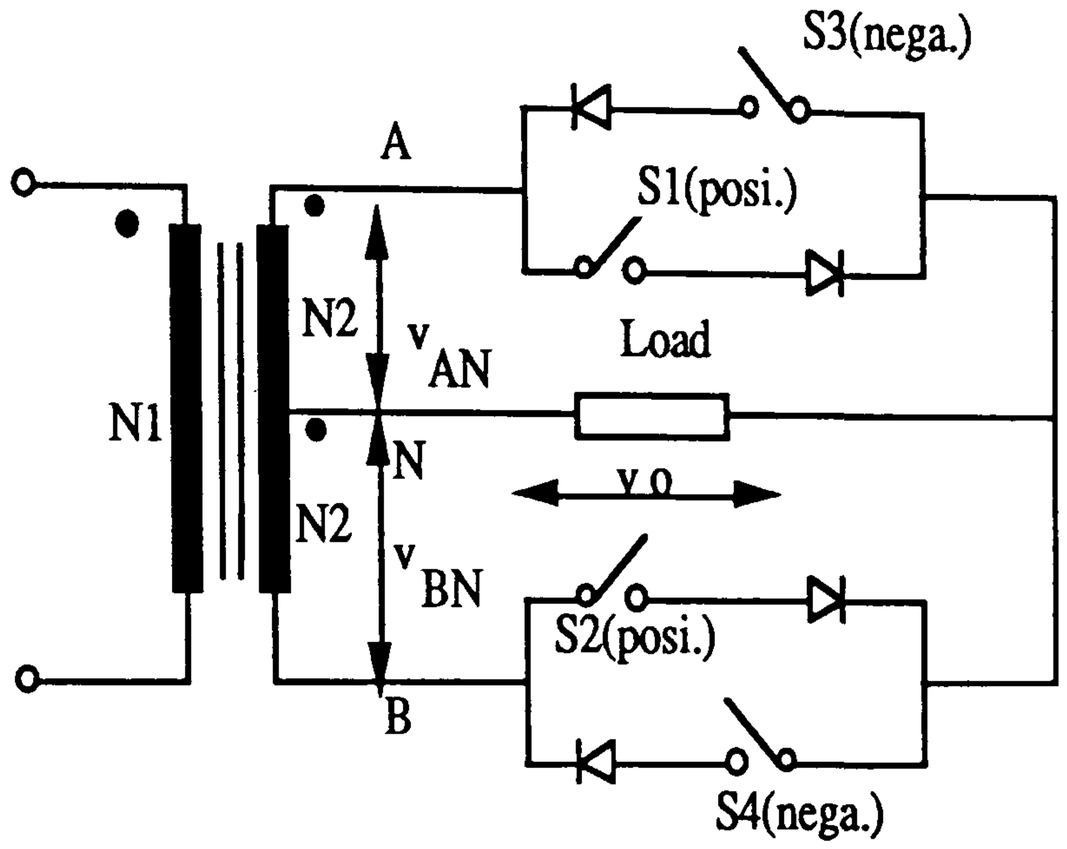

Figure 1 Circuit configuration for conventional modulation strategy

$$v_{AN} = V_m \sin(\omega_i t) \qquad (1)$$

$$u_{AN} = \frac{2}{\pi} V_m \cos(\omega_i t) \qquad (2)$$

$$v_{BN} = V_m \sin(\omega_i t - \pi) = -V_m \sin(\omega_i t) \qquad (3)$$

$$u_{BN} = -\frac{2}{\pi} V_m \cos(\omega_i t) \qquad (4)$$

$$v_o = M.V_m \sin(\omega_o t) \qquad (5)$$

v_o is the cycloconverter output voltage
M is the depth of modulation for output voltage and $0.1 < M < 2/\pi$
$\omega_o = 2\pi f_c$
f_o is the cycloconverter output frequency

R = fi/fo is the input/output frequency ratio. Refering to equations (1) to (5) it is clear that the firing angles are determined so that the average output voltage , produced across the load by a conducting switch , is equal to the instantaneous value of the required output voltage at that firing instant .

From equation (1), for triggering angle α , the average value of the output voltage is

$$v_{ave.} = \frac{1}{\pi}\int_{\alpha}^{\pi+\alpha} V_m \sin(\omega_i t)\, d(\omega_i t) = \frac{2}{\pi} V_m \cos(\alpha) \qquad (6)$$

$$\alpha = \omega_i t = 2\pi f_i t$$

Therefore the (5) and (6) values should be equal at any instant of conduction , so

$$\frac{2}{\pi} V_m \cos(\alpha) = M V_m \sin(\frac{\alpha}{R}) \qquad (7)$$

Equation (7) implies that the intersecting points of a sinusoidal reference voltage with a series of cosine timing waves[(2) and (4)] , which are derived from and synchronized to the ac input voltage , are the required switching points of the switches .

Depending on M, R and fi, equation (7) may be applied by appropriate implementation . For M = 0.63 , R = 20 , fi = 1 kHz and resistive load the full output modulated voltage and associated harmonic spectrum are presented in Figure 2.

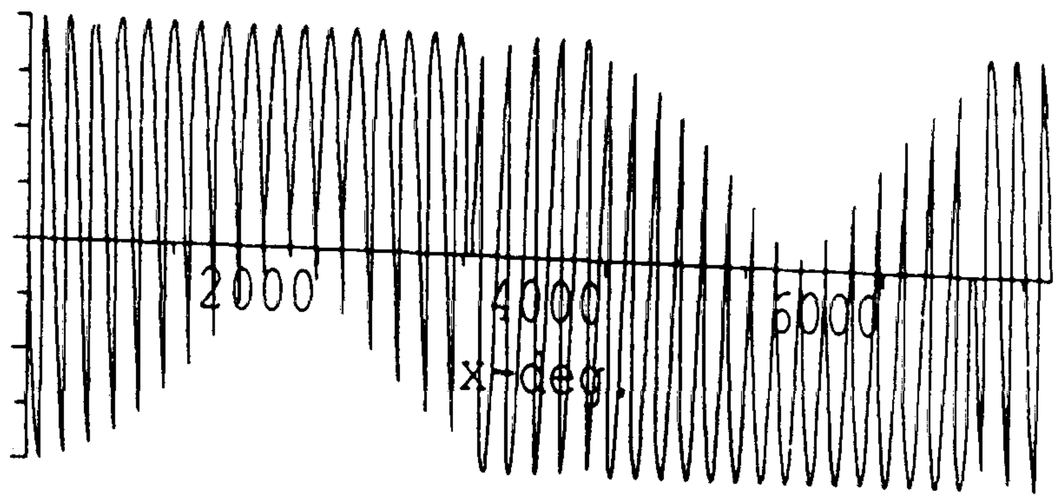

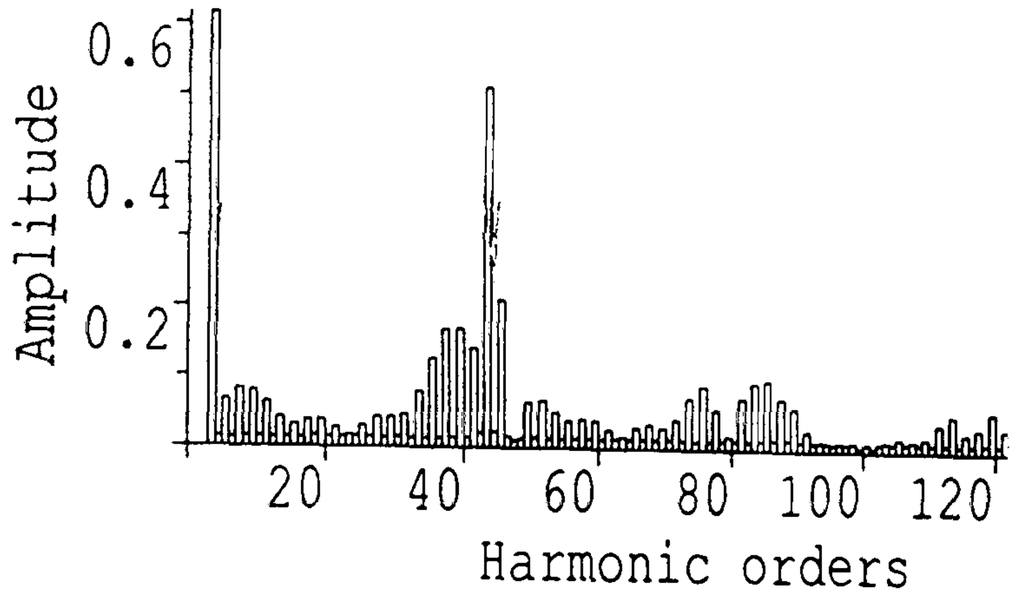

Figure 2 cycloconverter modulated output voltage and associated harmonic spectrum with conventional strategy

Proposed modulation strategy

Figure 3 shows the configuration suitable for implementing the new strategy. S1 to S4 are biletral switches as shown. S1 and S2 conduct when point A is positive with respect to B and similarly S3 and S4 conduct when point B is positive with respect to A, thereby producing the positive half-cycle of the cycloconverter

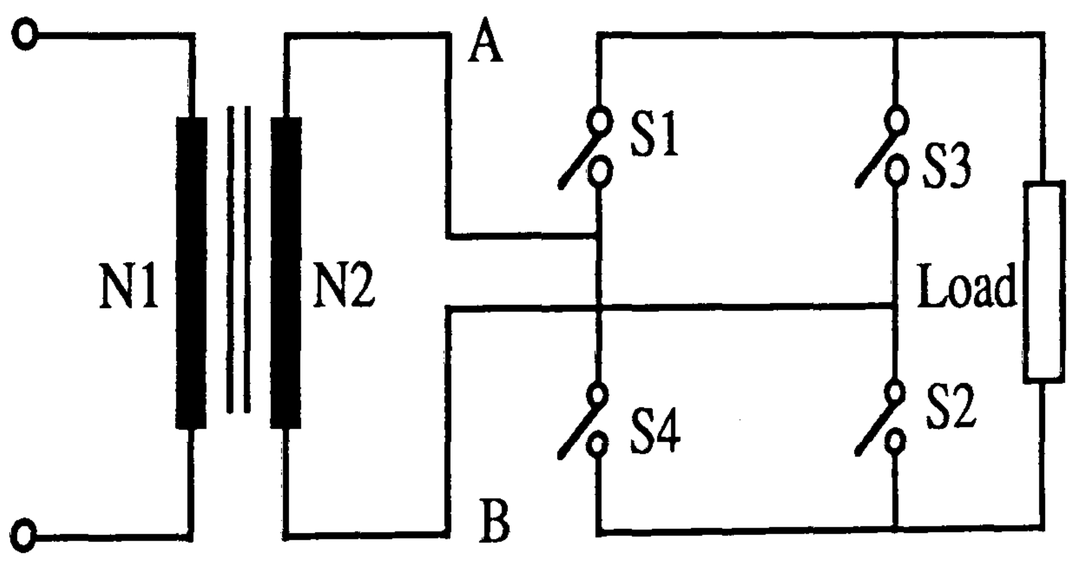

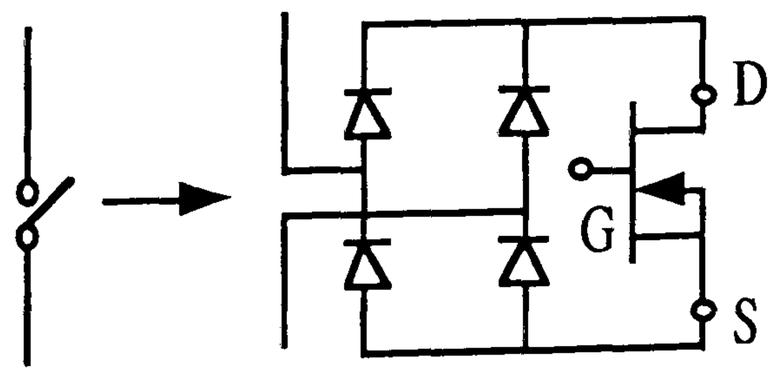

Figure 3 circuit configuration for proposed modulation strategy

output. The negative half-cycle of the output is produced in a similar fashion. Figure 4 illustrates the strategy for deriving the triggering angles of the switches which uses the "equal area crierion" i.e. the hatched area being equal to the dotted area. The two ares are given by the following expressions.

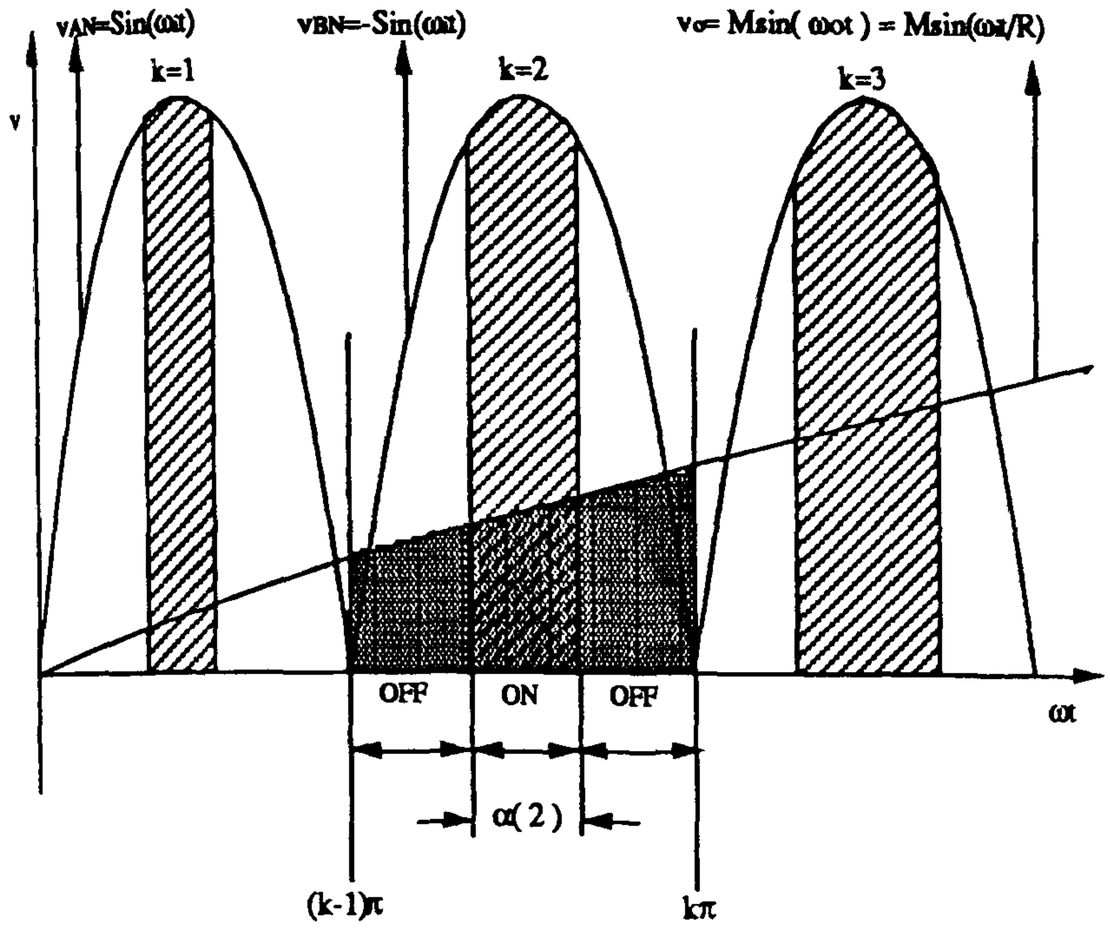

Figure 4 Equal area criterion for proposed modulation strategy

$$A_{dot} = \int_{\frac{(k-1)\pi}{\omega_i}}^{\frac{k\pi}{\omega_i}} MSin(\omega_o t)dt \qquad (8)$$

$$= \frac{M}{R}\left[Cos(k-1)\frac{\pi}{R} - Cos(k\frac{\pi}{R})\right]$$

$$A_{hatch.} = \int_{\frac{(k-1)\pi+\frac{\pi}{2}-\frac{\alpha}{2}}{\omega_i}}^{\frac{(k-1)\pi+\frac{\pi}{2}+\frac{\alpha}{2}}{\omega_i}} Sin(R\omega_o t)\,dt \qquad (9)$$

$$A_{hatch.} = \frac{1}{R\omega_o}\left\{ Cos\left[(k-0.5)\pi - \frac{\alpha}{2}\right] - Cos\left[(k-0.5)\pi + \frac{\alpha}{2}\right] \right\} \qquad (10)$$

Since :

$$Cos(Q) - Cos(P) = 2Sin(\frac{P+Q}{2})Sin(\frac{P-Q}{2}) \qquad (11)$$

Then :

$$A_{hatch.} = 2Sin(k-0.5)\pi.Sin(\frac{\alpha}{2}) \qquad (12)$$

By equating (8) with (12) :

$$A_{dot.} = A_{hatch}$$

or

$$\frac{M}{\omega_o}\left[Cos(k-1)\frac{\pi}{R} - Cos(k\frac{\pi}{R})\right] = \qquad (13)$$

$$= \frac{2}{R\omega_o}.Sin(k-0.5)\pi.Sin(\frac{\alpha}{2})$$

From equation (13) the value of $\alpha(k)$ can be determined from:

$$\alpha(k) = Sin^{-1}\left[\frac{X}{Y}\right].\frac{360}{\pi} \qquad (14)$$

Where

$$X = RM\left[Cos(k-1)\frac{\pi}{R} - Cos(k\frac{\pi}{R})\right] \qquad (15)$$

$$Y = 2(-1)^{k+1}Sin(k-0.5)\pi$$

Where

k = 1,2,3,.....2R

M = 0, ...$2/\pi$

For M = 0.63, R = 20 and fi = 1 kHz, the modulated output voltage and associated harmonic spectrum are presented in Figure 5.

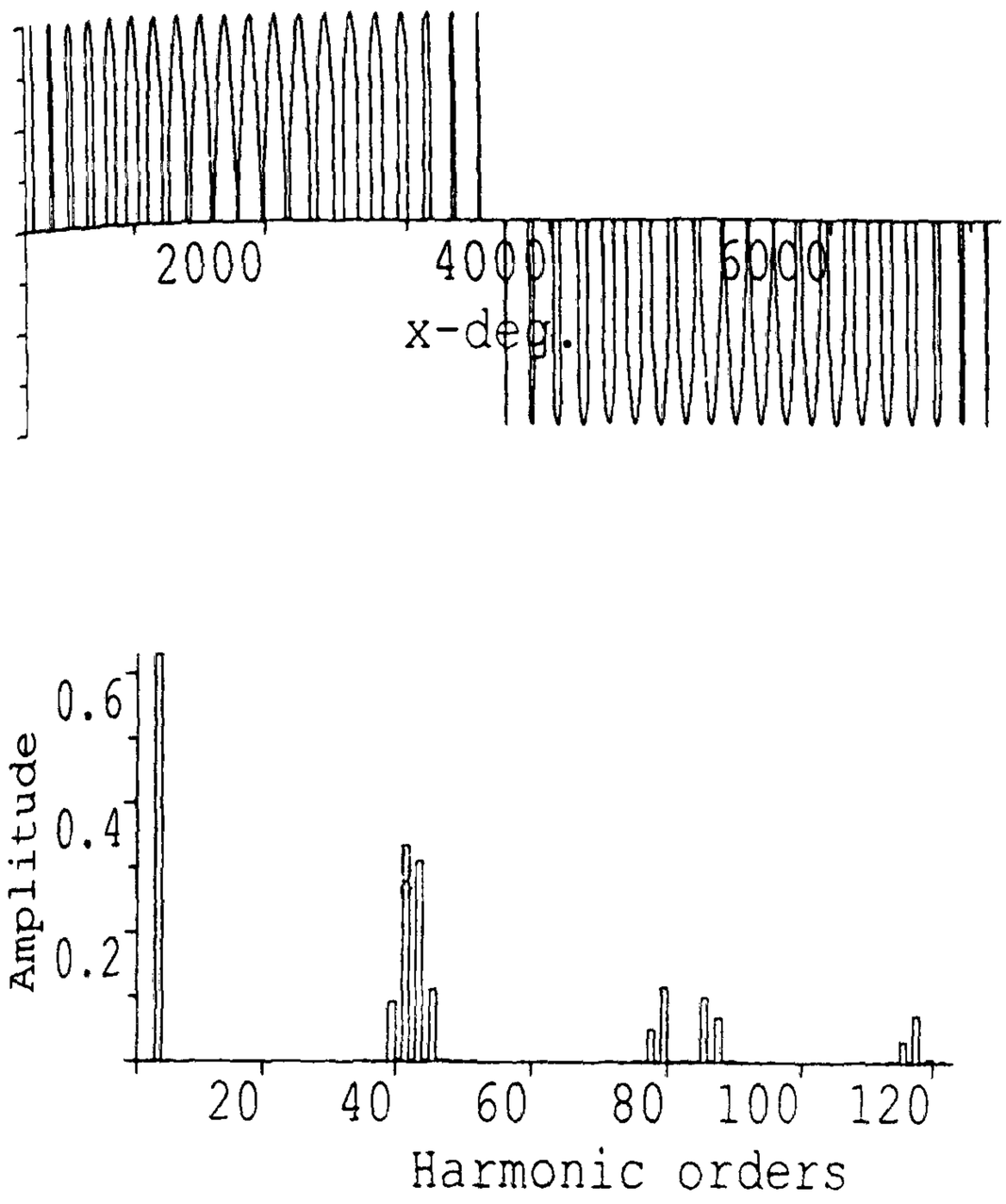

Figure 5 cycloconverter modulated output voltage and associated hamonic spectrum with proposed strategy

EXPERIMENTAL RESULTS

The proposed control strategy was verified on:

(i) a single-phase cycloconverter supplied from a 1 kHz source. Figure 6 (a) & (b) show the output voltage waveform(50 Hz fundamental) and harmonic content respectively .

(ii) a three-phase cycloconverter supplied at lkHz from a dc source via a 1kHz inverter-transformer system.

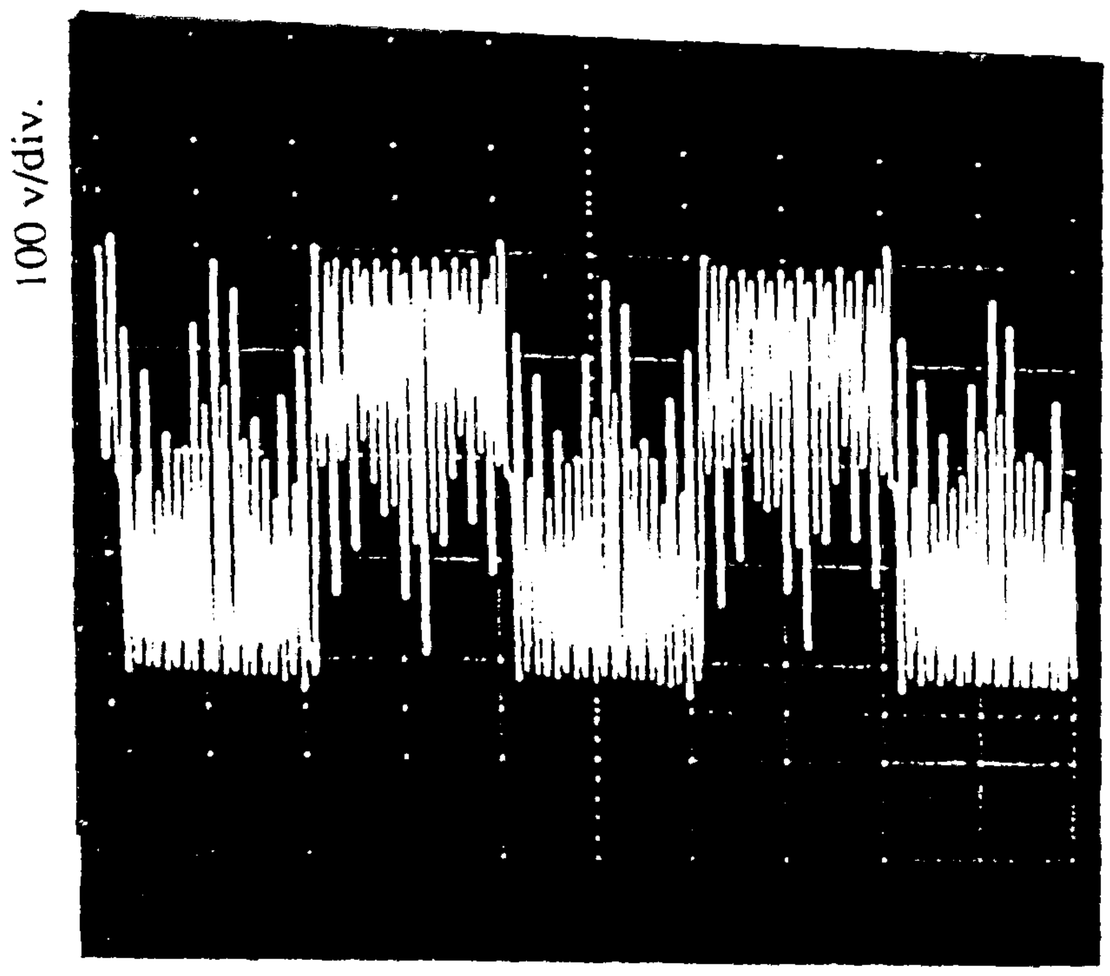

(a) 5 msec./div.

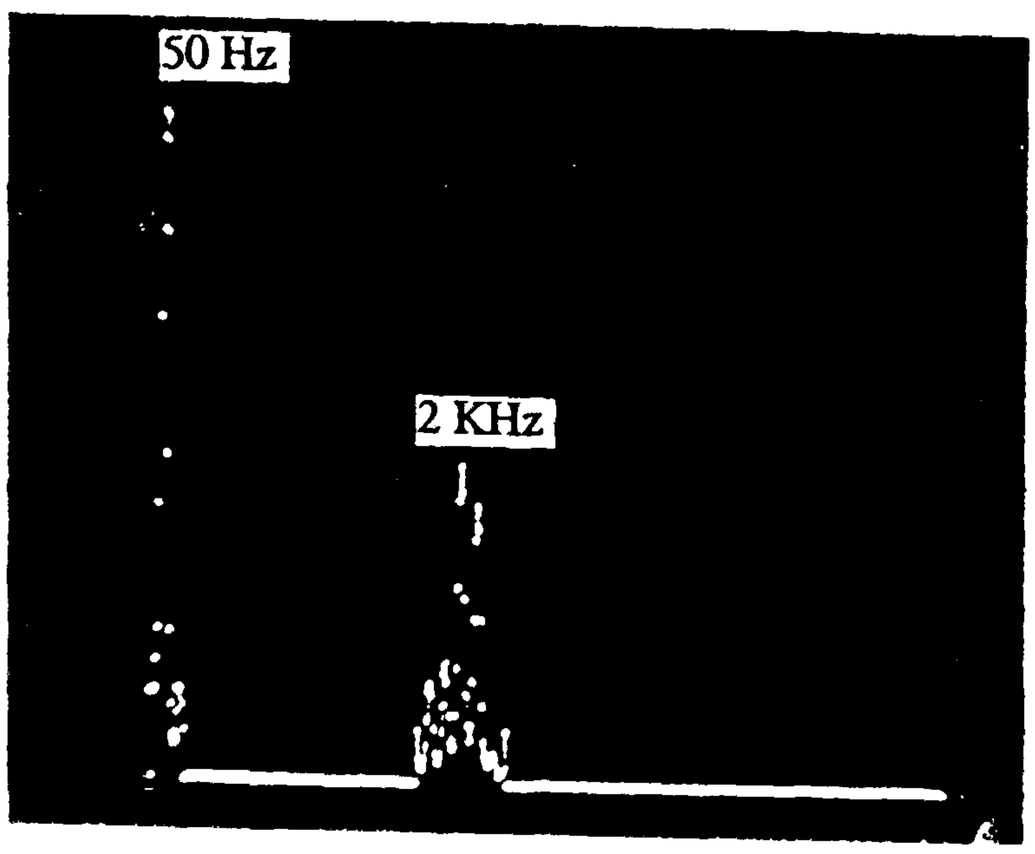

(b)

Figure 6 cycloconverter output voltage waveform(a) & associated harmonic contet(b)

Figure 7 shows the output voltage harmonic spectrum of the 50Hz output cycloconverter. As can be seen there are no significant harmonics below 2kHz for the input frequency of lkHz. Also this results compare very favourably with the predicted spectrum shown in Figure 5.

Figure 8 shows the three-phase voltage waveforms. For measurement purposes these oscillograms were obtained with a 2 microfarad capacitor connected across the output to filter out harmonics in excess of 1.8 kHz.

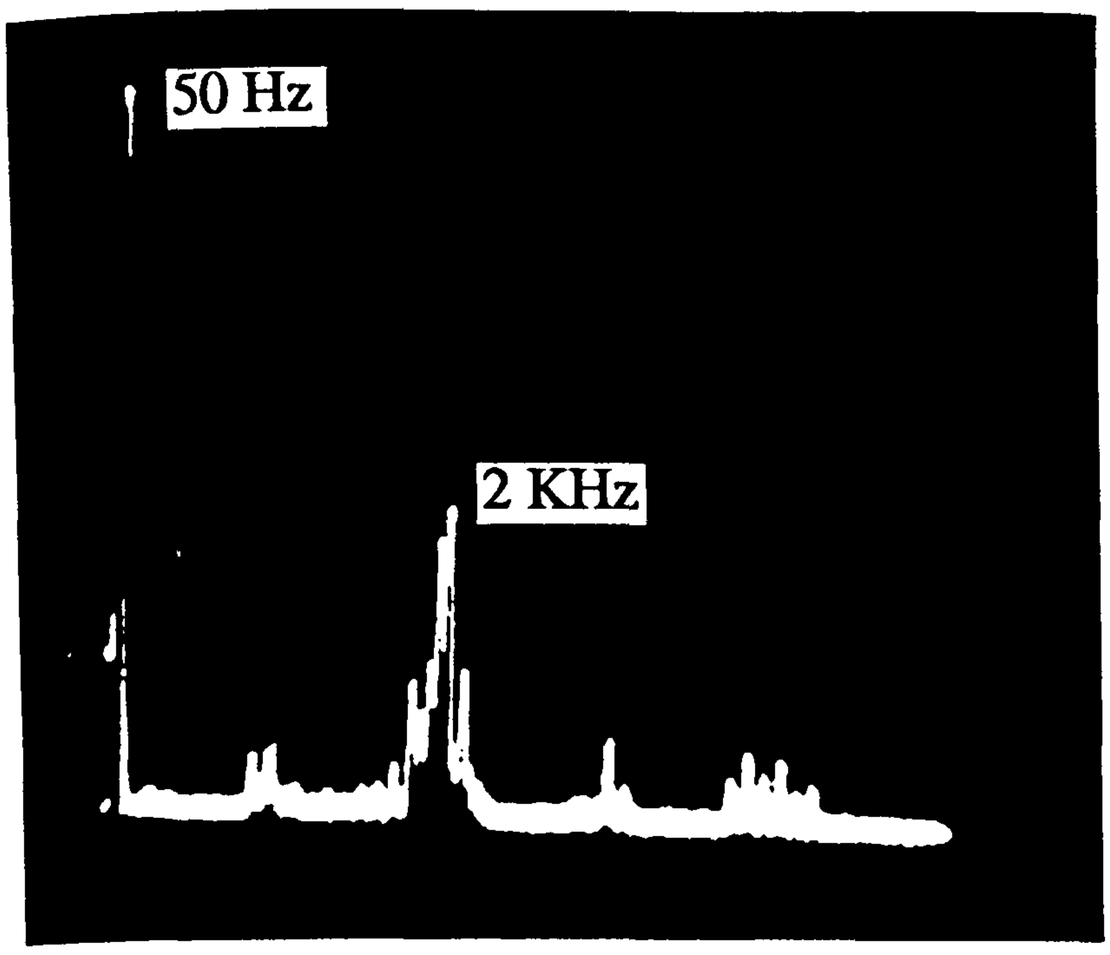

Figure 7 Output voltage harmonic spectrum

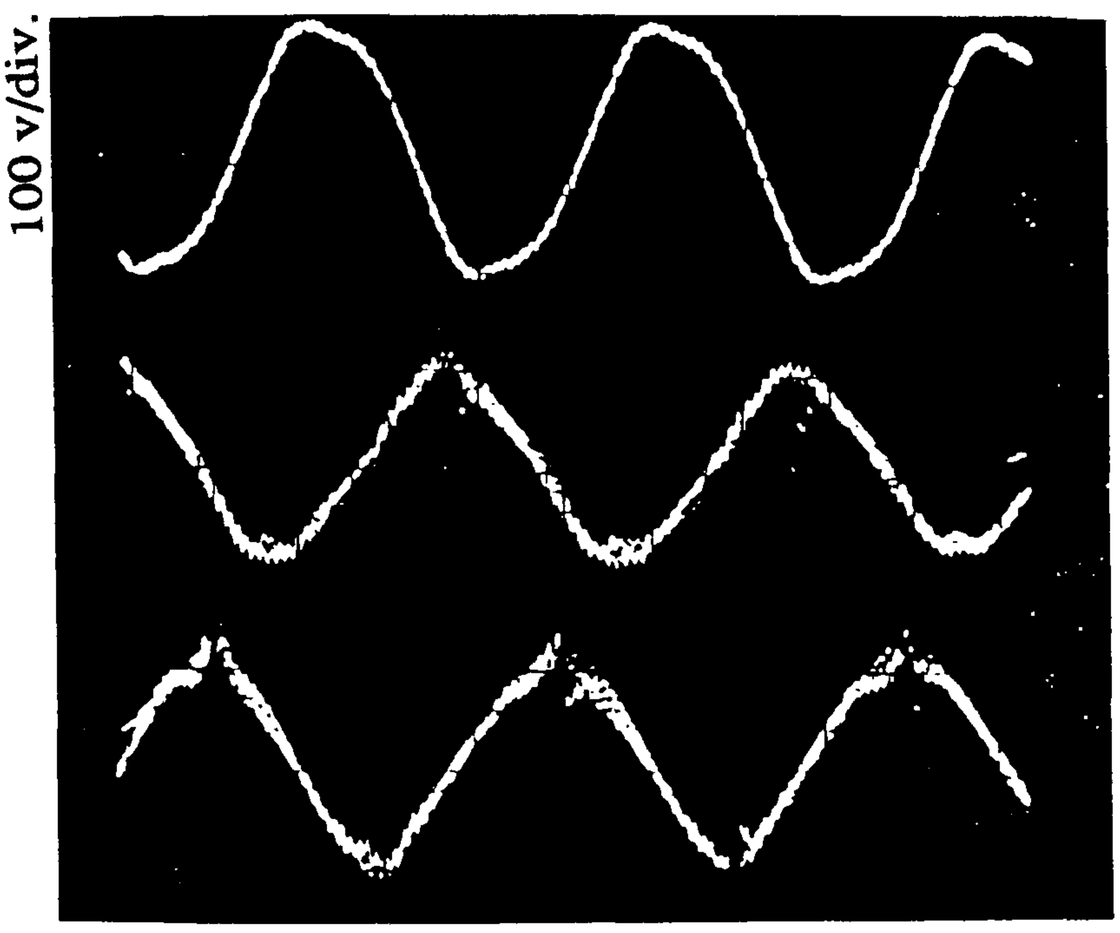

Figure 8 Three phase output voltage waveforms

CONCLUSIONS

The proposed control strtategy for a non-circulating current cycloconverter offers the following advantages:

1 Typically for a 1kHz input system the control strategy assures that there are no significant harmonics below 2kHz.

2 The strategy is amenable to implementation using on-line microprocessor control i.e. equation (14) can be programmed into the system.

3 Unlike conventional cycloconverter the proposed configuration does not require any centre-tapped windings.

ACKNOWLEDGEMENT

Mr. Asghar Karamat is grateful for a research award by University of Urmia-IRAN

REFERECES

1 I. Yamato , N. Tokunaga , Y. Matsuda , H. Amano , and Y. Suzuki "New conversion system for UPS using high frequency link" IEEE , PESC 1988 , pp.658-663 .

2 V.T. Ranganathan , P.D. Ziogas and U.R. Stefanovic "A DC-to-AC power conversion technique using twin resonant high freuency links" IEEE ,IA-19,No. 3,1983 ,pp.393-400

3 A.K.S Bhat , S.B. Dewan "DC to Utility interface using sinewave resonant inverter" IEE,Vol.135,pt. B,No. 5,sep. 88,pp.193-201

4 B.R. Pelly "Thyristor phase-controlled converters and cycloconverters,Wiley 1971

5 S. B. Dewan, A. Straughen "Power semiconductor circuits" Wiley 1975